CYANOCARBAZOLE-BASED ORGANIC MATERIALS FOR ELECTRONIC APPLICATIONS

Ph.D. THESIS

by

V. JOSEPH

DEPARMENT OF CHEMISTRY
INDIAN INSTITUTE OF TECHNOLOGY ROORKEE
ROORKEE - 247 667 (INDIA)
MARCH, 2018

CYANOCARBAZOLE-BASED ORGANIC MATERIALS FOR ELECTRONIC APPLICATIONS

A THESIS

Submitted in partial fulfilment of the requirements for the award of the degree

of

DOCTOR OF PHILOSOPHY

in

CHEMISTRY

by

V. JOSEPH

DEPARMENT OF CHEMISTRY
INDIAN INSTITUTE OF TECHNOLOGY ROORKEE
ROORKEE-247 667 (INDIA)
MARCH, 2018

INDIAN INSTITUTE OF TECHNOLOGY ROORKEE
ROORKEE

CANDIDATE'S DECLARATION

I hereby certify that the work which is being presented in the thesis entitled **"CYANOCARBAZOLE-BASED ORGANIC MATERIALS FOR ELECTRONIC APPLICATIONS"** in partial fulfilment of the requirements for the award of the Degree of Doctor of Philosophy and submitted in the Department of Chemistry of the Indian Institute of Technology Roorkee, Roorkee is an authentic record of my own work carried out during a period from July, 2013 to March, 2018 under the supervision of Dr. K. R. Justin Thomas, Associate Professor, Department of Chemistry, Indian Institute of Technology Roorkee, Roorkee.

The matter presented in the thesis has not been submitted by me for the award of any other degree of this or any other Institution.

(V. JOSEPH)

This is to certify that the above statement made by the candidate is correct to the best of my knowledge.

(K. R. Justin Thomas)
Supervisor

Dated:

ACKNOWLEDGEMENTS

First and foremost, I thank the Lord Jesus Christ for his blessings, without ***Him*** *it would not have been possible to bring out this thesis.*

It is my pleasure to extend my deepest sense of gratitude to my supervisor ***Dr. K. R. Justin Thomas****, for his meticulous guidance and continuous support throughout the work of this thesis. His perpetual energy, enthusiasm in research and constructive criticism motivated me during this tenure.*

I extend my thanks to SRC (Student Research Committee) members, ***Prof. M. R. Maurya*** *(Professor and Head, Department of Chemistry, IIT Roorkee),* ***Dr. R. K. Peddinti****, (Associate Professor, Department of Chemistry, IIT Roorkee),* ***Dr. B. S. S. Daniel****, (Professor, Department of Metallurgical and Materials Engineering, IIT Roorkee) for their valuable suggestions and constant support.*

I am thankful to Head, Department of Chemistry for providing necessary facilities to carry out the experiments.

I also thank ***Prof. Jwo-Huei Jou*** *and his group members, National Tsing Hua University, Taiwan for the device fabrication and characterizations.*

I convey my gratitude to lab mates: ***Sunil, Ankita, Ambika, Tina, Anupriya, Anuj, Abhishek, Dr. Snehasis, Dr. Bhaskar, Dr. Bala, Dr. Abhishek, Dr. Venkat, Dr. Babu, Dr. Karthik, Dr. Rajendra*** *for providing friendly environment and valuable scientific discussions.*

I take this opportunity to acknowledge the Ministry of Human Resource Development, New Delhi for providing financial assistance.

I extend my heartfelt thanks to ***Mrs. Jeyaseeli Justin*** *for her blessings and hospitality.*

I thank my parents for their blessings and encouragement to accomplish this thesis.

V. Joseph

Abstract

Organic materials have received immense attention in the last few decades owing to their utility in optoelectronic applications particularly organic light emitting diodes (OLED) and photovoltaics. The OLED serves as potentially energy saving technology when compared to their inorganic counterpart light sources such as liquid crystal displays and incandescent sources. Further, they provide low cost and environmental sustainability over their hazardous inorganic counterparts. The wide range of availability of organic chromophores and their facile functional modification leads to the development of library of organic emitters exhibiting primary colors such as red, green and blue. Despite of benchmark red and green emitters, blue emitters showing high efficiency and long durability are scarce in the literature owing to their associated wide band gap and improper charge injection and transportation. Thus, the pursuit of developing highly efficient blue emitters exhibiting good charge transport and better morphological stability is indispensable. In general, the efficacy of functional chromophore decides the fate of OLED device in terms of efficiency and durability. Carbazole is considered as a potential building block for the construction of fluorescent emitters since they possess high charge carrier mobility, good quantum yields, wide band gap and good electronic conjugation. The facile functionalization at various nuclear position of carbazole opens promising pathway for developing number of organic materials with tunable properties. The materials exhibiting bipolar character are desirable for realizing high efficiency because they provide balanced charge mobility. Generally, the incorporation of electron withdrawing group on carbazole results in bipolar nature. The modification at 3,6-position of carbazole gives good redox properties and the insertion of electron withdrawing group induces donor-acceptor interaction. The detrimental donor-acceptor interaction must be controlled otherwise which would quench the emission. On the other hand, 2,7-substitution of carbazole suppresses donor-acceptor interaction while providing extended conjugation. So, the carbazole-based materials containing 2,7-substitution got significant attention.

This thesis is classified into seven chapters. Chapter 1 presents the review of functional derivatives of carbazole in OLED applications as hole transporter, fluorescent emitter, thermally activated delayed fluorescence (TADF) emitter and phosphorescent host. Carbazole substitution at 3,6-position provides good redox properties, 2,7-substitution gives extended conjugation while 1,8-position results good morphological stability. However, *N*-functionalization did not

alter conjugation length, though increased the solubility of the materials. Chapter 2 deals with the aim and scope of the thesis in which cyanocarbazole-based derivatives are developed for fluorescent OLED applications. Chapter 3 to Chapter 6 presents the carbazole-based materials containing electron withdrawing cyano group and different chromophoric moieties as fluorescent emitters. The highlight of the thesis can be summarized as below.

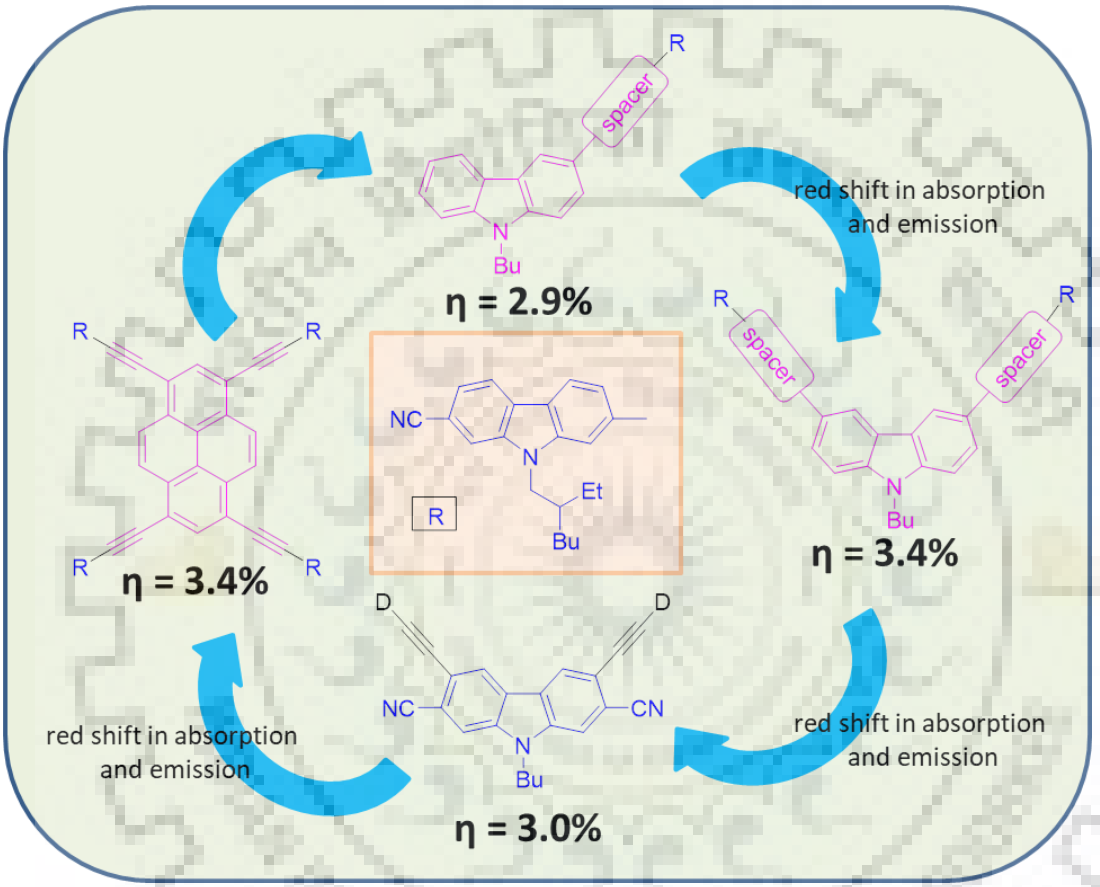

Chart 1. Pictorial representation of the work done in this thesis.

In chapter 3, asymmetrically 2,7-substituted carbazole derivatives are presented as fluorescent emitters. The photophysical properties of the dyes are dependent on the nature of chromophore attached. Further, the effect of acetylene/vinyl spacer between cyanocarbazole and the chromophore on optical, electrochemical and electroluminescent properties is elucidated. The absorption maxima of the compounds depending on the linker are in the order of direct < acetylene < vinyl. Carbazole/triphenylamine substituted dyes showed positive solvatochromism in emission spectra which is due to intramolecular charge migration from donor to acceptor. Electrochemical studies revealed high oxidation propensity for

triphenylamine substituted compounds among the substituents and for vinyl spacer among three different linkers. The high onset thermal decomposition temperature of carbazole substituted dyes is attributed to the presence of two rigid carbazole molecular back bones. All the dyes showed deep blue electroluminescence emission with the CIE coordinate of $0.15 \leq x \leq 0.17$ and $0.04 \leq y \leq 0.10$ while vinyl derivatives carbazole, triphenylamine and pyrene showed $0.12 \leq y \leq 0.33$. The best electroluminescence performance is realized for the device fabricated with a dye containing triphenylamine chromophore directly connected to cyanocarbazole chromophore exhibiting the maximum EQE of 4.1%.

In chapter 4, cyanocarbazole end-capped rigid and rod-like fluorophores containing fluorene or carbazole bridge are described. The optical and electroluminescence properties of the dyes are tuned by altering the bridge and the position/mode of linkage. The absorption maxima depends on the nature of bridge and follows the order 3,6-carbazole < 2,7-fluorene < 2,7-carbazole. The linear carbazole dyes displayed high thermal robustness when compared to fluorene analogs which is ascribed to three rigid carbazole units. Linear dyes showed typical π-π^* transition while V-shaped carbazole dyes showed intramolecular charge transfer transition. The largest Stokes shift is observed for directly connected dyes which indicate the involvement of high degree of structural reorganization of the dye molecules in the excited state. Despite of similar HOMO energy levels, dyes containing acetylene spacer showed low lying LUMO over directly connected dyes. It supports the electron withdrawing nature of acetylene spacer. The cyano end capping is found to be helpful in realizing balanced charge transport and thus better electroluminescence performance when compared to the known compounds in the literature. The devices fabricated with the dyes as emitting dopants in CBP host system showed deep blue emission with CIEy of 0.04. The electroluminescence performances of these dyes are superior to their analogous dyes containing only one cyanocarbazole unit (Chapter 3).

In chapter 5, pyrene appended cyanocarbazoles connected through acetylene spacer are presented. The optical and electroluminescence properties of the dyes are drastically changed as the number of cyanocarbazole units increased on the pyrene core. Particularly, 1,6- and 1,8-disubstituted dyes exhibited different optical and electroluminescence properties. 1,6-disubstitued dye showed hypsochromic absorption maxima when compared to mono-substituted dye while 1,8-disubstituted dye showed bathochromic shift. The solvent independent absorption and emission profiles of the dyes indicate the absence of donor-acceptor interactions. The

electroluminescence emission is tuned from deep blue to green color depending on cyanocarbazole density. The power and current efficiency of the dyes are linearly increased as the number of cyanocarbazole units increased on the pyrene core. It clearly indicates the role of cyanocarbazole in realizing the balanced charge transport and thus better device performance.

In chapter 6, a series of donor-acceptor configured arylamine donor substituted cyanocarbazoles linked through acetylene spacer is developed. The π electronic conjugation of triphenylamine dyes is increased as compared to their carbazole analogs. This leads to enhancement in thermal stability for them over rigid carbazole counterparts. The compounds containing arylamine acetylene at 2,7-position of core carbazole displayed negative absorption solvatochromism while the other isomers showed solvent independent absorption profiles. The positional variation of donor and acceptor tuned the optical and electroluminescence properties of the dyes. Despite of similar HOMO energy levels, 1,8-arylamine substituted dyes showed wide band gap over 2,7-substitued congeners which is due to the steric nature of the former. The high lying HOMO energy level of triphenylamine substituted dyes align well with the neighboring charge transporting layer which favors facile charge injection. As a result, low turn-on voltage and superior electroluminescence performance is observed. The best performance is obtained for the dye containing 3,6-dicyano and triphenylamine at 2,7-position of carbazole (3 wt%) exhibiting power efficiency, current efficiency and EQE of 5.3 lm/W, 6.7 cd/A and 4.1% respectively.

In chapter 7, summary of thesis is presented. The structure-property relationships among the dyes established in the thesis is critically analyzed. The outcome is used as a basis to predict the development of conceptually advanced emitters.

Table of Contents

List of Figures

List of Tables

List of Charts

List of Schemes

List of Abbreviations

ACN	Acetonitrile
ACQ	Aggregation caused quenching
ACT	Acetone
AFM	Atomic Force Microscopy
AIE	Aggregation induced emission
Al	Aluminium
Alq_3	Tris(8-hydroxyquinolinato)aluminium
BCP	Bathocuproine
$Bepp_2$	Bis(2-(2-hydroxyphenyl)pyridine)beryllium
BPBPA	*N,N,N'N'*-tetra[(1,1'-biphenyl)-4-yl]-(1,1'-biphenyl)-4,4'-diamine
Bphen	Bathophenanthroline
BP_4mPy	3,3',5,5'-tetra[(m-pyridyl)-phen-3-yl]biphenyl
Ca	Calcium
CBP	4,4'-N,N'-dicarbazolylbiphenyl
$CHCl_3$	Chloroform
CIE	Commission International de l'Ėclairage coordinates
Cs_2CO_3	Cesium carbonate
CsF	Cesium fluoride
CT	Charge transfer
CV	Cyclic voltammetry
C_4-DFQA	*N*,*N*'-di(nbutyl)-2,9-difluoroquinacridone
CzPS	9,9′-(sulfonylbis(4,1-phenylene))bis(9*H*-carbazole)
2CzPN	4,5-di(9*H*-carbazol-9-yl)phthalonitrile
4CzIPN	2,4,5,6-tetra(9*H*-carbazol-9-yl)isophthalonitrile)
D-A	Donor-acceptor
DBFTrz	2,8-bis(4,6-diphenyl-1,3,5-triazin-2-yl)- dibenzo[b,d]thiophene
DCM	Dichloromethane
DBE	Dibutyl ether
DFT	Density functional theory
DMF	*N*,*N*-dimethylformamide
DNTPD	*N,N'*-diphenyl-*N,N'*-bis-[4-(phenyl-m-tolyl-amino)-phenyl]-biphenyl-4,4'-diamine
DPDT-ICZ	Diphenyl indolo [3,2-*b*]carbazole
DPEPO	Bis[2-(diphenylphosphino)phenyl] ether oxide
DPPO	Diphenylphosphine oxide
DPV	Differential pulse voltammetry
DSSC	Dye sensitized solar cells
ΔE_{ST}	Singlet to triplet energy gap
EA	Ethyl acetate
EBU	European broadcast union
EML	Emissive layer
EL	Electroluminescence
EQE	External quantum efficiency
F_c/F_c^+	Ferrocene/ferrocenium
FIrpic	Bis[2-(4,6-difluorophenyl)pyridinato-C^2,*N*](picolinato)iridium(III)

FWHM	Full width at half maxima
HOMO	Highest occupied molecular orbital
HATCN	1,4,5,8,9,11-hexaazatriphenylenehexacarbonitrile
HLCT	Hybridized local and charge transfer
HRMS	High resolution mass spectrometry
HTL	Hole transporting layer
ICT	Intramolecular charge transfer
$Ir(dbi)_3$	Tris[1-(2,4-diisopropyldibenzo[b,d]furan-3-yl)-2-phenylimidazole] iridium(III)
$Ir(MDQ)_2(acac)$	Bis(2-methyldibenzo[f,h]quinoxaline)(acetylacetonate)iridium(III)
$Ir(mphmq)_2(tmd)$	bis[2-(3,5-dimethylphenyl)-4-methyl-quinoline](acetylacetonate)iridium(III)
$Ir(ppy)_3$	Tris[2-phenylpyridinato-C^2,*N*]iridium(III)
$Ir(2\text{-}phq)_3$	Tris(2-phenylquinoline)iridium(III)
ITO	Indium tin oxide
LE	Local excited state
LiF	Lithium fluoride
L_{max}	Maximum luminance
LUMO	Lowest unoccupied molecular orbital
mCBP	3,3-di(9*H*-carbazol-9-yl)biphenyl
mCP	1,3-bis(*N*-carbazolyl)benzene
MeOH	Methanol
MoO_3	Molybdenum trioxide
m-MTDATA	4,4',4"-tris[(3-methylphenyl)phenylamino]triphenylamine
NMR	Nuclear magnetic resonance spectroscopy
NPB	*N,N'*-di(1-naphthyl)-*N,N'*-diphenyl-(1,1'-biphenyl)-4,4'-diamine
NTSC	National television standards committee
η_c	Current efficiency
η_p	Power efficiency
OFET	Organic field effect transistors
OLED	Organic light emitting diodes
OPV	Organic photovoltaics
OXD-7	1,3-Bis[2-(4-tert-butylphenyl)-1,3,4-oxadiazo-5-yl]benzene
PAH	Polyaromatic hydrocarbons
PCZAc	9,9-dimethyl-10-(9-phenyl-9*H*-carbazol-3-yl)-9,10-dihydroacridine
PEDOT:PSS	Poly(3,4-ethylenedioxythiophene)-poly(styrenesulfonate)
PFN	Poly [(9,9-bis(3'-(*N*,*N*-dimethylamino)propyl)-2,7-fluorene)-alt-2,7-(9,9-dioctylfluorene)]
PhOLED	Phosphorescent organic light emitting diodes
PL	Photoluminescence
PLQY	Photoluminescence quantum yield
PPh_3CH_3Br	Methyltriphenylphosphonium bromide
RISC	Reverse intersystem crossing
TADF	Thermally activated delayed fluorescence
TAPC	4,4'-(cyclohexane-1,1-diyl)bis(*N*-phenyl-*N*-*p*-tolylaniline)
TBADN	2-*tert*-Butyl-9,10-di(naphth-2-yl)anthracene
TCTA	Tris(4-carbazoyl-9-ylphenyl)amine
TEA	Triethylamine

4TCzBN	2,3,5,6-tetrakis[3,6-bis(1,1-dimethylethyl)-9*H*-carbazol-9-yl]benzonitrile
T_g	Glass transition temperature
T_d	Thermal decomposition temperature
TGA	Thermogravimetric analysis
THF	Tetrahydrofuran
TOL	Toluene
TPBi	2,2′,2"-(1,3,5-benzinetriyl)-tris(1-phenyl-1-*H*-benzimidazole)
TPD	*N*,*N*′-bis(3-methylphenyl)-*N*,*N*′-diphenylbenzidine
TPE	Tetraphenylethene
TmPyPB	1,3,5-tri(m-pyridin-3-ylphenyl)benzene
TSPO1	Diphenyl-4-triphenylsilyl-phenylphosphine oxide
V_{on}	Turn-on voltage
ZADN	2-[4-(9,10-di-2-naphthalenyl-2-anthracenyl)phenyl]-1-phenyl

List of Publications

1. **Vellaichamy Joseph**, K. R. Justin Thomas, Meenu Singh, Snehasis Sahoo and Jwo-Huei Jou, "Manipulation of donor-acceptor interactions in carbazole-based emitters by chromophore choice to achieve near-UV emission" *Eur. J. Org. Chem.* **2017**, 6660-6670.
2. **Vellaichamy Joseph**, K. R. Justin Thomas, Snehasis Sahoo, Meenu Singh and Jwo-Huei Jou, "Simple carbazole based deep-blue emitters: The effect of spacer, linkage and end-capping cyano group on the photophysical and electroluminescent properties" *Dyes Pigm.* **2018**, *151*, 310-320.
3. Snehasis Sahoo, Deepak Kumar Dubey, Meenu Singh, **Vellaichamy Joseph**, K. R. Justin Thomas and Jwo-Huei Jou, "Highly efficient deep-blue organic light emitting diode with a carbazole based fluorescent emitter" *Jpn. J. Appl. Phys.* **2018**, DOI: 10.7567/JJAP.57.04FL08

CHAPTER 1

Carbazole-Based Functional Materials for OLED Applications: A Review

1.1 Introduction

Carbazole is a fused heterocyclic aromatic hydrocarbon containing nitrogen at 9-position. Carbazole is an inexpensive and widely available material. It is a white color solid which crystallizes as flakes in hot organic solvents such alcohol, glacial acetic acid, toluene and benzene [1]. Classically, carbazole was extracted from petroleum byproducts in 1878. Pure carbazole fluoresces slightly. The purification process of carbazole from coal tar product involves tedious steps and is difficult. Later, highly pure carbazole was prepared synthetically in laboratories. Graebe and Ullmann method of carbazole synthesis is widely employed to prepare carbazole [2]. The synthesis involves the treatment of *o*-aminodiphenylamine with nitrous acid to give 1-phenyl-1,2,3-benzotriazole which on heating would give carbazole quantitatively with the loss of nitrogen (Scheme 1.1).

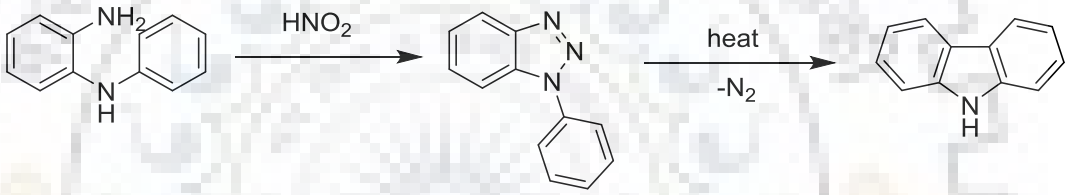

Scheme 1.1 Synthesis of carbazole.

The facile functionalization of carbazole at various nuclear positions makes them attractive in synthetic aspects as well as material property views [3-6]. Carbazole easily undergoes electrophilic substitution reaction at C3, C6, C1 and C8 positions owing to electron donating nature of nitrogen atom. The C3 and C6- positions are highly reactive while the reactivity of C1 and C8- positions is moderate due to steric reasons. N9 position can also be functionalized without altering the molecular backbone [7]. Since the meta- position of carbazole is deactivated, the functionalization at C2 and C7 position is difficult. However, the bottleneck has been overcome by following an indirect method. In material point of view, carbazole is an excellent hole transporter and thermally stable material [8-10]. In addition, carbazole is found to possess fluorescence quantum efficiency and high triplet energy value of about 3.02 eV [11]. The reactivity of carbazole is accelerated by the presence of nitrogen atom compared to the structural analog fluorene. Carbazole undergoes one electron oxidation attributed to the formation of stable dicarbazyl provided the C3 and C6 positions are blocked [12].

Carbazole can be considered as dibenzo pyrrole. Due to the symmetric nature of the fused benzene rings, the reactivity of both the benzene rings is same. The order of reactivity of nuclear positions follows C3,C6 > C1,C8. The bromination of carbazole at various nuclear positions makes them more attractive for the functional modification of carbazole by various metal-catalyzed reaction protocols using appropriate coupling partners. The mono-, di-, tri- and tetra- bromination of carbazole can be easily done by exploiting NBS as brominating reagent with the variation of reagent equivalents (Scheme 1.2) [5,13].

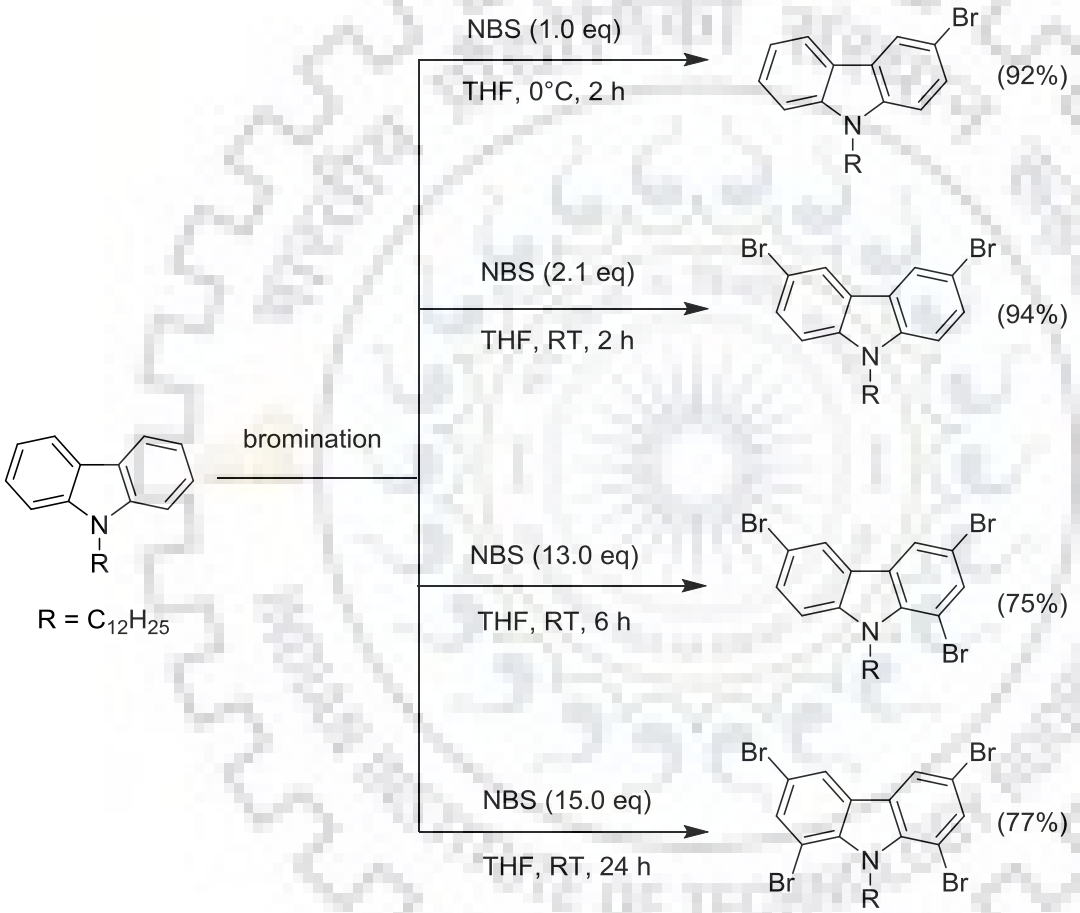

Scheme 1.2 Mono-, di-, tri- and tetra-bromination of carbazole.

The C2 and C7 position of carbazole cannot be functionalized by direct method because of deactivation by electron donating nature of nitrogen atom. However, the limitation was overcome by adopting an indirect synthetic protocol to synthesize 2,7-functionalized carbazole. The most efficient synthetic strategy was developed by Müllen and coworkers during the year 2003 [14]. The synthetic procedure involves the nitration of dibromo biphenyl followed by Cadogan cyclization reaction to yield target 2,7-dibromocarbazole (Scheme 1.3).

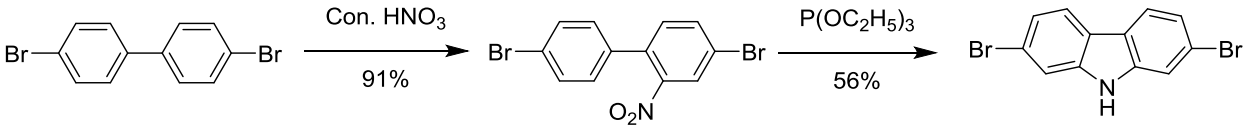

Scheme 1.3 Synthesis of 2,7-dibromo-9*H*-carbazole.

Similarly, the functionalization at bridge-head carbons such as C4 and C5 is also difficult by direct method of electrophilic substitution reactions. Using suitable precursors and appropriate synthetic procedures, Lee and coworkers reported the mono- bromination of carbazole at C4 position [15]. Here, 2-bromophenylboronic acid was reacted with 1-bromo-2-nitrobenzene under Suzuki coupling reaction condition to obtain 2-bromo-2'-nitro-1,1'-biphenyl which then underwent Cadogan ring closure reaction by using triphenylphosphine as reagent to yield 4-bromo-9*H*-carbazole (Scheme 1.4).

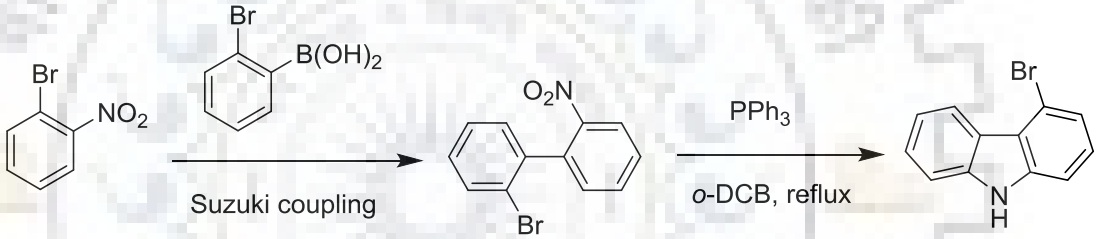

Scheme 1.4 Synthesis of 4-bromo-9*H*-carbazole.

Further, the asymmetric substitution functionalization of carbazole was established by Lee and coworkers [16]. Since the benzene rings of carbazole are equally reactive, asymmetric substitution of carbazole at C2 and C5 positions is realized through indirect method. The synthesis involves the Suzuki coupling reaction between 1,4-dibromo-2-nitrobenzene and 2-bromophenylboronic acid to yield 2′,4-bromo-2-nitro-1,1′-biphenyl which then converted into 2,5-dibromo-9*H*-carbazole by ring closure reaction using triphenylphosphine (Scheme 1.5). Also, they established the high thermal stability of 2,5-functionalzied carbazole over symmetrically 2,7-functionalized one.

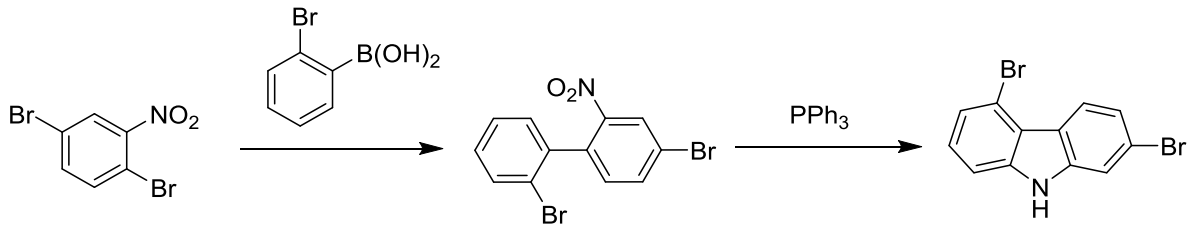

Scheme 1.5 Synthesis of 2,5-dibromo-9*H*-carbazole.

Later, multi-bromination of carbazole was reported by using 2,7-dibromocarbazole as a starting material. Tao and coworkers synthesized tetra, penta and hexa-bromocarbazole by changing the equivalent of bromine reagent at either low temperature (4 °C) or room temperature with good yields (Scheme 1.6) [17].

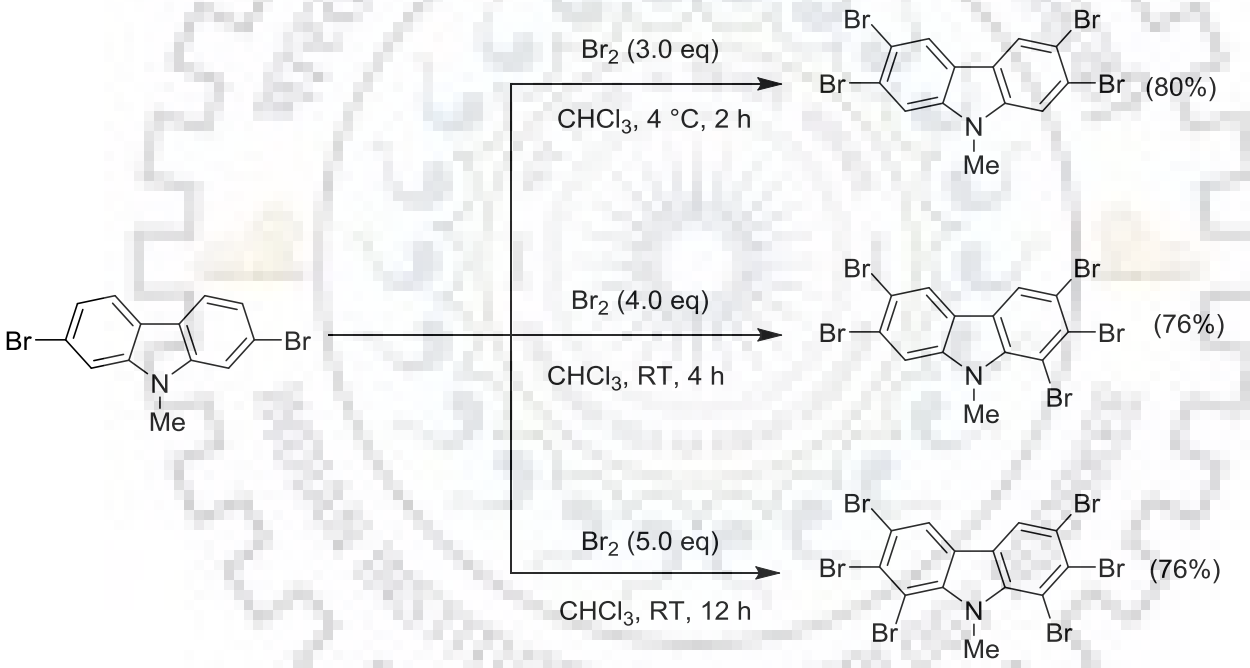

Scheme 1.6 Multi-bromination of carbazole.

The halogenated carbazole provides wide opportunity to functionally tune the carbazole using various conjugated chromophores. The halogenated carbazoles easily undergo a number of coupling reactions such as Suzuki coupling (boronic acids and boronic ester), Stille coupling (tin reagents), Heck coupling (vinyl compounds), Sonogashira coupling (terminal acetylenes) with suitable coupling partners. Further, they undergo C-N coupling reaction protocol developed by Buckwald-Hartwig reactions.

The advantageous material properties of carbazole-based compounds such as high thermal stability, hole transporting nature and high quantum yields are appealing to be exploited in optoelectronic applications. In addition, facile functional modification of carbazole offers library of compounds to functionally tune the material properties by studying the structure-property relationships [9,18,19]. Particularly, they found application in organic light emitting diodes (OLED). Carbazole has been utilized as potential building block for constructing OLED exhibiting desirable performances. Carbazole itself is a blue emitter. But, the emission intensity is weak and falls in ultra-violet region [20]. Moreover, they are prone to form aggregate in solid state. The abovementioned limitations make them unrealistic for the optoelectronic applications. However, these shortcomings can be overcome by the functional modification of carbazole with other conjugate chromophores. The extended conjugation of functionalized carbazole is beneficial to tune the emission color towards visible region from deep blue to red by careful design of molecules using choice of chromophores. Also, the detrimental aggregation could be controlled by incorporating non-planar chromophores [21]. Here, the role of carbazole in designing OLED device with different functional properties is briefly reviewed.

1.2 Carbazole functionalized molecules in fluorescent OLED

1.2.1 Carbazole-based hole transporting materials

Being electron rich, carbazole itself is a hole transporting material. However, the poor film morphology and tendency to form aggregates in solid state make them less attractive for applications in the OLED devices. But these limitations can be overcome by the functionalization of carbazole with bulky chromophoric units. Moreover, the incorporation of non-planar electron donating moieties on carbazole would not only alleviate detrimental aggregation but also enhance hole transporting character.

Recently, Jou and coworkers demonstrated phenyl or naphthyl substituted carbazole as an efficient hole transporting materials (**C1**-**C3**) for OLED applications (Chart 1.1) [22]. The fluorescent device utilizing these materials as hole transporting layer (HTL) exhibited better performance compared to the control device fabricated with conventional hole transporting material NPB. The increment in electroluminescence performance is attributed to good morphological stability of the hole transporting materials used. Atomic force microscopy (AFM) studies revealed that these compounds (**C1**-**C3**) are found to possess smooth thin film

compared to that of NPB. The high current efficiency of the device containing naphthyl (**C1**) and binaphthyl (**C2**) substituted carbazole were 4.5 and 4.0 cd/A respectively. This is 165% and 135% higher than the device made of NPB. Interestingly, naphthyl substituted carbazole (**C1**) exhibited high brightness of 10360 cd/m^2 which is attributed to facile hole transport arising from low energy barrier and the prevention of electron leakage at EML/HTL interface due to high lying LUMO. The high luminance of the device is also attributed to the smooth thin film morphology which would avoid undesirable current leakage at the interface. Furthermore, these materials are also used as hole transporting material in phosphorescent organic light emitting diodes (PhOLED) as they possess high triplet energy over CBP host. Here also, naphthyl substituted carbazole (**C1**) displayed high device performance compared to the control device fabricated with NPB hole transporting material. It is attributed to high hole transporting ability and low hole injection barrier of **C1** which facilitates the charge carrier injection into emissive layer.

Further, Grigalevicius and coworkers reported naphthyl/pyrenyl substituted carbazole containing phenyl linker as hole transporting materials (**C4**-**C5**) for red emitting phosphorescent OLED (Chart 1.1) [23]. Generally, low band gap emitters suffer high driving voltage due to serious carrier trapping and charge imbalance. The HOMO value of **C4** and **C5** is lower than that of NPB which eventually reduces the energy barrier for the hole injection into emissive layer. The calculated triplet energy of **C4** and **C5** is to be 2.39 and 2.48 eV respectively which clearly demonstrates their use in triplet harvesting OLED. The lack of characteristic emission of host and hole transporting layer in electroluminescence (EL) spectra indicates the origin of emission from the dopant and the effective carrier transporting nature of **C4** and **C5**. The EL performances of the devices constructed with these materials as HTL exhibited comparable EL performance with that of NPB. It is evident that the **C4** based device exhibited low current density due to poor injection of holes as a result of high energy barrier. The favorable HOMO level of **C5** resulted in efficient hole injection from ITO and lead to high luminance which is comparable to the control device fabricated with NPB.

Jou and coworkers developed 3,6-bis(4-vinylphenyl)-9*H*-ethylcarbazole (**C6**) and demonstrated as hole transporting material (Chart 1.1) for PhOLED devices [24]. They fabricated three different devices which emit primary colors such as red, green and blue. For comparison, they fabricated devices without hole transporting layer and presented their EL

performances for comparison. The power efficiency of 13.5 lm/W is observed for red emitting device without HTL. When the HTL layer **C6** is inserted, the power efficiency is raised to 20.6 lm/W at the brightness of 100 cd/m^2. The rise of power efficiency indicates the positive role of HTL made of **C6** in improving the device performance. The high efficiency of the device possessing HTL might arise from suitable HOMO and LUMO energy level of HTL which selectively allows the passage of hole carriers into emissive layers while forbidding the electron leakage at the interface owing to high LUMO level. Similarly, blue emitting device also gave improved efficiency when HTL is employed. It clearly demonstrates the electron confining nature of the hole transporting material which prevents overflowing of electron from host or guest into HTL. In contrast, green emitting device exhibited poor performance with low luminance of 3000 cd/m^2. At higher brightness, the efficiency increased because of the prevention of overflow of electrons into HTL. The poor performance of the devices without HTL is attributed to charge leakage at interface.

Yu and coworkers designed diphenylamine decorated bicarbazole (**C7;** Chart 1.1) and used as hole transporting material for both fluorescent and phosphorescent OLED devices [25]. This molecule showed high glass transition temperature of 170 °C which is exceedingly higher than that of widely used hole transporting materials such as NPB (95 °C), TPD (65 °C), TCTA (151 °C) and TAPC (78 °C). The excellent morphological stability of **C7** is attributed to its highly twisted orientation of bulky diphenylamine at peripheral position of carbazole. The fluorescent OLED device constructed with **C7** as hole transporting layer and C_4-DFQA doped Alq_3 as emitting layer exhibited the electroluminescence performance with the EQE of 2.14%, power efficiency of 7.73 lm/W and current efficiency of 7.63 cd/A. But, the device exhibited high efficiency roll-off at high luminance. It is reasoned that Alq_3 act as electron transporting host but not as bipolar host which result in imbalanced charge carrier mobility across the device. However, the performance is comparable with the NPB hole transporter based device. Further, the diphenylamine substituted bicarbazole **C7** is used as hole transporting layer in phosphorescence OLED with the device structure of ITO/HTL/DPDT-ICZ/ 5% $Ir(ppy)_2(tipg)$/ $Bepp_2$/LiF/Al. The device exhibited yellow color emission with the maximum current efficiency, power efficiency, and EQE of 48.3 cd/A, 57.0 lm/W and 13.2% respectively.

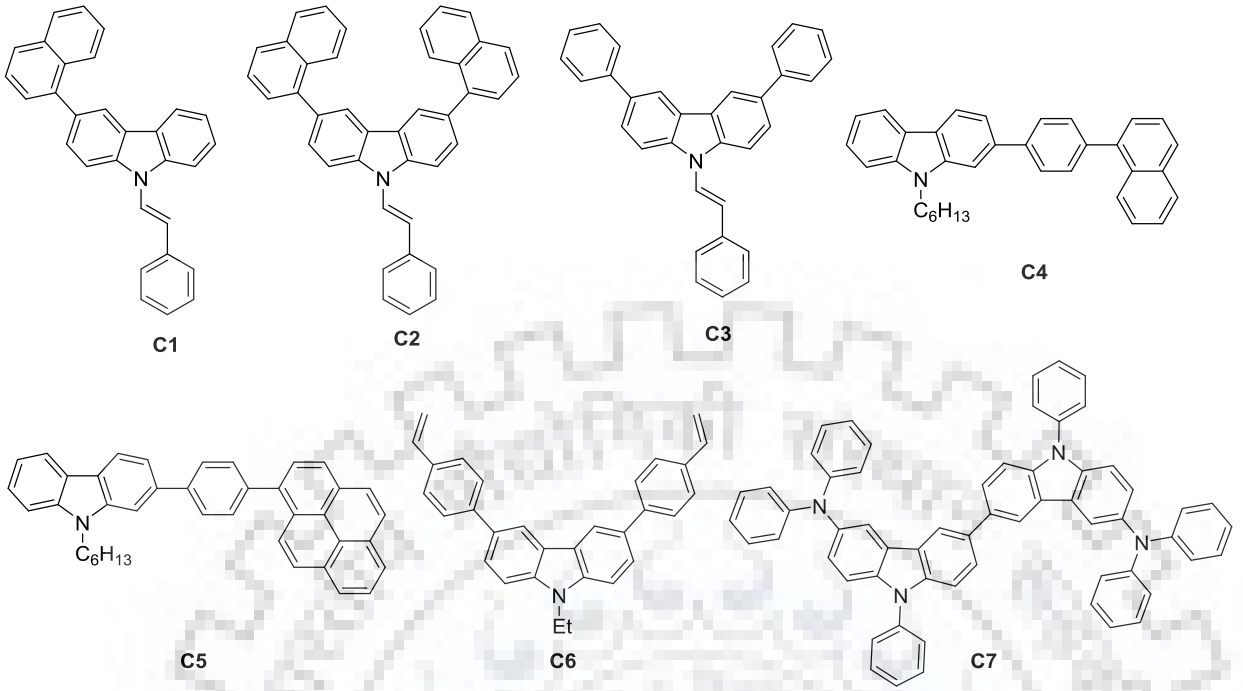

Chart 1.1 Carbazole-based derivatives as hole transporting materials in OLED.

Chai and coworkers reported arylamine substituted carbazoles (**C8-C10;** Chart 1.2) as hole transporting materials for red emitting phosphorescent OLED devices [26]. Generally, small molecules based hole transporters are highly desirable because they possess uniform thin film forming ability, high thermal stability and easy accessibility. The arylamine tethered carbazoles exhibited facile oxidation and constructed high lying HOMO energy level which is higher than that of NPB. As a result, the molecules possess low energy barrier for hole injection and exhibit superior hole transporting character over NPB. On the other hand, the high lying LUMO of the compounds is beneficial to prevent electron leakage and thus confine the charge carriers in emissive layer rather than at interface. Due to high hole transporting ability, **C8** exhibited comparable device performance with the device fabricated with NPB.

Since triphenylamine possesses high hole mobility and provides uniform thin film owing to its twisted structure, triphenylamine integrated carbazoles could be a choice of hole transporting materials. Promarak and coworkers reported di-, tri- and tetra- triphenylamine substituted carbazole (**C11-C13;** Chart 1.2) as hole transporting materials for fluorescent OLED devices [5]. The materials (**C11-C13**) exhibited high glass transition temperatures, thermal decomposition temperatures and hole transporting ability as compared to widely used NPB and

TPD. The identical electroluminescence spectra of the devices containing these materials as hole transporter with the device having NPB or TPD confirms the origin of electroluminescence is only from emitter. The electroluminescence data are similar to NPB and TPD devices. The durability of the devices is mainly dependent on stability of thin film of HTL. Since these triphenylamine-carbazole hybrids exhibited superior morphological stability, they are shown as potential hole transporting materials to realize stable device.

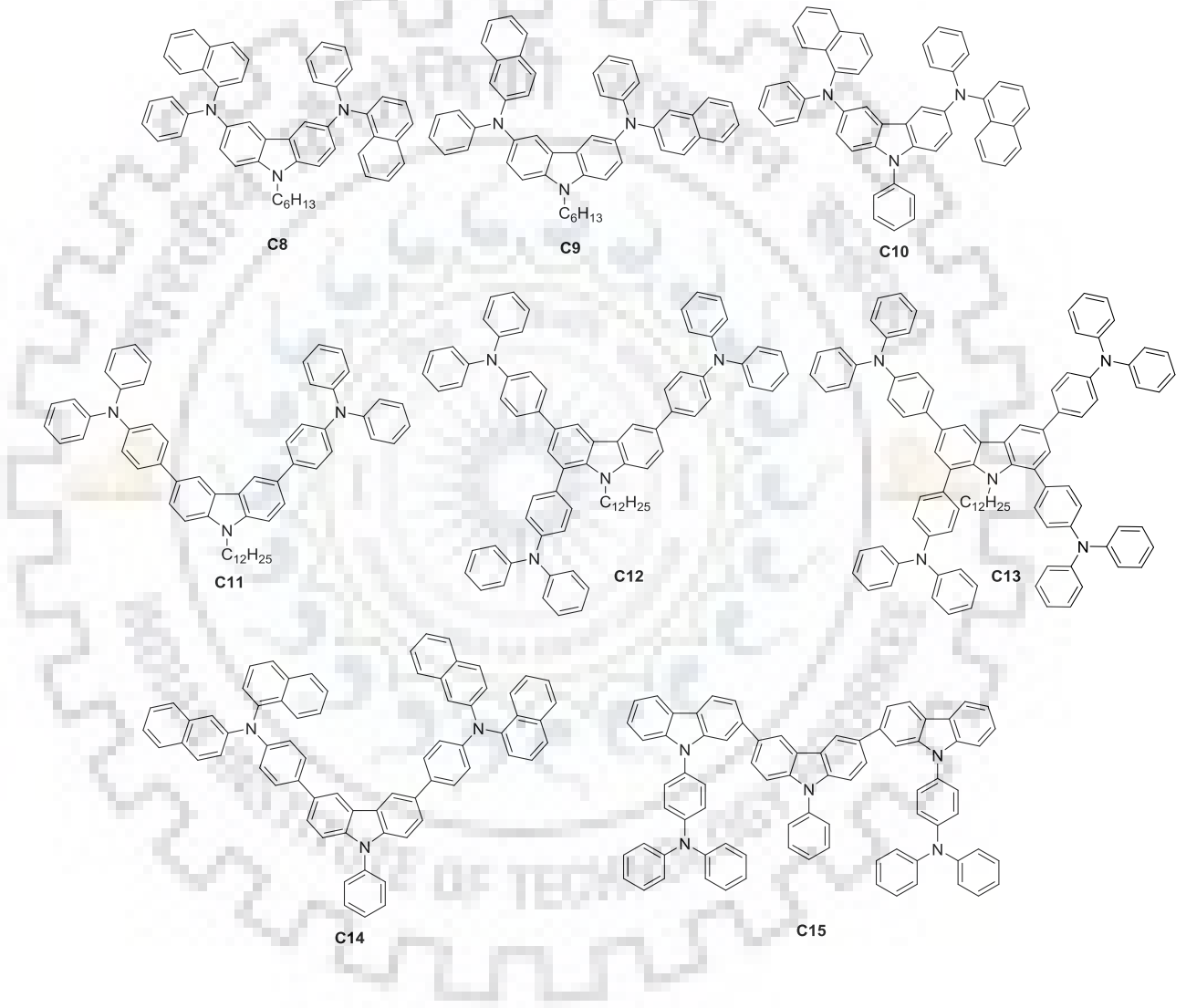

Chart 1.2 Carbazole-based derivatives as hole transporting materials in OLED.

Recently, Chai and coworkers reported arylamine substituted carbazoles (**C14-C15;** Chart 1.2) as hole transporting materials and employed them in red phosphorescent OLED devices [27]. The compounds (**C14** and **C15**) showed high glass transition temperature of 165 and 260 °C respectively which are promising for obtaining stable thin film and raise morphological

stability. Also, the high decomposition temperature of these compounds would be beneficial for realizing stable device. The HOMO and LUMO energy level of the compounds are in such a way that they allow hole injection due to low injection barrier while high lying LUMO which restricts the electron passage into HTL to confine the charge carriers in emissive layer. The phosphorescent OLED device fabricated with **C14** as HTM as hole transporting layer exhibited comparable EL performance with that of NPB based device. The poor performance of **C15** based device is attributed to poor hole mobility of **C15** when compared to **C14** and NPB.

Table 1.1 Photophysical and thermal properties of carbazole-based hole transporting materials

Dye	λ_{max} (nm)[a]	λ_{em} (nm)[a]	HOMO, eV[c]	LUMO, eV	$E_{0\text{-}0}$, eV[d]	T_g (°C)[e]	T_d (°C)[f]	Ref
C1	326[b]	381[b]	-5.27	-2.12	3.15	57	379	22
C2	308[b]	384[b]	-5.31	-2.21	3.10	107	461	22
C3	299[b]	384[b]	-4.93	-1.82	3.11	55	360	22
C4	318	404	-	-	3.34	58	344	23
C5	345	418	-	-	3.19	61	341	23
C6	-	-	-5.30	-2.30	3.30	109	350	24
C7	309, 370	429	-4.94	-1.94	3.00	170	481	25
C8	351	470	-5.16	-2.22	2.94	90	400	26
C9	316	435	-5.14	-2.19	2.95	86	380	26
C10	353	454	-5.06	-2.05	3.01	120	200	26
C11	320	415	-5.15	-1.86	3.29	-	334	5
C12	325	417	-5.16	-1.90	3.26	78	372	5
C13	328	419	-5.15	-1.91	3.24	122	415	5
C14	333	444	-5.55	-2.51	3.04	165	500	27
C15	313	402	-5.62	-2.31	3.31	260	575	27

[a] Measured in dichloromethane. [b] Measured in tetrahydrofuran. [c] Measured from cyclic voltammetry.

[d] Optical band gap obtained from intersection of absorption and emission. [e] Glass transition temperature.

[f] Thermal decomposition temperature at 5% weight loss.

Table 1.2 Electroluminescence properties of the devices containing carbazole-based derivatives as hole transporting layer.

Dye	Device structure	V_{on} (V)[a]	L_{max} (cd/m^2)[b]	η_c (cd/A)[c]	η_p (lm/W)[d]	EQE (%)[e]	$CIE_{(x,y)}$	Ref
C1	ITO/PEDOT:PSS/**HTL**/Alq_3/LiF/Al	3.9	10360	4.1/ 4.5	3.3	-	(0.33, 0.54)	22
C2	ITO/PEDOT:PSS/**HTL**/Alq_3/LiF/Al	3.8	4748	3.7	3.0	-	(0.34, 0.54)	22
C3	ITO/PEDOT:PSS/**HTL**/Alq_3/LiF/Al	4.1	5829	2.6	2.0	-	(0.34, 0.55)	22
C1	ITO/PEDOT:PSS/**HTL**/CBP+10% $Ir(ppy)_3$/ Alq_3/LiF/Al	3.5	15140	60.1	55.6	-	(0.31, 0.63)	22
C2	ITO/PEDOT:PSS/**HTL**/CBP+10% $Ir(ppy)_3$/ Alq_3/LiF/Al	3.4	9020	58.4	54.8	-	(0.30, 0.63)	22
C3	ITO/PEDOT:PSS/**HTL**/CBP+10% $Ir(ppy)_3$/ Alq_3/LiF/Al	3.5	12280	45.1	40.8	-	(0.31, 0.63)	22
C4	ITO/**HTL**/CBP:2% $Ir(MDQ)_2acac$/ BP_4mPy/ LiF/Al	11.3	5638	17.6	3.8	11.4	(0.61, 0.38)	23
C5	ITO/**HTL**/CBP:2% $Ir(MDQ)_2acac$/ BP_4mPy/ LiF/Al	6.3	19064	22.3	6.8	14.8	(0.62, 0.38)	23
C6	ITO/PEDOT:PSS/**HTL**/CBP:$Ir(2\text{-}phq)_3$/ TPBi/ LiF/Al	3.7	19310	24.0	20.6	10.8	(0.58,0.42)	24
C6	ITO/PEDOT:PSS/**HTL**/CBP:$Ir(ppy)_3$/TPBi/ LiF/Al	3.6	28470	48.8	42.7	13.4	(0.33,0.62)	24
C6	ITO/PEDOT:PSS/**HTL**/CBP:(FIrpic)/TPBi/ LiF/Al	4.6	11520	15.5	10.7	6.7	(0.17,0.40)	24
C7	ITO/**HTL**/Alq_3:1% C_4-DFQA/$Bepp_2$/LiF/Al	3.1	36680	7.63	7.73	2.1	(0.45, 0.53)	25
C7	ITO/**HTL**/DPDT-ICZ:5%$Ir(ppy)_2(tipg)$/ $Bepp_2$/LiF	2.4	46470	48.3	57.0	13.2	(0.44, 0.56)	25
C8	ITO/HATCN/**HTL**/$Bebq_2$:5%$Ir(mphmq)_2(tmd)$/ Bphen/LiF/Al	2.84	-	28.2	26.5	-	(0.65, 0.35)	26
C9	ITO/HATCN/**HTL**/$Bebq_2$:5%$Ir(mphmq)_2(tmd)$/ Bphen/LiF/Al	2.84	-	26.7	24.1	-	(0.65, 0.35)	26
C10	ITO/HATCN/**HTL**/$Bebq_2$:5%$Ir(mphmq)_2(tmd)$/ Bphen/LiF/Al	2.59	-	21.0	22.0	-	(0.65, 0.35)	26
C11	ITO/PEDOT:PSS/**HTL**/Alq_3/LiF/Al	2.4	28781	4.97	-	0.24	-	5
C12	ITO/PEDOT:PSS/**HTL**/Alq_3/LiF/Al	2.4	25052	5.00	-	0.24	-	5
C13	ITO/PEDOT:PSS/**HTL**/Alq_3/LiF/Al	2.5	22411	5.07	-	0.25	-	5
C14	ITO/DNTPD/**HTM**/$Bepq_2$:5% $Ir(mphmq)_2$ $(tmd)/Bepq_2$/LiF/Al	2.5	-	24.6	-	23.2	(0.65, 0.35)	27
C15	ITO/DNTPD/**HTM**/$Bepq_2$:5% $Ir(mphmq)_2$ $(tmd)/Bepq_2$/LiF/Al	2.5	-	17.6	-	16.3	(0.65, 0.34)	27

[a] Turn-on voltage. [b] Maximum luminance. [c] Current efficiency. [d] Power efficiency. [e] Maximum external quantum efficiency.

1.2.2 Carbazole-based materials as hole transporting emitters

Since carbazole-based materials exhibit excellent quantum yields, high thermal stability and good morphology, they have been actively researched as emitters for OLED. The materials possessing multifunctional characters are desirable for realizing the low cost OLED because they simplify the device structure. Thus, the carbazole-based materials exhibiting dual hole transporting and emission characteristics are briefly reviewed here.

You and coworkers reported a hole transporting emitter (**C16;** Chart 1.3) constituting carbazole connected to naphthalene through vinyl linker [28]. The materials possessing multi-functional behavior are highly desirable for obtaining low cost OLED since they reduce the number of layers in the device structure. Here, the hole transporting emitting material possessed high glass transition temperature of 117 °C which is advantageous for realizing defect free thin film formation and thus reduce the quenching of excitons at the interface. The high thermal decomposition temperature of 452 °C is beneficial for improving the thin film forming ability and thus expected to give long durable devices. The material exhibited high hole mobility of 3.24×10^{-4} cm^2 V^{-1} s^{-1} at the applied electric field of about 1.5×10^5 V cm^{-1}. Attracted by the high hole mobility and the intense emission, the compound is employed as hole transporting emitter in fluorescent OLED. The non-doped device exhibited low turn-on voltage of 3.0 V, maximum luminance of 1114 cd/m^2, current efficiency of 0.65 cd/A and EQE of 0.25%. Despite of high hole mobility, the performance of the device is poor which might be due to unfavorable energy barrier for charge carrier injection between charge transporting and emissive layers.

Promarak and coworkers developed pyrene decorated carbazoles (**C17**-**C19;** Chart 1.3) as hole transporting emitters [29]. As the number of pyrene unit increased on carbazole, the glass transition temperature is increased due to the increase of non-planarity. From, DFT calculation, it was found that pyrene at 1,8-position of carbazole did not contribute to conjugation. The Stokes shift of 5480 cm^{-1} of these materials indicates the less energy loss during excitation which would be beneficial for efficient fluorescence. The electroluminescence spectrum of the devices fabricated with the compounds (**C17**-**C19**) confined to blue region which attests the non-planar functionalization of carbazole at C1 and C8 positions. The bilayer device fabricated with tri-substituted carbazole (**C18**) as emitters in non-doped device exhibited high luminance,

current efficiency and low turn on voltage of 8235 cd/m^2, 2.53 cd/A and 3.0 V respectively. Further, they improved the device by incorporating additional hole transporting layer, TPD. The current efficiency and maximum luminance was greatly increased about three fold. In these device structures, di-substituted carbazole (**C17**) based device exhibited the lowest turn on voltage of 2.6 V which is one of the best low turn-on voltage realized so far. The stable emission from tri-substituted carbazole (**C18**) over wide range of driving voltage makes it a promising material for display and lighting applications.

Velasco and coworkers synthesized carbazole trimer (**C20;** Chart 1.3) connected with acetylene spacer and demonstrated as hole transporting blue emitter [30]. The *N*-alkylation of peripheral carbazole with 2-ethylhexyl chain was beneficial to suppress non-radiative fluorescence quenching when compared to *N*-arylation. Moreover, the rigid acetylene linker provided planar structure and effective conjugation across the molecular backbone and thus raise fluorescence quantum yield. The solid state quantum yield of **C20** is similar to the solution quantum yield which indicates the role of 2-ethylhexyl chain in suppressing non-radiative decay pathway as well as controlling the aggregation in solid state. So, the alkylation of peripheral carbazole is preferable over arylation at *N*- position of carbazole. The hole charge mobility is observed to be 2.8×10^{-4} cm^2 V^{-1} s^{-1} at an electric field of 6.4×10^5 V cm^{-1}. This relatively high charge carrier mobility indicates the hole transporting character of the material. Further, the non-doped device fabricated with the hole transporting emitter (**C20**) to evaluate the potentiality of the material for OLED applications. They optimized the device performance by varying the thickness of emitting layer from 25 nm to 55 nm. The device exhibited blue emission with current efficiency of 0.17 cd/A and maximum luminance of 39.46 cd/m^2 at 50 nm thickness of emitting layer.

Lu and coworkers reported asymmetrically functionalized carbazole with triphenylamine/pyrene (**C21**,**C22;** Chart 1.3) and employed them as hole transporting green emitters [31]. Though the chromophoric conjugation is increased in **C22**, it exhibited blue shifted absorption due to decrease of coplanarity as the increase of conjugation length. Similar results are obtained in emission spectra. Thin film emission spectra exhibited blue shifted emission compared to solution spectra which is attributed to the formation of *H*- aggregates in solid state. The bilayer devices employing these materials as hole transporting emitters displayed green emission with intense fluorescence. The device fabricated with **C21** exhibited

the maximum luminance, current efficiency of 13470 cd/m^2 and 1.18 cd/A, respectively. The poor device performance of **C22** is attributed to extended molecular length which eventually leads to the crystallization of thin film and thus leads to failure of the device.

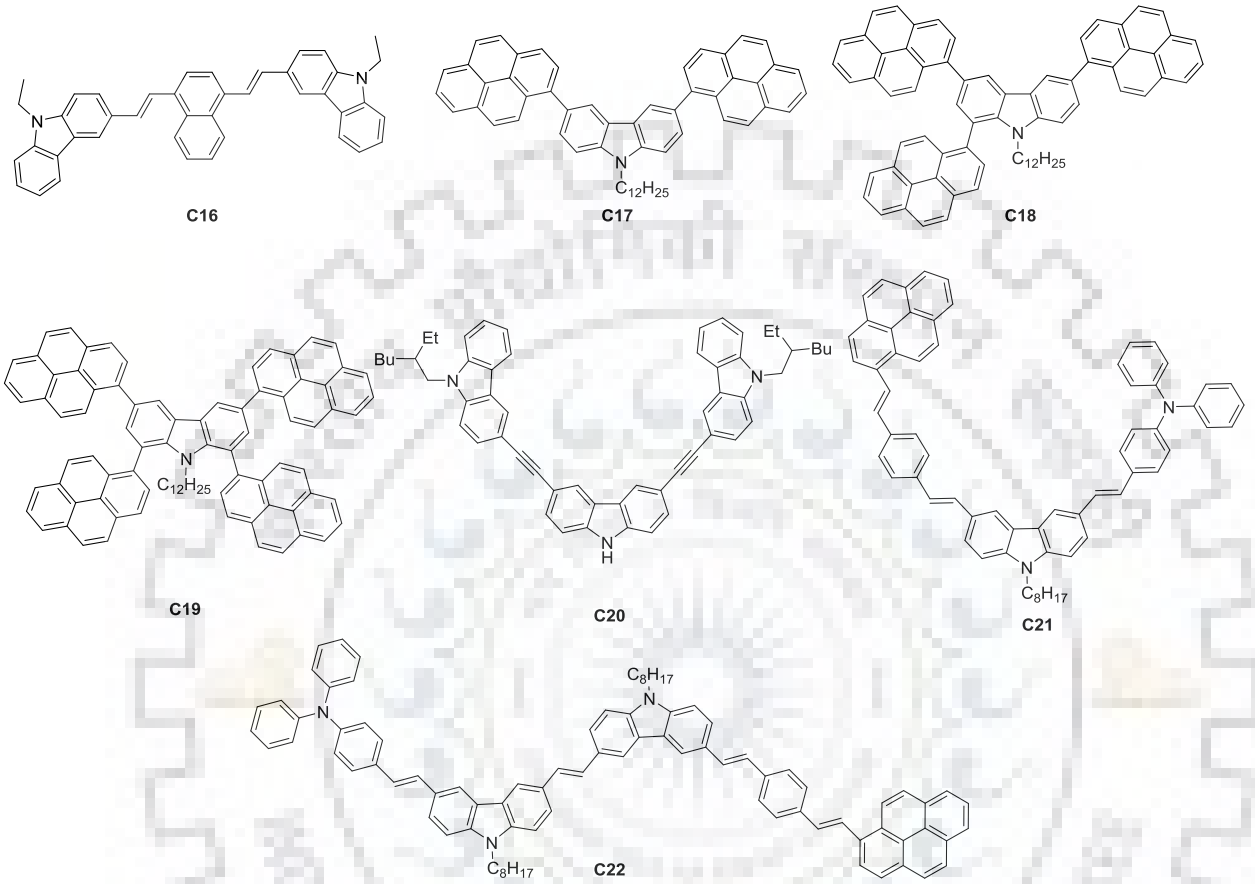

Chart 1.3 Carbazole-based materials as hole transporting emitters.

Li and coworkers developed triphenylethene and triphenylbenzene substituted carbazole as hole transporting emitters (**C23**, **C24;** Chart 1.4) for non-doped fluorescent OLED [32]. Owing to their twisted structure, the absorption and emission of these materials are restricted to blue region. Triphenylethene substituted carbazole (**C23**) exhibited aggregation induced emission (AIE) properties in emission spectra recorded in different THF/water ratio. In contrast, triphenylbenzene derivative (**C24**) exhibited aggregation caused quenching (ACQ) effect. The high lying HOMO values of these materials are comparable to the HOMO of NPB. Both of these carbazole derivatives gave high hole transporting ability of about 1×10^{-3} cm^2 V^{-1} s^{-1} which is the best hole mobility among the twisted molecules reported so far. Considering the superior hole mobilities and high quantum efficiency, they employed these molecules as hole

transporting emitter in bilayer device architecture. Interestingly, their EL spectra resembled to PL spectra recorded in THF and thin film which indicates the mitigation of π-π interaction in solid state ascribed to twisted triphenylethene and triphenylbenzene moiety. The best EL performance observed for triphenylbenzene derivative (**C24**) with current efficiency of 1.21 cd/A and EQE of 2.76% for the device containing TPBi as electron transporting layer. Further, the EL performance of the triphenylbezene tethered carbazole (**C24**) was improved by changing the electron transporting layer from TPBi to TmPyPB. The exciting EL performance for the device with current efficiency of 2.21 cd/A and EQE of 4.27% whose emission is confined to blue-violet region with electroluminescence maximum at 397 nm. This is the best EL device performance so far reported for deep blue emitting materials in double layer device.

Liu and coworkers demonstrated carbazole end-capped diphenylethene (**C25;** Chart 1.4) as hole transporting emitter [33]. Interestingly, the material is non-emissive in dilute solution but intensely emissive in aggregate form. When the hole transporting emitter is fabricated in the device which does not have exclusive hole transporting layer, it showed lower turn on voltage, high current efficiency and EQE. The current efficiency and luminance of the device without dedicated hole transporting layer (NPB) exhibited more than double of that device possessing HTL. The high performance of the device which does not possess HTL clearly demonstrates the role of bi-functional nature of carbazole based materials. The low turn-on voltage of the device is attributed to high-lying HOMO of the emitter which reduce energy barrier for hole injection into emissive layer.

Tang and coworkers studied carbazole tethered triphenylethene via *N*- and C3- position (**C26**, **C27;** Chart 1.4) as hole transporting emitters [34]. The high thermal stability and glass transition temperature are favorable for obtaining morphologically stable thin film and long durable devices. The devices containing these hole transporting emitters exhibited sky blue emission. The **C26** based device displayed the maximum luminance, current efficiency and EQE of 6300 cd/m^2, 1.1 cd/A and 0.6%, respectively. The better performance of **C26** is attributed to favorable energy alignment of the emitter with the work function of ITO anode. The low energy barrier for the injection of charge carriers allows the effective charge transfer into emissive layer, effective harvesting of excitons and thus high luminance.

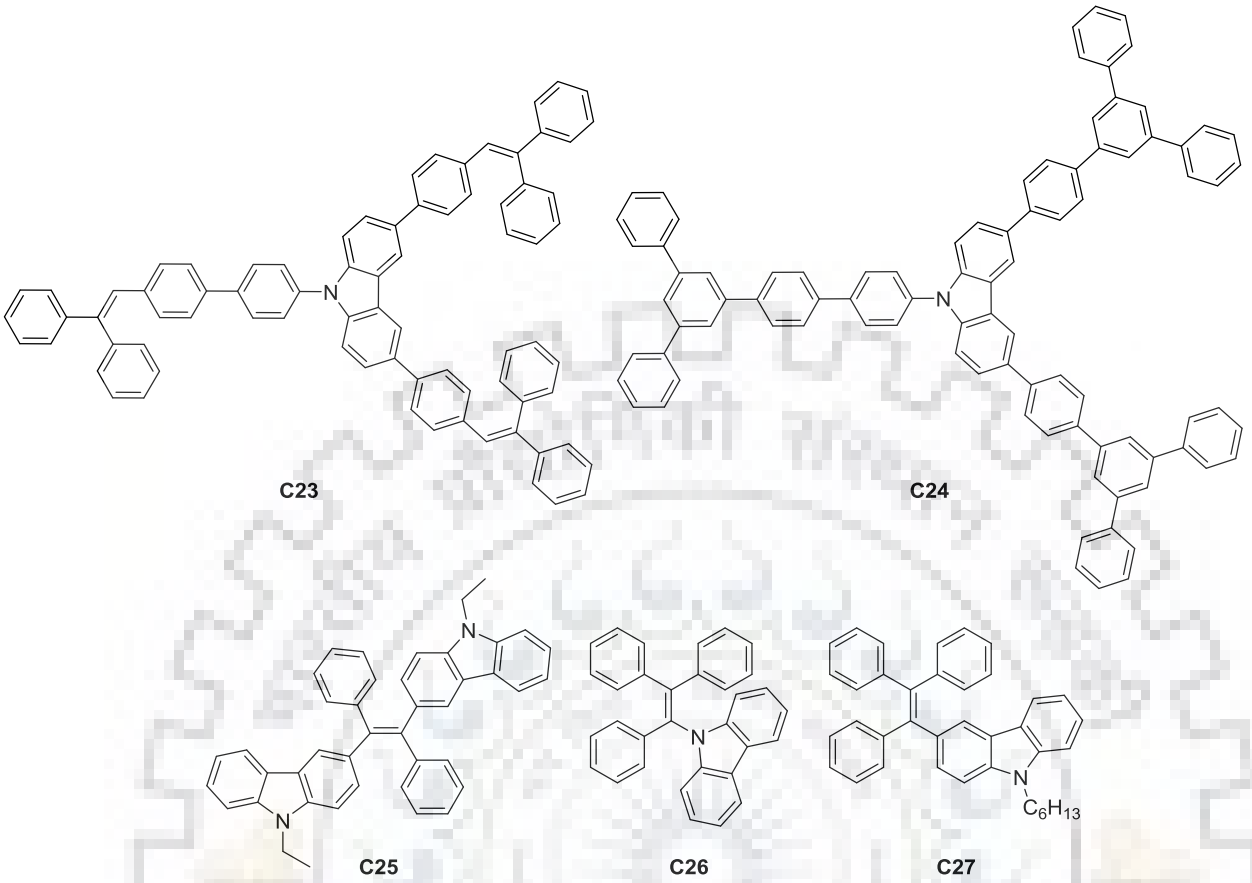

Chart 1.4 Carbazole-based materials as hole transporting emitters.

Zhu and coworkers studied the effect of tetraphenylethene (TPE) chromophore on carbazole (**C28**-**C32;** Chart 1.5) over AIE and EL properties systematically [9]. Due to high hole transporting property of carbazole and high solid state photoluminescence quantum yield of TPE, the combination of carbazole and TPE is a fruitful methodology to obtain efficient hole transporting emitting molecules. The glass transition temperature of the compounds progressively increased as the number of TPE loading on carbazole. All the compounds exhibit AIE properties in typical THF/water fluorescence measurements. As the number of TPE unit increases on carbazole, AIE property is observed at lower water percentage. This indicates the insolubility of TPE which tends to form nano aggregates and easily show AIE property at low water content. All of the materials are exploited as hole transporting emitters in OLED device. The EL performances and low turn on voltages of TPE decorated carbazole is much better than the TPE decorated fluorene analogs. It is ascribed to the proper alignment of HOMO energy level with the neighboring charge transporting layers.

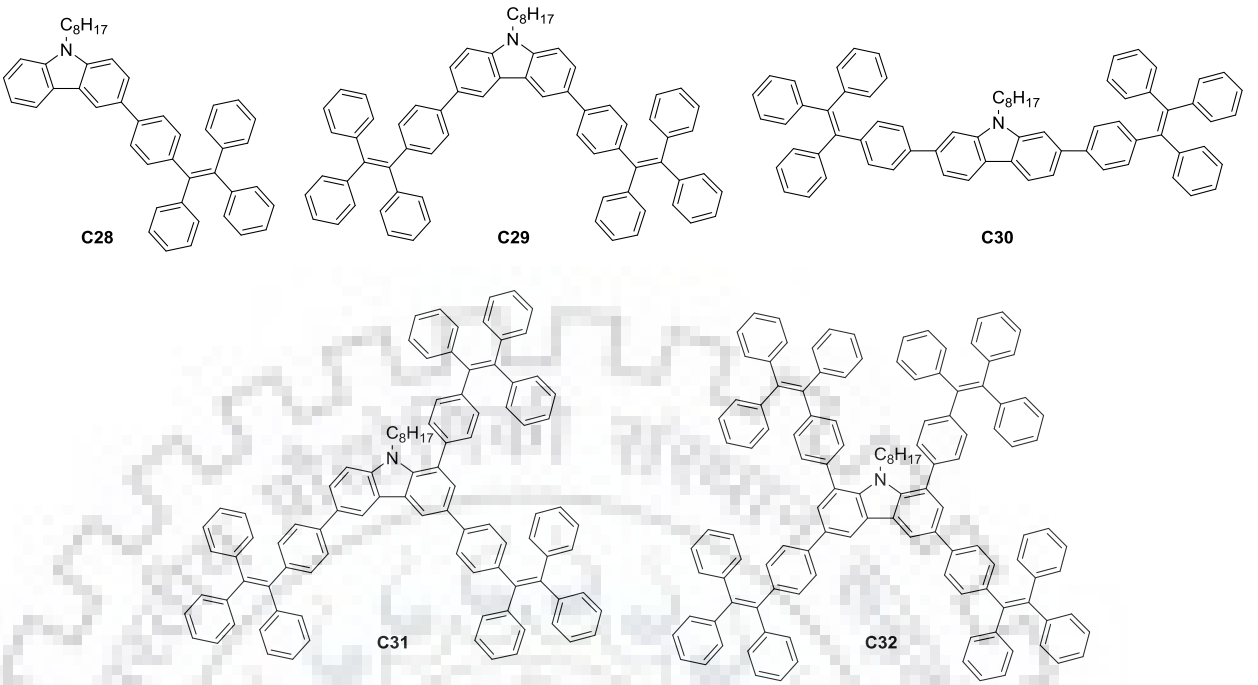

Chart 1.5 Carbazole-based materials as hole transporting emitters.

Table 1.3 Photophysical and thermal properties of the carbazole-based hole transporting emitters

Dye	λ_{max} (nm)[a]	λ_{em} (nm)[a] (Φ_F)[c]	HOMO (eV)[d]	LUMO (eV)	$E_{0\text{-}0}$, (eV)[f]	T_g (°C)[g]	T_d (°C)[h]	Ref
C16	407[b]	472[b] (0.71)	-5.26	-2.63	2.63	-	-	28
C17	348	430 (0.94)	-5.45	-2.33	3.12	70	375	29
C18	346	436 (0.72)	-5.46	-2.36	3.10	125	398	29
C19	347	439 (0.56)	-5.47	-2.40	3.09	170	407	29
C20	349	392 (0.39)	-5.89	-2.57	3.32	-	-	30
C21	408[b]	506[b] (0.52)	-4.94	-2.31	2.63	-	418	31
C22	401[b]	504[b] (0.59)	-4.97	-2.35	2.62	-	426	31
C23	350[b]	451[b] (0.08)	-5.37	-2.27	3.10	186	479	32
C24	330[b]	398[b] (0.72)	-5.47	-2.15	3.32	198	564	32
C25	-	502[b] (0.22)	-5.20	-2.10	3.10	119	370	33
C26	341[b]	466[b] (0.70)	-5.20[e]	-1.40	3.80	72	294	34
C27	342[b]	489[b] (0.27)	-4.93[e]	-1.08	3.85	50	301	34
C28	334[b]	483[b] (0.37)	-5.01	-1.21	3.80	21	331	9
C29	337[b]	487[b] (0.16)	-4.96	-1.25	3.71	65	449	9
C30	360[b]	483[b] (0.22)	-4.97	-1.39	3.58	138	443	9
C31	318[b]	488[b] (0.23)	-5.07	-1.43	3.64	70	493	9
C32	326[b]	485[b] (0.18)	-4.96	-1.37	3.59	94	463	9

[a] Measured in dichloromethane. [b] Measured in tetrahydrofuran. [c] Absolute quantum yield. [d] Calculated from cyclic voltammetry. [e] Calculated from DFT. [f] Band gap obtained from optical edge. [g] Glass transition temperature. [f] Thermal decomposition temperature at 5% weight loss.

Table 1.4 Electroluminescence properties of carbazole-based hole transporting emitters

Dye	Device structure	V_{on} (V)[a]	L_{max} (cd/m^2)[b]	η_c (cd/A)[c]	η_p (lm/W)[d]	EQE (%)[e]	$CIE_{(x,y)}$	Ref
C16	ITO/PEDOT:PSS/**HT-EML**/ PFN/Al	3.0	1114	0.65	-	0.25	(0.34, 0.59)	28
C17	ITO/PEDOT:PSS/**HT-EML**/ BCP/LiF/Al	3.2	7193	1.86	-	-	(0.15, 0.13)	29
C18	ITO/PEDOT:PSS/**HT-EML**/ BCP/LiF/Al	3.0	8235	2.53	-	-	(0.18, 0.26)	29
C19	ITO/PEDOT:PSS/**HT-EML**/ BCP/LiF/Al	3.1	9645	2.46	-	-	(0.21, 0.28)	29
C20	ITO/PEDOT:PSS/**HT-EML**/ TPBi/LiF/Al	3.2	39.5	0.17	-	-	-	30
C21	ITO/PEDOT:PSS/**HT-EML**/ Alq_3/LiF/Al	4.4	13470	1.18	0.35	-	-	31
C22	ITO/PEDOT:PSS/**HT-EML**/ Alq_3/LiF/Al	3.3	7767	1.00	0.66	-	-	31
C23	ITO/MoO_3/**HT-EML**/TPBi/ LiF/Al	3.2	5446	2.79	2.41	1.93	(0.16, 0.17)	32
C24	ITO/MoO_3/**HT-EML**/TPBi/ LiF/Al	3.8	4025	1.27	0.92	2.76	(0.17, 0.07)	32
C24	ITO/MoO_3/**HT-EML**/TmPyPB/LiF/Al	3.9	2587	2.21	1.83	4.27	(0.17, 0.08)	32
C25	ITO/**HT-EML**/TPBi/Alq_3/ LiF/Al	4.5	5060	5.7	3.4	2.3	-	33
C26	ITO/**HT-EML**/TPBi/LiF/Al	4.0	6300	1.1	0.4	0.6	-	34
C27	ITO/**HT-EML**/TPBi/LiF/Al	4.6	4390	1.0	0.5	0.4	-	34
C28	ITO/PEDOT/**HT-EML**/ TPBi/LiF/Al	3.5	2585	3.5	2.1	-	(0.18, 0.34)	9
C29	ITO/PEDOT/**HT-EML**/ TPBi/LiF/Al	3.5	1353	4.9	3.9	-	(0.20, 0.40)	9
C30	ITO/PEDOT/**HT-EML**/ TPBi/LiF/Al	4.2	1129	5.5	3.1	-	(0.20, 0.38)	9
C31	ITO/PEDOT/**HT-EML**/ TPBi/LiF/Al	3.3	986	3.1	2.2	-	(0.20, 0.39)	9
C32	ITO/PEDOT/**HT-EML**/ TPBi/LiF/Al	3.6	2088	3.1	1.8	-	(0.20, 0.38)	9

[a] Turn-on voltage. [b] Maximum luminance. [c] Maximum current efficiency. [d] Maximum power efficiency. [e] Maximum external quantum efficiency.

1.2.3 Carbazole-based bipolar emitting materials

The carrier mobility of holes is several orders higher than the mobility of electrons in thin film devices. Since the energy harvesting mechanism involves the recombination of hole and electron charge carrier at emissive layer to generate excitons at the emissive layer, the color of emission depends on the band gap of the materials used. Due to the unbalanced movement of charge carriers, the recombination may take place at the interface of emissive layer and charge transporting layer rather than emissive layer. This reduces the device efficiency and compromises color purity of the OLED device. Generally, unipolar materials suffer poor device performance due to unbalanced charge carrier mobility across the device. On the other hand, bipolar materials exhibit both hole and electron transporting character which would be helpful to realize balanced charge transport and improve the electroluminescence efficiency. Since carbazole is a hole transporter, tethering electron withdrawing moieties on carbazole would boost the transportation of electron carriers and thus provide bipolar nature.

Liu and coworkers recently reported carbazole-phenathroimidazole hybrids as bipolar materials (**C33** and **C34;** Chart 1.6) for non-doped fluorescent OLED (only **C34** is fabricated) [35]. Though both the compounds exhibited similar absorption profile, biphenyl bridged compound showed blue shifted emission to that of phenyl compound. Here, the local excited state (LE) component is dominant over charge transfer (CT) component in HLCT mechanism which results in blue shifted emission. The HLCT emission is confirmed by two independent linear relationships in Lippert-Mataga plot. Also, the PLQY recorded in thin film is 72% for biphenyl while 14% for phenyl. It indicates the supremacy of the biphenyl compound for OLED applications. The HOMO is dispersed over phenanthraimidazole-carbazole axis while LUMO is located on benzonitrile which indicates the effective charge separation in D-A molecules and renders bipolar nature. From the single charge carrier devices, these compounds are found to have bipolar nature by observing similar current densities over the voltage range for both hole only and electron only devices. The hole and electron mobility of the compounds are comparable to the conventional hole and electron transporters namely NPB and Alq_3 respectively. The non-doped device exhibited EQE of 4.71% and low efficiency roll-off (only 3.2% drop) at high luminance of 1000 cd/m^2 with EQE of 4.56%. Further, the device performance is enhanced by modulating HTL with different ratio of TCTA/MoO_3. The optimized device showed high EQE of 5.80% which is the best deep blue emitter known in the

literature for non-doped devices matching NTSC standard. The EQE exceeds the theoretical limit which is attributed to HLCT in emission mechanism.

You and coworkers developed D-π-A configured molecule as bipolar emitter (**C35;** Chart 1.6) which contains carbazole as donor, biphenyl as π bridge and triphenylimidazole as acceptor [36]. Due to twist structure of biphenyl linker, the emission of the molecule was restricted to blue region. From the single charge carrier devices, it is confirmed that the molecule exhibit both hole and electron transporting properties. The high current density of electron only device over the current density of hole only device indicates that this molecule possess good electron transporting character. The non-doped device fabricated with the dye as emitter exhibited deep blue emission with CIE_y coordinate of 0.064 which approaches EBU standard. The device gave maximum current efficiency of 2.30 cd/A, power efficiency of 1.52 lm/W which is the highest performance of the reported deep blue emitting materials meeting EBU standard color in non-doped devices.

Lu and coworkers demonstrated carbazole-phenanthroimidazole hybrids (**C36** and **C37;** Chart 1.6) as bipolar emitters [37]. Bis-phenanthroimidazole derivative **C37** exhibited high glass transition temperature of 207 °C and thermal decomposition temperature compared to mono- analog **C36** which guarantees stable and smooth thin film for device applications. Further, the smoothness of the materials are examined by AFM studies and found to possess smooth surface. The charge carrier current density is more for two PI carbazole compound **C37** compared to one PI carbazole **C36**. This would facilitate high charge carrier mobility and thus high electroluminescence performance due to balanced injection and transportation of charge carriers in the devices. The non-doped devices fabricated with these dyes as emitters exhibited high EQE of 3.02%, current efficiency of 1.53 cd/A and power efficiency of 0.86 lm/W. Interestingly, the full width at half maximum of the EL spectrum of both the dyes (40 nm) ensures the saturated color purity with CIEy coordinate of 0.056. This highly efficient violet emitting material will open up a way to generate energy saving OLED. Since these materials possess high triplet energy, they are exploited as host material for green phosphorescent OLED [38].

Jiang and coworkers reported diphenyl sulfone substituted at 3,6- and 2,7-positions of *N*-phenyl carbazoles (**C38** and **C39;** Chart 1.6) and studied their emitting nature in non-doped fluorescent devices [39]. The 2,7-substituted carbazole exhibited superior performance over 3,6-

analog. The absorption and emission wavelength of 2,7-substituted carbazole is higher than 3,6-substituted carbazole that coincides with the extended conjugation of the former compound. Further, the higher band gap of 2,7-substituted carbazole attests effective π electronic conjugation over 3,6-substituted counterpart. Both the compounds displayed high thermal decomposition temperature of about 430 °C and glass transition temperature of about 95 °C which ensures uniform film forming ability and long durability of the OLED device. From DFT calculation, it is found that HOMO is dispersed over *N*-phenyl carbazole unit while LUMO is concentrated over diphenylsulfone unit which presumes the ICT character. The high value of ΔE_{ST} confirmed the absence of TADF character. Interestingly, 2,7-substituted carbazole exhibited higher fluorescence quantum yield in thin film as compared to 3,6-analog. The OLED device fabricated with 2,7-carbazole showed maximum luminance of 3703 cd/m^2, current efficiency of 1.62 cd/A and EQE of 2.4%. The high performance of **C39** over **C38** might be due to suppression of aggregation and controlled π-π stacking in 2,7-functionalized carbazole which is also exemplified in high solid state fluorescence quantum yield.

Lee and coworkers synthesized carbazole-sulfone hybrids containing phenyl spacer (**C40** and **C41;** Chart 1.6) and studied their electroluminescent properties by employing them as emitters [40]. Carbazole acts as electron donor and sulfone as acceptor and phenyl as linker. Here, sulfone moiety acts as conjugation breaker due to its tetrahedral conformation as attached to phenyl linker and thereby restrict the emission to blue region. The PLQY in toluene solution even with aerated condition exhibited almost unity which indicates the suppression of non-radiative decay pathway significantly. The well separated HOMO and LUMO orbitals of the compounds indicate bipolar nature. The EL spectra of non-doped device resembled to thin film emission spectra which confirm the effective confinement of excitons in emissive layer and the origin of emission only from emitter. The dye **C41** based device exhibited low turn on voltage of 2.6 V and high current density and luminance attributed to facile charge injection into the emissive layer. The non-doped device fabricated with **C40** exhibited high EQE of 4.2% with blue-violet emission. The device exhibited relatively low efficiency roll-off with EQE of 3.2% at high luminance of 1000 cd/m^2. The low performance of **C41** based device can be explained by single carrier charge transport studies which showed unbalanced charge transport.

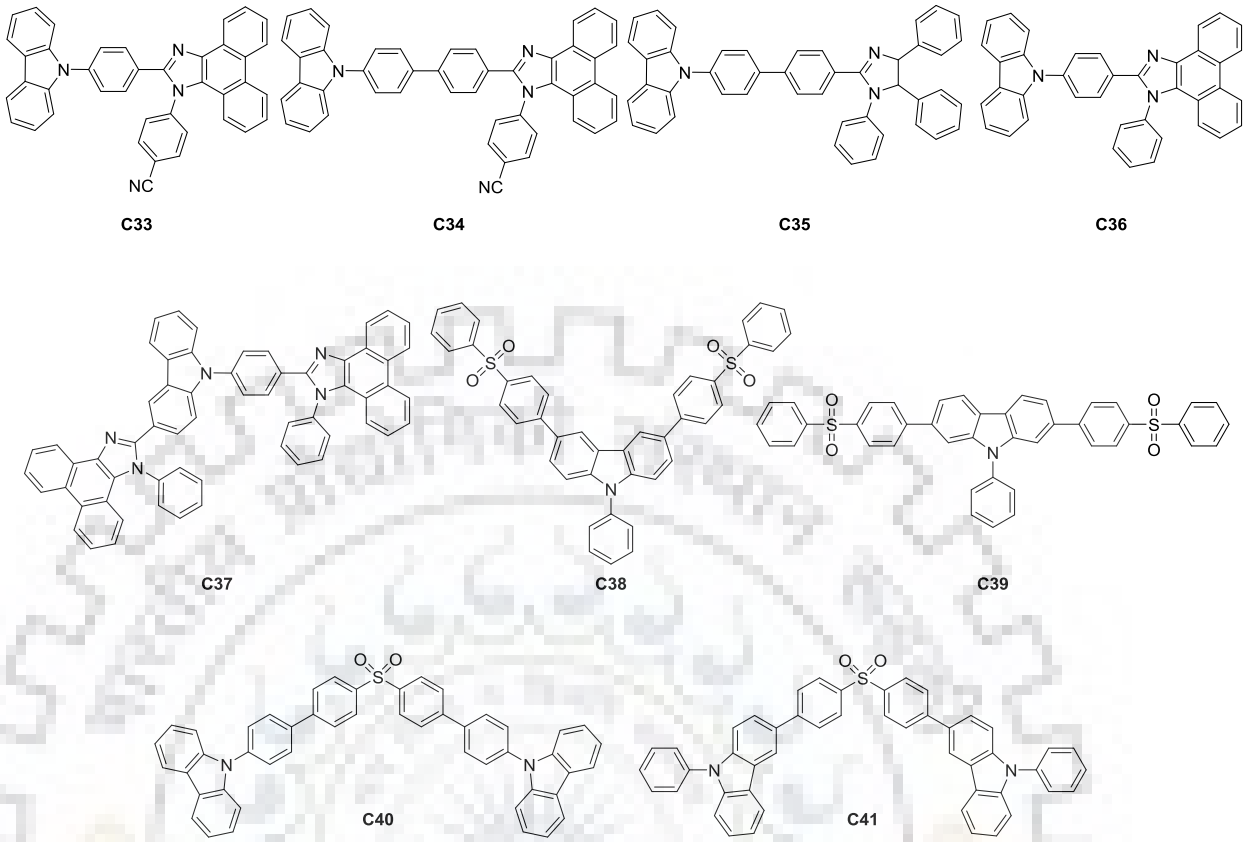

Chart 1.6 Carbazole-based materials as bipolar emitters.

Thomas and coworkers reported carbazole-benzimidazole hybrids containing phenyl/thiophene linker (**C42**-**C46;** Chart 1.7) as bipolar emitters [41]. The 2,7-functionalized carbazole dyes (**C44**,**C45**) exhibited longer wavelength absorption and emission over 3,6-analogs (**C42**,**C43**) ascribing to linear conjugation of the former compounds. Similarly, thiophene bridged compounds showed bathochromic shift over phenyl bridged compounds due to the electron richness and lower resonance energy of the former. The high lying HOMO of thiophene bridged compounds resulted in low turn-on voltage compared to phenyl bridged compounds due to favorable hole injection from neighboring HTL layer to emissive layer. Also, the low current density and low luminance of 2,7-functionalized carbazole is attributed to relatively high energy barrier for charge injection in non-doped devices. The high electroluminescence performance observed for the device containing **C46** doped in CBP with high EQE of 1.5%, power efficiency of 6.8 lm/W.

Yu and coworkers reported carbazole-coumarin hybrids having phenyl/thiophene linker (**C47**-**C50;** Chart 1.7) as bipolar light emitting materials [42]. Thiophene containing compounds

exhibited red shift in absorption and emission spectra while phenyl compounds exhibited blue shift due to the tilting phenyl ring which restricts the electronic delocalization. The electroluminescence performance of the devices was optimized by varying the doping concentration of emitter. The best performance was observed at 10% doping concentration with high brightness of 12910 cd/m^2, maximum current efficiency of 7.39 cd/A for mono- substituted phenyl bridged hybrid. Interestingly, all the di-substituted dyes exhibited inferior performance over mono- substituted dyes. It might be due to strong intermolecular interaction in thin films as the doping concentration is increased which resulted in self-quenching of fluorescence.

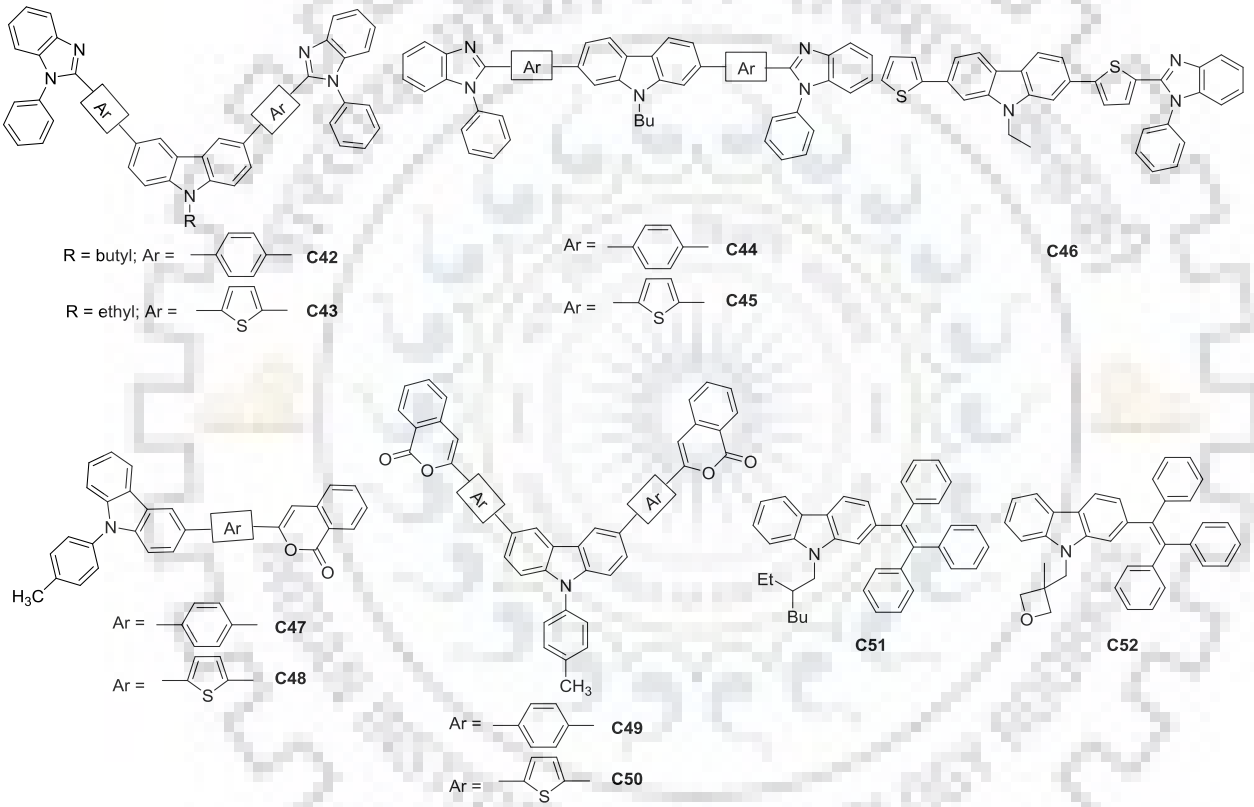

Chart 1.7 Carbazole-based materials as bipolar emitters.

Chang and coworkers reported triphenylethene substituted carbazole at C2 position (**C51** and **C52;** Chart 1.7) and studied the properties by varying alkyl chain [43]. For the first time, triphenylethene-based carbazole materials exhibiting bipolar character is reported. The high melting and glass transition temperature of oxetane based compound (**C52**) is attributed to its ability to form hydrogen bond in solid state and intermolecular interaction respectively. The presence of oxetanyl group was beneficial to improve glass transition temperature due to high

intermolecular interaction in solid state. But, it exhibited high charge drift mobility due to polar nature of oxetanyl group and thus lower carrier mobility. These compounds showed AIE property which was confirmed by conventional THF/water mixture emission spectra and observed enhanced emission as the water ratio is above 70%. The OLED device fabricated with these luminogen as emitters exhibited high EQE of 3.7% luminous efficiency of 8.8 cd/A, power efficiency of 7.0 lm/W at practical brightness of 100 cd/m^2 for the compound **C52**.

Table 1.5 Photophysical and thermal properties of carbazole-based bipolar emitters

Dye	λ_{max} (nm)[a]	λ_{em} (nm)[a] (Φ_F)[d]	HOMO (eV)[e]	LUMO (eV)	E_{0-0} (eV)[f]	T_g (°C)[g]	T_d (°C)[h]	Ref
C33	342	450	-5.86	-2.61	3.25	147	446	35
C34	343	429	-5.72	-2.52	3.20	169	487	35
C35	335[b]	409	-5.76	-2.45	3.31	134	413	36
C36	339[b]	381, 399[b] (0.65)	-5.52	-2.33	3.19	132	405	37
C37	346[b]	390, 407[b] (0.59)	-5.35	-2.22	3.13	207	515	37
C38	343	395 (0.38)	-5.62	-2.40	3.22	96	430	39
C39	339	411 (0.59)	-5.72	-2.58	3.14	95	427	39
C40	341[c]	428[c] (0.98)	-5.61	-2.45	3.16	157	498	40
C41	332[c]	416[c] (0.79)	-5.62	-2.46	3.16	143	486	40
C42	341	415 (0.61)	-5.53	-2.25	3.28	-	512	41
C43	388	449, 461 (0.75)	-5.36	-2.45	2.91	-	524	41
C44	349	410, 426 (0.62)	-5.83	-2.67	3.16	-	494	41
C45	406	454, 481 (0.89)	-5.44	-2.63	2.81	-	493	41
C46	372	458 (0.84)	-5.31	-2.36	2.95	-	438	41
C47	406	490 (0.84)	-5.63	-2.91	2.72	-	339	42
C48	451	524 (0.74)	-5.45	-3.04	2.41	-	311	42
C49	405	490 (0.79)	-5.60	-2.88	2.72	-	314	42
C50	445	524 (0.50)	-5.40	-3.02	2.38	-	276	42
C51	-	- (0.26)	-5.45	-3.57	1.88	49	302	43
C52	-	- (0.71)	-5.49	-3.58	1.91	87	307	43

[a] Measured in dichloromethane. [b] Measured in tetrahydrofuran. [c] Measured in toluene. [d] Absolute quantum yield. [e] Calculated from cyclic voltammetry. [f] Calculated from optical edge. [g] Glass transition temperature. [h] Thermal decomposition temperature at 5% weight loss.

Table 1.6 Electroluminescence properties of carbazole-based bipolar emitters

Dye	Device structure	V_{on} (V)[a]	L_{max} (cd/m^2)[b]	η_c (cd/A)[c]	η_p (lm/W)[d]	EQE (%)[e]	$CIE_{(x,y)}$	Ref
C34	ITO/MoO_3/TCTA:20%MoO_3/TCTA/**EML**/TPBi/LiF/Al	3.8	9755	3.82	2.86	5.80	(0.15, 0.08)	35
C35	ITO/NPB/TCTA/**EML**/TPBi/LiF/Al	4.75	-	2.30	1.52	-	(0.17, 0.06)	36
C36	ITO/NPB/**EML**/TPBi/LiF/Al	-	-	0.65	0.48	1.94	(0.17, 0.05)	37
C37	ITO/NPB/**EML**/TPBi/LiF/Al	-	-	1.53	0.86	3.02	(0.17, 0.06)	37
C38	ITO/NPB/mCP/**EML**/TPBi/Ca/Ag	5.6	2684	1.36	-	1.9	(0.18, 0.12)	39
C39	ITO/NPB/mCP/**EML**/TPBi/Ca/Ag	6.3	3703	1.62	-	2.4	(0.16, 0.18)	39
C40	ITO/NPB/mCP/**EML**/TPBi/LiF/Al	3.5	-	1.89	1.58	4.21	(0.16, 0.06)	40
C41	ITO/NPB/mCP/**EML**/TPBi/LiF/Al	2.8	-	0.82	0.84	2.70	(0.16, 0.04)	40
C42	ITO/PEDOT:PSS/**EML**(CBP:15%dopant)/TPBi/LiF/Al	6.3	522	0.3	0.1	0.4	(0.18, 0.11)	41
C43	ITO/PEDOT:PSS/**EML**(CBP:15%dopant)/TPBi/LiF/Al	6.2	549	0.4	0.2	0.2	(0.17, 0.22)	41
C44	ITO/PEDOT:PSS/**EML**(CBP:15%dopant)/TPBi/LiF/Al	6.0	734	0.6	0.3	0.6	(0.16, 0.12)	41
C45	ITO/PEDOT:PSS/**EML**(CBP:15%dopant)/TPBi/LiF/Al	6.0	815	0.4	0.2	0.2	(0.20, 0.34)	41
C46	ITO/PEDOT:PSS/**EML**(CBP:15%dopant)/TPBi/LiF/Al	5.8	944	0.7	6.8	1.5	(0.19, 0.31)	41
C47	ITO/TAPC/**EML**(TBADN:10%dopant)/TPBi/LiF/Al	-	12910	7.39	-	3.36	(0.29, 0.49)	42
C48	ITO/TAPC/**EML**(TBADN:10%dopant)/TPBi/LiF/Al	-	251	0.96	-	0.41	(0.40, 0.56)	42
C49	ITO/TAPC/**EML**(TBADN:10%dopant)/TPBi/LiF/Al	-	1641	1.86	-	0.84	(0.30, 0.46)	42
C50	ITO/TAPC/**EML**(TBADN:10%dopant)/TPBi/LiF/Al	-	95	0.29	-	0.33	(0.39, 0.50)	42
C51	ITO/TAPC:20%MoO_3/TAPC/**EML**/TmPyPB/LiF/Al	6125	2.9	8.8	8.5	3.5	(0.28, 0.42)	43
C52	ITO/TAPC:20%MoO_3/TAPC/**EML**/TmPyPB/LiF/Al	4311	2.9	9.0	8.4	3.8	(0.24, 0.37)	43

[a]Turn-on voltage. [b]Maximum luminance. [c]Maximum current efficiency. [d]Maximum power efficiency. [e]Maximum external quantum efficiency.

1.3 Carbazole functionalized materials in phosphorescence OLED

1.3.1 Carbazole-based materials as hole transporting host in PhOLED

Heavy metal-based phosphorescent emitters can harvest 100% of excitons through spin-orbit coupling and thus expected to give superior electroluminescence performance. But, the triplet emitters must be doped into the host material which would otherwise quench the emission by concentration quenching and triplet-polaron quenching mechanism [44]. The host materials should invariably possess high triplet energy, suitable HOMO and LUMO energy level with neighboring layers for facile charge injection and high thermal stability. Since carbazole possess high triplet energy and sufficient hole transporting ability, carbazole based materials are exploited for host materials in PhOLED. Here, we describe carbazole-based hole transporting hosts for PhOLED.

It is well known that the arylamines are good hole transporting moities. Owing to the twist structure, diphenylamine tethered carbazoles are beneficial for increasing the amorphous nature. Lee and coworkers reported carbazole functionalized at 1- and 8-position with diphenylamine and its TPD analog (**C53-C55;** Chart 1.8) and employed them as host material for PhOLED [45]. The triplet energy of these molecules are in the range of 2.45 – 2.68 eV which is higher than that of green emitter $Ir(mppy)_3$. The presence of diphenylamine raised the HOMO energy level on moving from mono- to di-substitution whereas it did not alter the LUMO energy level. Due to complete conjugation over entire backbone, these molecules exhibited low ICT character. The high lying HOMO decreased the turn-on voltage by favoring easy hole injection into host molecules. Though the device based on **C55** displayed low turn on voltage, it suffers poor performance due to low triplet energy of the host which allowed back energy transfer from dopant to host. The device fabricated with **C54** exhibited maximum current efficiency, power efficiency and EQE of 25.0 cd/A, 17.9 lm/W and 8.2% respectively. The better performance of **C54** is owing to its suitable energy level with neighboring layers and dopant.

Generally, low band gap emitters suffer serious carrier trapping at higher operating voltages. So, the development of host materials which mitigate concentration quenching, charge trapping and reduced power consumption is necessary. Chang and coworkers reported star-shaped carbazoles as hole transporting host materials (**C56-C58;** Chart 1.8) for red emitting PhOLED [46]. The hole drift mobility of the compound **C58** was about 3×10^{-3} cm^2 V^{-1} s^{-1}. All

of the compounds (**C56-C58**) exhibited high decomposition temperature which is attributed to the rigid carbazole. The devices employing these materials as host exhibited red emission with the $Ir(piq)_3$ dopant which is compared with the control device fabricated with TCTA host material in a similar device structure. The best device performance with the maximum EQE, current efficiency and power efficiency of 8.4%, 5.3 cd/A and 5.5 lm/W respectively was observed for the device fabricated with the host **C58**. The electroluminescence performance of the device was according to the high hole transporting ability of the host material. Low current density of the device containing the host **C56** is attributed to poor hole mobility as compared to other hosts, **C57** and **C58**. The high brightness of **C58** based device indicates the superior electrical stability. Moreover, the electroluminescence performance of **C58** based device was comparable to that of TCTA host owing to similar hole transporting ability and triplet energy level.

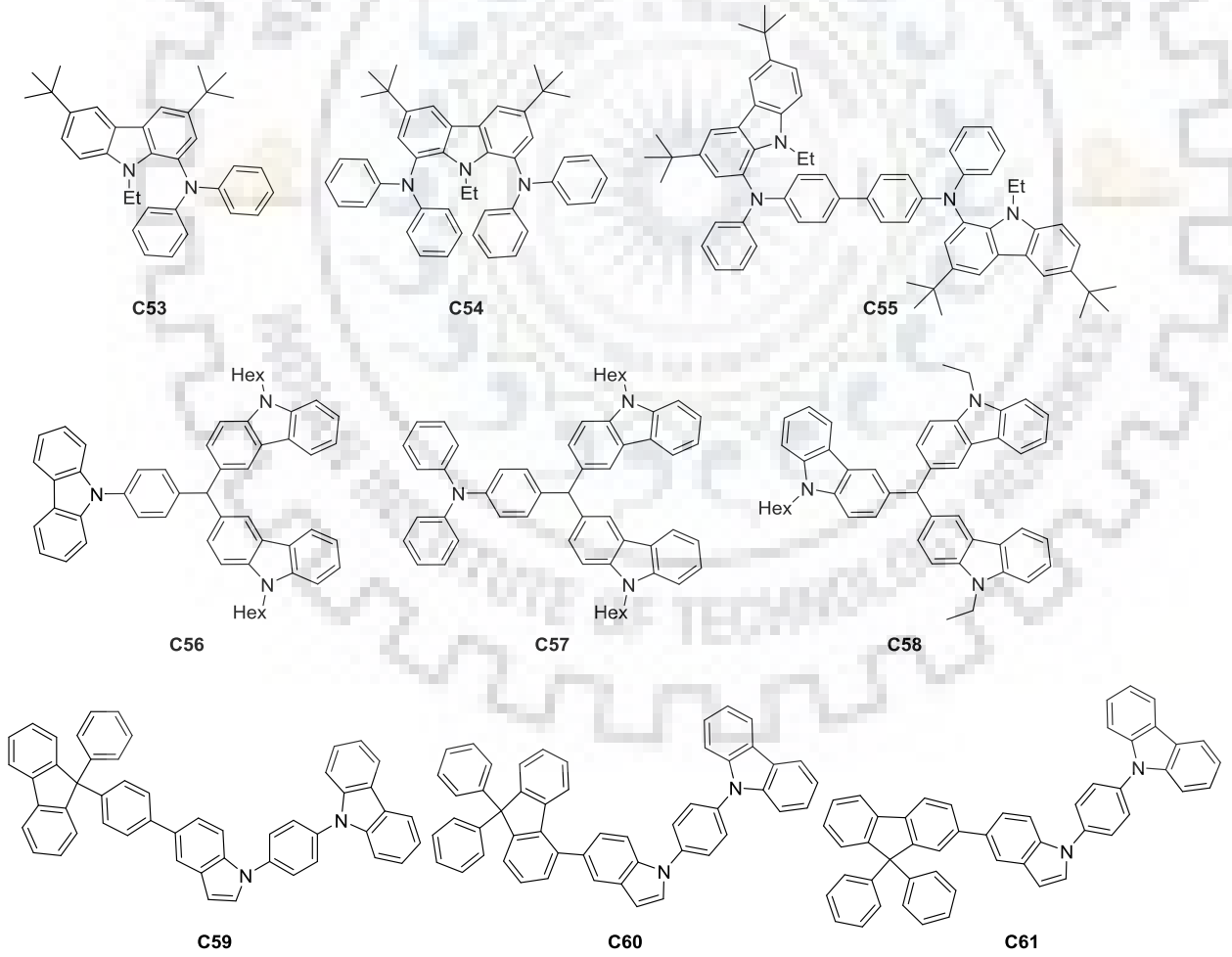

Chart 1.8 Carbazole-based hole transporting host materials for PhOLED.

The insertion of electron donating group and non-planar moieties usually increases hole transporting nature as well as amorphous nature. Dong and coworkers designed carbazole tethered with indole and spirofluorene (**C59**-**C61;** Chart 1.8) to enhance triplet energy by controlling the connection between spirofluorene and indole to induce distorted structure [47]. Since indole possess hole transporting character, carbazole tethered indole based materials are expected to show high hole mobility. The high glass transition temperature of **C61** (165 °C) is attributed to highly twisted structure. The triplet energies of the compounds **C59**, **C60**, **C61** determined from low temperature emission spectra are to be 3.20, 3.02, 3.20 respectively and high triplet energy is useful for fabricating green emitting devices. This would ensure exothermic energy transfer from host to dopant and restrict the back energy transfer from dopant to hosts. The OLED device fabricated with **C61** exhibited the maximum current efficiency of 45.2 cd/A, power efficiency of 23.2 lm/W, luminance of 61780 cd/m^2. The high performance of **C61** is due to effective energy transfer from host to the dopant and high glass transition temperature which raised the thin film forming ability.

Bagdziunas and coworkers reported phenothiazine decorated carbazole as host materials (**C62**, **C63;** Chart 1.9) for green and red emitting PhOLED [48]. The introduction of phenothiazine increased the HOMO energy level corresponding to the carbazole derivatives and thus facilitate easy injection of hole carriers. The green emitting devices employing these materials as host and Ir(ppy)$_3$ as dopant exhibited low performance when there is no hole transporting layer is used in device architecture. When the hole transporting layer is employed, the performance of the devices increased dramatically. The high performance was observed for mono-phenothiazine based device with maximum current efficiency, power efficiency and EQE of 74.1 cd/A, 47.5 lm/W and 20.0% respectively. The red emitting devices are also fabricated by using the dopant Ir(piq)$_2$(acac) and found high current efficiency of 37.4 cd/A and EQE of 10.5% for mono-phenothiazine based device. The probability of formation of excitons formation is inversely proportional to the root mean square roughness which is determined from Atomic force microscopy method. The high performance of mono-phenothiazine (**C62**) based devices can be attributed to low root mean square roughness value when dispersed in Ir(ppy)$_3$ and Ir(piq)$_2$(acac) which offers smooth surface and wider recombination zone.

Sun and coworkers developed carbazole-fluorene and carbazole-spirofluorene hybrid (**C64**, **C65;** Chart 1.9) as for solution processable host in PhOLED [49]. The spirofluorene tethered

carbazole (**C65**) exhibited slightly higher triplet energy due to twisted structure. Further, the high glass transition temperature of about 230 °C is beneficial to form uniform high quality thin film. From the AFM studies, it was confirmed that these molecules are able to form pin-hole free thin film. It suggests the effective suppression of aggregation and the absence of phase separation in solid state which would play positive role in boosting the device performance. The compounds (**C64**, **C65**) are employed as host for blue emitting device made of the dopant FIrpic. The host material is mixed with 30% of OXD-7 to improve electron carrier mobility in the device structure. The devices fabricated with both the host materials exhibited sky blue emission without additional peak indicating the efficient energy transfer from the host to dopant. The performance of the devices containing these hosts is superior to mCP-based devices. The best device performance is observed for fluorene-based host (**C65**) with maximum current efficiency of 21.2 cd/A and EQE of 10.5%. It is attributed to high triplet energy level, well matched HOMO and LUMO with neighboring layers and excellent film forming ability of the host materials.

CBP is a widely used host material in OLED device possessing host-guest system. The low glass transition temperature of CBP generally results in poor thin film. Jiang and coworkers designed carbazole dendronized CBP as a host material (**C66;** Chart 1.9) for blue PhOLED device [50]. The high triplet energy of the host is ascribed to twisted biphenyl core of the molecule. The HOMO of the host material is raised compared to CBP which approaches the work function of PEDOT and thus facilitate easy hole injection. The glass transition temperature of dendronized CBP is increased to 287 °C as compared to 62 °C of bare CBP host. The dihedral angle between biphenyl and carbazole is increased to 41 ° when compared to 37.7 ° of bare CBP which decrease the conjugation and thus raise the triplet energy. The twisted geometrical feature of host is beneficial to suppress intermolecular interaction and thereby prevent molecular recrystallization which improves the morphological stability of the thin film. The device fabricated with FIrpic doped in host exhibited the maximum luminance, current efficiency and EQE of 8600 cd/m^2, 5.8 cd/A and 2.8% respectively. The device performance is almost three times higher than the CBP based device of similar architecture.

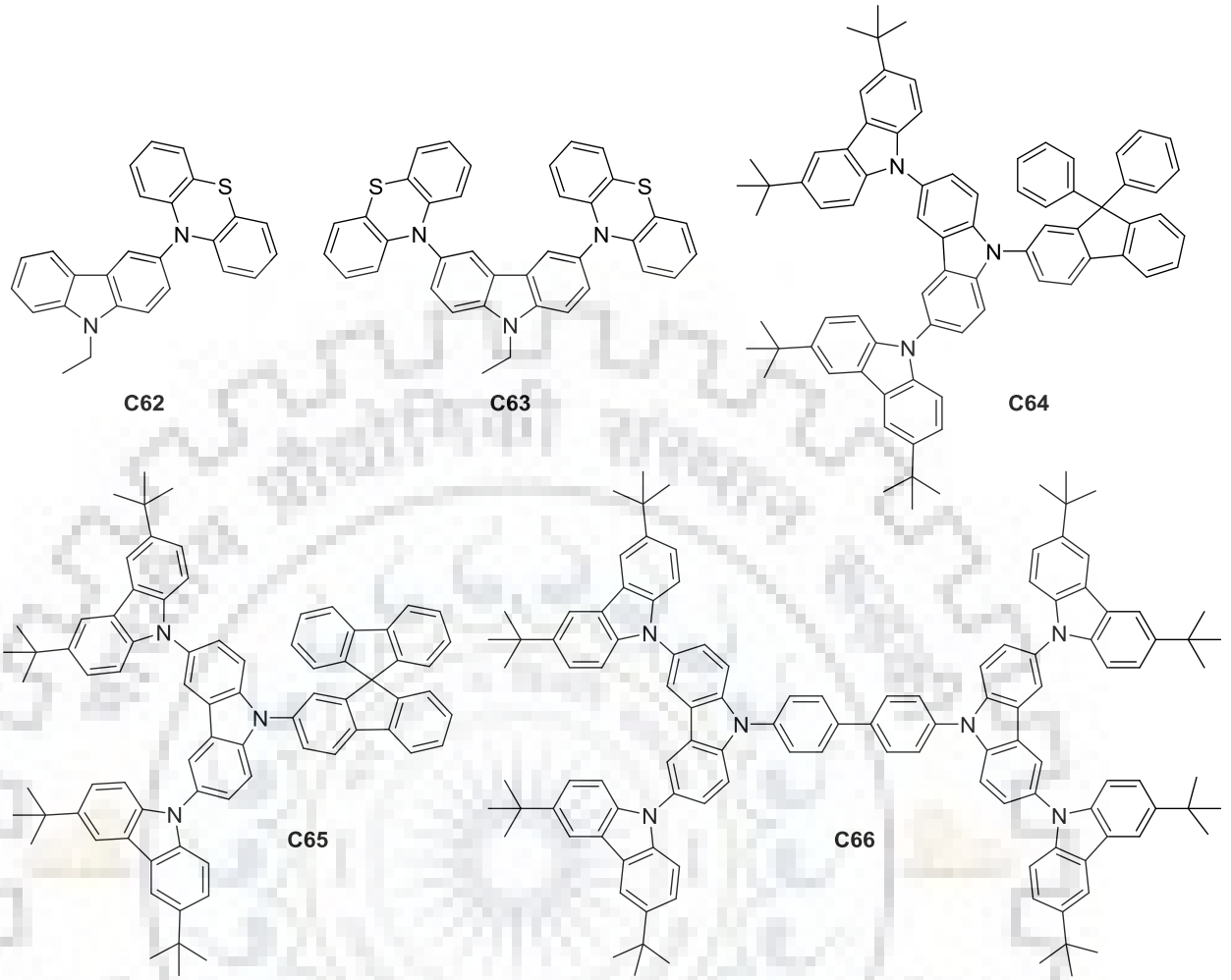

Chart 1.9 Carbazole-based hole transporting host materials for PhOLED.

Table 1.7 Photophysical and thermal properties of carbazole-based hole transporting host materials in PhOLED

Dye	λ_{max} (nm)[a]	λ_{em} (nm)[a]	HOMO (eV)[c]	LUMO (eV)	E_T (eV)[d]	E_{0-0} (eV)[e]	T_g (°C)[f]	T_d (°C)[g]	Ref
C53	360	396	-	-	2.68	3.25	65	-	45
C54	360	386	-	-	2.60	3.26	92	-	45
C55	348	420	-	-	2.45	3.14	165	-	45
C56	352	375, 396	-	-	2.97	3.43	73	417	46
C57	353	375, 397	-	-	2.97	3.35	54	413	46
C58	353	377, 397	-	-	2.97	3.42	93	411	46
C59	290[b]	350[b]	-5.42	-1.74	3.20	3.68	-	407	47
C60	290[b]	364[b]	-5.49	-1.86	3.02	3.64	-	405	47
C61	290[b]	364[b]	-5.43	-1.80	3.20	3.64	-	412	47
C62	330[b]	448[b]	-4.85	-1.45	2.60	3.40	-	-	48
C63	327[b]	483[b]	-4.86	-1.55	2.61	3.31	-	-	48
C64	327	400	-5.36	-1.94	2.72	-	231	459	49
C65	326	402	-5.32	-1.93	2.73	-	249	474	49
C66	350	402	-5.30	-1.98	2.68	3.42	287	475	50

[a] Measured in dichloromethane. [b] Meaured in tetrahydrofuran. [c] Calculated from cyclic voltammetry. [d] Triplet energy obtained from phosphorescence spectra. [e] Band gap obtained from optical edge. [f] Glass transition temperature. [g] Thermal decomposition temperature at 5% weight loss.

Table 1.8 Electroluminescence properties of carbazole-based hole transporting host materials in PhOLED

Dye	Dopant	Device structure	V_{on} (V)[a]	L_{max} [b] (cd/m^2)	ηc [c] (cd/A)	ηp [d] (lm/W)	EQE (%)[e]	$CIE_{(x,y)}$	Ref
C53	$Ir(mppy)_3$	ITO/PEDOT:PSS/**Host**:7% dopant/TPBi/CsF/Al	4.6	8050	24.5	14.1	8.0	(0.29, 0.60)	45
C54	$Ir(mppy)_3$	ITO/PEDOT:PSS/**Host**:7% dopant/TPBi/CsF/Al	3.7	6632	25.0	17.9	8.2	(0.29, 0.61)	45
C55	$Ir(mppy)_3$	ITO/PEDOT:PSS/**Host**:7% dopant/TPBi/CsF/Al	3.1	4936	11.2	10.1	3.6	(0.29, 0.61)	45
C56	$Ir(piq)_3$	ITO/NPB/**Host**:8%dopant/BP4mPy:8%dopant/ LiF/Al	5.3	3898	3.2	4.5	6.9	(0.68, 0.32)	46
C57	$Ir(piq)_3$	ITO/NPB/**Host**:8%dopant/BP4mPy:8%dopant/ LiF/Al	3.5	3610	4.2	4.9	7.1	(0.68, 0.32)	46
C58	$Ir(piq)_3$	ITO/NPB/**Host**:8%dopant/BP4mPy:8%dopant/ LiF/Al	3.5	8843	5.3	5.5	8.4	(0.68, 0.32)	46
C59	$Ir(piq)_3$	ITO/MoO3/TCTA/**Host**:8%dopant/TPBi/LiF/Al	4.2	33250	29.6	13.5	-	(0.31, 0.61)	47
C60	$Ir(piq)_3$	ITO/MoO3/TCTA/**Host**:8%dopant/TPBi/LiF/Al	4.7	42940	30.8	17.2	-	(0.30, 0.62)	47
C61	$Ir(piq)_3$	ITO/MoO3/TCTA/**Host**:8%dopant/TPBi/LiF/Al	4.5	61780	45.2	23.2	-	(0.30, 0.62)	47
C62	$Ir(piq)_3$	ITO/*m*-MTDATA/**Host**:7%dopant/Bphen/Ca:Al	2.5	58974	74.1	47.5	20.0	-	48
C63	$Ir(piq)_3$	ITO/*m*-MTDATA/**Host**:7%dopant/Bphen/Ca:Al	2.5	29913	49.4	34.1	12.9	-	48
C62	$Ir(piq)_2$ (acac)	ITO/*m*-MTDATA/**Host**:7%dopant/Bphen/Ca:Al	3.0	59110	37.4	29.6	10.5	-	48
C63	$Ir(piq)_2$ (acac)	ITO/*m*-MTDATA/**Host**:7%dopant/Bphen/Ca:Al	2.5	59558	28.2	40.6	7.2	-	48
C64	FIrpic	ITO/PEDOT:PSS/**Host**:30%OXD:7%dopant/ TPBi/Cs_2CO_3/Al	5.1	-	21.2	-	10.5	(0.17, 0.35)	49
C65	FIrpic	ITO/PEDOT:PSS/**Host**:30%OXD:7%dopant/ TPBi/Cs_2CO_3/Al	5.1	-	19.8	-	10.0	(0.16, 0.32)	49
C66	FIrpic	ITO/PEDOT:PSS/**Host**:30%OXD:10%dopant/ Cs_2CO_3/Al	5.6	8600	5.8	-	2.8	(0.16, 0.36)	50

[a] Turn-on voltage. [b] Maximum luminance. [c] Maximum current efficiency. [d] Maximum power efficiency. [e] Maximum external quantum efficiency.

1.3.2 Carbazole-based bipolar materials as host

Since carbazole-based materials possess high triplet energy, they have been exploited as triplet host materials in phosphorescent OLED. It is well known that the hole mobility is far faster than that of electron mobility. Unipolar materials lead to poor performance in OLED as a result of imbalanced charge carrier mobility. Bipolar host materials exhibit balanced charge transport arising from electron donor and electron acceptor moiety present in a single molecule and thus the device performances would be improved. The motive behind the development of bipolar host is to provide effective hole and electron charge transport, broaden the recombination zone, simplifying device structure and improve the device performance.

Lee and coworkers reported symmetrically substituted phosphine oxide on carbazole at C2- or C4-position (**C67**, **C68;** Chart 1.10) as bipolar hosts [15]. Here, electron donating carbazole act as hole transporter and electron withdrawing phosphine oxide as electron transporter to construct bipolar host materials. Carbazole connected via C4-position showed high glass transition temperature over C2-connected carbazole despite of the same molecular weight. The steric hindered position of C4-functionalized carbazole gave high glass transition temperature owing to more twisted structure while C2-connected compound results in less sterically hindered structure. The absorption maxima slightly increased for C4-functionalized carbazole, but it does not influence over triplet energy level. The substitution at C4-position of carbazole destabilized HOMO and LUMO while C2- position substitution brings HOMO and LUMO energy level stabilized. The blue emitting phosphorescent device fabricated with the host materials exhibited EQE of 15.0% and 9.5% for C4-substituted carbazole (**C68**) and C2-substituted carbazole (**C67**) respectively. The high performance of **C68** is evident from the similar current density observed for hole only and electron only device which ensures balanced charge transport. But, **C67** gave high hole current density over electron current and results in imbalanced charge transport across the device.

In another report, the same authors' demonstrated carbazole possessing diphenylphosphine oxide (**C69;** Chart 1.10) at C2 and C5-position as bipolar host for blue emitting PhOLED [16]. The asymmetric substitution of carbazole is beneficial for the suppression of aggregation in solid state by close molecular packing and thus enhances morphological stability. The glass transition temperature of **C69** is higher than symmetrically substituted carbazole at 2,7 and 3,6-

position [51]. The presence of diphenylphosphine oxide at C5-position of carbazole results in high morphological stability. The C2-functionalization results in reduction of energy band by stabilization of LUMO energy levels and thus low driving voltage and high power efficiency. On the whole, this design strategy increased the device performance with long durability. The device exhibited high EQE of 31.4% with blue emission at 10% dopant concentration. The efficiency roll-off is considerably less and EQE of 28.6% is observed at the brightness of 1000 cd/m^2. The high EL attributes to the high PL intensity of host:FIrpic film and absolute quantum yield of above 95% which confirms the efficient energy transfer from host to FIrpic and balanced charge carrier transport. Interestingly, the high power efficiency of 46.9 and 33.5 lm/W obtained at 100 cd/m^2 and 1000 cd/m^2 respectively without employing special electron or hole transporting layers in the device structure. It is ascribed to low driving voltage rendered by C2-substitution and high quantum efficiency by C5-substitution.

Generally, donor-acceptor (D-A) configuration of compounds will provide bipolar nature at the cost of lowering of triplet energy gap. For efficient energy transfer, the triplet energy of the host materials must be higher than that of dopant. So, the materials exhibiting both high triplet energy and bipolar nature are in demand for realizing highly efficient OLED devices. Xu and coworkers demonstrated the modulation of electroluminescent properties by D-A configured host materials (**C70**, **C71;** Chart 1.10) using short axis linkage [52]. When electron withdrawing group is attached at 1,8- position of carbazole, it would provide bipolar nature without altering the triplet energy level. The similar emission spectrum of these compounds in different solvents indicates the suppression of intra-molecular charge transfer from carbazole to phosphine oxide. Generally, when constructing bipolar materials, the electron current is increased at the cost of hole current and thereby bipolar character is achieved. It is interesting to note that hole only current (single layer device) is much higher than that of electron only current. The incorporation of phosphine oxide at 1,8-position did not alter the hole mobility of carbazole whereas it provides decent bipolar character by augmenting electron only current. Moreover, the electron mobility is drastically improved when compared to long-axis substituted analogs [53]. The modified D-A based host material for blue PhOLED exhibited low turn on voltage of 2.6 V with low efficiency roll-off performance at high brightness.

The insertion of diphenylphospine oxide (DPPO) with hole transporting unit stabilizes the HOMO level. As already stated, the hole mobility is faster than electron mobility. The

magnitude of electron mobility can be increased by the incorporation of high ratio of electron withdrawing unit in the molecules. Li and coworkers reported dual n-type bipolar host materials (**C72**, **C73;** Chart 1.10) for improving the electron mobility [54]. Here, DPPO on direct attachment with pyridine did not influence HOMO. The DPPO is tethered as second electron withdrawing group in addition to pyridine. The DPPO unit is grafted for its ability to retain triplet energy level and has no role in extending conjugation so that DPPO tethered host could be exploited for blue emitting materials. The role of second n- type unit (DPPO) was established by comparing the molecule without DPPO. The DPPO unit stabilized the LUMO while keep the HOMO intact. The thermal decomposition temperature sharply increased when DPPO is inserted. Since the triplet energy of these materials are higher than triplet energy of blue and green emitter FIrpic and $Ir(ppy)_3$ respectively, they were employed as host materials for blue and green emitting PhOLEDs. The DPPO did not participate in constructing HOMO and LUMO, so it does not have any role in conjugation whereas it pulls LUMO down due to strong electron withdrawing nature. From single carrier charge devices, the meta- and para-compounds (**C72** and **C73**) exhibited bipolar nature whereas the reference compound showed less electron current density. This indicates the role of DPPO in realizing bipolar nature. The EL performance of DPPO based compounds exhibited superior performance over the reference compound which contains only one n- type acceptor. The meta-substitued compound **C72** exhibited high EL performance over para- compound in FIrpic based blue devices with maximum current efficiency, power efficiency and EQE of 55.6 cd/A, 43.6 lm/W and 25.3% respectively.

Wang and coworkers reported carbazole substituted oxadiazole/benzimidazole at 1,8-position (**C74**, **C75;** Chart 1.10) to realize bipolar hosts [55]. The glass transition temperature of 138 and 154 °C respectively and decomposition temperature of these compounds are very high due to twisted configuration arises by steric hindered 1,8-substitution. Also, the electron deficient 1,8-position of carbazole leads to high triplet energy. From DFT calculation, it is found that oxadiazole/benzimidazole is perpendicular to carbazole core due to steric hindrance. The HOMO and LUMO orbitals are confined to carbazole and oxadiazole/benzimidazole respectively. The well separation of HOMO and LUMO guarantees the effective electronic charge transfer without back energy transfer. Benzimidazole-based host **C75** is used for blue emitting devices. The performance of the device is comparable to that of mCP based device in a

similar device configuration. When both the compounds are employed as host in green emitting devices, the oxadiazole-based device **C74** exhibited high current and power efficiency of 73.9 cd/A and 89.7 lm/W respectively and maximum luminance of 37920 cd/m^2 with low turn on voltage of 2.5 V. The high current and power efficiency of oxadiazole based device is attributed to balanced hole and electron transporting nature of the bipolar host material.

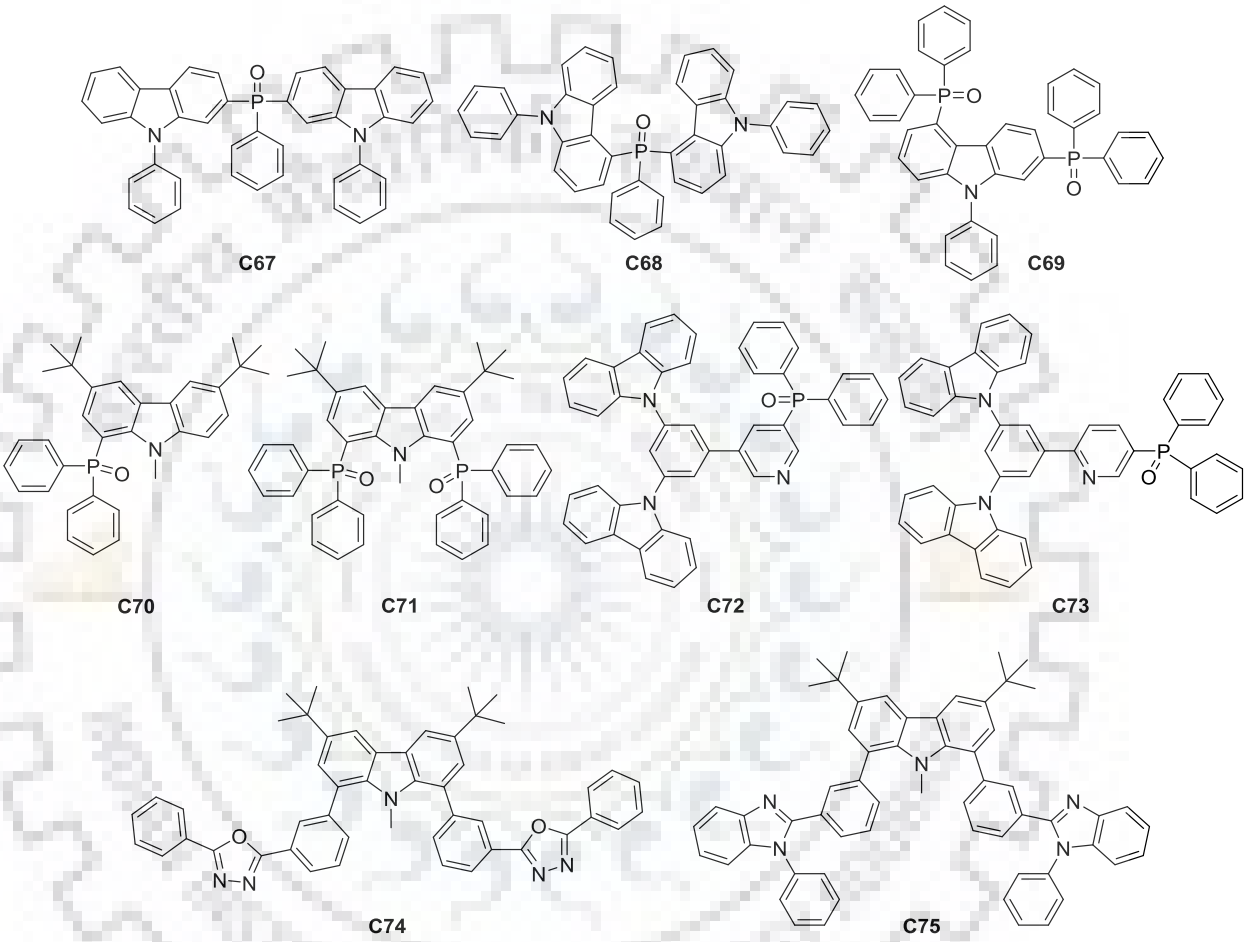

Chart 1.10 Carbazole-based bipolar host materials for PhOLED.

Lee and coworkers designed CN modified carbazole based bipolar host materials (**C76**, **C77;** Chart 1.11) by variation of *ortho* and *meta*-linkage with phenyl linker [56]. The observed EL and lifetime of the devices are superior to the devices employing universally known host mCBP. The blue shifted fluorescence and phosphorescence spectra of *ortho*-substituted compound compared to meta- compound is due to reduced degree of conjugation. Due to the distorted structure, *ortho*-substituted compound (**C76**) gave high triplet energy over meta-substituted and mCBP. According to DFT calculation, the HOMO of both the compounds is

similar to mCBP i.e. localized on phenylcarbazole while LUMO is concentrated on CN modified carbazole which would predict better electron transporting character over mCBP. The blue PhOLED employed $Ir(dbi)_3$ as dopant with 5 wt%. The meta-substituted host **C77** exhibited better efficiency over *ortho*- substituted analog **C76**. The good electron injection from lower LUMO level and the widening of recombination zone resulted in better performance and extended lifetime of the device.

Mu and coworkers reported bipolar host materials containing carbazole as donor, phenyl as linker and quinoxaline as acceptor (**C78**-**C80;** Chart 1.11) for red emitting PhOLED [57]. They tuned the optoelectronic properties of the host materials by modulating the linking mode with phenyl linker. The *ortho*-substituted compound (**C78**) showed high triplet energy compared to meta- and para- analogs due to highly twisted structure. All the isomers showed small efficiency roll-off at high luminance which attests the superiority of the host materials for practical applications. The device employed *para*-substituted compound **C80** exhibited the best EL performance with current efficiency, power efficiency and EQE of 21.9 cd/A, 15.4 lm/W and 12.2% respectively. Similarly, *ortho*-substituted compound (**C78**) exhibited almost similar magnitude of EL performances. The low performance of meta- compound can be explained from unbalanced charge transport which is evaluated from single carrier device where the hole mobility is much higher than electron mobility.

Li and coworkers designed carbazole tethered pyrazolyl pyridine as bipolar host materials (**C81-C83;** Chart 1.11) in which carbazole acts as hole transporter and pyrazolyl pyridine as electron transporter in the ratio of 1:2 to ensure effective balanced charge transport by increasing electron charge mobility [58]. The triplet energy of the materials was tuned by varying the linking position of phenyl linker. The *ortho*-functionalized compound (**C81**) exhibited high triplet energy of 2.95 eV compared to others due to its highly twisted structure. As the planarity of the compounds increases from *orho*- to *para*-, they are expected to give high current density owing to the raise of charge hopping and transporting character. The blue device employing FIrpic as dopant exhibited low performance for *ortho*-substituted compound owing to high energy barrier for charge injection. The small efficiency roll-off at practical luminance of 1000 cd/m^2 for **C82** is attributed to appropriate twisted conformation and triplet energy which forbids back energy transfer from dopant to host material. The *para*-substituted compound **C83** showed superior performance over *ortho*- and *meta*-compounds in green

devices fabricated with the dopant $Ir(ppy)_3$. It might be ascribed to proper energy level alignment for the transfer of charges from host to dopant and thus low driving voltage. However, meta-substituted compound (**C82**) exhibited low efficiency roll-off at high current density region which might be due to appropriate distortion and high film stability.

Fan and coworkers reported carbazole-pyridine hybrids linked through phenyl linker as bipolar hosts (**C84**, **C85;** Chart 1.11) for blue emitting PhOLED [59]. As the carbazole is appended, the glass transition and thermal decomposition temperature increased dramatically for **C85** when compared to **C84**. The device fabricated with **C84** as host exhibited the highest EQE of 17.8% at 100 cd/m^2. It also exhibited considerably low efficiency roll-off of 3.9% (EQE of 17.1%) even at high brightness of 1000 cd/m^2. The high performance is attributed to balanced charge transport achieved by the host material which is confirmed by the single charge carrier devices. Though **C85** exhibited high morphological properties, the efficiency is low due to unbalanced charge transport. The high hole only current density for **C85** over electron only current density resulted in unbalanced charge transport and thus poor performance.

Wang and coworkers reported carbazole tailored 1,2,4-thiadiazole through different linking position of phenylene linker (**C86-C88;** Chart 1.11) as bipolar host materials [60]. The triplet energy of the isomers followed the trend of *ortho-* > *meta-* > *para-*. The highly twisted and sterically hindered structure is responsible for high triplet energy level for ortho- substituted compound. The charge carrier mobility of the compounds was measured by time of flight technique. The *ortho-* and *meta-* substituted compounds exhibited almost similar hole and electron carrier mobility and acted as bipolar materials while *para*-substiuted compound exhibited high hole charge mobility. The high triplet energy and charge mobility of ortho-substituted compound **C86** was beneficial for suppressing back energy transfer and effective confinement of excitons and hence high device performance. The maximum EQE of 26.1% was observed and still it remained 20.3% at high brightness of 10,000 cd/m^2. The high performance of **C86** is attributed to high carrier mobility and balanced charge transport.

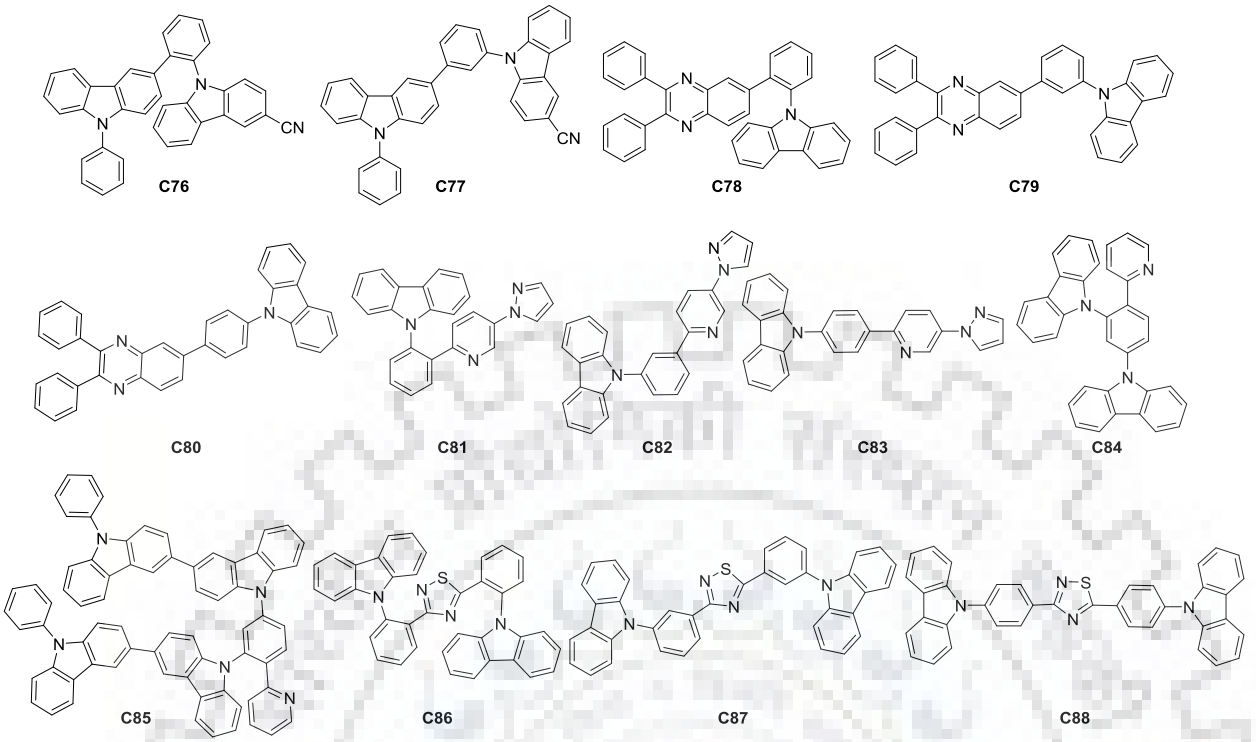

Chart 1.11 Carbazole-based bipolar host materials for PhOLED.

Table 1.9 Photophysical and thermal properties of carbazole-based bipolar host materials for PhOLED

Dye	λ_{max} (nm)[a]	λ_{em} (nm)[a]	HOMO (eV)[d]	LUMO (eV)	E_T (eV)[e]	E_{0-0} (eV)[f]	T_g (°C)[g]	T_d (°C)[h]	Ref
C67	354[b]	368, 382[b]	-5.97	-2.59	2.90	3.38	122	-	15
C68	354[b]	375, 389[b]	-5.90	-2.54	2.90	3.36	168	-	15
C69	371[b]	385, 398[b]	-6.17	-2.90	2.80	3.27	140	506	16
C70	363	391	-5.99	-2.63	2.98	3.36	175	323	52
C71	366	382, 390	-6.13	-2.87	2.98	3.26	-	394	52
C72	338	419	-5.66	-2.57	2.86	3.09	123	461	54
C73	339	455	-5.65	-2.79	2.78	2.86	130	442	54
C74	362[c]	385[c]	-5.58	-2.31	2.70	3.27	154	433	55
C75	365[c]	394[c]	-5.60	-2.34	2.60	3.26	138	416	55
C76	-	-	-6.10	-2.57	2.80	3.53	-	-	56
C77	-	-	-6.07	-2.57	2.78	3.50	-	-	56
C78	363	499	-5.82	-2.65	2.46	3.17	104	357	57
C79	363	516	-5.81	-2.65	2.40	3.16	107	390	57
C80	373	498	-5.72	-2.67	2.37	3.05	112	403	57
C81	339	397	-5.69	-2.26	2.95	3.43	58	301	58
C82	340	403	-5.63	-2.34	2.71	3.29	60	328	58
C83	340	396	-5.61	-2.35	2.67	3.26	-	336	58
C84	-	-	-5.54	-1.98	2.77	3.56	108	347	59
C85	-	-	-5.29	-1.88	2.72	3.41	192	571	59
C86	330	421	-5.64	-2.64	2.62	3.00	167	370	60
C87	338	428	-5.51	-2.50	2.58	3.01	170	394	60
C88	342	413	-5.50	-2.55	2.48	2.95	168	420	60

[a] Measured in dichloromethane. [b] Measured in tetrahydrofuran. [c] Measured in toluene. [d] Calculated from cyclic voltammetry. [e] Calculated from phosphorescence spectra. [f] Band gap obtained from optical edge. [g] Glass transition temperature. [h] Thermal decomposition temperature at 5% weight loss.

Table 1.10 Electroluminescent properties of carbazole-based bipolar host in PhOLED

Dye	Dopant	Device structure	V_{on} (V)[a]	L_{max} (cd/m^2)[b]	η_c (cd/A)[c]	η_p (lm/W)[d]	EQE (%)[e]	$CIE_{(x,y)}$	Ref
C67	FIrpic	ITO/PEDOT:PSS/TAPC/**Host**:10%dopant/ SPPO13/ LiF/Al	3.5	-	-	-	9.5	-	15
C68	FIrpic	ITO/PEDOT:PSS/TAPC/**Host**:10%dopant/ SPPO13/ LiF/Al	3.5	-	-	-	15.0	-	15
C69	FIrpic	ITO/PEDOT:PSS/TAPC/**Host**:10%dopant/ SPPO13/ LiF/Al	3.0	-	-	53.1	31.4	-	16
C70	FIrpic	ITO/MoOx/*m*-MTDATA:MoOx/*m*-MTDATA/ **Host**:10%FIrpic/Bphen/Cs_2CO_3/Al	2.6	-	16.0	16.8	8.7	-	52
C71	FIrpic	ITO/MoOx/*m*-MTDATA:MoOx/*m*-MTDATA/ **Host**:10%FIrpic/Bphen/Cs_2CO_3/Al	2.6	-	20.2	19.2	11.0	-	52
C72	FIrpic	ITO/PEDOT:PSS/TAPC/TCTA/**Host**:5%dopant/ TmPyPB/ LiF/Al	3.5	13970	55.6	43.6	25.3	(0.15, 0.38)	54
C73	FIrpic	ITO/PEDOT:PSS/TAPC/TCTA/**Host**:5%dopant/ TmPyPB/ LiF/Al	3.5	17230	47.4	37.2	19.1	(0.18, 0.42)	54
C74	FIrpic	ITO/MoO3/NPB/mCP/**Host**:6%dopant/TmPyPB/ LiF/Al	3.0	9565	27.6	27.0	11.6	(0.15, 0.31)	55
C74	$Ir(ppy)_3$	ITO/MoO3/NPB/TCTA/**Host**:9%dopant/ TmPyPB/LiF/Al	2.7	38440	64.0	70.0	17.5	(0.30, 0.63)	55
C75	$Ir(ppy)_3$	ITO/MoO3/NPB/TCTA/**Host**:9%dopant/ TmPyPB/LiF/Al	2.5	37920	73.9	89.7	20.3	(0.30, 063)	55
C76	$Ir(dbi)_3$	ITO/PEDOT:PSS/DNTPD/BPBPA/PCZAc/**Host**: 10% dopant/DBFTrz/ZADN/LiF/Al	-	-	-	-	17.1	-	56
C77	$Ir(dbi)_3$	ITO/PEDOT:PSS/DNTPD/BPBPA/PCZAc/**Host**: 10% dopant/DBFTrz/ZADN/LiF/Al	-	-	-	-	16.0	-	56
C78	$Ir(pic)_2$ (acac)	ITO/PEDOT:PSS/NPB/TCTA/**Host**:10%dopant/ TPBi/ LiF/Al	3.5	18426	21.2	13.4	12.2	(0.62, 0.38)	57
C79	$Ir(pic)_2$ (acac)	ITO/PEDOT:PSS/NPB/TCTA/**Host**:10%dopant/ TPBi/ LiF/Al	3.1	27049	15.7	11.9	9.2	(0.62, 0.38)	57

Table 1.10 (cont.)

Dye	Dopant	Device structure	V_{on} (V)[a]	L_{max} (cd/m^2)[b]	η_c (cd/A)[c]	η_p (lm/W)[d]	EQE (%)[e]	$CIE_{(x,y)}$	Ref
C80	$Ir(pic)_2(acac)$	ITO/PEDOT:PSS/NPB/TCTA/**Host**:10%dopant/ TPBi/ LiF/Al	3.2	19037	21.9	15.4	12.2	(0.61, 0.38)	57
C81	FIrpic	ITO/PEDOT:PSS/TAPC/TCTA/**Host**:5%dopant/ TmPyPB/LiF/Al	4.1	9750	38.7	30.4	17.4	(0.14, 0.33)	58
C82	FIrpic	ITO/PEDOT:PSS/TAPC/TCTA/**Host**:5%dopant/ TmPyPB/LiF/Al	3.9	14260	49.1	30.9	24.5	(0.15, 0.35)	58
C83	FIrpic	ITO/PEDOT:PSS/TAPC/TCTA/**Host**:5%dopant/ TmPyPB/LiF/Al	3.1	9727	50.2	45.1	25.3	(0.14, 0.31)	58
C81	$Ir(ppy)_3$	ITO/PEDOT:PSS/TAPC/TCTA/**Host**:8%dopant/ TmPyPB/LiF/Al	3.2	35360	71.3	56.5	20.9	(0.27, 0.63)	58
C82	$Ir(ppy)_3$	ITO/PEDOT:PSS/TAPC/TCTA/**Host**:8%dopant/ TmPyPB/LiF/Al	3.0	53840	80.3	72.0	23.3	(0.27, 0.63)	58
C83	$Ir(ppy)_3$	ITO/PEDOT:PSS/TAPC/TCTA/**Host**:8%dopant/ TmPyPB/LiF/Al	2.8	45010	91.8	96.1	27.3	(0.26, 0.63)	58
C84	FIrpic	ITO/HATCN/TAPC/TCTA/**Host**:15%dopant/ TmPyPB/Liq/Al	3.8	-	40.9	34.0	17.8	(0.17, 0.38)	59
C85	FIrpic	ITO/HATCN/TAPC/TCTA/**Host**:15%dopant/ TmPyPB/Liq/Al	3.4	-	34.5	33.2	14.4	(0.18, 0.41)	59
C86	$Ir(ppy)_3$	ITO/MoO3/TAPC/TCTA/**Host**:6%dopant/ TmPyPB/ LiF/Al	3.1	-	92.3	78.8	26.1	(0.30, 0.62)	60
C87	$Ir(ppy)_3$	ITO/MoO3/TAPC/TCTA/**Host**:6%dopant/ TmPyPB/ LiF/Al	3.4	-	86.4	61.8	24.0	(0.31, 0.62)	60
C88	$Ir(ppy)_3$	ITO/MoO3/TAPC/TCTA/**Host**:6%dopant/ TmPyPB/ LiF/Al	3.1	-	80.2	56.7	22.9	(0.30, 0.62)	60

[a] Turn-on voltage. [b] Maximum luminance. [c] Maximum current efficiency. [d] Maximum power efficiency. [e] Maximum external quantum efficiency.

1.4 Carbazole-based materials for TADF applications

Recently, Adachi and coworkers reported third generation OLED employing pure organic molecules that harvest 100% of excitons utilizing reverse intersystem crossing (RISC) [61]. The TADF process is potentially superior to the PhOLED technology which employs costly heavy metals such as iridium and platinum. For a molecule to be TADF active, it should possess well separated HOMO and LUMO levels and low singlet-triplet energy gap (ΔE_{ST}) which facilitates the RISC by means of thermal activation. Since carbazole-based materials exhibit small singlet-triplet energy gap for the rationally designed molecules, they are utilized in TADF as emitters as well as host materials.

1.4.1 Carbazole as donor in TADF emitters

Organic emitters exhibiting TADF character are generally constructed with D-A molecular structure. The well separated HOMO and LUMO is possible only when strong donor and acceptor moieties are tethered in the molecule in non-communicating positions to realize small energy difference between singlet and triplet energy for facile RISC. In this regard, carbazole is a good electron donor moiety which finds applications as they are tethered with electron withdrawing moieties to construct TADF emitters.

Adachi and coworkers designed a series of carbazolyl cyanobenzenes as TADF emitters (**C89**,**C90;** Chart 1.12) in which carbazole act as donor and cyanobenzene as acceptor [61]. Since the carbazole is distorted from cyanobenzene plane due to steric hindrance, the HOMO and LUMO orbitals are well separated at carbazole and cyanobenzene respectively. Also they tuned the emission color from sky blue to green color by modulating the number of electron donating carbazole unit in cyanobenzene core. From DFT calculation, it was demonstrated that the high dihedral angle between carbazole donor and cyanobenzene acceptor results in small ΔE_{ST} value for facile RISC process. The green OLED employing **C90** and and sky blue OLED of **C89** exhibited high EQE of 19.3% and 11.2% respectively, which are higher than conventional fluorescent OLEDs.

The introduction of strong electron withdrawing group would give well separated HOMO and LUMO energy level. Zhang and coworkers reported a TADF emitter (**C91;** Chart 1.12) containing carbazole-pyridine-carbonitrile with the distribution of carbazole and cyano group para- to each other at pyridine group [62]. The well separation of HOMO and LUMO generally

result in low ΔE_{ST}, but it would be detrimental for effective charge transfer. So, the TADF emitters possessing low ΔE_{ST} as well as high CT emission due to appropriate overlap of HOMO and LUMO orbitals are in high demand. By careful design of carbazole tethered pyridine-dicarbonitrile, low ΔE_{ST} of 0.04 eV and suitable overlap of HOMO and LUMO is realized. The large steric hindrance from carbazole and electron withdrawing cyano group on pyridine moiety suppressed the non-radiative decay to greater extent. The OLED device fabricated with **C91** as dopant (13 wt%) in mCP host exhibited high EQE of 21.2%, current efficiency and power efficiency of 47.7 cd/A and 42.8 lm/W respectively.

Lee and coworkers demonstrated carbazole-based TADF emitters **(C92-C94;** Chart 1.12) to generate high efficiency OLED and tuned the color of emission by increasing the number of carbazole donor unit on dicyanobenzene acceptor [63]. As the number of appended carbazole is increased, the donor strength of the materials is also increased. The molecule **C94** attained more twisted structure and low ΔE_{ST} among other compounds which is favorable for effective RISC. The OLED device fabricated with these compounds as emitters doped in PPT host exhibited blue and green emission for **C92**, **C93** and **C94** respectively. As the number of carbazole unit is appended, the emission color is bathochromically shifted from blue to green color for **C94** based devices. Also, the low ΔE_{ST} of **C94** ensured the conversion of triplet excitons into singlet excitons by RISC process. Thus, the best efficiency is observed for **C94** based device with high current efficiency, power efficiency, maximum brightness and EQE of 15.26 cd/A, 8.14 lm/W, 1526 cd/m^2 and 13.33% respectively.

Huang and coworkers designed non-conjugated trifluoromethyl substituted benzene containing electron donating carbazole (**C95**, **C96;** Chart 1.12) as TADF emitters to tune the electroluminescent properties [64]. From tetra- to penta-carbazole, the compound **C96** exhibited more desirable TADF characteristics such as low ΔE_{ST} for efficient RISC, high PLQY, and high lying HOMO for efficient charge injection. The devices fabricated with penta-carbazole **C96** showed high EL performances over tetra-carbazole **C95** which is attributed to effective RISC due to low ΔE_{ST}. The high lying HOMO of **C96** apparently reduces the energy barrier for hole injection and hence low turn-on voltage is observed. The best EL performance of **C96** with current efficiency of 11.8 cd/A and EQE of 5.2% which are about 10 times higher than the EL performance of **C95** in the same device architecture. The large difference in EL performance is attributed to ΔE_{ST} value of 0.24 and 0.02 eV for **C95** and **C96** respectively.

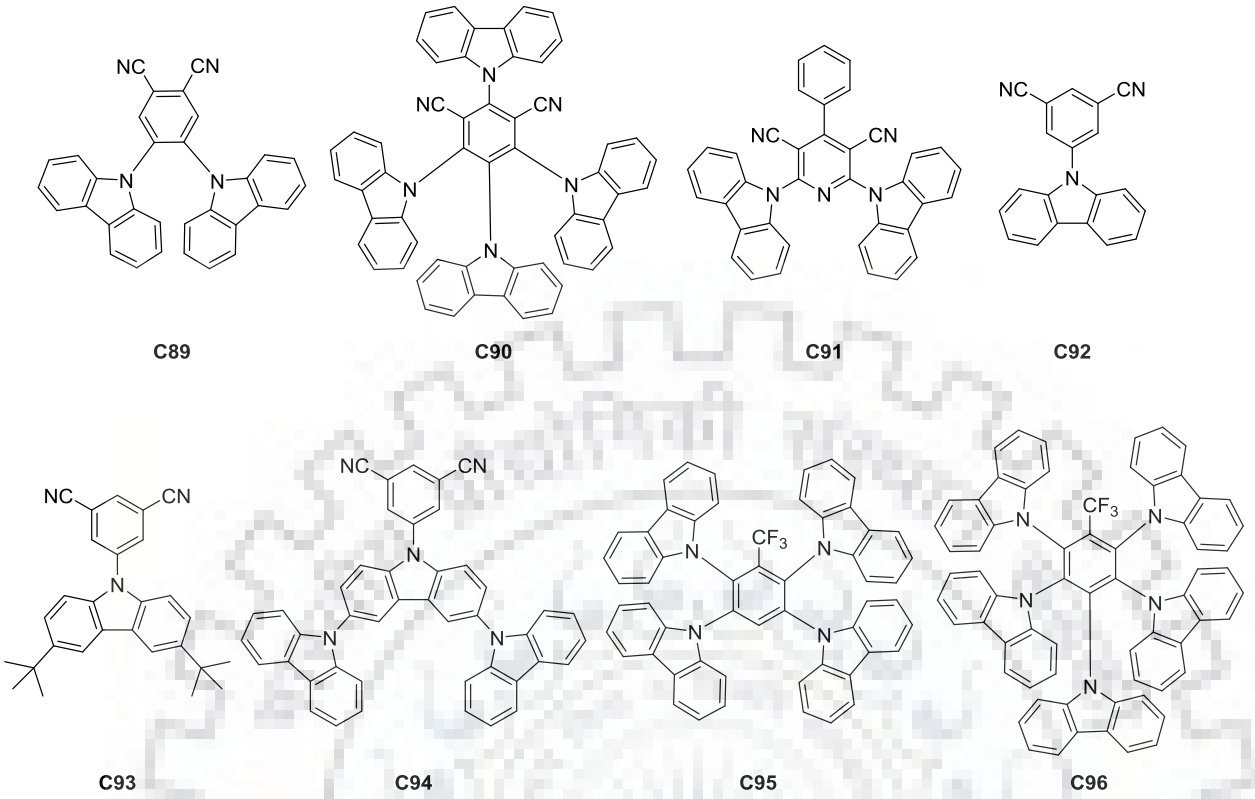

Chart 1.12 Carbazole as donors in TADF emitters.

Lee and coworkers designed TADF emitter **C97** (Chart 1.13) in which carbazole act as donor and diphenyl triazine as acceptor [65]. The device fabricated with the emitter displayed blue emission with high EL performances and long durability over PhOLED devices. The high stability of the device is attributed to molecular design containing stable carbazole donor and rigid triazine acceptor unit. The appropriate overlap of HOMO and LUMO orbitals at phenyl linker established the effective charge transfer excitons and thereby efficient light emission. The TADF based blue OLED fabricated with the emitter **C97** exhibited high EQE of 17.8%, power efficiency of 22.4 lm/W and current efficiency of 26.8 cd/A. The device also showed low efficiency roll-off at high brightness.

In another report, the same group reported two TADF emitters (**C98**, **C99;** Chart 1.13) containing three carbazoles as donor and diphenyl triazine as acceptor [66]. The phenyl linker is contributing to the construction of both HOMO and LUMO. The appropriate overlap of HOMO and LUMO levels enhance the radiative pathway and thus high PLQY observed. As the number of electron donating carbazole increases, the PLQY also doubly increased and approaches unity

in nitrogen purged solution. It is due to facile up-conversion of triplet excitons into singlet state. The EL performance of the device fabricated with three carbazole donor based dopant (**C98** and **C99**) exhibited dramatically improved performances over two carbazole donor based emitter (**C97**). The best performance is achieved for **C99** with power efficiency and EQE of 52.1 lm/W and 25.5% respectively.

Generally, the low ΔE_{ST} is realized in TADF molecules by increasing the twist angle between donor and acceptor. But, large twist angle suppress the radiative decay which is detrimental to the device performance. Alternatively, small ΔE_{ST} can be achieved by intramolecular space interaction between donor and acceptor. The spatial separation between donor and acceptor results in small ΔE_{ST} which is a pre-requisite for the molecule to exhibit TADF character. Cheng and coworkers designed D-A-D configured molecules (**C100**, **C101;** Chart 1.13) containing carbazole/t-butyl carbazole as donor and phenyl(pyridine-4-yl) methanone as acceptor [67]. The materials showed small ΔE_{ST} value of 0.03-0.04 eV due to spatial separation between donor and acceptor. The meta- positioned carbazole was beneficial to enhance EQE by widely dispersing the HOMO and to realize sufficient overlap between HOMO and LUMO. The blue OLED device fabricated with **C100** displayed sky blue emission with low turn on voltage of 2.8 V, high EQE of 24.0%, power efficiency of 57.2 lm/W and current efficiency of 54.7 cd/A. Likewise, green OLED using **C101** as dopant exhibited high EQE, power efficiency and current efficiency of 27.2%, 84.7 lm/W and 94.6 cd/A respectively.

In order to overcome the poor color purity of twisted TADF molecules, rigid and linear structured molecules are desirable for realizing high color purity especially deep blue emission. Cheng and coworkers designed a rigid and linear TADF emitters (**C102**, **C103;** Chart 1.13) containing t-butylcarbazole tethered di(pyridinyl) methanone [68]. They demonstrated that the structurally planar molecules are preferable for realizing pure blue emission unlike twisted structure which leads to red shifted emission. The HOMO and LUMO is concentrated over carbazole and di(pyridinyl)methanone respectively. Interestingly, for both the molecules pyridine constructs both HOMO and LUMO which is beneficial for enhancing radiative decay ascribed to substantial overlap of HOMO and LUMO. The planar and rigid structure is further confirmed by less Stokes shift of **C103** over flexible **C102**. The device doped with **C103** exhibited high EQE of 31.9% with pure blue emission which is the best EQE reported so far for

pure blue emitting materials whereas **C102** exhibited high EQE of 12.8% with green emission. The high EQE of the blue device is attributed to small ΔE_{ST} value which favors efficient RISC.

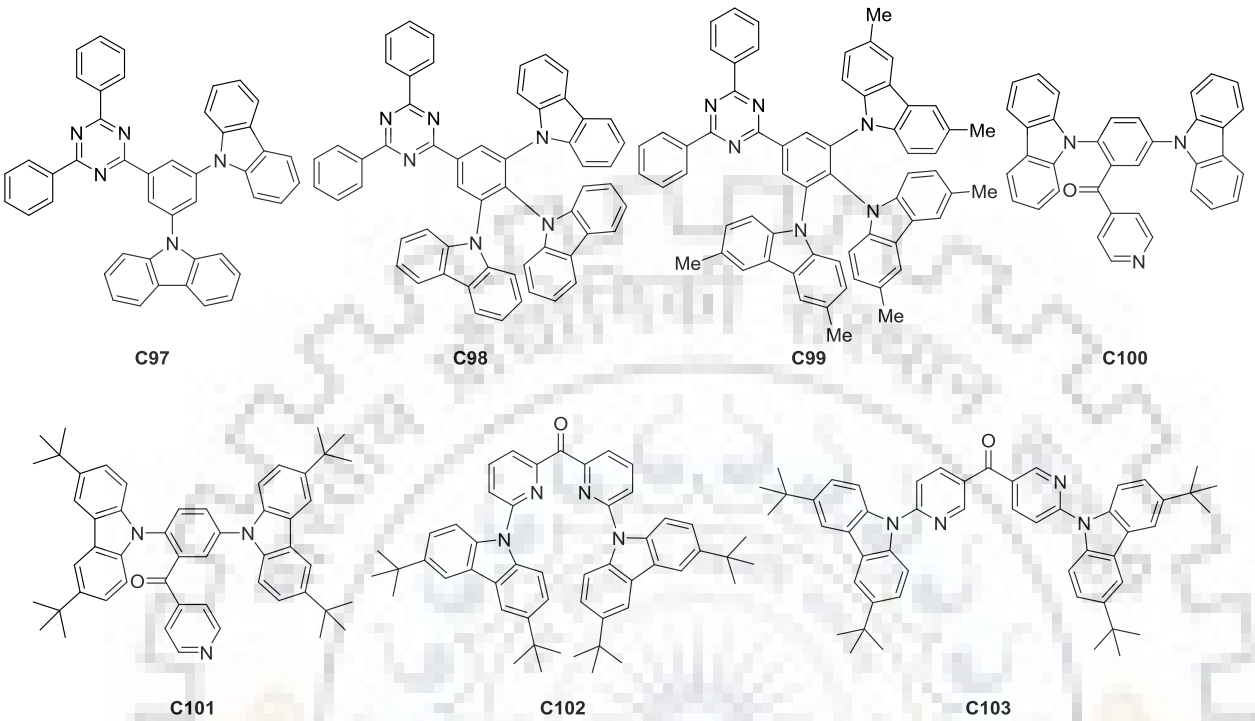

Chart 1.13 Carbazole as donors in TADF emitters.

Table 1.11 Photophysical and thermal properties of TADF emitters containing carbazole donors

Dye	λ_{max} (nm)[a]	λ_{em} (nm)[a] (Φ_F)[c]	HOMO/ LUMO (eV)[d]	Life time, τ		E_S, eV (exp/calc)	E_T, eV (exp/calc)	ΔE_{ST}, eV (exp/calc)	T_g (°C)[g]	T_d (°C)[h]	Ref
				τ_p (ns)[e]	τ_d (μs)[f]						
C89	-	473 (0.47)	-	28.5	166	-	-	0.08/-	-	-	61
C90	-	507 (0.94)	-	17.8	5.1	-	-		-	-	61
C91	374[b]	474[b]	-	9.7	46.6	2.77/-	2.73/-	0.04/-	-	350	62
C92	290[b]	437[b]	-5.87/-2.28	27	-	3.59/3.31	-/2.76	-/0.55	-	-	63
C93	295[b]	460[b]	-5.72/-2.22	45	-	3.50/3.22	-/2.61	-/0.61	86	-	63
C94	327[b]	482[b]	-5.57/-2.31	76	3.26	3.26/2.57	-/2.44	-/0.13	110	285	63
C95	332	440	-5.60/-2.62	-	9.31	3.02/-	2.78/-	0.24/-	-	417	64
C96	330	481	-5.57/-2.75	-	15.33	2.82/-	2.80/-	0.02/-	-	455	64
C97	-	- (0.66)[b]	-	-	3.1	2.89/-	2.64/-	0.25/-	160	397	65
C98	-	- (100)[b]	-	16.4	13.5	2.96/2.73	2.80/2.56	0.16/0.17	-	-	66
C99	-	- (0.99)[b]	-	15.1	13.3	2.86/2.61	2.79/2.45	0.07/0.16	-	-	66
C100	400[b]	490	-5.75/-2.88	15.0	0.6	2.87/-	2.84/-	0.03/-	109	382	67
C101	418[b]	508	-5.61/-2.87	18.0	1.0	2.74/-	2.70/-	0.04/-	140	412	67
C102	373[b]	520(0.02)	-5.63/-2.89	22.3	0.34	2.74/-	2.63/-	0.11/-	-	420	68
C103	384[b]	464(0.27)	-5.76/-2.76	26.4	0.27	3.00/-	2.98/-	0.02/-	-	484	68

[a] Measured in dichloromethane. [b] Measured in toluene. [c] Absolute quantum yield. [d] Calculated from cyclic voltammetry or DFT. [e] Prompt lifte time. [f] Delayed life time. [g] Glass transition temperature. [h] Decomposition temperature at 5% weight loss.

Table 1.12 Electroluminescence properties of TADF emitters containing carbazole donors

Dye	Device structure	Von (V)[a]	L_{max} (cd/m^2)[b]	η_c (cd/A)[c]	η_p (lm/W)[d]	EQE (%)[e]	$CIE_{(x,y)}$	Ref
C89	ITO/α-NPD/mCP/PPT:5% **dye**/PPT/LiF/Al	-	-	-	-	8.0	-	61
C90	ITO/α-NPD/CBP:5% **dye**/TPBi/LiF/Al	-	-	-	-	19.3	-	61
C91	ITO/TAPC/TCTA/mCP: 13% **dye**/TmPyPB/LiF/Al	3.2	-	47.7	42.8	21.2	(0.20, 0.35)	62
C92	ITO/HATCN/NPB/TAPC/PPT:10% **dye**/PPT/TPBi / LiF/Al	7.36	66.3	0.66	0.28	<1	(0.15, 0.12)	63
C93	ITO/HATCN/NPB/TAPC/PPT:10% **dye**/PPT/TPBi / LiF/Al	7.84	470.2	4.70	1.89	5.05	(0.16, 0.24)	63
C94	ITO/HATCN/NPB/TAPC/PPT:10% **dye**/PPT/TPBi / LiF/Al	5.89	1526	15.26	8.14	13.3	(0.20, 0.37)	63
C95	ITO/PEDOT:PSS/mCP:10% **dye**/TmPyPB/LiF/Al	4.8	1032	1.03	-	0.67	(0.17, 0.18)	64
C96	ITO/PEDOT:PSS/mCP:10% **dye**/TmPyPB/LiF/Al	3.9	2436	11.8	-	5.2	(0.21, 0.33)	64
C97	ITO/NPB/mCP/DPEPO:25% **dye**/TSPO1/ LiF/Al	5.9	-	26.8	22.4	17.8	(0.15, 0.16)	65
C98	ITO/NPB/mCP/DPEPO:40% **dye**/TSPO1/ LiF/Al	-	-	-	42.7	25.0	(0.18, 0.32)	66
C99	ITO/NPB/mCP/DPEPO:30% **dye**/TSPO1/ LiF/Al	-	-	-	52.1	25.5	(0.25, 0.50)	66
C100	ITO/NPB/mCP/CzPS:5%**dye**/DPEPO/TmPyPB/LiF/Al	2.8	10300	54.7	57.2	24.0	(0.17, 0.36)	67
C101	ITO/NPB/mCP/CBP:5% **dye**/PPT/TmPyPB/LiF/Al	3.1	37700	94.6	84.5	27.2	(0.30, 0.64)	67
C102	ITO/NPB/TAPC/mCBP:7% **dye**/TmPyPB/LiF/Al	3.5	3178	31.8	29.5	12.8	-	68
C103	ITO/NPB/TAPC/mCBP/mCBP:7% **dye**/DPEPO/ TmPyPB/LiF/Al	3.7	9670	37.6	37.3	31.9	-	68

[a] Turn-on voltage. [b] Maximum luminance. [c] Maximum current efficiency. [d] Maximum power efficiency. [e] Maximum external quantum efficiency.

1.4.2 Carbazole-based materials as TADF host

In order to be used as host materials for TADF based OLED, the host material should have high singlet and triplet energy compared to the dopant emitters, low energy barrier for the injection of charge carriers from the neighboring charge transport layers for effective confinement. Carbazole-based materials possess high triplet energy level and good charge transporting ability and low energy difference between singlet and triplet energy level. So, they are exploited as TADF host material in OLED devices.

Lee and coworkers reported carbazole functionalized with phosphine oxide at 2,7- position (**C104;** Chart 1.14) as host material for green emitting TADF devices [69]. Earlier, the same material was used as host bipolar material for phosphorescent OLED and found to exhibit high EL performances [51]. Since the molecule possessed low energy gap between singlet and triplet energy, it was exploited as host material for TADF emitter. The EL performance of the devices was tuned by varying the dopant concentration 4CzIPN. The best performance was observed for the device having 2% dopant with high EQE of 21.1%. The lower performance of the device containing 1% and 5% dopant concentration might be due to poor excitons harvesting and concentration quenching respectively. Also, at low doping concentration, due to poor energy transfer from host to dopant, additional EL peak at 390 nm was observed. However, the stability of device was short due to poor stability of host material.

Adachi and coworkers designed *N*-phenyl carbazole appended on mCP as host material (**C105;** Chart 1.14) for TADF applications [70]. The optoelectronic properties were compared with the conventional CBP host material. The compound **C105** exhibited high glass transition temperature of 165 °C which is much higher than that of CBP (62 °C). It would provide high morphological stability. Before fabricating device, they recorded PLQY for the 6 wt% 4CzIPN doped in **C105** spin coated film and found it to be 86%. The PLQY of spin coated film was higher than that of similar composition of vacuum deposited film. The solution processed host material based device exhibited high life time of 200 h at the brightness of 1000 cd/m^2. The observed device performance of 14.5% EQE at 100 cd/m^2 is comparable to the performance of vacuum processed emissive layer.

Lee and coworkers designed donor-acceptor configured host materials (**C106-C108;** Chart 1.14) by varying the interconnecting positions to optimize the carrier transport and thereby

realize high device performances [71]. The utility of these host materials for TADF application was confirmed by measuring transient PL decay of 4CzIPN doped host materials. The delayed lifetime fell in microsecond range of 3.6, 3.5 and 3.8 for *ortho*-, *meta*- and *para*-substituted carbazole respectively. The thin film PLQY of 4CzIPN doped host materials is in the order of *para*- (0.86) > *meta*- (1.00) > *ortho*- (0.75). The low quantum yield of para- and ortho-substituted compound might be due to low triplet energy and poor energy transfer despite of high triplet energy respectively. The device fabricated with the host materials exhibited the current density and luminance in the order of *para*- > *meta*- > *ortho*- which is coincided with band gap of the material. The low current density of *ortho*-substituted compound **C106** might arise from twist structure which disturbs the effective overlap of orbitals and thus less conjugation. The high EQE device performance was observed for *meta*-substituted compound **C107** which agreed well with the PLQY recorded for doped thin film. The donor-acceptor structure of the host materials induced intermolecular interaction in the thin film and thus red shifted the emission maximum from 502, 508, 510 nm for *ortho*, *meta*, *para*-substituted compound respectively.

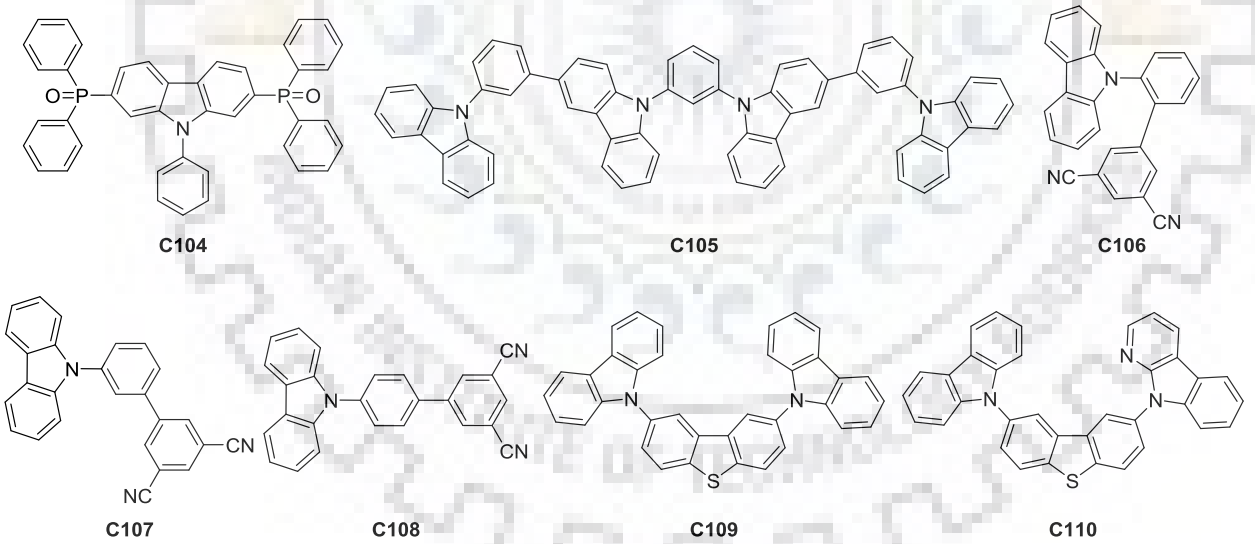

Chart 1.14 Carbazole-based materials as TADF host.

Choi and coworkers reported both symmetric and asymmetrically substituted dibenzothiophene (**C109-C110;** Chart 1.15) as host materials [72]. The materials showed high triplet energy (2.9 eV) which is higher than that of the emitter 2CzPN (2.5 eV). The transient PL decay of 2CzPN doped host materials exhibited larger rate constant for RISC process which

attributes to the superior performance of the devices at low current density. Remarkably, the maximum EQE of 25.7% was observed for asymmetric host **C110** at very low current density of 0.08 mA/cm^2. The observed high EQE is attributed to the balanced charge transport realized by the presence of electron withdrawing carboline unit. The maximum luminance is almost doubled from 3000 to 6000 cd/m^2 when the host changed from **C109** to **C110**. It is ascribed to characteristic electrical stability of the carboline unit which improved the luminance.

The favorable π-π stacking of the molecules is beneficial for improving charge carrier mobility. Duan and coworkers reported carbazole-triphenylene dyads (**C111-C113;** Chart 1.15) as host material for TADF applications [73]. They tuned the charge carrier mobility of the hosts by employing π-π stacking as effective strategy through varying the linking position. The electronic properties are modulated by changing the linking position. The *meta*-substituted host gave high electron mobility among the hosts. Generally, *para*-substituted molecules give high carrier mobility but here high mobility is observed for *meta*-compound. Single crystal structural arrangement of meta- compound **C112** showed favorable stacking for efficient carrier mobility. The lowest hole mobility of *para*-compound (**C113**) could be attributed to the dispersion of HOMO and its overlapping with LUMO. The devices fabricated with 4CzIPN doped ortho and meta- substituted hosts (**C111** and **C112**) exhibited high electroluminescence performances as compared to that of CBP host. The low performance of *para*-substituted compound (**C113**) is attributed to the formation of exciplex which is confirmed by the broad and red shifted emission peak for the film emission of 4CzIPN doped host. The best device performance is observed for *ortho*-substituted compound with high EQE of 16.3% and the very small efficiency roll-off at high brightness of 1000 cd/m^2.

The high EQE can be realized by not only of low ΔE_{ST} but also of high charge carrier mobility. Duan and coworkers designed bipolar host materials (**C114-C117;** Chart 1.15) exhibiting high carrier mobility by varying the linking position of carbazole on benzonitrile [74]. The EQE of the device fabricated with these host materials showed better efficiency compared to their conventional unipolar hosts such as CBP, mCP, DPEPO. The bipolar nature of all hosts is confirmed by time of flight measurements indicating electron mobility is higher than that of hole mobility. The high EQE of 21.5% is observed for the device containing **C114** host with the low turn-on voltage of 2.8 V. The high performance is attributed to the high PLQY of the emissive layer of 4TCzBN doped host and high charge carrier mobility of the host

material. The low turn-on voltage is attributed to proper energy level of frontier orbital of host which favors facile charge injection from the neighboring charge transport layers. The superior performance of these compounds over mCP host is due to bipolar nature of host materials and its resultant balanced charge transport. By varying the linking type of carbazole, they tuned the electroluminescent properties, especially **C116** based device exhibited low turn on voltage of 4.9 V even at high brightness of 1000 cd/m^2.

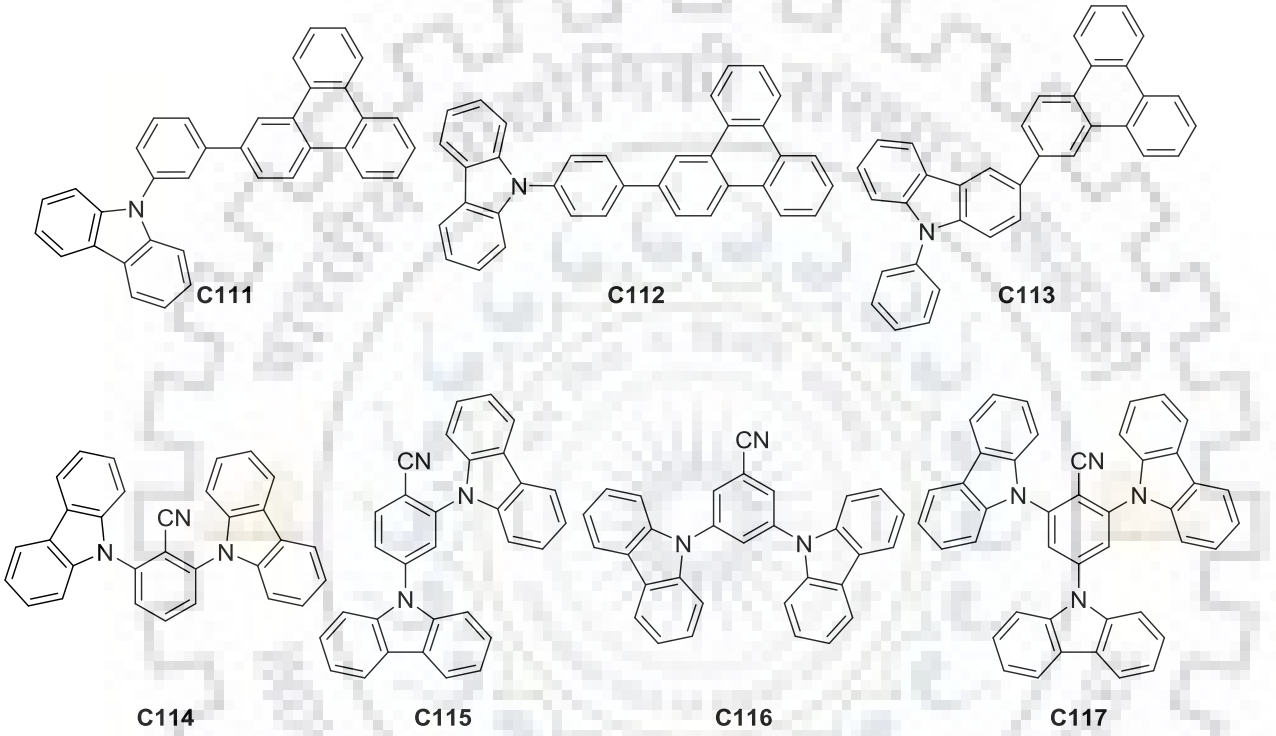

Chart 1.15 Carbazole-based materials as TADF host.

Table 1.13 Photophysical and thermal properties of the carbazole-based TADF host materials

Dye	λ_{max} (nm)[a]	λ_{em} (nm)	HOMO/ LUMO (eV)[d]	E_S (eV)	E_T (eV)[e]	ΔE_{ST} (eV)	Tg (°C)[f]	Td (°C)[g]	Ref
C104	-	392[c]		3.86	2.81	-	-	-	69
C105	-	390[b]	-6.20/-2.70	3.50	2.79	0.09	165	394	70
C106	-	-	-6.15/-3.13	3.02	2.99	0.03	-	-	71
C107	-	-	-6.07/-3.18	2.89	2.73	0.16	-	-	71
C108	-	-	-6.09/-3.21	2.88	2.58	0.30	-	-	71
C109	341	378	-5.71/-2.19	3.52	2.94	0.58	-	-	72
C110	341	378	-5.72/-2.27	3.45	2.92	0.53	-	-	72
C111	341[b]	367, 378[b]	-5.67/-2.10	3.57	2.66	0.91	102	399	73
C112	293[b]	371, 386[b]	-5.63/-2.13	3.50	2.60	0.91	111	374	73
C113	290[b]	376, 394[b]	-5.54/-2.10	3.44	2.61	0.83	107	369	73
C114	-	405[b]	-5.74/-2.45	3.34	2.95	0.39	101	-	74
C115	-	404	-5.73/-2.47	3.27	3.03	0.24	104	-	74
C116	-	396	-5.78/-2.54	3.39	3.03	0.36	96	-	74
C117	-	415	-5.75/-2.61	3.20	2.87	0.33	153	-	74

[a] Measured in chloroform. [b] Measured in toluene. [c] Measured in dichloromethane. [d] Calculated from cyclic voltammetry. [e] Calculated from phosphorescence spectra. [f] Glass transition temperature. [g] Decomposition temperature at 5% weight loss.

Table 1.14 Electroluminescence properties of carbazole-based TADF host materials

Dye	Dopant	Device structure	V_{on} (V)[a]	L_{max} (cd/m^2)[b]	η_c (cd/A)[c]	η_p (lm/W)[d]	EQE (%)[e]	$CIE_{(x,y)}$	Ref
C104	4CzIPN	ITO/PEDOT:PSS/TAPC/mCP/**Host**: 2%dopant/ TSPO1/ LiF/Al	-	-	-	42.1	21.1	(0.19, 0.46)	69
C105	4CzIPN	ITO/PEDOT:PSS/**Host**: 6% dopant/T2T/ Bpy-TP2/LiF/Al	6.0	-	-	-	14.5	-	70
C106	4CzIPN	ITO/PEDOT:PSS/TAPC/mCP/**Host**: 5%dopant/ TSPO1/LiF/Al	-	-	-	46.6	20.9	(0.24, 0.51)	71
C107	4CzIPN	ITO/PEDOT:PSS/TAPC/mCP/**Host**: 5%dopant/ TSPO1/LiF/Al	-	-	-	71.1	26.0	(0.24, 0.54)	71
C108	4CzIPN	ITO/PEDOT:PSS/TAPC/mCP/**Host**: 5%dopant/ TSPO1/LiF/Al	-	-	-	64.4	22.9	(0.26, 0.55)	71
C109	2CzPN	ITO/HATCN/TAPC/**Host**: 6%dopant/TmPyPB/LiF/Al	5.0	3231	31.8	-	18.5	(0.17, 0.34)	72
C110	2CzPN	ITO/HATCN/TAPC/**Host**: 6%dopant/TmPyPB/LiF/Al	4.7	6366	53.1	-	25.7	(0.19, 0.39)	72
C111	4CzIPN	ITO/HATCN/NPB/TCTA/**Host**:10%dopant/ Bphen/ LiF/Al	3.5	-	51.8	36.4	16.3	-	73
C112	4CzIPN	ITO/HATCN/NPB/TCTA/**Host**:10%dopant/ Bphen/ LiF/Al	3.1	-	50.7	41.4	15.9	-	73
C113	4CzIPN	ITO/HATCN/NPB/TCTA/**Host**:10%dopant/ Bphen/ LiF/Al	2.9	-	15.4	13.3	5.5	-	73
C114	4TCzBN	ITO/HATCN/NPB/TCTA/mCP/**Host**: 30%dopant/ DPEPO/Bphen/LiF/Al	2.8		-	42.0	21.5	(0.16, 0.26)	74
C115	4TCzBN	ITO/HATCN/NPB/TCTA/mCP/**Host**: 30%dopant/ DPEPO/Bphen/LiF/Al	3.3	-	-	23.3	13.0	(0.17, 0.29)	74
C116	4TCzBN	ITO/HATCN/NPB/TCTA/mCP/**Host**: 30%dopant/ DPEPO/Bphen/LiF/Al	2.8	-	-	34.5	20.1	(0.16, 0.23)	74
C117	4TCzBN	ITO/HATCN/NPB/TCTA/mCP/**Host**: 30%dopant/ DPEPO/Bphen/LiF/Al	2.8	-	-	29.5	14.8	(0.17, 0.28)	74

[a] Turn-on voltage. [b] Maximum luminance. [c] Current efficiency. [d] Power efficiency. [e] External quantum efficiency.

1.5 Conclusions and Future Prospects

The synthesis and functionalization of carbazole and the application of functional derivatives of carbazole in OLED as hole transporting material, fluorescent emitters, phosphorescent host and TADF emitter have been briefly reviewed. Generally, C3,C6-functionalized carbazoles showed good redox properties while induces donor-acceptor interaction. The C2,C7-functionalization of carbazole leads to the elongation of π conjugation. The insertion of chromophore at C1,C8 position of carbazole results in good amorphous nature and increases triplet energy. The functional modification at *N*-position did not alter the conjugation while improves solubility of the materials. Generally, the functionalization of carbazole at C3,C6 position have been reported. The functionalization at C2,C7-position of carbazole are exploited scarcely for the development of fluorescent emitters. However, the asymmetric functionalization of carbazole at C2 and C7 position has not been explored much owing to the involvement of tedious and difficult synthetic procedure and low yields. Similarly, multi-functionalized carbazole derivatives are seldom reported due to the lack of efficient synthetic protocol and purification methods. Also, multi-functionalization of carbazole with the same chromophore has been reported. But, the selective introduction of two different chromophores on multi-substituted carbazole is ill explored.

CHAPTER 2

Cyanocarbazole-Based Organic Materials for Electronic Applications: Aim and Scope

Organic π conjugate materials contributed significantly for the development of organic electronics. The structure-property relationships of organic molecules help to rationally develop organic materials for optoelectronic applications such as organic light emitting diodes (OLED), organic field effect transistors (OFET), organic photovoltaics (OPV) and chemical sensors [75-80]. Among them, OLED received much attention because they are considered as a potential power saving technology to the existing incandescent and liquid crystal display light sources. The advantage of OLED includes the cheap production cost, light weight, flexibility and less power consumption [81]. For full color solid state displays, highly efficient primary color (Red, Green and Blue) emitters are necessary. To date, numerous green and red emitting materials exhibiting high efficiency are developed [82, 83]. But, the realization of highly efficient blue emitting materials exhibiting long durability with high color purity is difficult owing to associated wide band gap and the resultant poor charge injection/transportation into the emitters. For better device performance and long lifetime of the device, organic emitters should have balanced transportation of charge carriers and good thermal and morphological stability respectively [84-86].

It is the need of the hour to develop highly efficient blue emitting materials for the realization of full color displays and to cut down power consumption. OLED can be defined as the thin film device which converts electricity into light. Ideally, OLED contains organic emitter sandwiched between anode and cathode [87]. In principle, when the external voltage is applied excitons are generated in the emitter as holes and electrons meet. The decay of excitons results in light emission. Fluorescent emitters can harvest only 25% of excitons and the remaining 75% triplet excitons go unused. But, the second generation phosphorescent OLED could harvest both singlet and triplet excitons through intersystem crossing by using heavy metal complexes [88]. However, they are inferior to fluorescent OLED due to high cost of heavy metals and its associated environmental unsustainability and poor color purity of blue emitters. Further, third generation thermally activated delayed fluorescence (TADF) OLED was developed. Though the organic materials harvest 100% excitons through reverse intersystem crossing by thermal activation, TADF emitters exhibiting high color purity for blue and deep blue color are yet to be developed [89]. So, it is necessary to develop deep blue emitting fluorescent emitters to fulfill the primary colors and to cut down the power consumption of light emitting sources.

In general, electroluminescence color and the performance of OLED devices are governed by the organic emitters employed in the device. So, the choice of suitable organic building block is necessary to construct efficient emitter. Carbazole is a promising organic building block for the construction of deep blue emitting fluorescent emitters because it possesses good charge transporting ability, and wide band gap [90-92]. Owing to high triplet energy and good charge transporting capability, carbazole-based materials are used as host material for phosphorescent OLED [93-94]. Further, small difference between singlet and triplet energy of suitably designed carbazole derivatives are beneficial to develop TADF and HLCT emitters [95-97]. Carbazole derivatives are extensively studied as fluorescent emitters. It is well known that hole mobility is faster than that of electron mobility. When carbazole is functionalized with electron donating chromophores, they show good hole transporting character but generally leads to inferior performance due to unbalanced charge transport. In order to improve electron mobility and to realize balanced charge transport, electron withdrawing groups can be inserted on carbazole. On the other hand, the incorporation of electron withdrawing moiety induces donor-acceptor interaction and thus red shift the emission by shrinking the band gap [98-100]. As a result, the color purity of electroluminescence would be compromised. Recently, donor-acceptor configured molecules linked through meta- linker showed deep blue emission with better performance. It is reasoned that meta- linkage suppressed donor-acceptor interaction and thus retained wide band gap while accelerating electron mobility by the presence of electron withdrawing group [101-102]. From the literature reports, it is clear that the materials possessing bipolar nature with rational design would be beneficial to realize efficient deep blue emitters.

In this thesis, we have chosen cyano group as electron withdrawing moiety to accelerate the electron mobility and thereby realize balanced charge transport. Since cyano group is rigid and small in size, it is beneficial to suppress the non-radiative decay arising from vibrational and structural relaxation. The bipolar nature of cyano decorated carbazole is reported in literature [103-105]. The insertion of electron withdrawing group at C3 and C6 position of carbazole induces donor-acceptor interaction arising from lone pair electron of nitrogen atom. As a result, the emission is bathochromically shifted and consequently dipolar quenching of fluorescence dramatically. On the other hand, 2,7- functionalization of carbazole with electron withdrawing group would not induce detrimental donor-acceptor interaction while boosting the electron

mobility. Keeping the above mentioned things in mind, we adopted the insertion of cyano group at meta- position of carbazole (C2 and C7) to alleviate donor-acceptor character and to boost electron transport for achieving balanced charge transport. In order to make the emitting molecules solution processable, we have incorporated alkyl group at *N*9- position of carbazole to enhance the solubility. We propose an efficient synthetic method for selective functionalization of carbazole particularly at C2/C7 position. The selective halogenation of carbazole at 1,3,6,8 and 2,3,6,7 position would open the door to new class of organic functional materials for optoelectronic applications by employing C-C coupling and C-N coupling reaction protocols.

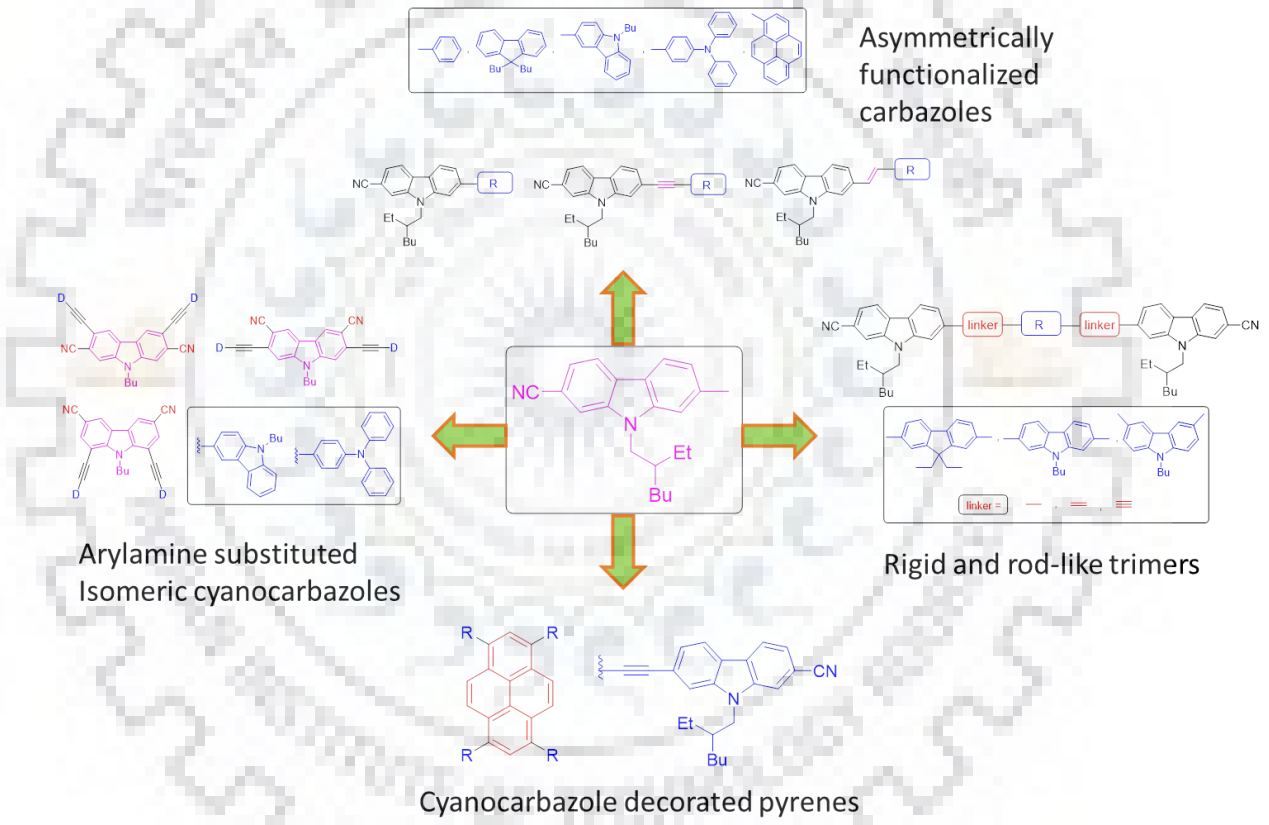

Chart 2.1 Outline of the compounds synthesized in the thesis.

Prompted by the above discussions, we have chosen 2-cyanocarbazole functionalized derivatives as emitters for fluorescent OLED devices. They were employed as non-doped fluorescent emitters and emitting dopant in host-guest devices. The optical and electroluminescence properties of the emitters are tuned by appending wide range of chromophores such as phenyl, fluorene, carbazole, triphenylamine and pyrene. Further, the

effects of conjugate π spacer on photophysical, electrochemical, thermal and electroluminescence properties are discussed. Chart 2.1 displays the outline of the work discussed in the thesis.

This thesis describes four different classes of compounds such as (a) asymmetrically functionalized carbazoles containing cyano group at one end and different chromophoric substituent at other end, (b) rigid and rod-like cyanocarbazole end capped trimers (c) cyanocarbazole appended pyrenes through acetylene spacer (d) carbazole containing donor and acceptor moieties. The structure-property relationships of the compounds are elucidated by studying optical, thermal, electrochemical and electroluminescence properties as the variation of spacer, linkage and cyano end capping.

The objective of the thesis can be outlined as follows

- To study the effect of cyano group on photophysical, electrochemical and electroluminescence properties
- To explore the effect of π spacer such as acetylene and vinyl for tuning the functional properties of organic materials
- To comprehend the effect of number of cyanocarbazole on photophysical and electroluminescence properties
- To study the effect of cyano group on positional isomers of carbazole derivatives and utilize them in organic light emitting diodes

CHAPTER 3

Asymmetrically 2,7-Disubstituted Carbazoles: Effect of Substituent and Linker on Photophysical and Electroluminescence Properties

3.1 Introduction

Recent advances in the development of organic semiconducting materials gave significant contribution to the modern organic electronics [106-110]. The development of new organic conjugate compounds became a booming field in the past decades since the organic materials found vast applications in optoelectronic devices. In addition, wide range of availability, facile synthesis and easy purification makes them more attractive for the real applications especially in lighting and display technologies. So, organic materials are considered to be a potential substitute for the existing lighting technology that employs inorganic semiconducting materials. Since organic materials are easy to synthesize, purification and are sustainable, they need special attention to fulfill the energy saving technology. Owing to their unique photophysical properties, thermal stability and charge transporting properties, organic conjugate materials found applications in optoelectronic devices such as organic photovoltaics, organic light emitting diodes, organic thin film transistors and chemical sensors. Among them, OLED technology got immense attention over existing liquid crystal display because OLED devices could provide energy saving technology. The OLED performance of the devices is predominantly dependent on the emitting materials used. So, the emitting materials possessing suitable material properties are highly desirable. Generally, polyaromatic hydrocarbons (PAH) are exploited for optoelectronic applications owing to their semi-conducting properties, wide variety of functionalization and excellent conjugation [111-114]. Among them, carbazole-based materials got immense attention for the OLED applications for their chemical and thermal stability, facile functionalization at various positions, excellent charge transporting capability and high fluorescence quantum yields [115-118]. Carbazole-based materials are exploited for OLED applications as hole transporters, fluorescent emitters, donors in TADF emitters. Since carbazole-based materials possess high triplet energy, they have been widely used as host materials for PhOLED and TADF too. Since carbazole possess multiple reactive sites for the functionalization, the functional tuning of carbazole by tethering various chromophores on it would be fruitful for the applications. Since the photophysical properties of the materials are dependent on the structure of the organic molecule, it is interesting to study the structure-property relationship of the organic molecules.

For the practical applications of OLED technology in light emitting sources such as displays and illuminating light sources, the OLED devices that emit primary colors with long

durability are necessary. So far, red and green emitting materials exhibiting superior performance and long lifetime have been established. But blue emitting materials possessing desirable device performances are yet to be developed. The bottleneck for realizing efficient blue emitting materials accompanies the inherent wide band gap and unfavorable energy level alignment with the neighboring molecular layers of OLED device. Alternatively, phosphorescent and TADF OLED devices exhibit high efficiency over fluorescent molecules but they suffer poor color purity and short lifetime which makes them potentially unrealistic for large applications. So the fluorescent materials exhibiting deep blue emission are highly in demand to fulfill the requirement of achieving primary colors. The mechanism involves in OLED device is the recombination of hole and electron charge carriers in emissive layer to form excitons which in turn produce light energy as it comes to the ground state. It is well known that the mobility of hole is faster than that of electron. Thus, recombination takes place at interface rather than in emissive layer and results in poor color purity. The prominent factor that controls the device performance is balanced charge transport. Bipolar materials that contain donor and acceptor moiety in a molecule are generally helpful to realize balanced charge transport. Since carbazole is electron donor, tethering electron deficient moieties would result in balanced charge transport. For example, Ma and coworkers reported carbazole/benzothiadiazole hybrid **CB1** (Chart 3.1) as red emitting material [100]. Zhao and coworkers reported carbazole connected benzothiadiazole via different linking position **CB2** and **CB3** (Chart 3.1) [119]. Subsequently, carbazole connected to different acceptor group such as tricyanovinyl, quinoxaline and maleimide (**CB4**-**CB7**) have been reported (Chart 3.1) by different research groups [120, 121, 98]. The devices employing these materials as emitters exhibited better performance ascribed to balanced charge transport. However, the D-A configuration induced intramolecular charge transfer and red shift in emission. An alternative methodology that satisfies both balanced charge transport and blue emission has to be developed. So far, much efforts have been put forth to bring out highly efficient blue emitting fluorescent materials. Since carbazole possess high band gap and good charge transporting capability, carbazole based materials are useful in developing blue emitters.

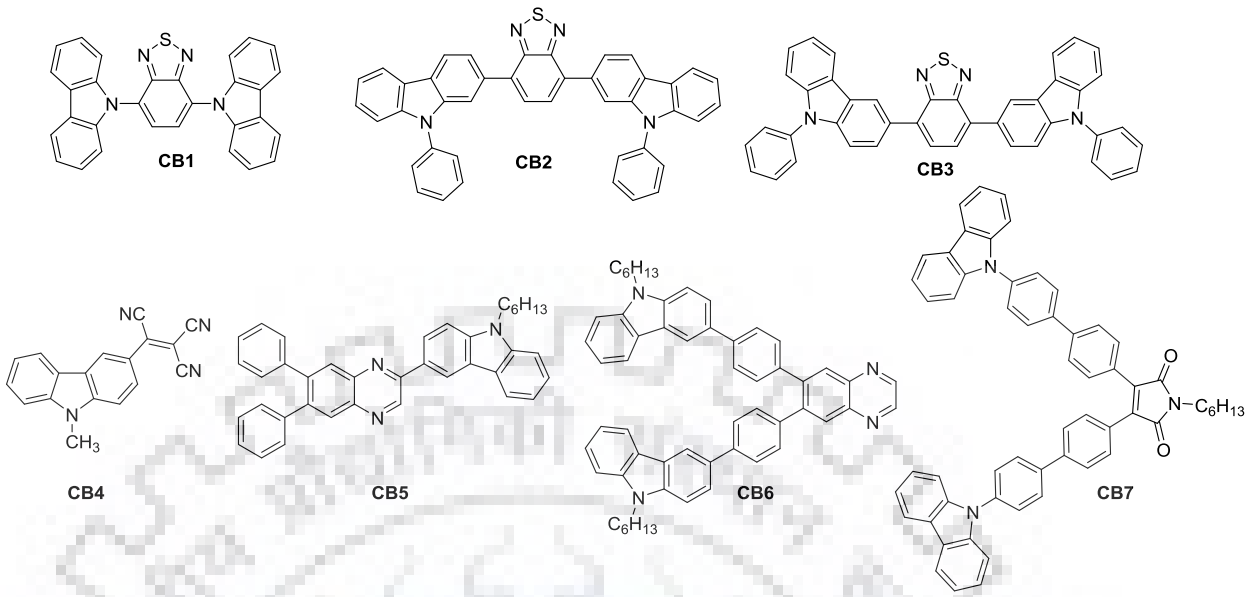

Chart 3.1 Green and red emitting D-A molecules containing carbazole as donor.

Since the strong electron withdrawing group induces ICT, the focus has been shifted to weaker donor and acceptor. Wei and coworkers reported carbazole functionalized triphenylamine [122]. They concluded that the hole transporting nature of **CB8** (Chart 3.2) could be utilized for hole transporter. However they have not utilized it in OLED device architecture either as emitter or charge transporting layer. Kazlauskas and coworkers reported carbazole functionalized with pyrene **CB9** and demonstrated as blue emitting material (Chapter 3.2) [123]. Jeng and coworkers reported carbazole tethered dimesityl boron (**CB10** and **CB11**) and utilized as a blue emitter [124]. When vinyl linker is inserted, the red-shifted absorption and emission spectra observed. This indicates the role of vinyl linker in raising the conjugation length. Bhalla and coworkers reported carbazole end capped biphenyl **CB12** and **CB13** (Chart 3.2) as blue emitter [125]. They also studied the role of acetylene linker on photophysical and electroluminescence properties by inserting acetylene linker between phenyl groups.

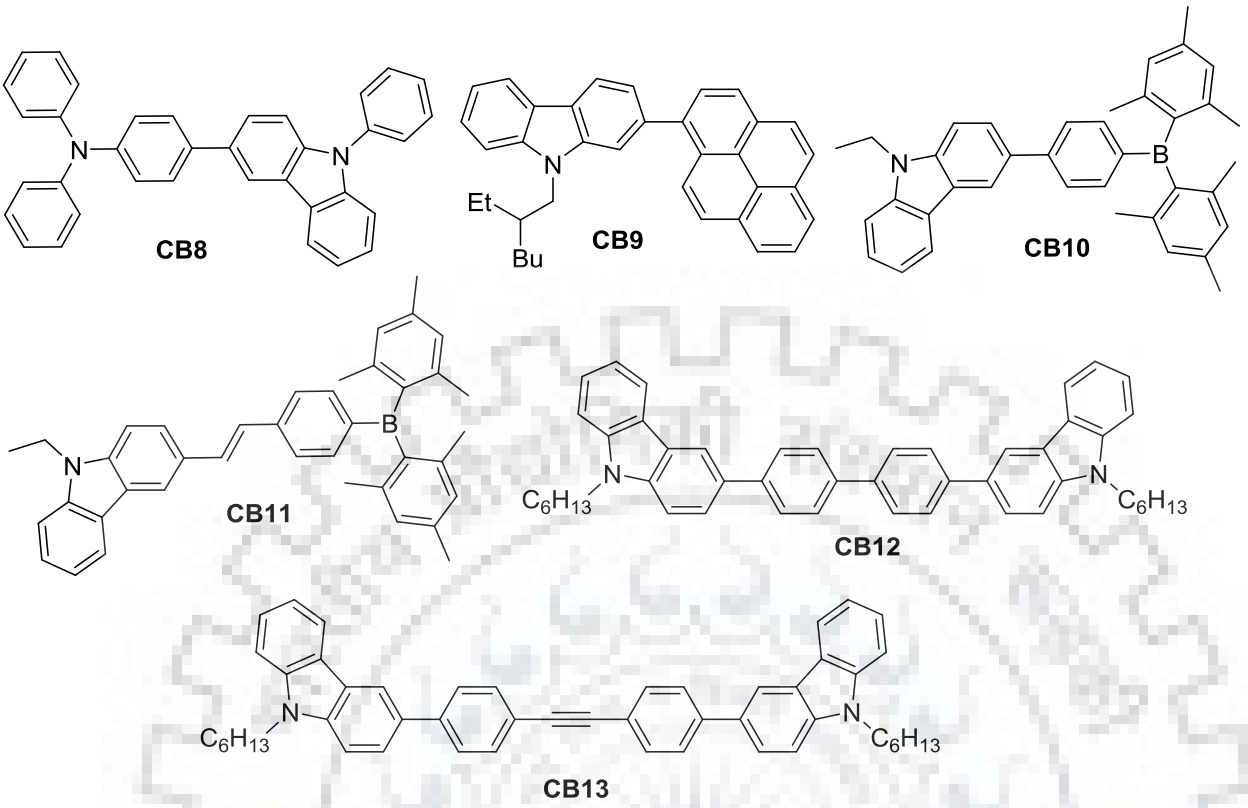

Chart 3.2 Carbazole functionalized blue emitting materials.

Nakamura and coworkers reported carbazole dimers **CB14**-**C19** (Chart 3.3) connected with different linking topology such as direct, acetylene and vinyl [126]. They studied the effect of mode of linker and their linking position either by C3 or C6- position of carbazole on photophysical properties. The C2- connected carbazole showed red shifted absorption owing to linear conjugation over C3- connections. The vinyl linker increased the donor strength and raised the HOMO level over acetylene linker. The high lying HOMO is beneficial for facile hole injection from hole transporting layer of OLED device. Durocher and coworkers reported carbazole/fluorene hybrid connected at C2- position as blue emitting material **CB20** (Chart 3.3). However, these materials are not used as emitter in OLED devices.

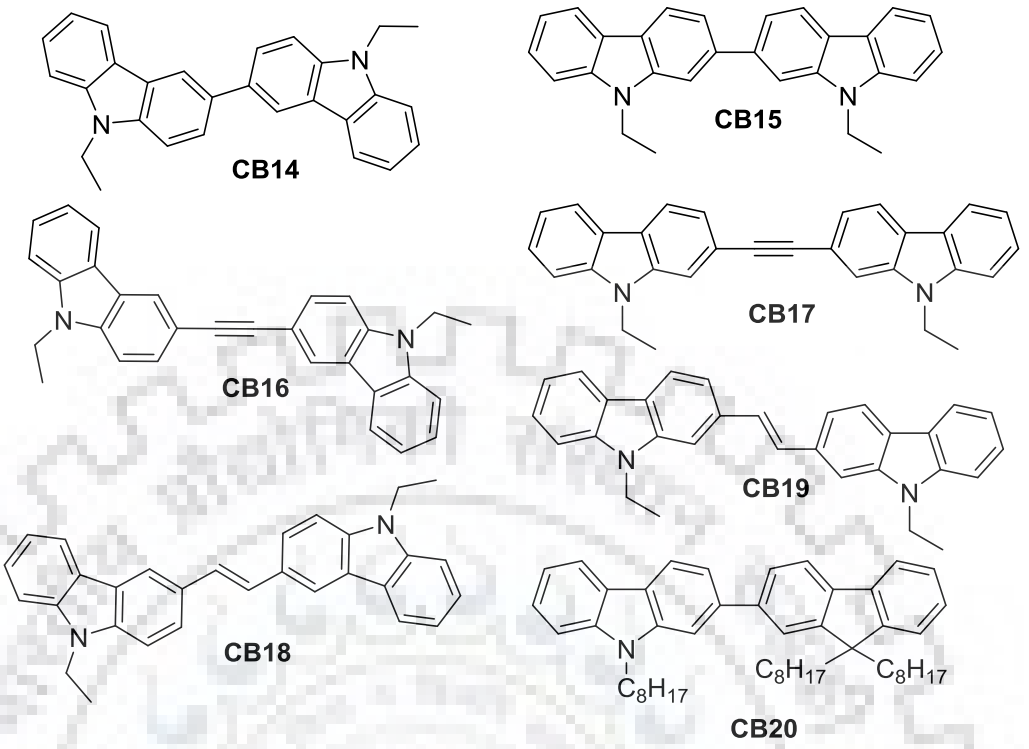

Chart 3.3 Carbazole-based materials as blue emitters.

The development of blue emitters possessing donor-acceptor configuration is beneficial to rule out the imbalanced charge transport. However, the resulting emission compromised color purity with the red shifted emission due to ICT. Lin and coworkers reported carbazole derivatives possessing cyano group at C3-position of carbazole **CB21**-**CB23** (Chart 3.4) as fluorescent emitters [103]. They concluded the presence of electron withdrawing cyano group was beneficial for realizing balanced charge transport by triggering electron transport. However, the electroluminescence spectra of the devices exhibited red shifted emission due to the donor-acceptor interaction. Later, Grazulevicius and coworkers reported cyanocarbazole tethered to carbazole via *N*-position **CB24**-**CB26** (Chart 3.4) and utilized them as blue emitting materials [127]. They found that the presence of cyano group in realizing balanced charge transport and thus better device performances. Similarly, cyanocarbazole based materials are utilized as bipolar host materials for PhOLED. Though the materials exhibit blue emission, their color purity is not up to the mark. It could be attributed to the presence of electron withdrawing cyano group at 3- position of carbazole which permits donor-acceptor interaction.

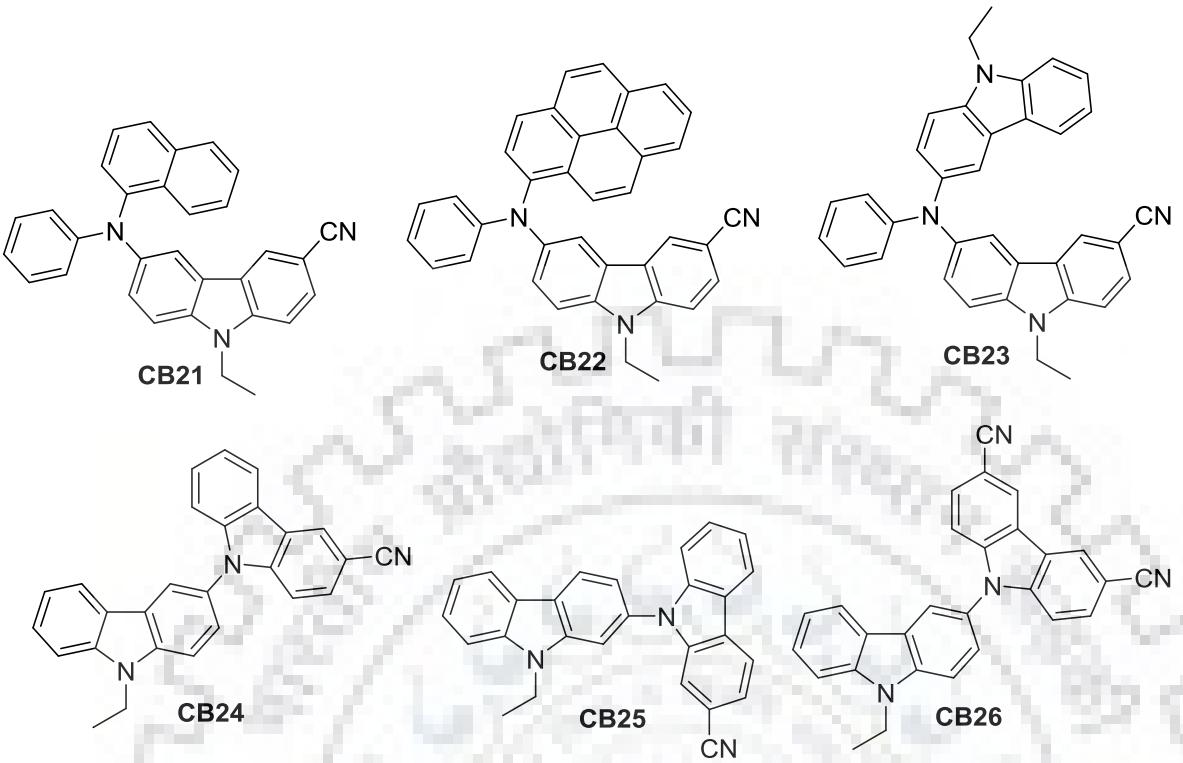

Chart 3.4 Carbazole-based materials possessing cyano group as emitting materials.

Lin and coworkers reported amine functionalized carbazoles **CB27**-**CB30** (Chart 3.5) as emitting materials [128]. They compared the photophysical and electroluminescence properties of 3,6-substituted carbazole with those of analogous 2,7-substituted one. They found that the latter compounds showed red shifted absorption and higher molar extinction coefficient owing to linear conjugation. Also, the device performances of 2,7-substituted carbazole are superior to that of 3,6-substituted analogs as a result of high charge carrier mobility. The different packing of 2,7-substituted carbazoles lead to different molecular packing density and thus high charge carrier hopping. So, tethering of donor and acceptor through *meta*- linkage would be an ideal methodology to have balanced charge transport and to retain the emission in blue region.

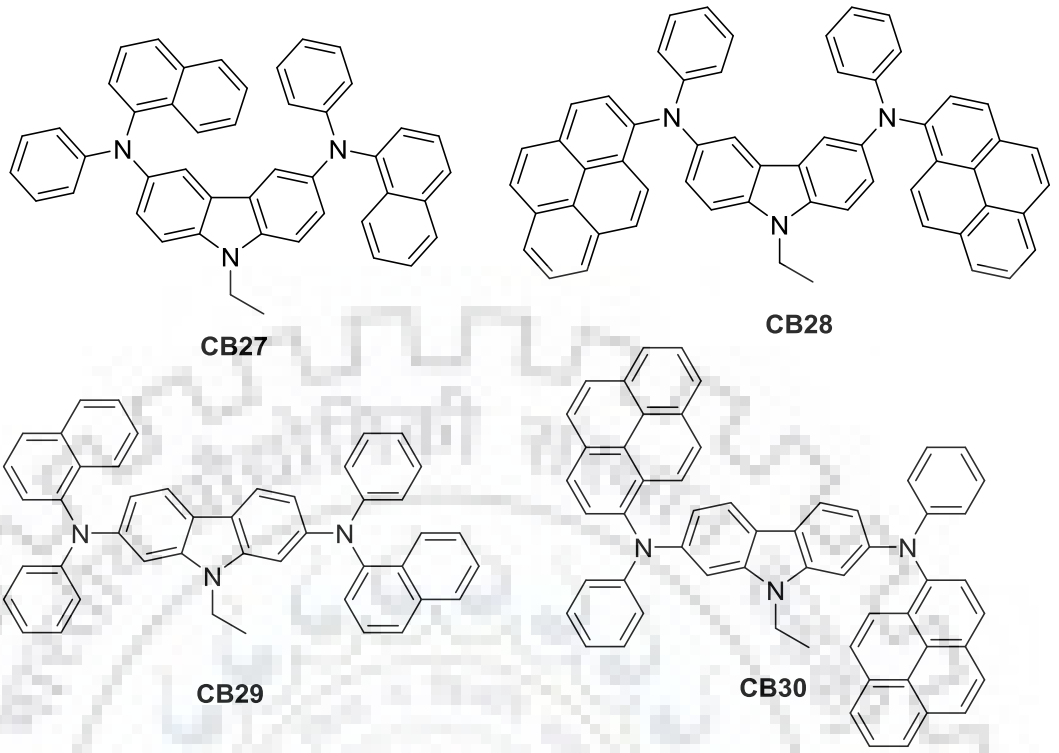

Chart 3.5 Comparison of 3,6 vs 2,7-functionalization of carbazole.

Recently, Ge and coworkers reported carbazole based D-A configured deep blue emitters **CB31** and **CB32** (Chart 3.6) by inserting phenyl linker between carbazole donor and thiazole acceptor [129]. The tilting of phenyl ring suppressed the ICT and thus emission is confined to blue color. Xu and coworkers reported carbazole/triazole hybrids (**CB33**, **CB34**) containing biphenyl linker to achieve blue emission (Chart 3.6) [102]. Lee and coworkers designed carbazole/phenathroimidazole conjugates (**CB35**, **CB36**) containing anthracene linker (Chart 3.6) [130]. The molecules exhibit deep blue emission with high EQE by exploiting the hybridized local and charge transfer excited state. Till date, many deep-blue emitting materials have been developed with D-A architecture. But carbazole-based deep blue emitters are scarcely known in the literature. It has been noticed that D-A designed molecules connected through *meta*-linkage would suppress the unwanted red shifted emission while retaining the emission to blue region.

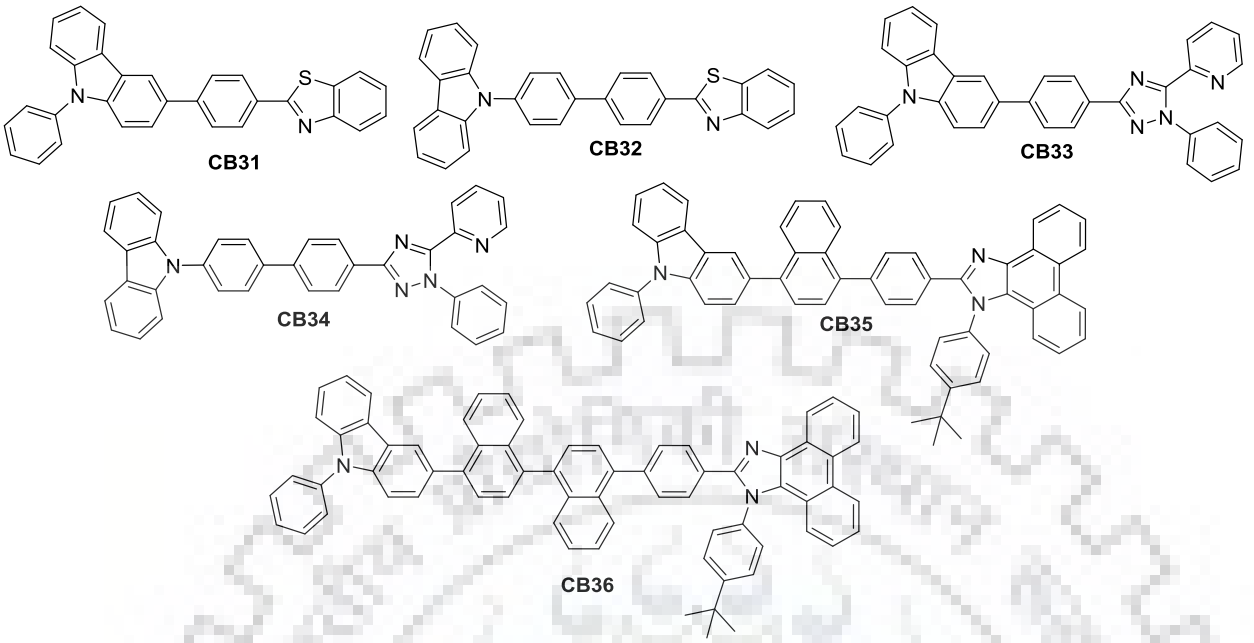

Chart 3.6 Deep blue emitting D-π-A configured materials containing carbazole donor.

Since the incorporation of electron withdrawing group on 2,7-position of carbazole does not participate in donor-acceptor interaction, however improve balance of charge transport without altering the emission towards red region. The functionalization of carbazole with cyano group at 2,7-position remains unexplored. In this chapter, we present the functionalization of carbazole at 2,7-position asymmetrically with electron donating group at one end and electron withdrawing cyano group at the other end (Chart 3.7). We envisioned that the functionalization at 2,7-position of carbazole would alleviate donor-acceptor interaction due to *meta*- linkage to electron donating nitrogen atom. Alternatively, 2,7-functionalization leads to effective π electronic conjugation across the molecular backbone [131]. We here present the synthesis of deep blue emitting materials possessing cyano at C2-position and different chromophore on C7-position of carbazole to functionally fine tune the material properties (Chart 3.7).

The linker part plays a vital role in deciding the photophysical properties. Acetylene linker provides planar conjugation between the donor and acceptor. The compounds possessing acetylene linker have been explored for OLED applications owing to their high quantum yields, rigid rod-like structure, and efficient π bridge between chromophores due to planarity [132-134]. Carbazole derivatives containing acetylene linker are found to possess superior quantum yields over directly linked compounds. With the aim of increasing quantum yields and to raise the electroluminescence performances, we synthesized cyanocarbazole derivatives possessing

acetylene linker and compared their photophysical and electroluminescence properties with the directly connected congeners. The effect of acetylene linker on photophysical, electrochemical and electroluminescence properties is elaborated. Organic compounds containing vinyl linker generally exhibit effective π conjugation owing to coplanarity of vinyl linker. The chromophoric effect of vinyl linker on the photophysical and electroluminescent properties of cyanocarbazole derivatives is also described.

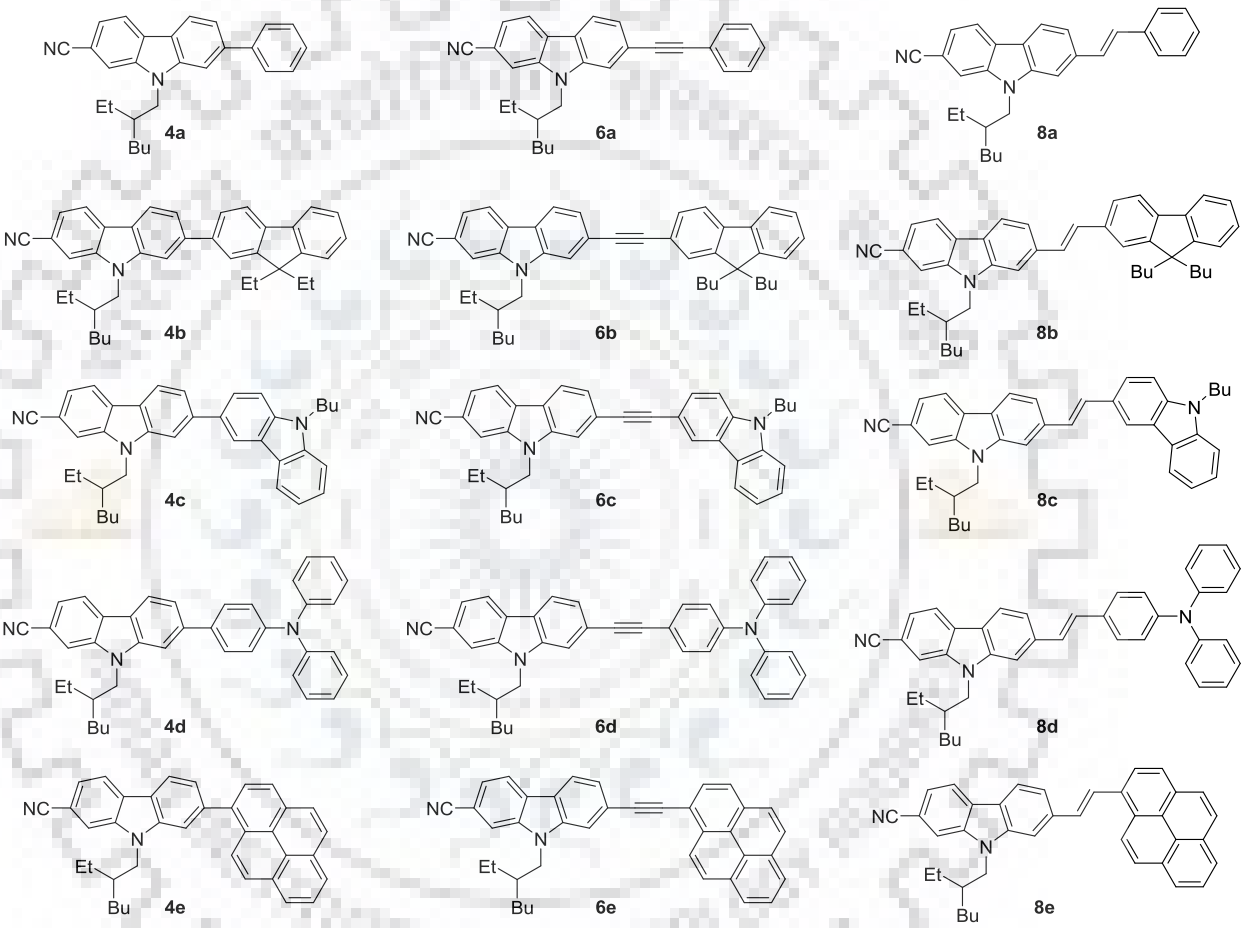

Chart 3.7 Structure of asymmetrically 2,7-disubstituted carbazole derivatives containing cyano acceptor.

3.2 Results and Discussion

3.2.1 Synthesis and Characterization

The synthetic protocols of the target dyes (Chart 3.7) and the intermediates are illustrated in Scheme 3.1. The 2,7-dibromocarbazole, **1** was selectively cyanated in a stoichiometrically controlled reaction with CuCN in DMF to obtain **2**. Then **2** was converted to the target dyes (**4a-4e**) by Suzuki coupling reaction with suitable boronic acid derivatives (**3a-3e**). Similarly the intermediate **2** was converted into target dyes (**6a-6e**) and (**8a-8e**) by Sonogashira and Heck coupling reaction using appropriate terminal acetylenes (**5a-5e**) and terminal alkenes (**7a-7e**) respectively. All the dyes were thoroughly characterized by ^{1}H and ^{13}C nuclear magnetic resonance (NMR) spectroscopy and high-resolution mass spectrometry (HRMS). The data is consistent with the proposed structures. All of the dyes are soluble in common organic solvents such as dichloromethane (DCM), toluene (TOL), tetrahydrofuran (THF), chloroform ($CHCl_3$), *N*,*N*-dimethylformamide (DMF), acetonitrile (ACN), and methanol (MeOH).

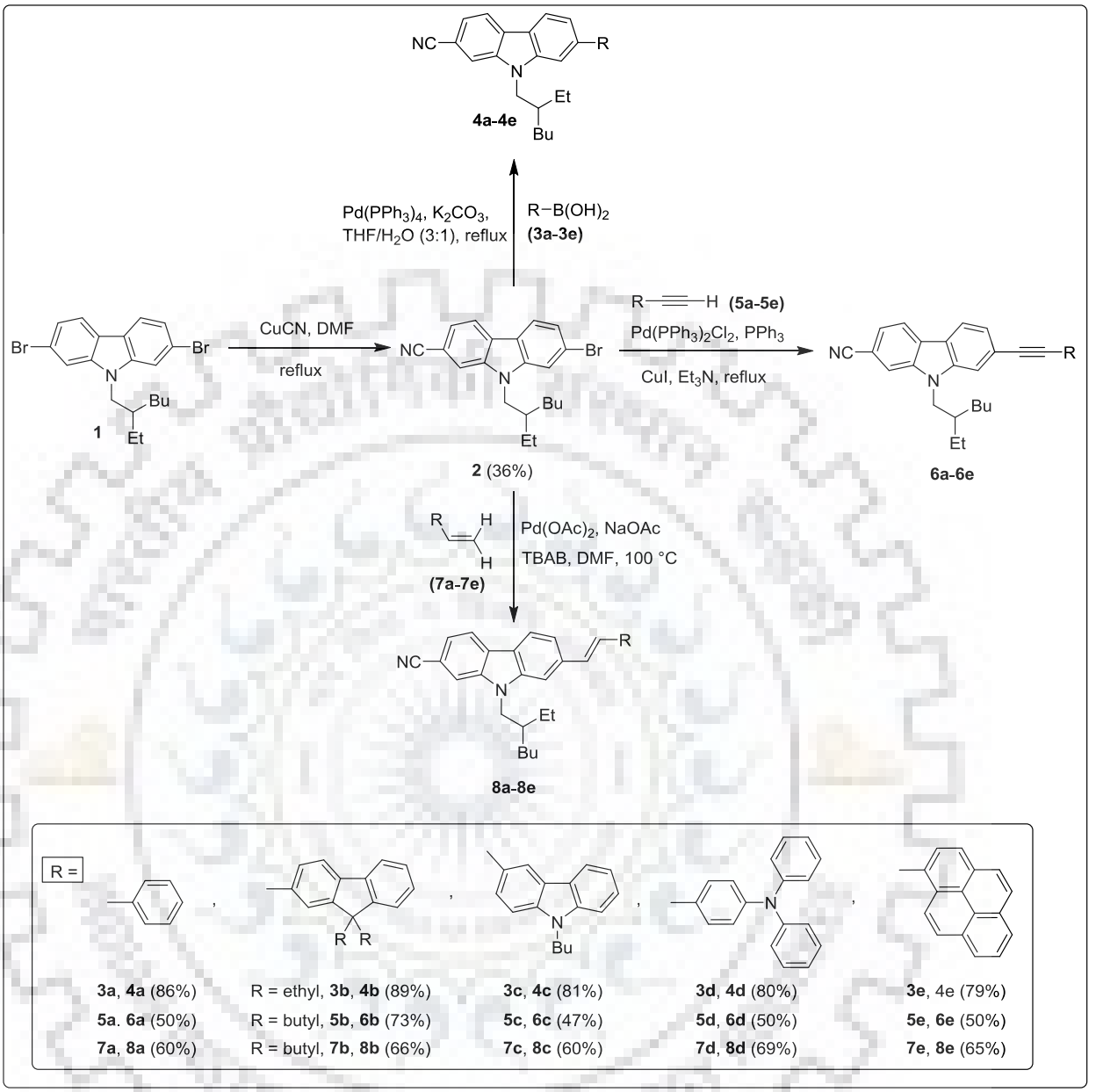

Scheme 3.1 Synthetic route for the target dyes.

3.2.2 Photophysical Properties

The absorption spectra of the dyes recorded in dichloromethane solution are displayed in Figure 3.1. And the relevant data are summarized in the Table 3.1. Depending on the nature of linker, the compounds can be classified into three sets namely directly connected, acetylene linker and vinyl linker connected compounds. In the first set of compounds, cyanocarbazole is tethered with different chromophoric units such as phenyl, fluorene, carbazole, triphenylamine

and pyrene. The second and the third set contain acetylene and vinyl bridges between cyanocarbazole and other chromophoric units respectively. Here, the common features of all classes of compounds are described. The absorption maximum is progressively increased according to the electron richness of tethered chromophoric units to cyanocarbazole. The trend in absorption maxima is phenyl (**4a**) < fluorene (**4b**) < carbazole (**4c**) < pyrene (**4e**) < triphenylamine (**4d**). But the trend is slightly modified for acetylene and vinyl linker congeners in which pyrene-based compounds exhibited red shifted absorption maxima as compared to triphenylamine substituted counterparts. The blue shift observed for pyrene substituted compound **4e** could be due to twisted conformation whereas conjugation is extended in acetylene and vinyl bridged counterparts ascribed to linearity of the spacers [126]. As a result, pyrene substituted compounds containing acetylene and vinyl linker showed the longest absorption maxima compared to their triphenylamine analogs. The absorption spectrum of all the compounds showed multiple absorption peaks. The absorption bands may be classified into two types. The band appearing below 300 nm corresponds to the π-π* transition of the chromophores such as carbazole, fluorene or triphenylamine present in the compounds while the lower energy band above 300 nm is attributed to delocalized π-π* transition of entire molecular segments [135]. The longer wavelength absorption observed for **4b**-**4e** when compared to **4a** is reflective of the extended conjugation in the former compounds owing to the presence of fused aromatics or amine units.

The red shifted absorption of **4c** when compared to the known compounds 9,9'-diethyl-9*H*,9'*H*-2,2'-bicarbazole and 9,9'-diethyl-9*H*,9'*H*-3,3'-bicarbazole indicates the chromophoric role of cyano group on carbazole [126]. Similarly, the absorption maximum of **4d** is red shifted when compared to the reported compound *N*,*N*-diphenyl-4-(9-phenyl-9*H*-carbazol-3-yl)aniline [122]. It could be due to the elongation of conjugation by functionalization at 2-position of carbazole and an additional cyano group which increases linear conjugation. However, the incorporation of cyano group on carbazole has insignificant change in absorption maxima of **4e** recorded in THF as compared to the reported compound 9-(2-ethylhexyl)-2-(pyren-1-yl)-9*H*-carbazole (Table 3.2) [123].

When the acetylene spacer is introduced, the absorption maximum of the compounds (**6a**-**6e**) is red shifted compared to their analogous directly linked compounds (**4a**-**4e**). The linear structure of acetylene linker offered effective conjugation and thus resulted in red shifted

absorption maximum. It is interesting to compare the absorption spectrum of **6b** with the reported compound containing cyanofluorene instead of cyanocarbazole. The slight increment in absorption maximum of **6b** is attributed to electron richness of carbazole over fluorene. The red shifted absorption of **6c** compared to reported dyes 1,2-bis(9-ethyl-9*H*-carbazol-2-yl)ethyne and 1,2-bis(9-ethyl-9*H*-carbazol-3-yl)ethyne [126] which do not have cyano group indicates the chromophoric effect of cyano group.

The compounds containing vinyl linker exhibited the largest bathochromic shifted absorption maxima compared to their direct and acetylene linked analogs. It is ascribed to sp^2 hybridization of carbon of both aromatic and aliphatic vinyl linker which results in effective overlap of π orbitals. Whereas the blue shifted absorption maximum is observed for acetylene counterparts. Different hybridization (sp^2 and sp) between aromatic carbon and acetylene linker leads to mismatch in energies of π orbitals and poor overlap [187-190]. The trend of absorption maxima followed the order of acetylene linked compounds. The red shifted absorption of **8c** when compared to reported compounds (*E*)-1,2-bis(9-ethyl-9*H*-carbazol-3-yl)ethene and (*E*)-1,2-bis(9-ethyl-9*H*-carbazol-2-yl)ethene indicates the chromophoric role of cyano group on carbazole [126, 136]. The above comparison reveals the role of cyano group on carbazole and the linking mode in raising the conjugation length. On the whole, the absorption maxima followed trend for each compound as direct (**4**) < acetylene (**6**) < vinyl (**8**).

Further, the nature of ground state of the molecules is evaluated by measuring absorption spectra in different solvents of varying polarity from non-polar toluene to polar methanol (Figure 3.3 to Figure 3.17). The negligible change in absorption maxima is observed for all the compounds irrespective of solvent polarity. It reveals that the ground state of the dyes is non-polar in nature and their insensitivity towards solvent polarity.

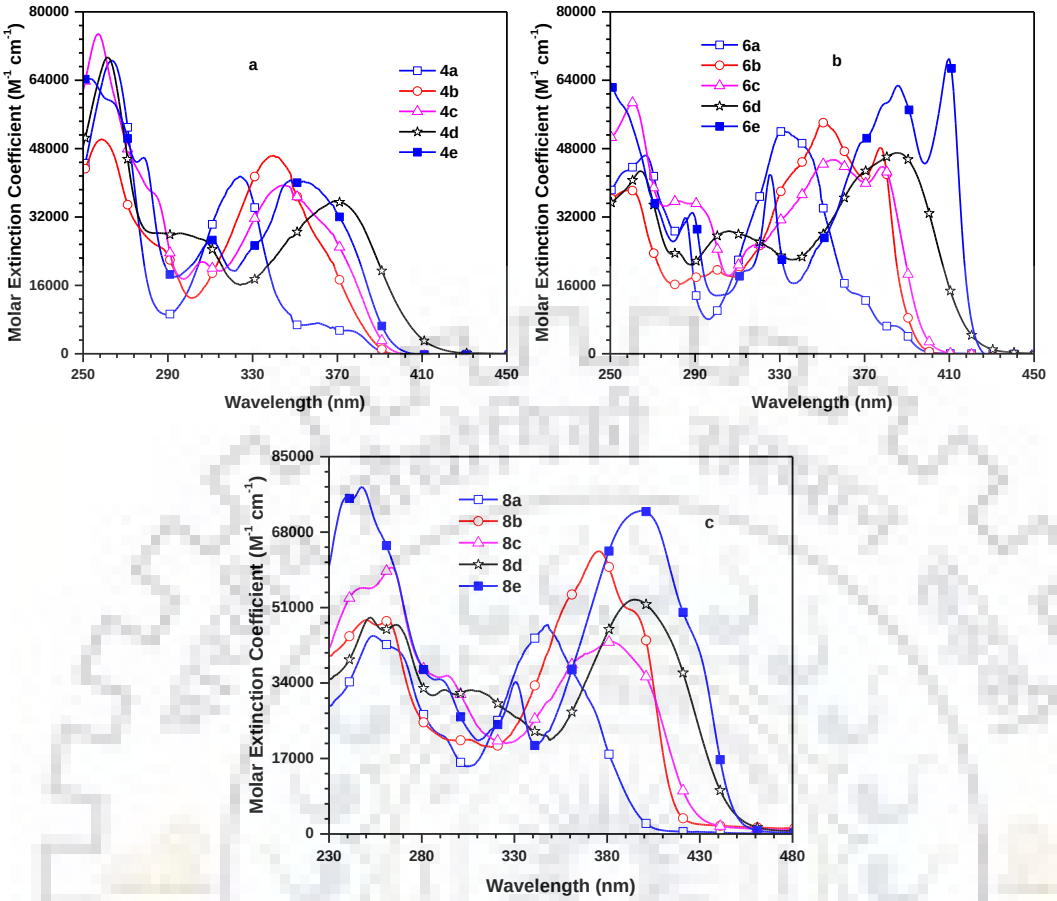

Figure 3.1 Absorption spectra of (a) direct, (b) acetylene and (c) vinyl linked dyes recorded in dichloromethane.

The emission spectra of the compounds recorded in dichloromethane are displayed in Figure 3.2, and the pertinent data compiled in Table 3.1. The emission spectra of **4a**-**4e** followed the same trend of absorption spectra. Triphenylamine substituted compound **4e** exhibited the largest bathochromic shift among the compounds. Phenyl and fluorene substituted compounds (**4a** and **4b**) have displayed structured emission while carbazole, triphenylamine and pyrene substituted compounds (**4c**, **4d** and **4e**) exhibited featureless broad spectra. The vibrational fine structure of **4a** and **4b** is due to rigid nature of the molecular framework. These dyes showed solvent independent emission revealing absence of selective stabilization of dyes in solvents. In contrast, the dyes **4c** and **4d** gave broad and structureless emission spectra sensitive to solvent polarity. The pronounced positive solvatochromic behavior of **4d** is ascribed to more structural reorganization and dipolar relaxation of the molecule in the excited state [137-139]. This result supports the polarized excited state of the molecules which is

preferentially stabilized by solvents of high polarity. It is interesting to note that the dye **4c** gave structured emission in toluene, whereas it collapsed into a broad emission in polar solvents. This points the two aspects about the nature of the excited state. Firstly, the molecule is more rigid due to the presence of carbazole. Secondly, the dipolar relaxation is less pronounced as the donor strength of carbazole is small when compared to triphenylamine [140-141]. Though **4e** exhibited structureless emission, it did not show preferential stabilization of excited state in selective solvents. The structureless emission is ascribed to large structural reorganization to attain planar structure at excited state compared to its twisted ground state.

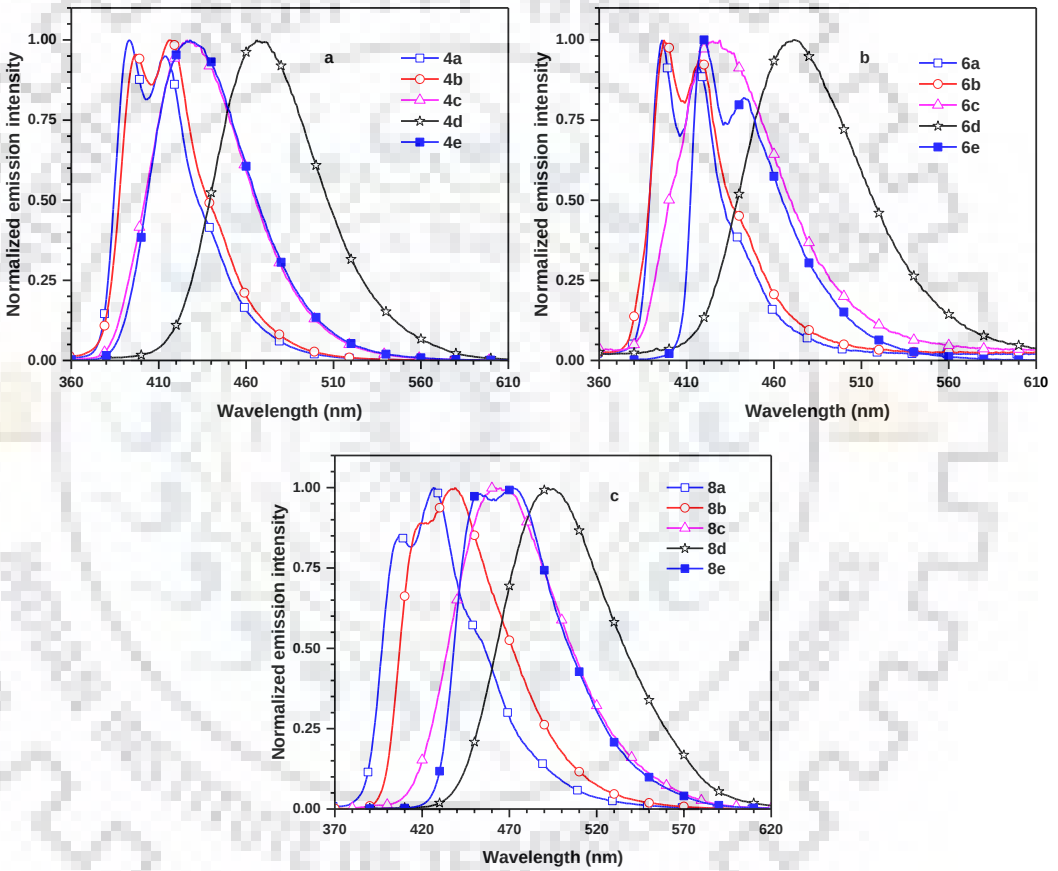

Figure 3.2 Emission spectra of (a) direct, (b) acetylene and (c) vinyl linked dyes recorded in dichloromethane.

The pattern and trend of emission maxima of acetylene and vinyl linker compounds is similar to the directly connected compounds. However, pyrene substituted compounds **6e** and **8e** exhibited structured emission which indicates the absence of structural reorganization and the rigidity of the molecules. The involvement of large structural changes in the former (**4e**) resulted in structureless emission. The trend of emission maxima among each set follows as

direct (**4**) < acetylene (**6**) < vinyl (**8**). Despite of blue shift in absorption, the directly connected compounds exhibited almost similar emission maxima compared to their acetylene analogs. It might be due to pronounced structural changes associated with the former compounds which stabilize the excited state and thus red shifted emission maxima whose values are comparable to their acetylene analogs. This indicates the planar nature of these molecules at excited compared to twist ground state.

Table 3.1 Optical properties of the dyes

Dye	λ_{max}, nm (ε_{max}, M^{-1} cm^{-1} $\times 10^3$)[a]	λ_{em}, nm (Φ_F)[a,b]	Stokes shift, cm^{-1}	λ_{em},[c] nm
4a	264 (68.6), 324 (41.5)	393, 414 (0.28)	5419	398, 418
4b	259 (50.2), 288 (24.5), 340 (46.4)	397, 416 (0.42)	4223	452
4c	257 (74.9), 306 (21.5), 346 (39.3)	426 (0.68)	5428	431
4d	262 (69.3), 296 (28.2), 368 (35.7)	466 (0.80)	5715	452
4e	243 (70.5), 279 (45.9), 310 (26.7), 348 (40.7)	428 (0.72)	5371	454
6a	267 (46.4), 286 (31.9), 331 (52.0)	396, 417 (0.40)	4959	451
6b	259 (38.3), 351 (54.2), 378 (48.2)	397, 417 (0.47)	1266	451
6c	261 (58.8), 290 (35.2), 355 (45.4), 379 (43.8)	425 (0.55)	2856	469
6d	264 (42.7), 306 (28.7), 385 (47.0)	471 (0.84)	4743	490
6e	246 (66.1), 289 (33.0), 313 (19.3), 325 (41.9), 386 (62.8), 410 (69.1)	420, 443 (0.59)	581	494
8a	254 (44.6), 348(47.2)	407, 427 (0.13)	4166	452
8b	261 (47.9), 376(63.7), 396sh (49.5)	419, 439 (0.66)	2729	459
8c	248 (55.4), 264 (60.1), 294sh (35.7), 383 (43.3)	462 (0.55)	4465	469
8d	252 (48.8), 266sh (47.1), 307 (32.5), 395 (52.8)	479 (0.83)	4991	470
8e	248 (78.2), 291sh (34.7), 331 (34.3), 399 (72.9)	453, 472 (0.89)	2988	469

[a]Measured in dichloromethane solution. [b]Absolute quantum yield measured using integrating sphere. [c]Measured for drop cast film.

The solvatochromic properties of the dyes are examined by recording the emission spectra in various solvents of different polarity (Figure 3.3 to Figure 3.17). Phenyl, fluorene and pyrene substituted compounds exhibited solvent independent emission maxima while pronounced red shift is observed for carbazole and triphenylamine substituted compounds as the polarity of the solvents increases for acetylene and vinyl linked compounds. The selective stabilization of excited state indicates the polar nature of excited state and results in the red shifted emission maximum as the polarity of solvents increases (Table 3.2). Pyrene functionalized compound **4e**

exhibited moderate red shift as the solvent polarity is increased whereas its acetylene and vinyl linker based analogs (**6e** and **8e**) showed solvent independent emission. The moderate shift of **4e** could be ascribed to structural changes in polar solvents.

The emission spectrum of **4c** exhibited red shifted emission when compared to known compounds 9,9'-diethyl-9*H*,9'*H*-2,2'-bicarbazole and 9,9'-diethyl-9*H*,9'*H*-3,3'-bicarbazole [126]. Similarly, the red shifted emission is observed for **6b** compared to its cyanofluorene analog reported in literature attests the effective π conjugation rendered by carbazole scaffold over fluorene. In a similar way, the compound **6c** also exhibited bathochromically shifted emission compared to 1,2-bis(9-ethyl-9*H*-carbazol-2-yl)ethyne and 1,2-bis(9-ethyl-9*H*-carbazol-3-yl)ethyne which do not have cyano group confirms the additive chromophoric density of cyano group on carbazole [126]. The red shifted emission spectrum is observed for **8c** when compared to reported compounds (*E*)-1,2-bis(9-ethyl-9*H*-carbazol-3-yl)ethene and (*E*)-1,2-bis(9-ethyl-9*H*-carbazol-2-yl)ethane [126]. It indicates the stabilization of excited state by intramolecular charge transfer from carbazole donor to cyanocarbazole acceptor. This is further attested by the presence of well separated HOMO and LUMO in carbazole and cyanocarbazole respectively.

The largest Stokes shift is observed for directly connected compounds (**4a**-**4e**) compared to their analogous compounds containing acetylene and vinyl linker (Table 3.3 and Table 3.4). This further confirms the large structural changes at excited state to attain planar structure compared to its twisted ground state. In each set of compounds, carbazole and triphenylamine substituted compounds (**3** and **4**) exhibited large Stokes shift compared to other compounds. It is attributed to the pronounced dipolar relaxation of excited state accompanying charge migration from carbazole/ triphenylamine donor to cyanocarbazole acceptor. The large Stokes shift is observed for triphenylamine derivatives in each set which supports the above argument.

Further the solvent dependence of excited state of molecules is studied by plotting Stokes shift against solvent orientation polarizability (Figure 3.18). The linear correlation observed in Lippert-Mataga plot for carbazole substituted compounds (**4c**, **6c** and **8c**) and triphenylamine substituted compounds (**4d**, **6d** and **8d**) with large slope values indicates the presence of single excited state namely charge transfer excited state and the involvement of sizeable change in dipole moment from ground to excited state. The positive slope obtained for the compounds indicates the positive solvatochromism in the emission spectra [142-144]. Thin film emission spectrum recorded by drop cast method displayed broad and red shifted emission for all the

dyes as compared to emission spectrum recorded in toluene (Figure 3.19 and Table 3.1). It might be due to the intermolecular interaction and the formation of *J*- aggregation of the dyes in the solid state [145-147].

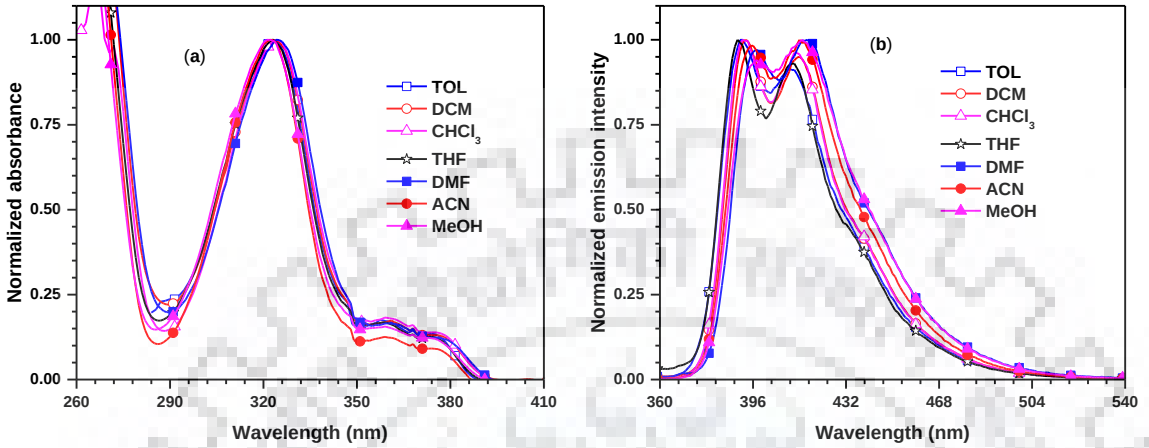

Figure 3.3 Absorption (a) and emission (b) spectra of **4a** recorded in different solvents.

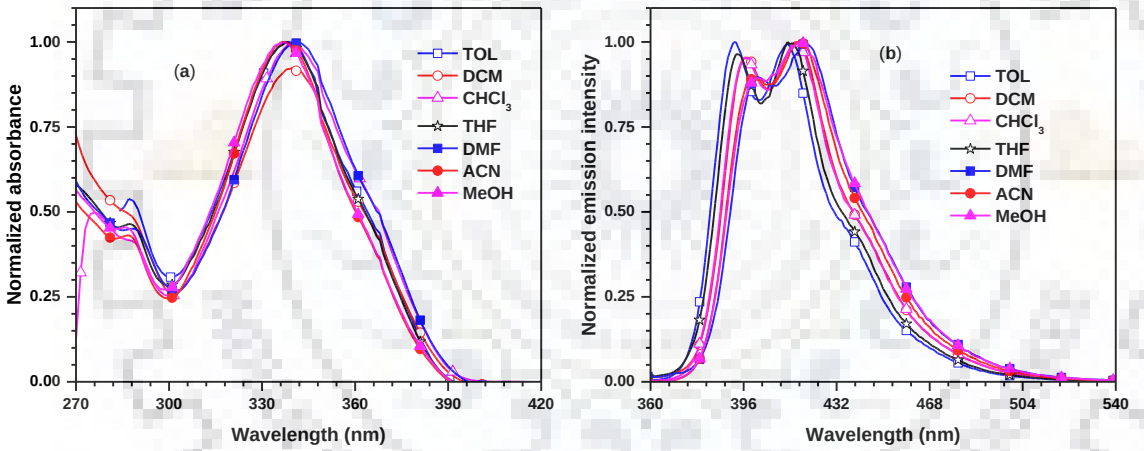

Figure 3.4 Absorption (a) and emission (b) spectra of **4b** recorded in different solvents.

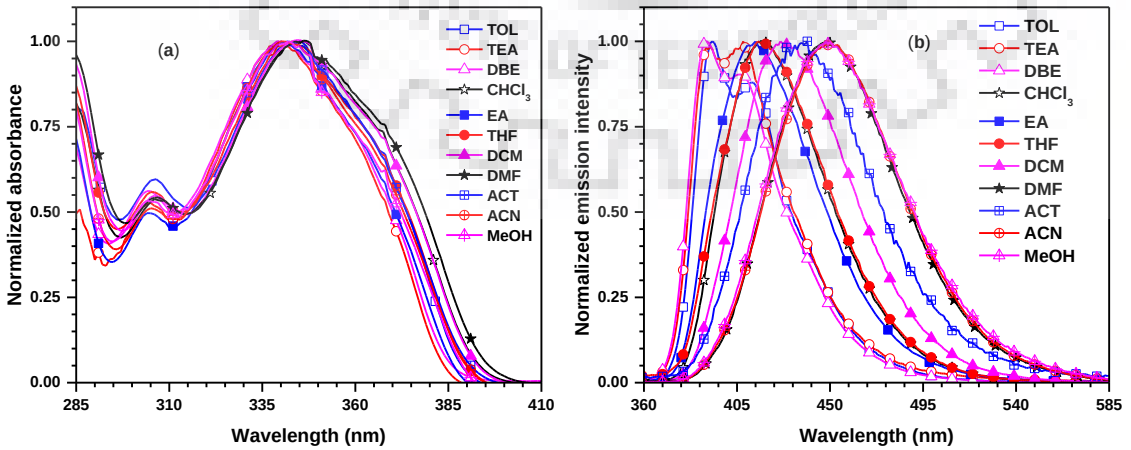

Figure 3.5 Absorption (a) and emission (b) spectra of **4c** recorded in different solvents.

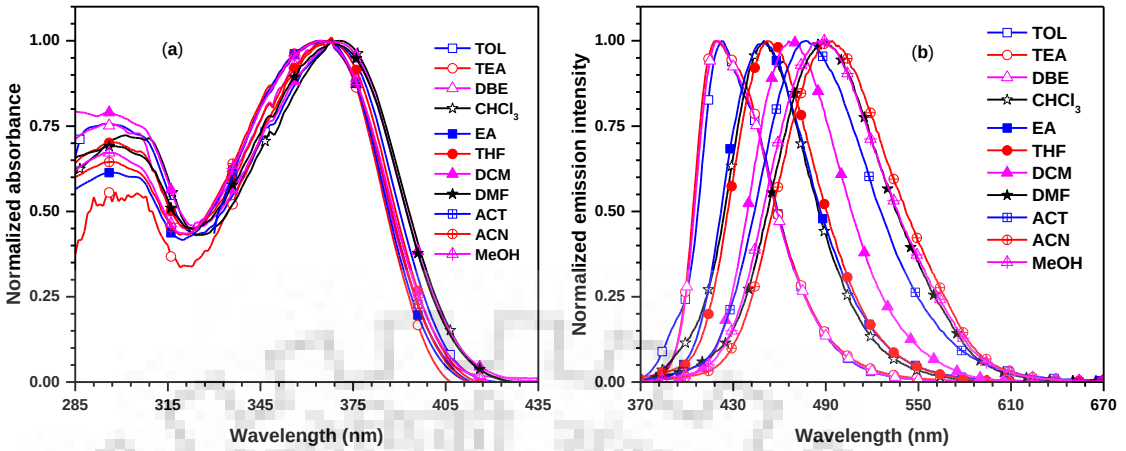

Figure 3.6 Absorption (a) and emission (b) spectra of **4d** recorded in different solvents.

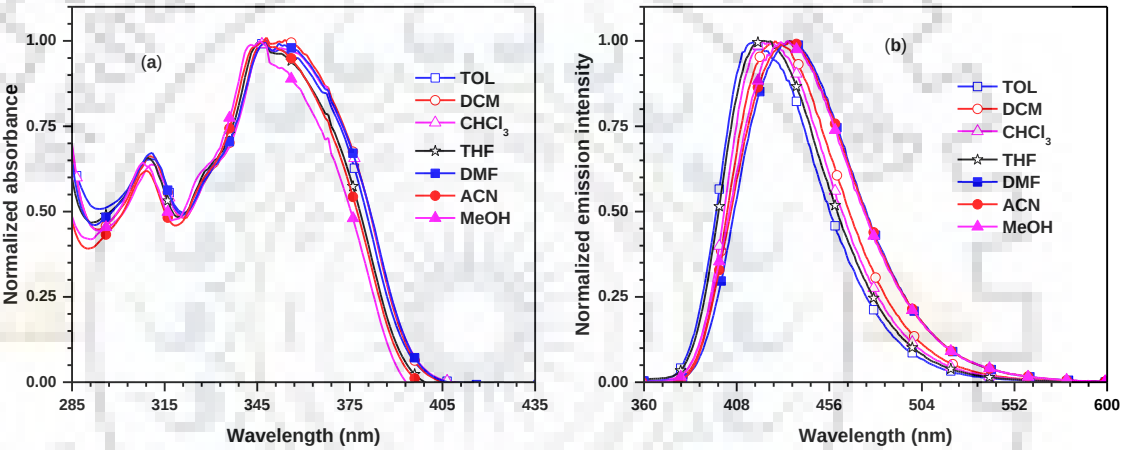

Figure 3.7 Absorption (a) and emission (b) spectra of **4e** recorded in different solvents.

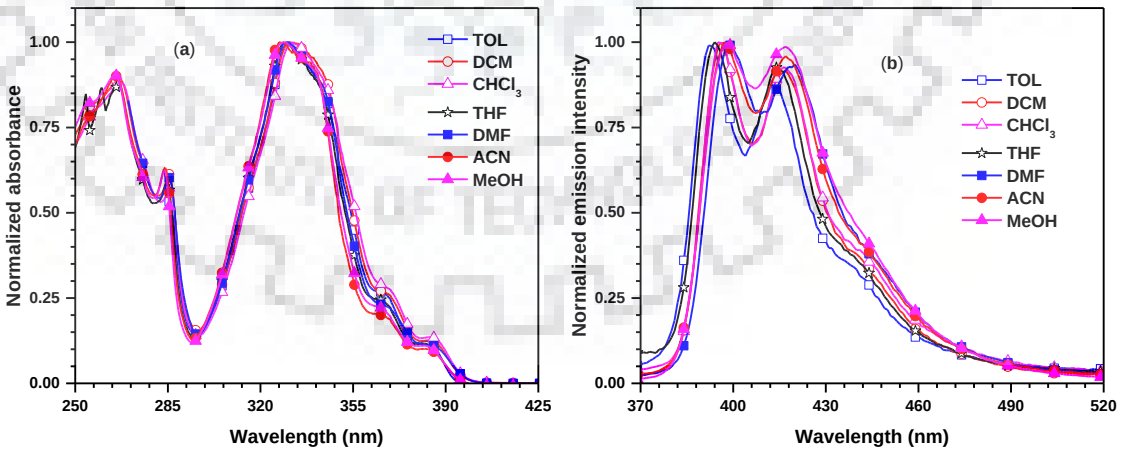

Figure 3.8 Absorption (a) and emission (b) spectra of **6a** recorded in different solvents.

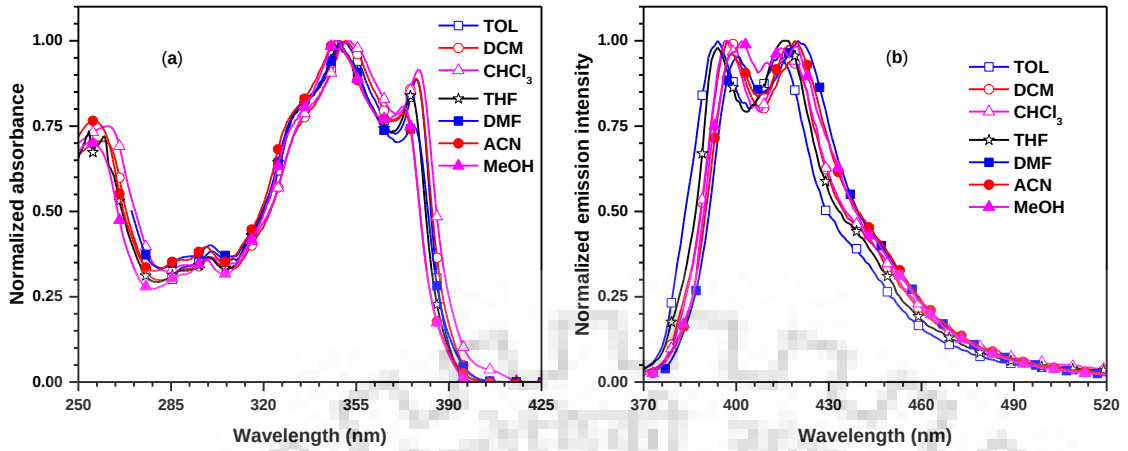

Figure 3.9 Absorption (a) and emission (b) spectra of **6b** recorded in different solvents.

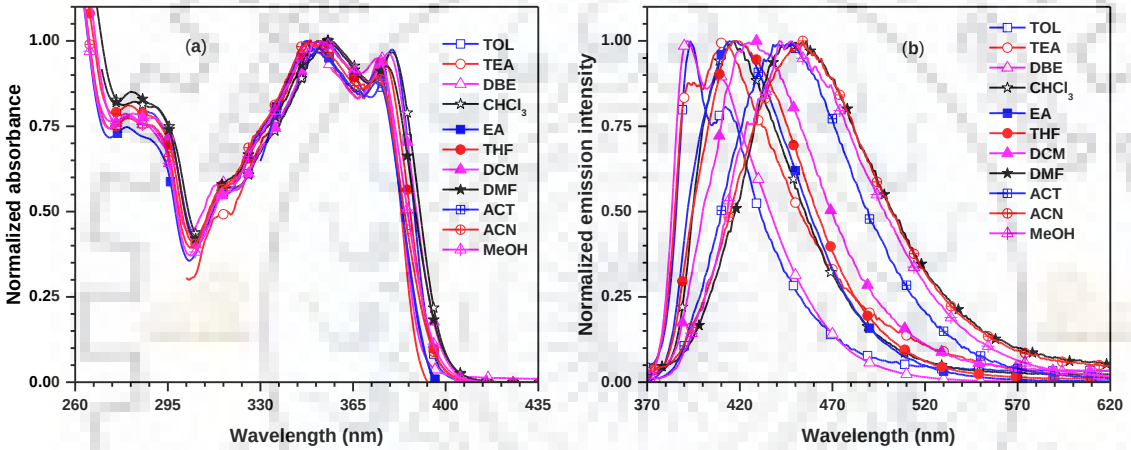

Figure 3.10 Absorption (a) and emission (b) spectra of **6c** recorded in different solvents.

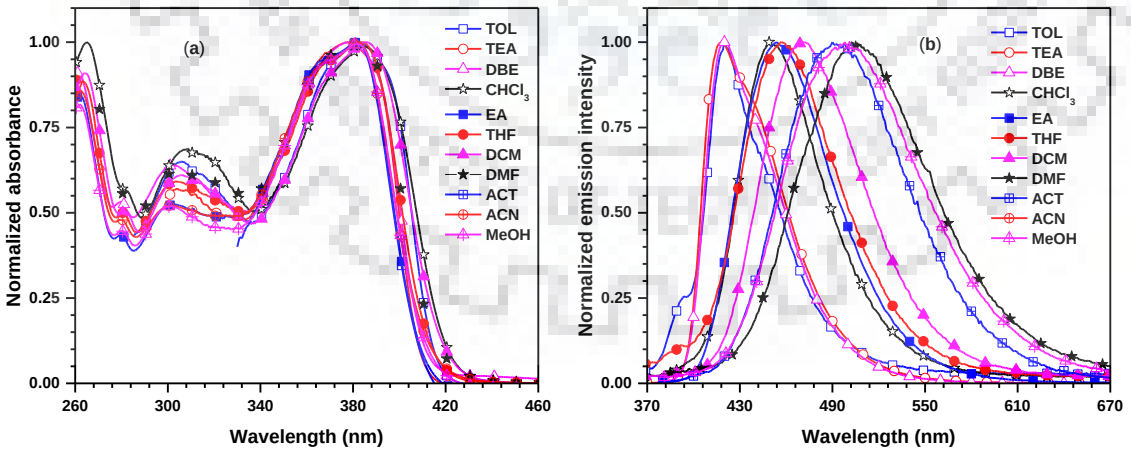

Figure 3.11 Absorption (a) and emission (b) spectra of **6d** recorded in different solvents.

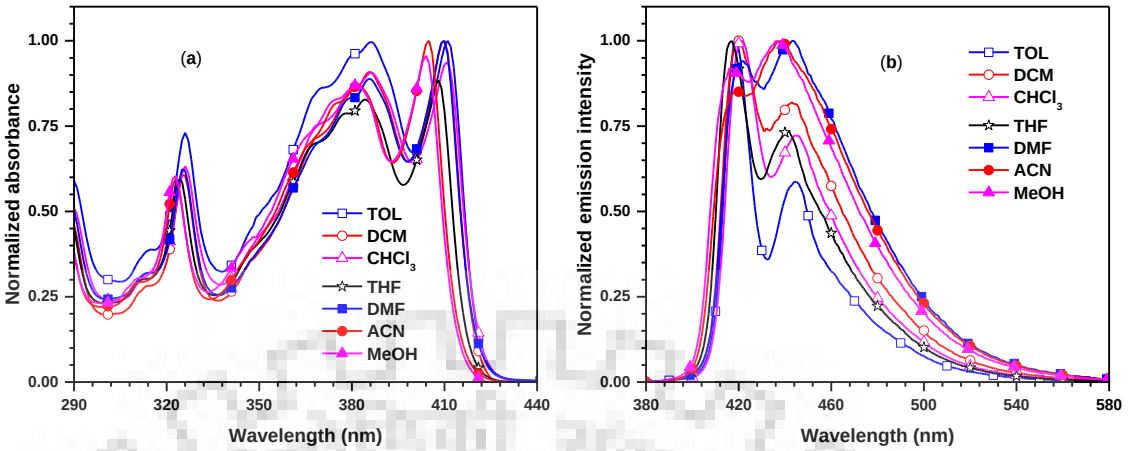

Figure 3.12 Absorption (a) and emission (b) spectra of **6e** recorded in different solvents.

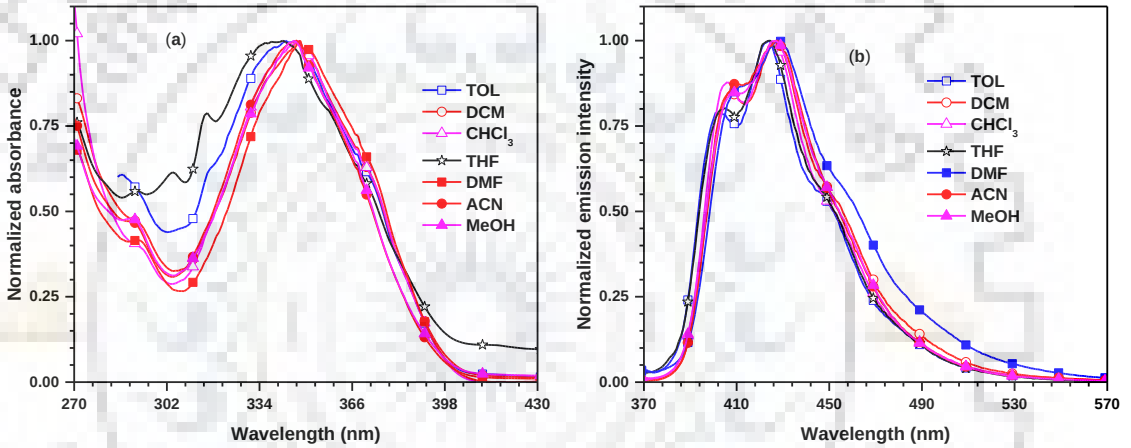

Figure 3.13 Absorption (a) and emission (b) spectra of **8a** recorded in different solvents.

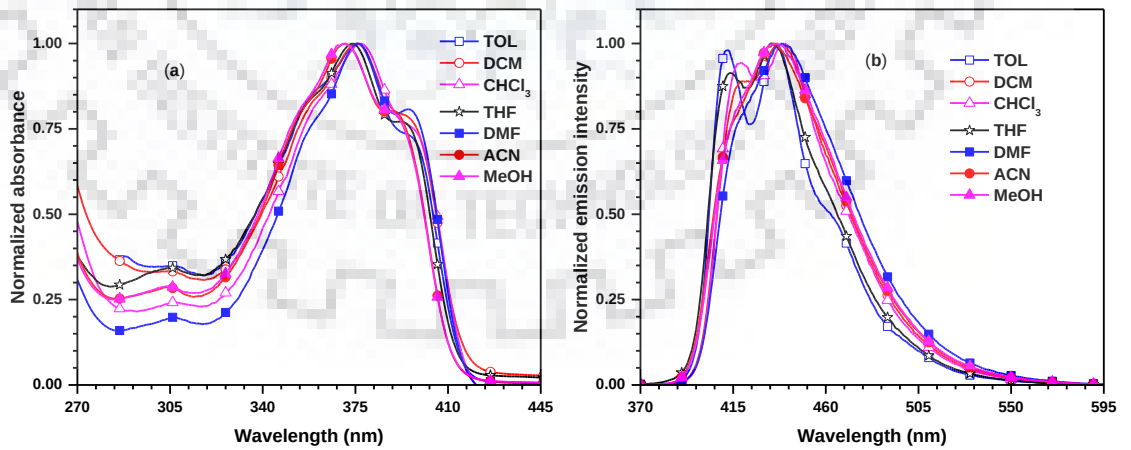

Figure 3.14 Absorption (a) and emission (b) spectra of **8b** recorded in different solvents.

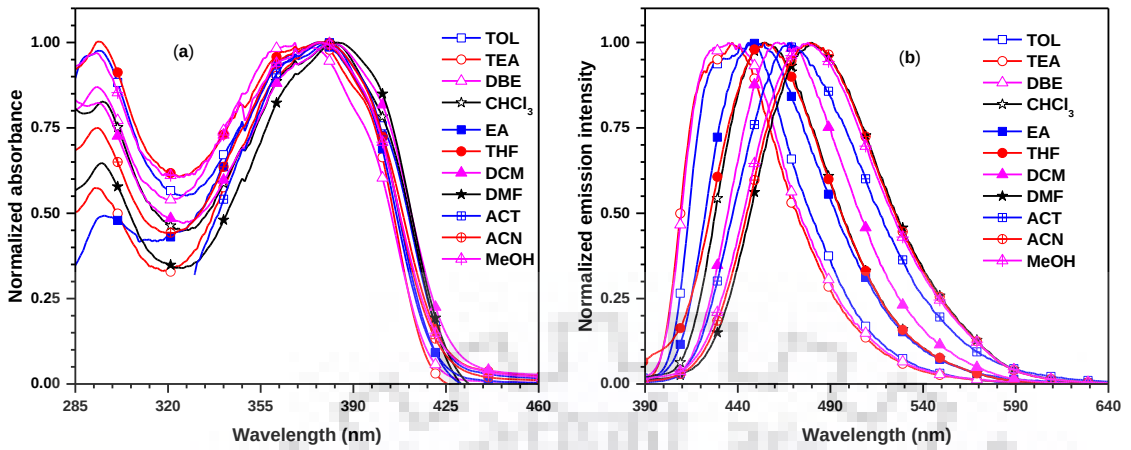

Figure 3.15 Absorption (a) and emission (b) spectra of **8c** recorded in different solvents.

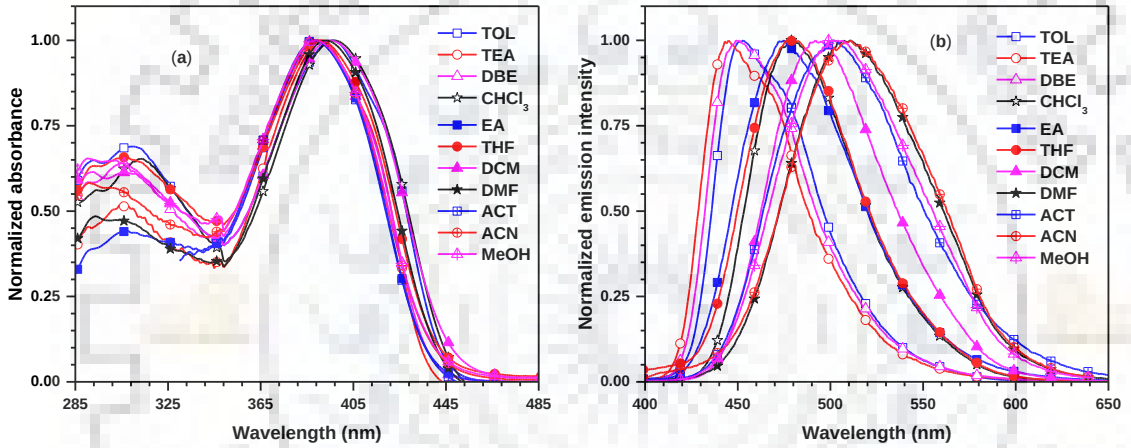

Figure 3.16 Absorption (a) and emission (b) spectra of **8d** recorded in different solvents.

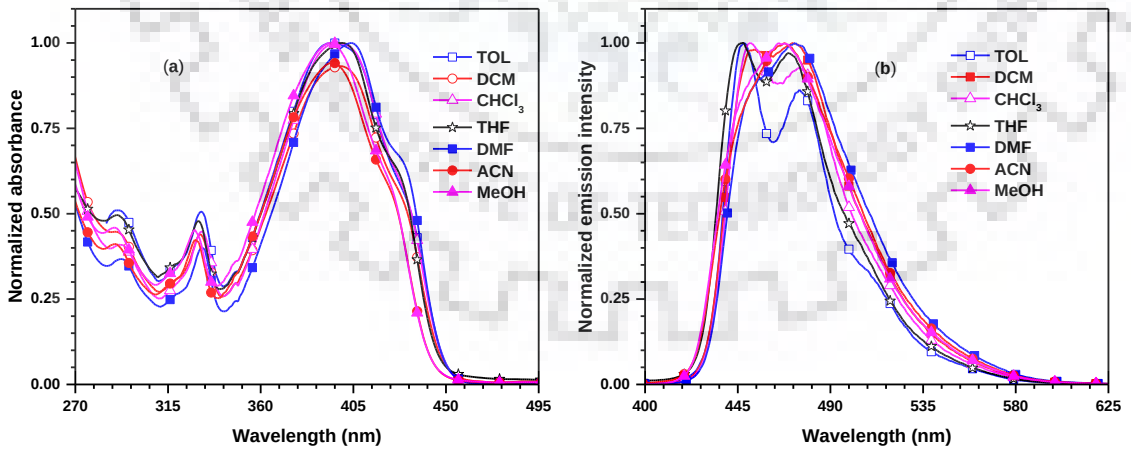

Figure 3.17 Absorption (a) and emission (b) spectra of **8e** recorded in different solvents.

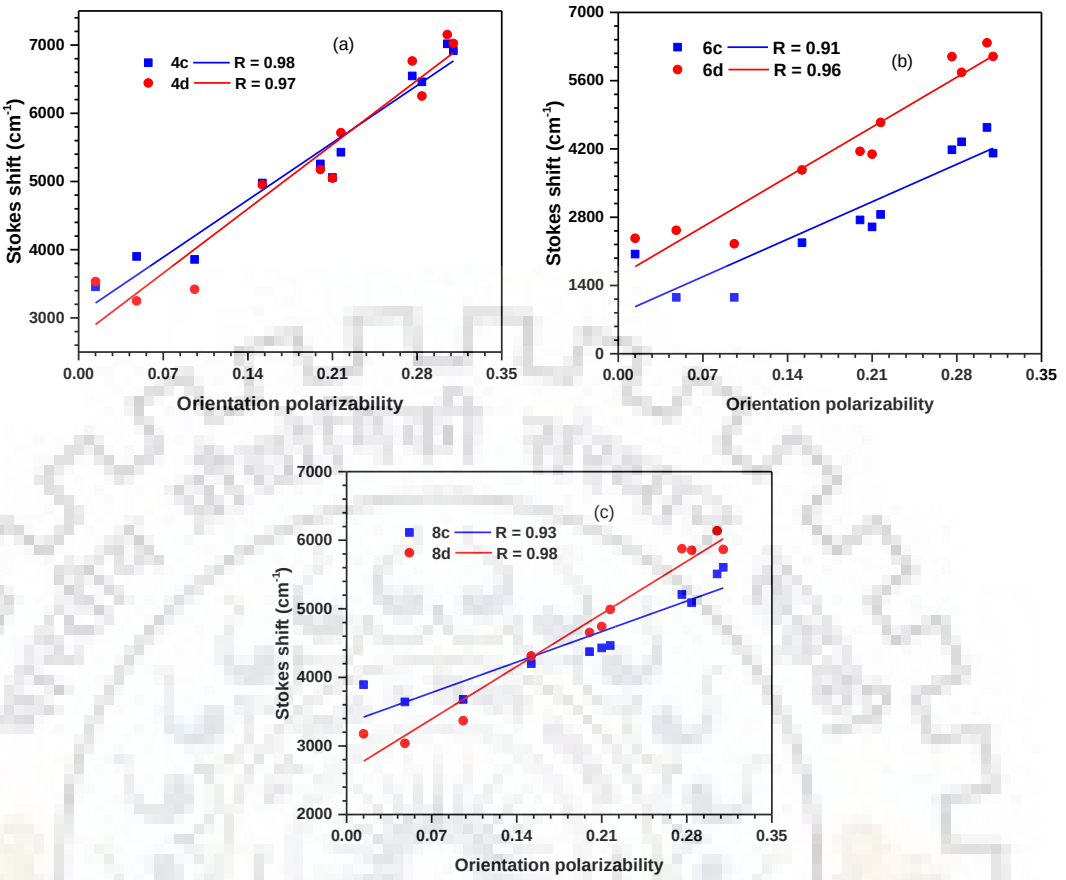

Figure 3.18 Lippert-Mataga plot of (a) direct, (b) acetylene and (c) vinyl linked dyes.

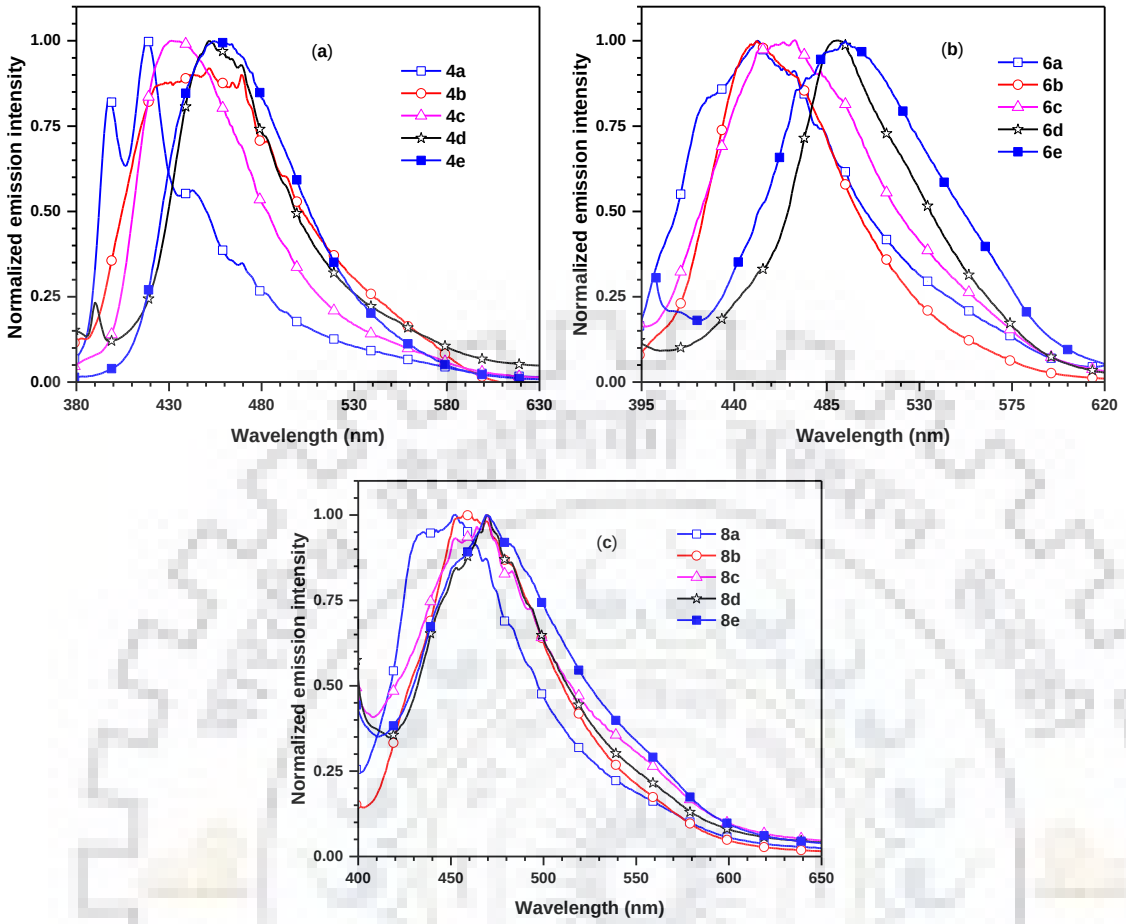

Figure 3.19 Thin film emission spectra of (a) direct, (b) acetylene (b) and (c) vinyl linked dyes recorded by drop cast method.

Table 3.2 Solvatochromic data of the dyes

Dye	Absorption maxima, λ_{max} (nm)						Emission maxima, λ_{em} (nm)					
	TOL	$CHCl_3$	THF	DMF	ACN	MeOH	TOL	$CHCl_3$	THF	DMF	ACN	MeOH
4a	323	266, 324	266, 323	324	262, 322	260, 321	392, 412	392, 412	390, 412	397, 417	396, 414	397, 415
4b	287, 338	288sh, 339	288sh, 338	290sh, 342	288sh, 337	287sh, 337	393, 413	396, 416	394, 415	402, 420	400, 417	401, 418
4c	306, 345	276, 307sh,346	306sh, 343	282,308sh 347	282,305sh 342	281,304sh, 342	393, 412	418	415	449	450	448
4d	296, 368	301, 368	298, 368	298, 368	297, 365	296, 364	423	450	452	490	494	489
4e	311, 348	279sh, 310, 348	277sh, 311, 347	278sh, 310, 348	277sh, 309, 348	277sh, 308, 346	417	421	422	436	436	434
6a	330, 367	267, 286, 332	267, 285, 329	286, 330	266, 284, 323	265, 284, 329	392, 413	395, 416	394, 414	398, 420	397, 417	398, 417
6b	351, 378	261, 353, 379	260, 349, 376	300, 349, 377	298, 347, 373	299, 348, 373	394, 414	397, 418	394, 416	401, 420	399, 419	402, 420
6c	288, 355, 380	282, 356, 380	281, 352, 377	281, 353, 378	280, 349, 375	280, 353, 374	393, 412	416	418	449	454	442
6d	306, 382	265, 309, 384	264, 302, 385	302, 385	263, 303, 382	262, 300, 382	420	452	457	503	505	498
6e	313, 326, 370, 386, 411	313, 326, 369, 386, 411	312, 324, 367, 384, 408	312, 325, 386, 410	323, 382, 405	323, 381, 404	419, 444	421, 445	417, 441	422, 443	419, 439	416, 436
8a	286, 343	262, 269sh 347	268, 316sh, 342	292sh, 348	251,291sh , 347	251, 291sh, 346	405, 424	406, 426	405, 424	412, 427	410, 427	410, 427
8b	376, 396s	262, 377, 397sh	267, 374, 393sh	306, 376, 397sh	259,371, 390sh	258, 371, 390	412, 436	419, 440	414, 434	439	436	437
8c	294, 380	265,295sh 382	267, 294s, 378	295sh, 384	262, 293, 379	261, 293, 377	446	455	454	480	479	478
8d	310, 396	267sh, 314, 397	271, 309, 391	306, 393	266sh, 300, 389	265sh, 303, 389	453	479	480	511	511	504
8e	291sh, 331, 395	291sh, 331, 397	290sh, 330, 400	292sh, 331, 404	289sh, 328, 395	289sh, 328, 394	448, 475	451, 475	447, 470	473	468	468

Table 3.3 Stokes shift value of the dyes

Dye		4a	4b	4c	4d	4e	6a	6b	6c	6d	6e	8a	8b	8c	8d	8e
Stokes shift (cm^{-1})	TOL	5450	4141	3456	3533	4755	4701	1074	2043	2368	465	4463	2324	3894	3177	2995
	$CHCl_3$	5354	4246	4978	4952	4983	4931	1196	2277	3770	465	4188	2659	4200	4312	3016
	THF	5319	4205	5058	5050	5122	5014	1215	2601	4092	465	4548	2583	4429	4742	2629
	DMF	5675	4364	6547	6766	5800	5177	1587	4183	6093	465	4464	3817	5208	5876	3611
	ACN	5803	4674	7018	7154	5800	5392	1747	4640	6376	465	4428	4018	5508	6137	3949
	MeOH	5964	4736	6918	7023	5860	5269	1934	4113	6097	465	4511	4071	5605	5866	4013

Table 3.4 Solvatochromic data of the dyes

Dye	Absorption maxima, λ_{max} (nm)				Emission maxima, λ_{em} (nm)				Stokes shift (cm^{-1})			
	TEA	DBE	EA	ACT	TEA	DBE	EA	ACT	TEA	DBE	EA	ACT
4c	305, 340	304, 339	304, 340	342	392, 408	390, 406	414	439	3902	3857	5257	6461
4d	305, 368	305, 368	305, 365	368	418	421	450	478	3250	3421	5175	6253
6c	347, 375	279, 345, 375	279, 348, 375	347, 375	392, 412	392, 410	418	448	1156	1156	2743	4345
6d	304, 378	261, 301, 382	300, 382	382	418	418	454	490	2532	2255	4152	5770
8c	292, 377	293, 375	295, 376	378	437	435	450	468	3642	3678	4374	5088
8d	307, 392	306, 390	307, 389	388	445	449	475	502	3038	3369	4654	5853

3.2.3 Electrochemical Properties

The redox behavior of the dye molecules plays a vital role in the electroluminescent characteristics since it has a direct influence on the charge injection and transport in the molecular layers of OLED device. The electrochemical properties of the dyes are studied by cyclic voltammetry and differential pulse voltammetry methods. All the compounds exhibited irreversible oxidation peak while triphenylamine substituted compounds (**4d**, **6d** and **8d**) exhibited quasi-reversible oxidation peak (Figure 3.20 to Figure 3.22). The irreversible oxidation peak corresponds to the oxidation of carbazole unit [148-150]. The oxidation potential of the dyes is reflective of electron richness of the chromophores tethered to cyanocarbazole. Thus the dyes containing triphenylamine moiety exhibited very low oxidation potential in the series.

Among the series, compounds containing vinyl linker exhibited low oxidation potential compared to their acetylene and directly linked counterparts (Table 3.5). It might be due to high oxidation propensity of vinyl linked compounds which arise from effective electronic coupling of orbitals between vinyl linker and aryl segments. The low oxidation potential of **4c** is attributable to the electron richness of carbazole over fluorene. In contrast, the compound **4c** gave high oxidation potential as compared to reported compound 1,2-bis(9-ethyl-9*H*-carbazol-3-yl)ethyne due to the electron withdrawing cyano group, while lower oxidation potential compared to 1,2-bis(9-ethyl-9*H*-carbazol-2-yl)ethyne due to the different position of linkage [126]. The relatively low oxidation potential of **6b** compared to its cyanofluorene analog instead of cyanocarbazole indicates the electron richness of carbazole core [151].

The HOMO energy level of the compounds is calculated by adding 4.8 eV with oxidation potential [152]. The LUMO energy level is obtained from the difference between HOMO and optical band gap. The optical band gap is estimated from the absorption edge of the compounds, which is taken from the intersection of absorption and emission spectra recorded in dichloromethane solution. The observed HOMO and LUMO energy values (Table 3.5) are well matching with the neighboring molecular layers of OLED device which would facilitate the facile injection and transport of charge carriers. The high lying HOMO is obtained for vinyl linked compounds while low-lying LUMO is obtained for acetylene linked compounds owing to electron withdrawing nature of acetylene linker [126]. Since the compounds containing vinyl

linker possessed relatively high lying HOMO and low lying LUMO, they exhibited low band gap compared to direct and acetylene linked congeners.

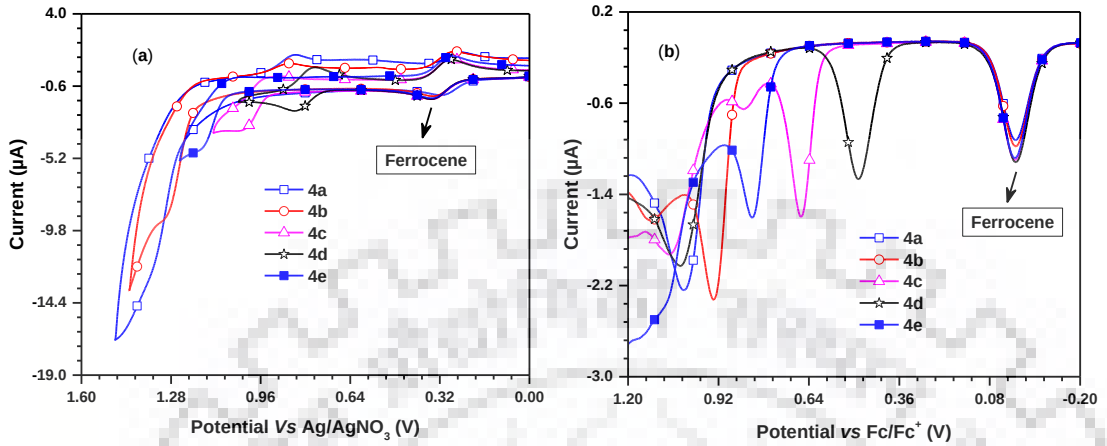

Figure 3.20 Cyclic voltammograms (a) and differential pulse voltammograms (b) of the directly connected compounds recorded in dichloromethane.

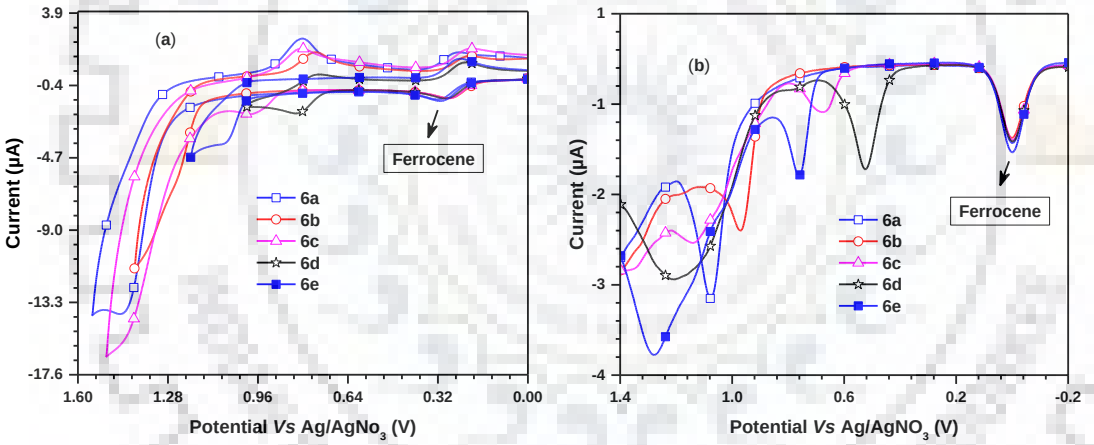

Figure 3.21 Cyclic voltammograms (a) and differential pulse voltammograms (b) of the acetylene linked compounds recorded in dichloromethane.

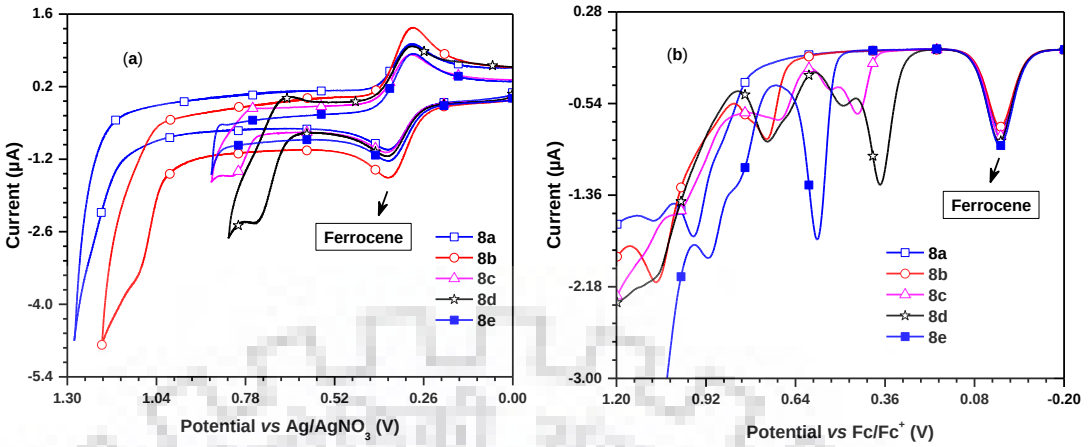

Figure 3.22 Cyclic voltammograms (a) and differential pulse voltammograms (b) of the vinyl linked compounds recorded in dichloromethane.

3.2.4 Thermal Properties

The thermal stability of the compounds was evaluated by thermo gravimetric analysis (TGA) recorded at the heating rate of 10 °C/min under nitrogen atmosphere. The thermogram is displayed in Figure 3.23. All the compounds exhibited high onset temperature (>330 °C) corresponding to 10% weight loss and high decomposition temperature in the range of 406-710 °C (Table 3.5). The high thermal stability of the compounds is attributed to rigid nature of carbazole unit present in each molecule. It is well documented that carbazole based materials exhibit high thermal decomposition temperature ascribed to the rigidity and robust nature of carbazole unit [153, 16]. The fluorene acetylene compound **6b** has shown appreciable increment in the decomposition temperature as compared to its cyanofluorene counterpart instead of cyanocarbazole reported in the literature. The high onset temperature of 411 °C is observed for triphenylamine derivative **8d** which stems from the non-planar nature of triphenylamine moiety in raising thermal stability [154]. The high decomposition temperature of acetylene compounds over other analogous compounds might arise from the restriction intramolecular rotation of acetylene linker which leads to better π-π stacking and thus high thermal stability.

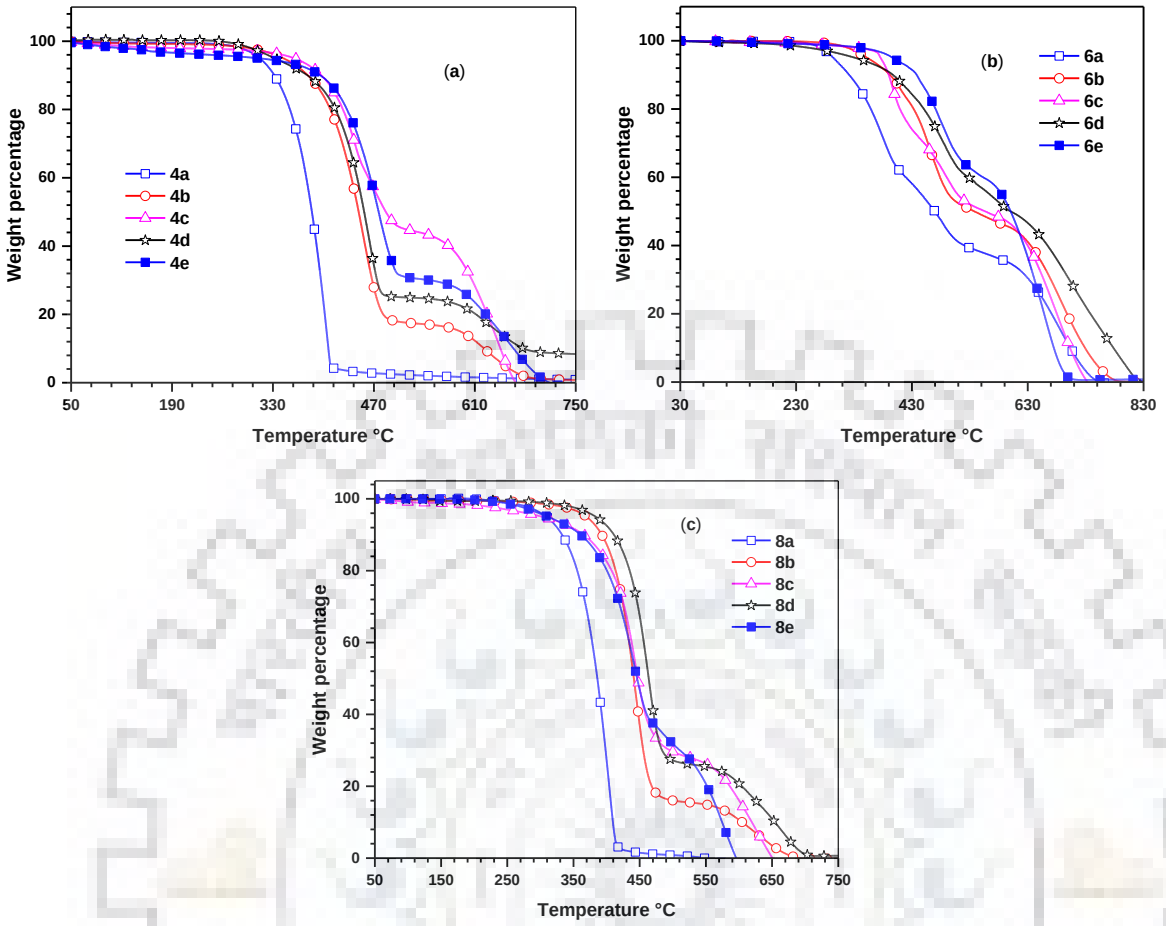

Figure 3.23 TGA plot of (a) direct, (b) acetylene and (c) vinyl linked compounds under nitrogen atmosphere.

Table 3.5 Thermal and electrochemical properties of the dyes

Dye	T_{onset}[a], ° C	T_d, ° C	E_{ox}[b], V	HOMO[c],eV	LUMO[d], eV	$E_{0\text{-}0}$[e], eV
4a	331	406	1.02	-5.82	-2.53	3.29
4b	378	627	0.93	-5.73	-2.48	3.25
4c	397	640	0.66	-5.46	-2.25	3.21
4d	378	632	0.49	-5.37	-2.35	3.02
4e	396	655	0.82	-5.62	-2.44	3.18
6a	322	686	1.08	-5.88	-2.64	3.24
6b	392	690	0.97	-5.77	-2.56	3.21
6c	390	680	0.68	-5.48	-2.32	3.16
6d	397	710	0.52	-5.32	-2.37	2.96
6e	436	652	0.76	-5.56	-2.56	3.00
8a	332	407	0.96	-5.76	-2.59	3.17
8b	393	446	0.73	-5.53	-2.47	3.06
8c	365	629	0.45	-5.25	-2.30	2.95
8d	411	464	0.38	-5.18	-2.39	2.79
8e	361	573	0.57	-5.37	-2.53	2.84

[a] Temperature corresponding to 10% weight loss. [b] Oxidation potential quoted reference to ferrocene internal standard. [c] HOMO= -(4.8 + E_{ox}). [d] LUMO = HOMO + $E_{0\text{-}0}$. [e] Optical band gap obtained from the intersection of normalized absorption and emission spectra (optical edge).

3.2.5 Theoretical Investigations

To get insight into the electronic structure and photophysical properties of the compounds, we have performed density functional theoretical calculations. The geometry of the molecules were optimized using B3LYP functional and using 6-31G(d,p) basis set [155,156]. The alkyl chains were approximated to methyl to reduce the cost of computational time. The approximation of alkyl chains to methyl may not affect the electronic properties of modeled compounds significantly. The trend of most probable longer wavelength absorption maxima matches well with the experimental data (Table 3.6 to Table 3.8). Furthermore, the oscillator strength corresponding to the HOMO to LUMO excitation of the compounds followed the trend of experimental molar extinction coefficients. The HOMO of **4a** is delocalized over carbazole unit and there is no contribution from phenyl unit because the phenyl ring is out of plane to cyanocarbazole unit. In contrast, the HOMO is concentrated over pyrene for **4e**. The LUMO is diffused over the entire molecule. The HOMO energy level of fluorene substituted dye **4b** is spread over the entire molecule which is the characteristics of π-π* transition. For **4c** and **4d**, HOMO is mainly concentrated over linker carbazole and triphenylamine moiety respectively and slightly extended up to cyanocarbazole moiety. The LUMO of these dyes is mainly

localized on cyanocarbazole unit (Figure 3.24). This indicates the charge transfer from carbazole/triphenylamine to cyanocarbazole moiety during electronic excitation [157-159]. It is evident that the LUMO of the phenyl substituted compounds (phenyl) is low lying because their LUMO orbitals are delocalized over more space compared to other compounds [160].

Likewise, the compounds containing acetylene and vinyl linker also exhibited characteristic π-π* transition for phenyl, fluorene and pyrene substituted compounds (Figure 3.25 and Figure 3.26). Carbazole and triphenylamine substituted compounds displayed intramolecular charge transfer transition arising from HOMO to LUMO electronic excitation. Interestingly, the HOMO of **4a** and **4e** are constituted by carbazole alone while its acetylene and vinyl congeners displayed the HOMO spreading over entire molecule. It might be due to planar nature of acetylene and vinyl linkers. It is characteristic of π-π* transition. The absorption maxima of computed data of each set followed the trend of experimental results. Further, the compounds containing acetylene and vinyl linker exhibited red shifted absorption maximum compared to directly connected compounds in keeping with experimental results.

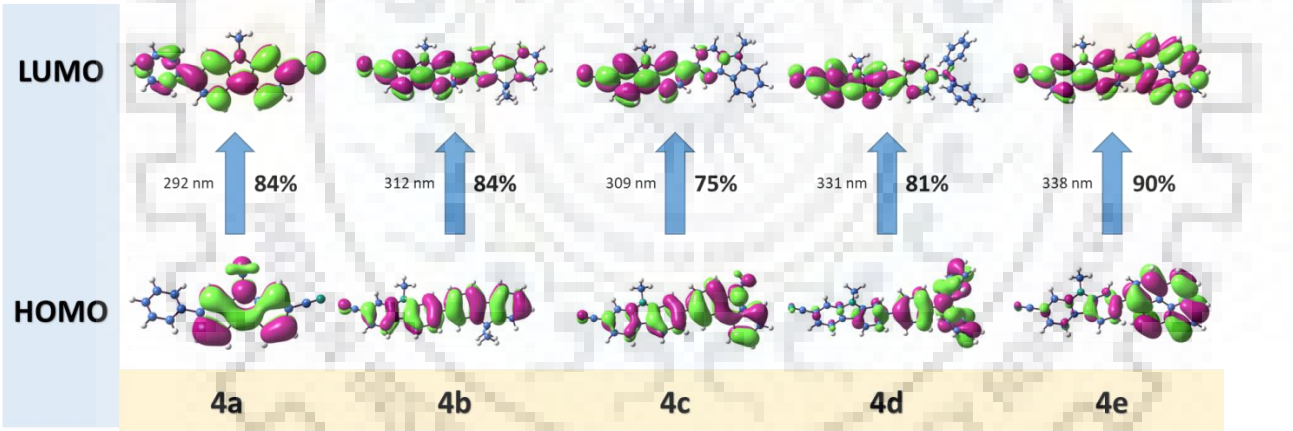

Figure 3.24 Frontier molecular orbital diagrams of the directly connected compounds (**4a-4e**).

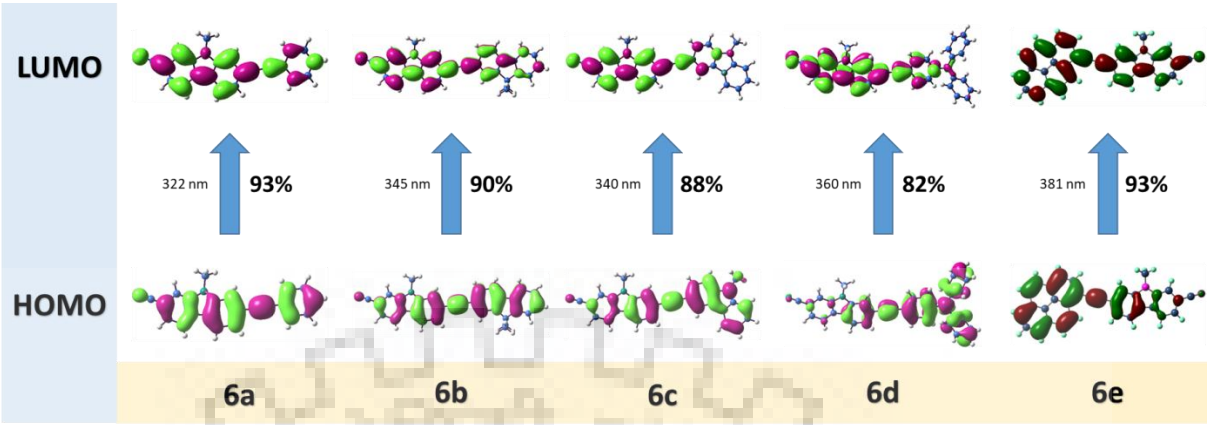

Figure 3.25 Frontier molecular orbital diagrams of the dyes containing acetylene spacer (**6a-6e**).

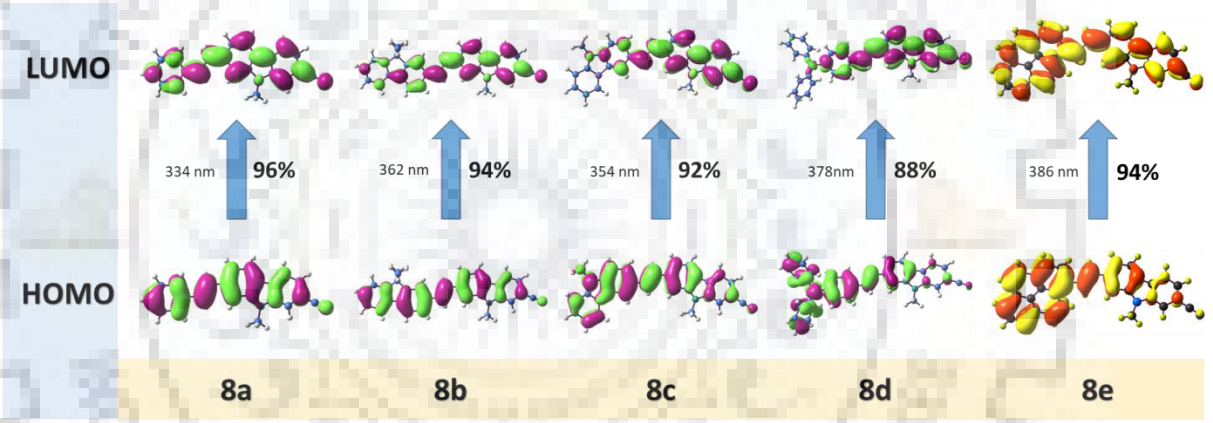

Figure 3.26 Frontier molecular orbital diagrams of the dyes containing vinyl spacer (**8a-8e**).

Table 3.6 Predicted vertical excitation obtained by B3LYP/6-31G (d,p) method for the directly connected dyes **4a-4e**

Dye	λ_{max} (nm)	*f*	Assignment
4a	292	0.8711	HOMO→LUMO (84%)
4b	312	1.4192	HOMO→LUMO (84%)
4c	251	0.1600	HOMO-2→LUMO (48%), HOMO-2→LUMO+1 (27%)
	266	0.1905	HOMO-2→LUMO+1 (41%), HOMO-2→LUMO (24%), HOMO-3→LUMO (14%)
	304	0.1423	HOMO-1→LUMO (81%)
	309	1.0209	HOMO→LUMO (75%)
4d	261	0.2899	HOMO→LUMO+1 (56%), HOMO-2→LUMO (17%), HOMO→LUMO (16%)
	271	0.2465	HOMO→LUMO+3 (92%)
	331	1.1728	HOMO→LUMO (81%)
4e	251	0.3162	HOMO→LUMO+2 (37%), HOMO-3→LUMO (32%)
	273	0.2645	HOMO-2→LUMO (47%), HOMO-3→LUMO (14%), HOMO→LUMO+1 (14%)
	290	0.1871	HOMO→LUMO+1 (70%), HOMO-2→LUMO (13%)
	338	0.9456	HOMO→LUMO (90%)

Table 3.7 Predicted vertical excitation obtained by B3LYP/6-31G (d,p) method for the acetylene linker dyes **6a-6e**

Dye	λ_{max} (nm)	*f*	Assignment
6a	254	0.1418	HOMO→LUMO+1 (41%), HOMO-2→LUMO (31%)
	322	1.5002	HOMO→LUMO (93%)
6b	229	0.1116	HOMO→LUMO+3 (22%), HOMO-1→LUMO+1 (18%), HOMO-6→LUMO (14%)
	345	2.0868	HOMO→LUMO (90%)
6c	250	0.4807	HOMO→LUMO+2 (22%), HOMO-3→LUMO (14%), HOMO-2→LUMO+1 (13%), HOMO-1→LUMO+1 (11%), HOMO-2→LUMO (10%), HOMO→LUMO+1 (10%)
	257	0.1822	HOMO-3→LUMO (28%), HOMO→LUMO+2 (13%), HOMO-1→LUMO (12%), HOMO-2→LUMO (10%)
	340	1.8056	HOMO→LUMO (88%)
6d	271	0.2283	HOMO→LUMO+3 (87%)
	273	0.2482	HOMO→LUMO+1 (58%), HOMO-1→LUMO (19%), HOMO→LUMO (14%)
	360	1.8568	HOMO→LUMO (82%)
6e	262	0.3640	HOMO→LUMO+2 (30%), HOMO-3→LUMO (22%), HOMO-2→LUMO+1 (16%)
	301	0.4208	HOMO→LUMO+1 (53%), HOMO-2→LUMO (32%)
	381	1.9439	HOMO→LUMO (93%)

Table 3.8 Predicted vertical excitation obtained by B3LYP/6-31G (d,p) method for the vinyl linker dyes **8a**-**8e**

Dye	λ_{max} (nm)	*f*	Assignment
8a	258	0.1506	HOMO→LUMO+1 (46%), HOMO-2→LUMO (29%)
	334	1.4892	HOMO→LUMO (96%)
8b	362	2.0171	HOMO→LUMO (94%)
8c	254	0.7744	HOMO-2→LUMO+1 (38%), HOMO→LUMO+2 (25%)
	354	1.7526	HOMO→LUMO (92%)
8d	273	0.2306	HOMO→LUMO+3 (86%)
	277	0.2090	HOMO→LUMO+1 (64%)
	295	0.1144	HOMO-1→LUMO (76%), HOMO→LUMO+1 (12%)
	378	1.8079	HOMO→LUMO (88%)
8e	264	0.1142	HOMO→LUMO+2 (32%), HOMO-3→LUMO (19%), HOMO→LUMO+5 (11%), HOMO-2→LUMO+1 (10%)
	293	0.1109	HOMO-2→LUMO (43%), HOMO-3→LUMO (17%), HOMO→LUMO+1 (16%)
	306	0.3337	HOMO→LUMO+1 (61%), HOMO-2→LUMO (24%)
	386	1.5666	HOMO→LUMO (94%)

3.2.6 Electroluminescence Properties

The electroluminescent properties of the dyes were examined by employing them as emitters in doped OLEDs having the configuration of ITO/PEDOT:PSS/CBP:dye(**4a-4e)**/TPBi/LiF/Al, in which ITO (Indium tin oxide) served as anode, PEDOT:PSS (Polyethylenedioxythiophene/ polystyrenesulfonate) as hole injecting layer, CBP (*N,N'*-dicarbazolyl-4,4'-biphenyl) as host, TBPi (1,3,5-tris(*N*-phenylbenzimidazol-2-yl)benzene) as electron transporting or hole blocking layer, LiF as an electron injecting layer and Al as cathode.

Firstly, the representative non-doped device was fabricated with **4c** which gave poor electroluminescence characteristics with broad and bathochromically shifted electroluminescence emission as compared to the photoluminescence spectrum recorded in toluene (Figure 3.32). The formation of aggregation of the dye in thin film could have resulted in poor thin film morphology and failure of the non-doped device [161-163]. Since the non-doped device exhibited poor electroluminescence performance ascribed to aggregation caused emission quenching and improper charge carrier movement, we turned our focus on doped device to improve the device performance by doping the dyes into CBP host. In the doped device, the luminance is substantially increased and electroluminescence emission spectra

restored to the pattern of photoluminescence spectra recorded in toluene solution. This clearly points out that the aggregation of dyes in CBP host is drastically controlled by dilution effect [164-166]. Further the performance of doped devices is optimized by varying the dopant concentration. The best electroluminescence performance was obtained for the devices fabricated with 3 wt% of dopants. At 1 wt% concentration, the devices exhibited poor performance due to more dilution and less number of dopants harvesting excitons whereas high concentration leads to the beginning of aggregation of dyes and concentration quenching of emission which eventually reduce the performance.

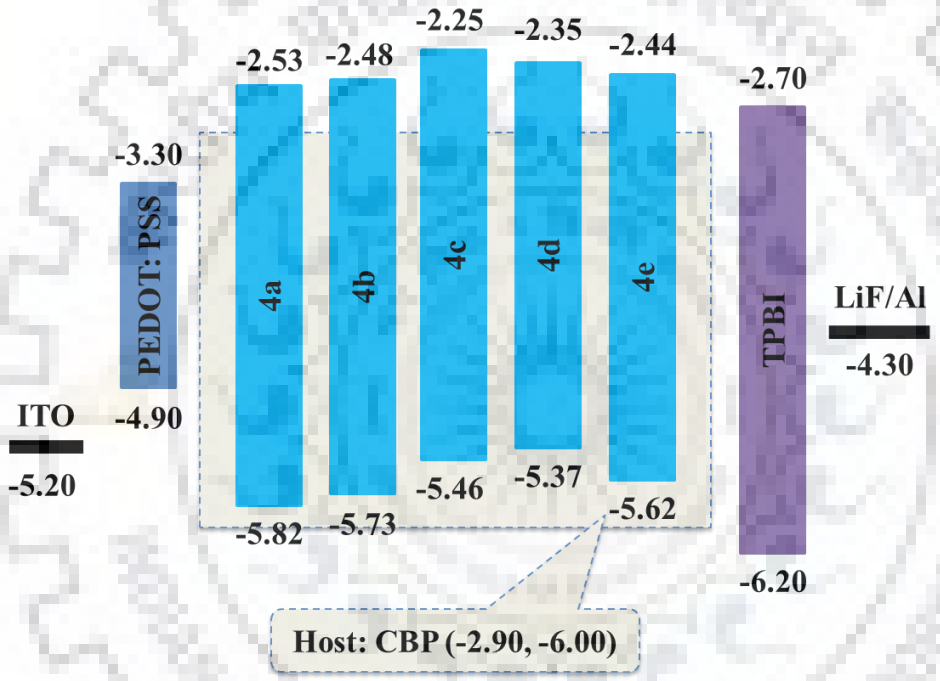

Figure 3.27 Energy level diagram of OLED device fabricated with the emitters (**4a**-**4e**).

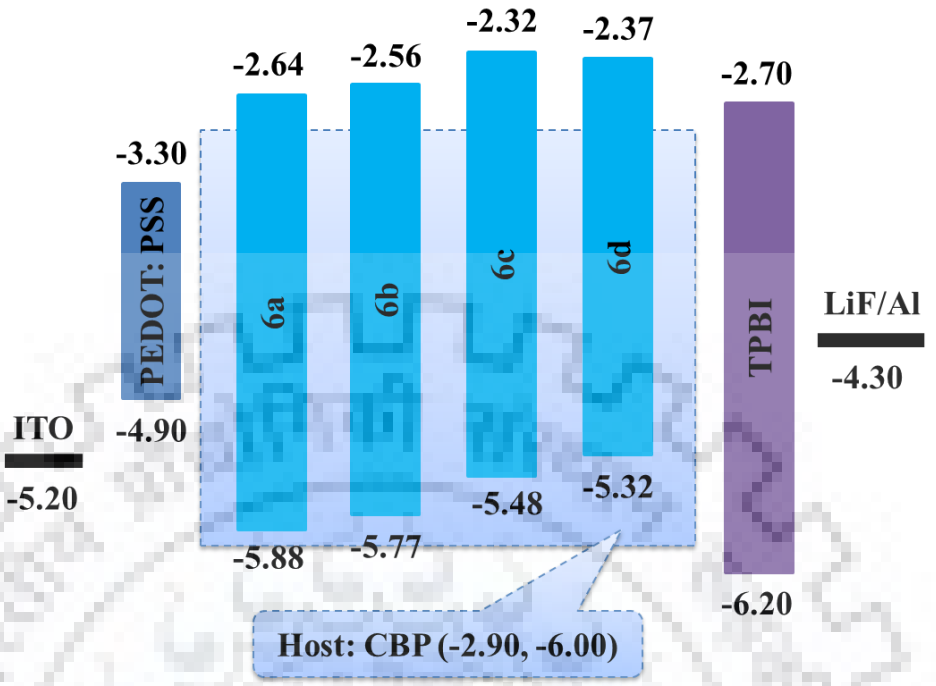

Figure 3.28 Energy level diagram of OLED device fabricated with the acetylene linked dyes (**6a-6d**).

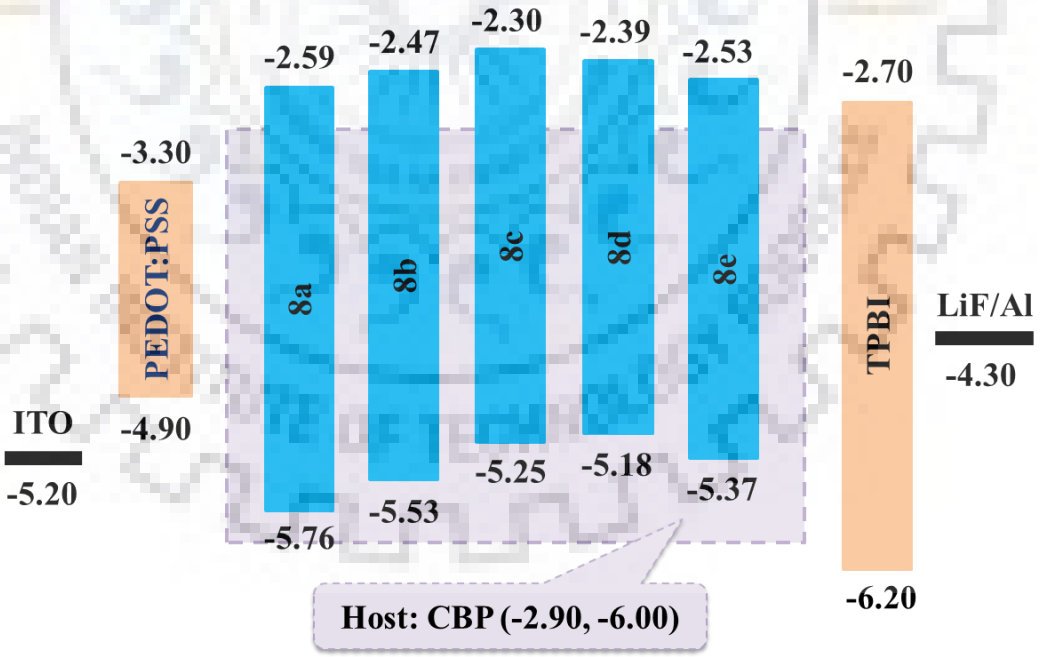

Figure 3.29 Energy level diagram of OLED device fabricated with the vinyl linked dyes (**8a-8e**).

Though the energy barrier for the injection of holes and electrons is little higher for these directly connected dyes compared to acetylene based dyes, these directly connected dyes exhibited superior performance. It could be due to the suppression of aggregation by twisted conformation of these dyes. The high color purity of the doped devices employing these emitters is attributed to narrow full width half maxima (FWHM) of the electroluminescence spectra (Table 3.9). It indicates that the proper dispersion of dopant into the host material and the suppression of aggregation in thin films. The resemblance of EL spectra of the doped devices with PL spectra indicates the origin of emission occurring completely from the dopant molecules and the control of aggregation drastically. The absence of emission from CBP even at low dopant concentrations suggests the effective energy transfer from host to the dopants [167].

The high current efficiency of the doped device containing **4d** is attributed to favorable energy level alignment of dye with hole and electron injection layers which facilitate better charge flow into emissive layers and effective confinement of excitons (Figure 3.27). The best electroluminescence performance is obtained for the device containing **4d** (3 wt%) with power efficiency of 1.3 lm/W, current efficiency of 2.0 cd/A, luminance of 1758 cd/m^2 and external quantum efficiency of 4.1% (Table 3.9). The high EQE of the dye **4d** could be attributed to high photoluminescence quantum yield, suitable energy barrier for balanced transport of charges and effective suppression of aggregation by twist structure of triphenylamine unit.

When we compare electroluminescence performance of directly connected dyes with the acetylene congeners, the former gave better performances. In acetylene based compounds, a non-doped device was fabricated with **6d** which gave high current density but low luminance with broad and bathochromically shifted electroluminescence emission as compared to the photoluminescence spectrum recorded in toluene (Figure 3.37 and Table 3.10). The formation of aggregation of the dye in thin film could have induced crystalline nature in thin film and resulted in poor performance. The doped devices were employed to improve device performance. The relatively low turn on voltage for the doped devices fabricated with the dopant **6d** is due to the high lying HOMO and low lying LUMO energy level which ensures the effective charge transport from the adjacent hole transporting and electron transporting layer, respectively (Figure 3.27). It is further attested by the high luminance, high current efficiency and power efficiency observed for the dye **6d** which confirms the balanced charge transport and confinement of excitons within the emissive layer. The highest luminance is observed for the

device containing **6d**. It is probably due to the high quantum yield and favorable alignment of HOMO and LUMO energy levels with the neighboring charge transporting layers.

In the third set of compounds which contain vinyl linker, the compound **8d** possessed high lying HOMO which is beneficial for facile transfer of hole carriers (Figure 3.28). The non-doped device exhibited high current density but low luminance with broad and red shifted electroluminescence spectrum compared to photoluminescence recorded in toluene. The high current density might be due to the hole only charge carrier leakage at cathode. Though the device possessed almost similar energy barrier for both hole and electron injection, the injection of hole carrier was facile due to downhill process over electron injection into emitter. Therefore, the injected hole carriers might have reached cathode before recombination occurs in emissive layer. Thus, the low luminance is observed. In the doped devices, the electroluminescence spectrum is resumed to photoluminescence spectrum recorded in toluene. It indicates the alleviation of aggregation due to dilution effect of emitter in CBP host. The origin of electroluminescence is from the emitting dopant which is approved by the absence of CBP host characteristic emission at around 400 nm.

The attractive electroluminescent properties of **8e** among other vinyl linker compounds in the doped device is due to proper energy level of **8e** with CBP host which ensures complete energy transfer from host to dopant (Table 3.11). The appropriate energy barrier prevents the back energy transfer from guest to host. The turn-on voltage of the non-doped device is very high whereas the doped device is drastically reduced. The low turn-on voltage and high power efficiency for the devices fabricated with **8e** is ascribed to low energy barrier for the transportation of charge carriers and effective harvesting of excitons. The balanced charge transport in **8e** is responsible for the high current efficiency observed among the series of dyes.

The turn-on voltage of doped devices containing **8d** is high compared to other compounds within the series (Table 3.11). It is ascribed to the high energy barrier for the transfer of holes from host to the dopant. Due to the non-planar structure of triphenylamine, molecular aggregation and the formation of aggregates are greatly reduced in thin film. As a result, **8d** exhibited increased efficiency as compared to rigid and planar carbazole substituted dye **8c**. The high performance can be attributed to high quantum yield, relatively low energy barrier for electron charge carrier transfer. The relatively poor performance of the devices containing **8b** and **8c** is due to the unfavorable alignment of HOMO and LUMO that hinders the balanced

charge transport. A shoulder peak in EL spectrum at 400 nm is observed for doped device fabricated with **8c** which is due to the residual emission of CBP host. It indicates the incomplete energy transfer from CBP host to the dopant **8c** and thus poor performance [168]. The best electroluminescence performance is observed for the dye **8e** doped in 3 wt% with the power efficiency of 4.3 lm/W, current efficiency of 6.5 cd/A, EQE of 3.3% and maximum luminance of 5701 cd/m^2 (Table 3.11). Also, the small efficiency roll-off is observed for **8e** at high brightness of 1000 cd/m^2. The high performance of **8e** based devices could be attributed to high quantum yield, high coplanarity of emitter which results in effective conjugation to provide high current density and brightness in the device. Generally, coplanarity induces quenching of emission in EL device. But, when **8e** is doped in CBP host aggregation is drastically reduced, so the high current density and brightness is observed. It is interesting to compare the performance of **8a** with **8d** which possess appended diphenylamine. The power and current efficiency of **8d** is increased drastically. It is due to balanced transportation of charge carriers into emitters and their effective confinement.

All the dyes except **4a** in the doped devices exhibited deep blue emission with CIE coordinates of $0.15<x<0.17$, $0.08<y<0.04$ which are agreeing well with deep blue emission (0.14, 0.08) prescribed by National Television System Committee (NTSC 1987). The high color purity of the doped devices employing these emitters is attributed to narrow full width half maxima (FWHM) of the electroluminescence spectra which is almost similar to PL spectra recorded in toluene (Table 3.9 to Table 3.11). It indicates that the proper dispersion of dopant into the host material and the suppression of aggregation in thin films. The resemblance of EL spectra of the doped devices with PL spectra indicates the origin of emission occurring completely from the dopant molecules and the control of aggregation drastically. The absence of emission from CBP host even at low dopant concentrations suggests the effective energy transfer from host to the dopants except **8c**.

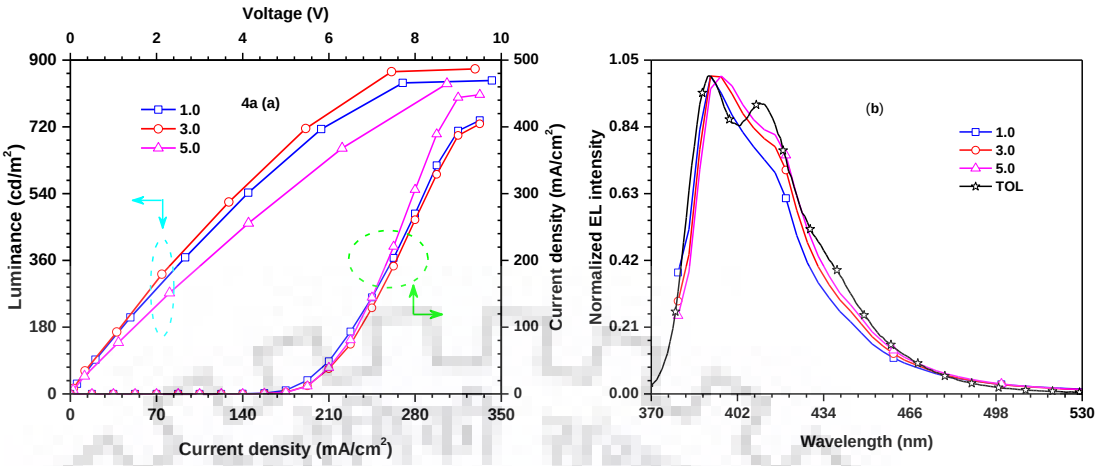

Figure 3.30 J-V-L characteristics and EL spectra of the dye **4a**.

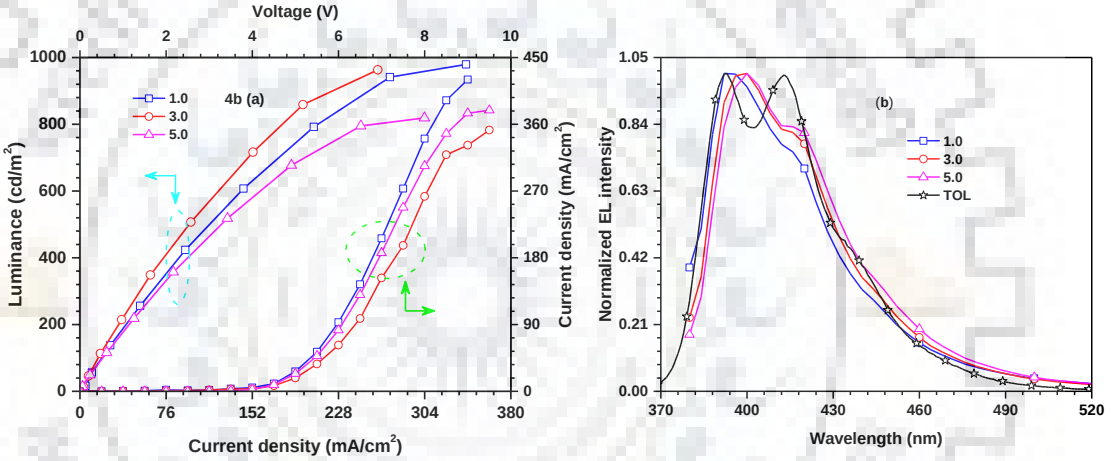

Figure 3.31 J-V-L characteristics and EL spectra of the dye **4b**.

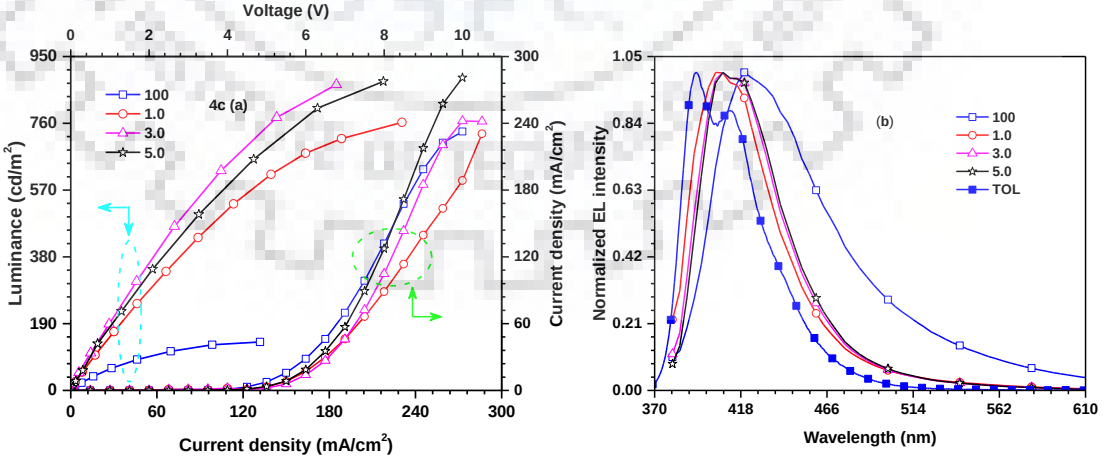

Figure 3.32 J-V-L characteristics and EL spectra of the dye **4c**.

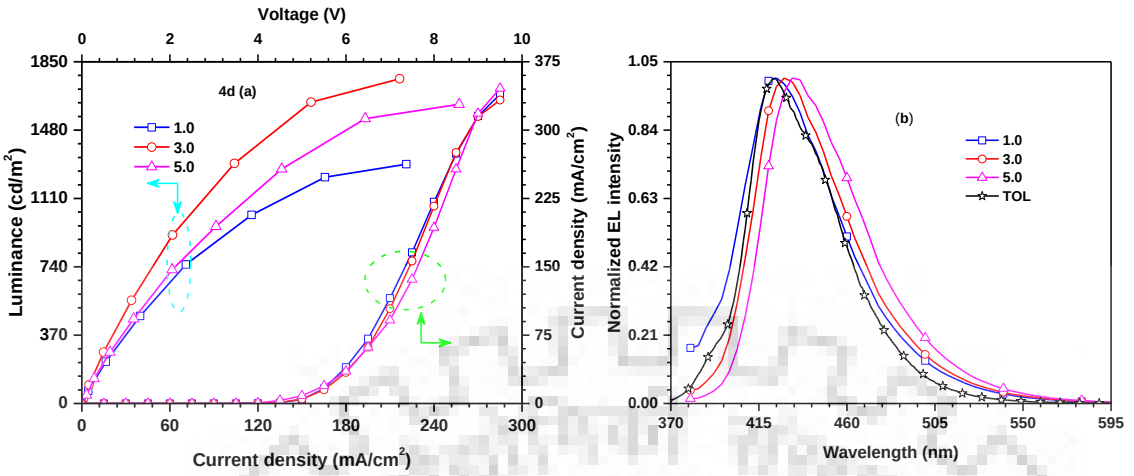

Figure 3.33 J-V-L characteristics and EL spectra of the dye **4d**.

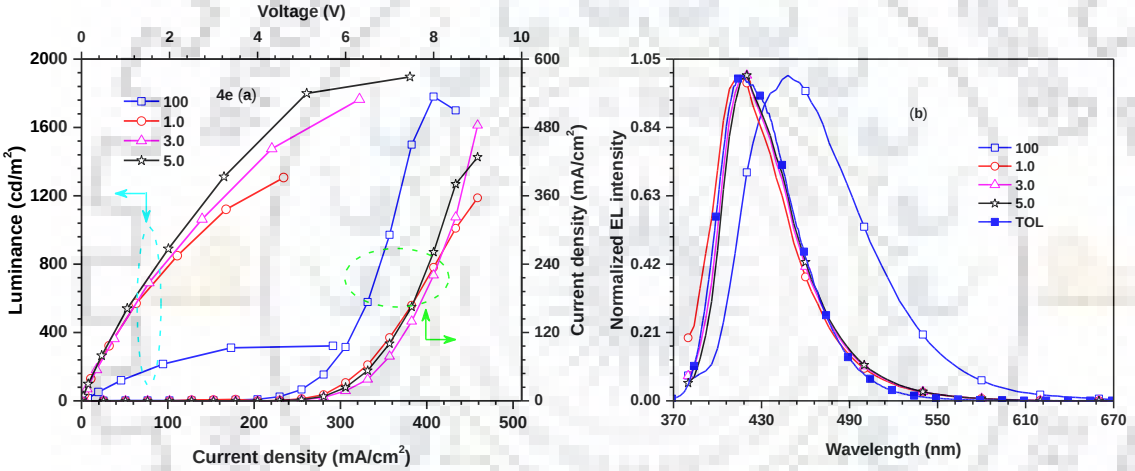

Figure 3.34 J-V-L characteristics and EL spectra of the dye **4e**.

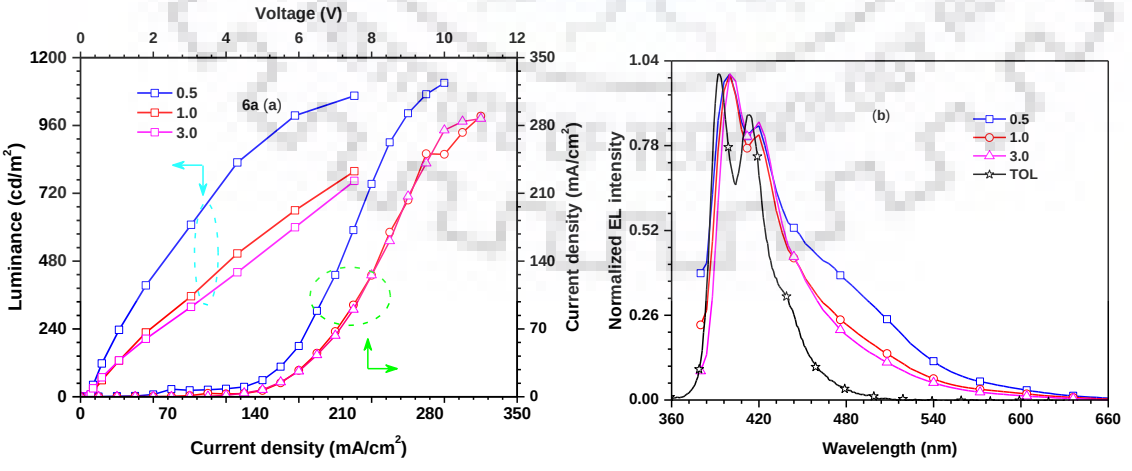

Figure 3.35 J-V-L characteristics and EL spectra of the dye **6a**.

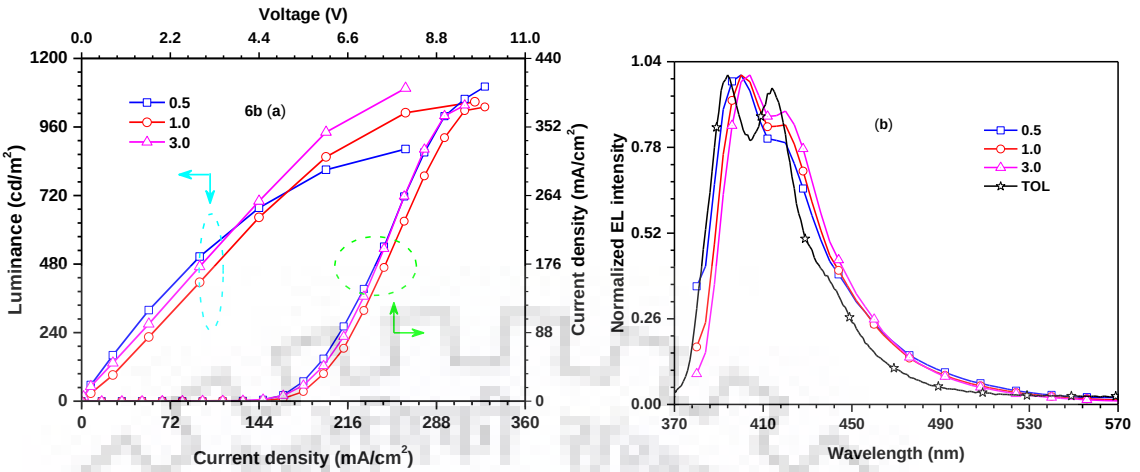

Figure 3.36 J-V-L characteristics and EL spectra of the dye **6b**.

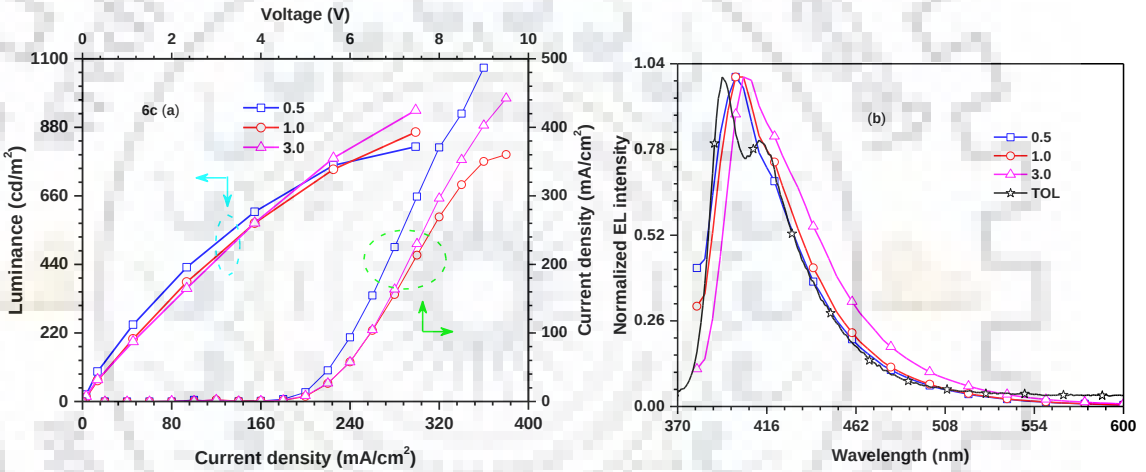

Figure 3.37 J-V-L characteristics and EL spectra of the dye **6c**.

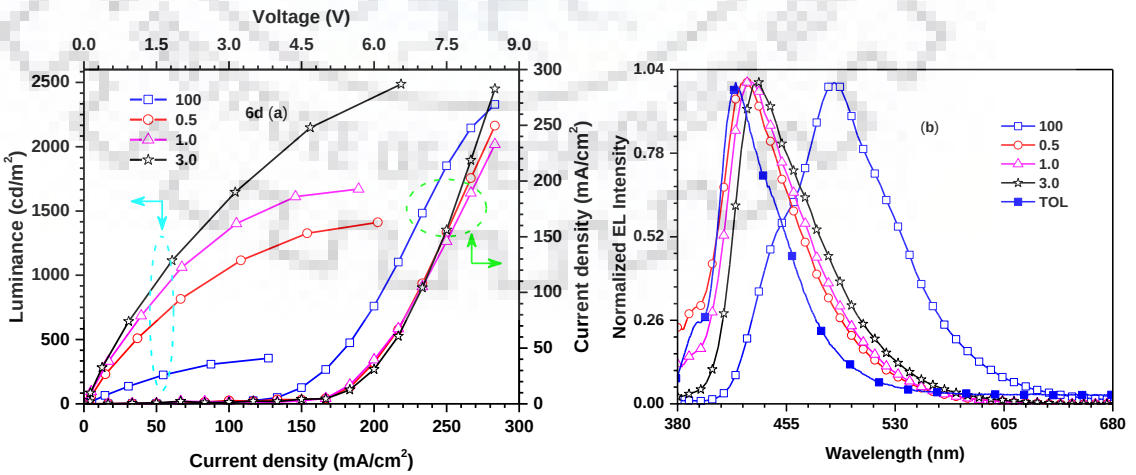

Figure 3.38 J-V-L characteristics and EL spectra of the dye **6d**.

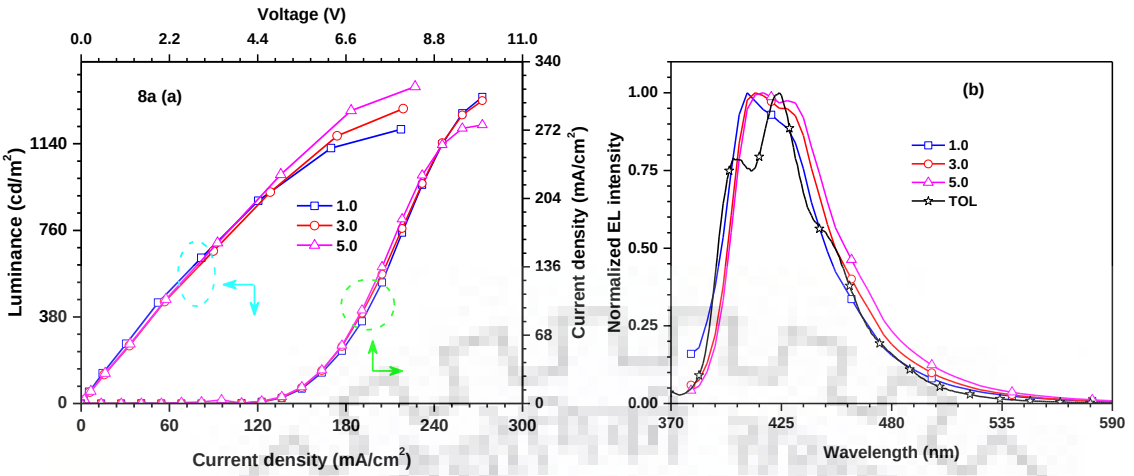

Figure 3.39 J-V-L characteristics and EL spectra of the dye **8a**.

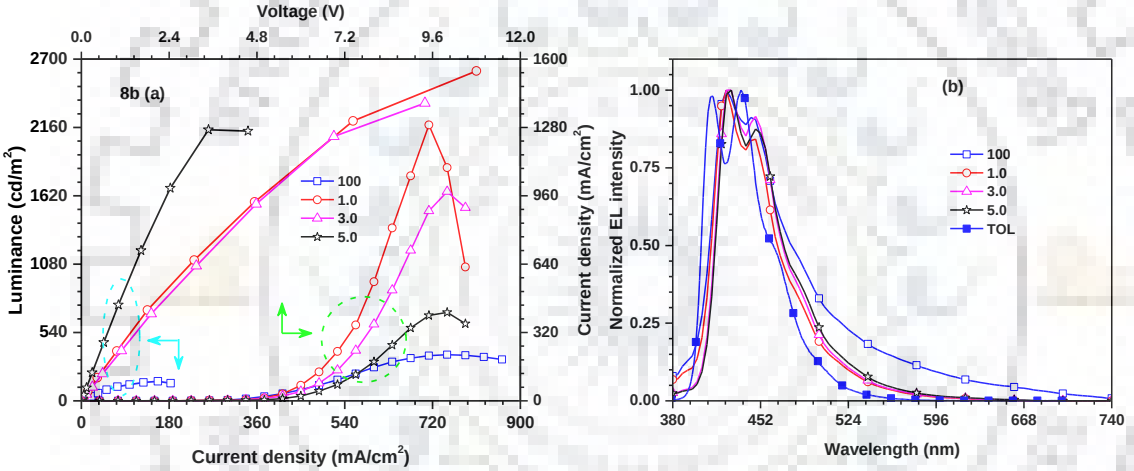

Figure 3.40 J-V-L characteristics and EL spectra of the dye **8b**.

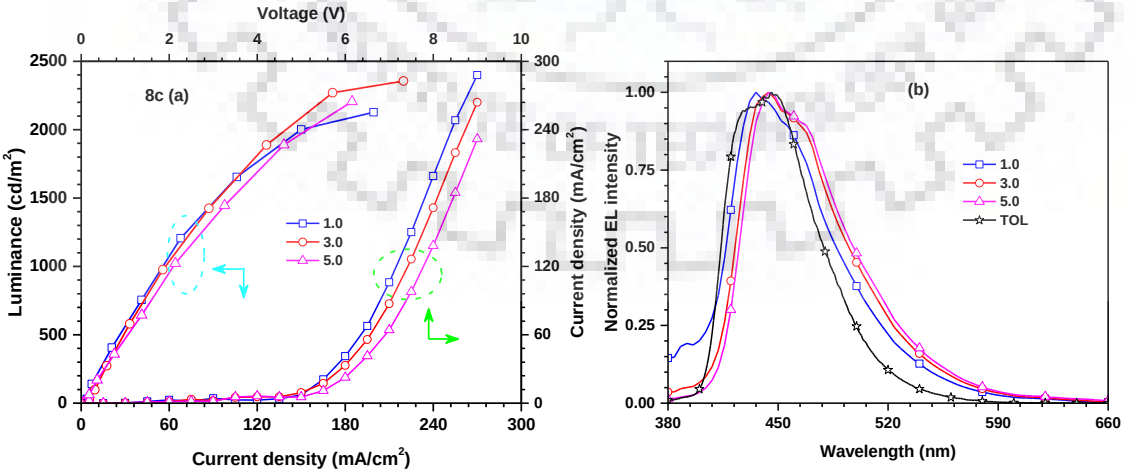

Figure 3.41 J-V-L characteristics and EL spectra of the dye **8c**.

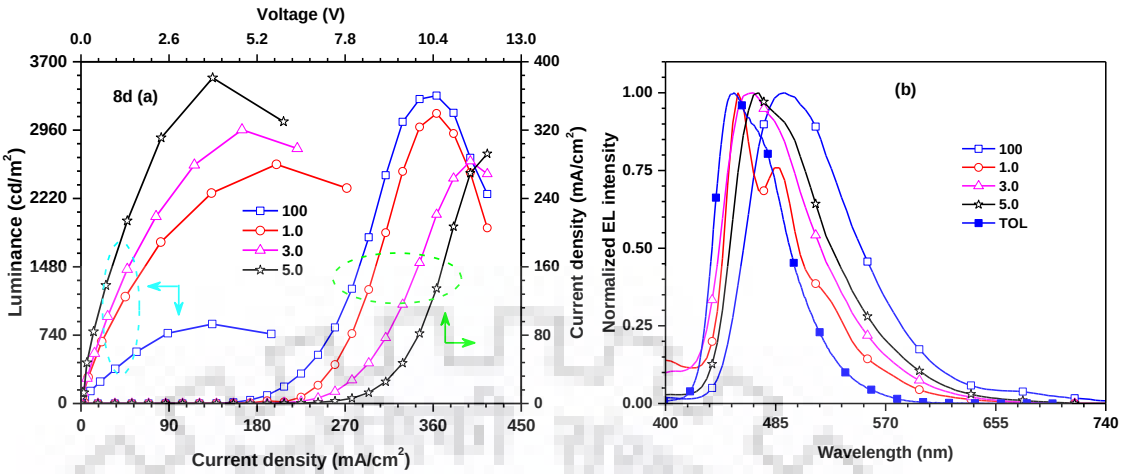

Figure 3.42 J-V-L characteristics and EL spectra of the dye **8d**.

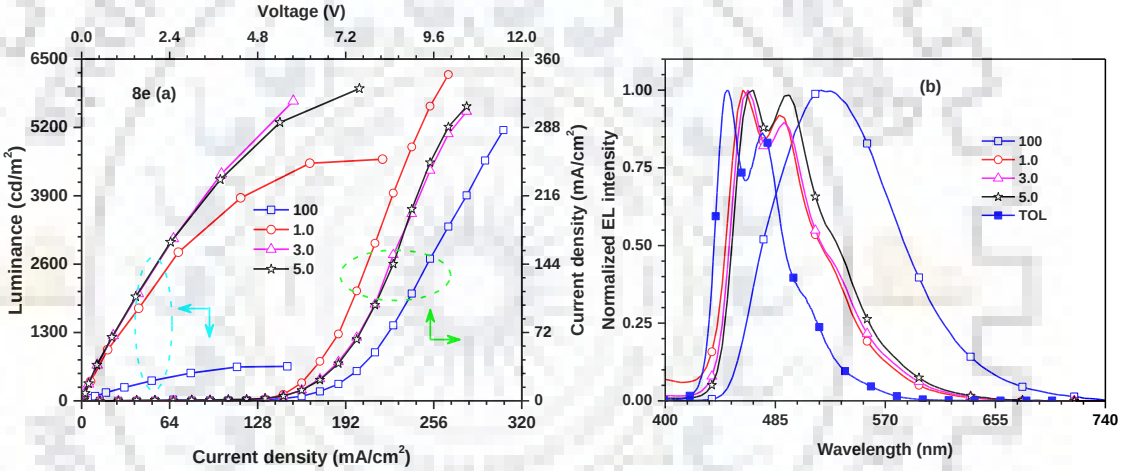

Figure 3.43 J-V-L characteristics and EL spectra of the dye **8e**.

Table 3.9 Electroluminescent properties of the dyes (**4a-4e**) [a]

Dye	wt %	Turn-on voltage (V)	Power efficiency (lm/w)	Current efficiency (cd/A)	EQE (%)	CIE (x,y)	Maximum luminance (cd/m^2)	λ_{EL} (nm)	FWHM (nm)
4a	1.0	5.5	0.3	0.4	2.6	(0.16, 0.05)	845	392	54
	3.0	5.7	0.3	0.5	2.8	(0.16, 0.05)	876	396	52
	5.0	5.8	0.2	0.4	2.1	(0.16, 0.04)	837	396	51
4b	1.0	4.8	0.3	0.5	2.4	(0.16, 0.05)	979	392	58
	3.0	4.9	0.4	0.6	3.0	(0.16, 0.04)	963	400	54
	5.0	4.9	0.3	0.5	2.3	(0.16, 0.04)	819	400	55
4c	1.0	6.0	0.3	0.6	2.0	(0.16, 0.06)	763	404	57
	3.0	5.9	0.4	0.8	2.6	(0.16, 0.05)	870	408	55
	5.0	5.8	0.4	0.7	2.2	(0.16, 0.05)	879	408	54
4d	1.0	5.1	0.9	1.5	3.6	(0.15, 0.05)	1296	424	64
	3.0	5.0	1.3	2.0	4.1	(0.15, 0.06)	1758	428	58
	5.0	4.8	1.0	1.5	2.4	(0.15, 0.07)	1620	432	60
4e	1.0	5.3	0.7	1.1	3.1	(0.16, 0.05)	1307	416	64
	3.0	5.6	0.6	1.1	2.7	(0.16, 0.05)	1765	420	59
	5.0	5.5	0.7	1.3	3.0	(0.16, 0.06)	1896	420	58

[a] values at 100 cd/m^2

Table 3.10 Electroluminescent properties of the dyes (**6a**-**6d**) [a]

Dye	wt %	Turn-on voltage (V)	Power efficiency (lm/w)	Current efficiency (cd/A)	EQE (%)	CIE (x,y)	Maximum luminance (cd/m^2)	λ_{EL} (nm)	FWHM (nm)
6a	0.5	4.9	0.4	0.6	0.8	(0.17, 0.14)	1065	400, 420	141
	1.0	5.3	0.5	0.9	1.5	(0.17, 0.11)	1006	400, 420	76
	3.0	5.3	0.5	0.9	1.7	(0.17, 0.09)	975	400, 420	60
6b	0.5	5.2	0.4	0.7	2.0	(0.17,0.07)	883	400, 418	66
	1.0	5.5	0.4	0.7	2.1	(0.16,0.06)	1048	400, 420	58
	3.0	5.3	0.4	0.7	2.2	(0.16,0.05)	1096	404, 420	55
6c	0.5	5.0	0.4	0.7	2.5	(0.16, 0.06)	818	400	64
	1.0	5.1	0.5	0.9	2.9	(0.16, 0.06)	889	404	60
	3.0	5.1	0.5	0.8	1.9	(0.16, 0.07)	935	404	61
6d	0.5	5.1	0.8	1.3	2.1	(0.16, 0.08)	1411	428	73
	1.0	5.0	1.2	1.9	2.8	(0.15, 0.08)	1671	432	69
	3.0	5.0	1.2	1.9	2.2	(0.15, 0.10)	2487	436	68

[a] values at 100 cd/m^2

Table 3.11 Electroluminescent properties of the dyes (**8a**-**8e**) [a]

Dye	wt%	Turn-on voltage (V)	Power Efficiency (lm/w)	Current Efficiency (cd/A)	EQE (%)	CIE (x,y)	Maximum Luminance (cd/m^2)	λ_{EL} (nm)	FWHM (nm)
8a	1.0	5.3/ 7.7	0.5/ 0.3	0.9/ 0.7	2.8/ -	(0.16, 0.05) / -	1203	408	57
	3.0	5.3/ 7.6	0.5/ 0.3	0.8/ 0.7	2.2/ -	(0.16, 0.05) / -	1294	412	56
	5.0	5.3/ 7.5	0.5/ 0.3	0.8/ 0.7	1.9/ -	(0.16, 0.06) / -	1391	416	58
8b	1.0	5.1/ 6.9	0.3/ 0.2	0.5/ 0.5	0.8/ 0.9	(0.16, 0.08) / -	2606	424, 448	63
	3.0	5.4/ 7.4	0.3/ 0.2	0.5/ 0.5	0.7/ 0.7	(0.16, 0.08) / -	2352	424, 448	60
	5.0	5.1/ 7.2	0.6/ 0.4	1.0/ 1.0	1.4/ 1.3	(0.16, 0.09) / -	2142	428, 448	62
8c	1.0	4.8/ 6.3	1.0/ 0.9	1.5/ 1.8	1.5/ 2.0	(0.16, 0.12)/ (0.16, 0.12)	2128	436	78
	3.0	5.0/ 6.5	0.7/ 0.8	1.1/ 1.7	0.9/ 1.6	(0.16, 0.14)/ (0.16, 0.13)	2356	444	75
	5.0	5.2/ 7.0	0.8/ 0.7	1.3/ 1.6	1.1/ 1.4	(0.16, 0.15)/ (0.16, 0.14)	2206	444	75
8d	1.0	5.6/ 7.9	2.2/ 0.5	3.9/ 1.2	2.8/ -	(0.16 ,0.20) / -	1047	456, 488	78
	3.0	6.4/ 8.1	2.4/ 1.3	4.9/ 3.4	2.7/ 2.0	(0.17, 0.24) / -	2964	468	82
	5.0	6.8/ 8.8	2.0/ 1.0	4.3/ 2.9	1.9/ 1.4	(0.18, 0.32) / -	3525	472	81
8e	100	6.6/ -	0.4/ -	0.9/ -	0.3/ -	(0.30, 0.52) / -	654	520	105
	1.0	5.0/ 6.0	3.7/ 2.7	5.8/ 5.1	3.2/ 3.0	(0.16, 0.26)/ (0.16, 0.25)	4594	460, 488	78
	3.0	4.8/ 6.3	4.3/ 2.8	6.5/ 5.7	3.3/ 2.9	(0.17, 0.29)/ (0.16, 0.28)	5701	464, 492	77
	5.0	4.8/ 6.3	2.8/ 2.9	4.4/ 5.7	2.0/ 2.7	(0.17, 0.33)/ (0.17, 0.32)	5940	468, 496	79

[a] values at 100/1000 cd/m^2.

3.3 Conclusions

A series of compounds containing cyanocarbazole tethered to various chromophores either directly or via acetylene or vinyl linker have been designed, synthesized and characterized. The effect of linker such as acetylene, vinyl on photophysical and electroluminescent properties is elaborated systematically. Carbazole and triphenylamine substituted dyes of all types showed positive solvatochromism in emission spectra ascribed to intramolecular charge transfer from donor to acceptor. The highest Stokes shift is observed for directly connected derivatives when compared to acetylene and vinyl linker analogs. It could be ascribed to large structural perturbation at excited state as compared to the twisted ground state. The superior thermal stability of acetylene linked compounds is attributed to rigid and rod-like acetylene spacer. The vinyl linked compounds showed high oxidation propensity owing to better electronic conjugation over the entire molecule and hence lead to high-lying HOMO energy level. All the compounds showed deep blue emission in electroluminescent devices. The low-lying LUMO of acetylene derivatives is ascribed to the electron withdrawing nature of acetylene spacer. Triphenylamine tethered cyanocarbazoles showed high power efficiency and current efficiency when compared to other chromophore substituted derivatives in each class of compounds. Among the dyes, the best performance is obtained for **4d** (3 wt%) which showed the power efficiency of 1.3 lm/W, current efficiency of 2.0 cd/A, 4.1% EQE and luminance of 1758 cd/m^2. It might be due to favorable energy barrier for hole and electron injection into the emissive layer which balanced charge transport.

3.4 Experimental Section

3.4.1 General Methods and Characterization

All the chemicals were purchased from commercial source and used without further purification. All the solvents were dried by standard procedures prior to use. Column chromatography purifications were performed by silica gel (120-230 mesh) as stationary phase. ^{1}H NMR and ^{13}C NMR were recorded on a JEOL RESONANCE instrument at 400 MHz and 100.3 MHz respectively. Deuterated chloroform ($CDCl_3$) was used as solvent to record ^{1}H NMR and ^{13}C NMR. The chemical shifts were calibrated using the residual peak of $CDCl_3$ at δ 7.26 for ^{1}H and δ 77.0 for ^{13}C. UV-Vis absorption spectra were recorded at room temperature in a quartz cuvette using Cary 100 spectrophotometer. The fluorescence spectra were recorded by

using Horiba scientific (Fluoromax-4) spectrofluorometer for air equilibrated solutions. The cyclic voltammetry (CV) and differential pulse voltammetry (DPV) measurements were recorded using BASi Epsilon electrochemical analyzer with conventional three electrode cells consisting of glassy carbon working electrode, $Ag/AgNO_3$ reference electrode and platinum wire counter electrode. The electrochemical measurements were performed for dichloromethane solutions with 0.1 M tetrabutylammonium perchlorate as supporting electrolyte at room temperature. The redox potentials were calibrated using ferrocene as an internal standard. The mass spectra were recorded by using HRMS ESI spectrometer (BruckerDaltonics) operating at the positive ion mode. The TGA results were obtained from Perkin-Elmer Pyris Diamond Analyzer at the heat rate of 10 °C min^{-1} and nitrogen was used as carrier gas.

3.4.2 Synthesis

Synthesis of 7-bromo-9-(2-ethylhexyl)-9*H*-carbazole-2-carbonitrile, 2

A mixture of 2,7-dibromo-9-(2-ethylhexyl)-9*H*-carbazole (5.0 g, 11.4 mmol), cuprous cyanide (1.5 g, 17.1 mmol) and *N*,*N*-dimethylformamide (30 mL) was refluxed for 12 h. After completion of the reaction, the mixture was cooled to room temperature and poured into ammonia solution to get precipitate. The precipitate was washed with water and extracted with chloroform. The organic layer was washed with brine solution and dried over anhydrous sodium sulphate. Finally, the solvent was removed under vacuum to yield a residue which was purified by column chromatography using hexane/chloroform (3:1) as eluant. Yellow solid. Yield 1.6 g (36%). mp 96-98 °C;IR (KBr, cm^{-1}) 2220 ($\nu_{C\equiv N}$); ^{1}H NMR ($CDCl_3$, 400 MHz) δ 8.10 (d, J= 8.4 Hz, 1 H), 7.96 (d, J = 8.0 Hz, 1 H), 7.67 (s, 1 H), 7.57 (d, J = 2.0 Hz, 1 H), 7.49 (dd, J = 8.0 Hz, 1.6 Hz, 1 H), 7.40 (dd, J = 8.4 Hz, 1.6 Hz, 1 H), 4.18-4.08 (m, 2 H), 2.05-1.98 (m, 1 H), 1.44-1.22(m, 8 H), 0.92 (t, J = 7.2 Hz, 3 H), 0.87 (t, J = 7.2 Hz, 3 H); ^{13}C NMR ($CDCl_3$, 100.3 MHz)δ 142.53, 139.65, 125.48, 123.03, 122.36, 122.15, 121.39, 120.79, 120.45, 120.01, 113.22, 112.49, 108.29, 47.61, 39.13, 30.66, 28.45, 24.21, 22.91, 13.91, 10.76; HRMS calcd for $C_{21}H_{23}BrN_2$ (m/z + Na) 405.0942, found 405.0938.

Synthesis of 9-(2-ethylhexyl)-7-phenyl-9*H*-carbazole-2-carbonitrile, 4a

A mixture of 7-bromo-9-(2-ethylhexyl)-9*H*-carbazole-2-carbonitrile (1.0 g, 2.6 mmol), phenylboronic acid (0.35 g, 2.9 mmol), $Pd(PPh_3)_4$ (90.1 mg, 0.08 mmol), potassium carbonate (1.1 g, 7.8 mmol) and 28 mL of THF: water (3:1) mixture was refluxed for 12 h under nitrogen

atmosphere. After completion of reaction, the mixture was poured into water and the organic compound was extracted by using chloroform. The organic layer was dried over sodium sulphate. Finally, the solvent was removed under vacuum to yield a residue which was then purified by column chromatography using hexane/chloroform (3:1) as eluent. White solid. Yield 0.85 g (86%). mp 126-128 °C; IR (KBr, cm^{-1}) 2226 ($\nu_{C\equiv N}$); ^1H NMR ($CDCl_3$, 400 MHz) δ 8.18-8.14 (m, 2 H), 7.72-7.68 (m, 3 H), 7.61 (s, 1 H), 7.55-7.48 (m, 4 H), 7.43-7.39 (m, 1 H), 4.27-4.17 (m, 2 H), 2.11-2.05 (m, 1 H), 1.46-1.22 (m, 8 H), 0.94 (t, *J* = 7.2 Hz, 3 H), 0.87 (t, *J* = 7.2 Hz, 3 H). ^{13}C NMR ($CDCl_3$, 100.3 MHz) δ 142.51, 141.54, 141.06, 140.13, 128.89, 128.64, 127.52, 125.95, 122.07, 121.36, 120.81, 120.34, 119.77, 119.61, 113.05, 107.87, 107.78, 47.56, 39.33, 30.84, 28.64, 24.35, 22.97, 13.95, 10.84. HRMS calcd for $C_{27}H_{28}N_2$ *m/z* 380.2247, found 380.2241.

Synthesis of 7-(9,9-diethyl-9*H*-fluoren-2-yl)-9-(2-ethylhexyl)-9*H*-carbazole-2-carbonitrile, 4b

It was prepared from 7-bromo-9-(2-ethylhexyl)-9*H*-carbazole-2-carbonitrile (0.65 g, 1.7 mmol), (9,9-diethyl-9*H*-fluoren-2-yl)boronic acid (0.5g, 1.9 mmol), $Pd(PPh_3)_4$ (58.9 mg, 0.05 mmol), potassium carbonate (0.7 g, 5.1 mmol) and 28 mL of THF: water (3:1) mixture by following the procedure described for **4a**. Yellow solid. Yield 0.8 g (89%). mp 96-98 °C; IR (KBr, cm^{-1}) 2222 ($\nu_{C\equiv N}$); ^1H NMR ($CDCl_3$, 400 MHz) δ 8.20-8.16 (m, 2 H), 7.82 (d, *J* = 8.0 Hz, 1 H), 7.77-7.75 (m, 1 H), 7.70-7.61 (m, 5 H), 7.50 (dd, *J* = 8.0 Hz, 1.2 Hz, 1 H), 7.39-7.33 (m, 3 H), 4.31-4.21 (m, 2 H), 2.13-2.08 (m, 5 H), 1.47-1.26 (m, 8 H), 0.97 (t, *J* = 7.2 Hz, 3 H), 0.88 (t, *J* = 7.2 Hz, 3 H), 0.41 (t, *J* = 7.2 Hz, 6 H). ^{13}C NMR ($CDCl_3$, 100.3 MHz) δ 150.72, 150.17, 142.63, 141.64, 141.13, 140.99, 140.41, 140.28, 127.19, 126.92, 126.46, 126.08, 122.95, 122.14, 121.97, 121.39, 120.87, 120.44, 120.00, 119.78, 113.12, 107.87, 107.75, 56.19, 47.59, 39.50, 32.77, 30.96, 28.76, 24.45, 23.02, 13.99, 10.91, 8.59. HRMS calcd for $C_{38}H_{40}N_2$ *m/z* 524.3186, found 524.3166.

Synthesis of 9'-butyl-9-(2-ethylhexyl)-9*H*,9'*H*-[2,3'-bicarbazole]-7-carbonitrile, 4c

It was prepared from 7-bromo-9-(2-ethylhexyl)-9*H*-carbazole-2-carbonitrile (0.65 g, 1.7 mmol), (9-butyl-9*H*-carbazol-3-yl)boronic acid (0.5 g, 1.9 mmol), $Pd(PPh_3)_4$ (58.9 mg, 0.051 mmol), potassium carbonate (0.7 g, 5.1 mmol) and 28 mL of THF: water (3:1) mixture by following the procedure described for **4a**. Pale orange solid. Yield 0.72 g (81%). mp 90-92 °C;

IR (KBr, cm^{-1}) 2216 ($\nu_{C\equiv N}$); ^1H NMR ($CDCl_3$, 400 MHz) δ 8.42 (d, J = 1.6 Hz, 1 H), 8.20-8.14 (m, 3 H), 7.82 (dd, J = 8.4 Hz, 1.6 Hz, 1 H), 7.71-7.66 (m, 3 H), 7.54-7.44 (m, 4 H), 7.30-7.28 (m, 1 H), 4.37 (t, J = 7.2 Hz, 2 H), 4.30-4.20 (m, 2 H), 2.15-2.09 (m, 1 H), 1.95-1.88 (m, 2 H), 1.49-1.25 (m, 10 H), 1.00-0.94 (m, 6 H), 0.88 (t, J = 7.2 Hz, 3 H). ^{13}C NMR ($CDCl_3$, 100.3 MHz) δ 142.79,142.22, 140.93, 140.12, 140.06, 132.54, 126.21, 125.91, 125.46, 123.41, 122.85, 122.05, 121.32, 120.67, 120.51, 120.37, 120.21, 120.00, 119.24, 118.97, 112.99, 109.02, 108.90, 107.84, 107.46, 47.61, 42.94, 39.37, 31.14, 30.91, 28.71, 24.40, 22.99, 20.56, 13.99, 13.87, 10.88. HRMS calcd for $C_{37}H_{39}N_3$ *m/z* 525.3139, found 525.3111.

Synthesis of 7-(4-(diphenylamino)phenyl)-9-(2-ethylhexyl)-9*H*-carbazole-2-carbonitrile, 4d

It was prepared from a mixture of 7-bromo-9-(2-ethylhexyl)-9*H*-carbazole-2-carbonitrile (0.50 g, 1.3 mmol), (4-(diphenylamino)phenyl)boronic acid (0.41 g, 1.43 mmol), $Pd(PPh_3)_4$ (45 mg, 0.08 mmol), potassium carbonate (0.54 g, 3.9 mmol) and 28 mL of THF: water (3:1) by following the procedure described for **4a**. Tan color solid. Yield 0.57 g (80%). mp 110-112 °C; IR (KBr, cm^{-1}) 2222 ($\nu_{C\equiv N}$); ^1H NMR ($CDCl_3$, 400 MHz) δ 8.15 (d, J = 3.6 Hz, 1 H), 8.12 (d, J = 3.2 Hz, 1 H), 7.67 (s, 1 H), 7.59-7.57 (m, 3 H), 7.53-7.47 (m, 2 H), 7.31-7.27 (m, 4 H), 7.20-7.16 (m, 6 H), 7.08-7.04 (m, 2 H), 4.23-4.20 (m, 2 H), 2.11-2.05 (m, 1 H), 1.44-1.23 (m, 8 H), 0.93 (t, J = 7.6 Hz, 3 H), 0.85 (t, J = 7.2 Hz, 3 H). ^{13}C NMR ($CDCl_3$, 100.3 MHz) δ 147.56, 147.49, 142.70, 140.62, 140.19, 135.22, 129.32, 128.15, 126.13, 124.55, 123.72, 123.11, 122.13, 121.38, 120.75, 120.54, 120.43, 119.29, 113.06, 107.64, 107.23, 47.65, 39.38, 30.91, 28.68, 24.39, 22.99, 13.97, 10.89. HRMS calcd for $C_{39}H_{37}N_3$ *m/z* 547.2982, found 547.2968.

Synthesis of 9-(2-ethylhexyl)-7-(pyren-1-yl)-9*H*-carbazole-2-carbonitrile, 4e

It was prepared from a mixture of 7-bromo-9-(2-ethylhexyl)-9*H*-carbazole-2-carbonitrile (0.60 g, 1.6 mmol), pyren-1-ylboronic acid (0.65 g, 1.7 mmol), $Pd(PPh_3)_4$ (55.4 mg, 0.09 mmol), potassium carbonate (0.54 g, 4.7 mmol) and 28 mL of THF: water (3:1) by following the procedure described for **4a**. Tan color solid. Yield 0.63 g (79%). mp 128-130 °C; IR (KBr, cm^{-1}) 2221 ($\nu_{C\equiv N}$); ^1H NMR ($CDCl_3$, 400 MHz) δ 8.29-8.27 (m, 2 H), 8.24-8.22 (m, 3 H), 8.20-8.18 (m, 1 H), 8.14 (s, 2 H), 8.10-8.02 (m, 3 H), 7.74-7.68 (m, 2 H), 7.60-7.54 (m, 2 H), 4.25-4.19 (m, 2 H), 2.14-2.08 (m, 1 H), 1.44-1.22 (m, 8 H), 0.92 (t, J = 7.2 Hz, 3 H), 0.82 (t, J = 7.2 Hz, 3 H). ^{13}C NMR ($CDCl_3$, 100.3 MHz) δ 142.22, 140.92, 140.15, 137.89, 131.47, 130.89, 130.71, 128.64, 127.78, 127.63, 127.60, 127.39, 126.11, 125.26, 125.16, 124.96, 124.91,

124.85, 124.62, 122.91, 122.22, 120.98, 120.79, 120.43, 113.25, 111.59, 107.93, 47.75, 39.41, 30.90, 28.63, 24.30, 22.99, 13.96, 10.86. HRMS calcd for $C_{37}H_{32}N_2$ *m/z* 504.2560, found 504.2557.

Synthesis of 9-(2-ethylhexyl)-7-(phenylethynyl)-9*H*-carbazole-2-carbonitrile, 6a

A mixture of 7-bromo-9-(2-ethylhexyl)-9*H*-carbazole-2-carbonitrile (0.8 g, 2.0 mmol), ethynylbenzene (0.23 g, 2.2 mmol), $Pd(PPh_3)_2Cl_2$ (14 mg, 0.02 mmol), PPh_3 (5.2 mg, 0.02 mmol), CuI (11.4 mg, 0.06 mmol) and triethylamine (30 mL) was refluxed for 12 h under nitrogen atmosphere. After completion of reaction, the reaction mixture was poured into water and extracted with chloroform. The organic layer was dried over anhydrous sodium sulphate. Finally, the solvent was removed under vacuum to yield a residue which was further purified by column chromatography using hexane/chloroform (3:2) as eluent. Off-white solid. Yield 0.4 g (50%); mp 118-120 °C; IR (KBr, cm^{-1}) 2223 ($\nu_{C\equiv N}$); ^{1}H NMR ($CDCl_3$, 400 MHz) δ 8.12 (d, *J* = 7.6 Hz, 1 H), 8.08 (d, *J* = 8.4 Hz, 1 H), 7.68 (s, 1 H), 7.61-7.59 (m, 3 H), 7.50-7.45 (m, 2 H), 7.42-7.36 (m, 3 H), 4.23-4.13 (m, 2 H), 2.11-2.02 (m, 1 H), 1.47-1.22 (m, 8 H), 0.93 (t, *J* = 7.2 Hz, 3 H), 0.87 (t, *J* = 6.8 Hz, 3 H); ^{13}C NMR ($CDCl_3$, 100.3 MHz) δ 141.52, 140.19, 131.57, 128.37, 125.68, 123.42, 123.00, 122.15, 122.06, 121.48, 120.99, 120.17, 113.17, 112.50, 108.18, 90.16, 90.03, 47.63, 39.19, 30.72, 28.51, 24.26, 22.95, 13.96, 10.81; HRMS calcd for $C_{29}H_{28}N_2$ (*m/z* + Na) 427.2150, found 427.2156.

Synthesis of 7-((9,9-dibutyl-9*H*-fluoren-2-yl)ethynyl)-9-(2-ethylhexyl)-9*H*-carbazole-2-carbonitrile, 6b

It was prepared from 7-bromo-9-(2-ethylhexyl)-9*H*-carbazole-2-carbonitrile (0.7 g, 1.8 mmol), 9,9-dibutyl-2-ethynyl-9*H*-fluorene (0.7 g, 2.2 mmol), $Pd(PPh_3)_2Cl_2$ (14 mg, 0.018 mmol), PPh_3 (5.2 mg, 0.018 mmol), CuI (3.8 mg, 0.054 mmol) and triethylamine (30 mL) by following the procedure described for **6a**. Yellow solid. Yield 0.8 g (73%); mp 100-102 °C; IR (KBr, cm^{-1}) 2219 ($\nu_{C\equiv N}$); ^{1}H NMR ($CDCl_3$, 400 MHz) δ 8.13 (d, *J* = 8.4 Hz, 1 H), 8.10 (d, *J* = 8.4 Hz, 1 H), 7.73-7.69 (m, 3 H), 7.64 (s, 1 H), 7.60-7.57 (m, 2 H), 7.52-7.49 (m, 2 H), 7.37-7.34 (m, 3 H), 4.25-4.15 (m, 2 H), 2.12-1.98 (m, 5 H), 1.46-1.25 (m, 8 H), 1.14-1.05 (m, 4 H), 0.94 (t, *J*= 7.2 Hz, 3 H), 0.88 (t, *J* = 7.2 Hz, 3 H), 0.70-0.54 (m, 10 H); ^{13}C NMR ($CDCl_3$, 100.3 MHz) δ 150.93, 150.77, 141.60, 140.27, 140.22, 130.65, 127.54, 126.85, 125.91, 125.73, 123.47, 122.82, 122.34, 122.15, 121.43, 121.16, 121.02, 120.94, 120.13, 119.95, 119.64,

113.14, 112.42, 108.21, 91.33, 90.22, 54.99, 47.69, 40.13, 39.19, 30.76, 28.54, 25.85, 24.33, 22.99, 13.93, 13.74, 10.81; HRMS calcd for $C_{44}H_{48}N_2$ (*m/z* + Na) 627.3715, found 627.3716.

Synthesis of 7-((9-butyl-9*H*-carbazole-3-yl)ethynyl)-9-(2-ethylhexyl)-9*H*-carbazole-2-carbonitrile, 6c

It was prepared from 7-bromo-9-(2-ethylhexyl)-9*H*-carbazole-2-carbonitrile (1.0 g, 2.8 mmol), 9-butyl-3-ethynyl-9*H*-carbazole (0.7 g, 2.8 mmol), $Pd(PPh_3)_2Cl_2$ (19.6 mg, 0.028 mmol), PPh_3 (7.3 mg, 0.028 mmol), CuI (16.0 mg, 0.084 mmol) and triethylamine (30 mL) by following the procedure described for **6a**. Pale yellow solid. Yield 0.7 g (47%); mp 106-108 °C; IR (KBr, cm^{-1}) 2218 ($\nu_{C\equiv N}$); ^{1}H NMR ($CDCl_3$, 400 MHz) δ 8.36-8.29 (m, 1 H), 8.20 (d, *J* = 2.0 Hz, 1 H), 8.13-8.08 (m, 1 H), 7.72-7.68 (m, 2 H), 7.63 (s, 1 H), 7.58-7.48 (m, 3 H), 7.44-7.39 (m, 1 H), 7.31-7.27 (m, 1 H), 4.34-4.27 (m, 2 H), 4.24-4.14 (m, 2 H), 2.12-2.06 (m, 1 H), 1.90-1.82 (m, 2 H), 1.46-1.25 (m, 2 H), 0.98-.93 (m, 6 H), 0.89 (t, *J* = 7.2 Hz, 3 H); ^{13}C NMR ($CDCl_3$, 100.3 MHz) δ 141.73, 140.25, 139.38, 129.85, 129.21, 128.76, 126.12, 124.22, 124.06, 123.45, 123.19, 122.72, 122.18, 121.06, 120.96, 120.46, 120.30, 119.34, 113.19, 112.35, 110.40, 109.04, 108.95, 108.77, 108.05, 91.28, 88.76, 47.75, 43.08, 39.27, 30.99, 30.81, 28.59, 24.35, 23.02, 20.47, 14.02, 13.82, 10.89; HRMS calcd for $C_{39}H_{39}N_3$ *m/z* 549.3144, found 549.3157.

Synthesis of 7-((4-(diphenylamino)phenyl)ethynyl)-9-(2-ethylhexyl)-9*H*-carbazole-2-carbonitrile, 6d

It was prepared from 7-bromo-9-(2-ethylhexyl)-9*H*-carbazole-2-carbonitrile (0.84 g, 2.2 mmol), 4-ethynyl-*N*,*N*-diphenylaniline (0.6 g, 2.2 mmol), $Pd(PPh_3)_2Cl_2$ (15.4 mg, 0.022 mmol), PPh_3 (5.7 mg, 0.022 mmol), CuI (12.5 mg, 0.066 mmol) and triethylamine (30 mL) by following the procedure described for **6a**. Yellow solid. Yield 0.6 g (50 %); mp 128-130 °C; IR (KBr, cm^{-1}) 2216 ($\nu_{C\equiv N}$); ^{1}H NMR ($CDCl_3$, 400 MHz) δ 8.11 (d, *J* = 7.6 Hz, 1 H), 8.06 (d, *J* = 8.4 Hz, 1 H), 7.67 (s, 1 H), 7.57 (s, 1 H), 7.49-7.43 (m, 4 H), 7.31-7.27 (m, 4 H), 7.15-7.03 (m, 8 H), 4.22-4.12 (m, 2 H), 2.09-2.01 (m, 1 H), 1.45-1.24 (m, 8 H), 0.93 (t, *J* = 7.2 Hz, 3 H), 0.87 (t, *J* = 7.6 Hz, 3 H); ^{13}C NMR ($CDCl_3$, 100.3 MHz) δ 147.96, 146.98, 141.53, 140.11, 132.49, 129.33, 125.68, 124.94, 123.56, 123.33, 122.49, 122.04, 121.16, 120.89, 120.84, 120.12, 115.65, 113.05, 112.19, 108.03, 90.51, 89.47, 47.56, 39.14, 30.70, 28.47, 24.25, 22.90, 13.92, 10.78; HRMS calcd for $C_{41}H_{37}N_3$ *m/z* 571.2987, found 571.2994.

Synthesis of 9-(2-ethylhexyl)-7-(pyren-1-ylethynyl)-9*H*-carbazole-2-carbonitrile, 6e

It was prepared from a mixture of 1-bromopyrene (0.5 g, 1.78 mmol), 9-(2-ethylhexyl)-7-ethynyl-9*H*-carbazole-2-carbonitrile (0.59 g, 1.78 mmol), $Pd(PPh_3)_2Cl_2$ (12.5 mg, 0.018 mmol), PPh_3 (9.4 mg, 0.036 mmol), CuI (3.5 mg, 0.018 mmol), triethylamine (30 mL) by following the procedure described for **6a**. Yield 0.47 g (50%). mp 146-148 °C; IR (KBr, cm^{-1}) 2219 ($\nu_{C\equiv N}$); ^{1}H NMR ($CDCl_3$, 400 MHz) δ 8.72 (d, J = 9.2 Hz, 2 H), 8.27-8.20 (m, 4 H), 8.17-8.12 (m, 4 H), 8.08-8.03 (m, 2 H), 7.75 (s, 1 H), 7.67-7.64 (m, 2 H), 7.49 (dd, J = 7.6 Hz, 1.2 Hz, 1 H), 4.22-4.14 (m, 2 H), 2.13-2.06 (m, 1 H), 1.49-1.25 (m, 8 H), 0.96 (t, J = 7.2 Hz, 3 H), 0.90 (t, J = 7.6 Hz, 3 H), ^{13}C NMR ($CDCl_3$, 100.3 MHz) δ 141.65, 140.23, 131.85, 131.27, 131.19, 130.97, 129.56, 128.32, 128.21, 127.18, 126.26, 125.75, 125.64, 125.38, 124.51, 124.42, 124.22, 123.59, 122.36, 122.18, 121.62, 121.15, 120.99, 120.24, 117.56, 113.18, 112.54, 108.22, 96.05, 89.40, 47.62, 39.30, 30.82, 28.61, 24.39, 23.01, 14.02, 10.89; HRMS calcd for $C_{39}H_{32}N_2$ *m/z* 528.2565, found 528.2564.

Synthesis of (*E*)-9-(2-ethylhexyl)-7-styryl-9*H*-carbazole-2-carbonitrile, 8a

A mixture of 7-bromo-9-(2-ethylhexyl)-9*H*-carbazole-2-carbonitrile (0.7 g, 1.83 mmol), styrene (0.23 g, 2.2 mmol), $Pd(OAc)_2$ (8.3 mg, 0.037 mmol), sodium acetate (1.5 g, 18.3 mmol), tetrabutylammonium bromide (120 mg, 0.37 mmol) in 20 mL of DMF was heated to 100 °C for 24 h under nitrogen atmosphere in the pressure tube under sealed condition. After completion of the reaction, the reaction mixture was poured into water and extracted with chloroform. The organic layer was dried over sodium sulphate. Finally, the solvent was removed under vacuum to yield a residue which was then purified by column chromatography using hexane/chloroform (3:2) as eluent. Colorless solid. Yield 0.44 g (60%). mp 158-160 °C; IR (KBr, cm^{-1}) 2226 ($\nu_{C\equiv N}$); ^{1}H NMR ($CDCl_3$, 400 MHz) δ 8.09 (dd, J = 9.6 Hz, J = 1.2 Hz, 2 H), 7.66 (s, 1 H), 7.58 (d, J = 7.2 Hz, 2 H), 7.53-7.46 (m, 3 H), 7.42-7.38 (m, 2 H), 7.33-7.27 (m, 3 H), 4.25-4.15 (m, 2 H), 2.11-2.05 (m, 1 H), 1.45-1.24 (m, 8 H), 0.95 (t, J = 7.6 Hz, 3 H), 0.88 (t, J = 7.2 Hz, 3 H). ^{13}C NMR ($CDCl_3$, 100.3 MHz) δ 142.48, 140.21, 137.09, 129.32, 129.11, 128.71, 127.79, 126.54, 126.06, 122.14, 122.07, 121.28, 121.24, 120.69, 120.36, 118.46, 113.05, 113.01, 107.68, 107.57, 107.49, 47.56, 39.33, 30.84, 28.65, 24.38, 22.97, 13.99, 10.87; HRMS calcd for $C_{29}H_{30}N_2$ *m/z* 406.2409, found 406.2401.

Synthesis of (*E*)-7-(2-(9,9-dibutyl-9*H*-fluoren-2-yl)vinyl)-9-(2-ethylhexyl)-9*H*-carbazole-2-carbonitrile, 8b

It was prepared from a mixture of 7-bromo-9-(2-ethylhexyl)-9*H*-carbazole-2-carbonitrile (0.5 g, 1.3 mmol), 9,9-dibutyl-2-vinyl-9*H*-fluorene (0.44 g, 1.43 mmol), $Pd(OAc)_2$ (5.8 mg, 0.026 mmol), sodium acetate (1.07 g, 13.0 mmol), tetrabutylammonium bromide (84 mg, 0.26 mmol) in 20 mL of DMF by following the procedure described for **8a**. Pale yellow solid. Yield 0.52 g (66%). mp 114-116 °C; IR (KBr, cm^{-1}) 2220 ($\nu_{C\equiv N}$); ^{1}H NMR ($CDCl_3$, 400 MHz) δ 8.11 (dd, J = 8.0 Hz, J = 2.0 Hz, 2 H), 7.73-7.67 (m, 3 H), 7.58-7.54 (m, 4 H), 7.48 (d, J = 8.0 Hz, 1 H), 7.36-7.29 (m, 5 H), 4.27-4.17 (m, 2 H), 2.11-2.00 (m, 5 H), 1.47-1.26 (m, 8 H), 1.15-1.06 (m, 4 H), 0.96 (t, J = 8 Hz, 3 H), 0.90 (t, J = 7.2 Hz, 3 H), 0.71-0.58 (m, 10 H). ^{13}C NMR ($CDCl_3$, 100.3 MHz) δ 151.30, 150.95, 142.63, 141.23, 140.71, 140.28, 137.43, 136.04, 130.10, 128.33, 127.14, 126.81, 126.18, 125.66, 122.86, 122.15, 121.35, 121.18, 120.79, 120.70, 120.42, 119.93, 119.71, 118.57, 113.05, 107.67, 107.38, 54.95, 47.68, 40.30, 39.39, 30.90, 28.74, 25.94, 24.48, 23.08, 23.03, 14.03, 13.81, 10.94; HRMS calcd for $C_{44}H_{50}N_2$ *m/z* 606.3974, found 606.3971.

Synthesis of (*E*)-7-(2-(9-butyl-9*H*-carbazol-3-yl)vinyl)-9-(2-ethylhexyl)-9*H*-carbazole-2-carbonitrile, 8c

It was prepared from a mixture of 7-bromo-9-(2-ethylhexyl)-9*H*-carbazole-2-carbonitrile (0.5 g, 1.3 mmol), 9-butyl-3-vinyl-9*H*-carbazole (0.36 g, 1.43 mmol), $Pd(OAc)_2$ (5.8 mg, 0.026 mmol), sodium acetate (1.1 g, 13.0 mmol), tetrabutylammonium bromide (84 mg, 0.26 mmol) in 20 mL of DMF by following the procedure described for **8a**. Yellow solid. Yield 0.43 g (60%). mp 130-132 °C; IR (KBr, cm^{-1}) 2218 ($\nu_{C\equiv N}$); ^{1}H NMR ($CDCl_3$, 400 MHz) δ 8.29 (s, 1 H), 8.16-8.08 (m, 3 H), 7.73 (d, J = 8.0 Hz, 1 H), 7.66 (s, 1H), 7.58-7.41 (m, 7 H), 7.36-7.28 (m, 2 H), 4.33 (t, J = 7.6 Hz, 2 H), 4.27-4.16 (m, 2 H), 2.12-2.07 (m, 1 H), 1.92-1.85 (m, 2 H), 1.47-1.26 (m, 10 H), 0.97 (t, J = 7.6 Hz, 6 H), 0.90 (t, J = 7.2 Hz, 3 H). ^{13}C NMR ($CDCl_3$, 100.3 MHz) δ 142.66, 140.82, 140.32, 140.17, 137.88, 130.38, 128.23, 126.36, 126.23, 125.85, 124.44, 123.19, 122.77, 122.06, 121.26, 120.76, 120.56, 120.36, 119.03, 118.75, 118.37, 112.96, 108.91, 107.38, 107.06, 47.58, 42.92, 39.35, 31.12, 30.88, 28.70, 24.41, 23.03, 20.54, 14.05, 13.87, 10.92; HRMS calcd for $C_{39}H_{41}N_3$ (*m/z* +1) 552.3373, found 552.3368.

Synthesis of (*E*)-7-(4-(diphenylamino)styryl)-9-(2-ethylhexyl)-9*H*-carbazole-2-carbonitrile, 8d

It was prepared from a mixture of 7-bromo-9-(2-ethylhexyl)-9*H*-carbazole-2-carbonitrile (0.5 g, 1.3 mmol), *N*,*N*-diphenyl-4-vinylaniline (0.39 g, 1.43 mmol), $Pd(OAc)_2$ (5.8 mg, 0.026 mmol), sodium acetate (1.07 g, 13.0 mmol), tetrabutylammonium bromide (84 mg, 0.26 mmol) in 20 mL of DMF by following the procedure described for **8a**. Greenish yellow solid. Yield 0.52 g (69%). mp 132-134 °C; IR (KBr, cm^{-1}) 2225 ($\nu_{C\equiv N}$); ^1H NMR ($CDCl_3$, 400 MHz) δ 8.08 (dd, J = 12.8 Hz, J = 4.4 Hz, 2 H), 7.66 (s, 1 H), 7.51-7.44 (m, 5 H), 7.30-7.28 (m, 4 H), 7.20 (s, 2 H), 7.13 (d, J = 8.8 Hz, 4 H), 7.09-7.03 (m, 4 H), 4.25-4.14 (m, 2 H), 2.10-2.04 (m, 1 H), 1.45-1.24 (m, 8 H), 0.94 (t, J = 8.0 Hz, 3 H), 0.88 (t, J = 7.2 Hz, 3 H). ^{13}C NMR ($CDCl_3$, 100.3 MHz) δ 147.57, 147.44, 142.61, 140.23, 137.51, 131.18, 129.40, 129.23, 128.82, 127.53, 127.37, 126.17, 124.69, 124.48, 124.42, 123.51, 123.27, 123.04, 122.18, 122.01, 121.34, 121.21, 120.99, 120.71, 120.56, 120.43, 118.29, 113.08, 112.96, 107.58, 107.37, 107.13, 47.61, 39.36, 30.88, 28.69, 24.41, 23.00, 14.02, 10.90; HRMS calcd for $C_{41}H_{39}N_3$ (*m/z* +1) 574.3217, found 574.3199.

Synthesis of (*E*)-9-(2-ethylhexyl)-7-(2-(pyren-1-yl)vinyl)-9*H*-carbazole-2-carbonitrile, 8e

It was prepared from a mixture of 7-bromo-9-(2-ethylhexyl)-9*H*-carbazole-2-carbonitrile (0.6 g, 1.6 mmol), 1-vinylpyrene (0.41 g, 1.8 mmol), $Pd(OAc)_2$ (7.2 mg, 0.032 mmol), sodium acetate (1.31 g, 16.0 mmol), tetrabutylammonium bromide (103 mg, 0.32 mmol) in 20 mL of DMF by following the procedure described for **8a**. Greenish yellow solid. Yield 0.55 g (65%). mp 148-150 °C; IR (KBr, cm^{-1}) 2227 ($\nu_{C\equiv N}$); ^1H NMR ($CDCl_3$, 400 MHz) δ 8.53 (d, J = 9.2 Hz, 1 H), 8.40-8.31 (m, 2 H), 8.21-8.14 (m, 6 H), 8.12-8.00 (m, 3 H), 7.72-7.61 (m, 3 H), 7.57-7.48 (m, 2 H), 4.25-4.15 (m, 2 H), 2.13-2.07 (m, 1 H), 1.48-1.26 (m, 8 H), 0.97 (t, J = 7.6 Hz, 3 H), 0.90 (t, J = 7.6 Hz, 3 H). ^{13}C NMR ($CDCl_3$, 100.3 MHz) δ 142.45, 140.17, 137.39, 132.05, 131.51, 131.45, 130.90, 130.82, 128.35, 127.57, 127.34, 126.01, 125.37, 125.05, 124.84, 123.43, 122.72, 122.08, 121.33, 120.64, 120.40, 118.45, 112.99, 107.87, 107.65, 47.41, 39.36, 30.88, 28.70, 24.41, 23.00, 14.02, 10.89; HRMS calcd for $C_{39}H_{34}N_2$ *m/z* 530.2717, found 530.2728.

3.4.3 Computational Methods

All theoretical calculations were performed by using Gaussian 09 program package. The ground state geometries were fully optimized without any symmetry constraints at the DFT level with Becke's three parameters hybrid functional and Lee, Yang and Parr's correlational functional B3LYP and MPW1K using the 6-31G* basis set on all atoms. Vibrational analyses on the optimized structures were performed to confirm the structure. The excitation energies and oscillator strengths for the lowest singlet-singlet transitions at the optimized geometry in the ground state were obtained by TD-DFT calculations using the hybrid functional model namely B3LYP.

3.4.4 OLED Fabrication and Characterization

The device fabrication process initially involved spin coating of an aqueous solution of PEDOT: PSS at 4000 rpm for 20 s to form a 35 nm hole injection layer on pre-cleaned ITO anode. Before depositing the following emissive layer (EML), the solution was prepared by dissolving the host and guest molecules in tetrahydrofuran at 40 ^{o}C for 0.5 h with stirring. The resulting EML solutions were deposited by spin-coating at 2500 rpm for 20 s under nitrogen. The electron-transporting layer of 1,3,5-tris(*N*-phenylbenzimidazol-2-yl)benzene (TPBi) (32 nm), electron injection layer of LiF (1 nm), and 100 nm layer of Al as a cathode were deposited by using thermal deposition method in high vacuum chamber at respective rates of 0.3, 0.1 and 10 Ås^{-1}. The current density-voltage and luminance (*J-V-L*) characteristics of the resultant devices were measured through a Keithley 2400 electrometer by using Minolta CS-100A luminance-meter, while spectrum and CIE color chromatic coordinates were measured by using PR-655 spectroradiometer. The emission area of devices was 25 mm^2, and only the luminance in forward direction was measured.

CHAPTER 4

Rigid Rod-Like Carbazole Fluorophores: Effect of End Capping Cyano Group, Spacer and Linkage on Optical and Electroluminescence Properties

4.1 Introduction

Organic materials exhibiting tunable optical properties, high thermal and morphological stability have received much attention for OLED applications. Generally, linear and rod-like conjugates display high stability owing to rigid structure which could be beneficial to realize long durable devices. Since carbazole is an electron rich building block, carbazole end capped chromophores have been utilized as hole transporting materials in OLED devices. Owing to the rigidity of backbone and amorphous nature, they serve as highly stable hole transporter. Carbazole end-capped electron-rich chromophores such as thiophene, fluorene and carbazole (**CE1-CE5**) through different linking topology and varying linker (Chart 4.1) have exhibited promising hole transporting characteristics [169-171].

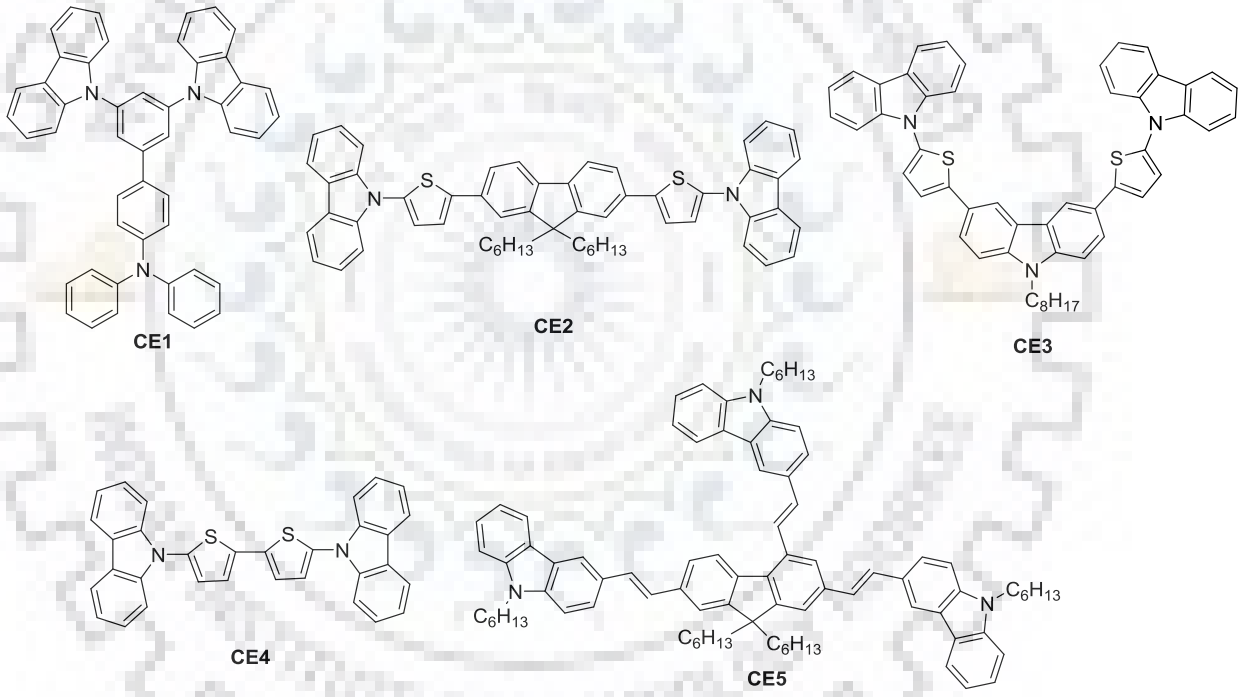

Chart 4.1 Carbazole end capped hole transporting materials.

Fluorene is another fruitful chromophore extensively explored for optoelectronic applications. It is a fused aromatic hydrocarbon and prone to facile functionalization at C2, C7 and C9 position (**CE6-CE13;** Chart 4.2). Owing to rigid chromophoric nature, high fluorescence good charge transporting ability and high chemical and thermal stability, fluorene based compounds are exploited in OLED applications. The tailoring of carbazole and fluorene would result in more desirable material characteristics [172-174, 148]. Over the past decades,

various carbazole-fluorene trimers (Chart 4.2) having different linking topology and carbazole trimers with different end capping carbazole via C2, C3 and *N*-position were reported. These materials are demonstrated as hole transporting materials in OLED devices.

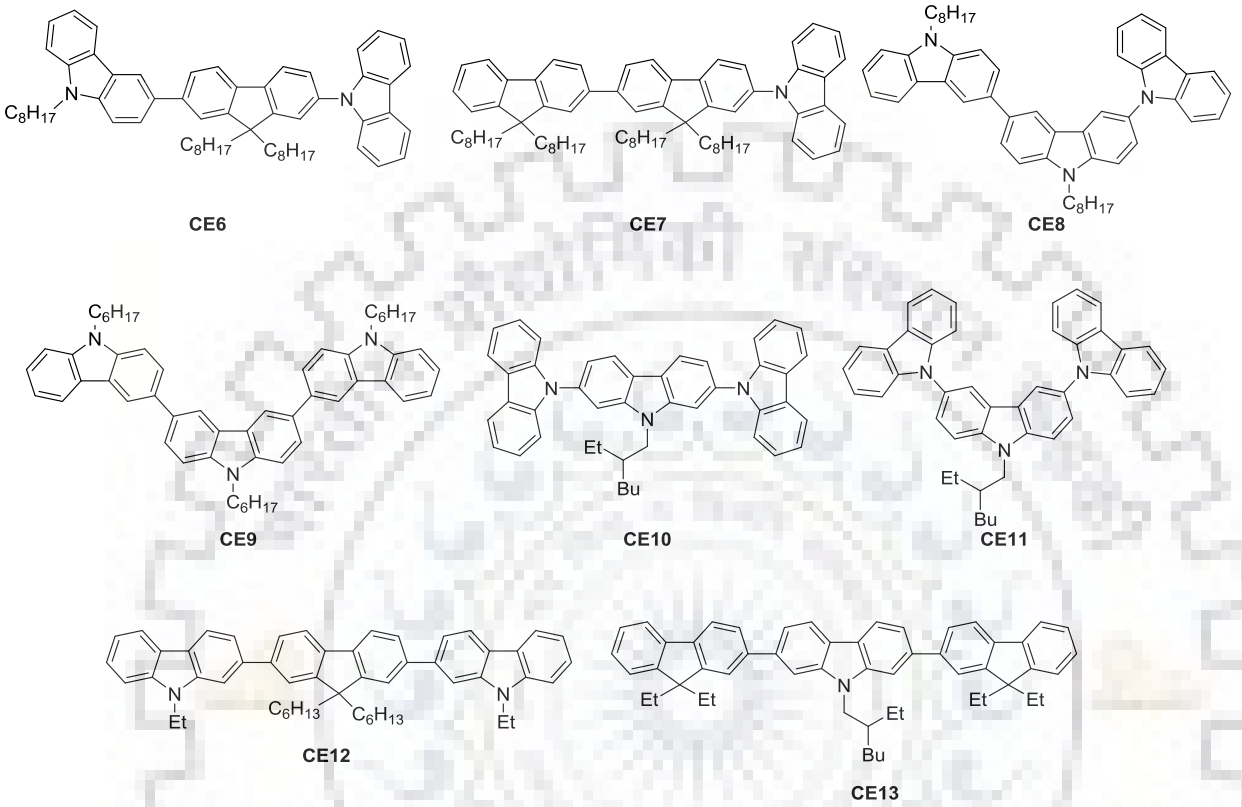

Chart 4.2 Hole transporting carbazole/fluorene trimers containing different linking topology.

Since carbazole possess high triplet energy and excellent hole transporting character, carbazole trimers can be utilized as a host material for PhOLED. For example, Chen and coworkers reported *N*-carbazole end capped fluorene via 2,7-position (**CE14**) and demonstrated as host material (Chart 4.3) [175]. Qiu and coworkers reported *N*-carbazole end capped carbazole at 2,7- and 3,6-positions (**CE15**,**CE16;** Chart 4.3) [176]. Owing to twisted structure, these materials exhibited high triplet energy of about 3.0 eV. In addition, the high lying HOMO of the compounds was beneficial for facile hole transportation. The high glass transition temperature leads to good morphological stability. Brunner and coworkers designed carbazole/fluorene end capped carbazole at different linking position (**CE17-CE19;** Chart 4.3) and employed them as host material for PhOLED [177].

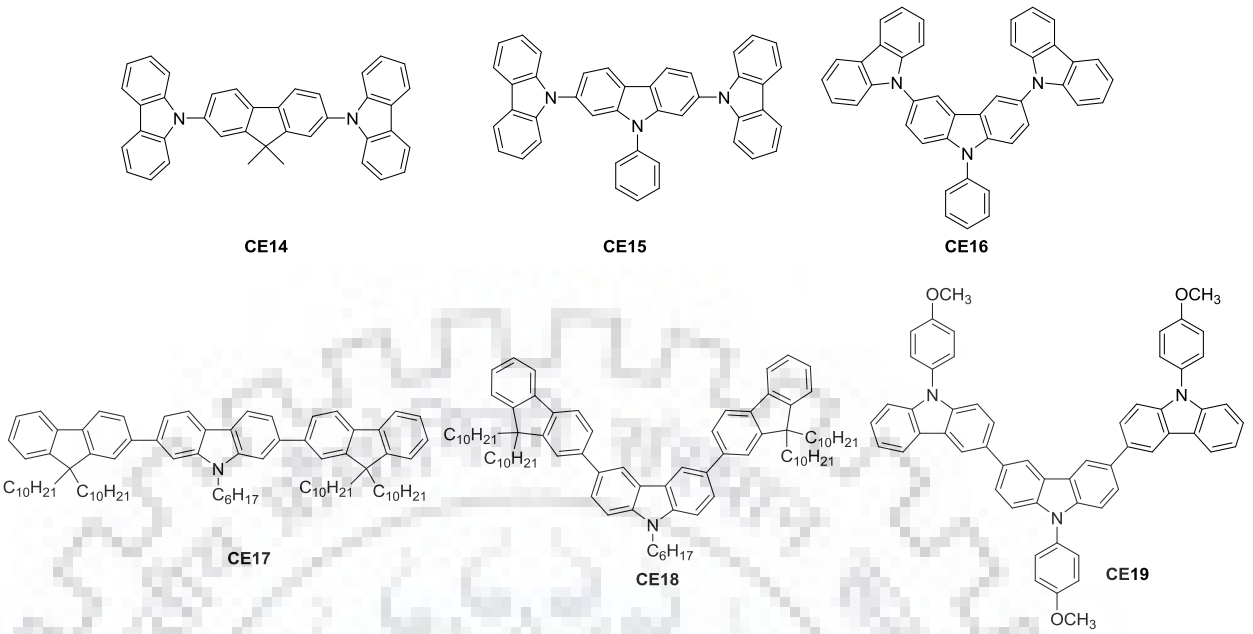

Chart 4.3 Carbazole/fluorene and carbazole trimers as host materials.

Further, carbazole end capped materials are utilized as emitting materials in OLED as they are found to exhibit intense emission in solution. Strohriegl and coworkers reported linear and angular carbazole trimers (**CE20**,**CE21;** Chart 4.4) connected at 2,7 and 3,6-positions respectively [178]. The linear carbazole trimer showed better conjugation over angularly substituted congener. Also, linear derivative exhibited intense blue emission while 3,6-substituted trimer gave pale and weak emission. Dias and coworkers reported C2-carbazole end capped C3, C6-carbazole core (**CE22;** Chart 4.4) and demonstrated as blue emitter [179]. Shimasaki and coworkers reported carbazole trimers containing acetylene linker (**CE23;** Chart 4.4) and presented as blue emitting material [180]. However, the above reported compounds have not been used as emitter in OLED device. Recently, Velasco and coworkers reported angularly 3,6-substituted carbazole connected to end capped carbazole acetylene (**CE24;** Chart 4.4) and employed it as non-doped emitter in OLED device [30]. Owing to rigid acetylene linker, the compound showed better quantum yield in solution. However, the non-doped device fabricated with emitter exhibited poor performance owing to the formation of aggregates in thin film.

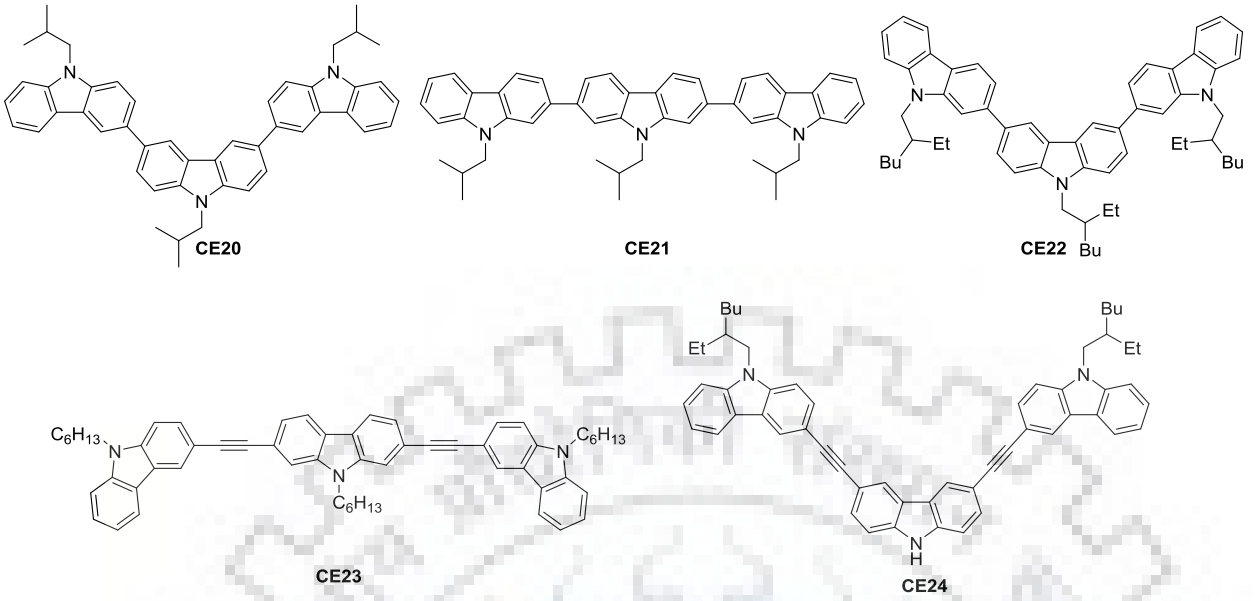

Chart 4.4 Carbazole end capped trimers as emitting materials.

In addition, Kazlauskas and coworkers reported carbazole trimers (**CE25-CE30**) connected with different linking topology (Chart 4.5). They are demonstrated as hole transporting materials and displayed low threshold amplified spontaneous emission in electrically driven organic lasers [181]. Though central carbazole trimers and carbazole end capped fluorene trimers are reported, their use in device application is limited. Also, carbazole trimer possessing acetylene linker showed poor device performance owing to inappropriate charge carrier mobility across the device.

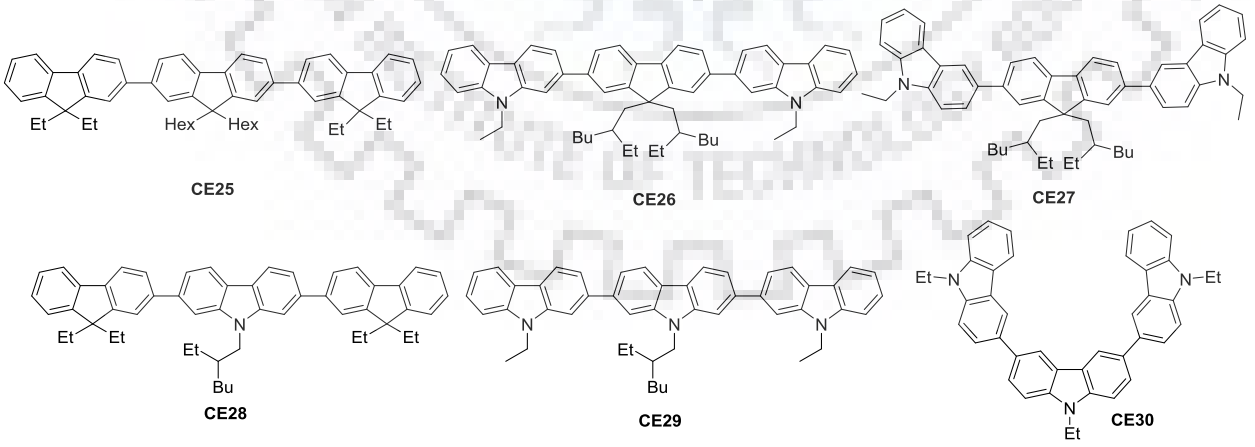

Chart 4.5 Hole transporting carbazole/fluorene trimers with different linking topology.

Xue and coworkers studied the carbazole end capped anthracene connected through vinyl linker as aggregation induced luminogen (**CE31;** Chart 4.6) [182]. The compound was non-emissive in solution while emissive in aggregate form. When the luminogen was employed as non-doped emitter in OLED device, it exhibited green emission. It was also employed as emitting dopant in host matrix, the efficiency of the device increased about eight fold owing to the suppression of aggregation. Matussek and coworkers synthesized carbazole end capped anthracene having acetylene linker (**CE32;** Chart 4.6) and demonstrated as red emitter in OLED device [134]. The presence of rigid acetylene linker was beneficial to raise the quantum yield and provide effective electronic conjugation. Oh and coworkers reported carbazole trimers having vinyl linker as emitters (**CE33**,**CE34;** Chart 4.6) [183]. Also the cyano end capping on peripheral carbazole leads to better performance due to the realization of balanced charge transport by accelerating the electron mobility.

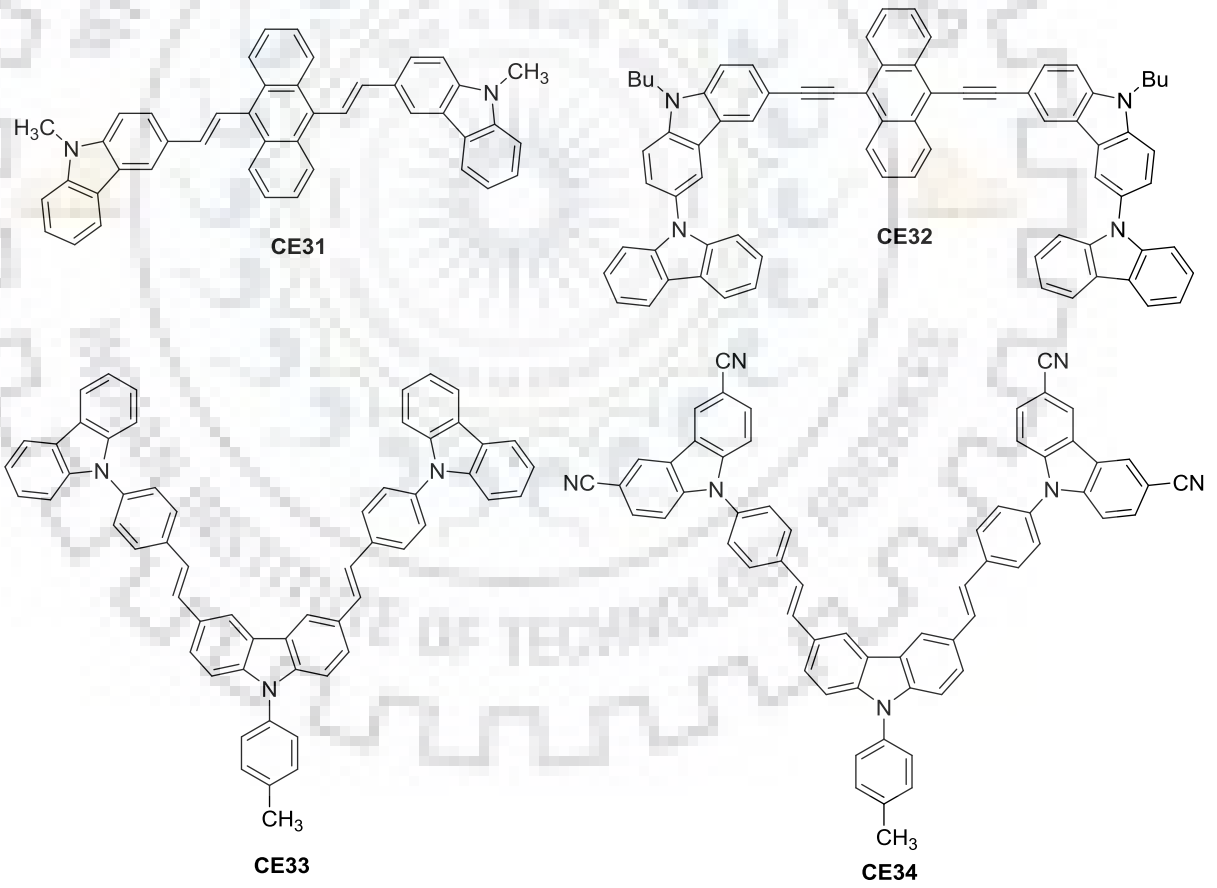

Chart 4.6 Carbazole and cyanocarbazole end capped materials as emitters.

From the above discussions, it is clear that carbazole end capped trimers are beneficial for good charge transport and to realize better thermal stability. Further, as discussed in previous chapter, cyano substitution on carbazole would have tremendous impact in realizing increased electron transport and thus achieve balanced charge transport. So, we intended to explore the effect of cyano group on peripheral carbazole of carbazole trimers to attain balanced charge transport. In this chapter, we describe synthesis and characterization of cyanocarbazole end capped carbazole or fluorene trimers and their photophysical and electroluminescence properties (Chart 4.7). Further, we studied the effect of conjugating spacer (acetylene and vinyl) on optical, electrochemical and electroluminescence properties.

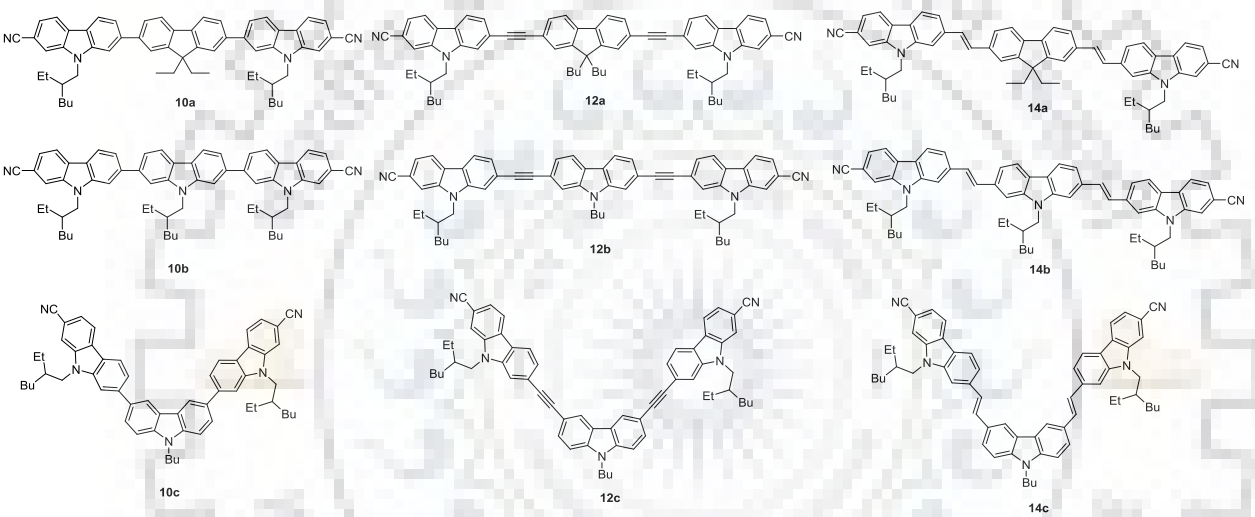

Chart 4.7 Structure of cyanocarbazole end capped rigid molecules.

4.2 Results and Discussion

4.2.1 Synthesis and Characterization

The synthesis of an intermediate **2** is described in Chapter 3. The intermediate **2** was converted into desired final compounds (**10a**-**10c**) by adopting Suzuki coupling reaction protocol using appropriate diboronic acids (**9a**-**9c**). The target acetylene compounds (**12a**-**12c**) were obtained from the intermediate **2** by Sonogashira reaction with suitable terminal diacetylenes (**11a**-**11c**). The vinyl linked target compounds (**14a**-**14c**) were synthesized by employing Heck coupling reaction using appropriate terminal vinylene intermediates (**13a**-**13c**). All the new compounds were obtained in moderate to good yields. The newly prepared

compounds were thoroughly characterized by ^{1}H NMR, ^{13}C NMR, IR and HRMS techniques. The data is consistent with the proposed structures of the compounds. All the compounds are soluble in common organic solvents such as toluene (TOL), dichloromethane (DCM), chloroform ($CHCl_3$), tetrahydrofuran (THF), *N*,*N*-Dimethylformamide (DMF) and sparingly soluble in acetonitrile (ACN) and methanol (MeOH).

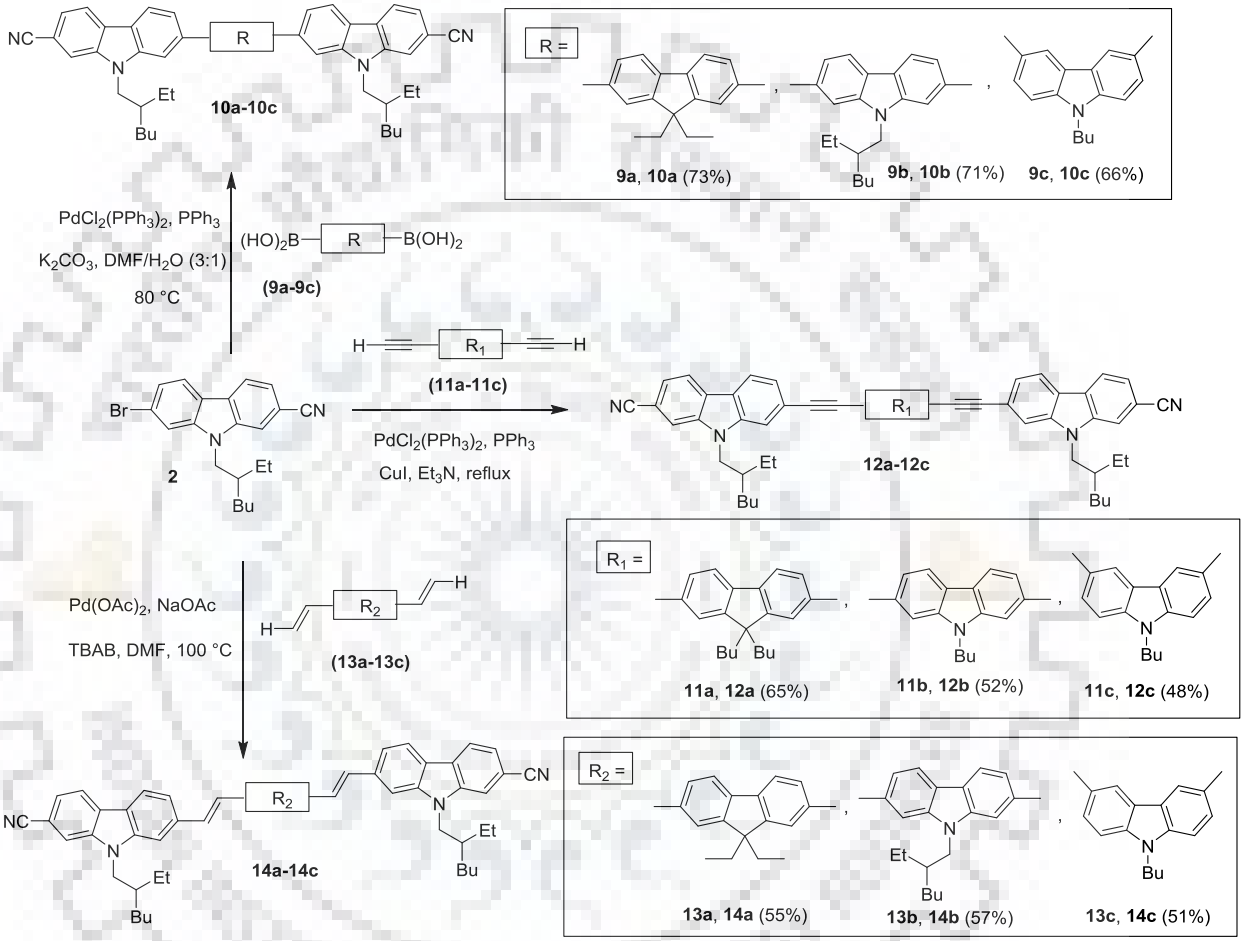

Scheme 4.1 Synthetic procedure for the target compounds (**10a**-**10c**, **12a**-**12c** and **14a**-**14c**).

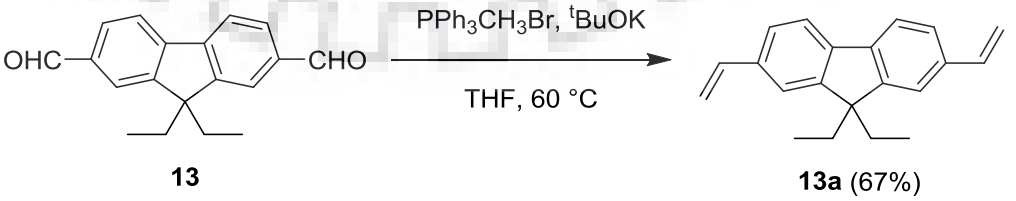

Scheme 4.2 Synthesis of the intermediate **13a**.

4.2.2 Photophysical Properties

The absorption spectra of the compounds recorded in dichloromethane are depicted in Figure 4.1. And the relevant data are compiled in Table 4.1. The absorption spectrum of each compound contains two distinct bands. The higher energy band, ca. below 300 nm, arises from π-π* transition of either carbazole or fluorene unit [184-186]. The lower energy band is assigned to the delocalized π-π* transition of entire molecular backbone. The absorption maxima of the dyes are dependent on the nature of the spacer and linkage mode. The absorption maxima of the compounds followed the order of vinyl > acetylene > direct for the same chromophore. Due to the sp^2 hybridized carbon of vinyl linker and aromatic moieties, the overlapping of molecular orbital is effective in vinyl compounds. This provides efficient delocalization of π electron and thus red shifted absorption maximum. In contrast, mismatching of energy levels of sp hybridized acetylene and sp^2 hybridized aromatic segments lead to poor overlapping. As a result, the electronic delocalization is relatively less for acetylene derivatives and thus blue shifted absorption maxima compared to analogous vinyl linker compounds [187-190]. The blue shifted absorption maxima of directly linked compounds could be attributed to twisting of end capped cyanocarbazole from the core fluorene or carbazole moiety.

Within a set of compounds, the absorption maxima progressively increased reflective of the nature of core which is connected to the peripheral cyanocarbazole such as 2,7-carbazole (**b**) > 2,7-fluorene (**a**) > 3,6-carbazole (**c**). The linear 2,7-substituted carbazole derivatives show extended conjugation over V-shaped angularly substituted 3,6-carbazole analogs. The salient features of the absorption characteristics can be summarized as follows: (i) Generally, the vinyl linked compounds (**14a-14c**) showed longer wavelength absorption when compared to the acetylene linked compounds (**12a-12c**) which in turn longer than the directly tethered derivatives (**10a-10c**). (ii) Within a class, the absorption maxima progressively increased with the nature of the spacer as, 2,7-carbazole (**b**) > 2,7-fluorene (**a**) > 3,6-carbazole (**c**). It is probable that in the directly linked derivatives the tilting between the core and the peripheries disrupt the electronic delocalization across the molecule. Among the spacers, vinyl linker and carbazole 2,7-linkage render extended conjugation [191-192].

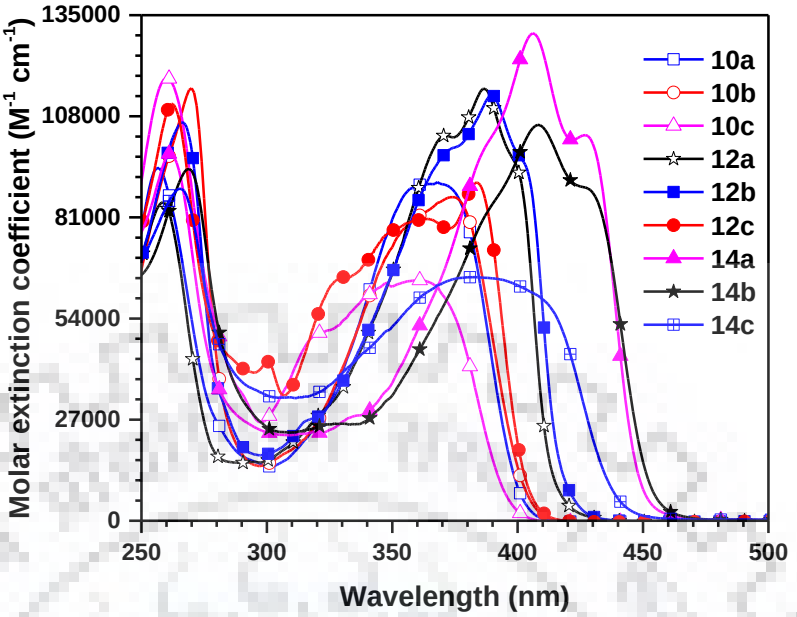

Figure 4.1 Absorption spectra of the dyes recorded in dichloromethane.

It is interesting to compare the absorption spectrum of **10a** with that of the known compound 2,7-bis(9-ethylcarbazol-2-yl)-9,9-dihexylfluorene which lacks CN group on peripheral carbazole units [174]. The compound **10a** exhibited bathochromically shifted absorption peak, which clearly attests the role of cyano substitution in extending the conjugation. In the same way, **10b** also exhibited red shifted absorption maximum when compared to the trimeric carbazole, 9,9′,9″-tri-*sec*-butyl[2,2′;7′,2″]-tercarbazole known in the literature [178]. Similarly, compound **12c** displayed red-shift over 3,6-bis[2-(9-(2-ethylhexyl)-9*H*-carbazol-3-yl)-ethynyl]-9*H*-carbazole attributable to the linkage of terminal carbazoles via C3 and absence of cyano group on carbazole [30]. However, the chromophoric effect is less significant when **12a** is compared to the reported dye, 7,7'-((9,9-dibutyl-9*H*-fluorene-2,7-diyl)bis(ethyne-2,1-diyl))bis(9,9-dipropyl-9*H*-fluorene-2-carbonitrile) which features cyanofluorene at terminal ends instead of cyanocarbazole [151]. This indicates that cyano substitution on 2,7-carbazole and 2,7-fluorene makes the resultant chromophores similar in electronic characteristics.

Further, the optical response of the dyes towards the polarity of the solvents was elucidated by studying the solvatochromism of the dyes (Figure 4.3 to Figure 4.11). The dyes showed less significant variations in the absorption properties on changing the solvent polarity indicative of nonpolar nature of the ground state in these molecules.

Table 4.1 Optical properties of the dyes

Dye	λ_{max}, nm (ε_{max}, M^{-1} cm^{-1} $\times 10^3$)[a]	λ_{em}, nm (Φ_F)[a,b]	Stokes shift,[a] cm^{-1}	$\lambda_{em,}$[c] nm
10a	257 (94.2), 368 (90.4)	410, 430 (0.70)	2784	445
10b	270 (115.5), 374 (86.4)	415, 433 (0.61)	2642	456
10c	260 (118.2), 362 (64.2)	431 (0.66)	4422	452
12a	259(85.0), 371(102.9), 387(115.3)	411, 433 (0.63)	1509	446, 470
12b	267(106.5), 372(98.7), 390(113.6)	414, 437 (0.82)	1486	459
12c	262(111.3), 300(42.5), 360(80.3), 384(90.3)	422 (0.54)	2345	452
14a	261(98.0), 406(130.2), 427sh(103.0)	448, 476 (0.92)	2309	484
14b	269(93.9), 408(105.7), 429(88.3)	454, 479 (0.90)	2483	469
14c	265(88.7), 383(65.1)	465 (0.73)	4604	470

[a] Measured in dichloromethane solution. [b] Absolute quantum yield using integrating sphere. [c] Measured for drop cast film.

The emission spectra of the compounds recorded in dichloromethane are displayed in Figure 4.2. And the corresponding data are registered in Table 4.1. The emission maxima of the compounds followed the similar trend as observed in absorption spectra among the series as direct < acetylene < vinyl. Despite of shorter wavelength absorption for the directly connected compounds **10a**-**10c**, they showed almost similar emission maximum as that of acetylene congeners (**12a**-**12c**). Probably, it might be due to pronounced structural reorganization in the excited state which eventually resulted in larger Stokes shift for **10a**-**10c** over their rigid acetylene counterparts [138]. Also, the vinyl linked compounds gave comparable Stokes shift to that of directly linked compounds. However, the Stokes shift is larger than that of acetylene analogs. It is attributed to flexibility of vinyl linker which undergoes structural reorganization. In each class of compounds, V-shaped carbazole derivatives showed the largest Stokes shift over their linear carbazole and fluorene counterparts. It is ascribed to significant structural reorganization in the excited state induced by intramolecular charge transfer from core carbazole to peripheral cyanocarbazole [193-195]. The emission spectral characteristic can be summarized as below. (i) The emission maxima of the compounds varied depending upon the nature of linker which is similar to absorption trend as well, vinyl (**14**) > acetylene (**12**) > direct (**10**). (ii) Within a set of compounds, the emission maxima followed the trend of 3,6-carbazole (**c**) > 2,7-carbazole (**b**) > 2,7-fluorene (**a**). V-shaped carbazole derivatives exhibited the largest red shift emission maxima unlike their shortest absorption maxima compared to their linear analogs. It is attributed to pronounced structural perturbation at excited state due to the development of intramolecular charge migration from carbazole donor to cyano acceptor. The

emission spectra of the compounds **10a**, **10b** and **12c** showed red-shift as compared to their reported analogs which lack CN group on peripheral carbazole.

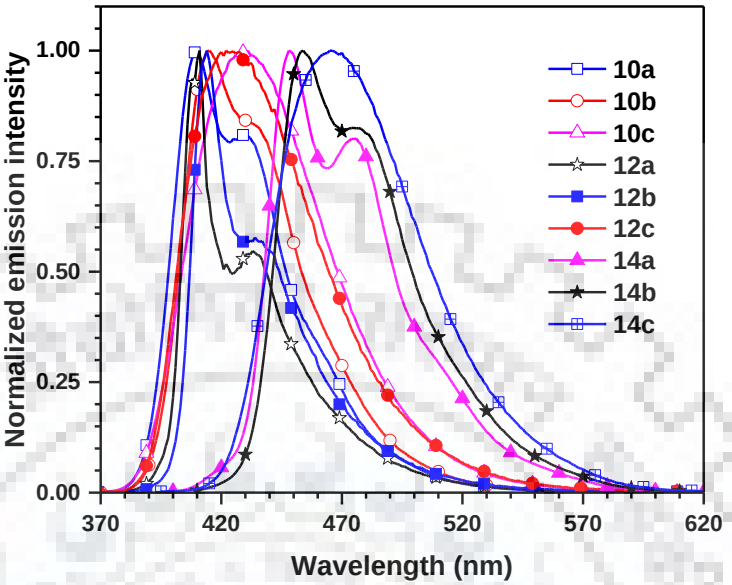

Figure 4.2 Emission spectra of the dyes recorded in dichloromethane.

The nature of the excited state was probed by measuring emission spectra of the dyes in the solvents of different polarity (Figure 4.3 to Figure 4.11). The linear fluorene and carbazole core derivatives, **10a**, **10b**, **12a**, **12b**, **14a** and **14b** displayed insignificant changes in emission spectra with respect to the solvent polarity while the V-shaped dyes **10c**, **12c** and **14c** exhibited positive solvatochromism (Table 4.2). It suggests the stabilization of V-shaped dyes in polar solvents at excited state, probably due to intramolecular charge transfer from carbazole donor to peripheral cyanocarbazole acceptor. Furthermore, the significant increase in FWHM for V-shaped dyes in polar solvents attest the presence of structural reorganization and dipolar relaxation (Table 4.3). Whereas the linear compounds did not show appreciable change in FWHM of emission spectra as the polarity of solvent is increased.

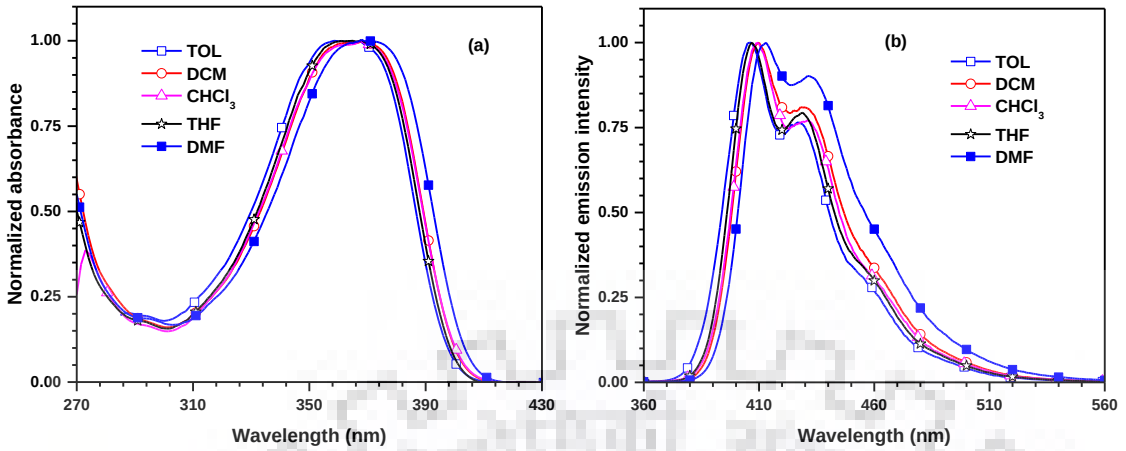

Figure 4.3 Absorption (a) and emission (b) spectra of **10a** recorded in different solvents.

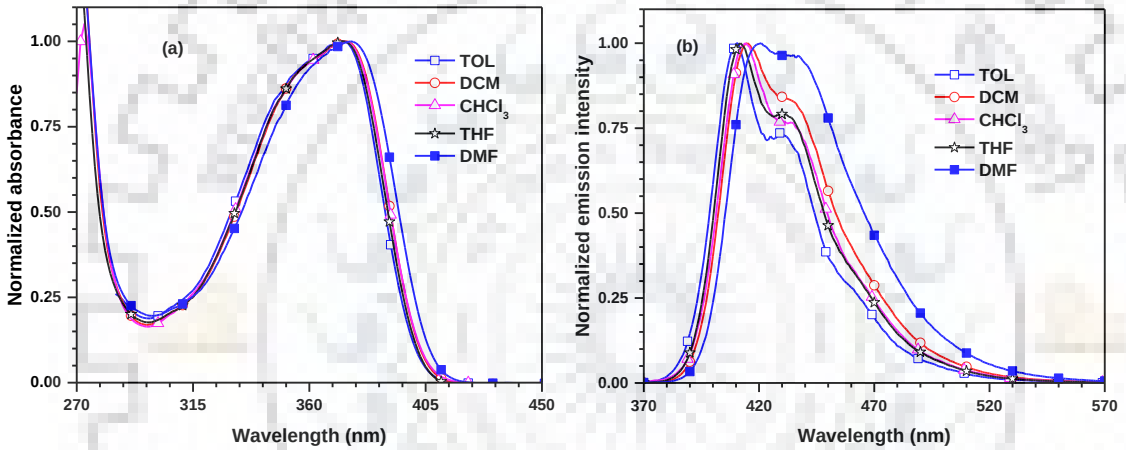

Figure 4.4 Absorption (a) and emission (b) spectra of **10b** recorded in different solvents.

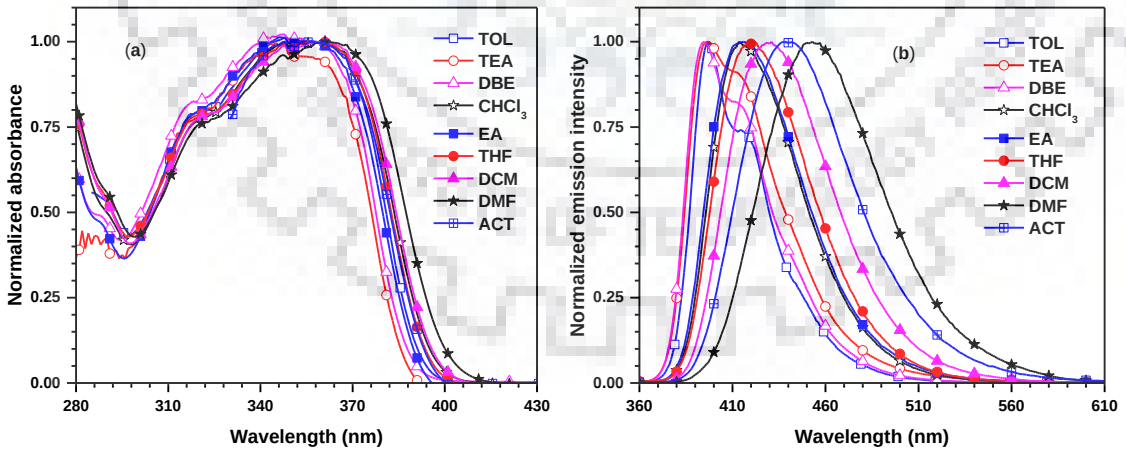

Figure 4.5 Absorption (a) and emission (b) spectra of **10c** recorded in different solvents.

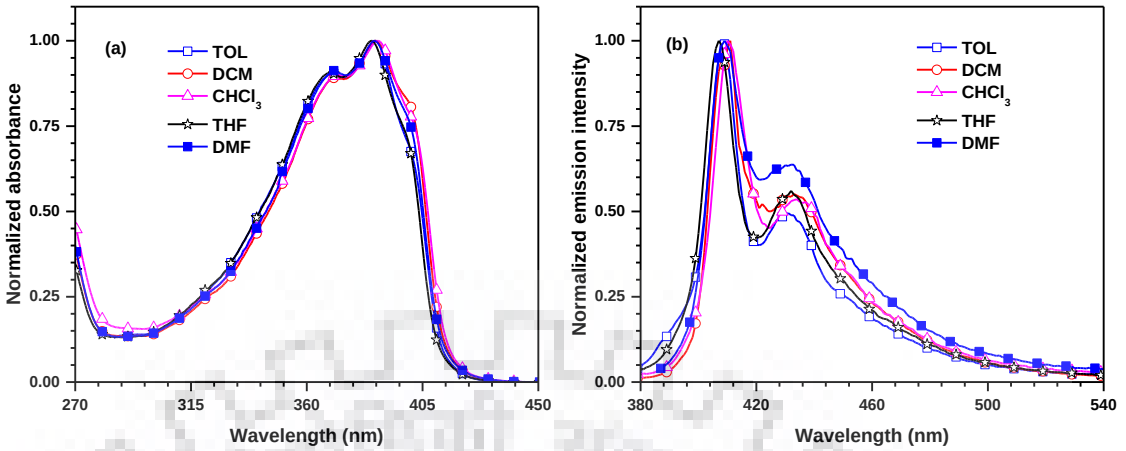

Figure 4.6 Absorption (a) and emission (b) spectra of **12a** recorded in different solvents.

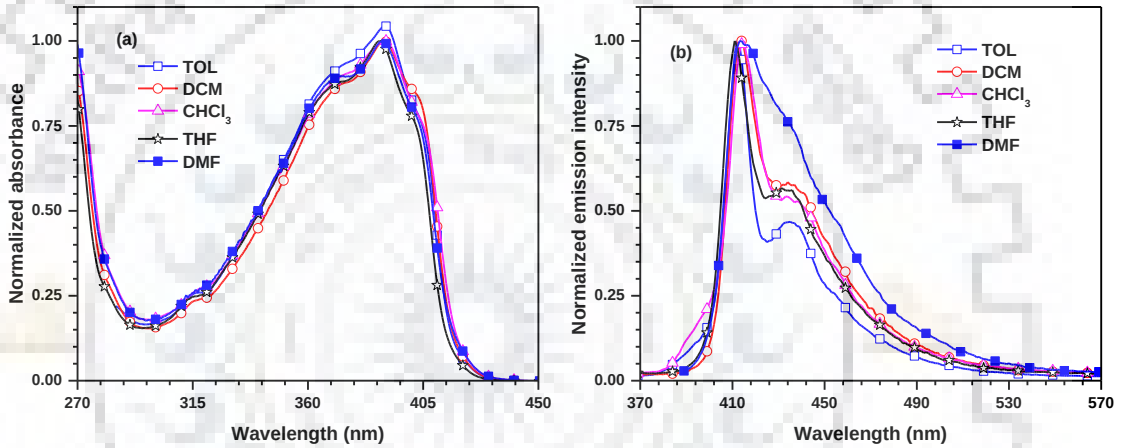

Figure 4.7 Absorption (a) and emission (b) spectra of **12b** recorded in different solvents.

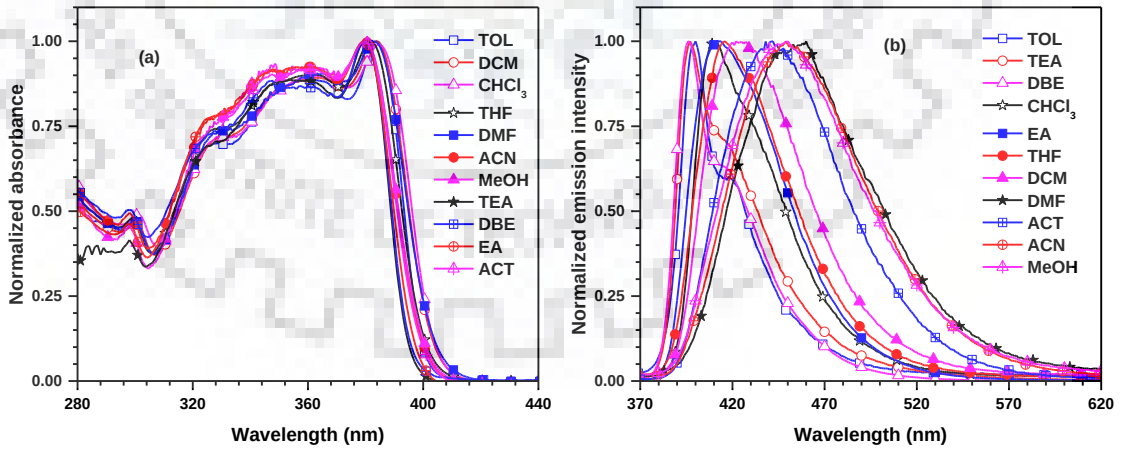

Figure 4.8 Absorption (a) and emission (b) spectra of **12c** recorded in different solvents.

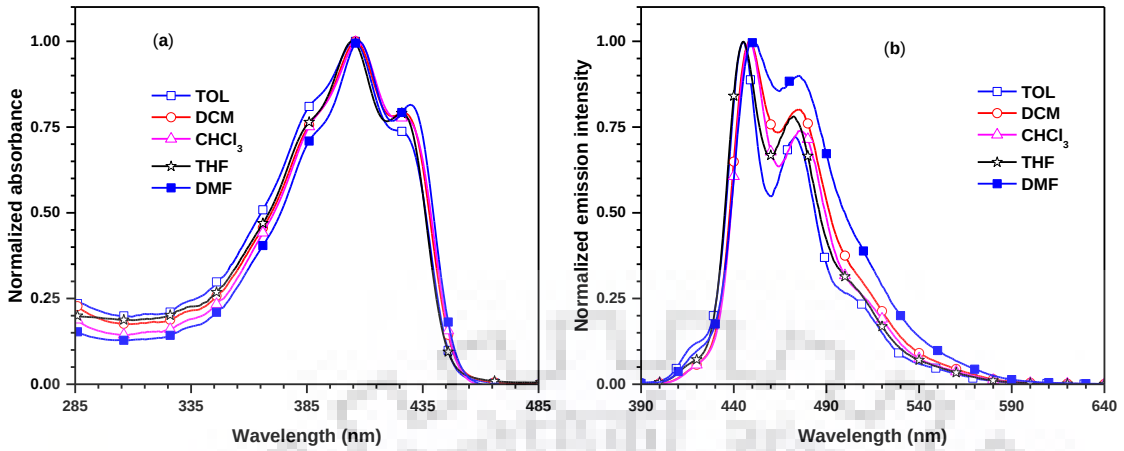

Figure 4.9 Absorption (a) and emission (b) spectra of **14a** recorded in different solvents.

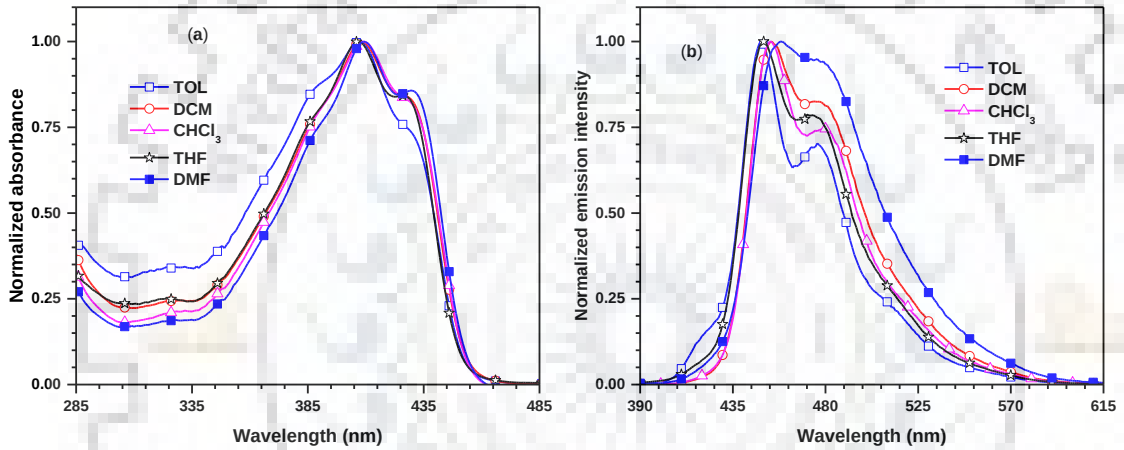

Figure 4.10 Absorption (a) and emission (b) spectra of **14b** recorded in different solvents.

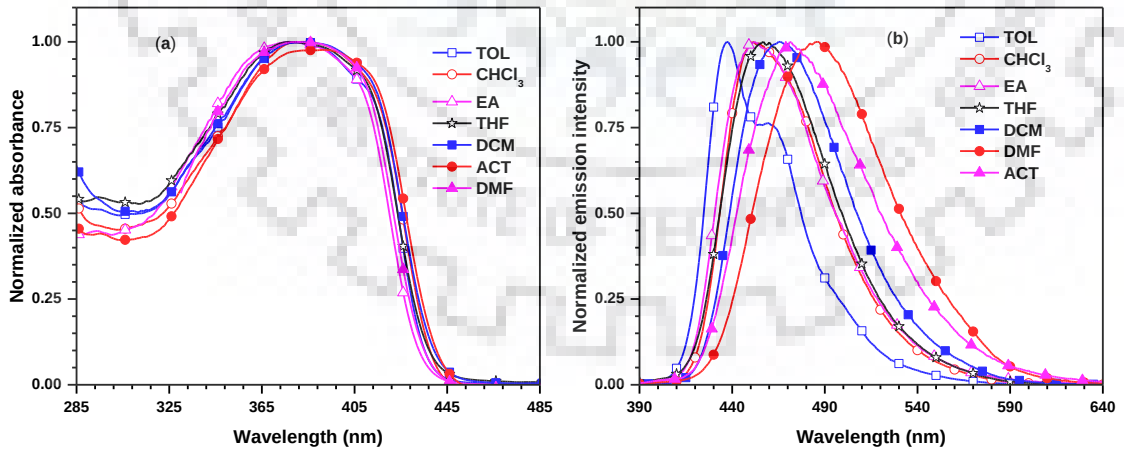

Figure 4.11 Absorption (a) and emission (b) spectra of **14c** recorded in different solvents.

Table 4.2 Solvatochromic data of the dyes

Dye	Absorption maxima, λ_{max} (nm)				Emission maxima, λ_{em} (nm)			
	TOL	$CHCl_3$	THF	DMF	TOL	$CHCl_3$	THF	DMF
10a	359	367	368	370	406, 427	409, 431	407, 429	413, 431
10b	372	374	373	376	411, 429	414, 435	412, 433	421, 436
10c	359	359	359	362	397, 414	414	422	453
12a	369,387	371, 388	369, 385	371, 387	408, 431	410, 434	407, 432	409, 432
12b	371, 390	372, 390	371, 388	371, 389	412, 435	415, 433	411, 431	414
12c	300,325, 357,384	301, 360, 384	300, 362, 382	300, 361, 383	400, 418	411	416	460
14a	405, 427sh	407, 429sh	405, 428sh	407, 430sh	445, 473	449, 475	445, 472	451, 475
14b	408, 428sh	270, 409, 429sh	269, 407, 427sh	409, 431sh	449, 476	453, 480	450, 474	458, 479
14c	376	266, 383	267, 377	383	437, 462	451	457	485

Table 4.3 Stokes shift and full width at half maxima values of the dyes

Dye	Stokes shift (cm^{-1})					FWHM (nm)				
	TOL	DCM	$CHCl_3$	THF	DMF	TOL	DCM	$CHCl_3$	THF	DMF
10a	3225	2784	2798	2604	2814	44	45	44	45	48
10b	2551	2642	2583	2538	2843	43	46	44	44	50
10c	2666	4422	3701	4158	5549	40	54	47	50	63
12a	1330	1509	1383	1404	1390	41	42	42	44	46
12b	1369	1486	1544	1442	1552	40	41	41	41	44
12c	1041	2345	1643	2139	4370	37	52	44	49	70
14a	2219	2309	2298	2219	2397	61	60	59	60	65
14b	2238	2483	2375	2348	2616	61	60	59	60	66
14c	3712	4604	3937	4643	5491	57	67	62	64	80

Table 4.4 Solvatochromic data of the dyes **10c**, **12c** and **14c**

Dye	Absorption maxima, λ_{max} (nm)				Emission maxima, λ_{em} (nm)				Stokes shift (cm^{-1})			
	TEA	DBE	EA	ACT	TEA	DBE	EA	ACT	TEA	DBE	EA	ACT
10c	359	357	357	360	397, 412	395, 412	416	442	2666	2695	3973	5153
12c	298, 347, 380	298, 347, 380	298, 348, 380	347, 380	397, 415	397, 414	412	442	1127	1127	2044	3691
14c	-	-	377	380	-	-	452	471	-	-	4401	5084

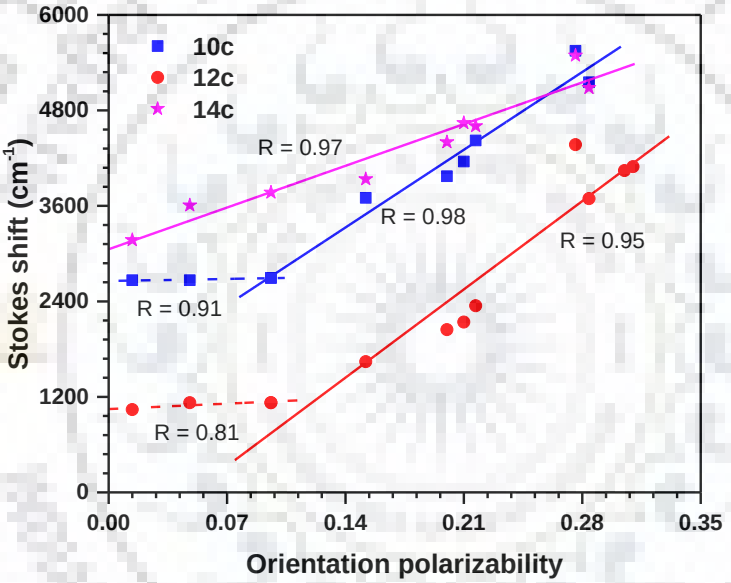

Figure 4.12 Lippert-Mataga plot for the dyes **10c**, **12c** and **14c**.

The Lippert-Mataga plot of the V-shaped dyes **10c**, **12c** and **14c** is displayed in Figure 4.12. The Stokes shift remains constant in the non-polar solvent region and increases rapidly as the polarity of the solvent increases for **10c** and **12c**. Such two linear correlations indicate the presence of two excited states namely local (LE) and charge transfer (CT) excited state and stabilization of CT state in polar solvents [196-197]. Moreover, this observation is consistent with the progression of LE state into CT state as the solvent polarity progresses. In contrast, linear progression of Stokes shift with respect to solvent polarity resulted in single linear correlation in Lippert-Mataga plot for **14c** comprising polar and non-polar solvents which indicate the presence of single excited state namely charge transfer excited state. Drop cast thin films of the compounds displayed emission in the longer wavelength when compared to that of

solution (Figure 4.13). It is probably originating from the intermolecular association or *J*-aggregation of the dyes in the solid state [145-147].

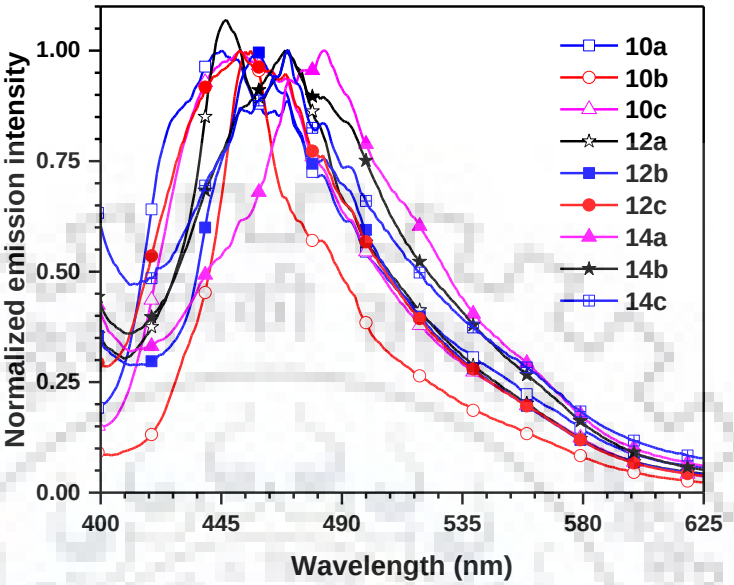

Figure 4.13 Thin film emission spectra of the dyes recorded for drop cast films.

4.2.3 Electrochemical Properties

The favorable HOMO and LUMO energy level alignment of the emitting materials with the neighboring charge injecting molecular layers of OLED devices determines the flow of charge carriers in the device. In order to estimate the HOMO and LUMO energy levels, the redox potentials of the dyes were measured by cyclic voltammetry studies. All the dyes exhibited an irreversible oxidation peak while **10c** showed quasi-reversible oxidation couple (Figure 4.14). Generally, the carbazole derivatives display irreversible oxidation attributable to the large reorganization energy associated with the oxidation arising from the rigid structure of carbazole [148-150]. When we compare the oxidation propensity of the fluorene compounds **10a**, **12a** and **14a** with their carbazole analogs **10b**, **12b** and **14b**, the latter compounds gave low oxidation potentials due to the electron richness of carbazole over fluorene moiety. The V-shaped dyes exhibited lowest oxidation potential compared to their linear carbazole analogs in each set of compounds and thus upwardly shifted the HOMO. This is due to the activation of 3,6-position of carbazole by nitrogen atom. Similar results are documented in the literature for 3,6-functionalized carbazoles [198, 116, 126]. Among the series, vinyl compounds exhibited the lowest oxidation potential compared to their acetylene and directly linked counterparts. It

further attests the availability of electron through delocalization of π conjugation in vinyl derivatives.

The HOMO energy level of the compounds is calculated by adding 4.8 eV with oxidation potential. The LUMO energy level is obtained from the difference between HOMO and optical band gap. The optical band gap is estimated from the absorption edge of the compounds, which is taken from the intersection of absorption and emission spectra recorded in dichloromethane. The directly linked and acetylene linked compounds gave similar HOMO values while vinyl linked compounds showed high-lying HOMO. Due to electron withdrawing nature of acetylene linker, the compounds (**12a-12c**) showed deeper LUMO levels than their direct and vinyl linked counterparts. The compounds possessing vinyl linker (**14a-14c**) constructed high-lying HOMO and the LUMO is similar to that of acetylene counterparts. Thus **14a-14c** exhibited low band gap compared to their direct and acetylene analogs. The observed HOMO and LUMO energy values are well matching with the neighboring molecular layers of OLED device which would facilitate the facile injection of charge carriers.

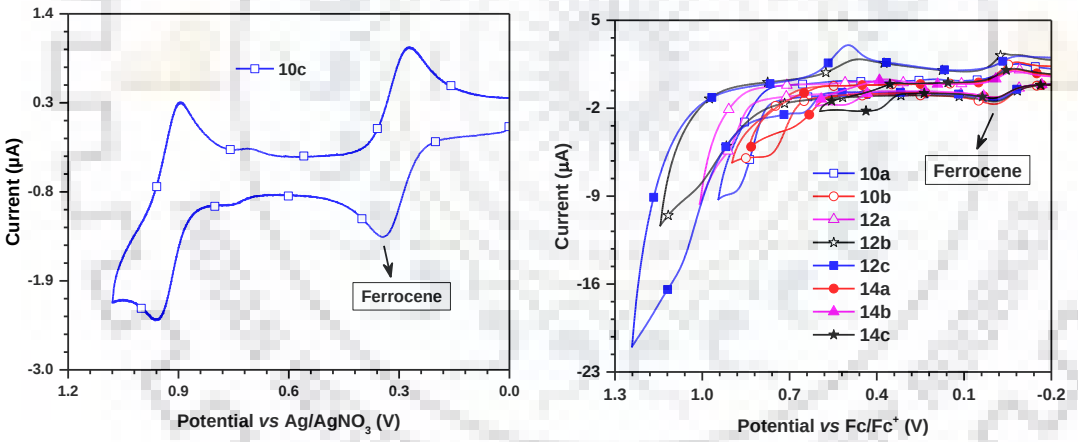

Figure 4.14 Cyclic voltammograms of the dyes recorded in dichloromethane.

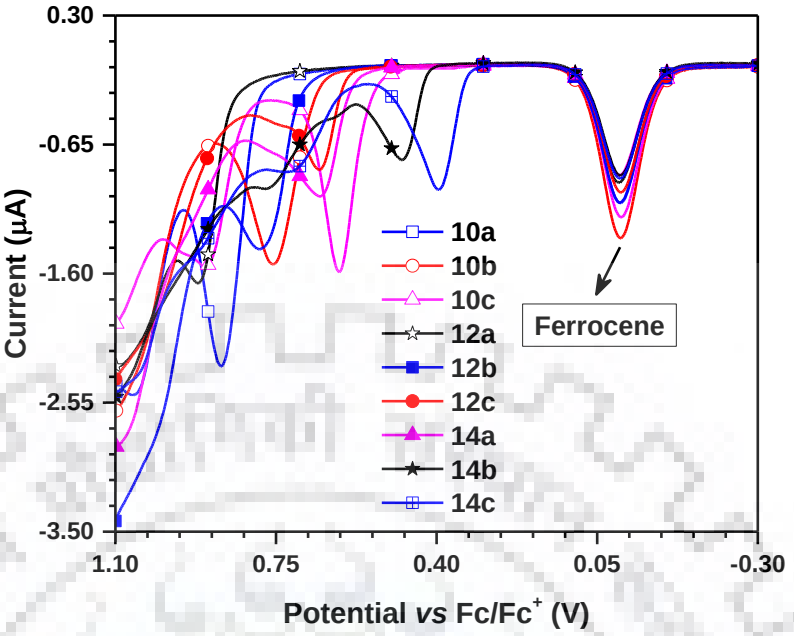

Figure 4.15 Differential pulse voltammograms of the dyes recorded in dichloromethane.

4.2.4 Thermal Properties

The thermal stability of the compounds was evaluated by thermogravimetric analysis (TGA) under nitrogen atmosphere at a heating rate of 10 °C/min. The TGA plot is depicted in Figure 4.16 and the relevant data summarized in Table 4.5. All the dyes exhibited high thermal stability with the onset temperature of 386-463 °C corresponding to 10% weight loss. Carbazole trimers exhibited superior thermal decomposition temperature over fluorene/carbazole hybrids. It is ascribed to the presence of three rigid carbazole units. The exceptional thermal stability of the carbazole-based materials is well documented in the literature [16, 153]. It is interesting to compare the thermal stability of compounds (**12b**, **12c**) containing acetylene linker with those directly linked compounds (**10b**, **10c**) and vinyl linked compounds (**14b**, **14c**). Due to the rigid-rod like acetylene linkage, the former compounds exhibited superior decomposition onset temperatures. Exceptionally, **12a** exhibited poor thermal stability when compared to **10a** and **14a**. It might arise from the decomposition of labile butyl chains present in **12a**. Generally, vinyl linked compounds exhibited inferior thermal decomposition temperature over direct and acetylene linked compounds. It might be attributed to the flexibility of vinyl linker. Interestingly, **10b** showed high decomposition temperature than the reported carbazole trimer 9,9′,9″-tri-*sec*-butyl[2,2′;7′,2″]-tercarbazole [178]. This attests the beneficial role cyano group in improving the thermal robustness of carbazole. Similarly, thermal decomposition temperature

of **12a** is higher when compared to the reported dye, 7,7'-((9,9-dibutyl-9*H*-fluorene-2,7-diyl)bis(ethyne-2,1-diyl))bis(9,9-dipropyl-9*H*-fluorene-2-carbonitrile) which contains cyanofluorene instead of cyanocarbazole [151]. It suggests the role of rigid carbazole in improving thermal decomposition temperature in **12a**. The remarkable thermal stability of these compounds is beneficial to increase the durability of the light-emitting devices.

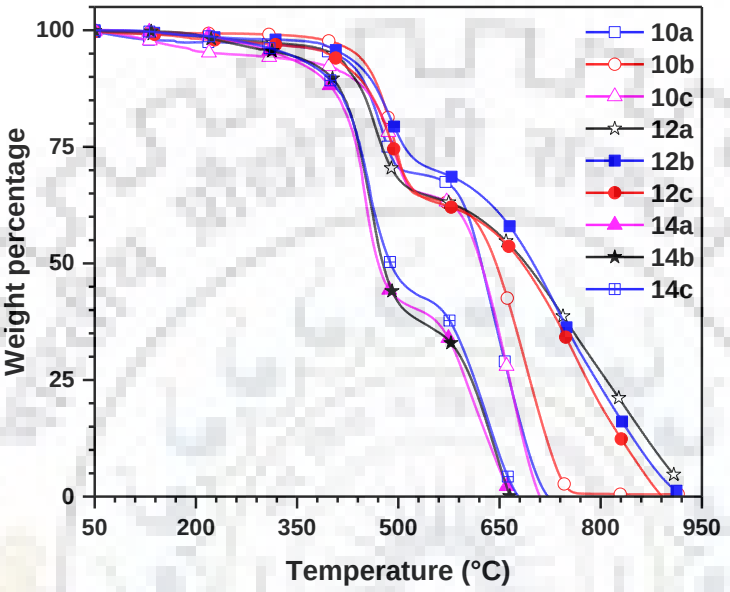

Figure 4.16 TGA plot of the dyes.

Table 4.5 Thermal and electrochemical properties of the dyes

Dye	T_{onset}, °C[a]	T_d, °C	E_{ox}, V[b]	HOMO, eV[c]	LUMO, eV[d]	$E_{0\text{-}0}$, eV[e]
10a	445	639	0.87	-5.67	-2.52	3.15
10b	463	688	0.76	-5.56	-2.43	3.13
10c	429	667	0.61	-5.41	-2.24	3.17
12a	434	467	0.92	-5.72	-2.65	3.07
12b	457	742	0.79	-5.59	-2.55	3.04
12c	440	768	0.65	-5.45	-2.33	3.12
14a	386	604	0.65	-5.45	-2.62	2.83
14b	400	647	0.48	-5.28	-2.47	2.81
14c	394	634	0.39	-5.19	-2.31	2.88

[a] Temperature corresponding to 10% weight loss. [b] Oxidation potential quoted reference to ferrocene internal standard. [c] HOMO = -(4.8 + E_{ox}). [d] LUMO = HOMO + $E_{0\text{-}0}$. [e] Optical band gap obtained from the intersection of normalized absorption and emission spectra (optical edge).

4.2.5 Theoretical Investigations

To get insight into the electronic structure and photophysical properties of these materials, we have performed density functional theoretical calculations. The geometry of the molecules were optimized using B3LYP functional and 6-31G(d,p) basis set [155-156]. The alkyl chains were approximated to methyl to reduce the cost of computational time and it may not affect the point of discussion. The computed absorption maxima and oscillator strength of the most prominent electronic transitions of the compounds are listed in Table 4.6. The frontier molecular orbital diagrams of the dyes are represented in Figure 4.17 to Figure 4.19.

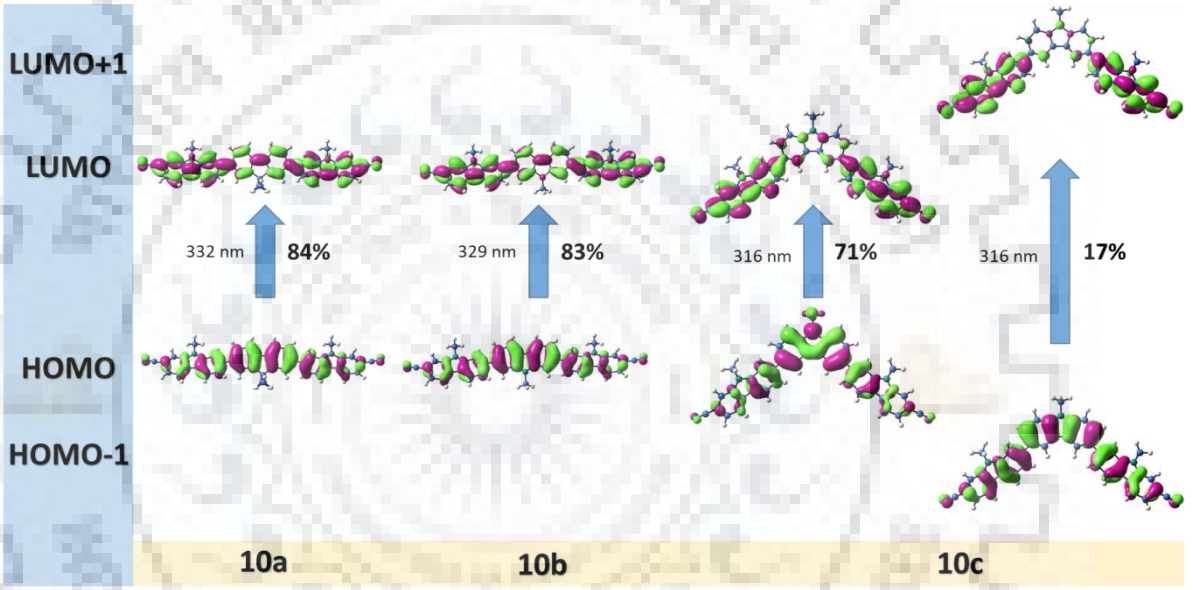

Figure 4.17 Frontier molecular orbital diagrams of the dyes (**10a**-**10c**) and their contribution to prominent absorptions.

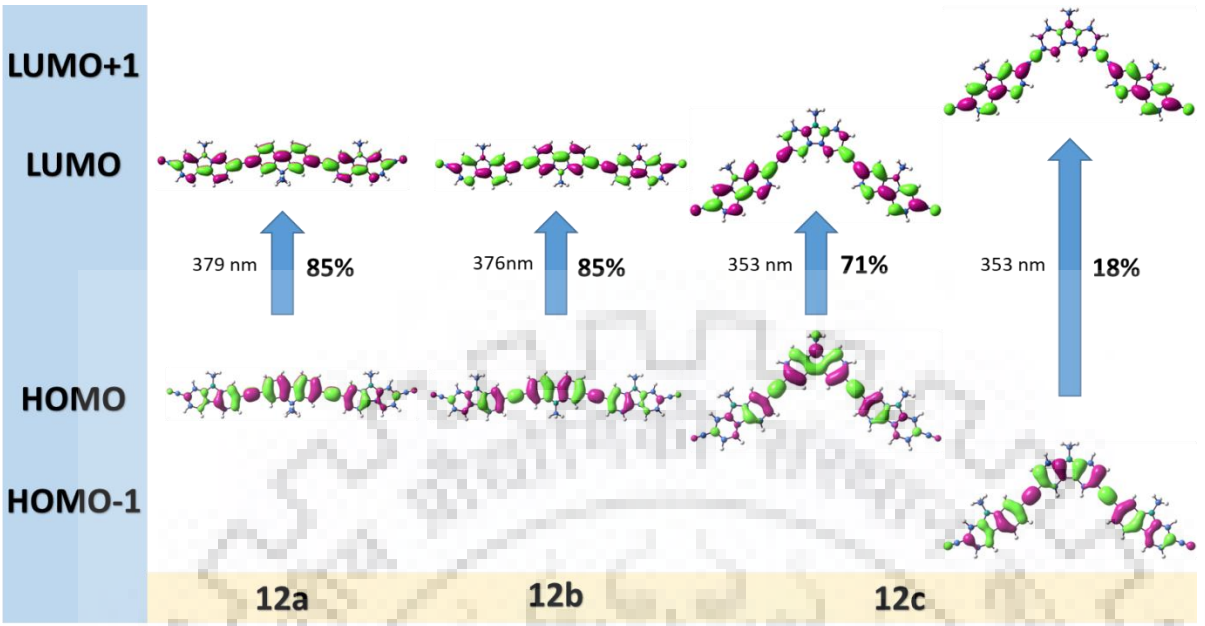

Figure 4.18 Frontier molecular orbital diagrams of the dyes (**12a-12c**) and their contribution to prominent absorptions.

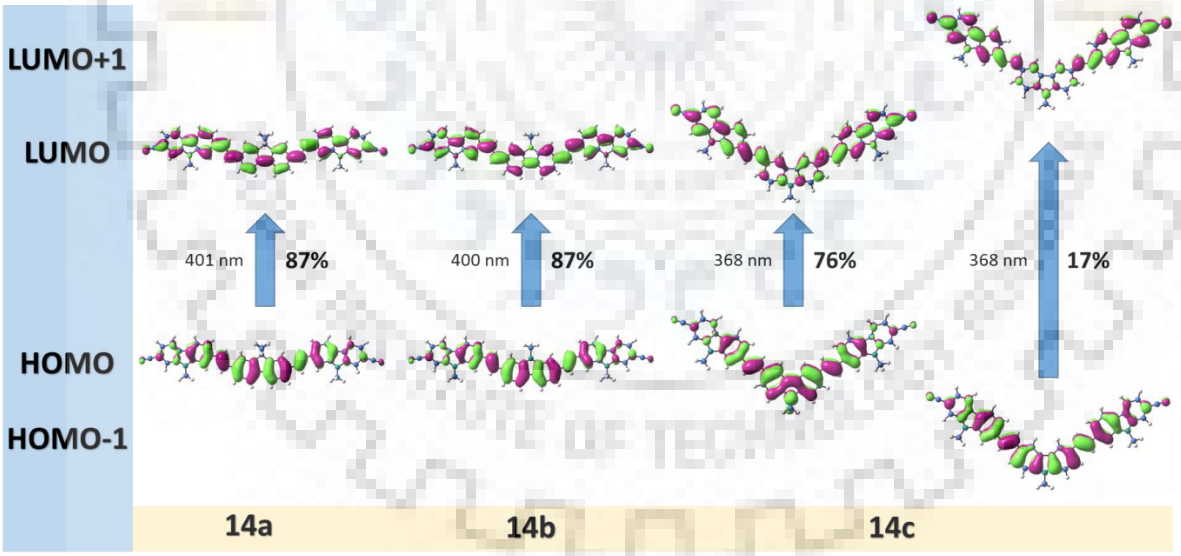

Figure 4.19 Frontier molecular orbital diagrams of the dyes (**14a-14c**) and their contribution to prominent absorptions.

Table 4.6 Predicted vertical excitation obtained by B3LYP/6-31G (d,p) method for the dyes

Dye	λ_{max} (nm)	*f*	Assignment
10a	332	2.8121	HOMO→LUMO (84%)
10b	329	2.7813	HOMO→LUMO (83%)
10c	274	0.3769	HOMO-1→LUMO+2 (32%), HOMO-1→LUMO+1 (29%), HOMO-5→LUMO (11%)
	297	0.2529	HOMO→LUMO+2 (57%), HOMO→LUMO+1 (19%)
	300	0.2288	HOMO→LUMO+1 (39%), HOMO-1→LUMO (24%), HOMO→LUMO+2 (23%)
	305	0.1415	HOMO-3→LUMO (31%), HOMO-2→LUMO+1 (29%), HOMO-2→LUMO (14%), HOMO-3→LUMO+1 (11%)
	316	1.6974	HOMO→LUMO (71%), HOMO-1→LUMO+1 (17%)
12a	282	0.1057	HOMO→LUMO+2 (35%), HOMO-1→LUMO+1 (32%), HOMO-4→LUMO (15%)
	379	3.8309	HOMO→LUMO (85%)
12b	283	0.1533	HOMO→LUMO+2 (35%), HOMO-2→LUMO+1 (23%), HOMO-5→LUMO (13%), HOMO-1→LUMO+1 (11%)
	376	3.8746	HOMO→LUMO (85%)
12c	288	0.2601	HOMO-1→LUMO+1 (46%), HOMO-1→LUMO+2 (16%), HOMO→LUMO (10%)
	325	0.9616	HOMO→LUMO+1 (56%), HOMO-1→LUMO (34%)
	353	2.6004	HOMO→LUMO (71%), HOMO-1→LUMO+1 (18%)
14a	288	0.1613	HOMO-1→LUMO+1 (38%), HOMO→LUMO+2 (30%), HOMO-4→LUMO (16%)
	401	3.5255	HOMO→LUMO (87%)
14b	271	0.1327	HOMO→LUMO+2 (55%), HOMO-5→LUMO (17%), HOMO-1→LUMO+1 (11%)
	290	0.2054	HOMO-1→LUMO+1 (39%), HOMO→LUMO+2 (29%), HOMO-5→LUMO (14%)
	334	0.1105	HOMO-2→LUMO (50%), HOMO→LUMO+1 (41%)
	400	3.4885	HOMO→LUMO (87%)
14c	295	0.3176	HOMO-1→LUMO+1 (53%), HOMO-1→LUMO+2 (11%), HOMO→LUMO (10%)
	333	0.9315	HOMO→LUMO+1 (59%), HOMO-1→LUMO (33%)
	368	3.0010	HOMO→LUMO (76%), HOMO-1→LUMO+1 (17%)

The trend of absorption maxima of the compounds is similar to that of experimental results which depend on the nature of linker as direct (**10**) < acetylene (**12**) < vinyl (**14**). Similarly, within the series, absorption maxima followed the trend for central aromatic linkage as 3,6-carbazole (**c**) < 2,7-fluorene (**a**) < 2,7-carbazole (**b**). The HOMO and LUMO of the linear compounds (**10a**, **10b**, **12a**, **12b** and **14a**, **14b**) are dispersed over the entire molecule. Therefore, the HOMO to LUMO excitation in these linear compounds is assigned to typical π-

π* absorption. In contrast, for V-shaped compounds (**10c**, **12c** and **14c**), HOMO is mainly localized on central carbazole and spread into end-capped cyanocarbazole units to some extent. However, the LUMO is concentrated mainly on peripheral cyanocarbazoles. This clearly indicates the drifting of electron density from central carbazole to terminal cyanocarbazoles during electronic excitation [157-159].

4.2.6 Electroluminescence Properties

To evaluate the electroluminescence performance of the dyes, we fabricated the OLED devices with the configuration, ITO/PEDOT:PSS/CBP:dye/TPBi/LiF/Al. Here, indium doped tin oxide (ITO) serves as anode, polyethylenedioxythiophene/polystyrenesulfonate (PEDOT:PSS) as hole injecting layer, *N,N'*-dicarbazolyl-4,4'-biphenyl (CBP) as host material into which the dyes are doped, 1,3,5-tris(*N*-phenylbenzimidazol-2-yl)benzene (TPBi) as electron transporting or hole blocking layer, LiF as electron injecting layer and aluminum as cathode.

Initially, we fabricated a non-doped device with the dye **12c** as emitting layer. We observed high current density and low luminance. In addition, we noted broad and red shifted electroluminescence spectra as compared to its photoluminescence recorded in toluene. It might be due to the formation of *J*- aggregates in solid state, which resulted in poor quality of thin film [145,163,199]. The observation of high current density probably arises from the hole only current. Due to the fast injection of hole carriers and imbalanced charge transport, the hole carriers could have reached cathode before the recombination takes place in emissive layer [199]. As a result, the recombination zone formed at the interface rather than at emissive layer leading to the quenching of excitons without electroluminescence. Thus, low luminance is observed. However, the observed electroluminescence performance is better than the reported device fabricated with 3,6-bis[2-(9-(2-ethylhexyl)-9*H*-carbazol-3-yl)-ethynyl]-9*H*-carbazole in a similar device configuration [30]. The improved luminance could be attributed to the electron withdrawing CN group which boosted the electron transport while retarding hole mobility. Since the non-doped device gave poor performance probably due to the aggregation of the dyes in solid state, we changed our focus for doped devices by using these emitters as dopants into CBP host to alleviate the intermolecular interactions. The energy level diagram of doped device configuration is represented in Figure 4.20. The current density-voltage-luminance (J-V-L) plots and the electroluminescence spectra of the devices are displayed in Figures 4.21 to 4.26.

The electroluminescent data is collected in Table 4.7. In the doped devices, the emission maximum of electroluminescence is blue shifted when compared to that of non-doped device and it closely resembles to emission maximum of photoluminescence spectrum recorded in toluene (Figure 4.26). It clearly indicates that the dispersion of dye molecules into CBP host suppressed the formation of aggregation by dilution effect and the emission originates from the dopants [164]. As the doping concentration is increased, electroluminescence emission maximum slightly shifts to the longer wavelength region because of aggregation.

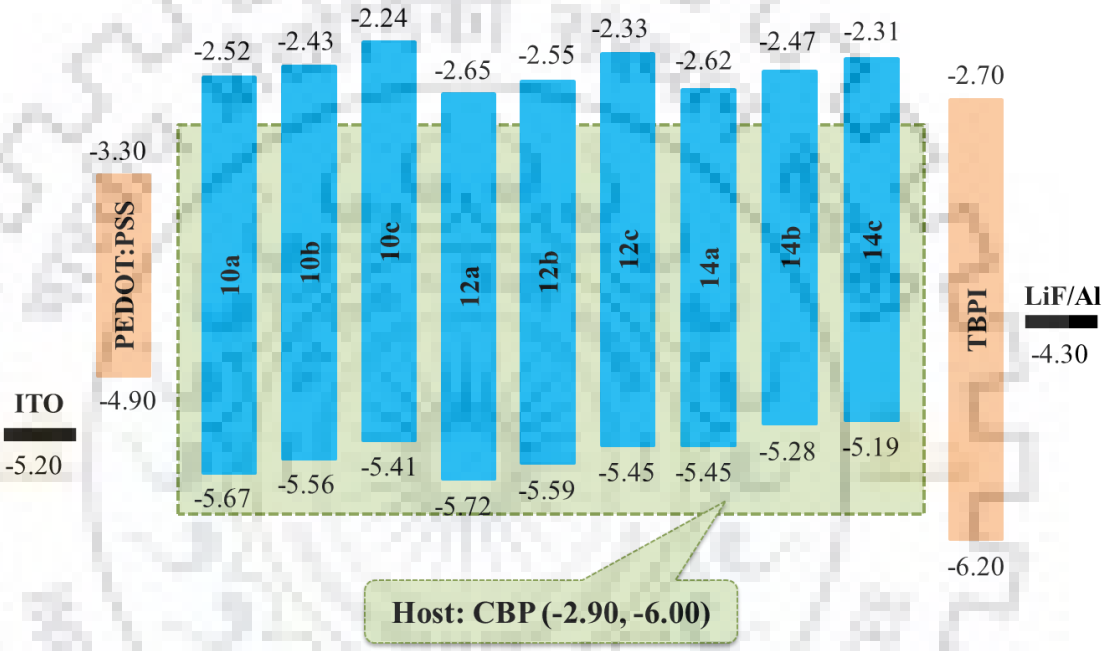

Figure 4.20 Energy level diagram of the materials used in OLED device (all values are in eV with reference to vacuum).

The doped devices fabricated with the acetylene congeners (**12a-12c**) exhibited higher power and current efficiencies when compared to those of directly linked analogs (**10a-10c**). The energy barrier (Figure 4.20) for the injection of holes and electrons is relatively less for the acetylene dyes, which could facilitate balanced transport of charge carriers. Particularly, the low- lying LUMO of acetylene derivatives is beneficial for achieving balanced charge transport and thus maximum harvesting of excitons and better electroluminescence performance. The relatively high-energy barrier of **10c** for the injection of holes and electrons restricted the performance of the corresponding device within the series. This may be due to the incomplete energy transfer from CBP host to the dopant [200]. Furthermore, high energy barrier for the

injection of charge carriers from host to dopant resulted in high turn-on voltage for **10c** compared to other dyes. 3,6-carbazole substituted compounds showed high turn-on voltage in each set of derivatives owing to high energy barrier for charge injection. In contrast, 2,7-fluorene and 2,7-carbazole derivatives gave similar turn-on voltage.

The doped devices containing vinyl linked compounds showed high electroluminescence performances compared to both acetylene and directly linked counterparts. The superior current and power efficiency of **14a**-**14c** might be due to low energy barrier for the transportation of charge carriers and effective harvesting and confinement of excitons in emissive layer. The low turn-on voltage of vinyl linked compounds is attributed to high-lying HOMO energy level which facilitates the easy injection of hole charge carriers from PEDOT into emissive layer. Also, linear carbazole compound **14b** showed almost two-fold increase in power and current efficiency when compared to that of fluorene analog **14a**. It is due to more favorable energy barrier for the transportation of charge carriers for linear carbazole compound than fluorene analog.

All the direct and acetylene linked compounds (**10a**-**10c** and **12a**-**12c**) exhibited deep blue emission with the CIE coordinate of x = 0.16, and y in the range of 0.04 to 0.07. These values match well with the standard deep blue emission (0.14, 0.08) prescribed by National Television System Committee (NTSC 1987). The narrow full width half maxima (FWHM) of the EL spectra are responsible for the high color purity of OLED light. This further confirms the suppression of detrimental aggregation of the dyes in the solid state. The best electroluminescence performance which meets the NTSC deep blue emission standard is obtained for the device fabricated with the dye, **12a** (1 wt%). It showed the power efficiency of 1.2 lm/W, current efficiency of 2.0 cd/A and EQE of 4.4%. It might be due to the lowest energy barrier of **12a** with adjacent layers and host, which favors balanced charge transport, and effective transfer of energy from CBP host to the dopant.

On the whole, the best electroluminescence efficiency is observed for the device fabricated with **14b** (3 wt%) with power efficiency of 6.2 lm/W, current efficiency of 8.5 cd/A, EQE of 4.6% and maximum luminance of 9314 cd/m^2. The high performance is attributed to favorable energy barrier of the compound with neighboring charge transporting layers and host which results in balanced charge transport and effective energy transfer from CBP host to the dopant. However, the color purity of vinyl linked compounds is compromised to some extent due to

higher FWHM of electroluminescence spectra. The electroluminescence emission falls in bluish green color. Since the vinyl linker-based compounds possessed low band gap, the electroluminescence spectrum is red shifted compared to their direct and acetylene linked counterparts. As a result, they exhibited bluish green emission. Further, the relatively larger FWHM value attests the compromise of color purity to some extent. Interestingly, the cyanocarbazole end capped trimers exhibited superior performance over their corresponding mono- substituted cyanocarbazole (Chapter 3). It could be ascribed to the presence of two cyanocarbazole units which is beneficial to realize balanced charge transport and thus effective harvesting of excitons.

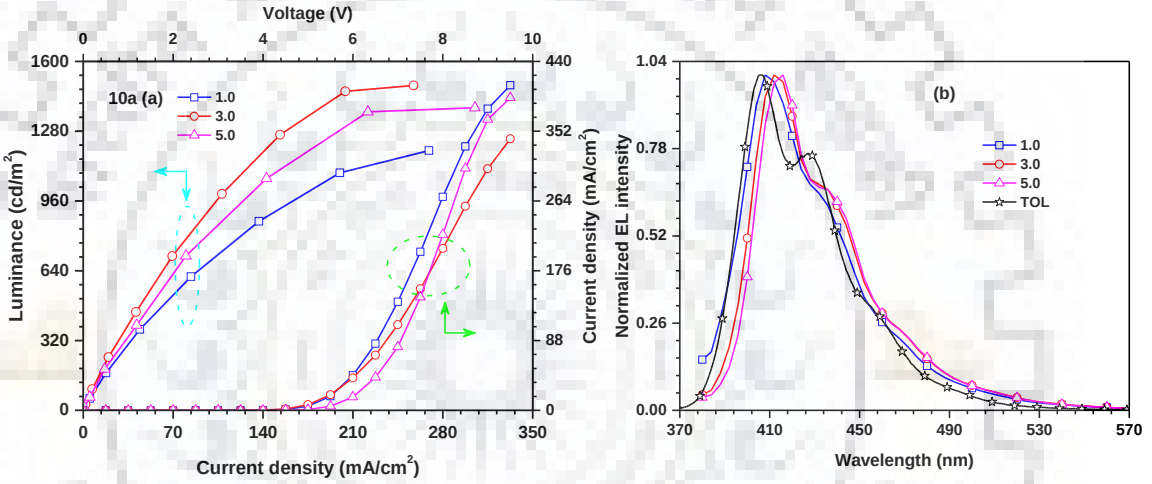

Figure 4.21 J-V-L characteristics and comparison of EL spectra and PL of the dye **10a**.

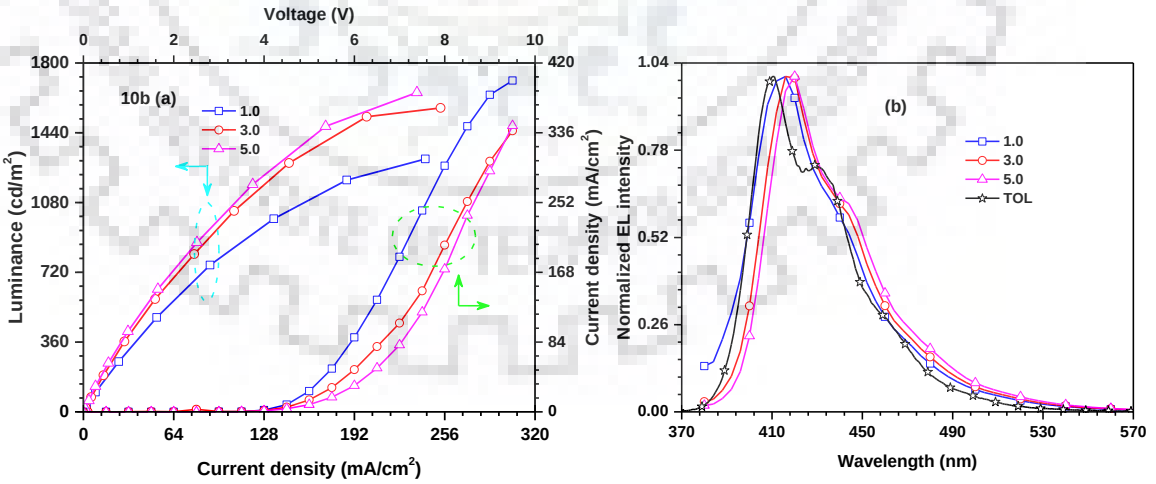

Figure 4.22 J-V-L characteristics and comparison of EL spectra and PL of the dye **10b**.

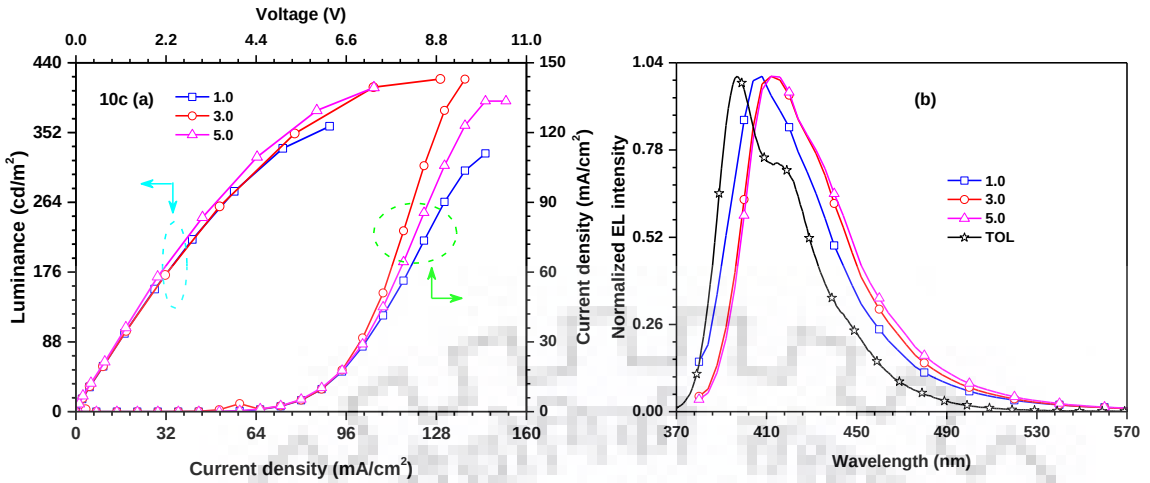

Figure 4.23 J-V-L characteristics and comparison of EL spectra and PL of the dye **10c**.

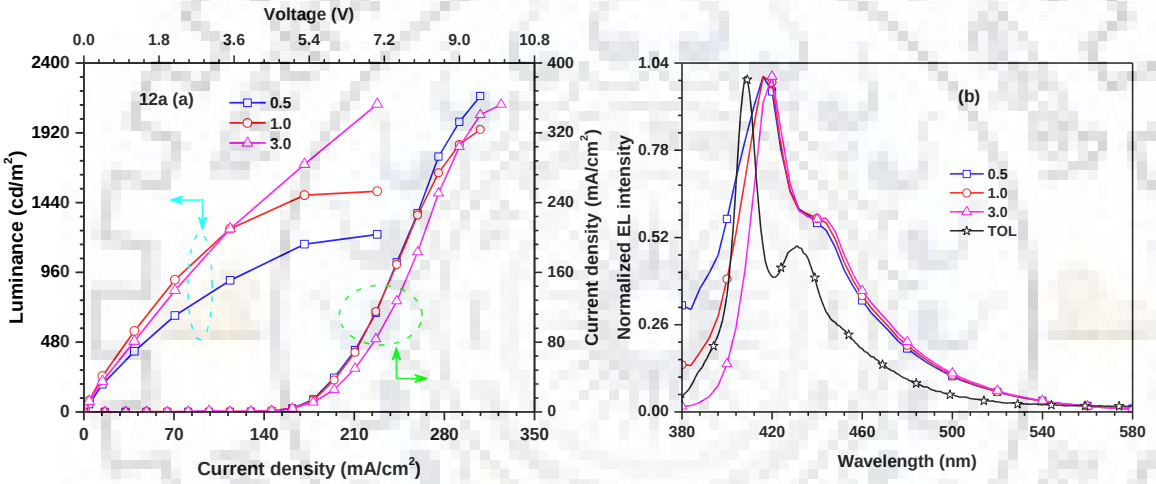

Figure 4.24 J-V-L characteristics and comparison of EL spectra and PL of the dye **12a**.

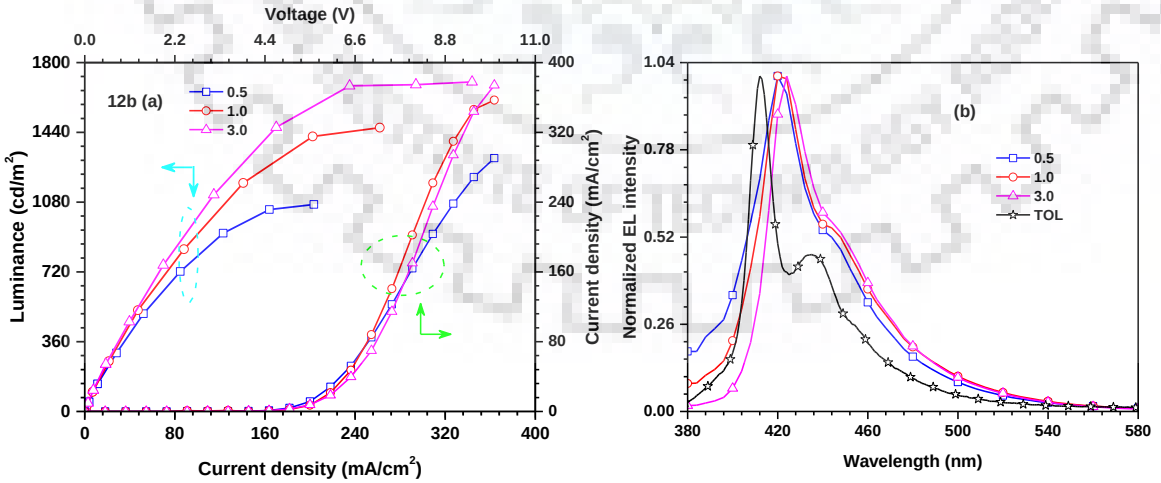

Figure 4.25 J-V-L characteristics and comparison of EL spectra and PL of the dye **12b**.

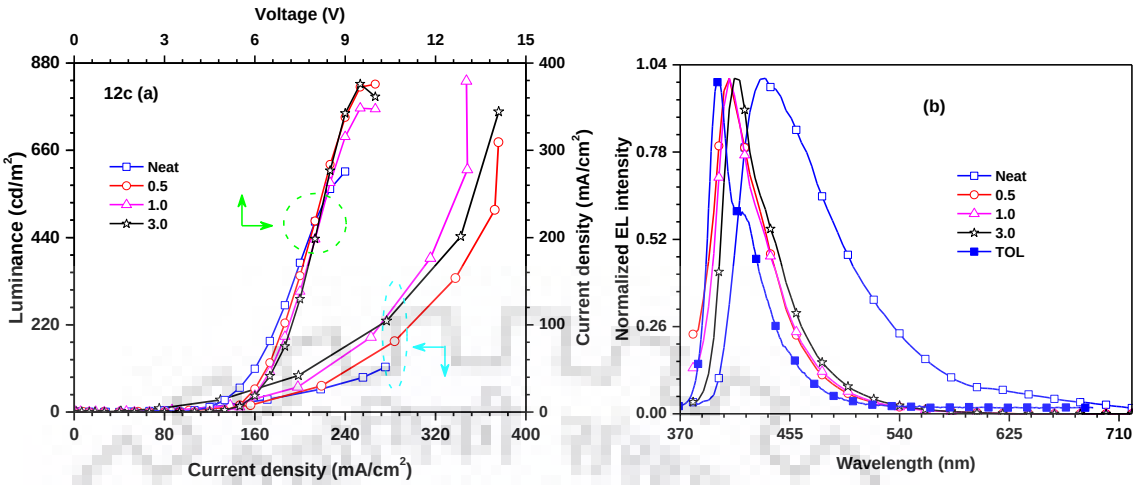

Figure 4.26 J-V-L characteristics and comparison of EL spectra and PL of the dye **12c**.

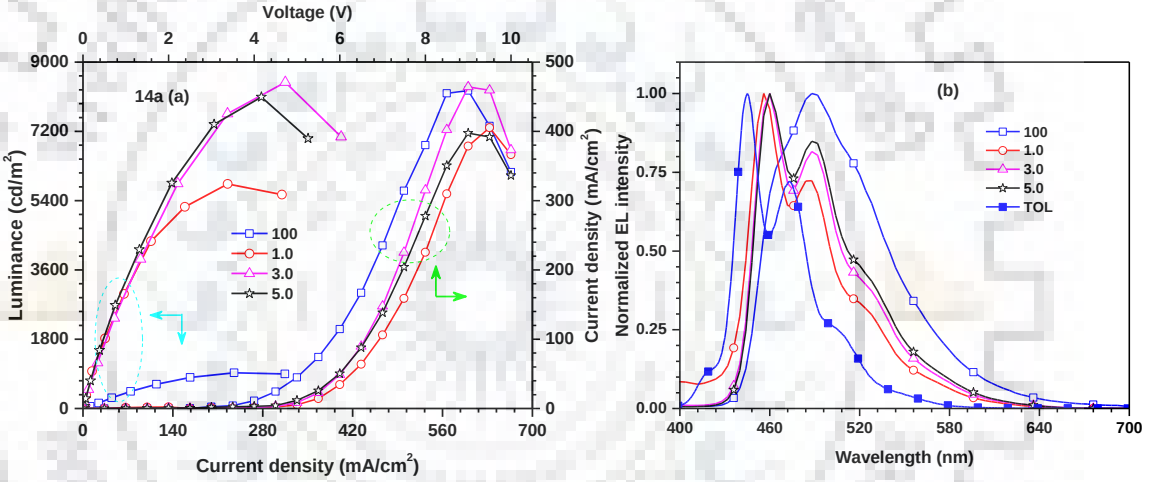

Figure 4.27 J-V-L characteristics and comparison of EL spectra and PL of the dye **14a**.

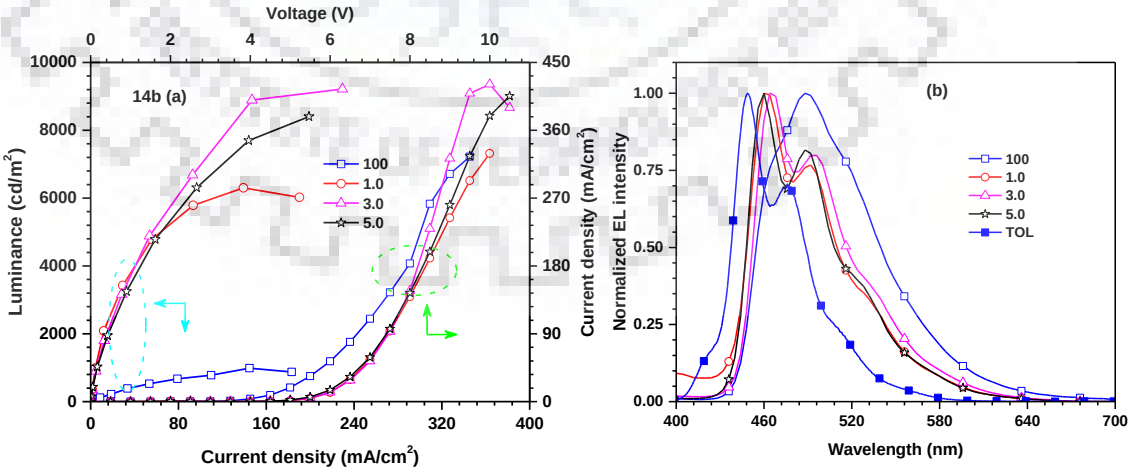

Figure 4.28 J-V-L characteristics and comparison of EL spectra and PL of the dye **14b**.

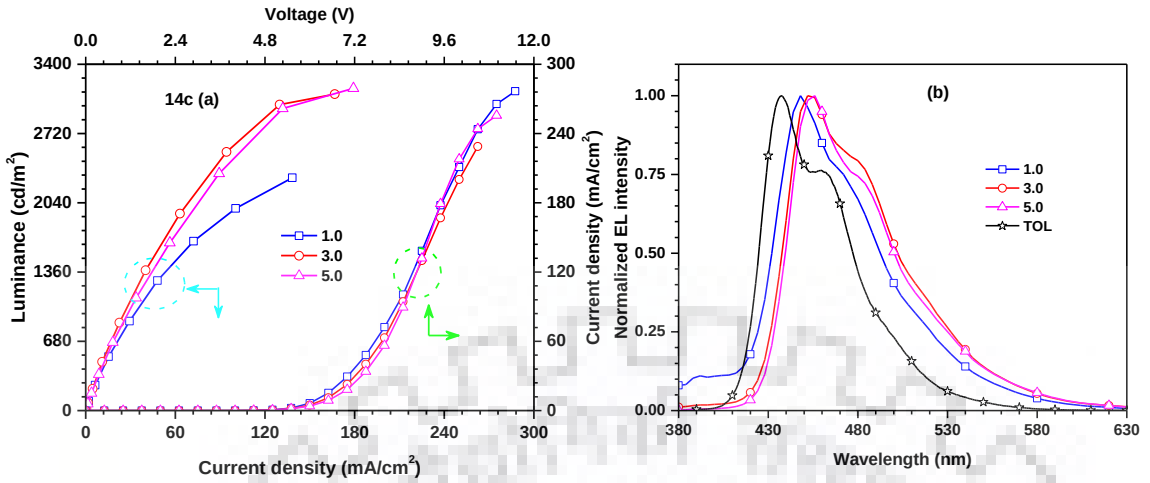

Figure 4.29 J-V-L characteristics and comparison of EL spectra and PL of the dye **14c**.

Table 4.7 Electroluminescent parameters of the dyes [a]

Dye	wt%	Turn-on voltage (V)	Power Efficiency (lm/w)	Current Efficiency (cd/A)	EQE (%)	CIE (x,y)	Maximum Luminance (cd/m^2)	λ_{EL} (nm)	FWHM (nm)
10a	1.0	5.2	0.6	1.0	3.7	(0.16, 0.05)	1191	408	55
	3.0	5.0	0.9	1.4	4.2	(0.16, 0.05)	1490	412	53
	5.0	5.7	0.7	1.2	3.6	(0.16, 0.05)	1388	416	51
10b	1.0	4.5	0.8	1.2	3.7	(0.16, 0.04)	1305	416	54
	3.0	4.6	0.9	1.3	3.9	(0.16, 0.05)	1568	418	50
	5.0	4.8	1.0	1.5	4.0	(0.16, 0.05)	1648	420	51
10c	1.0	6.5	0.3	0.6	2.0	(0.16, 0.05)	360	408	54
	3.0	6.5	0.3	0.6	1.8	(0.16, 0.05)	420	412	52
	5.0	6.4	0.3	0.6	1.7	(0.16, 0.05)	409	412	53
12a	0.5	5.2	0.8	1.3	3.2	(0.16, 0.07)	1221	416	68
	1.0	5.1	1.2	2.0	4.4	(0.16, 0.07)	1518	416	60
	3.0	5.1	1.1	1.9	3.5	(0.16, 0.07)	2276	420	54
12b	0.5	5.3	0.7	1.2	3.0	(0.16, 0.06)	1068	420	56
	1.0	5.5	0.8	1.4	3.0	(0.16, 0.06)	1464	420	53
	3.0	5.4	0.8	1.4	2.8	(0.16, 0.06)	1700	424	47
12c	0.5	5.7	0.4	0.8	2.6	(0.16, 0.05)	864	408	55
	1.0	5.6	0.6	1.1	3.4	(0.16, 0.05)	1085	408	52
	3.0	5.5	0.8	1.4	3.6	(0.16, 0.06)	1706	412	49
14a	1.0	4.5	3.2	4.6	3.0	(0.16, 0.21)	5834	456, 488	73
	3.0	4.3	3.2	4.3	2.6	(0.16, 0.26)	8478	460, 488	73
	5.0	4.1	2.6	3.4	1.8	(0.16, 0.28)	7810	460, 488	75
14b	1.0	4.4	5.7	8.0	4.4	(0.16, 0.26)	6304	460, 492	75
	3.0	4.3	6.2	8.5	4.6	(0.16, 0.30)	9314	464, 496	75
	5.0	4.3	5.3	7.4	4.5	(0.16, 0.26)	8404	460, 488	73
14c	1.0	5.5	2.4	4.2	3.5	(0.15, 0.14)	2286	448	70
	3.0	5.6	2.7	4.8	3.4	(0.15, 0.18)	3107	452	70
	5.0	5.7	2.6	4.6	3.1	(0.15, 0.18)	3163	456	67

[a] values at 100 cd/m^2

4.3 Conclusions

Cyanocarbazole end capped fluorene/carbazole trimers have been designed, synthesized and characterized by their photophysical and electroluminescent properties. The effect of core unit, spacer and linking topology on photophysical, electrochemical and electroluminescent properties is studied elaborately. The linear compounds showed solvent independent emission while V-shaped compounds displayed positive solvatochromism attributable to intramolecular charge transfer excited state. The linear carbazole derivatives showed high thermal decomposition temperature compared to their analogous fluorene compounds which attest the role of carbazole. Also, acetylene linked compounds show better thermal stability over directly connected and vinyl compounds owing to rigid and rod-like spacer. Despite of similar HOMO energy level for direct and acetylene derivatives, the LUMO of acetylene derivatives are stabilized due to the electron withdrawing nature of acetylene spacer. The vinyl derivatives gave high lying HOMO and low lying LUMO which was beneficial for facile transportation of charge carriers. As a result, vinyl linked compounds showed high power efficiency and current efficiency. The effect of cyano- group of peripheral carbazole on photophysical and electroluminescent properties is established by comparing the known compounds in the literature. The balanced charge transport of charge carriers was obtained by the presence of cyano- group without compromising color purity of electroluminescence and hence better OLED performance.

4.4 Experimental Section

4.4.1 General Materials and Methods

Computational methods, OLED device fabrication and characterization methods are similar to that are in chapter 3.

4.4.2 Synthesis

Synthesis of 7,7'-(9,9-diethyl-9*H*-fluorene-2,7-diyl)bis(9-(2-ethylhexyl)-9*H*-carbazole-2-carbonitrile), 10a

A mixture of 7-bromo-9-(2-ethylhexyl)-9*H*-carbazole-2-carbonitrile (0.74 g, 1.94 mmol), (9,9-diethyl-9*H*-fluorene-2,7-diyl)diboronic acid (0.3 g, 0.97 mmol), $PdCl_2(PPh_3)_2$ (13.6 mg, 0.019 mmol), PPh_3 (10.2 mg, 0.038 mmol), potassium carbonate (0.8 g, 5.8 mmol) and DMF/

water (21:7 mL) is heated to 80 °C for 12 h under nitrogen atmosphere. After completion of the reaction, the mixture is poured to water and extracted with chloroform. The organic layer was dried over anhydrous sodium sulphate. Finally, the solvent was removed under vacuum to yield a residue which was further purified by column chromatography using hexane/chloroform (2:3) as eluant. Tan color solid. Yield 0.58 g (73%). mp 146-148 °C; IR (KBr, cm^{-1}) 2221 ($\nu_{C\equiv N}$); ^1H NMR ($CDCl_3$, 400 MHz) δ 8.21-8.16 (m, 4 H), 7.88 (d, J = 7.6 Hz, 2 H), 7.74-7.63 (m, 10 H), 7.51 (d, J = 8.4 Hz, 2 H), 4.32-4.21 (m, 4 H), 2.22-2.11 (m, 6 H), 1.48-1.25 (m, 16 H), 0.98 (t, J = 7.2 Hz, 6 H), 0.89 (t, J = 7.6 Hz, 6 H), 0.51 (t, J = 7.6 Hz, 6 H). ^{13}C NMR ($CDCl_3$, 100.3 MHz) δ 151.08, 142.62, 141.49, 140.62, 140.28, 126.64, 126.05, 122.15, 122.03, 121.43, 120.87, 120.40, 120.21, 119.75, 113.12, 107.86, 107.79, 56.36, 47.57, 39.50, 32.84, 30.97, 28.76, 24.45, 23.01, 13.99, 10.91, 8.74. HRMS calcd for $C_{59}H_{62}N_4$ *m/z* 826.4969, found 826.4948.

Synthesis of 9,9',9''-tris(2-ethylhexyl)-9*H*,9'*H*,9''*H*-[2,2':7',2''-tercarbazole]-7,7''-dicarbonitrile, 10b

It was prepared from a mixture of 7-bromo-9-(2-ethylhexyl)-9*H*-carbazole-2-carbonitrile (0.73 g, 1.90 mmol), (9-(2-ethylhexyl)-9*H*-carbazole-2,7-diyl)diboronic acid (0.35 g, 0.95 mmol), $PdCl_2(PPh_3)_2$ (13.3 mg, 0.019 mmol), PPh_3 (10.0 mg, 0.038 mmol), potassium carbonate (0.8 g, 5.8 mmol) and DMF/water (21:7 mL) by following the procedure described for **10a**. Greenish yellow solid. Yield 0.6 g (71%); mp 214-216 °C; IR (KBr, cm^{-1}) 2222 ($\nu_{C\equiv N}$); ^1H NMR ($CDCl_3$, 400 MHz) δ 8.25-8.17 (m, 6 H), 7.75-7.68 (m, 8 H), 7.63-7.61 (m, 2 H), 7.53-7.51 (m, 2 H), 4.35-4.27 (m, 6 H), 2.24-2.13 (m, 3 H), 1.51-1.27 (m, 24 H), 0.98 (t, J = 8.0 Hz, 9 H), 0.88 (t, J = 6.8 Hz, 9 H). ^{13}C NMR ($CDCl_3$, 100.3 MHz) δ 142.65, 142.12, 142.06, 140.24, 139.57, 126.07, 122.18, 122.02, 121.46, 120.87, 120.81, 120.75, 120.42, 120.11, 119.16, 113.12, 108.30, 108.01, 107.78, 47.66, 47.39, 39.52, 39.44, 31.07, 30.96, 28.83, 28.73, 24.38, 23.09, 23.03, 14.05, 14.01, 10.97, 10.91. HRMS calcd for $C_{62}H_{69}N_5$ *m/z* 883.5547, found 883.5531.

Synthesis of 9'-butyl-9,9''-bis(2-ethylhexyl)-9*H*,9'*H*,9''*H*-[2,3':6',2''-tercarbazole]-7,7''-dicarbonitrile, 10c

It was prepared from a mixture of 7-bromo-9-(2-ethylhexyl)-9*H*-carbazole-2-carbonitrile (0.74 g, 1.94 mmol), (9-butyl-9*H*-carbazole-3,6-diyl)diboronic acid (0.3 g, 0.97 mmol),

$PdCl_2(PPh_3)_2$ (13.6 mg, 0.019 mmol), PPh_3 (10.2 mg, 0.038 mmol), potassium carbonate (0.8 g, 5.8 mmol) and DMF/water (21:7 mL) by following the procedure described for **10a**. Yellow solid. Yield 0.53 g (66%); mp 172-174 °C; IR (KBr, cm^{-1}) 2222 ($\nu_{C\equiv N}$); ^{1}H NMR ($CDCl_3$, 400 MHz) δ 8.49 (s, 2 H), 8.22-8.15 (m, 4 H), 7.87-7.85 (m, 2 H), 7.72-7.68 (m, 6 H), 7.59-7.49 (m, 4 H), 4.42 (t, *J* = 6.8 Hz, 2 H), 4.31-4.21 (m, 4 H), 2.13 (t, *J* = 5.6 Hz, 2 H), 2.00-1.93 (m, 2 H), 1.51-1.26 (m, 16 H), 1.04-0.85 (m, 17 H). ^{13}C NMR ($CDCl_3$, 100.3 MHz) *δ* 142.79, 142.10, 140.58, 140.13, 132.92, 126.19, 125.89, 123.51, 122.13, 121.39, 120.73, 120.48, 120.32, 120.02, 119.36, 113.05, 109.32, 107.88, 107.55, 47.63, 43.14, 39.38, 31.22, 30.90, 28.69, 24.39, 23.01, 20.60, 14.02, 13.92, 10.91. HRMS calcd for $C_{58}H_{61}N_5$ *m/z* 827.4921, found 827.4948.

Synthesis of 7,7'-(9,9-dibutyl-9*H*-fluorene-2,7-diyl)bis(ethyne-2,1-diyl))bis(9-(2-ethylhexyl)-9*H*-carbazole-2-carbonitrile), 12a

A mixture of 9,9-dibutyl-2,7-diethynyl-9*H*-fluorene (0.5 g, 1.5 mmol), 7-bromo-9-(2-ethylhexyl)-9*H*-carbazole-2-carbonitrile (1.1 g, 3.0 mmol), $Pd(PPh_3)_2Cl_2$ (21.1 mg, 0.03 mmol), PPh_3 (7.9 mg, 0.03 mmol), CuI (17.1 mg, 0.09 mmol) and triethylamine (30 mL) was refluxed for 12 h under nitrogen atmosphere. After completion of the reaction, the mixture was poured into water and extracted with chloroform. The organic layer was dried over anhydrous sodium sulphate. Finally, the solvent was removed under vacuum to yield a residue which was further purified by column chromatography using hexane/chloroform (1:4) as eluant. Brown solid. Yield 0.85 g (65%); mp 194-196 °C; IR (KBr, cm^{-1}) 2221 ($\nu_{C\equiv N}$); ^{1}H NMR ($CDCl_3$, 400 MHz) *δ* 8.14 (d, *J* = 8.4 Hz, 1 H), 8.11 (d, *J* = 8.0 Hz, 1 H), 7.74-7.69 (m, 4 H), 7.65-7.59 (m, 6 H), 7.53-7.49 (m, 4 H), 4.26-4.15 (m, 2 H), 2.12-2.02 (m, 6 H), 1.46-1.25 (m, 16 H), 1.17-1.08 (m, 4 H), 0.94 (t, *J* = 7.2 Hz, 6 H), 0.89 (t, *J* = 7.2 Hz, 6 H), 0.70 (t, *J* = 7.6 Hz, 6 H), 0.65-0.62 (m, 4 H); ^{13}C NMR ($CDCl_3$, 100.3 MHz) *δ* 151.14, 141.71, 140.82, 140.37, 130.88, 125.96, 125.84, 123.55, 122.29, 122.20, 121.83, 121.62, 121.16, 121.10, 120.21, 120.09, 113.31, 112.55, 108.32, 91.11, 90.69, 55.21, 47.84, 40.28, 39.31, 30.83, 28.62, 25.89, 24.40, 23.07, 23.03, 14.02, 13.85, 10.91; HRMS calcd for $C_{67}H_{70}N_4$ (*m/z* + 1) 931.5673, found 931.5694.

Synthesis of 7,7'-((9-butyl-9*H*-carbazole-2,7-diyl)bis(ethyne-2,1-diyl))bis(9-(2-ethylhexyl)-9*H*-carbazole-2-carbonitrile), 12b

It was prepared from a mixture of 9-butyl-2,7-diethynyl-9*H*-carbazole (0.5 g, 1.8 mmol), 7-bromo-9-(2-ethylhexyl)-9*H*-carbazole-2-carbonitrile (1.4 g, 3.6 mmol), $Pd(PPh_3)_2Cl_2$ (25.3 mg,

0.036 mmol), PPh_3 (9.4 mg, 0.036 mmol), CuI (20.6 mg, 0.108 mmol) and triethylamine (30 mL) by following the procedure described for **12a**. Yellow solid. Yield 0.81 g (52%); mp 266-268 °C; IR (KBr, cm^{-1}) 2225 ($\nu_{C\equiv N}$); ^1H NMR ($CDCl_3$, 400 MHz) δ 8.14-8.07 (m, 6 H), 7.68 (d, J = 11.2 Hz, 6 H), 7.55-7.49 (m, 6 H), 4.34 (t, J = 7.6 Hz, 2 H), 4.25-4.15 (m, 4 H), 2.12-2.06 (m, 2 H), 1.96-1.89 (m, 2 H), 1.51-1.25 (m, 18 H), 1.03-0.87 (m, 15 H); ^{13}C NMR ($CDCl_3$, 100.3 MHz) δ 141.71, 140.74, 140.35, 125.83, 123.57, 123.00, 122.64, 122.32, 122.27, 121.57, 121.12, 121.06, 120.68, 120.54, 120.36, 120.21, 113.28, 112.56, 112.02, 108.30, 91.51, 90.28, 47.81, 43.10, 39.30, 31.12, 30.84, 29.67, 28.62, 24.40, 23.02, 20.64, 14.01, 10.90; HRMS calcd for $C_{62}H_{61}N_5$ *m/z* 875.4927, found 875.4914.

Synthesis of 7,7'-((9-butyl-9*H*-carbazole-3,6-diyl)bis(ethyne-2,1-diyl))bis(9-(2-ethylhexyl)-9*H*-carbazole-2-carbonitrile), 12c

It was prepared from a mixture of 9-butyl-3,6-diethynyl-9*H*-carbazole (0.5 g, 1.8 mmol), 7-bromo-9-(2-ethylhexyl)-9*H*-carbazole-2-carbonitrile (1.4 g, 3.6 mmol), $Pd(PPh_3)_2Cl_2$ (25.3 mg, 0.036 mmol), PPh_3 (9.4 mg, 0.036 mmol), CuI (20.6 mg, 0.108 mmol) and triethylamine (30 mL) by following the procedure described for **12a**. Yellow solid. Yield 0.75 g (48%); mp 184-186 °C; IR (KBr, cm^{-1}) 2221 ($\nu_{C\equiv N}$); ^1H NMR ($CDCl_3$, 400 MHz) δ 8.34 (s, 2 H), 8.13-8.09 (m, 4 H), 7.73 (d, J = 8.8 Hz, 2 H), 7.66 (d, J = 13.2 Hz, 4 H), 7.53-7.48 (m, 4 H), 7.42 (d, J = 8.4 Hz, 2 H), 4.33 (t, J = 7.6 Hz, 2 H), 4.24-4.14 (m, 4 H), 2.09 (t, J = 6.4 Hz, 2 H), 1.93-1.86 (m, 2 H), 1.46-1.26 (m, 18 H), 1.00-0.93 (m, 9 H), 0.89 (t, J = 6.8 Hz, 6 H); ^{13}C NMR ($CDCl_3$, 100.3 MHz) δ 141.60, 140.30, 140.08, 129.63, 125.72, 124.01, 123.36, 122.67, 122.30, 122.03, 121.13, 120.93, 120.79, 120.19, 113.65, 113.01, 112.22, 108.96, 107.94, 91.38, 88.83, 47.57, 42.96, 39.18, 30.98, 30.75, 28.52, 24.29, 22.94, 20.41, 13.95, 13.76, 10.80; HRMS calcd for $C_{62}H_{61}N_5$ *m/z* 875.4927, found 875.4926.

Synthesis of 7,7'-((1*E*,1'*E*)-(9,9-diethyl-9*H*-fluorene-2,7-diyl)bis(ethene-2,1-diyl))bis(9-(2-ethylhexyl)-9*H*-carbazole-2-carbonitrile), 14a

A mixture of 9,9-diethyl-2,7-divinyl-9*H*-fluorene (0.25 g, 0.91 mmol), 7-bromo-9-(2-ethylhexyl)-9*H*-carbazole-2-carbonitrile (0.74 g, 1.93 mmol), $Pd(OAc)_2$ (8.2 mg, 0.036 mmol), sodium acetate (1.5 g, 18.2 mmol), tetrabutylammonium bromide (116 mg, 0.36 mmol) in 20 mL of DMF was heated to 100 °C for 24 h under nitrogen atmosphere in the pressure tube under sealed condition. After completion of the reaction, the reaction mixture was poured into

water and extracted with chloroform. The organic layer was dried over sodium sulphate. Finally, the solvent was removed under vacuum to yield a residue which was then purified by column chromatography. Yellow solid. Yield 0.44 g (55%). mp 202-204 °C; IR (KBr, cm^{-1}) 2218 ($\nu_{C\equiv N}$); ^{1}H NMR ($CDCl_3$, 400 MHz) δ 8.10 (dd, J = 14 Hz, J = 2.8, 4 H), 7.73 (d, J = 8.0 Hz, 2 H), 7.67 (s, 2 H), 7.59-7.54 (m, 8 H), 7.48 (d, J = 8.0 Hz, 2 H), 7.37 (s, 4 H), 4.27-4.17 (m, 4 H), 2.18-2.08 (m, 6 H), 1.47-1.26 (m, 16 H), 0.96 (t, J = 7.6 Hz, 6 H), 0.90 (t, J = 7.2 Hz, 6 H), 0.42 (t, J = 7.6 Hz, 6 H). ^{13}C NMR ($CDCl_3$, 100.3 MHz) δ 150.76, 142.52, 141.19, 140.19, 137.29, 136.20, 129.89, 128.47, 126.07, 121.97, 121.35, 121.15, 120.66, 120.37, 119.97, 118.55, 118.44, 113.03, 112.92, 107.62, 107.32, 56.07, 47.57, 39.31, 32.91, 30.85, 28.67, 24.41, 22.99, 14.00, 10.89, 8.59; HRMS calcd for $C_{63}H_{66}N_4$ (*m/z* +1) 879.5360, found 879.5341.

Synthesis of 7,7'-((1*E*,1'*E*)-(9-(2-ethylhexyl)-9*H*-carbazole-2,7-diyl)bis(ethene-2,1-diyl))bis(9-(2-ethylhexyl)-9*H*-carbazole-2-carbonitrile), 14b

It was prepared from a mixture of 9-(2-ethylhexyl)-2,7-divinyl-9*H*-carbazole (0.3 g, 0.90 mmol), 7-bromo-9-(2-ethylhexyl)-9*H*-carbazole-2-carbonitrile (0.73 g, 1.90 mmol), $Pd(OAc)_2$ (8.2 mg, 0.036 mmol), sodium acetate (1.5 g, 18.0 mmol) and tetrabutylammonium bromide (116 mg, 0.36 mmol) in 20 mL of DMF by following the procedure described for **14a**. Yellow solid. Yield 0.48 g (57%). mp 298-300 °C; IR (KBr, cm^{-1}) 2222 ($\nu_{C\equiv N}$); ^{1}H NMR ($CDCl_3$, 400 MHz) δ 8.12-8.06 (m, 6 H), 7.66 (s, 2 H), 7.59-7.38 (m, 14 H), 4.25-4.15 (m, 6 H), 2.17-2.08 (m, 3 H), 1.49-1.26 (m, 24 H), 1.00-0.86 (m, 18 H). ^{13}C NMR ($CDCl_3$, 100.3 MHz) δ 142.61, 142.01, 140.27, 137.35, 134.98, 130.49, 128.60, 126.15, 122.60, 122.18, 121.37, 121.18, 120.73, 120.49, 120.46, 118.50, 117.84, 113.09, 107.66, 107.50, 107.35, 47.64, 39.39, 30.88, 28.72, 24.44, 23.04, 14.09, 10.94; HRMS calcd for $C_{66}H_{73}N_5$ *m/z* 935.5860, found 935.5859.

Synthesis of 7,7'-((1*E*,1'*E*)-(9-butyl-9*H*-carbazole-3,6-diyl)bis(ethene-2,1-diyl))bis(9-(2-ethylhexyl)-9*H*-carbazole-2-carbonitrile), 14c

It was prepared from a mixture of 9-butyl-3,6-divinyl-9*H*-carbazole (0.25 g, 0.91 mmol), 7-bromo-9-(2-ethylhexyl)-9*H*-carbazole-2-carbonitrile (0.74 g, 1.93 mmol), $Pd(OAc)_2$ (8.2 mg, 0.036 mmol), sodium acetate (1.5 g, 18.0 mmol) and tetrabutylammonium bromide (116 mg, 0.36 mmol) in 20 mL of DMF by following the procedure described for **14a**. Yellow solid. Yield 0.41 g (51%). mp 170-172 °C; IR (KBr, cm^{-1}) 2216 ($\nu_{C\equiv N}$); ^{1}H NMR ($CDCl_3$, 400 MHz) δ

8.33 (s, 1 H), 8.11 (d, *J* = 8.0 Hz, 4 H), 7.76-7.67 (m, 4 H), 7.59-7.55 (m, 4 H), 7.49-7.35 (m, 8 H), 4.34 (t, *J* = 6.8 Hz, 2 H), 4.27-4.17 (m, 4 H), 2.12-2.10 (t, *J* = 5.6 Hz, 2 H), 1.94-1.87 (m, 2 H), 1.45-1.27 (m, 18 H), 0.98 (t, *J* = 6.8 Hz, 9 H), 0.91 (t, *J* = 7.2 Hz, 6 H). ^{13}C NMR ($CDCl_3$, 100.3 MHz) δ HRMS calcd for $C_{62}H_{65}N_5$ *m/z* 879.5234, found 879.5243.

Synthesis of 9,9-diethyl-2,7-divinyl-9*H*-fluorene, 13a

A mixture of methyltriphenylphosphonium bromide (1.9 g, 5.3 mmol), potassium tertiary butoxide (0.74 g, 6.6 mmol) and 40 mL of THF is purged under nitrogen atmosphere for 10 minutes. 9,9-diethyl-9*H*-fluorene-2,7-dicarbaldehyde (0.6 g, 2.4 mmol) dissolved in 10 mL of THF was injected to the above mixture and heated to 60 °C for 24 h. After completion of reaction, the reaction mixture was filtered by Celite powder. The organic layer was collected, washed with water and extracted by chloroform. The organic layer was dried over sodium sulphate and purified by column chromatography. Colorless solid. Yield 0.4 g, (67%). mp 38-40 °C. ^{1}H NMR ($CDCl_3$, 400 MHz) δ 7.63 (d, *J* = 8.0 Hz, 1 H), 7.39-7.36 (m, 4 H), 6.79 (dd, *J* = 17.2 Hz, *J* = 6.4 Hz, 2 H), 5.80 (d, *J* = 17.6 Hz, 2 H), 5.25 (d, *J* = 10.8 Hz, 2 H), 2.04 (q, *J* = 7.6 Hz, 2 H), 0.33 (t, *J* = 7.6 Hz, 2 H). ^{13}C NMR ($CDCl_3$, 100.3 MHz) δ 150.52, 141.14, 137.34, 136.49, 125.41, 120.49, 119.66, 113.04, 55.96, 32.78, 8.51; HRMS calcd for $C_{21}H_{22}$ *m/z* 274.1716, found 274.1716.

CHAPTER 5

Cyanocarbazole Decorated Pyrenes: Tuning the Functional Properties by Varying Chromophore Density

5.1 Introduction

Pyrene is a polyaromatic fused hydrocarbon. Since pyrene offers good optical properties, high thermal stability and wide range of functional modification at various nuclear positions, pyrene-based materials are extensively exploited for optoelectronic applications especially in OLED. Pyrene itself is an emitter. But the emission falls on ultra-violet region. In addition, planar structure of pyrene is prone to detrimental intermolecular π-π stacking. Since the optoelectronic applications demand the organic materials to show the absorption and emission in visible region of electromagnetic spectrum, pyrene alone cannot be a good candidate for the applications. However, the tethering of conjugate chromophores on pyrene generally alleviates the above mentioned limitation. As a result, the emission falls on visible region and suppresses the aggregate formation by the peripheral bulky structures.

As mentioned in the previous chapters, carbazole is a potential building block for the construction of efficient hole transporting and fluorescent molecules. Pyrene-carbazole conjugates exhibit good charge transporting property and excellent emissive nature. For example, Kazlauskas and coworkers reported pyrene-carbazole conjugates (**PC1** and **PC2**) as hole transporting materials (Chart 5.1) [123]. Grazulevicius and coworkers reported tetra-substituted pyrene with carbazole (**PC3** and **PC4**) through C3 and C2-linking position (Chart 5.1) [201]. These compounds showed high quantum yield in solution. Also they gave high thermal stability due to the presence of rigid pyrene and carbazole. Promarak and coworkers designed pyrene-carbazole conjugates (**PC5-PC7;** Chart 5.1) as hole transporting blue emitters [29]. As the number of pyrene unit increased, the molecule showed better thermal and morphological stability. Müllen and coworkers designed *N*-phenyl carbazole decorated over 2,7-position of pyrene (**PC8;** Chart 5.1) and demonstrated as fluorescent emitter [202]. The material exhibited exceptional deep blue emission. The presence of two carbazole increased the hole transporting ability of pyrene and controlled the formation of excimers. Further, Ni and coworkers reported symmetrically substituted carbazole on pyrene (**PC9**) as fluorescent emitter (Chart 5.1) [203]. They found that the multi-substitution of pyrene suppressed the intermolecular interaction effectively and thereby increased the fluorescent quantum yields.

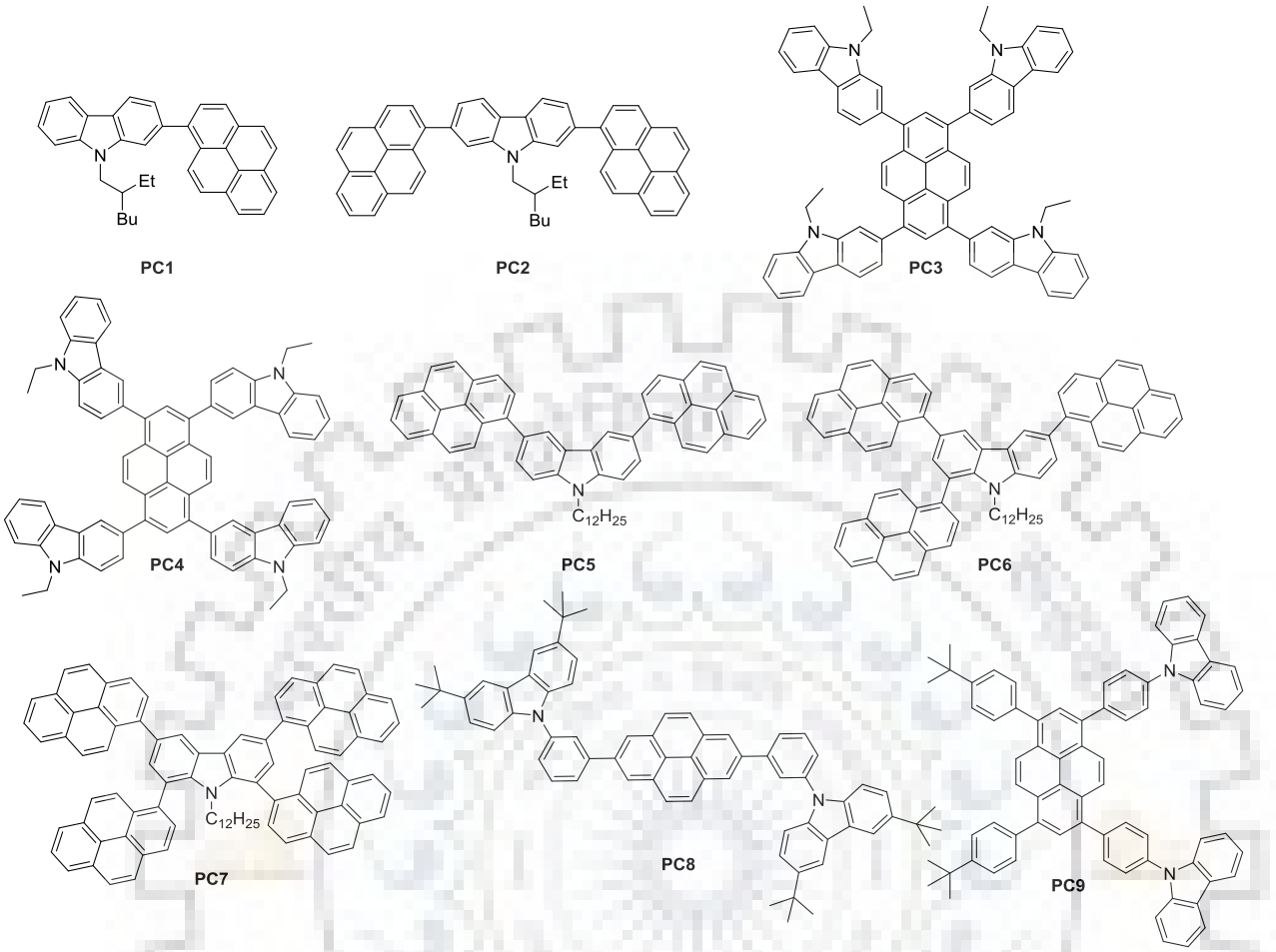

Chart 5.1 Pyrene-carbazole conjugates demonstrated in OLED applications.

The suitable conjugate spacer is beneficial to increase the π conjugation length across the molecular backbone. Acetylene serves as a rigid and linear spacer often used in organic chromophores to raise the conjugation length. Pyrene-carbazole conjugates connected through acetylene spacer are used as fluorescent emitters and found that the presence of acetylene spacer resulted in increases thermal stability and red shifts the absorption and emission maxima. For example, Lu and coworkers reported carbazole end capped pyrenes (**PC10**-**PC13**) linked through acetylene spacer (Chart 5.2) as fluorescence emitters [204-205]. Owing to the rigid and planar acetylene spacer, the emitters showed good electronic conjugation, high quantum yield. The OLED device showed blue emission with reasonable electroluminescence performance. On the other hand, planar structure of acetylene spacer would lead to the formation of π aggregates and fluorescence quenching. However, the π-π stacking improves charge carrier mobility [199]. For example, Tao and coworkers reported carbazole appended pyrene connected through

acetylene linker (**PC14;** Chart 5.2) as fluorescent emitter [206]. They demonstrated the beneficial role of acetylene spacer to extend the intramolecular π electronic conjugation and better charge carrier mobility by proper intermolecular interaction. However, the electroluminescence performance of the devices is not up to the mark.

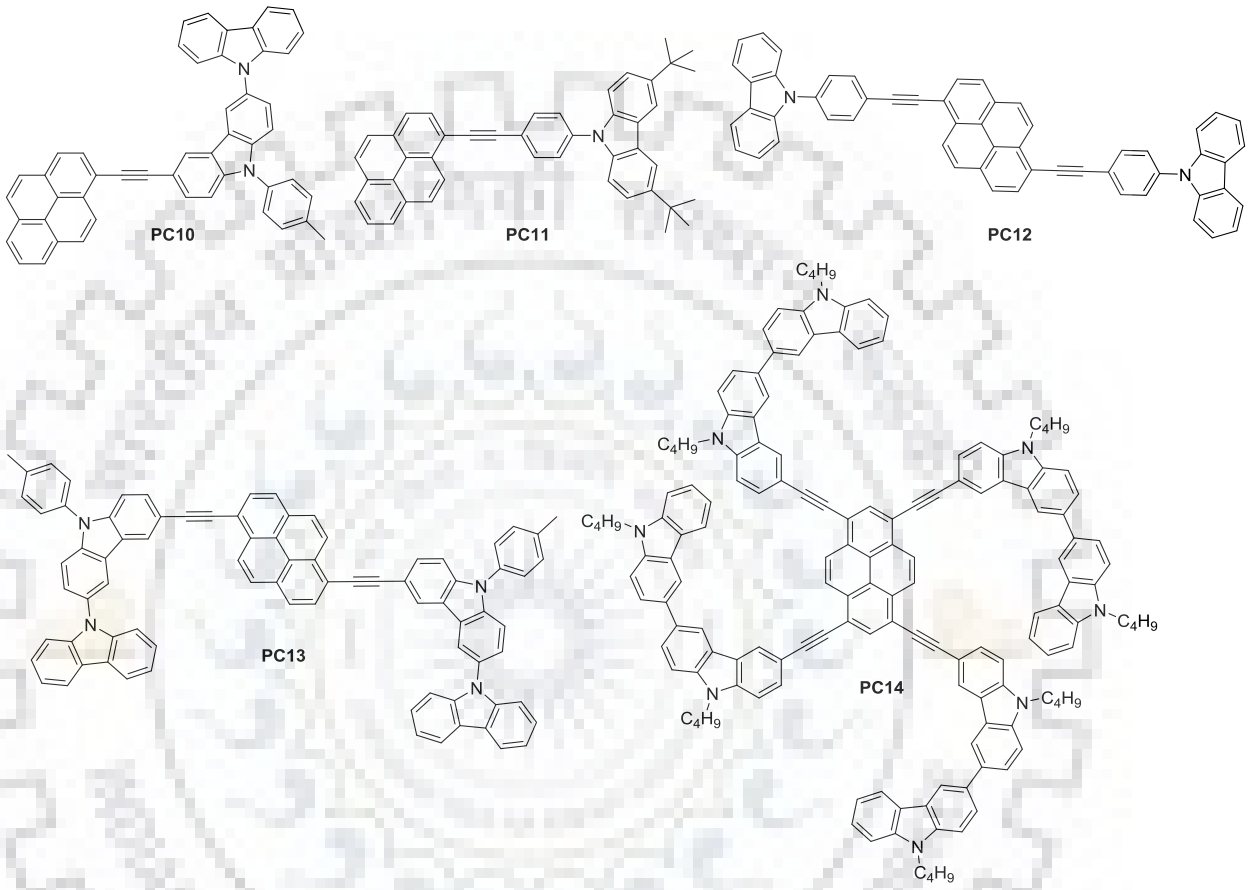

Chart 5.2 Pyrene-carbazole conjugates containing acetylene linker for OLED applications.

The poor OLED device performance is attributed to improper transport of charge carriers. The imbalanced transport of hole and electron charge carriers leads to less number of recombination sites in emissive layer. As a result, the luminance and current efficiency of the devices dropped. This limitation can be overcome by accelerating the electron mobility through insertion of electron withdrawing group. We used cyanocarbazole in previous chapters, to increase electron mobility and thereby realized balanced charge mobility and better device performance. We presume that the cyanocarbazole appended pyrene would give desirable material characteristics and better device performance owing to the realization of balanced charge transport. So far, the systematic study of pyrene-carbazole conjugates is not explored.

Thus, the study of structure-property relationships of the materials containing pyrene-carbazole conjugates connected through acetylene linker would shed a light on the molecular design for highly efficient emitters (Chart 5.3). Moreover, C2-functionalized carbazole decorated pyrenes are not known in the literature. We presume that rigid structures of pyrene, carbazole and acetylene would increase thermal robustness of the materials and the electron withdrawing cyano group would be beneficial to accelerate electron carrier mobility. The acetylene spacer would give better electronic conjugation due to planar arrangement and may help to increase the charge mobility through intermolecular interaction.

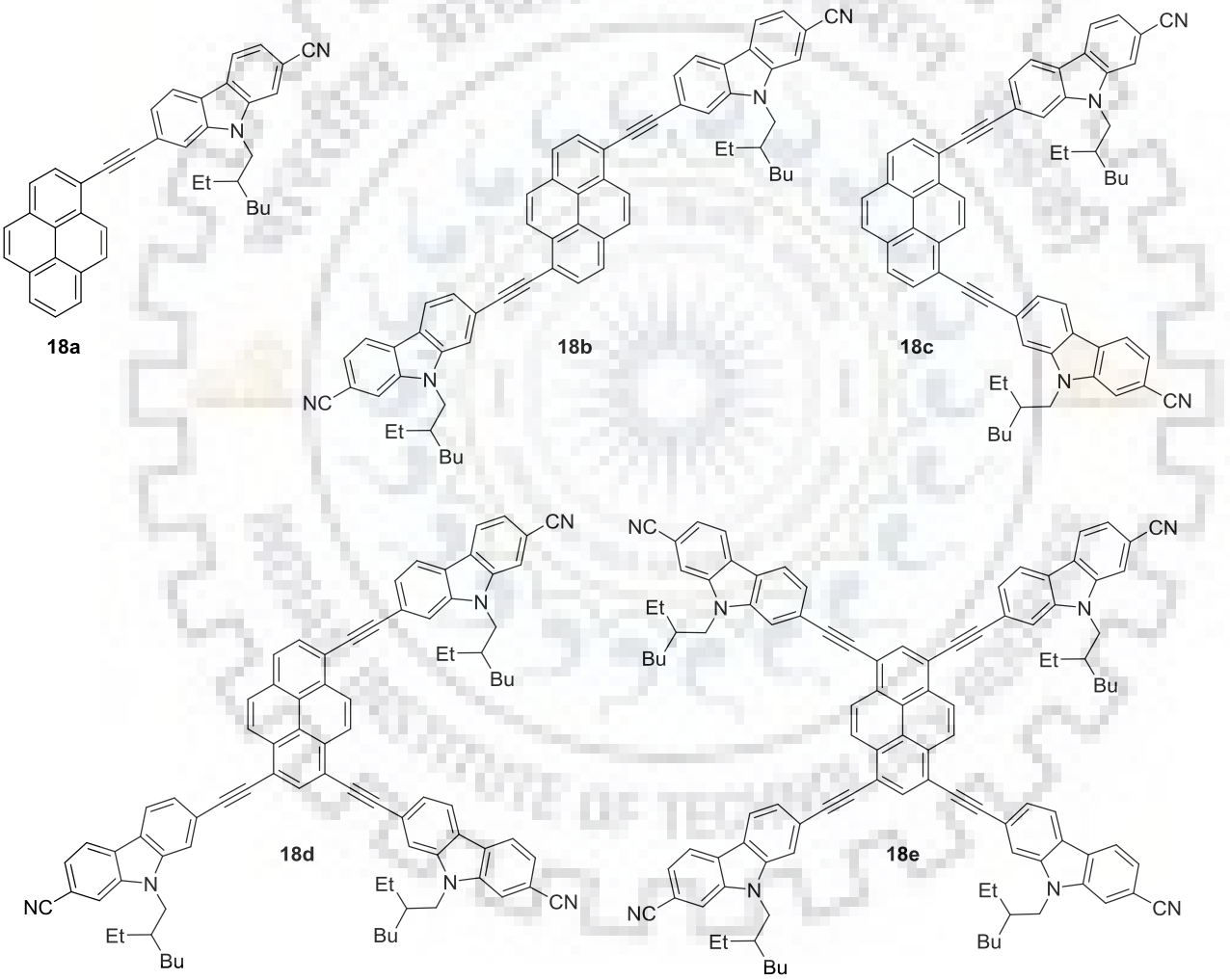

Chart 5.3 Structure of the cyanocarbazole decorated pyrene derivatives **18a-18e**.

5.2 Results and Discussion

5.2.1 Synthesis and Characterization

The synthetic route of the target dyes is illustrated in Scheme 5.1. The starting material 7-bromo-9-(2-ethylhexyl)-9*H*-carbazole-2-carbonitrile **2** was converted into **15** by following Sonogashira coupling reaction protocol using trimethylsilylacetylene as a coupling partner. Further, **15** was converted to **16** by desilylation reaction using Bu_4NBr, KF in MeOH. The intermediate **16** was converted into target compounds **18a-18e** by Sonogashira coupling reaction using appropriate bromo derivative of pyrene **17a-17e**. All the dyes were thoroughly characterized by ^1H and ^{13}C nuclear magnetic resonance (NMR) spectroscopy and high resolution mass spectrometry (HRMS) analysis. The spectral data is consistent with the proposed structures. All of the dyes are soluble in common organic solvents such as dichloromethane (DCM), toluene (TOL), tetrahydrofuran (THF), chloroform ($CHCl_3$), *N*,*N*-dimethylformamide (DMF) but sparingly soluble in acetonitrile (ACN) and methanol (MeOH).

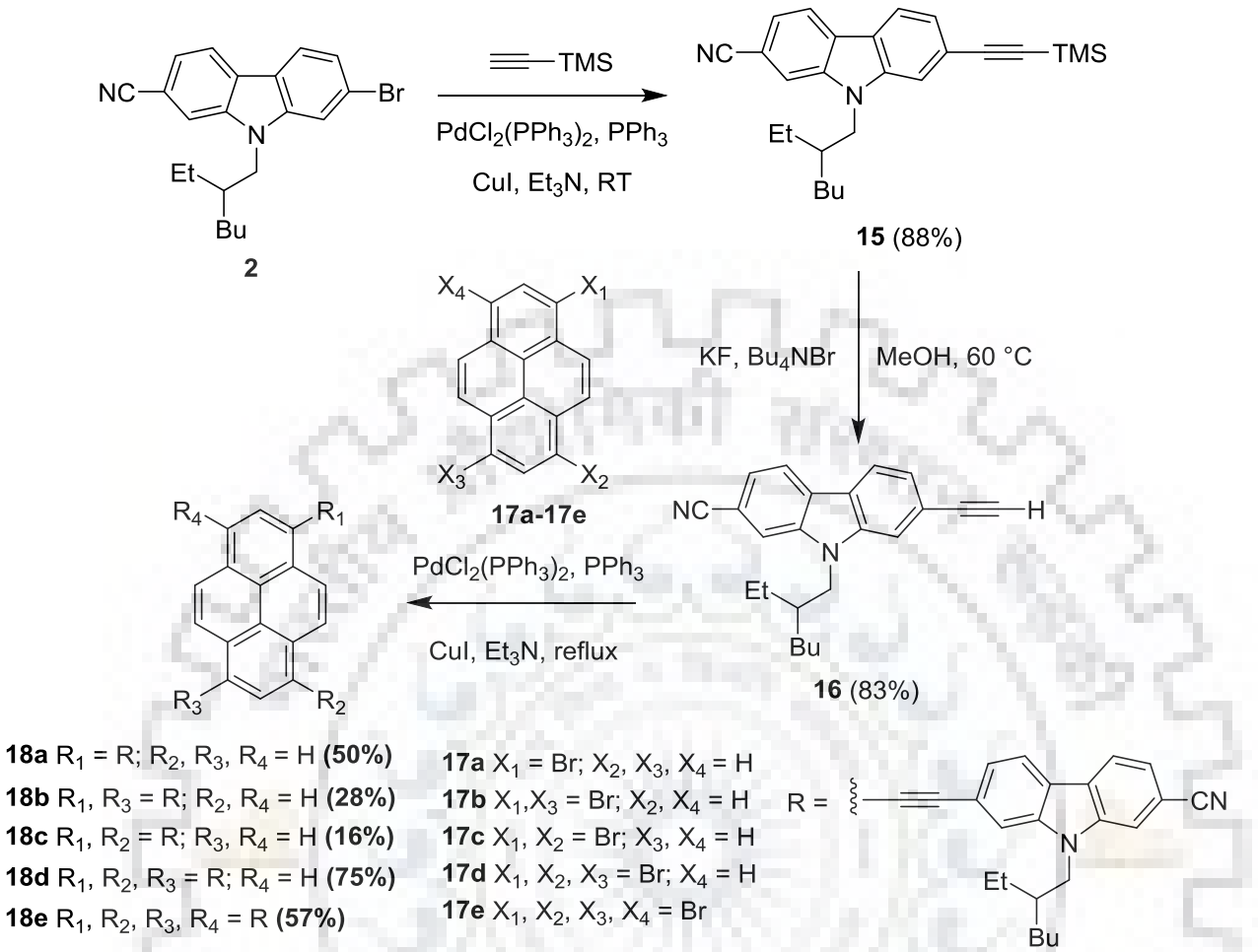

Scheme 5.1 Synthetic route of the target dyes **18a**-**18e**.

5.2.2 Photophysical Properties

The absorption spectra of the compounds recorded in dichloromethane solution are displayed in Figure 5.1, and the relevant data collected in Table 5.1. Absorption spectra consist of two distinguishable bands with multiple shoulder peaks for all the dyes. The higher energy band ca. below 290 nm is dominated by π-π* transition of pyrene and/or of carbazole [207-208]. The lower energy band can be assigned to the π-π* transition arising from delocalized structure. It is interesting to compare the absorption spectrum of **18a** with that of the known compound 9-(2-ethylhexyl)-2-(pyren-1-yl)-9*H*-carbazole which does not have acetylene linker and CN group [123]. The compound **18a** exhibited red shifted absorption maxima (61 nm) in THF solution (Table 5.2). The presence of linear conjugated acetylene linker relieves the molecule from twisting and thus it affords effective π electronic conjugation. Despite of

increase in chromophoric loading on pyrene core, the 1,6-disubstituted compound **18b** exhibited blue shifted absorption maximum as compared to that of **18a**. On the other hand, 1,8-disubstituted compound **18c** displayed red shifted absorption maximum compared to mono-substituted compound **18a**. This anomalous behavior can be understood in terms of excitonic coupling of transition dipoles. According to Kasha's molecular excitons theory, the angle difference between transition dipoles and their interconnected axis (θ) determines the direction and magnitude of spectral shift [209-211]. The excitonic coupling of transition dipoles results in a pair of excitonic states in first excited state namely lower excitonic level and upper excitonic level. If the angle between transition dipoles and their interconnected axis is greater than 54.7°, the allowed electronic transition is from ground state to upper excitonic level of first excited state. The optical excitation of trans- isomer might be due to the electronic coupling of transition dipoles of this kind and the molecules are arranged in side-by-side stacking fashion which resulted in blue shift in absorption maximum. Alternatively, if θ is less than 54.7°, the electronic excitation populates the lower excitonic level of first excited state, thereby red shifted absorption is observed. The observed red shifted absorption maximum for 1,8-disubstituted compound **18c** could be due to low θ value between the transition dipoles and interconnecting axis which leads to head-to-tail stacking arrangement. The parallel arrangement of 1,6-disubstituted compound in solution may be responsible for blue shift in absorption whereas the head to tail arrangement of 1,8-disubstituted compound in solution leads to red shift in absorption spectra. Similar results are reported in the literature [210,211]. Further, the tri-substituted compound **18d** exhibited similar absorption profile and the same absorption maxima of 1,8-disubstituted compound **18c**. It could be understood that the incorporation of additional ethynyl cyanocarbazole at trans- position of **18c** offset the change in absorption profile.

Tetra-substituted compound **18e** gave the longest wavelength absorption among the compounds which is attributed to the high chromophoric loading. Interestingly, the compound **18e** exhibited large bathochromic shift in absorption maximum (64 nm) recorded in THF solution when compared to its analogous compound 1,3,6,8-tetra(9-ethyl-9*H*-carbazol-2-yl)pyrene which does not have acetylene spacer and cyano group at periphery of carbazole (Table 5.2) [201]. It clearly demonstrates the auxochromic role of cyano group and linear acetylene linker in raising the conjugation length. Further, the nature of ground states of the compounds is evaluated by measuring absorption spectra in various solvents of different

polarity from non-polar toluene to polar DMF (Figure 5.3 to Figure 5.7). All the compounds exhibited similar absorption maxima for all solvents of different polarity. It indicates that the ground state of the molecules is non-polar in nature and the polarity of the solvents does not have any influence over the absorption profile.

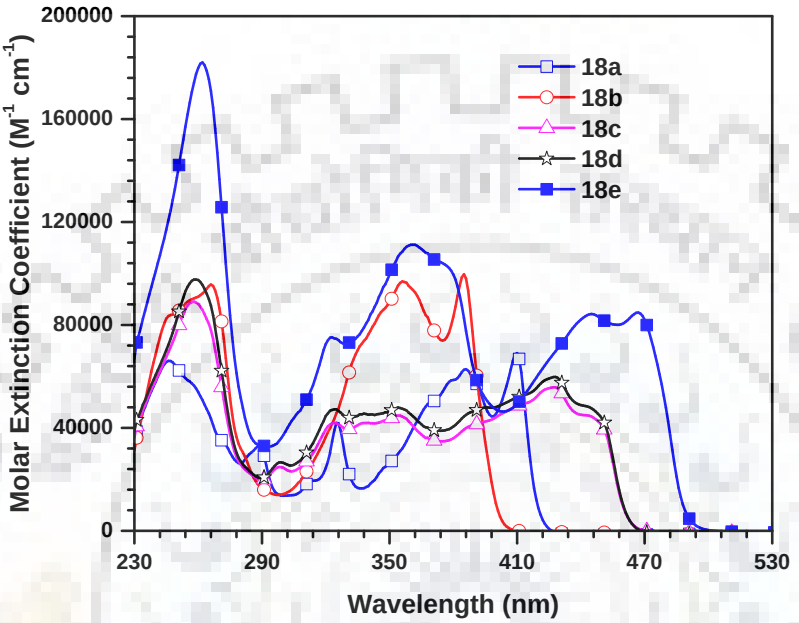

Figure 5.1 Absorption spectra of the dyes (**18a-18e**) recorded in dichloromethane.

The emission spectra of the compounds recorded in dichloromethane are displayed in Figure 5.2, and the pertinent data listed in Table 5.1. All the compounds exhibited structured emission with two distinct emission maxima. The emission profile of the compounds followed the trend of absorption spectrum. The structured emission indicates the rigid nature of molecules at excited state. Moreover, the observation of small Stokes shift value indicates rigid structure of compounds and its control over non-radiative excited state energy loss arising from structural relaxation. Tetra-substituted pyrene **18e** exhibited the longest emission among the dyes which comes from the high chromophoric loading and extended conjugation. The compound **18a** exhibited red shifted emission maxima (7 nm) when compared to that of known compound 9-(2-ethylhexyl)-2-(pyren-1-yl)-9*H*-carbazole which does not have acetylene linker and cyano group (Table 5.2) [123]. The well resolved vibronic peaks of **18a** indicate the rigidity of the compound and the absence of structural reorganization in excited state. Similarly, the compound **18e** exhibited large bathochromic shift (28 nm) when compared to its reported congener 1,3,6,8-tetra(9-ethyl-9*H*-carbazol-2-yl)pyrene which does not possess acetylene

spacer and cyano group (Table 5.2) [201]. It demonstrates the role of cyano group and acetylene linker in raising the conjugation of the molecules. All the compounds exhibit moderate Stokes shift in solution spectra. It is apparent that the remarkable Stokes shift observed for the compounds is useful for effective energy transfer and to suppress unwanted self-absorption process in OLED devices [212-213].

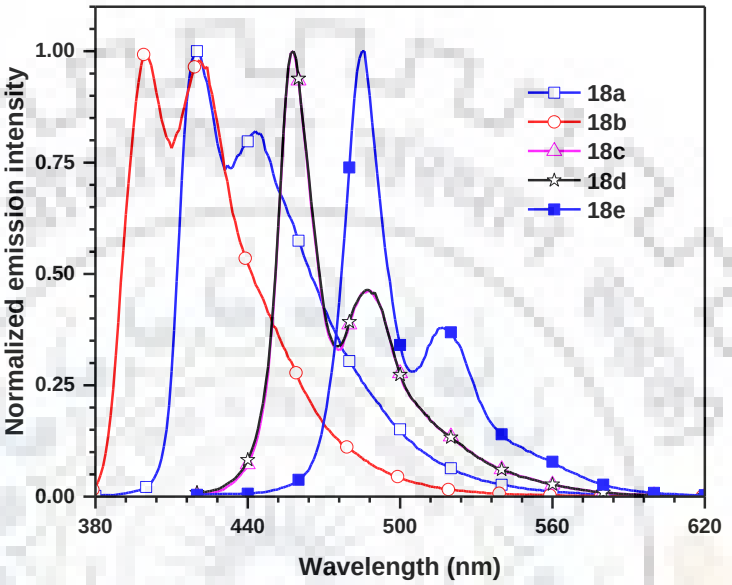

Figure 5.2 Emission spectra of the dyes (**18a-18e**) recorded in dichloromethane.

Table 5.1 Optical properties of the dyes

Dye	λ_{max}, nm (ε_{max}, M^{-1} cm^{-1} $\times 10^3$)[a]	λ_{em}, nm (Φ_F)[a,b]	Stokes shift, cm^{-1}	λ_{em},[c] nm
18a	246 (66.1), 289 (33.0), 313 (19.3), 325 (41.9), 386 (62.8), 410 (69.1)	420, 443 (0.59)	581	494
18b	266 (95.7), 356 (96.9), 385 (99.7)	400, 421 (0.38)	974	471, 501
18c	258 (89.1), 298 (24.8), 324 (41.9), 354 (44.8), 427 (55.7), 447 (43.3)	458, 488 (0.51)	1585	470
18d	259 (97.7), 299 (26.6), 324 (47.2), 354 (47.9), 391 (46.9), 428 (59.8), 447 (46.3)	458, 488 (0.64)	1530	470
18e	262 (182.0), 323 (75.2), 361 (111.2), 445 (84.2), 467 (84.8)	486, 517 (0.61)	837	569

[a] Measured in dichloromethane solution. [b] Absolute quantum yield using integrating sphere. [c] Measured for drop cast film.

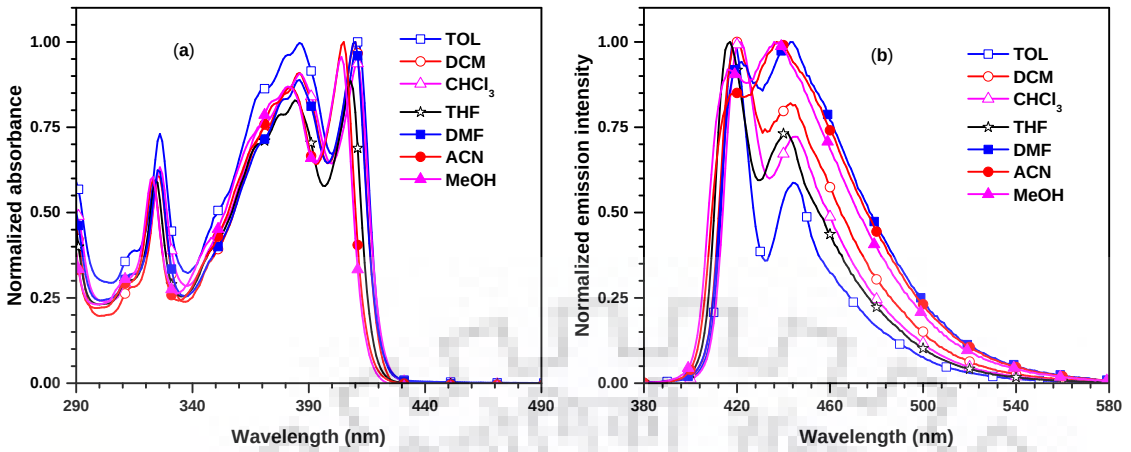

Figure 5.3 Absorption (a) and emission (b) spectra recorded in different solvents for **18a**.

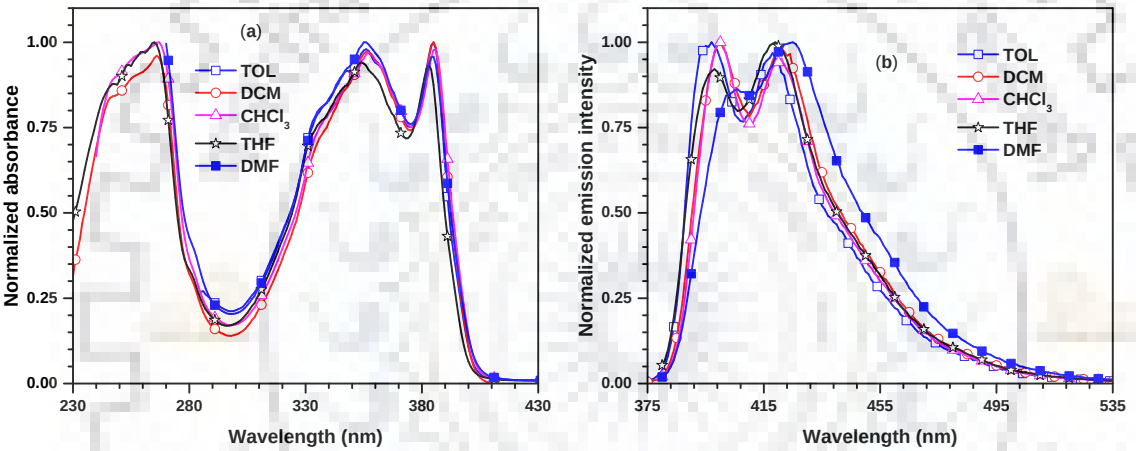

Figure 5.4 Absorption (a) and emission (b) spectra recorded in different solvents for **18b**.

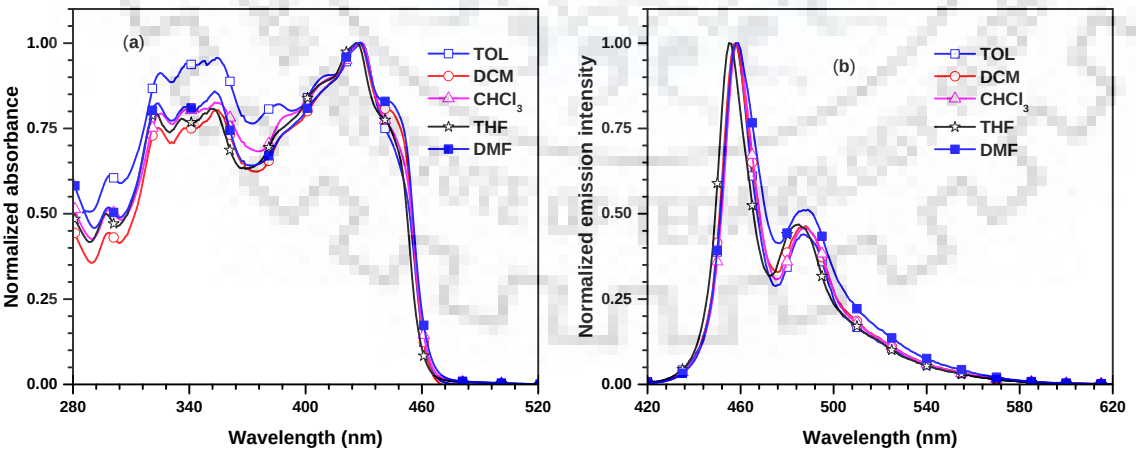

Figure 5.5 Absorption (a) and emission (b) spectra recorded in different solvents for **18c**.

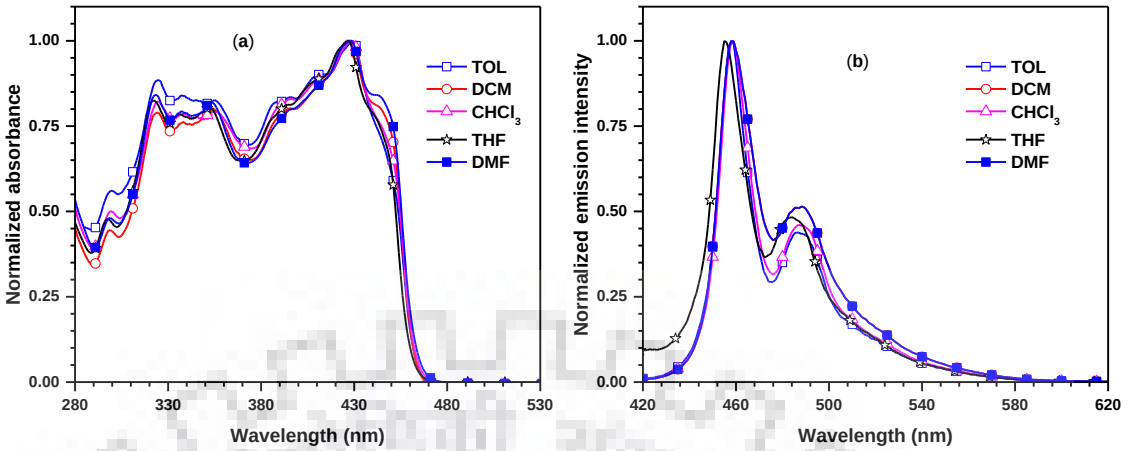

Figure 5.6 Absorption (a) and emission (b) spectra recorded in different solvents for **18d**.

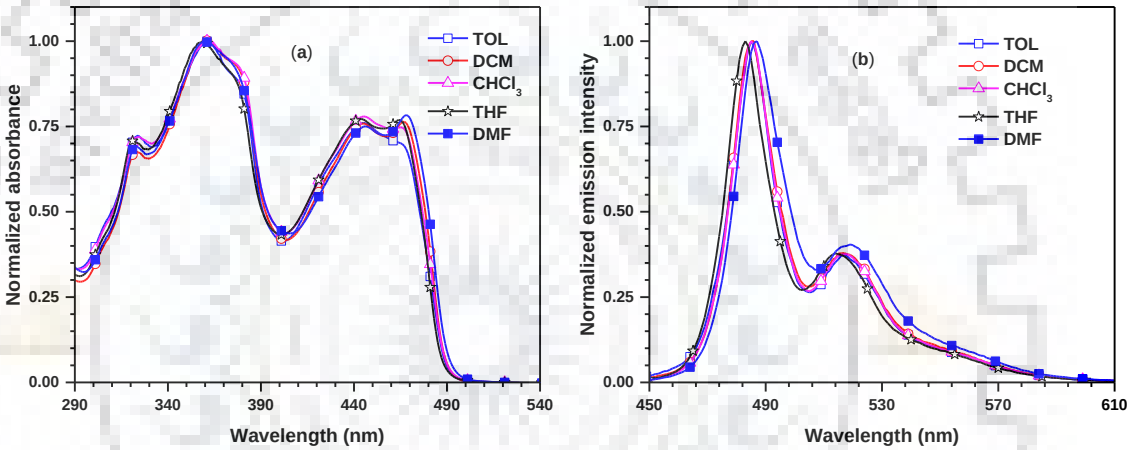

Figure 5.7 Absorption (a) and emission (b) spectra recorded in different solvents for **18e**.

Table 5.2 Solvatochromic data of the dyes

Dye	Absorption maxima, λ_{max} (nm)						Emission maxima, λ_{em} (nm)					
	TOL	$CHCl_3$	THF	DMF	ACN	MeOH	TOL	$CHCl_3$	THF	DMF	ACN	MeOH
18a	313, 326, 370, 386, 411	313, 326, 369, 386, 411	312, 324, 367, 384, 408	312, 325, 386, 410	323, 382, 405	323, 381, 404	419, 444	421, 445	417, 441	422, 443	419, 439	416, 436
18b	356, 385	267, 357, 386	265, 354, 383	356, 385	-	-	397, 418	400, 421	398, 419	406, 425	-	-
18c	299, 325, 355, 386, 408, 429	299, 325, 355, 387, 408, 429, 444s	297, 323, 353, 385, 407, 426, 443s	298, 323, 353, 428, 446s	-	-	458, 487	458, 487	455, 485	458, 489	-	-
18d	299, 325, 388, 409, 429	299, 325, 391, 411, 429, 443	298, 322, 389, 408, 427, 441	298, 324, 393, 413, 428, 444	-	-	458, 486	459, 487	455, 484	458, 488	-	-
18e	324, 361, 445, 463	324, 362, 445, 465	321, 359, 443, 464	323, 359, 446, 468	-	-	485, 517	485, 518	483, 514	487, 519	-	-

Table 5.3 Stokes shift value of the dyes

Dye	Stokes Shift (cm^{-1})						
	TOL	DCM	$CHCl_3$	THF	DMF	ACN	MeOH
18a	465	581	578	529	694	825	714
18b	785	974	907	984	1343	-	-
18c	1476	1585	1476	1496	1530	-	-
18d	1476	1530	1524	1441	1530	-	-
18e	980	837	887	848	834	-	-

To ascertain the nature of excited state, solvatochromism studies have been carried out by measuring the emission spectra in different solvents from non-polar toluene to polar methanol (Figure 5.3 to 5.7). The insignificant change of emission maximum value (5 nm) is observed for the dyes as the solvent polarity increases. It suggests the non-polar excited state of these molecules and thus solvent independent fluorescence spectra. It indicates the absence of structural changes and dipolar relaxation in the excited state. Thin film emission spectrum recorded by drop cast method is shown in Figure 5.8. All the dyes displayed red shift in emission as compared to that of solution spectrum recorded in toluene solution. It might be attributed to intermolecular interaction and *J*- aggregation of the molecules in solid state [145-147].

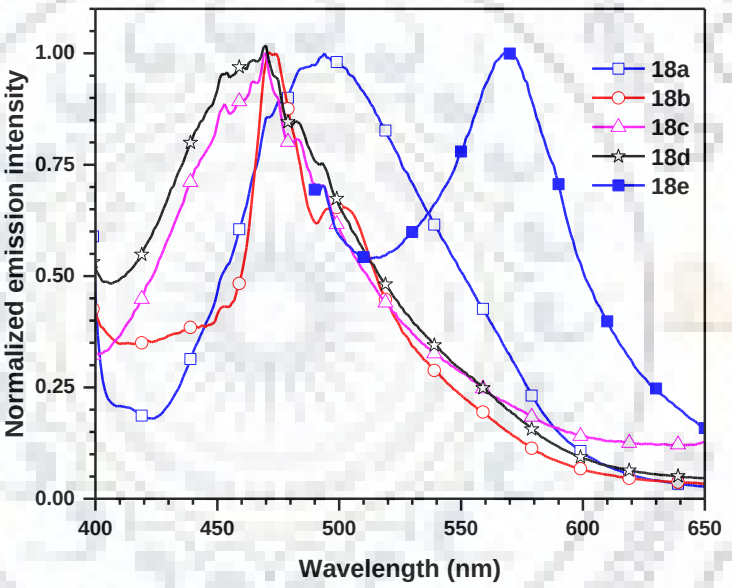

Figure 5.8 Thin film emission spectra of the dyes (**18a-18e**) recorded for drop cast films.

5.2.3 Electrochemical Properties

For realizing high performance OLED, the favorable energy level arrangements of emitting molecules with the adjacent charge transporting molecular layers is a crucial parameter. The HOMO and LUMO energy levels of the compounds are estimated by carrying out cyclic voltammetry studies. All the compounds displayed irreversible oxidation peak except **18e** which gave quasi-reversible oxidation peak (Figure 5.9). The irreversibility in oxidation peak stems from the oxidation of rigid carbazole moiety. It is evident that leaving 3,6-position of carbazole unprotected generally leads to irreversible oxidation [150]. The highest oxidation potential observed for **18b** which coincided with blue shifted absorption maxima observed in solution

spectra among the compounds. Similarly, the 1,8-disubstituted compound **18c** and tri-substituted compound **18d** showed similar oxidation potential. Due to the extended conjugation, **18e** gave lowest oxidation potential among the dyes. The superior π electronic conjugation in **18e** resulted in quasi-reversible oxidation peak [214]. The HOMO energy level of the compounds is calculated by adding 4.8 eV with oxidation potential. The LUMO energy level is obtained from the difference between HOMO and optical band gap. The optical band gap is estimated from the absorption edge of the compounds, which is taken from the intersection of absorption and emission spectra recorded in dichloromethane solution. The HOMO level is upwardly shifted as the number of substituent increases with an exception for **18b** while LUMO is downwardly shifted. The high lying HOMO is attributed to the increasing conjugation length and the low lying LUMO is attributed to the increasing number of electron withdrawing acetylene spacer on moving from mono- to tetra-substitution. The observed HOMO and LUMO energy values are well matching with the neighboring molecular layers of OLED device which would be beneficial for facile injection and transportation of charge carriers.

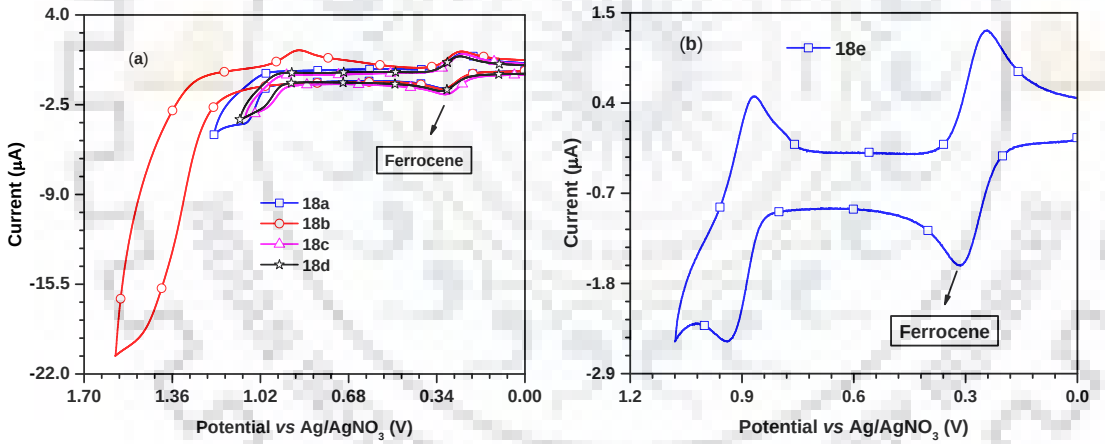

Figure 5.9 Cyclic voltammograms of **18a-18d** (a) and **18e** (b) recorded in dichloromethane.

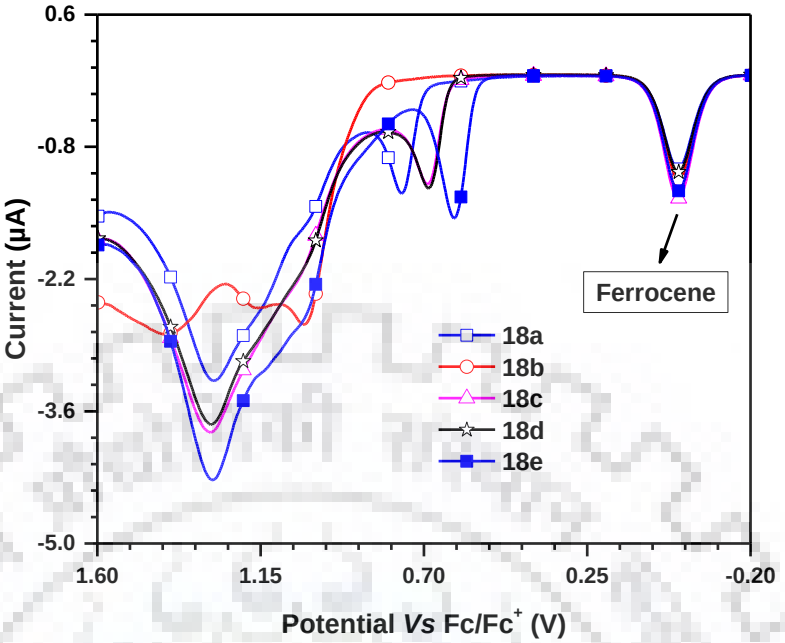

Figure 5.10 Differential pulse voltammograms of the dyes (**18a-18e**) recorded in dichloromethane.

5.2.4 Thermal Properties

The thermal stability of the compounds is evaluated by thermo gravimetric analysis (TGA) under nitrogen atmosphere with heating rate of 10 °C/min. The onset decomposition temperature corresponds to 10% weight loss fall in the range of 325-436 °C. The TGA plot of the dyes are displayed in Figure 5.11 and the relevant data summarized in Table 5.4. The high thermal decomposition temperature of these compounds could be attributed to the presence of both rigid carbazole and pyrene moiety. The high thermal decomposition temperature of pyrene functionalized carbazole compounds are well documented in the literature [201, 207]. The high thermal stability of carbazole tethered pyrene acetylene compounds can be exploited for the better performance of OLEDs. The rigidity of acetylene linker plays a vital role in raising thermal stability. The lowest onset temperature is observed for tetra-substituted compound **18e** which might be due to thermal degradation of alkyl chains.

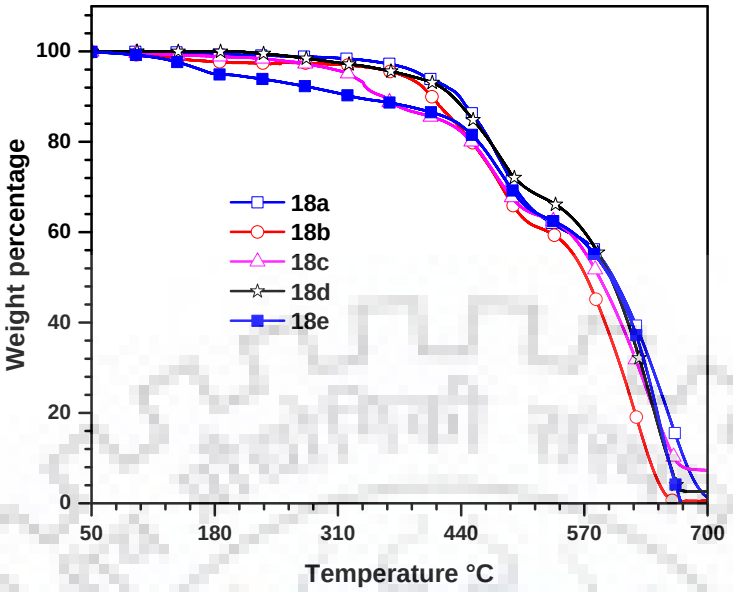

Figure 5.11 TGA curves of the compounds **18a-18e**.

Table 5.4 Thermal and electrochemical properties of the dyes

Dye	T_{onset}, °C[a]	T_d, °C	E_{ox}, V[b]	HOMO, eV[c]	LUMO, eV[d]	$E_{0\text{-}0}$, eV[e]
18a	436	652	0.76	-5.56	-2.56	3.00
18b	408	625	1.03	-5.83	-2.66	3.17
18c	359	638	0.69	-5.49	-2.73	2.76
18d	431	643	0.69	-5.49	-2.73	2.76
18e	325	649	0.62	-5.42	-2.81	2.61

[a] Temperature corresponding to 10% weight loss. [b] Oxidation potential quoted reference to ferrocene internal standard. [c] HOMO = -(4.8 + E_{ox}). [d] LUMO = HOMO + $E_{0\text{-}0}$. [e] Optical band gap obtained from the intersection of normalized absorption and emission spectra (optical edge).

5.2.5 Theoretical Investigations

To get deep insight into the electronic structure and photophysical properties of the compounds, we have performed density functional theoretical calculations. The geometry of the molecules was optimized using B3LYP functional and using 6-31G(d,p) basis set [155,156]. The alkyl chains were approximated to methyl to reduce the cost of computational time. The approximation of alkyl chains to methyl may not affect the electronic properties discussed here. The computed absorption maxima, oscillator strength and most prominent electronic transitions of the compounds are listed in Table 5.5. The electronic distribution in the frontier molecular orbitals is displayed in Figures 5.12 and 5.13. The trend of computed absorption maxima

follows the experimental results from mono- substitution to tri-substitution. Interestingly, di-substituted compounds (both 1,6- and 1,8-isomers) exhibited the similar absorption maxima unlike the different absorption maxima of experimental results. The different absorption pattern in solution spectra might be due to the different conformational arrangement of the compounds adopted in solution state [215]. The oscillator strength of most probable longer wavelength absorption followed the same trend of experimental molar extinction coefficient observed for the compounds in solution spectra. Despite of similar wavelength, the 1,6-disubstituted compound **18b** showed high oscillator strength compared to that of 1,8-disubstituted compound **18c** which is coincided the experimental results. The HOMO of the compounds is mainly concentrated on pyrene core and diffused to carbazole arm to some extent while the LUMO is localized on pyrene core for the compounds. This indicates a typical π-π* absorption during electronic excitation.

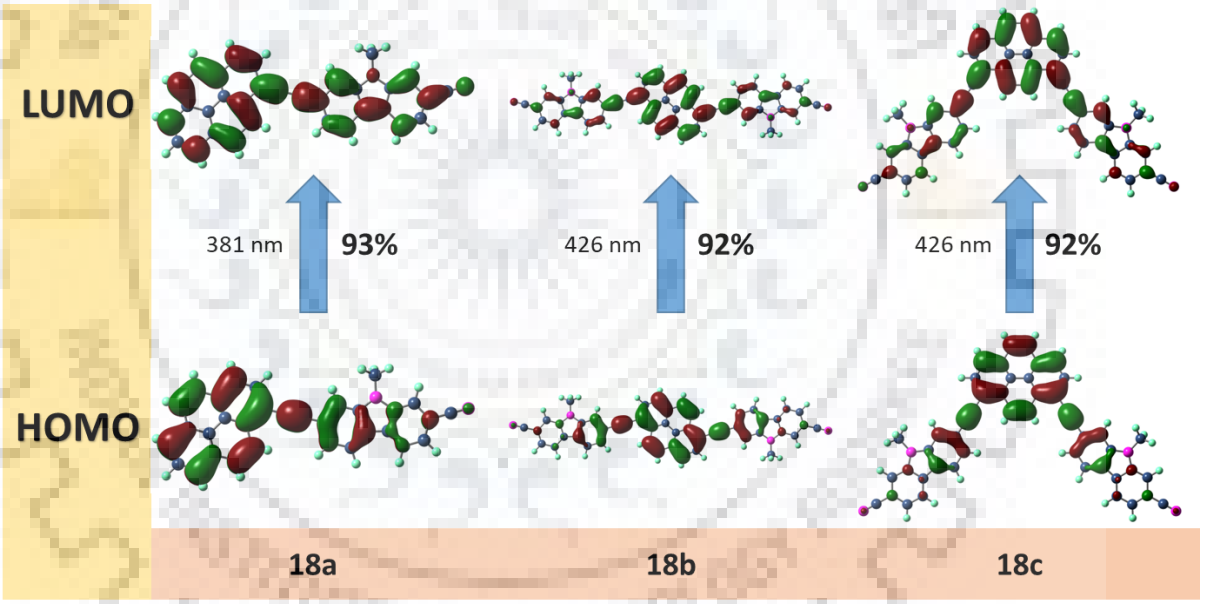

Figure 5.12 Frontier molecular orbital diagrams of the dyes **18a-18c** showing contribution to prominent absorption.

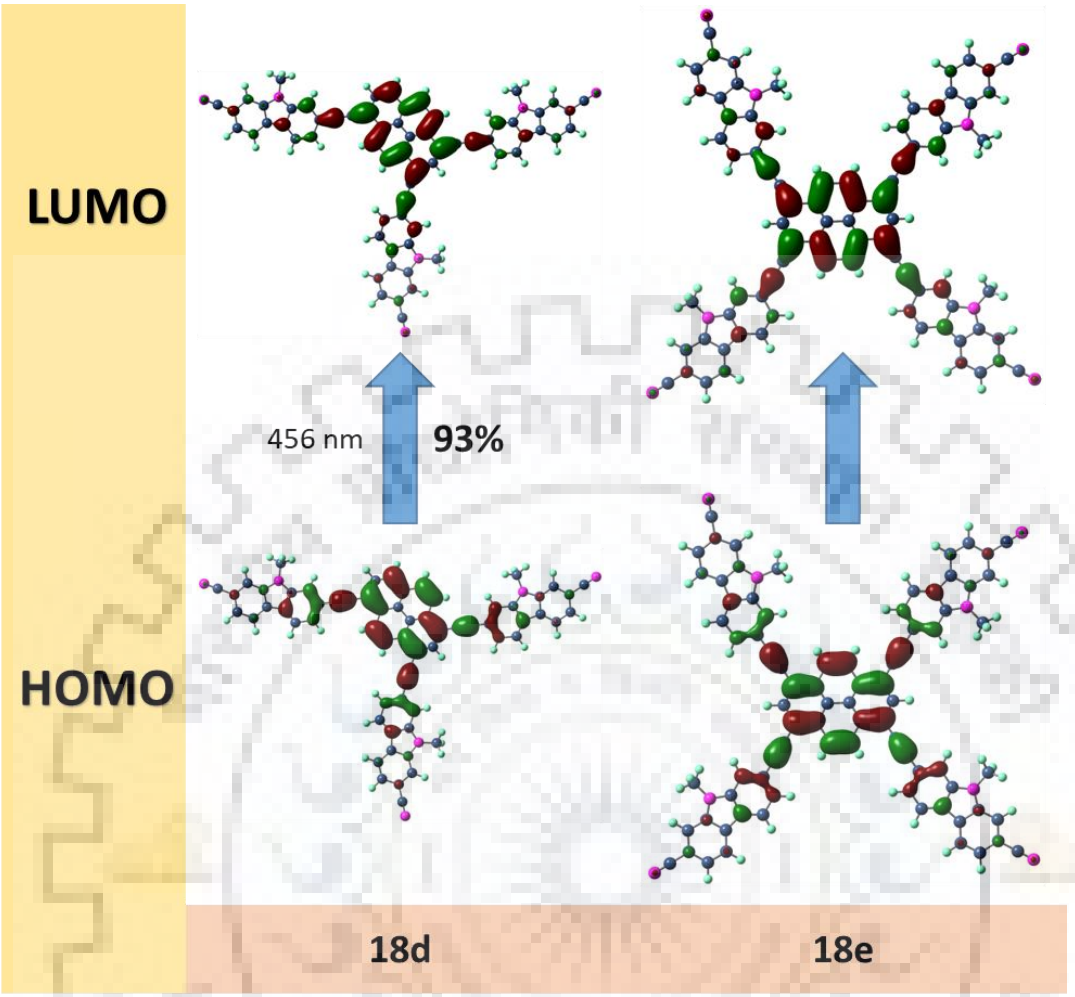

Figure 5.13 Frontier molecular orbital diagrams of the dyes **18d** and **18e** showing contribution to prominent absorption.

Table 5.5 Predicted vertical excitation obtained by B3LYP/6-31G (d,p) method for the dyes

Dye	λ_{max} (nm)	*f*	Assignment
18a	262	0.3640	HOMO→LUMO+2 (30%), HOMO-3→LUMO (22%), HOMO-2→LUMO+1 (16%)
	301	0.4208	HOMO→LUMO+1 (53%), HOMO-2→LUMO (32%)
	381	1.9439	HOMO→LUMO (93%)
18b	267	0.1524	HOMO-5→LUMO (27%), HOMO→LUMO+2 (17%), HOMO-2→LUMO (16%)
	270	0.2995	HOMO→LUMO+3 (36%), HOMO-4→LUMO (36%), HOMO→LUMO+2 (18%)
	299	1.2544	HOMO→LUMO+2 (39%), HOMO-1→LUMO+1 (27%), HOMO-4→LUMO (18%)
	327	0.1299	HOMO-2→LUMO (41%), HOMO-3→LUMO+1 (34%), HOMO-2→LUMO+2 (15%)
	426	3.0570	HOMO→LUMO (92%)
18c	271	0.1007	HOMO-5→LUMO (25%), HOMO→LUMO+3 (21%), HOMO-1→LUMO+2 (15%), HOMO-4→LUMO+1 (14%)
	299	0.3911	HOMO→LUMO+2 (40%), HOMO-1→LUMO+1 (25%), HOMO-4→LUMO (20%)
	337	0.8495	HOMO→LUMO+1 (54%), HOMO→LUMO+3 (22%), HOMO-5→LUMO (11%)
	339	1.2003	HOMO-1→LUMO (65%), HOMO-5→LUMO (10%)
	426	1.9505	HOMO→LUMO (92%)
18d	297	0.7724	HOMO→LUMO+3 (29%), HOMO-1→LUMO+1 (17%), HOMO-6→LUMO (14%), HOMO-5→LUMO+2 (12%)
	336	0.4495	HOMO→LUMO+2 (33%), HOMO-5→LUMO (30%)
	352	0.3814	HOMO→LUMO+1 (41%), HOMO→LUMO+4 (23%), HOMO-7→LUMO (13%)
	355	2.3759	HOMO-1→LUMO (54%), HOMO→LUMO+1 (14%)
	456	2.2869	HOMO→LUMO (93%)

5.2.6 Electroluminescence Properties

The electroluminescent characteristics of the compounds (**18a**-**18e**) were evaluated by utilizing them as emitter in the OLED device. The configuration of OLED device is ITO/PEDOT:PSS/mCBP:emitter(**18a-18e**)/TPBi/LiF/Al. Here, indium doped tin oxide (ITO) is served as anode, PEDOT:PSS (polyethylenedioxythiophene/polystyrenesulfonate) as hole injecting layer, mCBP 3,3-di(9*H*-carbazol-9-yl)biphenyl as the host material into which emitting materials are doped, TPBi (1,3,5-tris(*N*-phenylbenzimidazol-2-yl)benzene) as electron transporting or hole blocking layer, LiF as electron injecting layer and aluminium as a cathode.

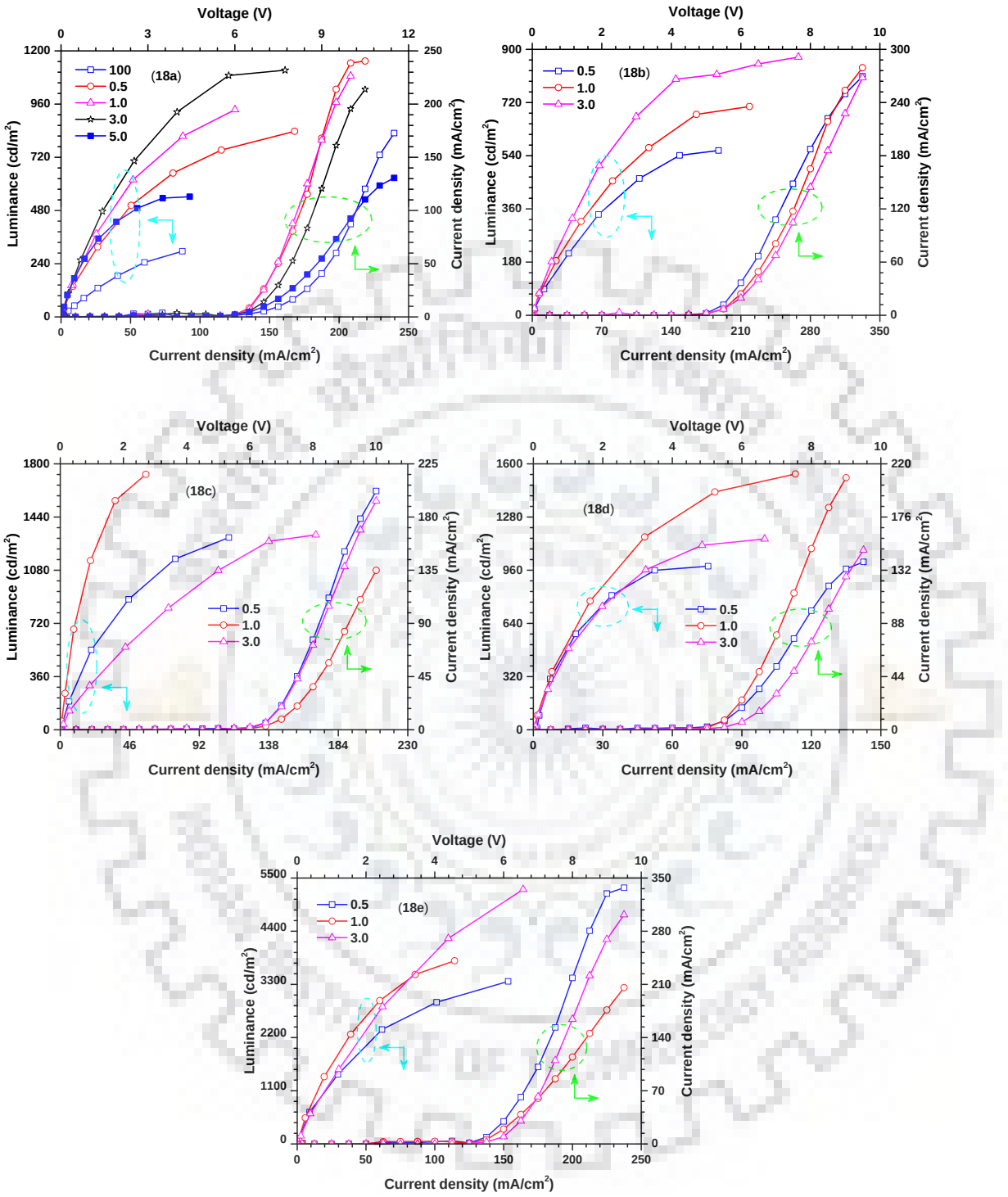

Figure 5.14 Current density-Voltage-Luminance (J-V-L) plots for the dyes **18a-18e**.

In order to evaluate the electroluminescence properties of these compounds, we fabricated a non-doped device with a representative compound **18a**. We observed high current density but low luminance for the non-doped device (Figure 5.14). The high current density might be due to

electron charge carriers due to the low energy barrier for electron injection from TPBI to emissive layer (0.11 eV). In contrast, hole injection energy barrier between PEDOT:PSS and emissive layer is very high (0.66 eV) which could have restricted the injection of hole carriers into emissive layer (Figure 5.15). As a result, the electron charge carriers might reach anode without recombination. The high energy barrier for the injection of charge carriers into emissive layer restricted the recombination of holes and electrons, but it allowed the leakage of charge carriers at the interface. Thus, low luminance is observed with high current density. Further, the electroluminescence spectrum of non-doped device of **18a** is broad and red shifted compared to the photoluminescence spectrum recorded in toluene (Figure 5.16). It might be due to the formation of aggregates in solid state [162]. The formation of aggregates induces the crystalline nature in thin film which eventually leads to the failure of the non-doped device.

Since the non-doped device exhibited poor electroluminescence performance ascribed to aggregation of dye molecules, we employed them as emitting dopant in the doped devices to improve electroluminescence performances. When the emitter **18a** is doped in to mCBP host, the electroluminescence spectrum restored in the blue region and it is comparable to photoluminescence spectrum recorded in toluene (Figure 5.16). It suggests the suppression of aggregation, when the emitter is doped into mCBP host. As the dopant concentration is increased to 3 wt%, the luminance is increased as a result of increased number of emitting molecules increased. But, at 5 wt% dopant concentration, the luminance began to decrease due to the formation of aggregation. The device performance is optimized at 1 wt% of dopant in mCBP host (Table 5.6). When we compare the power and current efficiency of **18a** with **18b**, **18a** exhibited superior performance. The high current density and low luminance observed for **18b** in doped device suggest imbalanced charge transport. Furthermore, the poor performance of **18b** could be attributed to the non-confinement of excitons in dopant molecules and the probable back energy transfer from dopant to host due to less energy barrier (0.17 eV) for holes (Figure 5.15). But, for the rest of the compounds, the considerable high energy barrier for hole and electron injection would refrain back transfer of energy from dopant to host. The appropriate energy gap favors complete energy transfer from host to the dopant and forbids back energy transfer and thus effective capture of excitons.

The power and current efficiency of the devices containing dye **18c** is three times higher than that **18b**. The energy barrier for hole injection from HTL to dopant is small as compared to

18b which facilitates efficient charge transport. Also, the back energy transfer would be completely controlled due to higher energy barrier between host and guest. The superior performance of **18c** might be due to the proper energy transfer from the host to guest and the absence of back energy transfer. Similarly, power and current efficiency of **18d** is superior to **18c**, despite of similar energy barriers for charge injection. Further, tetra-substituted compound **18e** exhibited almost two-fold increment in power and current efficiencies than that of **18d**. From the above discussion, we could infer that the number of cyanocarbazole unit on pyrene regulates the charge transport and contributes to the hike in device efficiency. As the number of cyanocarbazole loaded over pyrene moiety increases, the current and power efficiency of the devices increased progressively except for **18b**. It suggests the role of cyanocarbazole unit in achieving balanced charge transport and thus effective harvesting of excitons. The inferior and the odd performance of **18b** from the trend might be due to unfavorable energy levels which restricted the effective harvesting of excitons.

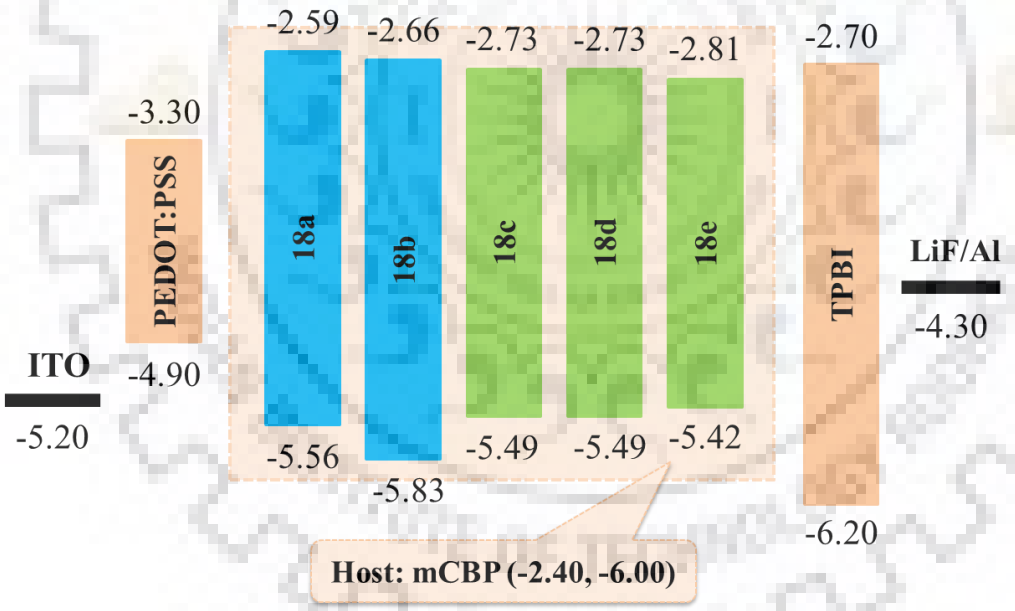

Figure 5.15 Energy level diagram for the OLED devices of the dyes (**18a-18e**) doped in mCBP host (values are in eV relative to vacuum level).

The best performance is achieved for the device fabricated with the dye **18e** (1 wt%) exhibiting power efficiency of 5.8 lm/w, current efficiency of 9.2 cd/A, maximum luminance of 3788 cd/m^2 and external quantum efficiency of 3.4%. The high performance of this device can

be attributed to four cyanocarbazole unit which ensures balanced charge transport and the favorable energy level alignment of **18e** with host material for effective trapping of excitons.

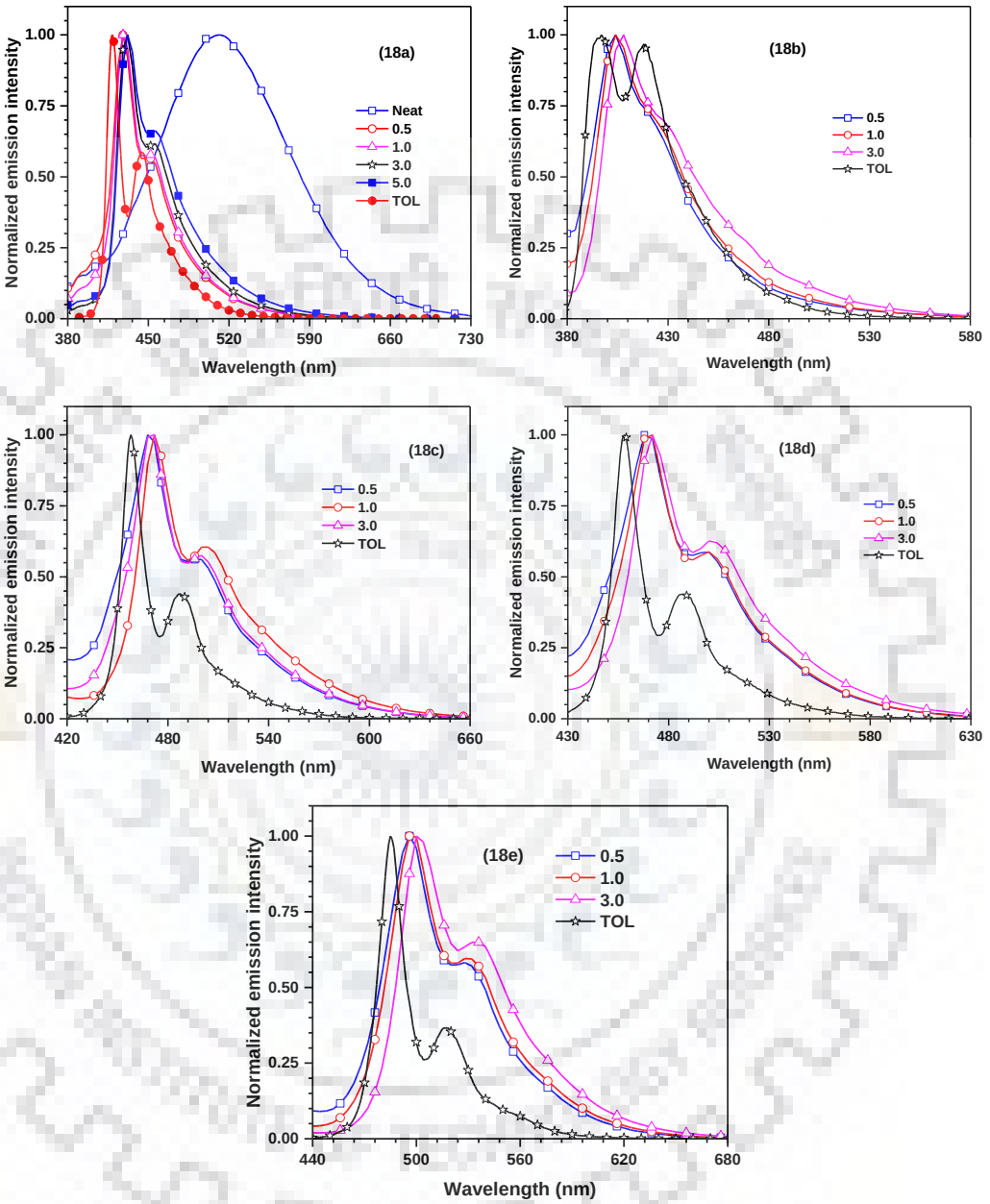

Figure 5.16 Comparison of EL and PL spectra of the dyes (**18a-18e**).

Table 5.6 Electroluminescent parameters of the dyes [a]

Dye	wt%	Turn on voltage (V)	Power Efficiency (lm/W)	Current Efficiency (cd/A)	EQE (%)	CIE (x,y)	Maximum Luminance (cd/m^2)	λ_{EL} (nm)
18a	100	8.2	0.2	0.5	0.2	(0.26, 0.40)	296	512
	0.5	6.3	0.8	1.7	2.7	(0.16, 0.08)	837	428
	1.0	6.3	1.0	1.9	2.9	(0.16, 0.08)	935	432
	3.0	6.5	1.0	2.0	2.6	(0.16, 0.09)	1113	432
18b	0.5	5.5	0.4	0.7	2.4	(0.16, 0.06)	558	404
	1.0	5.6	0.5	0.9	2.9	(0.16, 0.06)	707	404
	3.0	5.6	0.6	1.1	2.3	(0.16, 0.17)	874	408
18c	0.5	6.2	1.6	3.2	2.1	(0.16, 0.22)	1301	468, 500
	1.0	6.1	1.6	3.1	1.8	(0.16, 0.25)	1729	472, 504
	3.0	6.3	2.0	4.0	2.0	(0.18, 0.32)	1319	468, 500
18d	0.5	5.0	2.1	3.4	2.5	(0.15, 0.22)	984	468, 500
	1.0	5.0	3.3	5.2	3.2	(0.15, 0.24)	1539	472, 500
	3.0	5.5	2.4	4.2	2.3	(0.16, 0.30)	1148	472, 500
18e	0.5	4.9	4.4	7.0	2.7	(0.20, 0.47)	3362	496, 528
	1.0	5.0	5.8	9.2	3.4	(0.21, 0.51)	3788	496, 528
	3.0	5.2	3.8	6.3	2.0	(0.25, 0.58)	5264	500, 534

[a] values at 100 cd/m^2.

5.3 Conclusions

In summary, we have developed a series of pyrene-cyanocarbazole hybrids possessing acetylene linker by adopting Sonogashira coupling reaction. The structure-property relationship of the compounds is established by photophysical, electrochemical, thermal, theoretical and electroluminescence investigations. The solvent-independent absorption and emission spectra of the compounds indicate the absence of donor-acceptor interactions and structural perturbation in both ground and excited states. 1,8-disubstituted compound exhibited red shifted absorption and emission wavelength while 1,6-disubstituted compound exhibited blue shifted absorption and emission wavelength as compared to that mono-substituted compound. The high thermal stability of these dyes is attributed to rigid segments present in a molecule such as carbazole, pyrene, acetylene spacer and polar CN group. The electroluminescence properties of dyes are fine-tuned from deep blue to green emission by increasing the number of cyanocarbazole units on pyrene core. Except 1,6-disubstituted compound, the current and power efficiency of the compounds increased progressively as the number of cyanocarbazole increased on pyrene. This supports the positive role of cyanocarbazole in achieving balanced charge transport. The high

electroluminescence performance of **18e** is attributed to balanced charge transport due to the presence of four cyanocarbazole units and effective harvesting of excitons from the host.

5.4 Experimental Section

5.4.1 General Methods and Characterizations

Computational methods and other characterization methods are as described in chapter 3. OLED fabrication involves the similar fabrication method as described in chapter 3 with an exception of mCBP host instead of CBP host.

5.4.2 Synthesis

Synthesis of 9-(2-ethylhexyl)-7-((trimethylsilyl)ethynyl)-9*H*-carbazole-2-carbonitrile, 15

A mixture of 7-bromo-9-(2-ethylhexyl)-9*H*-carbazole-2-carbonitrile (2.0 g, 5.2 mmol), $Pd(PPh_3)_2Cl_2$ (36.5 mg, 0.052 mmol), PPh_3 (27.3 mg, 0.104 mmol), CuI (9.9 mg, 0.052 mmol), triethylamine (40 mL) and ethynyltrimethylsilane (0.9 mL, 6.25 mmol) was stirred at room temperature for 24 h under nitrogen atmosphere. After completion of the reaction, the reaction mixture was poured into water and extracted with chloroform. The organic layer was dried over sodium sulphate. Finally, the solvent was removed under vacuum to yield a residue which was then purified by column chromatography. Pale yellow solid. Yield 1.85 g (88%). mp 102-104 °C; IR (KBr, cm^{-1}) 2331 ($\nu_{C\equiv C}$); ^{1}H NMR ($CDCl_3$, 400 MHz) δ 8.11 (d, J = 7.6 Hz, 1 H), 8.03 (d, J = 8.4 Hz, 1 H), 7.67 (s, 1 H), 7.53 (s, 1 H), 7.49-7.45 (m, 1 H), 7.40-7.38 (m, 1 H), 4.21-4.11 (m, 2 H), 2.07-2.01 (m, 1 H), 1.42-1.23 (m, 8 H), 0.91 (t, J = 7.2 Hz, 3 H), 0.87 (t, J = 7.2 Hz, 3 H), 0.29 (s, 9 H). ^{13}C NMR ($CDCl_3$, 100.3 MHz) δ 141.44, 140.29, 125.71, 123.83, 122.18, 121.89, 121.12, 120.95, 120.19, 113.28, 112.99, 108.28, 105.71, 94.90, 47.70, 39.21, 30.72, 29.67, 28.53, 24.32, 22.98, 13.99, 10.87; HRMS calcd for $C_{25}H_{33}NSi$ (*m/z* +Na) 423.2227, found 423.2211.

Synthesis of 9-(2-ethylhexyl)-7-ethynyl-9*H*-carbazole-2-carbonitrile, 16

A mixture of 9-(2-ethylhexyl)-7-((trimethylsilyl)ethynyl)-9*H*-carbazole-2-carbonitrile (1.85 g, 4.6 mmol), potassium fluoride (0.27 g, 4.6mmol), tetrabutylammonium bromide (1.48 g, 4.6 mmol), methanol (10 mL) and chloroform (5 mL) was stirred for 30 minutes at 60 °C. After completion of the reaction, the mixture was poured into water and extracted with chloroform. The organic layer was dried over sodium sulphate. Finally, the solvent was removed under

vacuum to yield a residue which was purified by column chromatography. Yellow solid. Yield 1.25 g (83%). mp 90-92 °C; IR (KBr, cm^{-1}) 2219 ($\nu_{C\equiv C}$); ^{1}H NMR ($CDCl_3$, 400 MHz) δ 8.12 (dd, J = 8.0 Hz, 1.2 Hz, 1 H), 8.07-8.04 (m, 1 H), 7.68 (s, 1 H), 7.57 (s, 1 H), 7.49 (d, J = 8.0 Hz, 1 H), 7.42 (d, J = 8.0 Hz, 1 H), 4.21-4.10 (m, 2 H), 3.21 (s, 1 H), 2.06-1.99 (m, 1 H), 1.41-1.25 (m, 8 H), 0.92 (t, J = 7.6 Hz, 3 H), 0.86 (t, J = 6.8 Hz, 3 H). ^{13}C NMR ($CDCl_3$, 100.3 MHz) δ 141.25, 140.17, 125.50, 123.66, 122.15, 121.86, 121.07, 120.95, 120.75, 120.05, 113.20, 108.39, 84.28, 77.73, 47.57, 39.18, 30.70, 29.62, 28.48, 24.22, 22.91, 13.91, 10.75; HRMS calcd for $C_{22}H_{25}N$ (m/z +1) 329.2018, found 329.2022.

Synthesis of 9-(2-ethylhexyl)-7-(pyren-1-ylethynyl)-9*H*-carbazole-2-carbonitrile, 18a

A mixture of 1-bromopyrene (0.5 g, 1.78 mmol), 9-(2-ethylhexyl)-7-ethynyl-9*H*-carbazole-2-carbonitrile (0.59 g, 1.78 mmol), $Pd(PPh_3)_2Cl_2$ (12.5 mg, 0.018 mmol), PPh_3 (9.4 mg, 0.036 mmol), CuI (3.5 mg, 0.018 mmol), triethylamine (30 mL) was refluxed for 12 h under nitrogen atmosphere. After completion of the reaction, the reaction mixture was poured into water and extracted with chloroform. The organic layer was dried over sodium sulphate. Finally, the solvent was removed under vacuum to yield a residue which was then purified by column chromatography. Yield 0.47 g (50%). mp 146-148 °C; IR (KBr, cm^{-1}) 2219 ($\nu_{C\equiv N}$); ^{1}H NMR ($CDCl_3$, 400 MHz) δ 8.72 (d, J = 9.2 Hz, 2 H), 8.27-8.20 (m, 4 H), 8.17-8.12 (m, 4 H), 8.08-8.03 (m, 2 H), 7.75 (s, 1 H), 7.67-7.64 (m, 2 H), 7.49 (dd, J = 7.6 Hz, 1.2 Hz, 1 H), 4.22-4.14 (m, 2 H), 2.13-2.06 (m, 1 H), 1.49-1.25 (m, 8 H), 0.96 (t, J = 7.2 Hz, 3 H), 0.90 (t, J = 7.6 Hz, 3 H), ^{13}C NMR ($CDCl_3$, 100.3 MHz) δ 141.65, 140.23, 131.85, 131.27, 131.19, 130.97, 129.56, 128.32, 128.21, 127.18, 126.26, 125.75, 125.64, 125.38, 124.51, 124.42, 124.22, 123.59, 122.36, 122.18, 121.62, 121.15, 120.99, 120.24, 117.56, 113.18, 112.54, 108.22, 96.05, 89.40, 47.62, 39.30, 30.82, 28.61, 24.39, 23.01, 14.02, 10.89; HRMS calcd for $C_{39}H_{32}N_2$ m/z 528.2565, found 528.2564.

Synthesis of 7,7'-(pyrene-1,6-diylbis(ethyne-2,1-diyl))bis(9-(2-ethylhexyl)-9*H*-carbazole-2-carbonitrile), 18b and 7,7'-(pyrene-1,8-diylbis(ethyne-2,1-diyl))bis(9-(2-ethylhexyl)-9*H*-carbazole-2-carbonitrile), 18c

It was prepared from a mixture of dibromopyrene (mixture of isomers namely 1,6-dibromopyrene and 1,8-dibromopyrene) (0.3 g, 0.83 mmol), 9-(2-ethylhexyl)-7-ethynyl-9*H*-carbazole-2-carbonitrile (0.55 g, 1.66 mmol), $Pd(PPh_3)_2Cl_2$ (11.7 mg, 0.017 mmol), PPh_3 (8.7

mg, 0.033 mmol), CuI (3.2 mg, 0.017 mmol), triethylamine (30 mL) by following the procedure described for **18a**.

For **18b**: Yield 0.13 g (28%). mp 184-186 °C; IR (KBr, cm^{-1}) 2219 ($\nu_{C\equiv N}$); ^1H NMR ($CDCl_3$, 400 MHz) δ 8.16-8.08 (m, 6 H), 7.70-7.64 (m, 7 H), 7.54-7.46 (m, 7 H), 4.24-4.18 (m, 4 H), 2.10-2.07 (m, 2 H), 1.46-1.25 (m, 16 H), 0.95 (t, J = 7.2 Hz, 6 H), 0.88 (t, J = 7.2 Hz, 6 H). ^{13}C NMR ($CDCl_3$, 100.3 MHz) δ 141.71, 140.41, 125.82, 124.10, 123.59, 122.35, 122.01, 121.77, 121.36, 121.21, 121.16, 120.19, 113.77, 113.45, 113.37, 112.67, 108.45, 90.96, 47.85, 39.34, 30.85, 28.63, 24.40, 23.03, 14.02, 10.92; HRMS calcd for $C_{62}H_{54}N_4$ *m/z* 854.4343, found 854.4358.

For **18c**: Yield 0.11 g (16%). mp 146-148 °C; IR (KBr, cm^{-1}) 2222 ($\nu_{C\equiv N}$); ^1H NMR ($CDCl_3$, 400 MHz) δ 8.80 (s, 1 H), 8.73 (d, J = 9.2 Hz, 1 H), 8.28 (d, J = 7.6 Hz, 2 H), 8.20-8.08 (m, 8 H), 7.74 (d, J = 3.2 Hz, 2 H), 7.67-7.63 (m, 4 H), 7.51-7.47 (m, 2 H), 4.20-4.14 (m, 4 H), 2.10-2.08 (m, 2 H), 1.47-1.25 (m, 16 H), 0.98-0.87 (m, 12 H), ^{13}C NMR ($CDCl_3$, 100.3 MHz) δ 141.69, 140.34, 131.99, 131.75, 131.36, 131.15, 129.99, 128.12, 128.01, 126.31, 125.78, 125.19, 124.14, 123.64, 122.29, 121.76, 121.21, 121.10, 120.21, 118.38, 113.29, 112.61, 112.55, 108.36, 96.56, 89.26, 47.73, 39.35, 30.86, 28.65, 24.43, 23.03, 14.05, 10.94; HRMS calcd for $C_{62}H_{54}N_4$ *m/z* 854.4343, found 854.4358.

Synthesis of 7,7',7''-(pyrene-1,3,6-triyltris(ethyne-2,1-diyl))tris(9-(2-ethylhexyl)-9*H*-carbazole-2-carbonitrile), 18d

It was prepared from a mixture of 1,3,6-tribromopyrene (0.3 g, 0.68 mmol), 9-(2-ethylhexyl)-7-ethynyl-9*H*-carbazole-2-carbonitrile (0.67 g, 2.04 mmol), $Pd(PPh_3)_2Cl_2$ (14.4 mg, 0.02 mmol), PPh_3 (10.7 mg, 0.04 mmol), CuI (3.9 mg, 0.02 mmol), triethylamine (30 mL) by following the procedure described for **18a**. Yield 0.60 g (75 %). mp 132-134 °C; IR (KBr, cm^{-1}) 2223 ($\nu_{C\equiv N}$); ^1H NMR ($CDCl_3$, 400 MHz) δ 8.85 (s, 1 H), 8.75 (d, J = 9.2 Hz, 2 H), 8.29 (d, J = 8.0 Hz, 2 H), 8.23-8.10 (m, 10 H), 7.76-7.73 (m, 2 H), 7.70-7.63 (m, 6 H), 7.54-7.48 (m, 3 H), 4.81-4.70 (m, 2 H), 4.23-4.16 (m, 4 H), 2.11-2.03 (m, 3 H), 1.43-1.25 (m, 24 H), 0.99-0.87 (m, 18 H), ^{13}C NMR ($CDCl_3$, 100.3 MHz) δ 141.66, 140.25, 131.96, 131.70, 131.33, 131.11, 129.96, 128.08, 127.98, 126.26, 125.76, 125.16, 124.04, 123.62, 122.27, 121.73, 121.17, 121.07, 121.02, 120.20, 118.33, 113.23, 112.59, 112.53, 108.33, 96.61, 89.23, 47.69, 39.33,

30.85, 28.64, 24.43, 23.03, 14.04, 10.93; HRMS calcd for $C_{85}H_{76}N_6$ *m/z* 1180.6126, found 1180.6119.

Synthesis of 7,7',7'',7'''-(pyrene-1,3,6,8-tetrayltetrakis(ethyne-2,1-diyl))tetrakis(9-(2-ethylhexyl)-9*H*-carbazole-2-carbonitrile), 18e

It was prepared from a mixture of 1,3,6,8-tetrabromopyrene (0.3 g, 0.58 mmol), 9-(2-ethylhexyl)-7-ethynyl-9*H*-carbazole-2-carbonitrile (0.76 g, 2.32 mmol), $Pd(PPh_3)_2Cl_2$ (16.3 mg, 0.023 mmol), PPh_3 (12.2 mg, 0.046 mmol), CuI (4.4 mg, 0.023 mmol), triethylamine (30 mL) by following the procedure described for **18a**. Yield 0.50 g (57 %). mp 174-176 °C; IR (KBr, cm^{-1}) 2223 ($\nu_{C\equiv N}$); ^1H NMR ($CDCl_3$, 400 MHz) δ 8.79-8.63 (m, 3 H), 8.49 (s, 1 H), 8.27 (d, *J* = 7.6 Hz), 8.18-8.15 (m, 1 H), 8.13-8.07 (m, 8 H), 7.72-7.62 (m, 12 H), 7.50-7.46 (m, 4 H), 4.16-4.09 (m, 8 H), 2.08-2.03 (m, 4 H), 1.46-1.25 (m, 32 H), 0.99-0.86 (m, 24 H), ^{13}C NMR ($CDCl_3$, 100.3 MHz) δ 141.51, 140.17, 140.11, 133.22, 131.61, 1331.54, 131.26, 131.00, 130.19, 128.53, 126.69, 125.83, 125.60, 123.78, 123.55, 122.25, 122.03, 121.94, 121.75, 121.09, 120.97, 120.15, 118.98, 118.17, 118.10, 113.19, 112.50, 108.39, 97.19, 96.87, 89.13, 88.48, 88.39, 47.59, 39.30, 30.85, 28.63, 24.43, 23.03, 14.06, 10.93; HRMS calcd for $C_{108}H_{98}N_8$ *m/z* 1506.7909, found 1506.7937.

CHAPTER 6

Tetra-Substituted Carbazoles Containing Donor and Acceptor: Variation in Optical and Electroluminescent Properties Arising From Positional Isomerism

6.1 Introduction

Emitting molecules play a significant role in organic light emitting diodes since the electroluminescence performance of the OLED device is dependent on the functional properties of emitters. After the evolution of new concepts of hybridized local and charge transfer (HLCT) and thermally activated delayed fluorescence (TADF), the development of donor-acceptor (D-A) configured materials became a hot topic in the field of OLED. The systematic study of structure-property relationship of the organic materials contributed to the development of exciting OLED performances. The D-A materials behave as bipolar materials and thus exhibit better device performance. Therefore, the development of suitable materials possessing D-A moieties with desirable photophysical and electroluminescence properties is crucial. Generally, mismatched tailoring of donor and acceptor moieties lead to bathochromically shifted emission and fluorescence quenching. It is imperative that D-A molecules with rational design exhibit the emission confined to blue region with high performance owing to bipolar nature.

Arylamines (carbazole and triphenylamine) are considered as potential building blocks for the construction of organic emitter. When the suitable acceptor moieties are tethered on arylamines, their thermal stability is increased. Cyano group is one of the strong electron withdrawing groups. Since the size of cyano group is small, the non-radiative decay owing to vibrational and structural relaxation at excited state is greatly suppressed [216,217]. It is easy to introduce cyano group at different nuclear positions of carbazole. In order to exploit the advantages of above mentioned functional properties, many attempts have been reported where carbazole/triphenylamine donor integrated with cyano acceptor through phenyl spacer. For example, Adachi and coworkers reported carbazole substituted cyanobenzene (**DA1**-**DA6**) as highly efficient TADF emitters [61]. They tuned the color from sky blue to green and orange by appending carbazole moieties on cyanobenzene. The sky blue (**DA2**), green (**DA3**) and orange (**DA5**) emitters exhibited the external quantum efficiency of 8.0%, 19.3% and 11.2% respectively which are quite superior to the performance of conventional fluorescent devices. Zhang and coworkers designed carbazole substituted cyanopyridine (**DA7**) as blue TADF emitter [62]. Owing to large steric hindrance, well separated HOMO and LUMO energy level is realized with low ΔE_{ST} of 0.04 eV. The steric crowding and electron withdrawing cyano group suppressed non-radiative decay to greater extent. The device fabricated with **DA7** showed high EQE of 21.2% in mCP host system at 13 wt% concentration. Lee and coworkers developed

carbazole substituted dicyanobenzenes (**DA8**-**D10**) to tune the color and device performance [63]. As the number of carbazole increased, the donor strength of the molecule increased and thus emission color got tuned from sky blue to green.

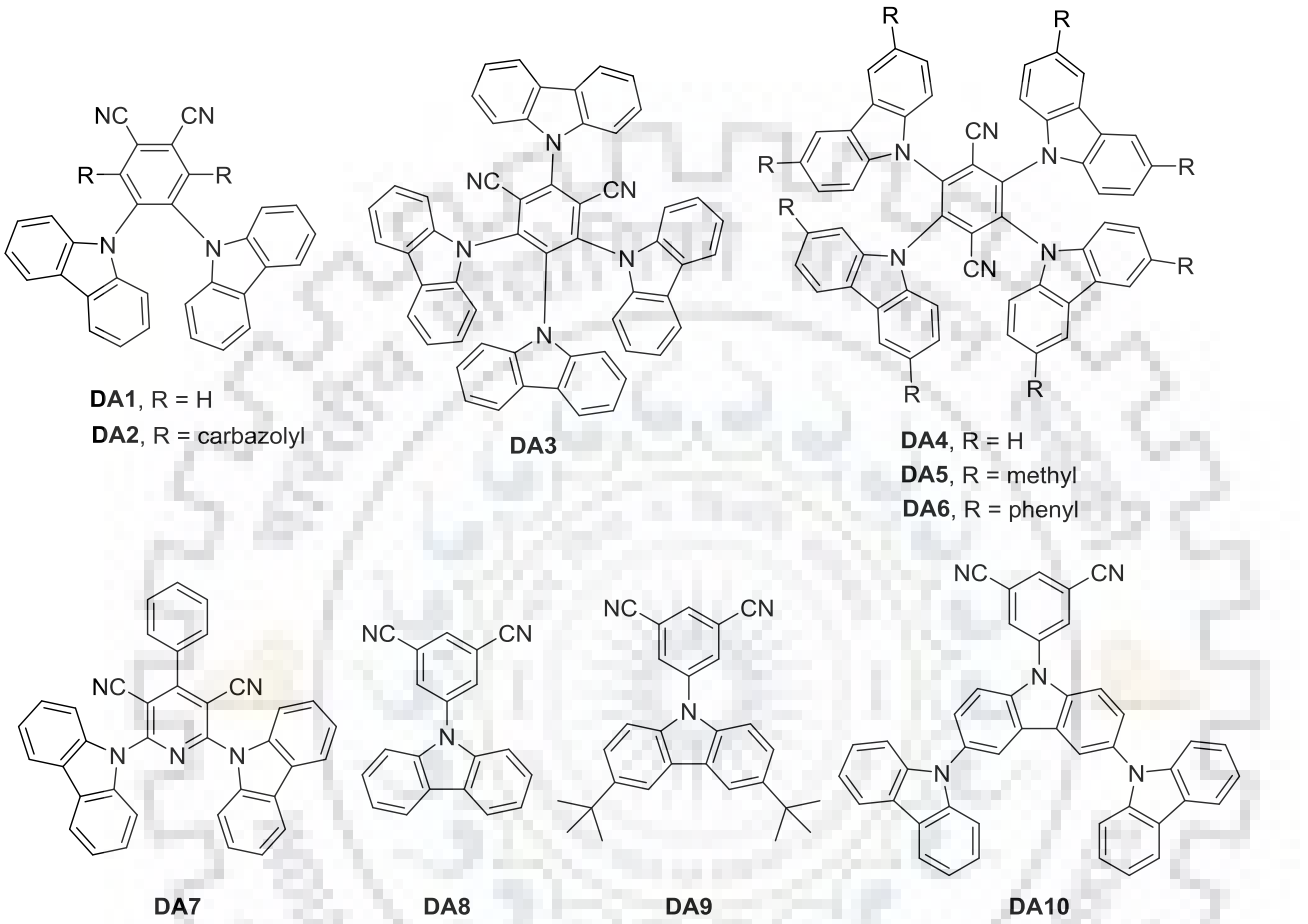

Chart 6.1 Carbazole-based compounds as TADF emitters.

Since the carbazole compounds containing cyano substituent exhibit high triplet energy and bipolar characteristics, they are utilized as host material for phosphorescence and TADF devices. Lee and coworkers demonstrated the utility of carbazole tethered cyanobenzene linked through phenyl spacer (**DA11**-**DA13**) as host materials [72]. The best device performance of 26.0% EQE with green emission was obtained for the device fabricated with meta-phenyl linked compound (**DA12**) as host. The high EQE is ascribed to high PLQY of the emitter doped thin film. Mostly, high performance OLED devices suffer due to short lifetime. To overcome this limitation, Lee and coworkers reported cyanocarbazole tailored carbazole through phenyl spacer with different linking topology (**DA14**-**D15**) [56]. Due to electron withdrawing nature

and stable molecular structure, the meta- linked compound (**DA15**) showed high EQE of 15.0% and almost double the life time of device based on ortho- phenyl substituted compound (**DA14**). Lin and coworkers reported arylamine decorated cyanocarbazole (**DA16**-**DA20**) as bipolar emitting materials [103]. They concluded that the bulkier arylamines are helpful to increase thermal and morphological stability. The cyano- substituted compounds showed superior performance which is due to the boosting of electron transport. Recently, Thomas and coworkers reported dicyanocarbazole possessing triphenylamine donor (**DA22**) as HLCT emitter [97]. They compared the parent compound which does not have cyano group (**DA21**). They found that the insertion of cyano group induced HLCT in **DA22**. As a result, the compound showed high EQE of 6.5% which is higher than that of parent compound.

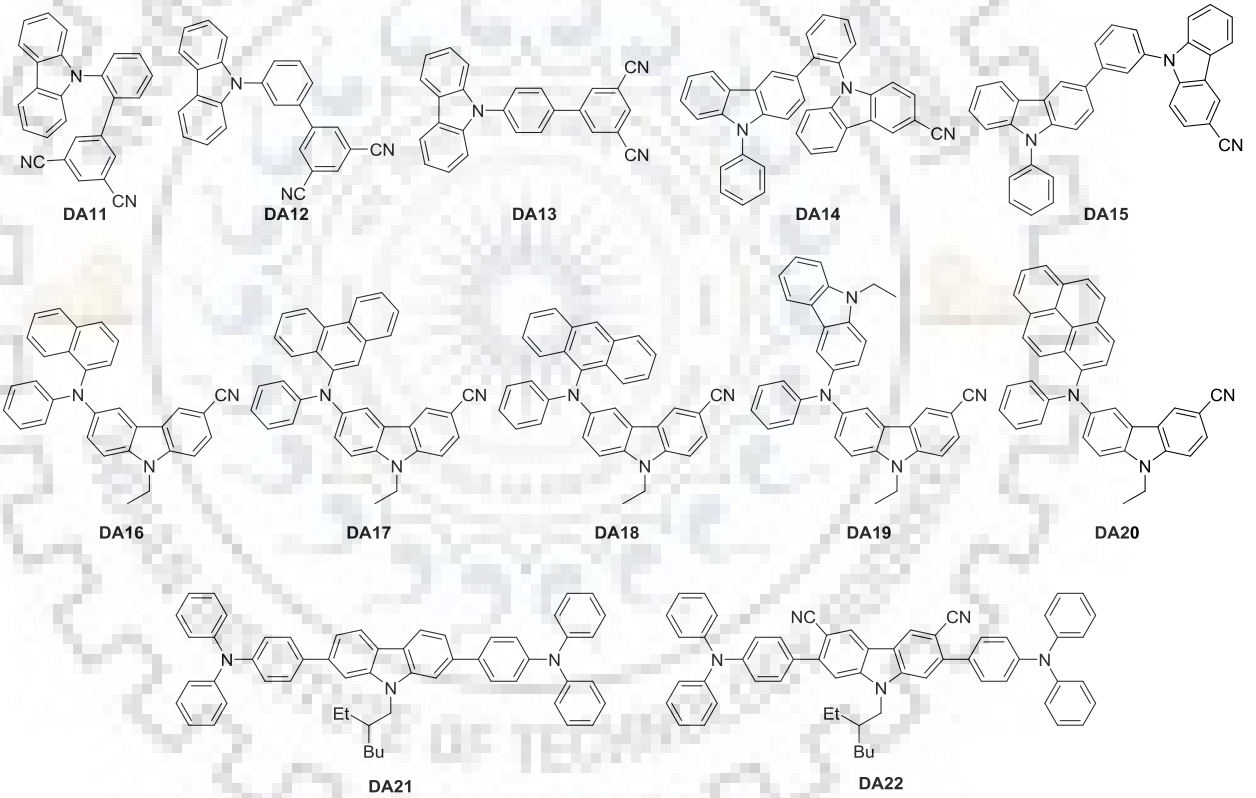

Chart 6.2 Arylamine functionalized cyanocarbazoles for electroluminescence applications.

Tailoring aromatic groups together through a choice of spacer would be a good method to elongate the conjugation of the molecule. Acetylene spacer is rigid and its rod-like shape facilitates the electronic delocalization through coplanarity and provides high quantum yield [180]. The tailoring of carbazole with other arylamines such as carbazole or triphenylamine

would be interesting to increase conjugation length and functionally tune the material properties. However, the combination of arylamine-cyanocarbazole conjugates containing acetylene spacer is not explored in the literature. As the continuous endeavor for the study of structure-property relationship in organic materials, we studied the effect of positional isomers on photophysical, electrochemical and electroluminescent properties of arylamine functionalized cyanocarbazole (Chart 6.3). In this chapter, we have studied the photophysical, electrochemical and electroluminescent properties of arylamine functionalized isomeric cyanocarbazoles. The structure-property relationship among the positional isomers is established. All the materials exhibited blue emission.

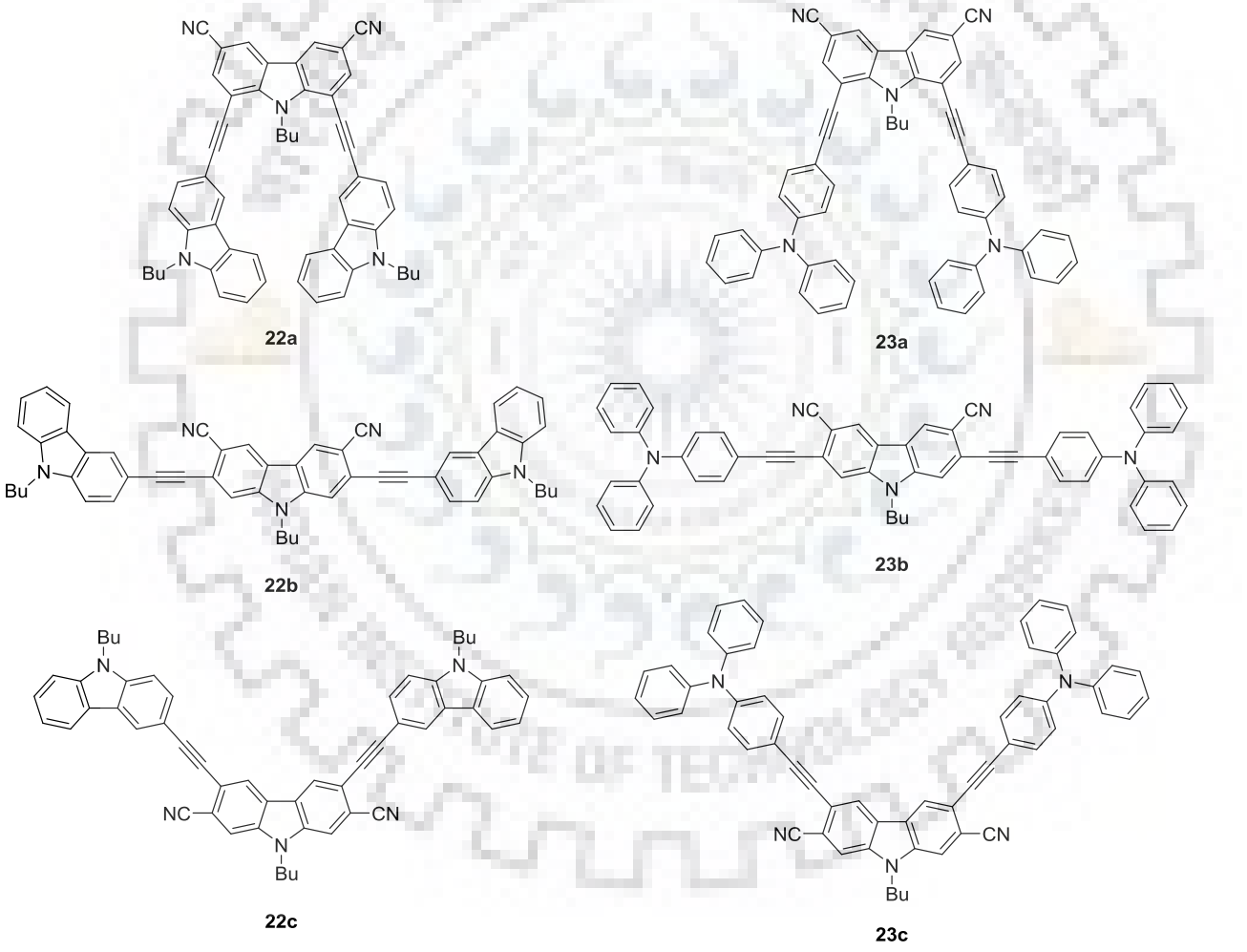

Chart 6.3 Structure of the isomeric cyanocarbazole dyes.

6.2 Results and Discussion

6.2.1 Synthesis and Characterization

The synthesis of target molecules is described in Scheme 6.1. 3,6-Dibromo-9-butyl-9*H*-carbazole (**19a**) and 2,7-dibromo-9-butyl-9*H*-carbazole (**19b**) were converted to corresponding cyanocarbazoles (**20a** and **20c**) by von-brown reaction. The cyano carbazoles obtained were iodinated to get **21a** and **21c**. In another synthetic route, **19b** was iodinated to get **20b** which then further selectively cyanated by using CuCN in DMF under reflux condition to yield **21b**. Finally, the intermediates **21a**-**21c** were converted to target dyes (**22a**-**22c** and **23a**-**23c**) by Sonogashira coupling reaction protocol using suitable terminal carbazole/triphenylamine acetylenes (**22** and **23**). All the dyes were obtained in moderate to good yields. All the compounds were thoroughly characterized by ^{1}H NMR, ^{13}C NMR and high resolution mass spectrometry measurements. The data are consistent with the proposed structures of the compounds. All the dyes are soluble in common organic solvents such as toluene (TOL), dichloromethane (DCM), chloroform ($CHCl_3$), tetrahydrofuran (THF), *N*,*N*-dimethylformamide (DMF) and sparingly soluble in acetonitrile (ACN) and methanol (MeOH).

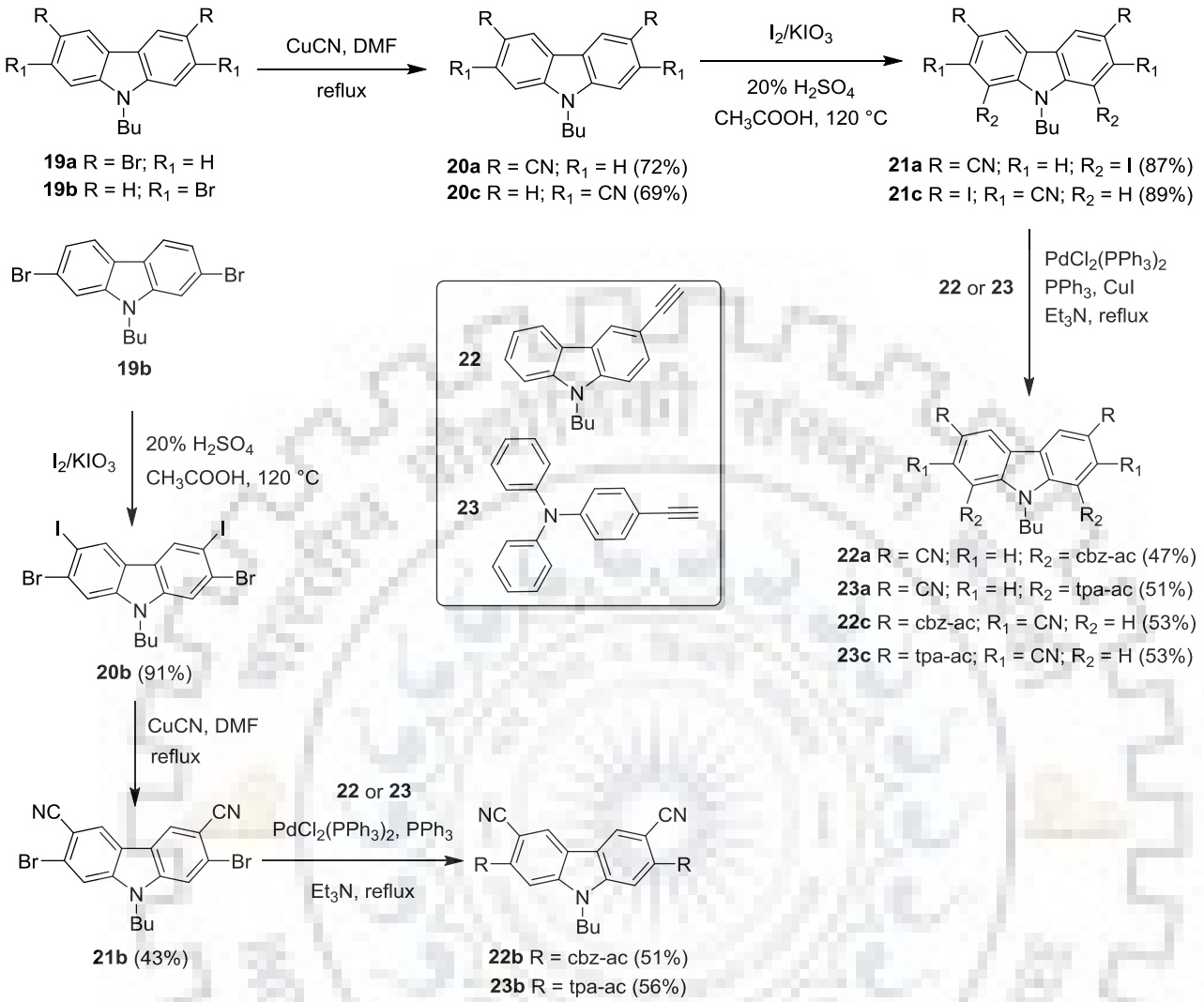

Scheme 6.1 Synthetic procedure for the target compounds **22a**-**22c** and **23a**-**23c**.

6.2.2 Photophysical Properties

The absorption spectra of the compounds recorded in dichloromethane solution are presented in Figure 6.1, and the relevant data summarized in Table 6.1. There are two or three distinct absorption bands with multiple shoulder peaks observed for each of the compounds. The higher energy absorption band ca. below 330 nm is ascribed to π-π* transition of carbazole and/ or triphenylamine while the lower energy absorption band arises from π-π* transition of entire molecular structure [218,219]. The substitution at 1,8-positions of carbazole generally does not influence the conjugation length. Accordingly, the introduction of acetylene at 1,8-position of carbazole (**22a** and **23a**) exhibited blue shifted absorption when compared to other positional isomers. When the acetylene is inserted at 2,7-position, the compounds **22b** and **23b** displayed bathochromic shift as compared to the corresponding 1,8-substituted isomers (**22a**

and **23a**). It could be attributed to the elongation of conjugation along the linear axis of carbazole [220]. Interestingly, when acetylene is tailored at 3,6-position of central carbazole, the compounds **22c** and **23c** exhibited weak charge transfer band at about 430 nm. It might arise from the intra-molecular charge migration from peripheral carbazole/triphenylamine to cyanocarbazole core [221]. Since the acceptor strength of carbazole is moderate, the intensity of observed charge transfer peak is low. Generally, triphenylamine substituted compounds (**23a-23c**) exhibited red shifted absorption maximum when compared to their corresponding carbazole analogs (**22a-22c**) which could be attributed the electron richness of triphenylamine over carbazole. It is interesting to compare the absorption maximum of **22b** with the known compound 3,3'-((9-hexyl-9*H*-carbazole-2,7-diyl)bis(ethyne-2,1-diyl))bis(9-hexyl-9*H*-carbazole) which does not have cyano group at 3,6-position of carbazole core [180]. The compound **22b** exhibited red shifted absorption maximum (12 nm). Similarly, when we compare **22c** with the known compound 3,3'-((9-hexyl-9*H*-carbazole-3,6-diyl)bis(ethyne-2,1-diyl))bis(9-hexyl-9*H*-carbazole) which lacks cyano group at 2,7-position of core carbazole, **22c** showed slight red shift of about 2 nm and an additional weak intra-molecular charge transfer band [180]. It is reasoned that the presence of cyano group in **22c** might induce the electron deficient nature of carbazole core and thereby induces weak intramolecular charge transfer. The above results indicate the auxochromic role of cyano group in extending the π conjugation. In order to study the nature of ground state of the molecules, we recorded absorption spectrum of the compounds in different polarity of various solvents from non-polar toluene to polar methanol (Figure 6.3 to Figure 6.8). All the dyes exhibited solvent independent absorption maximum while **22b** and **23b** showed blue shift in absorption spectra as the polarity of the solvent increases. The negative solvatochromism of the compounds containing carbazole/triphenylamine along the linear axis of carbazole core (**22b** and **23b**) might be due to high dipole moment at ground state [222-225].

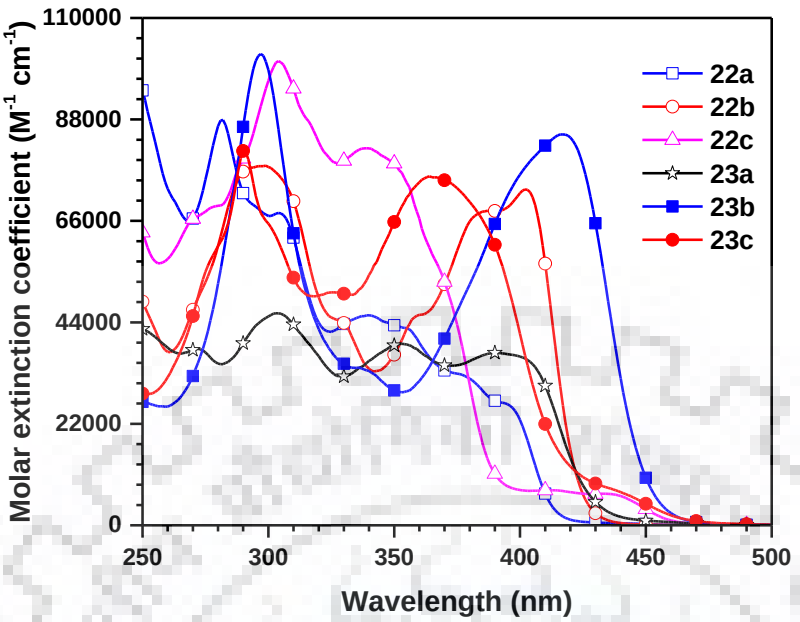

Figure 6.1 Absorption spectra of the dyes (**22a-22c** and **23a-23c**) recorded in dichloromethane.

Table 6.1 Optical properties of the dyes

Dye	λ_{max}, nm (ε_{max}, M^{-1} cm^{-1} $\times 10^3$)[a]	λ_{em}, nm (Φ_F)[a,b]	Stokes shift, cm^{-1}	λ_{em},[c] nm
22a	282(87.8), 304(67.7), 340(45.6), 380s(31.8), 395sh (26.3)	418 (0.37)	1393	484
22b	299(78.0), 329s(44.3), 359sh (45.4), 383sh (67.5), 402(72.8)	442 (0.71)	2251	494
22c	275sh (68.0), 304(100.7), 339(81.7), 433sh (6.8)	471 (0.73)	1863	500
23a	272sh (38.3), 303(45.9), 353(39.4), 390(37.4)	475 (0.41)	4588	501
23b	297(102.2), 337sh (34.0), 417(84.7)	492 (0.42)	3656	493
23c	290(81.2), 325sh (50.5), 364(75.7), 439sh (7.4)	510 (0.56)	3171	517

[a] Measured in dichloromethane solution. [b] Absolute quantum yield using integrating sphere. [c] Measured for drop cast film.

Figure 6.2 displays the emission spectra of the compounds recorded in dichloromethane and the pertinent data registered in Table 6.1. The emission maxima of the compounds followed the trend of absorption profile. All the compounds displayed structureless emission spectra with single emission maximum. Triphenylamine substituted dyes (**23a-23c**) showed broad and red shifted emission maximum when compared to their carbazole analogs (**22a-22c**). It might be due to structural reorganization associated with flexible triphenylamine units over rigid

carbazole at excited state [226]. Further, the above assumption is confirmed by increase of full width half maximum (FWHM) values for triphenylamine substituted compounds. When we compare the emission maximum of **22b** with the known compound 3,3'-((9-hexyl-9*H*-carbazole-2,7-diyl)bis(ethyne-2,1-diyl))bis(9-hexyl-9*H*-carbazole) which does not have cyano group at 3,6-position of carbazole core, the compound **22b** exhibited bathochromically shifted emission maximum [180]. Likewise, **22c** exhibited red shifted emission compared to its analogous compound 3,3'-((9-hexyl-9*H*-carbazole-3,6-diyl)bis(ethyne-2,1-diyl))bis(9-hexyl-9*H*-carbazole) which lacks cyano group at 2,7-position of carbazole core [180]. The nature of excited state of the dyes was studied by recording emission spectra in the solvents of different polarity (Figures 6.3-6.8). All the dyes exhibited positive solvatochromic character except **22a** which showed similar emission in all solvents, but **22a** also exhibited red shift in DMF. Triphenylamine substituted compounds (**23a**-**23c**) displayed high magnitude of spectral shift in emission solvatochromism as compared to their carbazole analogs (**22a**-**22c**). It might be due to the pronounced dipolar relaxation of triphenylamine substituted compounds at excited state over carbazole congeners [227]. The highest spectral shift of 80 nm is observed for **23c** in emission solvatochromism which is ascribed to the stabilization of charge transfer excited state. However, carbazole counterpart **22c** showed small solvatochromic spectral shift as a result of weak electron donating ability of carbazole and thus less dipolar stabilization of excited state. The nature of excited state species is studied by Lippert-Mataga plot (Figure 6.9). All the carbazole- based dyes (**22a** and **22c**) exhibited linear relationship which implies the presence of single excited state. In contrast, triphenylamine-based dyes **23a**-**23c** and **22b** exhibited two linear relationships attributable to local (LE) and charge transfer (CT) excited species [142-144]. Thin film emission spectra displayed red shifted emission maximum when compared to solution spectra recorded in toluene (Figure 6.10). It could be due to the intermolecular interaction or the formation of *J*- aggregates in solid state [228,229].

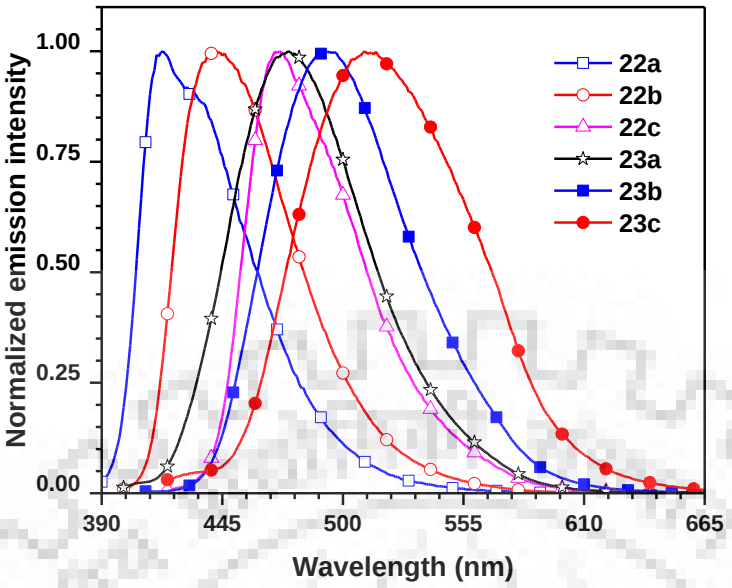

Figure 6.2 Emission spectra of the dyes (**22a-22c**) and (**23a-23c**) recorded in dichloromethane.

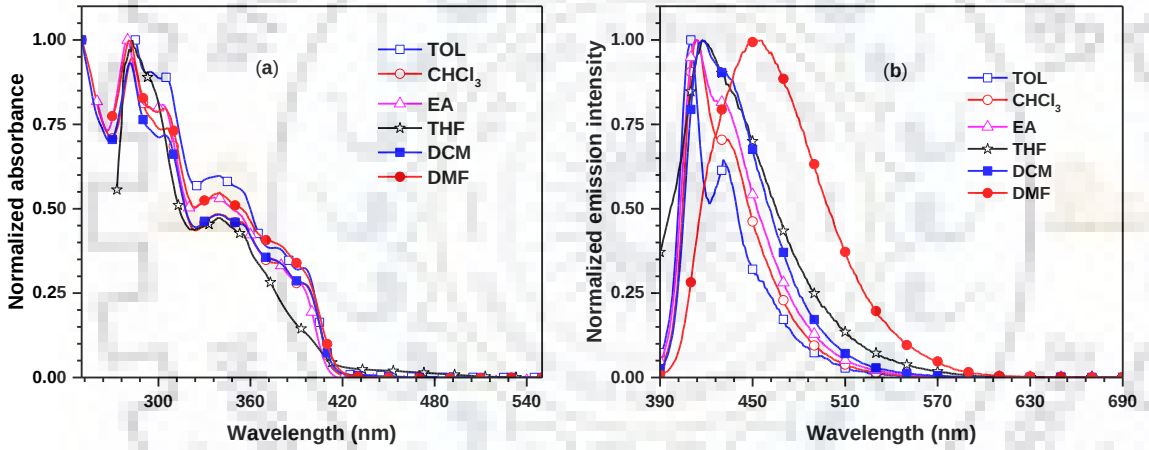

Figure 6.3 Absorption (a) and emission (b) spectra of **22a** recorded in different solvents.

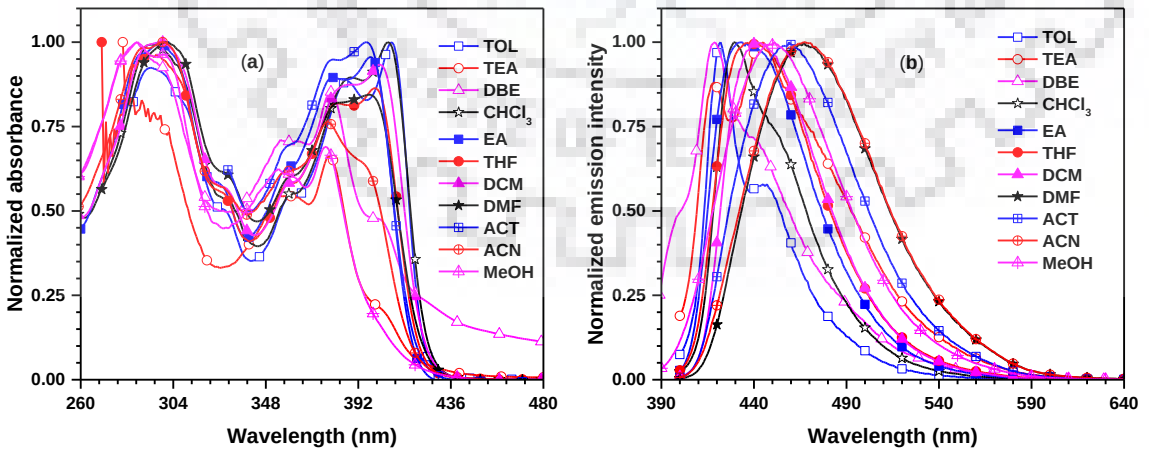

Figure 6.4 Absorption (a) and emission (b) spectra of **22b** recorded in different solvents.

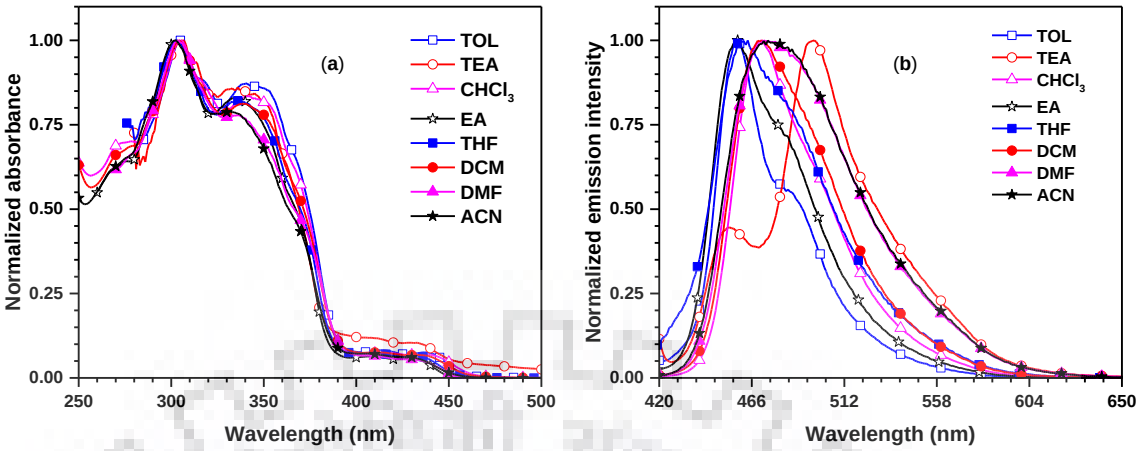

Figure 6.5 Absorption (a) and emission (b) spectra of **22c** recorded in different solvents.

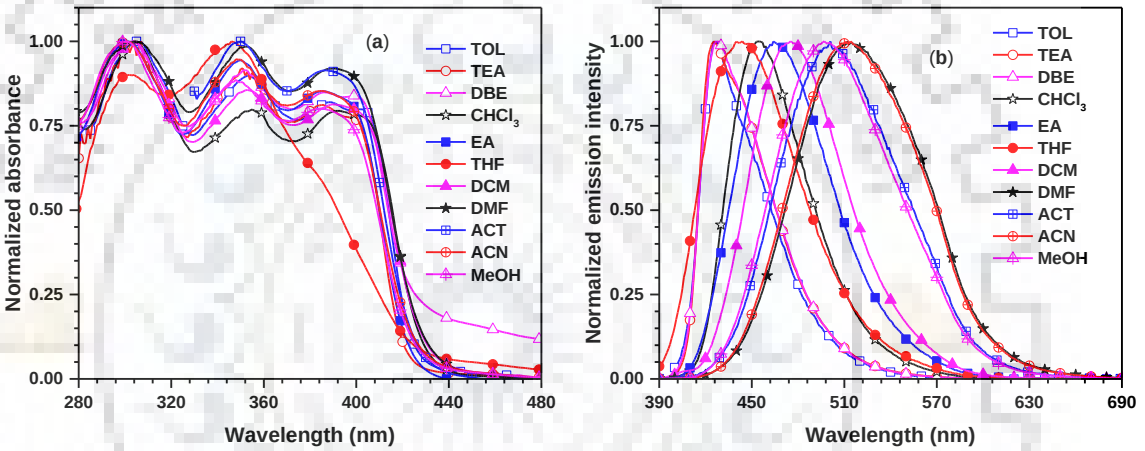

Figure 6.6 Absorption (a) and emission (b) spectra of **23a** recorded in different solvents.

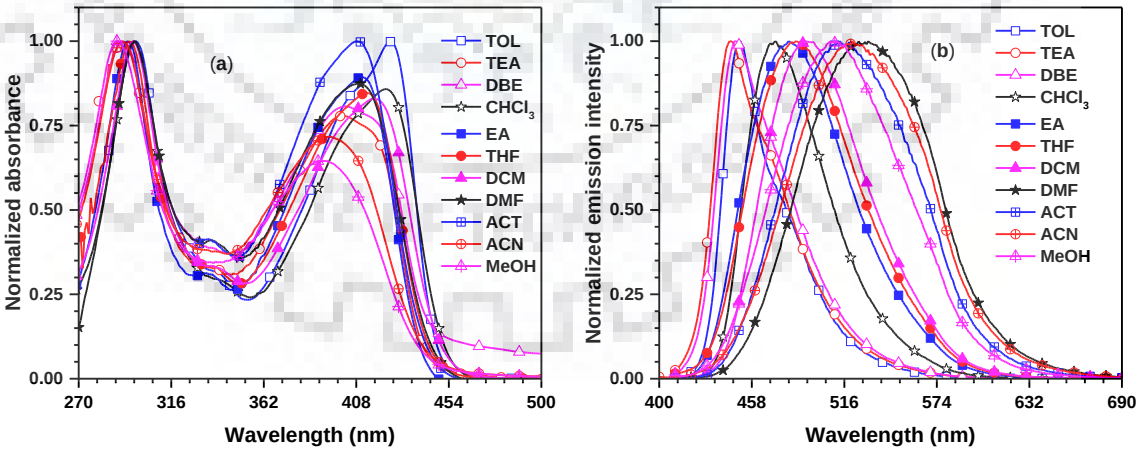

Figure 6.7 Absorption (a) and emission (b) spectra of **23b** recorded in different solvents.

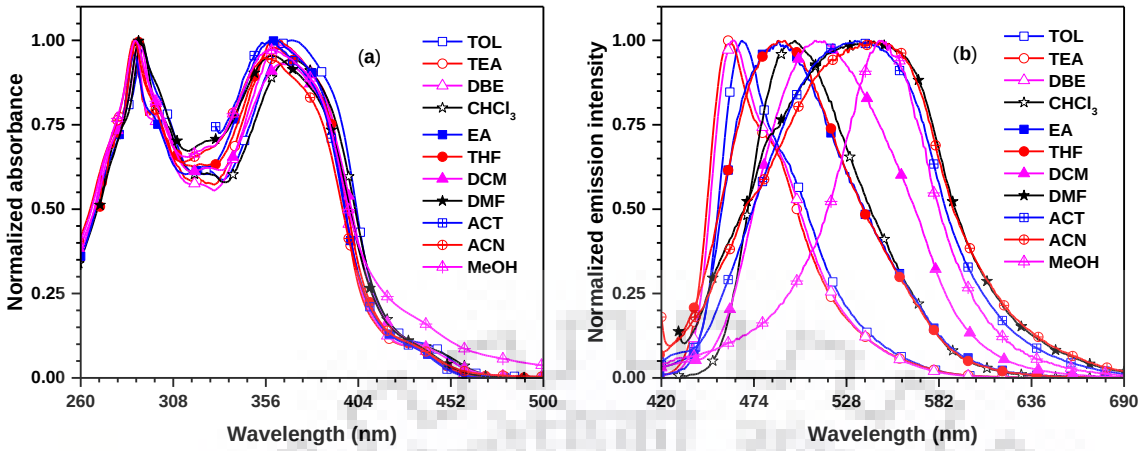

Figure 6.8 Absorption (a) and emission (b) spectra of **23c** recorded in different solvents.

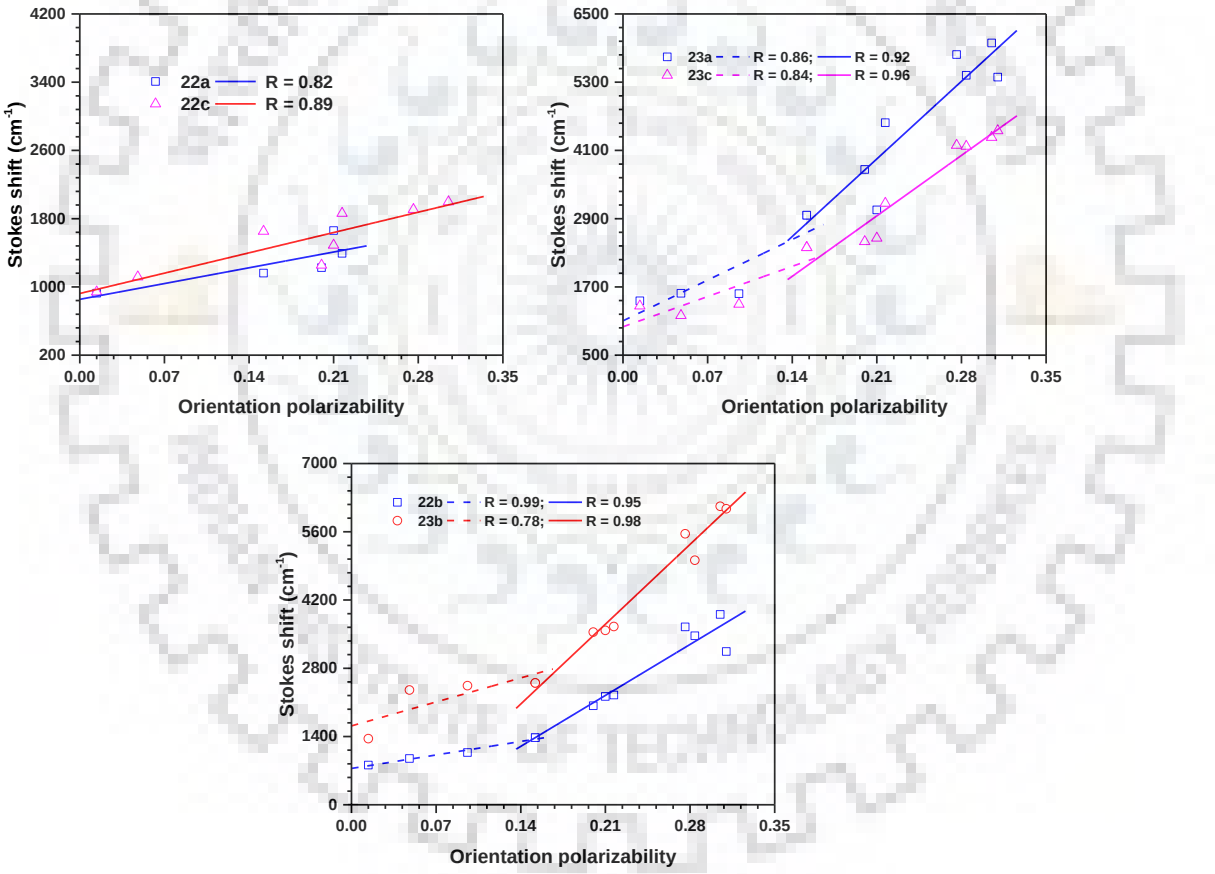

Figure 6.9 Lippert-Mataga plot of the dyes (**22a-22c** and **23a-23c**).

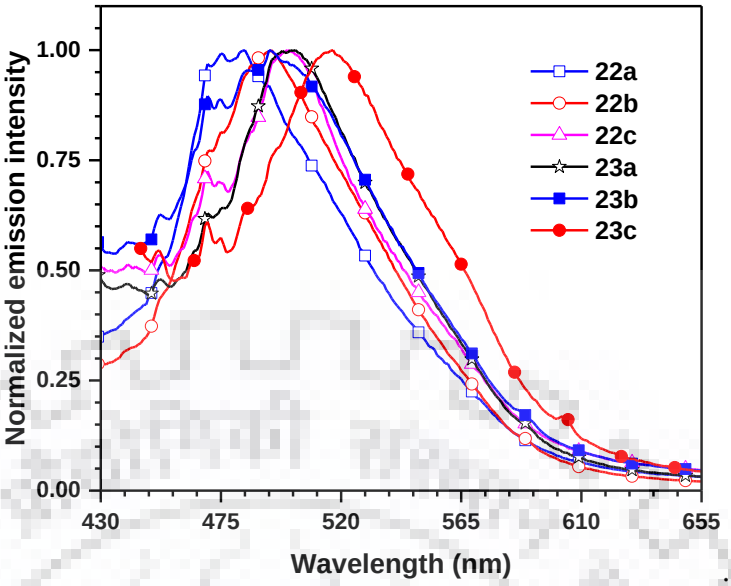

Figure 6.10 Thin film emission spectra of the dyes (**22a-22c** and **23a-23c**) recorded for drop cast films.

Table 6.2 Solvatochromic absorption data of the dyes

Dye	Absorption maxima, λ_{max} (nm)									
	TOL	TEA	DBE	$CHCl_3$	EA	THF	DMF	ACT	ACN	MeOH
22a	304, 339, 379, 395	-	-	289, 306sh, 339, 378, 395sh	280, 303, 336, 376sh, 394sh	283, 339, 390sh	281, 304, 339, 378sh, 394sh	-	-	-
22b	294, 327sh, 359sh, 387	295, 354sh, 378, 403sh	379, 401	296, 330sh, 361sh, 388	298, 325sh, 357sh, 379sh	296, 327sh, 358sh, 381sh	300, 329sh, 358sh, 381sh, 399	358sh, 379sh, 396	299, 326sh, 356sh, 377, 395	287, 354, 376, 395sh
22c	305, 340, 440sh	306, 336, 433sh	-	271sh, 305, 341, 437sh	271sh, 303, 336, 434	303, 336, 434sh	304, 337, 433sh	-	302, 332, 433sh	-
23a	305, 354, 389, 402	307, 350, 385, 399	303, 352, 386, 400	304, 355, 401	301, 350, 395	303, 346, 391sh	304, 352, 395	350, 394	301, 348, 393	301, 348, 392
23b	298, 425	289, 402	291, 403	297, 423	294, 335sh, 411	295, 337sh, 414	298, 336sh, 410	334sh, 408	292, 395	289, 390
23c	292, 370, 439sh	287, 364, 436sh	288, 321sh, 363, 434sh	292, 326sh, 369, 445sh	288, 360, 435sh	289, 360, 437sh	291, 358, 441sh	358, 436sh	288, 356, 439sh	288, 358, 440

Table 6.3 Solvatochromic emission data of the dyes

Dye	Emission maxima, λ_{em} (nm)									
	TOL	TEA	DBE	$CHCl_3$	EA	THF	DMF	ACT	ACN	MeOH
22a	410, 431	-	-	414, 434	414, 431	417	456	-	-	-
22b	422, 445	419, 445	419	430	433	439	467	459	467	451
22c	459, 484s	455, 497	-	471	459	464	472	-	474	-
23a	427	426	427	455	464	444	512	501	514	497
23b	451	444	447	473	481	486	531	513	521	511
23c	467	460	462	498	488	492	541	533	542	547

Table 6.4 Stokes shift value of the dyes

Dye	Stokes shift (cm^{-1})									
	TOL	TEA	DBE	$CHCl_3$	EA	THF	DMF	ACT	ACN	MeOH
22a	926	-	-	1162	1226	1660	3451	-	-	-
22b	813	948	1071	1375	2031	2221	3649	3466	3903	3144
22c	941	1117	-	1652	1255	1490	1908	-	1998	-
23a	1456	1588	1581	2960	3765	3053	5785	5421	5990	5389
23b	1356	2353	2443	2499	3541	3578	5558	5017	6123	6072
23c	1366	1197	1396	2392	2497	2558	4191	4174	4329	4446

6.2.3 Electrochemical Properties

The suitable HOMO and LUMO energy level of the compound facilitates the effective charge carrier mobility in the OLED device. In order to estimate the energy levels of HOMO and LUMO levels and to investigate the redox properties of the dyes, we carried out electrochemical experiment by cyclic voltammetry measurements. All the carbazole substituted compounds (**22a**-**22c**) exhibited irreversible oxidation while triphenylamine substituted compounds (**23a**-**23c**) gave quasi-reversible oxidation (Figure 6.11). The oxidation originates from carbazole and triphenylamine segments. The irreversible oxidation peak of carbazole substituted compounds is ascribed to large reorganization energy associated with stabilization of carbazole radical cation during the oxidation process [148,149]. The high oxidation propensity of triphenylamine-based compounds arises from electron richness of triphenylamine when compared to carbazole. The similar oxidation potential of 1,8-substituted compounds (**22a** and **23a**) with 2,7-substituted analogous compounds (**22b** and **23b**) indicates the similar electronic influence. But, the oxidation potential is slightly dropped for 3,6-substituted analogs **22c** and **23c**. The lower oxidation potential of 3,6-substituted analogs might be due to elongation of conjugation and strengthening of electron richness. The HOMO energy values are calculated by comparing the oxidation potential of ferrocene (-4.8 eV). The LUMO energy values are deduced by subtracting band gap value from HOMO energy values. The band gap values are estimated from the absorption edge which is the intersection of absorption and emission spectra of the dyes recorded in dichloromethane. The observed energy levels are well matching with the neighboring molecular layers of device which would be beneficial for facile charge transport.

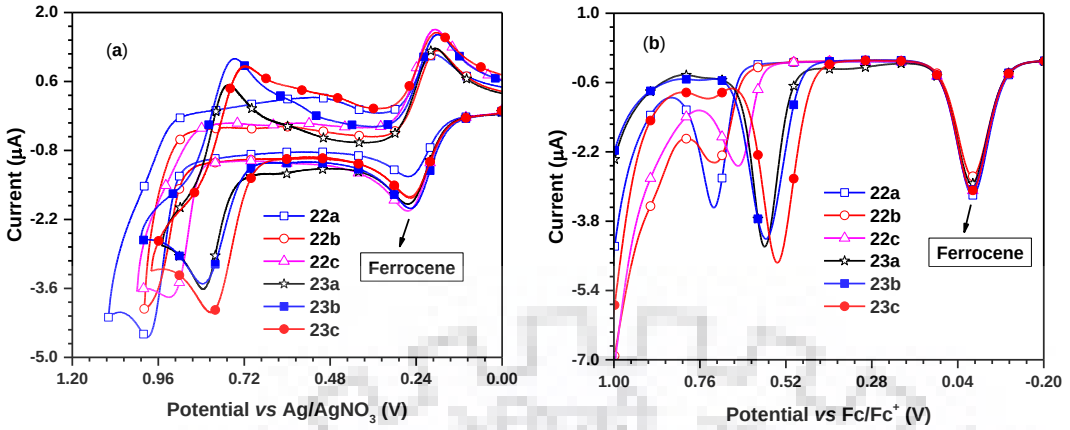

Figure 6.11 Cyclic voltammograms (a) and differential pulse voltammograms (b) of the dyes recorded in dichloromethane.

6.2.4 Thermal Properties

The thermal stability of the compounds was studied by thermo gravimetric analysis (TGA) under nitrogen atmosphere at the heating rate of 10 °C/min. The thermogram is displayed in Figure 6.12 and the relevant data summarized in Table 6.5. All the compounds exhibited high onset temperature of 375-504 °C corresponding to 10% weight loss. The high thermal stability of the compounds is ascribed to rigid nature of carbazole moiety. The high onset temperature of triphenylamine-based dyes arises from non-planar nature of triphenylamine [230]. The high thermal stability of molecules possessing rigid carbazole, polar cyano group and rod-like acetylene spacer is well documented in the literature [16, 153]. The 2,7-substituted compounds (**22b** and **23b**) showed high onset decomposition temperature when compared to analogous isomers.

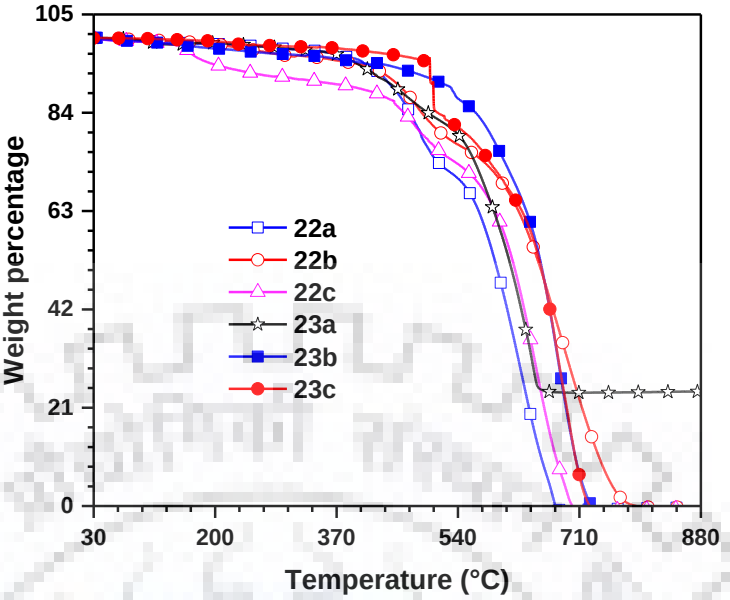

Figure 6.12 TGA plot of the dyes (**22a**-**22c** and **23a**-**23c**).

Table 6.5 Thermal and electrochemical properties of the dyes

Dye	$T_{onset,}$ °C[a]	T_d, °C	E_{ox}, V[b]	HOMO, eV[c]	LUMO, eV[d]	$E_{0\text{-}0}$, eV[e]
22a	444	628	0.72	-5.52	-2.43	3.09
22b	456	682	0.72	-5.52	-2.55	2.97
22c	375	646	0.65	-5.45	-2.63	2.82
23a	447	638	0.58	-5.38	-2.48	2.90
23b	522	680	0.58	-5.38	-2.60	2.78
23c	501	689	0.54	-5.34	-2.57	2.77

[a] Temperature corresponding to 10% weight loss. [b] Oxidation potential quoted reference to ferrocene internal standard. [c] HOMO = -(4.8 + E_{ox}). [d] LUMO = HOMO + $E_{0\text{-}0}$. [e] Optical band gap obtained from the intersection of normalized absorption and emission spectra (optical edge).

6.2.5 Theoretical Investigations

In order to have deep insight on the electronic structures and photophysical properties of the compounds, we have performed density functional theory calculation at B3LYP/6-31G(d,p) level [155,156]. The alkyl chains are shortened to methyl chain for reducing the cost of computational time. The computed absorption maxima, oscillator strength and most prominent electronic transitions of the compounds are listed in Table 6.6. The electronic distribution in the frontier molecular orbitals is displayed in Figure 6.13 and Figure 6.14. The trend of computed absorption maxima matched with the trend of experimental results. The HOMO is concentrated on peripheral donor and extended to central carbazole for **22a**/**22b** and **23a**/**23b** while the

LUMO is spread over cyano substituted carbazole core and slightly diffused to phenyl ring of peripheral carbazole/triphenylamine but not on cyano group. It indicates the involvement of π-π* transition during electronic excitation of these molecules. On the other hand, for **22c** and **23c**, the HOMO is dispersed over peripheral carbazole/triphenylamine and extends to carbazole core while the LUMO is completely concentrated on carbazole core and cyano group. It indicates the migration of charge from peripheral carbazole/triphenylamine to core carbazole containing cyano group which is due to characteristic ICT transition [157-159]. Since the overlap between HOMO and LUMO is observed for **22c** and **23c**, the intensity of ICT is weak. The similar results are obtained in experimental absorption spectroscopy where **22a**, **22b**, **23a** and **23b** exhibited π-π* transition while **22c** and **23c** displayed weak intramolecular charge transfer band.

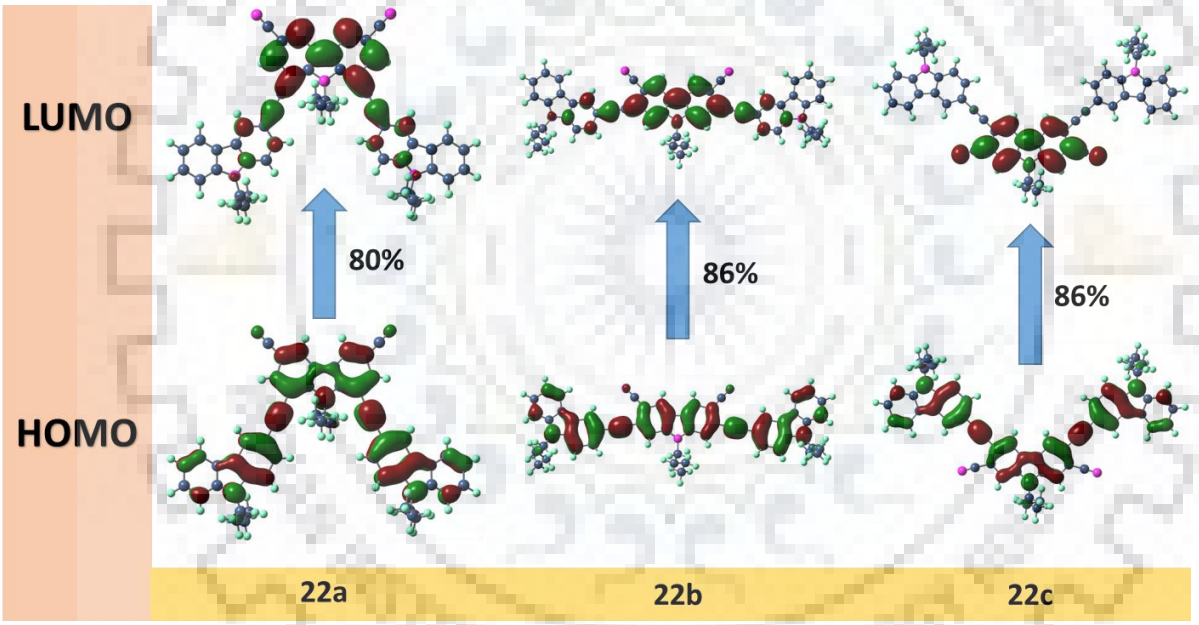

Figure 6.13 Frontier molecular orbitals of the dyes **22a-22c**.

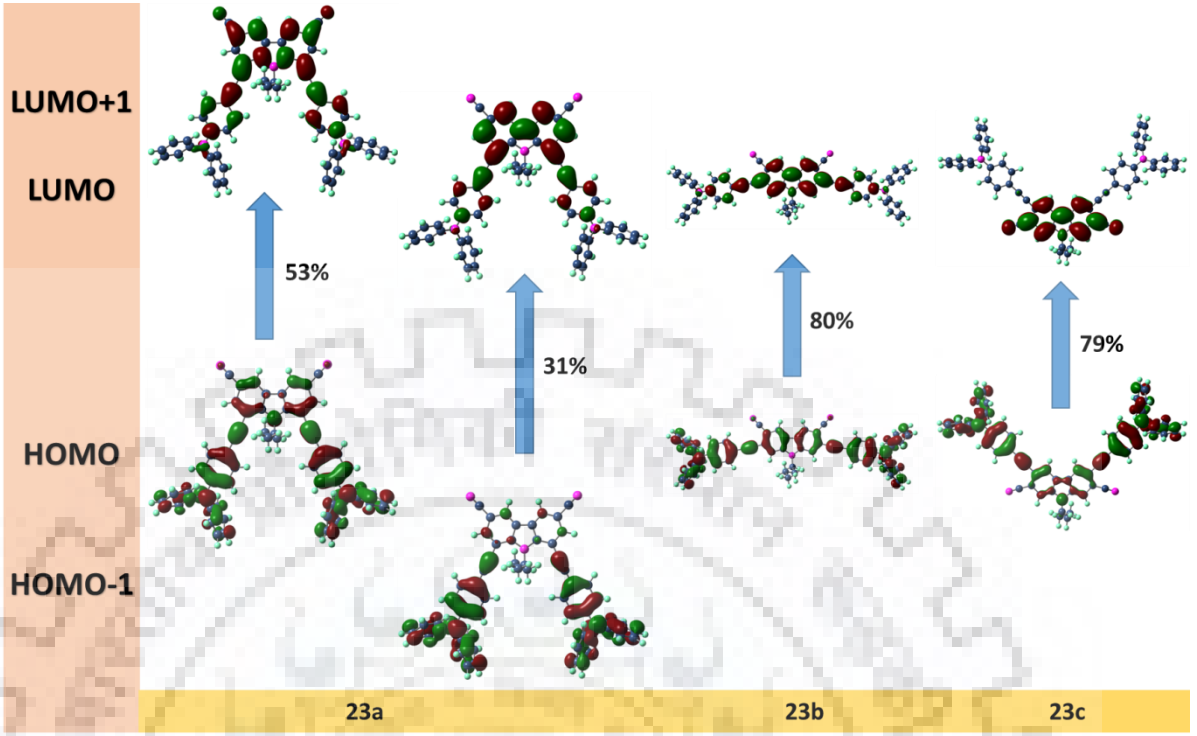

Figure 6.14 Frontier molecular orbitals of the dyes **23a-23c**.

Table 6.6 Predicted vertical excitation obtained by B3LYP/6-31G (d,p) method for the dyes

Dye	λ_{max} (nm)	*f*	Assignment
22a	266	0.3161	HOMO-2→LUMO (28%), HOMO-3→LUMO+1 (11%), HOMO-2→LUMO+3 (10%), HOMO-3→LUMO+2 (10%)
	268	0.1715	HOMO-2→LUMO+1 (18%), HOMO-3→LUMO (15%), HOMO-3→LUMO+2 (12%), HOMO-2→LUMO+3 (11%)
	274	0.2390	HOMO-5→LUMO (33%), HOMO→LUMO+4 (24%), HOMO-1→LUMO (16%), HOMO-6→LUMO (10%)
	293	0.2950	HOMO-1→LUMO+2 (15%), HOMO→LUMO+2 (15%), HOMO-1→LUMO+1 (14%), HOMO→LUMO+3 (13%), HOMO-1→LUMO+3 (11%)
	297	0.3503	HOMO-1→LUMO+1 (44%), HOMO-4→LUMO (10%)
	335	1.1000	HOMO→LUMO+1 (63%), HOMO-1→LUMO (23%)
	337	0.5988	HOMO→LUMO (80%)

Table 6.6 (cont.)

Dye	λ_{max} (nm)	*f*	Assignment
22b	265	0.4533	HOMO-4→LUMO+1 (36%), HOMO-5→LUMO (25%)
	275	0.2813	HOMO-2→LUMO (45%)
	286	0.1189	HOMO→LUMO+1 (44%), HOMO-4→LUMO (33%), HOMO-1→LUMO (15%)
	291	0.2566	HOMO-1→LUMO+1 (40%), HOMO→LUMO+4 (21%), HOMO-4→LUMO+1 (14%)
	371	2.9444	HOMO→LUMO (86%)
22c	272	0.2287	HOMO-3→LUMO (71%), HOMO-5→LUMO (10%)
	281	0.1108	HOMO-2→LUMO (40%), HOMO-4→LUMO (33%), HOMO→LUMO (10%)
	282	0.7387	HOMO-5→LUMO (40%), HOMO-6→LUMO (15%), HOMO-3→LUMO (10%), HOMO-1→LUMO+2 (10%)
	309	0.6219	HOMO-1→LUMO+1 (57%), HOMO→LUMO+2 (29%)
	326	1.3885	HOMO-1→LUMO (48%), HOMO→LUMO+1 (34%), HOMO-1→LUMO+2 (10%)
	349	0.8304	HOMO→LUMO+1 (46%), HOMO-1→LUMO (41%)
	380	0.1362	HOMO→LUMO (86%)
23a	268	0.2903	HOMO→LUMO+8 (47%), HOMO-1→LUMO+8 (38%)
	273	0.1068	HOMO-2→LUMO+1 (40%), HOMO-4→LUMO (23%)
	317	0.4871	HOMO-1→LUMO+1 (57%), HOMO-2→LUMO (20%)
	352	1.2440	HOMO→LUMO (75%)
	360	0.8664	HOMO→LUMO+1 (53%), HOMO-1→LUMO (31%)
23b	269	0.1066	HOMO→LUMO+6 (33%), HOMO-1→LUMO+7 (29%), HOMO-1→LUMO+6 (13%), HOMO→LUMO+7 (11%)
	270	0.1202	HOMO→LUMO+7 (25%), HOMO-1→LUMO+6 (20%), HOMO→LUMO+3 (17%), HOMO-1→LUMO+7 (11%)
	287	0.1606	HOMO-2→LUMO (59%), HOMO-1→LUMO+1 (15%), HOMO→LUMO (13%)
	298	0.1025	HOMO-3→LUMO (38%), HOMO→LUMO+1 (37%), HOMO-1→LUMO (14%)
	303	0.1441	HOMO-1→LUMO+1 (48%), HOMO-2→LUMO (18%), HOMO→LUMO+2 (12%), HOMO-3→LUMO+1 (10%)
	394	3.1392	HOMO→LUMO (80%)
23c	295	0.2984	HOMO-3→LUMO (35%), HOMO-2→LUMO+1 (21%), HOMO-1→LUMO+2 (18%), HOMO-4→LUMO (10%)
	335	0.9628	HOMO-1→LUMO+1 (58%), HOMO→LUMO+2 (31%)
	343	0.6902	HOMO-1→LUMO (66%), HOMO→LUMO+1 (17%)
	368	1.3018	HOMO→LUMO+1 (55%), HOMO-1→LUMO (24%), HOMO-1→LUMO+2 (11%)
	385	0.2148	HOMO→LUMO (79%), HOMO-2→LUMO (15%)

6.2.6 Electroluminescence Properties

To evaluate the electroluminescence performance of the dyes, the multilayered OLED devices were fabricated with the configuration of ITO/PEDOT:PSS/CBP:emitter (**22a-22c** and **23a-23c**)/TBPi/LiF/Al, where ITO (indium doped tin oxide) served as anode, PEDOT:PSS (polyethylenedioxythiophene/polystyrenesulfonate) as hole injecting layer, *N,N'*-dicarbazolyl-4,4'-biphenyl (CBP) as host material into which the dyes were doped, TBPi (1,3,5-tris(*N*-phenylbenzimidazol-2-yl)benzene) and LiF as electron transporting and electron injecting layer respectively, and Al as cathode. Initially, non-doped devices were fabricated by employing the dyes as emitting layer. All the non-doped devices displayed high current density but low luminance. It might be due to imbalanced charge transport and migration of charge carriers towards electrode interface before recombination takes place. Due to this charge leakage at interface/electrode, we observed high current density and low luminance value. Furthermore, the non-doped devices showed broad and red shifted electroluminescence spectrum as compared to their corresponding solution photoluminescence spectrum. It could be attributed to the formation of aggregates in solid state. The poor thin film stability of the emitter could have induced crystalline nature of the dyes and ends up with the failure of device [231,232]. However, the performance of non-doped device comprising **22c** is superior to the reported carbazole acetylene which does not have cyano group, in similar device architecture. It indicates the role of cyano group in improving the balanced transport of charge carriers [103].

Since the non-doped devices showed unsatisfactory electroluminescence performances due to the formation of aggregates in solid state and poor thin film quality, we fabricated doped devices to mitigate aggregation caused emission quenching and to improve the electroluminescence performances. The current density-voltage-luminance plots of the devices are presented in Figure 6.15. The electroluminescence spectra of the devices are shown in Figure 6.16 and the electroluminescence data compiled in Table 6.7. For the doped devices, we doped the emitters on CBP host at different concentrations. In the doped devices, the electroluminescence spectrum is narrow and blue shifted similar to the photoluminescence spectra recorded in toluene. It clearly indicates the suppression of aggregation of dye molecules in solid state due to dilution effect of fluorophores [164]. The absence of CBP emission at ca. 400 nm in electroluminescence spectrum suggests the origin of emission is solely from the emitters. However, the dye **22c** exhibited small hump around 400 nm. It might be due to the

CBP host emission which indicates the incomplete energy transfer from CBP host to the dopant. This is evident from the decreasing intensity of hump at higher concentration of dopant as the number of emitting molecules to capture excitons from CBP host increased. The doped devices exhibited high luminance compared to their analogous non-doped devices. It might be due to the effective capture of excitons formed in CBP host by dopants through favorable energy barrier. The power efficiency and current efficiency of the devices are progressively increased from **22a** to **22c**. It could be attributed to the decreasing energy barrier for electron injection owing to low-lying LUMO while HOMO is almost similar for all the dyes. The power and current efficiency of **22b** is about 2-3 fold increased as compared to its isomer **22a**. Despite of similar HOMO energy level, **22b** possessed low lying LUMO which facilitated easy injection of electrons into the emissive layer and thus balanced charge transport and effective capture of excitons realized. As a result, high luminance is observed. When the concentration of the dopants is increased, the electroluminescence performance is increased as a result of increasing number of emitting species. However, the electroluminescence performance dropped to some extent at higher concentration which could be due to the formation of aggregates. The best device performance is observed for the doped devices fabricated with 3 wt% of dopants. In non-doped devices, triphenylamine substituted dyes showed relatively low turn-on voltage when compared to their analogous carbazole dyes. It might be due to high lying HOMO of triphenylamine substituted dyes which facilitates the easy injection of hole charge carriers (Figure 6.17) [233,234]. As a result, triphenylamine substituted dyes showed better power efficiency, current efficiency and luminance over carbazole analogs. Similar results are observed for other doped devices also.

The color purity of the electroluminescence devices is attributed to small full width at half maxima values of the electroluminescence spectrum. The 2,7-substituted compounds (**22b** and **23b**) showed better electroluminescence performance when compared to their analogous isomers. It is ascribed to the favorable energy level alignment of dopant with host and neighboring charge transporting layers which ensure balanced charge transport and effective harvesting of excitons. The highest power and current efficiency and luminance are observed for **23c**. It is ascribed to low energy barrier for the injection of charge carriers and effective excitons harvesting from the host. The best electroluminescence performance is observed for the device fabricated with **23b** (3 wt%) with power efficiency of 5.3 lm/W, current efficiency of

6.7 cd/A, EQE of 4.0% and luminance of 4642 cd/m^2. The device containing **23b** gave the lowest turn-on voltage of 3.9 V which can be attributed to low energy barrier for charge injection.

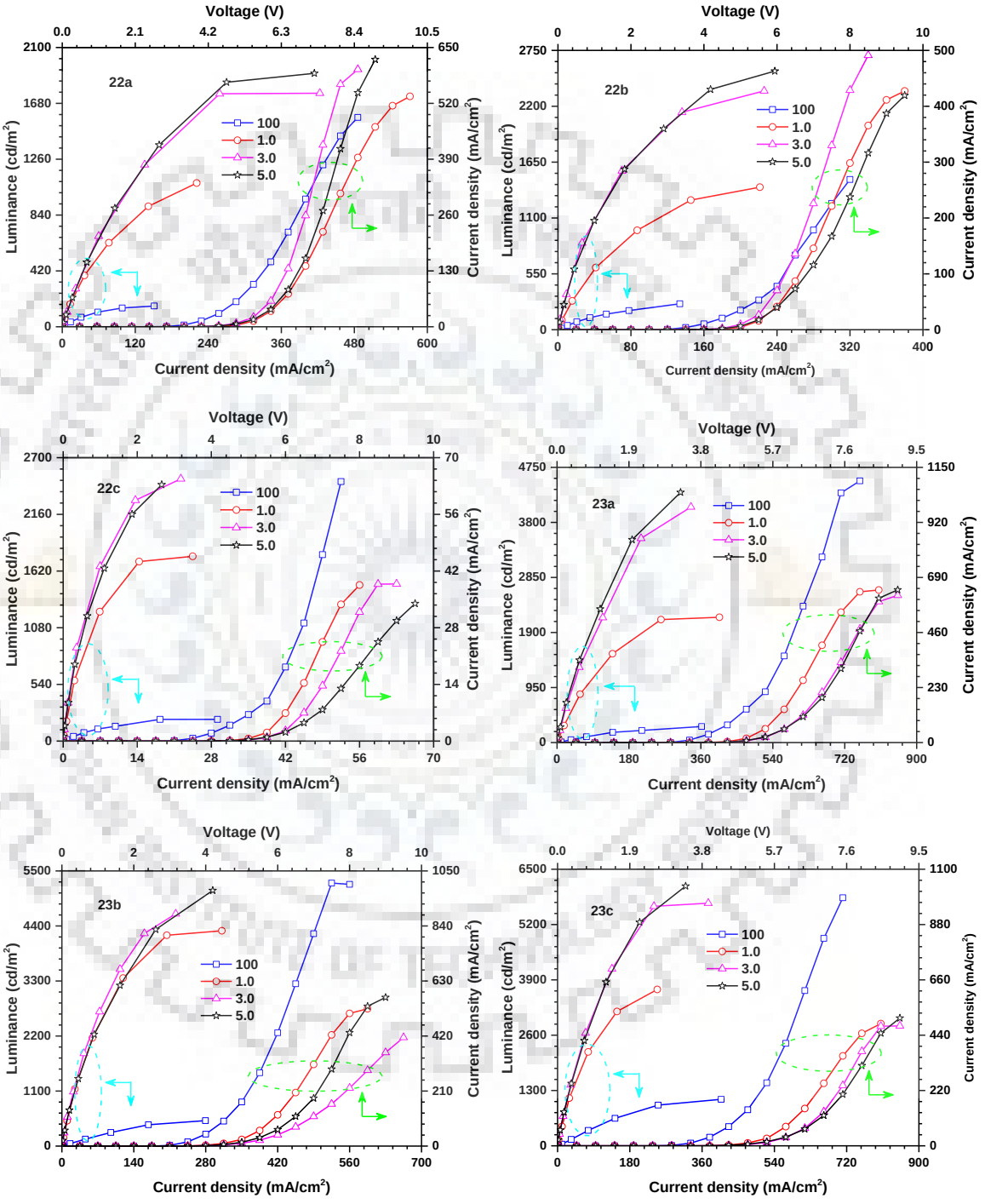

Figure 6.15 J-V-L characteristics of the electroluminescent devices fabricated with the dyes (**22a**-**22c** and **23a**-**23c**).

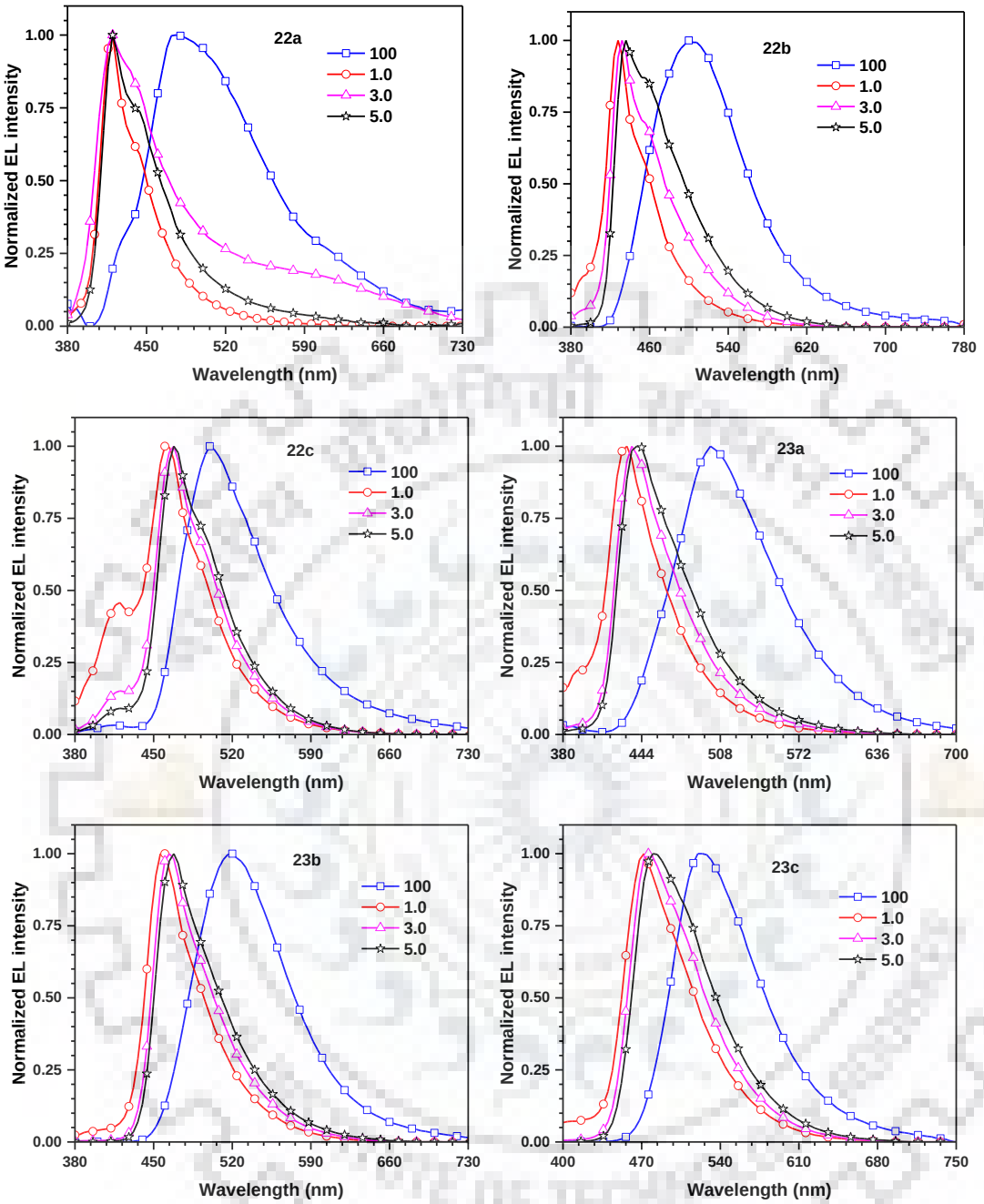

Figure 6.16 Electroluminescence spectra of the devices fabricated with the dyes (**22a**-**22c** and **23a**-**23c**).

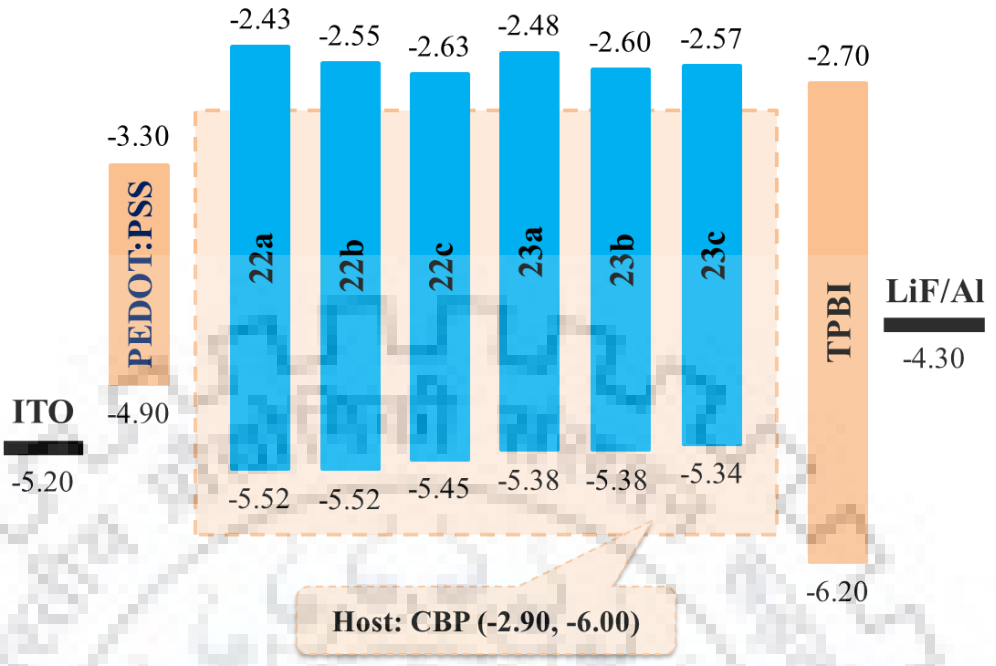

Figure 6.17 Energy level diagrams of the dyes (**22a-22c** and **23a-23c**) in OLED device (all values are in eV with reference to vacuum).

Table 6.7 Electroluminescent parameters of the dyes [a]

Dye	wt%	Turn-on voltage (V)	Power Efficiency (lm/w)	Current Efficiency (cd/A)	EQE (%)	CIE (x,y)	Maximum Luminance (cd/m^2)	λ_{EL} (nm)	FWHM (nm)
22a	100	4.9/ -	0.1/ -	0.2/ -	0.1/ -	(0.23, 0.33)/ -	156	476	111
	1	5.2/ 7.3	0.9/ 0.2	1.4/ 0.6	2.9/ 1.0	(0.16, 0.07)/ (0.17, 0.09)	1081	420	51
	3	4.9/ 6.3	0.9/ 0.5	1.4/ 1.0	2.4/ 1.6	(0.16, 0.07)/ (0.17, 0.09)	1756	420	67
	5	5.0/ 6.6	0.9/ 0.5	1.4/ 1.0	2.0/ 1.3	(0.16, 0.09)/ (0.17, 0.1)	1906	420	60
22b	100	4.8/ -	0.2/ -	0.4/ -	0.1/ -	(0.24, 0.41)/ -	256	500	104
	1	5.0/ 6.5	1.4/ 0.5	2.2/ 1.1	3.2/ 1.6	(0.16, 0.08)/ (0.17, 0.1)	1403	428	61
	3	4.5/ 5.6	3.0/ 1.7	4.3/ 3.0	4.1/ 3.1	(0.16, 0.12)/ (0.16, 0.12)	2351	432	70
	5	4.6/ 5.9	2.9/ 1.5	4.1/ 2.8	3.2/ 2.3	(0.16, 0.16)/ (0.16, 0.15)	2546	436	78
22c	100	4.8/ -	0.1/ -	0.2/ -	0.1/ -	(0.26, 0.49)/ -	207	500	85
	1	4.7/ 5.8	2.1/ 1.0	3.2/ 1.9	2.7/ 1.6	(0.15, 0.16)/ (0.16, 0.16)	1760	460	90
	3	4.9/ 6.1	2.9/ 1.6	4.6/ 3.0	2.8/ 2.0	(0.15, 0.23)/ (0.16, 0.21)	2498	468	68
	5	4.8/ 6.3	3.1/ 1.3	4.7/ 2.6	2.6/ 1.5	(0.16, 0.27)/ (0.16, 0.25)	2443	468	68
23a	100	4.5/ -	0.1/ -	0.1/ -	0.1/ -	(0.24, 0.45)/ -	277	500	96
	1	4.6/ 5.6	1.2/ 0.8	1.8/ 1.4	2.7/ 2.0	(0.16, 0.08)/ (0.16, 0.09)	2162	432	63
	3	4.7/ 5.8	2.0/ 1.4	3.0/ 2.5	3.2/ 2.8	(0.16, 0.10)/ (0.16, 0.11)	4065	436	60
	5	4.6/ 5.7	2.4/ 1.5	3.5/ 2.8	3.2/ 2.6	(0.16, 0.12)/ (0.16, 0.13)	4318	440	65
23b	100	3.8/ -	0.3/ -	0.3/ -	0.1/ -	(0.30, 0.55)/ -	509	520	93
	1	3.7/ 4.9	4.5/ 3.0	5.4/ 4.6	3.9/ 3.6	(0.15, 0.17)/ (0.15, 0.16)	4303	460	60
	3	3.9/ 5.4	5.3/ 2.9	6.7/ 4.9	4.0/ 3.2	(0.16, 0.22)/ (0.16, 0.21)	4642	464	62
	5	3.9/ 5.2	5.2/ 2.8	6.5/ 4.6	3.5/ 2.6	(0.16, 0.26)/ (0.16, 0.24)	5109	468	66
23c	100	3.8/ 5.7	0.3/ 0.2	0.4/ 0.3	0.1/ 0.1	(0.33, 0.58)/ (0.31, 0.57)	1092	524	88
	1	4.3/ 5.4	3.7/ 2.3	5.1/ 3.9	2.8/ 2.3	(0.17, 0.28)/ (0.16, 0.26)	3675	472	72
	3	4.5/ 5.7	4.6/ 2.6	6.6/ 4.8	2.9/ 2.3	(0.18, 0.35)/ (0.17, 0.32)	5702	476	73
	5	4.3/ 5.7	5.4/ 2.6	7.3/ 4.7	3.0/ 2.0	(0.19, 0.40)/ (0.18, 0.37)	6104	480	77

[a] values at 100/1000 cd/m^2.

6.3 Conclusions

In summary, we have designed and synthesized isomeric tetra-substituted carbazoles containing arylamine donors and cyano acceptors. The variations of optical, electrochemical and electroluminescence properties among the positional isomers are elaborated. Triphenylamine substituted compounds showed bathochromically shifted absorption and emission maxima as compared to their analogous carbazole congeners. The positive emission solvatochromism of the compounds is evaluated by Lippert-Mataga plots and DFT correlations. The superior thermal stability of triphenylamine substituted compounds (**23a**-**23c**) is ascribed to non-planar nature of triphenylamine moieties. The 1,8-arylamine substituted compounds showed wide band gap compared to other isomers which could be due to the steric congestion. The best electroluminescence device performance is observed for the device fabricated with the dyes **22b** which could be due to the favorable energy level alignment for effective harvesting of excitons In brief we have shown a method to modulate the functional properties of carbazole derivative by cyano substitution at different nuclear positions.

6.4 Experimental Section

6.4.1 General Methods and Characterization

Computational methods, OLED device fabrication and characterization are similar to the procedure described in chapter 3.

6.4.2 Synthesis

Synthesis of 9-butyl-1,8-bis((9-butyl-9*H*-carbazol-3-yl)ethynyl)-9*H*-carbazole-3,6-dicarbonitrile, 22a

A mixture of 9-butyl-1,8-diiodo-9*H*-carbazole-3,6-dicarbonitrile (0.55 g, 1.0 mmol), 9-butyl-3-ethynyl-9*H*-carbazole (0.52 g, 2.1 mmol), $Pd(PPh_3)_2Cl_2$ (14 mg, 0.02 mmol), PPh_3 (5.2 mg, 0.02 mmol), CuI (11.4 mg, 0.06 mmol) and triethylamine (30 mL) was refluxed for 12 h under nitrogen atmosphere. After completion of reaction, the reaction mixture was poured into water and extracted with chloroform. The organic layer was dried over anhydrous sodium sulphate. Finally, the solvent was removed under vacuum to yield a residue which was further purified by column chromatography using hexanes/chloroform (3:2) as eluant. Yellow solid. Yield 0.36 g (47%); mp 270-272 °C; IR (KBr, cm^{-1}) 2219 ($\nu_{C\equiv N}$); ^1H NMR ($CDCl_3$, 400 MHz) δ

8.32 (d, *J* = 1.6 Hz, 4 H), 8.09 (d, *J* = 7.6 Hz, 2 H), 8.01 (d, *J* = 1.6 Hz, 2 H), 7.67 (dd, *J* = 8.8 Hz, 1.2 Hz, 2 H), 7.53-7.49 (m, 2 H), 7.45-7.41 (m, 4 H), 7.28-7.24 (m, 2 H), 5.67 (t, *J* = 8.0 Hz, 2 H), 4.32 (t, *J* = 7.6 Hz, 4 H), 2.14-2.10 (m, 2 H), 1.91-1.85 (m, 4 H), 1.48-1.37 (m, 6 H), 0.96 (t, *J* = 7.6 Hz, 6 H), 0.90 (t, *J* = 7.6 Hz, 3 H); ^{13}C NMR ($CDCl_3$, 100.3 MHz) δ 140.79, 140.43, 135.78, 128.80, 126.40, 123.96, 123.83, 123.06, 122.93, 122.17, 120.43, 119.58, 118.93, 111.94, 109.03, 108.61, 103.82, 97.29, 82.99, 45.31, 42.98, 34.38, 31.05, 20.51, 19.91, 14.19, 13.83; HRMS calcd for $C_{54}H_{45}N_5$ (*m/z*+1) 764.3748, found 764.3774.

Synthesis of 9-butyl-2,7-bis((9-butyl-9*H*-carbazol-3-yl)ethynyl)-9*H*-carbazole-3,6-dicarbonitrile, 22b

It was prepared from a mixture of 2,7-dibromo-9-butyl-9*H*-carbazole-3,6-dicarbonitrile (0.37 g, 0.7 mmol), 9-butyl-3-ethynyl-9*H*-carbazole (0.38 g, 1.5 mmol), $Pd(PPh_3)_2Cl_2$ (10 mg, 0.01 mmol), PPh_3 (3.7 mg, 0.01 mmol), CuI (8.2 mg, 0.04 mmol) and triethylamine (30 mL) by following the procedure described for **22a**. Yellow solid. Yield 0.27 g (51%); mp 292-294 °C; IR (KBr, cm^{-1}) 2223 ($\nu_{C\equiv N}$); ^{1}H NMR ($CDCl_3$, 400 MHz) δ 8.33 (s, 2 H), 8.27 (s, 2 H), 8.12 (d, *J* = 7.6 Hz, 2 H), 7.72 (d, *J* = 8.0 Hz, 2 H), 7.58 (s, 2 H), 7.54-7.50 (m, 2 H), 7.44-7-7.36 (m, 4 H), 7.31-7.28 (m, 2 H), 4.31 (t, *J* = 7.6 Hz, 6 H), 1.94-1.83 (m, 6 H), 1.50-1.39 (m, 6 H), 1.03 (t, *J* = 7.6 Hz, 3 H), 0.96 (t, *J* = 7.6 Hz, 6 H); ^{13}C NMR ($CDCl_3$, 100.3 MHz) δ 142.51, 140.67, 140.24, 129.25, 126.28, 125.26, 125.07, 124.08, 122.59, 122.11, 120.53, 120.30, 119.52, 118.85, 111.94, 111.71, 109.16, 108.52, 106.10, 97.48, 85.31, 42.88, 30.99, 20.46, 13.79; HRMS calcd for $C_{54}H_{45}N_5$ (*m/z*+1) 764.3748, found 764.3733.

Synthesis of 9-butyl-3,6-bis((9-butyl-9*H*-carbazol-3-yl)ethynyl)-9*H*-carbazole-2,7-dicarbonitrile, 22c

It was prepared from a mixture of 9-butyl-3,6-diiodo-9*H*-carbazole-2,7-dicarbonitrile (0.37 g, 0.7 mmol), 9-butyl-3-ethynyl-9*H*-carbazole (0.38 g, 1.5 mmol), $Pd(PPh_3)_2Cl_2$ (10 mg, 0.01 mmol), PPh_3 (3.7 mg, 0.01 mmol), CuI (8.2 mg, 0.04 mmol) and triethylamine (30 mL) by following the procedure described for **22a**. Yellow solid. Yield 0.28 g (53%); mp 280-282 °C; IR (KBr, cm^{-1}) 2223 ($\nu_{C\equiv N}$); ^{1}H NMR ($CDCl_3$, 400 MHz) δ 8.36-8.34 (m, 4 H), 8.12 (d, *J* = 8.0 Hz, 2 H), 7.76-7.72 (m, 4 H), 7.52-7.48 (m, 2 H), 7.44-7.39 (m, 4 H), 7.29 (d, *J* = 8.0 Hz, 2 H), 4.34-4.28 (m, 6 H), 1.91-1.84 (m, 6 H), 1.45-1.39 (m, 6 H), 1.02-0.95 (m, 9 H); ^{13}C NMR ($CDCl_3$, 100.3 MHz) δ 140.80, 140.39, 139.50, 129.45, 126.18, 124.72, 124.20, 112.84, 122.39,

120.60, 119.44, 118.70, 118.48, 114.08, 113.28, 112.28, 108.98, 108.83, 95.87, 84.55, 43.71, 42.99, 31.08, 29.68, 22.68, 20.54, 13.85, 13.75; HRMS calcd for $C_{54}H_{45}N_5$ (*m/z*+1) 764.3748, found 764.3715.

Synthesis of 9-butyl-1,8-bis((4-(diphenylamino)phenyl)ethynyl)-9*H*-carbazole-3,6-dicarbonitrile, 23a

It was prepared from a mixture of 9-butyl-1,8-diiodo-9*H*-carbazole-3,6-dicarbonitrile (0.37 g, 0.7 mmol), 4-ethynyl-*N*,*N*-diphenylaniline (0.41 g, 1.5 mmol), $Pd(PPh_3)_2Cl_2$ (10 mg, 0.014 mmol), PPh_3 (3.7 mg, 0.014 mmol), CuI (8.2 mg, 0.04 mmol) and triethylamine (30 mL) by following the procedure described for **22a**. Yellow solid. Yield 0.29 g (51%); mp 138-140 °C; IR (KBr, cm^{-1}) 2219 ($\nu_{C\equiv N}$); ^{1}H NMR ($CDCl_3$, 400 MHz) δ 8.31 (d, *J* = 2.0 Hz, 2 H), 7.93 (d, *J* = 1.2 Hz, 2 H), 7.39 (d, *J* = 8.4 Hz, 4 H), 7.32-7.29 (m, 6 H), 7.15-7.08 (m, 14 H), 7.03 (d, *J* = 9.2 Hz, 4 H), 5.54 (t, *J* = 8.0 Hz, 2 H), 1.99-1.96 (m, 2 H), 1.43-1.34 (m, 2 H), 0.85 (t, *J* = 7.6 Hz, 3 H); ^{13}C NMR ($CDCl_3$, 100.3 MHz) δ 148.81, 146.83, 140.87, 135.89, 132.32, 129.51, 125.36, 124.20, 124.03, 123.16, 121.59, 118.78, 114.21, 108.44, 104.01, 96.23, 83.82, 45.16, 34.15, 19.76, 14.10; HRMS calcd for $C_{58}H_{41}N_5$ (*m/z*+Na) 830.3254, found 830.3252.

Synthesis of 9-butyl-2,7-bis((4-(diphenylamino)phenyl)ethynyl)-9H-carbazole-3,6-dicarbonitrile, 23b

It was prepared from a mixture of 2,7-dibromo-9-butyl-9*H*-carbazole-3,6-dicarbonitrile (0.37 g, 0.7 mmol), 4-ethynyl-*N*,*N*-diphenylaniline (0.41 g, 1.5 mmol), $Pd(PPh_3)_2Cl_2$ (10 mg, 0.014 mmol), PPh_3 (3.7 mg, 0.014 mmol), CuI (8.2 mg, 0.04 mmol) and triethylamine (30 mL) by following the procedure described for **22a**. Yellow solid. Yield 0.32 g (56%); mp 318-320 °C; IR (KBr, cm^{-1}) 2222 ($\nu_{C\equiv N}$); ^{1}H NMR ($CDCl_3$, 400 MHz) δ 8.34 (s, 2 H), 7.60 (s, 2 H), 7.49 (d, *J* = 8.4 Hz, 4 H), 7.32-7.28 (m, 8 H), 7.15-7.07 (m, 12 H), 7.02 (d, *J* = 9.2 Hz, 4 H), 4.32 (t, *J* = 7.6 Hz, 2 H), 1.93-1.85 (m, 2 H), 1.48-1.39 (m, 2 H), 0.99 (t, *J* = 7.6 Hz, 3 H); ^{13}C NMR ($CDCl_3$, 100.3 MHz) δ 148.83, 146.91, 142.87, 133.02, 129.46, 125.92, 125.32, 123.92, 121.68, 121.05, 118.44, 114.25, 112.42, 112.37, 106.92, 96.87, 86.01, 43.65, 30.91, 20.51, 13.79; HRMS calcd for $C_{58}H_{41}N_5$ (*m/z*+Na) 830.3254, found 830.3260.

Synthesis of 9-butyl-3,6-bis((4-(diphenylamino)phenyl)ethynyl)-9*H*-carbazole-2,7-dicarbonitrile, 23c

It was prepared from a mixture of 9-butyl-3,6-diiodo-9*H*-carbazole-2,7-dicarbonitrile (0.37 g, 0.7 mmol), 4-ethynyl-*N*,*N*-diphenylaniline (0.41 g, 1.5 mmol), $Pd(PPh_3)_2Cl_2$ (10 mg, 0.014 mmol), PPh_3 (3.7 mg, 0.014 mmol), CuI (8.2 mg, 0.04 mmol) and triethylamine (30 mL) by following the procedure described for **22a**. Yellow solid. Yield 0.30 g (53%); mp 228-230 °C; IR (KBr, cm^{-1}) 2223 ($\nu_{C\equiv N}$); ^1H NMR ($CDCl_3$, 400 MHz) δ 8.31 (s, 2 H), 7.75 (s, 2 H), 7.48 (d, J = 9.2 Hz, 4 H), 7.31-7.27 (m, 8 H), 7.14-7.12 (m, 8 H), 7.10-7.02 (m, 8 H), 4.33 (t, J = 7.6 Hz, 2 H), 1.91-1.84 (m, 2 H), 1.46-1.37 (m, 2 H), 0.99 (t, J = 7.2 Hz, 3 H); ^{13}C NMR ($CDCl_3$, 100.3 MHz) δ 148.47, 147.00, 139.59, 132.78, 129.43, 125.18, 125.09, 124.83, 124.61, 123.76, 121.97, 121.89, 118.45, 118.20, 114.83, 114.19, 113.46, 94.71, 85.33, 43.80, 31.01, 20.52, 13.73; HRMS calcd for $C_{58}H_{41}N_5$ (*m/z*+Na) 830.3254, found 830.3258.

Synthesis of 9-butyl-9*H*-carbazole-3,6-dicarbonitrile, 20a

A mixture of 3,6-dibromo-9-butyl-9*H*-carbazole (4.0 g, 10.5 mmol), copper cyanide (4.7 g, 52.5 mmol) and DMF (30 mL) was refluxed under nitrogen atmosphere. After 24 h, the reaction mixture was poured into water and extracted with chloroform. The organic layer was dried over anhydrous sodium sulphate. Finally, the solvent was removed under vacuum to yield a residue which was further purified by column chromatography using hexane/chloroform (3:2) as eluant. Colorless solid. Yield 2.1 g (72%); mp 220-222 °C; IR (KBr, cm^{-1}) 2223 ($\nu_{C\equiv N}$); ^1H NMR ($CDCl_3$, 400 MHz) δ 8.41 (d, J = 1.2 Hz, 2 H), 7.79 (dd, J = 8.4 Hz, 1.6 Hz, 2 H), 7.52 (d, J = 8.4 Hz, 2 H), 4.37 (t, J = 7.6 Hz, 2 H), 1.91-1.83 (m, 2 H), 1.45-1.35 (m, 2 H), 0.97 (t, J = 7.6 Hz, 3 H); ^{13}C NMR ($CDCl_3$, 100.3 MHz) δ 142.63, 130.17, 125.59, 122.00, 119.72, 110.16, 103.29, 43.46, 30.85, 20.37, 13.69; HRMS calcd for $C_{18}H_{15}N_3$ (*m/z*+Na) 296.1158, found 296.1162.

Synthesis of 2,7-dibromo-9-butyl-3,6-diiodo-9*H*-carbazole, 20b

A mixture of 2,7-dibromo-9-butyl-9*H*-carbazole (2.0 g, 5.2 mmol), potassium iodide (2.4 g, 14.6 mmol), potassium iodate (1.6 g, 6.4 mmol) and 50 mL of acetic acid was heated at 80 °C. After 8 h, the reaction mixture was cooled room temperature and quenched by addition of water. The obtained solid is filtered and dried. Off-white powder. Yield 3.0 g (91%); mp 190-192 °C; IR (KBr, cm^{-1}) 2223 ($\nu_{C\equiv N}$); ^1H NMR ($CDCl_3$, 400 MHz) δ 8.45 (s, 2 H), 7.68 (s, 2 H),

4.15 (t, *J* = 7.6 Hz, 2 H), 1.83-1.76 (m, 2 H), 1.41-1.31 (m, 2 H), 0.95 (t, *J* = 7.6 Hz, 3 H); ^{13}C NMR ($CDCl_3$, 100.3 MHz) δ 141.10, 131.46, 126.74, 122.30, 113.04, 88.86, 43.32, 30.76, 20.44, 13.78; HRMS calcd for $C_{16}H_{13}Br_2I_2N$ *m/z* 630.7499, found 630.7493.

Synthesis of 9-butyl-9*H*-carbazole-2,7-dicarbonitrile, 20c

It was prepared from a mixture of 2,7-dibromo-9-butyl-9*H*-carbazole (4.0 g, 10.5 mmol), copper cyanide (4.7 g, 52.5 mmol) and DMF (30 mL) by following the procedure described for **20a**. Colorless solid. Yield 2.0 g (69%); mp 216-218 °C; IR (KBr, cm^{-1}) 2222 ($\nu_{C\equiv N}$); ^{1}H NMR ($CDCl_3$, 400 MHz) δ 8.20 (d, *J* = 8.8 Hz, 2 H), 7.78 (s, 2 H), 7.54 (d, *J* = 8.0 Hz, 2 H), 4.35 (t, *J* = 7.6 Hz, 2 H), 1.91-1.83 (m, 2 H), 1.46-1.36 (m, 2H), 0.98 (t, *J* = 8.0 Hz, 3 H); ^{13}C NMR ($CDCl_3$, 100.3 MHz) δ 140.39, 124.99, 122.80, 121.99, 119.55, 113.61, 110.15, 43.52, 30.97, 20.51, 13.74; HRMS calcd for $C_{18}H_{15}N_3$ (*m/z*+1) 274.1339, found 274.1351.

Synthesis of 2,7-dibromo-9-butyl-9*H*-carbazole-3,6-dicarbonitrile, 21b

It was prepared from a mixture of 2,7-dibromo-9-butyl-3,6-diiodo-9*H*-carbazole (2.0 g, 3.2 mmol), copper cyanide (0.57 g, 6.4 mmol) and DMF (30 mL) by following the procedure described for **2a**. Colorless powder. Yield 0.6 g (43%). mp 216-218 °C; IR (KBr, cm^{-1}) 2222 ($\nu_{C\equiv N}$); ^{1}H NMR ($CDCl_3$, 400 MHz) δ 8.36 (s, 2 H), 7.73 (s, 2 H), 4.28 (t, *J* = 7.6 Hz, 2 H), 1.90-1.82 (m, 2 H), 1.44-1.38 (m, 2 H), 0.99 (t, *J* = 7.6 Hz, 3 H); ^{13}C NMR ($CDCl_3$, 100.3 MHz) δ 127.06, 125.75, 123.14, 120.78, 117.82, 114.22, 113.94, 43.90, 30.78, 20.44, 13.71; HRMS calcd for $C_{18}H_{13}Br_2N_3$ (*m/z*+1) 429.9549, found 429.9560.

Synthesis of 9-butyl-3,6-diiodo-9*H*-carbazole-2,7-dicarbonitrile, 21c

A mixture of 9-butyl-9H-carbazole-2,7-dicarbonitrile (0.5 g, 1.8 mmol), iodine (1.0 g, 4.0 mmol), potassium iodate (0.39 g, 1.8 mmol) and 20% sulfuric acid/acetic acid (3:30 mL) was heated to 110 °C. After 24 h, the reaction mixture was cooled to room temperature and the obtained solid was filtered and dried. Pale green powder. Yield 0.85 g (89%); mp 180-182 °C; IR (KBr, cm^{-1}) 2223 ($\nu_{C\equiv N}$); ^{1}H NMR ($CDCl_3$, 400 MHz) δ 8.58 (s, 2 H), 7.77 (s, 2 H), 4.30 (t, *J* = 7.2 Hz, 2 H), 1.88-1.80 (m, 2 H), 1.42-1.33 (m, 2 H), 0.97 (t, *J* = 7.6 Hz, 3 H); ^{13}C NMR ($CDCl_3$, 100.3 MHz) δ 139.84, 132.19, 125.45, 119.79, 117.78, 115.89, 85.21, 43.83, 30.93, 20.51, 13.71; HRMS calcd for $C_{18}H_{13}I_2N_3$ (*m/z*+Na) 547.9091, found 547.9096.

CHAPTER 7

Conclusions and Outlook

In summary, we have designed and developed a new class of carbazole-based organic materials containing electron withdrawing cyano group and different electron rich chromophores such as phenyl, fluorene, carbazole, triphenylamine and pyrene. The material properties of the dyes are optimized by inserting spacer units such as acetylene and vinyl. The absorption and emission maxima of the compounds are highly dependent on the nature of chromophoric substituent and the spacer units. The optical properties of the dyes are correlated by performing density functional theory calculations. The HOMO and LUMO energy level of the dyes are fine-tuned by the introduction of spacer units between cyanocarbazole and other chromophores. Both asymmetric and symmetrically functionalized carbazole-based materials are developed. All the dyes are used as fluorescent emitting dopant in OLED devices. We observed that 2,7-functionalization of carbazole mitigate the donor-acceptor interaction and enhanced the electroluminescence performances substantially when compared to their analogous known compounds which do not have cyano end capping. The electroluminescence performances of the dyes are influenced by the number of cyanocarbazole present on the molecules. The structure-property relationships of the compounds are established by correlating their optical, electrochemical, thermal and electroluminescence characteristics.

Chapter 3

- Asymmetrically 2,7-disubstiuted carbazoles containing cyano group at one end and different chromophores at another side either directly or via acetylene or vinyl linker have been synthesized.
- The absorption spectra of the dyes are highly dependent on the electron donating nature of substituent and the π linker.
- Triphenylamine substituted dyes gave red shifted absorption and emission maxima in each set of compounds. The insertion of vinyl linker lead to red shifted absorption and emission maxima when compared to their analogous acetylene and directly connected dyes.
- Carbazole and triphenylamine substituted dyes showed positive emission solvatochromism attributed to charge migration from donor (carbazole/triphenylamine) to cyanocarbazole acceptor.
- The highest structural reorganization of directly connected compounds at excited state resulted in large Stokes shifts.

- Low lying LUMO of acetylene derivatives is attributed to electron withdrawing nature of acetylene linker.
- Carbazole and triphenylamine substituted dyes showed high thermal decomposition temperatures. Acetylene derivatives gave superior thermal stability due to its rigid linkage mode.
- The best electroluminescence performance is observed for the device fabricated with **4d** (3 wt%) exhibiting the power efficiency 1.3 lm/w, current efficiency 2.0 cd/A, EQE of 4.1% and luminance of 1758 cd/m^2.

Chapter 4

- Cyanocarbazole end capped fluorene/carbazole trimers either directly or via acetylene or vinyl linker have been synthesized.
- 2,7-carbazole substituted dyes showed drastic change in photophysical and electroluminescence properties when compared to their 3,6-substituted analogs.
- Linearly substituted compounds (2,7-fluorene and 2,7-carbazole) exhibited red shifted absorption maxima and high molar extinction coefficient attributed to the elongation of conjugation along the linear axis.
- Despite of blue shifted absorption maxima, directly connected derivatives gave large Stokes shift which is attributed to the involvement of large structural reorganization at excited state.
- Intramolecular charge transfer from carbazole donor to cyanocarbazole acceptor induced positive solvatochromism in emission spectra for 3,6-substituted carbazoles.
- The Lippert-Mataga plot for 3,6-carbazole derivatives indicates the presence of two excited state (local and charge transfer) for **10b** and **12b** (direct and acetylene derivatives) while for **14c** (vinyl derivative) single (charge transfer) excited state.
- The rigid and rod-like structure of linear compounds containing acetylene linker gave high thermal stability over rest of the dyes.
- The dyes (2,7-fluorene and 3,6-carbazole) showed superior electroluminescence performance compared to their analogous asymmetrically substituted dyes containing only one cyanocarbazole unit (Chapter 3).

- The best device performance is realized for the device containing the emitter **14b** (3 wt%) with power efficiency 6.2 lm/W, current efficiency 8.5 cd/A, EQE of 4.6% and maximum luminance of 9314 cd/m^2.

Chapter 5

- Cyanocarbazole decorated pyrenes with different cyanocarbazole density have been designed and synthesized.
- 1,6-isomer showed blue shifted absorption maxima while 1,8-isomer gave red shifted absorption maxima when compared to mono-substituted dye. It is ascribed to different stacking interaction of molecules arising from two different electronic coupling of transition dipoles.
- The rigid nature of the molecular frame suppressed the structural perturbation at excited state and thus solvent independent emission is observed for all the dyes.
- The color of the electroluminescence emission is tuned from deep blue to green.
- The power efficiency and current efficiency of the emitters increased linearly as the number of cyanocarbazole units increased on pyrene core. It clearly demonstrates the role of cyanocarbazole for realizing balanced charge transport and effective harvesting of excitons.
- Tetra-substituted pyrene containing four cyanocarbazole **18e** (1 wt%) exhibited green emission with better electroluminescence performance with current efficiency of 9.2 cd/A, power efficiency of 5.8 lm/W, EQE of 3.4% and maximum luminance of 3788 cd/m^2

Chapter 6

- Arylamine substituted isomeric cyanocarbazoles have been designed, synthesized and characterized.
- Triphenylamine substituted compounds exhibited red shifted absorption and emission maxima when compared to their analogous carbazole derivatives.
- The negative absorption solvatochromism of 2,7-arylamine substituted dyes is attributed to large dipole moment of the dyes at ground state.
- Non-planar nature of triphenylamine dyes led to high thermal decomposition temperature as compared to rigid and planar carbazole.

- Despite of similar HOMO energy level of 1,8 and 2,7-arylamine substituted dyes, the former dyes showed wide band gap owing to steric hindrance induced inhibition of conjugation extention into 1,8-substituents.
- The high lying HOMO energy level of triphenylamine dyes facilitated facile charge injection due to the favorable alignment with neighboring charge transporting layers and eventually gave low turn-on voltage in non-doped devices.
- The best device performance is observed for the OLED device fabricated with **23b** (3 wt%) exhibiting power efficiency of 5.3 lm/W, current efficiency of 6.7 cd/A, EQE of 4.0% and maximum luminance of 4642 cd/m^2.

Future Prospects

From our reports, it is clear that cyanocarbazole moiety exhibit electron deficient nature. The tethering of donor-acceptor chromophores having high degree of dihedral angle would lead to low ΔE_{ST} and thus the molecules may exhibit TADF or HLCT characteristics. Also, carbazole-based HLCT emitters are ill reported in the literature. We propoe the isomeric cyanocarbazoles connected to phenanthroimidazole through phenyl linker (Chart 7.1). The structure-property relationships of the materials can be modulated by varying the position of linker.

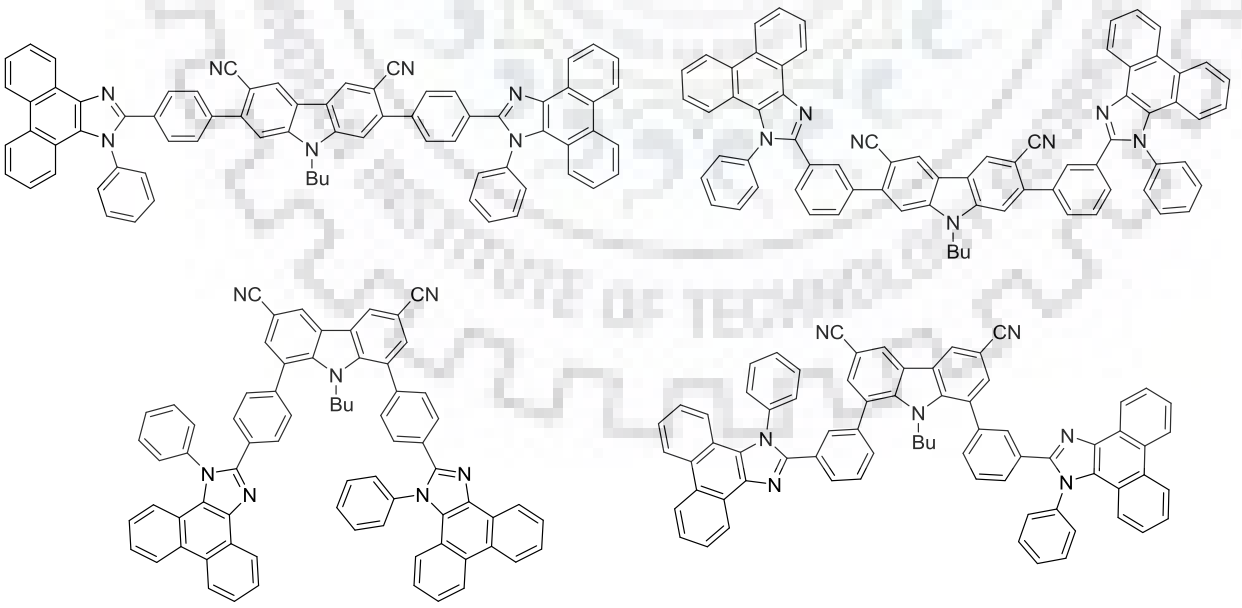

Chart 7.1 Isomeric cyanocarbazoles as TADF/HLCT emitters.

References

1. Sumpter, W. G. and Miller, F. M. *The Chemistry of Heterocyclic Compounds*, John Wiley and Sons, Inc: NJ, USA, 2008, Vol. 8, pp 70-109.
2. Campbell, N. and Barclay, B. M. "Recent advances in the chemistry of carbazole" *Chem. Rev*. **1947**, *40*, 359-380.
3. Wang, H.-Y.; Liu, F.; Xie, L.-H.; Tang, C.; Peng, B.; Huang, W.; Wei, W. "Topological arrangement of fluorenyl-substituted carbazole triads and starbursts: Synthesis and optoelectronic properties" *J. Phys. Chem. C*. **2011**, *115*, 6961-6967.
4. Gong, W.-L.; Zhong, F.; Aldred, M. P.; Fu, Q.; Chen, T.; Huang, D.-K.; Shen, Y.; Qiao, X.-F.; Ma, D.; Zhu, M.-Q. "Carbazole oligomers revisited: new additions at the carbazole 1- and 8-positons" *RSC Adv.* **2012**, *2*, 10821-10828.
5. Kochapradist, P.; Prachumrak, N.; Tarsang, R.; Keawin, T.; Jungsuttiwong, S.; Sudyoadsuk, T.; Promarak, V. "Multi-triphenylamine-substituted carbazoles: Synthesis characterization, properties, and applications as hole-transporting materials" *Tetrahedron Lett.* **2013**, *54*, 3683-3687.
6. Bluoin, N.; Leclerc, M. "Poly(2,7-carbazole)s: Structure-property relationships" *Acc. Chem. Res.* **2008**, *41*, 1110-1119.
7. Holmes, R. J.; D'Andrade, B. W.; Forrest, S. R. "Efficient, deep blue electrophosphorescence by guest charge trapping" *Appl. Phys. Lett.* **2003**, *83*, 3818-3820.
8. Moonsin, P.; Prachumrak, N.; Rattanawan, R.; Keawin, T.; Jungsuttiwong, S.; Sudyoadsuk, T.; Promarak, V. "Carbazole dendronised triphenylamines as solution processed high T_g amorphous hole-transporting materials for organic electroluminescent devices" *Chem. Commun.* **2012**, *48*, 3382-3384.
9. Gong, W.-L; Wang, B.; Aldred, M. P.; Li, C.; Zhang, G.-F.; Chen, T.; Wang, L.; Zhu, M.-Q. "Tetraphenylethene-decorated carbazoles: synthesis, aggregation-induced emission, photo-oxidation and electroluminescence" *J. Mater. Chem. C.* **2014**, *2*, 7001-7012.
10. Gantenbein, M.; Hellstern, M.; Pleux, L. L.; Neuburger, M.; Mayor, M. "New 4,4′-bis(9-carbazolyl)-biphenyl derivatives with locked carbazole-biphenyl junctions: High-triplet state energy materials" *Chem. Mater.* **2015**, *27*, 1772-1779.

11. Tsai, M.-H.; Lin, H.-W.; Su, H.-C.; Ke, T.-H.; Wu, C.; Fang, F.-C.; Liao, Y.-L.; Wong, K.-T.; Wu, C.-I. "Highly efficient organic blue electrophosphorescent devices based on 3,6-bis(triphenylsilyl)carbazole as the host material" *Adv. Mater.* **2006**, *18*, 1216-1220.
12. Vacareanu, L.; Grigoras, M. "Electrochemical characterization of arylene vinylene oligomers containing triphenylamine and carbazole units" *J. Appl. Electrochem.* **2010**, *40*, 1967-1975.
13. Pansay, S.; Prachumrak, N.; Jungsuttiwong, S.; Keawin, T.; Sudyoadsuk, T.; Promarak, V. "Multibromo-N-alkylcarbazoles: synthesis, characterization, and their benzo[b]thiophene derivatives" *Tetrahedron Lett.* **2012**, *53*, 4568-4572.
14. Dierschke, F.; Grimsdale, F. C.; Mullen, K. "Efficient synthesis of 2,7-dibomocarbazoles as components for electroactive materials" *Synthesis* **2003**, *16*, 2470-2472.
15. Kim, M.; Lee, J. Y. "Synthesis of 2- and 4-substituted carbazole derivatives and correlation of substitution position with photophysical properties and device performances of host materials" *Org. Electron.* **2013**, *14*, 67-73.
16. Kim, M.; Lee, J. Y. "Engineering the substitution position of diphenylphosphine oxide at carbazole for thermal stability and high external quantum efficiency above 30% in blue phosphorescent organic light-emitting diodes" *Adv. Funct. Mater.* **2014**, **24**, 4164-4169.
17. Kumar, S.; Tao, Y.-T. "Synthesis of Polyarylated Carbazoles: Discovery toward Soluble Phenanthro- and Tetraceno-Fused Carbazole Derivatives" *J. Org. Chem.* **2015**, *80*, 5066-5076.
18. Konidena, R. K.; Thomas, K. R. J.; Sahoo, S.; Dubey, D. K.; Jou, J.-H. "Multi-substituted deep-blue emitting carbazoles: Comparative study on photophysical and electroluminescence characteristics" *J. Mater. Chem. C.* **2017**, *5*, 709-726.
19. Niu, F.; Niu, H.; Liu, Y.; Lian, J.; Zeng, P. "Synthesis, characterization and application of starburst 9-alkyl-1,3,6,8- tetraaryl-carbazole derivatives for blue-violet to UV OLEDs" *RSC Adv.* **2011**, *1*, 415-423.
20. Romero-Ale, E. E.; Olives, A. I.; Martín, M. A.; del Castillo, B.; Lopez-Alvarado, P.; Menendez, J. C. "Environmental effects on the fluorescence behaviour of carbazole derivatization reagents" *Luminescence* **2005**, *20*, 162-169.

21. Thomas, K. R. J.; Lin, J. T.; Tao, Y.-T.; Ko, C.-W. "Light-emitting carbazole derivatives: Potential electroluminescent materials" *J. Am. Chem. Soc.* **2001**, *123*, 9404-9411.

22. Kumar, S.; An, C.-C.; Sahoo, S.; Griniene, R.; Volyniuk, D.; Grazulevicius, J. V.; Grigalevicius, S.; Jou, J.-H. "Solution-processable naphthalene and phenyl substituted carbazole core based hole transporting materials for efficient organic light-emitting diodes" *J. Mater. Chem. C.* **2017**, *5*, 9854-9864.

23. Chang, C.-H.; Krucaite, G.; Lo, D.; Chen, Y.-L.; Su, C.-C.; Lin, T.-C.; Grazulevicius, J. V.; Peciulyte, L.; Grigalevicius, S. "Naphthyl or pyrenyl substituted 2-phenylcarbazoles as hole transporting materials for organic light-emitting diodes" *Dyes Pigm.* **2017**, *136*, 302-311.

24. Jou, J.-H.; Li, T.-H.; Kumar, S.; An, C.-C.; Agrawal, A.; Chen, S. Z.; Fang, P.-H.; Krucaite, G.; Grigalevicius, S.; Grazulevicius, J.; Sung, C.-F. "Enabling high-efficiency organic light-emitting diodes with a cross-linkable electron confining hole transporting material" *Org. Electron.* **2015**, *24*, 254-262.

25. Chen, S.; Jiang, S.; Yu, H. "Diphenylamino-substituted bicarbazole derivative: Hole-transporting material with high glass-transition temperature, good electron and triplet exciton blocking capabilities and efficient hole injection" *Chem. Phys. Lett.* **2017**, *674*, 109-114.

26. Fan, J. G.; Kim, M. J.; Nguyen, Q. P. B.; Braveenth, R.; Ko, H. M.; Han, J.-H.; Kim, G. W.; Kwon, J. H.; Chai, K. Y. "Synthesis and characterization of carbazole core-based small molecular-hole-transporting materials for red phosphorescent OLEDs" *Bull. Korean Chem. Soc.* 2016, *37*, 1710-1716.

27. Braveenth, R.; Bae, H. W.; Ko, I. J.; Qiong, W.; Nguyena, Q. P. B.; Jayashantha, P. G. S.; Kwon, J. H.; Chai, K. Y. "Thermally stable efficient hole transporting materials based on carbazole and triphenylamine core for red phosphorescent OLEDs" *Org. Electron.* **2017**, *51*, 463-470.

28. Liu, X.; Liang, J.; You, J.; Ying, L.; Xiao, Y.; Wang, S.; Li, X. "Small molecular hole-transporting and emitting materials for hole-only green organic light-emitting devices" *Dyes Pigm.* **2016**, *131*, 41-48.

29. Kotchapradist, P.; Prachumrak, N.; Tarsang, R.; Jungsuttiwong, S.; Keawin, T.; Sudyoadsuk, T.; Promarak, V. "Pyrene-functionalized carbazole derivatives as non-

doped blue emitters for highly efficient blue organic light-emitting diodes" *J. Mater. Chem. C*. **2013**, *1*, 4916-4924.

30. Reig, M.; Bubniene, G.; Cambarau, W.; Jankauskas, V.; Getautis, V.; Palomares, E.; Martinez-Ferrero, E.; Velasco, D. "New solution-processable carbazole derivatives as deep blue emitters for organic light-emitting diodes" *RSC Adv*. **2016**, *6*, 9247-9253.
31. Zhan, Y.; Peng, J.; Ye, K.; Xue, P.; Lu, R. "Pyrene functionalized triphenylamine-based dyes: synthesis, photophysical properties and applications in OLEDs" *Org. Biomol. Chem.* **2013**, *11*, 6814-6823.
32. Yang, J.; Guo, Q.; Ren, Z.; Gao, X.; Peng, Q.; Li, Q.; Ma, D.; Li, Z. "New insight into intramolecular conjugation in the design of efficient blue materials: from the control of emission to absorption" *J. Mater. Chem. C*. **2017**, *5*, 6185-6192.
33. Liu, Y.; Ye, X.; Liu, G.; Lv, Y.; Zhang, X.; Chen, S.; Lam, J. W. Y.; Kwok, H. S.; Tao, X.; Tang, B. Z. "Structural features and optical properties of a carbazole-containing ethene as a highly emissive organic solid" *J. Mater. Chem. C*. **2014**, *2*, 1004-1009.
34. Chan, C. Y. K.; Lam, J. W. Y.; Zhao, Z.; Chen, S.; Lu, P.; Sung, H. H. Y.; Kwok, H. S.; Ma, Y.; Williams, I. D.; Tang, B. Z. "Aggregation-induced emission, mechanochromism and blue electroluminescence of carbazole and triphenylamine-substituted ethenes" *J. Mater. Chem. C.* **2014**, *2*, 4320-4327.
35. Tan, Y.; Zhao, Z.; Shang, L.; Liu, Y.; Wei, C.; Li, J.; Wei, H.; Liu, Z.; Bian, Z.; Huang, C. "Novel bipolar D-π-A type phenanthroimidazole/carbazole hybrid material for high efficiency nondoped deep-blue organic light-emitting diodes with NTSC CIEy and low efficiency roll-off" *J. Mater. Chem. C*. **2017**, *5*, 11901-11909.
36. Fan, S; You, J.; Miao, Y.; Wang, H.; Bai, Q.; Liu, X.; Li, X.; Wang, S. "A bipolar emitting material for high efficient non-doped fluorescent organic light-emitting diode approaching standard deep blue" *Dyes Pigm*. **2016**, *129*, 34-42.
37. Gao, Z.; Liu, Y.; Wang, Z.; Shen, F.; Liu, H.; Sun, G.; Yao, L.; Lv, Y.; Lu, P.; Ma, Y. "High-efficiency violet-light-emitting materials based on phenanthro[9,10-*d*]imidazole" *Chem. Eur. J.* **2013**, *19*, 2602-2605.
38. Gao, Z.; Wang, Z.; Shan,T.; Liu, Y.; Shen, F.; Pan, Y.; Zhang, H.; He, X.; Lu, P.; Yang, B.; Ma, Y. "High-efficiency deep blue fluorescent emitters based on

phenanthro[9,10-*d*]imidazole substituted carbazole and their applications in organic light emitting diodes" *Org. Electron*. **2014**, *15*, 2667-2676.

39. Huang, B.; Yin, Z.; Ban, X.; Ma, Z.; Jiang, W.; Tian, W.; Yang, M.; Ye, S.; Lin, B.; Sun, Y. "Nondoped deep blue OLEDs based on Bis-(4-benzenesulfonyl-phenyl)-9-phenyl-9*H*-carbazoles" *J. Lumin*. **2016**, *172*, 7-13.
40. Ye, J.; Chen, Z.; Fung, M.-K.; Zheng, C.; Ou, X.; Zhang, X.; Yuan, Y.; Lee, C.-S. "Carbazole/sulfone hybrid D-π-A-structured bipolar fluorophores for high-efficiency blue-violet electroluminescence" *Chem. Mater*. **2013**, *25*, 2630-2637.
41. Karthik, D.; Thomas, K. R. J.; Jou, J.-H.; Chen, Y.-L. "Synthesis, characterization and electroluminescence of carbazole-benzimidazole hybrids with thiophene/phenyl linker" *Dyes Pigm*. **2016**, *133*, 132-142.
42. Yu, T.; Zhu, Z.; Bao, Y.; Zhao, Y.; Liu, X.; Zhang, H. "Investigation of novel carbazole-functionalized coumarin derivatives as organic luminescent materials" Dyes Pigm. 2017, 147, 260-269.
43. Lo, D.; Chang, C.-H.; Krucaite, G.; Volyniuk, D.; Grazulevicius, J. V.; Grigalevicius, S. "Sky-blue aggregation-induced emission molecules for non-doped organic light-emitting diodes" *J. Mater. Chem. C*. **2017**, *5*, 6054-6060.
44. Tao, Y.; Yang, C.; Qin, J. "Organic host materials for phosphorescent organic light-emitting diodes" *Chem. Soc. Rev*. **2011**, *40*, 2943-2970.
45. Ameen, S.; Lee, S. B.; Yoon, S. C.; Lee, J.; Lee, C. "Diphenylaminocarbazoles by 1,8-functionalization of carbazole: Materials and application to phosphorescent organic light-emitting diodes" *Dyes Pigm*. **2016**, *124*, 35-44.
46. Chang, C.-H.; Griniene, R.; Su, Y.-D.; Yeh, C.-C.; Kao, H.-C.; Grazulevicius, J. V.; Volyniuk, D.; Grigalevicius, S. "Efficient red phosphorescent OLEDs employing carbazole-based materials as the emitting host" *Dyes Pigm*. **2015**, *122*, 257-263.
47. Dong, Q.; Lian, H.; Gao, Z.; Guo, Z.; Xiang, N.; Zhong, Z.; Guo, H.; Huang, J.; Wong, W.-Y. "Novel spirofluorene/indole/carbazole-based hole transport materials with high triplet energy for efficient green phosphorescent organic light-emitting diodes" *Dyes Pigm.* **2017**, *137*, 84-90.
48. Bagdziunas, G.; Grybauskaite, G.; Kostiv, N.; Ivaniuk, K.; Volyniuka, D.; Lazauskas, A. "Green and red phosphorescent organic light-emitting diodes with ambipolar hosts

based on phenothiazine and carbazole moieties: photoelectrical properties, morphology and efficiency" *RSC Adv.* **2016**, *6*, 61544-61554.

49. Tang, J.; Chen, Y.; Cong, L.; Lin, B.; Sun, Y. "Novel tri-carbazole modified fluorene host material for highly efficient solution-processed blue and green electrophosphorescent devices" Tetrahedron 2014, 70, 3847-3853.
50. Yang, W.; Chen, Y.; Jiang, W.; Ban, X.; Huang, B.; Dai, Y.; Sun, Y. "A carbazole-based dendritic host material for efficient solution-processed blue phosphorescent OLEDs" *Dyes Pigm*. **2013**, *97*, 286-290.
51. Son, H. S.; Seo, C. W.; Lee, J. Y. "Correlation of the substitution position of diphenylphosphine oxide on phenylcarbazole and device performances of blue phosphorescent organic light-emitting diodes" *J. Mater. Chem.* **2011**, *21*, 5638-5644.
52. Yang, W.; Zhang, Z.; Han, C.; Zhang, Z.; Xu, H.; Yan, P.; Zhao, Y.; Liu, S. "Controlling optoelectronic properties of carbazole-phosphine oxide hosts by short-axis substitution for low-voltage-driving PHOLEDs" *Chem. Commun*. **2013**, *49*, 2822-2824.
53. Jeon, S. O.; Yook, K. S.; Joo, C. W.; Lee, J. Y. "Phenylcarbazole-based phosphine oxide host materials for high efficiency in deep blue phosphorescent organic light-emitting diodes" *Adv. Funct. Mater*. **2009**, *19*, 3644-3649.
54. Li, W.; Li, J.; Liu, D.; Li, D.; Zhang, D. "Dual n-type units including pyridine and diphenylphosphine oxide: effective design strategy of host materials for high-performance organic light-emitting diodes" *Chem. Sci*. **2016**, *7*, 6706-6714.
55. Huang, H.; Wang, Y.; Pan, B.; Yang, X.; Wang, L.; Chen, J.; Ma, D.; Yang, C. "Simple bipolar hosts with high glass transition temperatures based on 1,8-disubstituted carbazole for efficient blue and green electrophosphorescent devices with "ideal" turn-on voltage" *Chem. Eur. J*. **2013**, *19*, 1828-1834.
56. Byeon, S. Y.; Kim, J. H.; Lee, J. Y. "CN-modified host materials for improved efficiency and lifetime in blue phosphorescent and thermally activated delayed fluorescent organic light-emitting diodes" *ACS Appl. Mater. Interfaces* **2017**, *9*, 13339-13346.
57. Mingming, H.; Qihao, X.; Yongxin, J.; Haichuan, M.; Lei, G.; Peijun, H.; Jinhai, H.; Jianhua, S. "Bipolar carbazole/quinoxaline-based host materials for efficient red PhOLEDs" *Dyes Pigm*. **2018**, *150*, 185-192.

58. Li, W.; Li, J.; Liu, D.; Jin, Q. "Simple bipolar host materials for high-efficiency blue, green, and white phosphorescence OLEDs" *ACS Appl. Mater. Interfaces* **2016**, *8*, 22382-22391.

59. Bian, C.; Wang, Q.; Ran, Q.; Liu, X.-Y.; Fan, J.; Liao, L.-S. "New carbazole-based bipolar hosts for efficient blue phosphorescent organic light-emitting diodes" *Org. Electron.* **2018**, *52*, 138-145.

60. Jin, J.; Zhang, W.; Wang, B.; Mu, G.; Xu, P.; Wang, L.; Huang, H.; Chen, J.; Ma, D. "Construction of high T_g bipolar host materials with balanced electron-hole mobility based on 1,2,4-thiadiazole for phosphorescent organic light-emitting diodes" *Chem. Mater.* **2014**, *26*, 2388-2395.

61. Uoyama, H.; Goushi, K.; Shizu, K.; Nomura, H.; Adachi, C. "Highly efficient organic light-emitting diodes from delayed fluorescence" *Nature* **2012**, *492*, 234-238.

62. Liu, W.; Zheng, C.-J.; Wang, K.; Chen, Z.; Chen, D.-Y.; Li, F.; Ou, X.-M.; Dong, Y.-P.; Zhang, X.-H. "Novel carbazol-pyridine-carbonitrile derivative as excellent blue thermally activated delayed fluorescence emitter for highly efficient organic light-emitting devices" *ACS Appl. Mater. Interfaces* **2015**, *7*, 18930-18936.

63. Park, W. J.; Lee, Y.; Kim, J. Y.; Yoon, D. W.; Kim, J.; Chae, S. H.; Kim, H.; Lee, G.; Shim, S.; Yang, J. H.; Lee, S. J. "Effective thermally activated delayed fluorescence emitter and its performance in OLED device" *Synth. Met.* **2015**, *209*, 99-104.

64. Mei, L.; Hu, J.; Cao, X.; Wang, F.; Zheng, C.; Tao, Y.; Zhang, X.; Huang, W. "The inductive-effect of electron withdrawing trifluoromethyl for thermally activated delayed fluorescence: tunable emission from tetra- to penta-carbazole in solution processed blue OLEDs" *Chem. Commun.* **2015**, *51*, 13024-13027.

65. Kim, M.; Jeon, S. K.; Hwang, S.-H.; Lee, J. Y. "Stable blue thermally activated delayed fluorescent organic light-emitting diodes with three times longer lifetime than phosphorescent organic light-emitting diodes" *Adv. Mater.* **2015**, *27*, 2515-2520.

66. Lee, D. R.; Kim, M.; Jeon, S. K.; Hwang, S.-H.; Lee, C. W.; Lee, J. Y. "Design strategy for 25% external quantum efficiency in green and blue thermally activated delayed fluorescent devices" *Adv. Mater.* **2015**, *27*, 5861-5867.

67. Rajamalli, P.; Senthilkumar, N.; Gandeepan, P.; Huang, P.-Y.; Huang, M.-J.; Ren-Wu, C.-Z.; Yang, C.-Y.; Chiu, M.-J.; Chu, L.-K.; Lin, H.-W.; Cheng, C.-H. "A new

molecular design based on thermally activated delayed fluorescence for highly efficient organic light emitting diodes" *J. Am. Chem. Soc*. **2016**, *138*, 628-634.

68. Rajamalli, P.; Senthilkumar, N.; Huang, P.-Y.; Ren-Wu, C.-C.; Lin, H.-W.; Cheng, C.-H. "New molecular design concurrently providing superior pure blue, thermally activated delayed fluorescence and optical out-coupling efficiencies" *J. Am. Chem. Soc*. **2017**, *139*, 10948-10951.
69. Kim, B. S.; Lee, J. Y. "Phosphine oxide type bipolar host material for high quantum efficiency in thermally activated delayed fluorescent device" *ACS Appl. Mater. Interfaces* **2014**, *6*, 8396-8400.
70. Suzuki, Y.; Zhang, Q.; Adachi, C. "A solution-processable host material of 1,3-bis{3-[3-(9-carbazolyl)phenyl]-9-carbazolyl}benzene and its application in organic light-emitting diodes employing thermally activated delayed fluorescence" *J. Mater. Chem. C.* **2015**, *3*, 1700-1706.
71. Lee, C. W.; Lee, J. Y. "Systematic control of photophysical properties of host materials for high quantum efficiency above 25% in green thermally activated delayed fluorescent devices" *ACS Appl. Mater. Interfaces* **2015**, *7*, 2899-2904.
72. Kang, J. S.; Hong, T. R.; Kim, H. J.; Son, Y. H.; Lampande, R.; Kang, B. Y.; Lee, C.; Bin, J.-K.; Lee, B. S.; Yang, J. H.; Kim, J.; Park, S.; Cho, M. J.; Kwon, J. H.; Choi, D. H. "High-performing bipolar host materials for blue thermally activated delayed fluorescent devices with excellent external quantum efficiencies" *J. Mater. Chem. C*. **2016**, *4*, 4512-4520.
73. Cai, M.; Song, X.; Zhang, D.; Qiao, J.; Duan, L. "π-π stacking: a strategy to improve the electron mobilities of bipolar hosts for TADF and phosphorescent devices with low efficiency roll-off" *J. Mater. Chem. C.* **2017**, *5*, 3372-3381.
74. Zhang, D.; Cai, M.; Bin, Z.; Zhang, Y.; Zhang, D.; Duan, L. "Highly efficient blue thermally activated delayed fluorescent OLEDs with record-low driving voltages utilizing high triplet energy hosts with small singlet-triplet splittings" *Chem. Sci*. **2016**, *7*, 3355-3363.
75. Bedi, A.; Zade, S. S. "Electrochemical route to solution-processable polymers of thiophene/selenophene capped didodecyloxybenzo[1,2-b:4,3-b′]dithiophene and their optoelectronic properties" *Macromolecules* **2013**, *46*, 8864-8872.

76. Dhar, J.; Venkataramaiah, N.; Anitha, A.; Patil, S. "Photophysical, electrochemical and solid state properties of diketopyrrolopyrrole based molecular materials: importance of the donor group*" J. Mater. Chem. C.* **2014**, *2*, 3457-3466.

77. Prathapan, S.; Johnson, T. E.; Lindsey, J. S. "Building-block synthesis of porphyrin light harvesting arrays" *J. Am. Chem. Soc.***1993**,*115*, 7519-7520.

78. Singh, R.; Tharion, J.; Murugan, S.; Kumar, A. "ITO-free solution-processed flexible electrochromic devices based on PEDOT:PSS as transparent conducting electrode" *ACS Appl. Mater. Interfaces* **2017**, *9*, 19427-19435.

79. Pati, P. B.; Zade, S. S. "Dicyanovinyl terthiophene as a reaction based colorimetric and ratiometric fluorescence probe for cyanide anions" *RSC Adv.* **2013**, *3*, 13457-13462.

80. Dudhe, R. S.; Tiwari, S. P.; Raval, H. N.; Khaderbad, M. A.; Singh, R.; Sinha, J.; Yedukondalu, M.; Ravikanth, M.; Kumar, A.; Rao, V. R. "Explosive vapor sensor using poly(3-hexylthiophene) and Cu(II) tetraphenylporphyrin composite based organic field effect transistors" *Appl. Phys. Lett.* **2008**, *93*, 263306-263309.

81. Duan, L.; Hou, L.; Lee, T.-W.; Qiao, J.; Zhang, D.; Dong, G.; Wang, L.; Qiu, Y. "Solution processable small molecules for organic light-emitting diodes" *J. Mater. Chem.* **2010**, *20*, 6392-6407.

82. Velasco, D.; Castellanos, S.; Lopez, M.; Lopez-Calahorra, F.; Brillas, E.; Julia, L. "Red organic light-emitting radical adducts of carbazole and tris(2,4,6-trichlorotriphenyl)methyl radical that exhibit high thermal stability and electrochemical amphotericity" *J. Org. Chem.* **2007**, *72*, 7523-7532.

83. Vanga, D. G.; Santra, M.; Keerthi, A.; Valiyaveettil, S. "Synthesis and photophysical properties of pyrene-based green fluorescent dyes: butterfly-shaped architectures" *Org. Biomol. Chem.* **2014**, *12*, 7914-7918.

84. Liu, B.; Yuan, Y.; He, D.; Huang, D.-Y.; Luo, C.-Y.; Zhu, Z.-L.; Lu, F.; Tong, Q.-X.; Lee, C.-S. "High-performance blue OLEDs based on phenanthroimidazole emitters via substitutions at the C6- and C9-positions for improving exciton utilization" *Chem. Eur. J.* **2016**, *22*, 12130-12137.

85. Tang, X.; Bai, Q.; Peng, Q.; Gao, Y.; Li, J.; Liu, Y.; Yao, L.; Lu, P.; Yang, B.; Ma, Y. "Efficient deep blue electroluminescence with an external quantum efficiency of

6.8% and CIEy < 0.08 based on a phenanthroimidazole-sulfone hybrid donor-acceptor molecule" *Chem. Mater*. **2015**, *27*, 7050-7057.

86. Xue, M.-M.; Huang, C.-C.; Yuan, Y.; Zhang, Y.-X.; Fung, M.-K.; Liao, L.-S. "A novel electron-acceptor moiety as a building block for efficient donor–acceptor based fluorescent organic lighting-emitting diodes" *Chem. Commun*. **2017**, *53*, 263-265.
87. Tang, C. W.; VanSlyke, S. A. "Organic electroluminescent diodes" *Appl. Phys. Lett.* **1987**, *51*, 913-915.
88. Yang, X.; Zhou, G.; Wong, W.-Y. "Functionalization of phosphorescent emitters and their host materials by main-group elements for phosphorescent organic light-emitting devices" *Chem. Soc. Rev*, **2015**, *44*, 8484-8575.
89. Godumala, M.; Choi, S.; Cho, M. J.; Choi, D. H. "Thermally activated delayed fluorescence blue dopants and hosts: from the design strategy to organic light-emitting diode applications" *J. Mater. Chem. C.* **2016**, *4*, 11355-11381.
90. Kim, S. H.; Cho, I.; Sim, M. K.; Park, S.; Park, S.Y. "Highly efficient deep-blue emitting organic light emitting diode based on the multifunctional fluorescent molecule comprising covalently bonded carbazole and anthracene moieties" *J. Mater. Chem.* **2011**, *21*, 9139-9148.
91. Lanke, S. K.; Sekar, N. "Aggregation induced emissive carbazole-based push-pull NLOphores: synthesis, photophysical properties and DFT studies" *Dyes Pigm*. **2016**, *124*, 82-92.
92. Reig, M.; Gozalvez, C.; Bujaldon, R.; Bagdziunas, G.; Ivaniuk, K.; Kostiv, N.; Volyniuk, D.; Grazulevicius, J. V.; Velasco, D. "Easy accessible blue luminescent carbazole-based materials for organic light-emitting diodes" *Dyes Pigm*. **2017**, *137*, 24-35.
93. Xiang, C.; Fu, X.; Wei, W.; Liu, R.; Zhang, Y.; Balema, V.; Nelson, B.; So, F. "Efficiency roll-off in blue emitting phosphorescent organic light emitting diodes with carbazole host materials" *Adv. Funct. Mater*. **2016**, *26*, 1463-1469.
94. Siraj, N.; Hasan, F.; Das, S.; Kiruri, L. W.; Gall, K. E. S.; Baker, G. A.; Warner, I. M. "Carbazole-derived group of uniform materials based on organic salts: solid state fluorescent analogues of ionic liquids for potential applications in organic-based blue light-emitting diodes" *J. Phys. Chem. C.* **2014**, *118*, 2312-2320.

95. Tao, Y.; Yuan, K.; Chen, T.; Xu, P.; Li, H.; Chen, R.; Zheng, C.; Zhang, L.; Huang, W. "Thermally activated delayed fluorescence materials towards the breakthrough of organoelectronics" *Adv. Mater*. **2014**, *26*, 7931-7958.

96. Wu, S.; Aonuma, M.; Zhang, Q.; Huang, S.; Nakagawa, T.; Kuwabara, K.; Adachi, C. "High-efficiency deep-blue organic light-emitting diodes based on a thermally activated delayed fluorescence emitter" *J. Mater. Chem. C*. **2014**, *2*, 421-424.

97. Konidena, R. K.; Thomas, K. R. J.; Dubey, D. K.; Sahoo, S.; Jou, J.-H. "A new molecular design based on hybridized local and charge transfer florescence for highly efficient (>6%) deep-blue organic light emitting diodes" *Chem. Commun*. **2017**, *53*, 11802-11805.

98. Sharma, N.; Kumar, S.; Chandrasekaran, Y.; Patil, S. "Maleimideebased donor-π-acceptor-π-donor derivative for efficient organic light-emitting diodes" *Org. Electron.* **2016**, *38*, 180-185.

99. Ledwon, P.; Zassowski, P.; Jarosz, T.; Lapkowski, M.; Wagner, P.; Cherpak, V.; Stakhira, P. "A novel donor–acceptor carbazole and benzothiadiazole material for deep red and infrared emitting applications" *J. Mater. Chem. C*. **2016**, *4*, 2219-2227.

100. Ni, F.; Wu, Z.; Zhu, Z.; Chen, T.; Wu, K.; Zhong, C.; An, K.; Wei, D.; Ma, D.; Yang, C. "Teaching an old acceptor new tricks: rationally employing 2,1,3-benzothiadiazole as input to design a highly efficient red thermally activated delayed fluorescence emitter" *J. Mater. Chem. C*. **2017**, *5*, 1363-1368.

101. Liu, H.; Bai, Q.; Yao, L.; Zhang, H.; Xu, H.; Xu, H.; Zhang, S.; Li, W.; Gao, Y.; Li, J.; Lu, P.; Wang, H.; Yang, B.; Ma, Y. Highly efficient near ultraviolet organic light-emitting diode based on a meta-linked donor-acceptor molecule" *Chem. Sci.* **2015**, *6*, 3797–3804.

102. Xu, H.; Sun, P.; Wan, K.; Li, J.; Wang, F.; Miao, Y.; Wang, H.; Xu, B.; Wong, W.-Y. "Bipolar hosts and non-doped deep-blue emitters (CIEy = 0.04) based on phenylcarbazole and 2-(2-phenyl-2H-1,2,4-triazol-3-yl)pyridine groups" *J. Mater. Chem. C*. **2017**, *5*, 4455-4462.

103. Thomas, K. R. J.; Velusamy, M.; Lin, J. T.; Tao, Y.-T.; Chuen, C.-H. "Cyanocarbazole derivatives for high performance electroluminescent devices" *Adv. Funct. Mater*. **2004**, *14*, 387-392.

104. Deng, L.; Li, J.; Wang, G.-X.; Wu, L.-Z. "Simple bipolar host materials incorporating CN group for highly efficient blue electrophosphorescence with slow efficiency roll-off" *J. Mater. Chem. C*. **2013**, *1*, 8140-8145.

105. Lin, M.-S.; Yang, S.-J.; Chang, H.-W.; Huang, Y.-H.; Tsai, Y.-T.; Wu, C.-C.; Chou, S.-H.; Mondal, E.; Wong, K.-T. "Incorporation of a CN group into mCP: a new bipolar host material for highly efficient blue and white electrophosphorescent devices" *J. Mater. Chem*. **2012**, *22*, 16114-16120.

106. Gupta, V. D.; Padalkar, V. S.; Phatangare, K. R.; Patil, V. S.; Umape, P. G.; Sekar, N. "The synthesis and photo-physical properties of extended styryl fluorescent derivatives of N-ethyl carbazole" *Dyes Pigm*. **2011**, *88*, 378-384.

107. Mukherjee, S.; Singh, R.; Gopinathan, S.; Murugan, S.; Gawali, S.; Saha, B.; Biswas, J.; Lodha, S.; Kumar, A. "Solution-processed poly(3,4-ethylenedioxythiophene) thin films as transparent conductors: Effect of *p*-toluenesulfonic acid in dimethyl sulfoxide" *ACS Appl. Mater. Interfaces* **2014**, *6*, 17792-17803.

108. Pati, P. B.; Senanayak, S. P.; Narayan, K. S.; Zade, S. S. "Solution processable benzooxadiazole and benzothiadiazole based D-A-D molecules with chalcogenophene: Field effect transistor study and structure property relationship" *ACS Appl. Mater. Interfaces* **2013**, *5*, 12460-12468.

109. Prathapan, S.; Yang, S. I.; Seth, J.; Miller, M. A.; Bocian, D. F.; Holten, D.; Lindsey, J. S. "Synthesis and excited-state photodynamics of perylene-porphyrin dyads. 1. parallel energy and charge transfer via a diphenylethyne linker" *J. Phys. Chem. B* **2001,** *105,* 8237-8248.

110. Moreshead, W. V.; Przhonska, O. V.; Bondar, M. V.; Kachkovski, A. D.; Nayyar, I. H.; Masunov, A. E.; Woodward, A. W.; Belfield, K. D. "Design of a new optical material with broad spectrum linear and two-photon absorption and solvatochromism" *J. Phys. Chem. C* **2013**, *117*, 23133-23147.

111. Jain, V.; Sahoo, R.; Mishra, S. P.; Sinha, J.; Montazami, R.; Yochum, H. M.; Heflin, J. R.; Kumar, A. "Synthesis and characterization of regioregular water-soluble 3,4-propylenedioxythiophene derivative and its application in the fabrication of high-contrast solid-state electrochromic devices" *Macromolecules* **2009**, *42*, 135-140.

112. Dhar, J.; Mukhopadhay, T.; Yaacobi-Gross, N.; Anthopoulos, T. D.; Salzner, U.; Swaraj, S.; Patil, S. "Effect of chalcogens on electronic and photophysical properties

of vinylene-based diketopyrrolopyrrole copolymers" *J. Phys. Chem. B* **2015**, *119*, 11307-11316.

113. Morales, A. R.; Frazer, A.; Woodward, A. W.; Ahn-White, H.-Y.; Fonari, A.; Tongwa, p.; Timofeeva, T.; Belfield, K. D. "Design, synthesis, and structural and spectroscopic studies of push-pull two-photon absorbing chromophores with acceptor groups of varying strength" *J. Org. Chem.* **2013**, *78*, 1014-1025.
114. Yang, S. I.; Lammi, R. K.; Prathapan, S.; Miller, M. A.; Seth, J.; Diers, J. R.; Bocian, D. F.; Lindsey, J. S.; Holten, D. "Synthesis and excited state photodynamics of perylene-porphyrin dyads Part 3: Effects of perylene, linker and connectivity on ultrafast energy transfer" *J. Mater. Chem*. **2001**, *11*, 2420-2430.
115. Kundu, P.; Thomas, K. R.; Lin, J. T.; Tao, Y.-T.; Chien, C.-H. "High Tg carbazole derivatives as blue-emitting hole-transporting materials for electroluminescent devices" *Adv. Funct. Mater*. **2003**, *13*, 445-452.
116. Konidena, R. K.; Thomas, K. R. J.; Kumar, S.; Wang, Y.-C.; Li, C.-J.; Jou, J.-H. "Phenothiazine decorated carbazoles: Effect of substitution pattern on the optical and electroluminescent characteristics" *J. Org. Chem*. **2015**, *80*, 5812-5823.
117. Divya, K. P.; Sreejith, S.; Suresh, C. H.; Philips, D. S.; Ajayaghosh, A. "Chain folding controlled by an isomeric repeat unit: Helix formation versus random aggregation in acetylene-bridged carbazole-bipyridine co-oligomers" *Chem. Asian J.* **2013**, *8*, 1579-1586.
118. Reig, M.; Gozalvez, C.; Jankauskas, V.; Gaidelis, V.; Grazulevicius, J. V.; Fajari, L.; Julia, L.; Velasco, D. "Stable all organic radicals with ambipolar charge transport" *Chem. Eur. J.* **2016**, *22*, 18551-18558.
119. Song, X.; Wang, M.; Kong, L.; Zhao, J. "Effects of the acceptor pattern and substitution position on the properties of *N*-phenyl-carbazolyl based donor–acceptor–donor molecules" *RSC Adv*. **2017**, *7*, 18189-18198.
120. Wang, H.; Chen, G.; Liu, Y.; Hu, L.; Xu, X.; Ji, S. "The synthesis and characterization of novel dipolar fluorescent materials based on a quinoxaline core" *Dyes Pigm*. **2009**, *83*, 269-275.
121. Reig, M.; Bagdziunas, G.; Volyniuk, D.; Grazulevicius, J. V.; Velasco, D. "Tuning the ambipolar charge transport properties of tricyanovinyl-substituted carbazole-based materials" *Phys. Chem. Chem. Phys.* **2017**, *19*, 6721-6730.

122. Zhu, C.-C.; Guo, K.-P.; Liu, W.-B.; He, Y.-B.; Li, Z.-M.; Gao, X.-C.; Deng, F. J.; Wei, B. "Synthesis of asymmetric biphenyl derivatives for optoelectronic applications" *Opt. Mater*. **2013**, *35*, 2095-2101.

123. Krotkus, S.; Kazlauskas, K.; Miasojedovas, A.; Gruodis, A.; Tomkeviciene, A.; Grazulevicius, J. V.; Jursenas, S. "Pyrenyl-functionalized fluorene and carbazole derivatives as blue light emittes" *J. Phys. Chem. C*. **2012**, *116*, 7561-7572.

124. Lin, S.-L.; Chan, L.-H.; Lee, R.-H.; Yen, M.-Y.; Kuo, W.-J.; Chen, C.-T.; Jeng, R.-J. "Highly efficient carbazole-π-dimesitylborane bipolar fluorophores for nondoped blue organic-light emitting diodes" *Adv. Mater*. **2008**, *20*, 3947-3952.

125. Bhalla, V.; Singh, G.; Kumar, M.; Singh, C.; Rawat, M.; Anand, R. S. "Carbazole-based linear conjugated molecules: structure–property relationships and device properties" *RSC Adv*. **2013**, *3*, 14722-14730.

126. Kato, S.-i.; Noguchi, H.; Kobayashi, A.; Yoshihara, T.; Tobita, S.; Nakamura, Y. "Bicarbazoles: systematic structure-property investigations on a series of conjugated carbazole dimers" *J. Org. Chem*. **2012**, *77*, 9120-9133.

127. Skuodis, E.; Tomkeviciene, A.; Reghu, R.; Peciulyte, L.; Ivaniuk, K.; Volyniuk, D.; Bezvikonnyi, O.; Bagdziunas, G.; Gudeika, D.; Grazulevicius, J. V. "OLEDs based on the emission of interface and bulk exciplexes formed by cyano-substituted carbazole derivative" *Dyes Pigm*. **2017**, *139*, 795-807.

128. Shen, J.-Y.; Yang, X.-L.; Huang, T.-H.; Lin, J. T.; Ke, T.-H.; Chen, L.-Y.; Wu, C.-C.; Yeh, M.-C. P. "Ambipolar conductive 2,7-carbazole derivatives for electroluminescent devices" *Adv. Funct. Mater*. **2007**, *17*, 983-995.

129. Bai, Y.; Wei, B.; Ouyang, X.; Liu, Z.; Jiang, W.; Li, W.; Zhang, L.; Hong, L.; He, G.; Chen, Y.; Ge, Z. "Tunable crystal packing for enhanced electroluminescent properties based on novel thiazole derivatives with different connecting positions of carbazole" *Dyes Pigm*. **2016**, *130*, 319-326.

130. Chen, W.-C.; Yuan, Y.; Ni, S.-F.; Tong, Q.-X.; Wong, F.-L.; Lee, C.-S. "Achieving efficient violet-blue electroluminescence with CIEy <0.06 and EQE >6% from naphthyl-linked phenanthroimidazole-carbazole hybrid fluorophores" *Chem. Sci*. **2017**, *8*, 3599-3608.

131. Venkateswararao, A.; Thomas, K. R. J.; Lee, C.-P.; Li, C.-T.; Ho, K.-C. "Organic Dyes Containing Carbazole as Donor and π-Linker: Optical, Electrochemical, and Photovoltaic Properties" *ACS Appl. Mater. Interfaces* **2014**, *6*, 2528-2539.

132. Liu, Y.; Wang, H.-Y.; Chen, G.; Xu, X.-P.; Ji, S.-J. "Synthesis and properties of novel 'ethyne-linked' compounds containing carbazole and 1,8-naphthalimide groups" *Aust. J. Chem.* **2009**, *62*, 934–940.

133. Zhang, H.; Wan, X.; Xue, X.; Li, Y.; Yu, A.; Chen, Y. "Selective tuning of the HOMO–LUMO gap of carbazole-based donor–acceptor–donor compounds toward different emission colors" *Eur. J. Org. Chem.* **2010**, 1681-1687.

134. Slodek, A.; Filapek, M.; Schab-Balcerzak, E.; Grucela, M.; Kotowicz, S.; Janeczek, H.; Smolarek, K.; Mackowski, S.; Malecki, J. G.; Jedrzejowska, A.; Szafraniec-Gorol, G.; Chrobok, A.; Marcol, B.; Krompiec, S.; Matussek, M. "Highly luminescence anthracene derivatives as promising materials for OLED applications" *Eur. J. Org. Chem.* **2016**, 4020-4031.

135. Liu, X.; Zhang, T.; Ni, T.; Jiang, N.; Liu, Z.; Bian, Z.; Lu, Z.; Huang, C. "Co-deposited Cu(I) complex for tri-layered yellow and white organic light-emitting diodes" *Adv. Funct. Mater.* **2014**, *24*, 5385-5392.

136. Song, Y.; Di, C.-a.; Wei, Z.; Zhao, T.; Xu, W.; Liu, Y.; Zhang, D.; Zhu, D. "Synthesis, characterization and field-effect transistor properties of carbazolenevinylene oligomers: from linear to cyclic architectures" *Chem. Eur. J.* **2008**, *14*, 4731-4740.

137. Nandy, R.; Sankararaman, S. "Donor-acceptor substituted phenylethynyltriphenylenes – excited state intramolecular charge transfer, solvatochromic absorption and fluorescence emission" *Beilstein J. Org. Chem.* **2010,** *6*, 992-1001.

138. Grabowski, Z. R.; Rotkiewicz, K. "Structural changes accompanying intramolecular electron transfer: focus on twisted intramolecular charge-transfer states and structures" *Chem. Rev.* **2003,** *103,* 3899-4031.

139. Valchanov, G.; Ivanova, A.; Tadjer, A.; Chercka, D.; Baumgarten, M. "Understanding the Fluorescence of TADF Light-Emitting Dyes" *J. Phys. Chem. A.* **2016**, *120*, 6944-6955.

140. Keerthi, A.; Sriramulu, D.; Liu, Y.; Timothy, C. T. Y.; Wang, Q.; Valiyaveettil, S. "Architectural influence of carbazole push-pull-pull dyes on dye sensitized solar cells" *Dyes Pigm*. **2013**, *99*, 787-797.

141. Shaydyuk, Y. O.; Levchenko, S. M.; Kurhuzenkau, S. A.; Anderson, D.; Masunov, A. E.; Kachkovsky, O. D.; Slominsky, Y. L.; Bricks, J. L.; Belfield, K. D.; Bondar, M. V. "Linear photophysics, two-photon absorption and femtosecond transient absorption spectroscopy of styryl dye bases" *J. Lumin.* **2017**, *183*, 360-367.

142. Mataga, N.; Kaifu, Y.; Koizumi, M. "The solvent effect on fluorescence spectrum. Change of solute-solvent interaction during the lifetime of excited solute molecule" *Bull. Chem. Soc. Jpn*. **1955**, *28*, 690-691.

143. Mataga, N.; Kaifu, Y.; Koizumi, M. "Solvent effects upon fluorescence spectra and the dipolemoments of excited molecules" *Bull. Chem. Soc. Jpn*. **1956**, *29*, 465-470.

144. Lanke, S. K.; Sekar, N. "AIE based coumarin chromophore - Evaluation and correlation between solvatochromism and solvent polarity parameters" *J Fluoresc*. **2016**, *26*, 497-511.

145. Naik, M. A.; Venkatramaiah, N.; Kanimozhi, C.; Patil, S. "Influence of side-chain on structural order and photophysical properties in thiophene based diketopyrrolopyrroles: A systematic study" *J. Phys. Chem. C*. **2012**, *116*, 26128-26137.

146. Gopi, V.; Varma, S. J.; Kumar, M. V. M.; Prathapan, S.; Jayalekshmi, S.; Joseph, R. "Semiconducting thienylene-biphenylenevinylene hybrid polymers: synthesis, characterization and application prospects in polymer LEDs" *Dyes Pigm*. **2016**, *126*, 303-312.

147. Gupta, J.; Vadukumpully, S.; Valiyaveettil, S. "Synthesis and property studies of linear and kinked poly(pyreneethynylene)s" *Polymer* **2010**, *51*, 5078-5086.

148. Paliulis, O.; Ostrauskaite, J.; Gaidelis, V.; Jankauskas, V.; Strohriegl, P. "Synthesis of conjugated carbazole trimers and pentamers by Suzuki coupling" *Macromol. Chem. Phys*. **2003**, *204*, 1706-1712.

149. Panthi, K.; Adhikari, R. M; Kinstle, T. H. "Carbazole donor-carbazole linker-based compounds: Preparation, photophysical properties, and formation of fluorescent nanoparticles" *J. Phys. Chem. A.* **2010,** *114*, 4550-4557.

150. Karon, K.; Lapkowski, M. "Carbazole electrochemistry: a short review" *J Solid State Electrochem*. **2015**, *19*, 2601-2610.

151. Jou, J.-H.; Kumar, S.; Fang, P.-H.; Venkateswararao, A.; Thomas, K. R. J.; Shyue, J.-J.; Wang, Y.-C.; Li, T.-H.; Yu, H.-H. "Highly efficient ultra-deep blue organic light emitting diodes with a wet- and dry-process feasible cyanofluorene acetylene based emitter" *J. Mater. Chem. C*. **2015**, *3*, 2182-2194.

152. Pomrnerehne, J.; Vestweber, H.; Guss, W.; Mahrt, R. F.; Bassler, H.; Porsch, M.; Daub, J. "Efficient two layer LEDs on a polymer blend basis" *Adv. Mater*. **1995**, *7*, 551-554.

153. Thomas, K. R. J.; Lin, J. T.; Tao, Y.-T.; Ko, C. W. "Novel green light-emitting carbazole derivatives: Potential electroluminescent materials" *Adv. Mater*. **2000**, *12*, 1949-1951.

154. Park, H.; Lee, J.; Kang, I.; Chu, H. Y.; Lee, J.-I.; Kwon, S.-K.; Kim, Y.-H. "Highly rigid and twisted anthracene derivatives: a strategy for deep blue OLED materials with theoretical limit efficiency" *J. Mater. Chem*. **2012**, *22*, 2695-2700.

155. Becke, A. D. "Densityfunctional thermochemistry. III. The role of exact exchange" *J. Chem. Phys*. **1993**, *98*, 5648-5652.

156. Lee, C.; Yang, W.; Parr, R. G. "Development of the Colle-Salvetti correlation energy formula into a functional theory of the electron density" *Phys. Rev. B Condens. Matter*. **1988**, *37*, 785-789.

157. Ran, X.-Q.; Feng, J.-K.; Ren, A. M.; Li, W.-C.; Zou, L.-Y. Sun, C.-C. "Theoretical study on photophysical properties of ambipolar spirobifluorene derivatives as efficient blue-light-emitting materials" *J. Phys. Chem. A*. **2009,** *113*, 7933-7939.

158. Tang, S.; Li, B.; Zhang, J. "Photophysical properties of phenyl- or thiophene-cored branched molecules with thiophene and/or thienylenevinylene arms toward broad absorption spectra for solar cells: A theoretical study" *J. Phys. Chem. C*. **2013**, *117*, 3221-3231.

159. Pati, P. B.; Zade, S. S. "Highly emissive triphenylamine based fluorophores for detection of picric acid" *Tetrahedron Lett*. **2014**, *55*, 5290-5293.

160. Lee, S. J.; Park, J. S.; Yoon, K.-J.; Kim, Y.-I.; Jin, S.-H.; Kang, S. K.; Gal, Y.-S.; Kang, S.; Lee, J. Y.; Kang, J.-W.; Lee, S.-H.; Park, H.-D.; Kim, J.-J. "High-

efficiency deep-blue light-emitting diodes based on phenylquinoline/carbazole-based compounds" *Adv. Funct. Mater*. **2008**, *18*, 3922-3930.

161. Spano, F. C. "The spectral signatures of Frenkel polarons in H- and J- aggregates" *Acc, Chem. Res.* **2010**, *43*, 429-439.
162. Chen, Y.-H.; Lin, S.-L.; Chang, Y.-C.; Chen, Y.-C.; Lin, J.-T.; Lee, R.-H.; Kuo, W.-J.; Jeng, R.-J. "Efficient non-doped blue light emitting diodes based on novel carbazole-substituted anthracene derivatives" *Org. Electron.* **2012**, *13*, 43-52.
163. Xu, X.; Chen, S.; Yu, G.; Di, C.; You, H.; Ma, D.; Liu, Y. "High-efficiency blue light-emitting diodes based on a polyphenylphenyl compound with strong electron-accepting groups" *Adv. Mater.* **2007**, *19*, 1281-1285.
164. Zhen, C.-G.; Dai, Y.-F.; Zeng, W.-J.; Ma, Z.; Chen, Z.-K.; Kieffer, J. "Achieving highly efficient fluorescent blue organic light emitting diodes through optimizing molecular structures and device configuration" *Adv. Funct. Mater.* **2011**, *21*, 699-707.
165. Li, G.; Zhao, Y.; Li, J.; Cao, J.; Zhu, J.; Sun, X. W.; Zhang, Q. "Synthesis, characterization, physical properties and OLED application of single BN-fused perylene diimide" *J. Org. Chem*. **2015**, *80*, 196-203.
166. Venkatramaiah, N.; Kumar, G. D.; Chandrasekaran, Y.; Ganduri, R.; Patil, S. "Efficient Blue and Yellow Organic Light-Emitting Diodes Enabled by aggregation induced emission" *ACS Appl. Mater. Interfaces* **2018**, *10*, 3838-3847.
167. Kumar, D.; Thomas, K. R. J.; Lin, C.-C.; Jou, J.-H. "Pyrenoimidazole-based deep-blue-emitting materials: Optical, electrochemical and electroluminescent characteristics" *Chem. Asian J*. **2013**, *8*, 2111-2124.
168. Jou, J.-H.; Chen, Y.-L.; Tseng, J.-R.; Wu, R.-Z.; Shyue, J. J.; Thomas, K. R. J.; Kapoor, N.; Chen, C.-T.; Lin, Y.-P.; Wang, P.-H.; Hung, H.-W.; Li, J.-Y.; Chen, S.-P. "The use of a polarity matching and high-energy exciton generating host in fabricating efficient purplish-blue OLEDs from a sky-blue emitter" *J. Mater. Chem*. **2012**, *22*, 15500-15506.
169. Kim, B. M.; Nguyen, Q. P. B.; Fan, J. G.; Kim, M. J.; Braveenth, R.; Kim, G. W.; Kwon, J. H.; Chai, K. Y. "Novel star-shaped hole-transporting materials based on triphenylamine cores end-capped with carbazole and triarylamine derivatives for use in OLEDs" *Bull. Korean Chem. Soc.* **2015**, *36*, 1303-1306.

170. Promaraka, V.; Ruchirawat, S. "Synthesis and properties of *N*-carbazole end-capped conjugated molecules" *Tetrahedron* **2007**, *63*, 1602-1609.

171. Wu, C.-S.; Fang, S.-W.; Chen, Y. "Solution-processable hole-transporting material containing fluorenyl core and triple-carbazolyl terminals: synthesis and application to enhancement of electroluminescence" *Phys. Chem. Chem. Phys.* **2013**, *15*, 15121-15127.

172. Irfan, M.; Belfield, K. D.; Saeed, A. "Carbazole/fluorene based conjugated small molecules: synthesis and comparative studies on the optical, thermal and electrochemical properties" *RSC Adv*. **2015**, *5*, 48760-48768.

173. Tomkeviciene, A.; Grazulevicius, J. V.; Kazlauskas, K.; Gruodis, A.; Jursenas, S.; Ke, T.-H.; Wu, C.-C. "Impact of linking topology on the properties of carbazole trimers and dimers" *J. Phys. Chem. C*. **2011**, *115*, 4887-4897.

174. Tomkeviciene, A.; Grazulevicius, J. V.; Volyniuk, D.; Jankauskas, V.; Sini, G. "Structure–properties relationship of carbazole and fluorene hybrid trimers: experimental and theoretical approaches" *Phys. Chem. Chem. Phys.* **2014**, *16*, 13932-13942.

175. Yin, J.; Zhang, S.-L.; Chen, R.-F.; Ling, Q.-D.; Huang, W. "Carbazole endcapped heterofluorenes as host materials: theoretical study of their structural, electronic, and optical properties" *Phys. Chem. Chem. Phys.* **2010**, *12*, 15448-15458.

176. Jiang, W.; Duan, L.; Qiao, J.; Dong, G.; Zhang, D.; Wang, L.; Qiu, Y. "High-triplet-energy tri-carbazole derivatives as host materials for efficient solution-processed blue phosphorescent devices" *J. Mater. Chem.* **2011**, *21*, 4918-4926.

177. Brunner, K.; van Dijken, A.; Borner, H.; Bastiaansen, J. J. A. M.; Kiggen, N. M. M.; Langeveld, B. M. W. "Carbazole compounds as host materials for triplet emitters in organic light-emitting diodes: Tuning the HOMO Level without influencing the triplet energy in small molecules" *J. Am. Chem. Soc*. **2004**, *126*, 6035-6042.

178. Sonntag, M.; Strohriegl, P. "Novel 2,7-linked carbazole trimers as model compounds for conjugated carbazole polymers" *Chem. Mater*. **2004**, *16*, 4736-4742.

179. Dias, F. B.; Bourdakos, K. N.; Jankus, V.; Moss, K. C.; Kamtekar, K. T.; Bhalla, V.; Santos, J.; Bryce, M. R.; Monkman, A. P. "Triplet harvesting with 100% efficiency by way of thermally activated delayed fluorescence in charge transfer OLED emitters" *Adv. Mater.* **2013**, *25*, 3707-3714.

180. Shimasaki, T.; Iwasawa, R.; Watanabe, M.; Teramoto, N.; Shibata, M. "Ethynylene-bridged conjugate carbazole trimers: synthesis and their structural, photophysical, and electrochemical properties" *Asian J. Org. Chem*. **2017**, *6*, 841-851.

181. Baronas, P.; Kazlauskas, K.; Kreiza, G.; Jankauskas, V.; Tomkeviciene, A.; Simokaitiene, J.; Grigalevicius, S.; Grazulevicius, J. V.; Jursenas, S. "Differently linked fluorene-carbazole triads for light amplification" *Dyes Pigm*. **2015**, *123*, 370-379.

182. Liu, W.; Ying, S.; Sun, Q.; Qiu, X.; Zhang, H.; Xue, S.; Yang, W. "9,10-Bis(*N*-methylcarbazol-3-yl-vinyl-2)anthracene: High contrast piezofluoro-chromism and remarkably doping-improved electroluminescence performance" *Dyes Pigm*. **2016**, *125*, 8-14.

183. Oh, D. K.; Hong, S. M.; Lee, C. E.; Kim, B.-S.; Jin, J.-I. "Dispersive charge transport due to strong charge–dipole interactions of cyano-group in the cyano-carbazole based molecular glass" *Solid State Commun*. **2005**, *136*, 585-590.

184. Venkateswararao, A.; Thomas, K. R. J.; Lee, C.-P.; Ho, K.-C. "Effect of auxiliary chromophores on the optical, electrochemical and photovoltaic properties of carbazole-based dyes" *Asian J. Org. Chem*. **2015**, *4*, 69-80.

185. Baheti, A.; Thomas, K. R. J.; Li, C.-T.; Lee, C.-P.; Ho, K.-C. "Fluorene-based sensitizers with a phenothiazine donor: Effect of mode of donor tethering on the performance of dye-sensitized solar cells" *ACS Appl. Mater. Interfaces* **2015**, *7*, 2249-2262.

186. Gupta, V. D.; Tathe, A. B.; Padalkar, V. S.; Patil, V. S.; Phatangare, K. R.; Umape, P. G.; Ramasami, P.; Sekar, N. "TDDFT investigation of the electronic structures and photophysical properties of fluorescent extended styryl push-pull chromophores containing carbazole unit" *J Fluoresc*. **2013**, *23*, 1121-1138.

187. Wang, Y.; Ma, J.; Jiang, Y. "Tuning of electronic structures of poly(*p*-phenylenevinylene) analogues of phenyl, thienyl, furyl, and pyrrolyl by double-bond linkages of group 14 and 15 elements" *J. Phys. Chem. A.* **2005,** *109*, 7197-7206.

188. Beeby, A.; Findlay, K.; Low, P. J.; Marder, T. B. "A re-evaluation of the photophysical properties of 1,4-bis(phenylethynyl)benzene: A model for poly(phenyleneethynylene)" J. *Am. Chem. Soc*. **2002**, *124*, 8280-8284.

189. Song, M.; Park, J. S.; Yoon, M.; Yoon, H. W.; Kim, A. J.; Jin, S.-H. "Synthesis and characterization of poly(carbazolyl-2,7-vinylene) derivatives for organic light-emitting diode applications" *Macromol Res*. **2010**, *18*, 1088-1095.

190. Wang, T.-T.; Chung, S.-M.; Wu, F.-Y.; Shu, C.-F.; Diau, E. W.-G. "Relaxation dynamics of 2,7- and 3,6-distyrylcarbazoles in solutions and in solid films: Mechanism for efficient nonradiative deactivation in the 3,6-linked carbazole" *J. Phys. Chem. B.* **2005,** *109*, 23827-23835.

191. Wu, F.-I.; Shih, P. -I.; Yuan, M.-C.; Dixit, A. K.; Shu, C.-F.; Chung, Z.-M.; Diau. E. W.-G. "Novel distyrylcarbazole derivatives as hole-transporting blue emitters for electroluminescent devices" *J. Mater. Chem.* **2005**, *15*, 4753-4760.

192. Bhaskar, A.; Ramakrishna, G.; Lu, Z.; Twieg, R.; Hales, J. M.; Hagan, D. J.; Stryland, E. V.; Goodson, T. "Investigation of two-photon absorption properties in branched alkene and alkyne chromophores" *J. Am. Chem. Soc*. **2006**, *128*, 11840-11849.

193. McNamara, L. E.; Liyanage, N.; Peddapuram, A.; Murphy, J. S.; Delcamp, J. H.; Hammer, N. I. "Donor-Aceptor-Donor thienopyrazines via Pd-catalyzed C-H activation as NIR fluorescent materials" *J. Org. Chem.* **2016**, *81*, 32-42.

194. Gong, S.; Zhao, Y.; Wang, M.; Yang, C.; Zhong, C.; Qin, J.; Ma, D. "Versatile benzimidazole/triphenylamine hybrids: Efficient nondoped deep blue electroluminescence and good host materials for phosphorescent emitters" *Chem. Asian J.* **2010**, *5*, 2093-2099.

195. Keerthi, A.; Valiyaveettil, S. "Regioisomers of perylenediimide: synthesis, photophysical, and electrochemical properties" *J. Phys. Chem. B*. **2012**, *116*, 4603-4614.

196. Yang, S.-W.; Elangovan, A.; Hwang, K.-C.; Ho, T.-I. "Electronic polarization reversal and excited state intramolecular charge transfer in donor/acceptor ethynylpyrenes" *J. Phys. Chem. B.* **2005,** *109*, 16628-16635.

197. Adhikari, R. M.; Mondal, R.; Shah, B. K.; Neckers, D. C. "Synthesis and photophysical properties of carbazole-based blue light-emitting dendrimers" *J. Org. Chem.* **2007**, *72*, 4727-4732.

198. Zhu, L.; Shan, Y.; Wang, R.; Liu, D.; Zhong, C.; Song, Q.; Wu, F. "High-efficiency perovskite solar cells based on new TPE compounds as hole transport materials: The

role of 2,7- and 3,6- substituted carbazole derivatives" *Chem. Eur. J.* **2017**, *23*, 4373-4379.

199. Chandrasekaran, N.; Gann, E.; Jain, N.; Kumar, A.; Gopinathan, S.; Sadhanala, A.; Friend, R. H.; Kumar, A.; McNeill, C. R.; Kabra, D. "Correlation between photovoltaic performance and interchain ordering induced delocalization of electronics states in conjugated polymer blends" *ACS Appl. Mater. Interfaces* **2016**, *8*, 20243-20250.
200. Thomas, K. R. J.; Kapoor, N.; Bolisetty, M. N. K. P.; Jou, J.-H.; Chen, Y.-L.; Jou, Y.-C. "Pyrene-fluorene hybrids containing acetylene linkage as color tunable emitting materials for organic light-emitting diodes" *J. Org. Chem.* **2012**, *77*, 3921-3932.
201. Reghu, R. R.; Grazulevicius, J. V.; Simokaitiene, J.; Miasojedovas, A.; Kazlauskas, K.; Jursenas, S.; Data, P.; Karon, K.; Lapkowski, M.; Gaidelis, V.; Jankauskas, V. "Glass-forming carbazolyl and phenothiazinyl tetra substituted pyrene derivatives: Photophysical, electrochemical and photoelectrical Properties" *J. Phys. Chem. C.* **2012**, *116*, 15878-15887.
202. Chercka, D.; Yoo, S.-J.; Baumgarten, M.; Kim, J.-J.; Mullen, K. "Pyrene based materials for exceptionally deep blue OLEDs" *J. Mater. Chem. C.* **2014**, *2*, 9083-9086.
203. Zhang, R.; Zhao, Y.; Zhang, T.; Xu, L.; Ni, Z. "A series of short axially symmetrically 1,3,6,8-tetrasubstituted pyrene-based green and blue emitters with 4-*tert*-butylphenyl and arylamine attachments" *Dyes Pigm.* **2016**, *130*, 106-115.
204. Xing, Y.; Xu, X.; Zhang, P.; Tian, W.; Yu, G.; Lu, P.; Liu, Y.; Zhu, D. "Carbazole–pyrene-based organic emitters for electroluminescent device" Chem. Phys. Lett. 205, 408, 169-173.
205. Zhao, Z.; Zhang, P.; Wang, F.; Wang, Z.; Lu, P.; Tian, W. "Blue light-emitting, electron-transporting materials based on ethynyl-linked D–A systems" *Chem. Phys. Lett.* **2006**, *423*, 293-296.
206. Liang, Z.-Q.; Chu, Z.-Z.; Yang, J.-X.; Yuan, C.-X.; Tao, X.-T.; Zou, D.-C. "X-shaped tetra-substituted pyrenes: Synthesis, photophysics, and electroluminescence" *Synth. Met.* **2011**, *161*, 1691-1698.

207. Salunke, J. K.; Wong, F. L.; Feron, K.; Manzhos, S.; Lo, M. F.; Shinde, D.; Patil, A.; Lee, C. S.; Roy, V. A. L.; Sonar, P.; Wadgaonkar, P. P. "Phenothiazine and carbazole substituted pyrene based electroluminescent organic semiconductors for OLED devices*" J. Mater. Chem. C*. **2016**, *4*, 1009-1018.

208. Konidena, R. K.; Thomas, K. R. J.; Singh, M.; Jou, J.-H. "Thienylphenothiazine integrated pyrenes: an account on the influence of substitution patterns on their optical and electroluminescence properties" *J. Mater. Chem. C*. **2016**, *4*, 4264-4258.

209. Kasha, M. "Energy transfer mechanisms and the molecular exciton model for molecular aggregates" *Radiat. Res.* **1963**, *20*, 55-70.

210. de Halleux, V.; Calbert, J.-P.; Brocorens, P.; Cornil, J.; Declercq, J.-P.; Bredas, J.-L.; Geerts, Y. "1,3,6,8-tetraphenylpyrene derivatives: towards fluorescent liquid-crystalline columns?" *Adv. Funct. Mater*. **2004**, *14*, 649-659.

211. Patalag, L. J.; Ho, L. P.; Jones, P. G.; Werz, D. B. "Ethylene-bridged oligo-BODIPYs: Access to intramolecular *J*-aggregates and superfluorophores" *J. Am. Chem. Soc*. **2017**, *139*, 15104-15113.

212. Mahar, J.; Saeed, A.; Belfield, K. D.; Iqbal, A.; Irfan, M.; Shabir, G.; Larik, F. A.; Channar, P. A. "An investigation of the effect of conjugation on fluorene based chromophores: Optoelectronic and electrochemical behavior" *Dyes Pigm*. **2017**, *147*, 385-392.

213. Miller, M. A.; Lammi, R. K.; Prathapan, S.; Holten, D.; Lindsey, J. S. "A tightly coupled linear array of perylene Bis(porphyrin) and phthalocyanine units that function as a photoinduced energy transfer cascade" *J. Org. Chem*. **2000**, *65*, 6634-6649.

214. Lee, Y. O.; Pradhan, T.; Yoo, S.; Kim, T. H.; Kim, J.; Kim, J. S. "Enhanced electrogenerated chemiluminescence of phenylethynylpyrene derivatives: Use of weakly electron-donating group as a substituent" *J. Org. Chem*. **2012**, *77*, 11007-11013.

215. Toyota, S. "Rotational isomerism involving acetylene carbon" *Chem. Rev*. **2010**, *110*, 5398-5424.

216. Kim, M.; Jeon, S. K.; Hwang, S.-H.; Lee, S.-S.; Yu, E.; Lee, J. Y. "Highly efficient and color tunable thermally activated delayed fluorescent emitters using a "twin emitter" molecular design" *Chem. Commun*, **2016**, *52*, 339-342.

217. Taneda, M.; Shizu, K.; Tanaka, H.; Adachi, C. "High efficiency thermally activated delayed fluorescence based on 1,3,5-tris(4-(diphenylamino)phenyl)-2,4,6-tricyanobenzene" *Chem. Commun.* **2015**, *51*, 5028-5031.

218. Pati, P. B.; Yang, W.; Zade, S. S. "New dyes for DSSC containing triphenylamine based extended donor: Synthesis, photophysical properties and device performance" *Spectrochim. Acta A.* **2017**, *178*, 106-113.

219. Iqbal, A.; Lee, S. H.; Park, O. O.; Siddiqi, H. M.; Akhter, T. "Synthesis and characterization of blue light emitting redox-active polyimides bearing a noncoplanar fused carbazole-triphenylamine unit" *New J. Chem.* **2016**, *40*, 5285-5293.

220. Venkateswararao, A.; Thomas, K. R. J.; Lee, C.-P.; Ho, K.-C. "Synthesis and characterization of organic dyes containing 2,7-disubstituted carbazole π-linker" *Tetrahedron Lett.* **2013**, *54*, 3985-3989.

221. Thiery, S.; Tondelier, D.; Geffroy, B.; Jeannin, O.; Berthelot, J. R.; Poriel, C. "Modulation of the physicochemical properties of donor-spiro-acceptor derivatives through donor unit planarisation: Phenylacridine versus indoloacridine-new hosts for green and blue phosphorescent organic light-emitting diodes (PhOLEDs)" *Chem. Eur. J.* **2016**, *22*, 10136-10149.

222. Reichardt, C. "Solvatochromic dyes as solvent polarity indicators" *Chem. Rev.* **1994**, *94*, 2319-2358.

223. Jacques, P. "On the relative contributions of nonspecific and specific interactions to the unusual solvatochromism of a typical merocyanine dye" *J . Phys. Chem.* **1986**, *90*, 5535-5539.

224. Palayangoda, S. S.; Cai, X.; Adhikari, R. M.; Neckers, D. C. "Carbazole-based donor-acceptor compounds: Highly fluorescent organic nanoparticles" *Org. Lett.* **2008**, *10*, 281-284.

225. Li, H.; Parameswaran, M.; Nurmawati, M. H.; Xu, Q.; Valiyaveettil, S. "Synthesis and structure-property investigation of polyarenes with conjugated side chains" *Macromolecules* **2008**, *41*, 8473-8482.

226. Lu, X.; Fan, S.; Wu, J.; Jia, X.; Wang, Z.-S.; Zhou, G. "Controlling the charge transfer in D-A-D chromophores based on pyrazine derivatives" *J. Org. Chem.* **2014**, 79, 6480-6489.

227. Thomas, K. R. J.; Lin, J. T.; Tao, Y.-T.; Chuen, C.-H. "Star shaped thieno-[3,4-b]-pyrazines: A new class of red emitting electroluminescent materials*" Adv. Mater*. **2002**, *14*, 822-826.

228. Deng, Y.; Yuan, W.; Jia, Z.; Liu, G. "H- and J-aggregation of fluorene-based chromophores" *J. Phys. Chem. B* **2014**, *118*, 14536-14545.

229. Sherwood, G. A.; Cheng, R.; Smith, T. M.; Werner, J. H.; Shreve, A. P.; Peteanu, L. A.; Wildeman, J. "Aggregation effects on the emission spectra and dynamics of model oligomers of MEH-PPV" *J. Phys. Chem. C* **2009,** *113*, 18851-18862.

230. Gupta, V. D.; Tathe, A. B.; Padalkar, V. S.; Umape, P. G.; Sekar, N. "Red emitting solid state fluorescent triphenylamine dyes: Synthesis, photo-physical property and DFT study" *Dyes Pigm*. **2013**, *97*, 429-439.

231. Salbeck, J.; Yu, N.; Bauer, J.; Weissortel, F.; Bestgen, H. "Low molecular organic glasses for blue electroluminescence" *Synth. Met*. **1997**, *91*, 209-215.

232. Yu, F.; Wang, M.; Sun, H.; Shan, Y.; Du, M.; Khan, A.; Usman, R.; Zhang, W.; Shana, H.; Xu, C. "Tuning the solid-state fluorescence of chalcone crystals via molecular coplanarity and J-aggregate formation" *RSC Adv*. **2017**, *7*, 8491-8503.

233. Zhao, X.; Wang, S.; You, J.; Zhang, Y.; Li, X. "Solution-processed thermally stable amorphous films of small molecular hole injection/transport bi-functional materials and their application in high efficiency OLEDs" *J. Mater. Chem. C*. **2015**, *3*, 11377-11384.

234. Khunchalee, J.; Tarsang, R.; Prachumrak, N.; Jungsuttiwong, S.; Keawin, T.; Sudyoadsuk, T.; Promarak, V. "Synthesis and properties of oligofluorene-thiophenes as emissive materials for organic electroluminescent devices: color-tuning from deep blue to orange" *Tetrahedron* **2012**, *68*, 8416-8423.

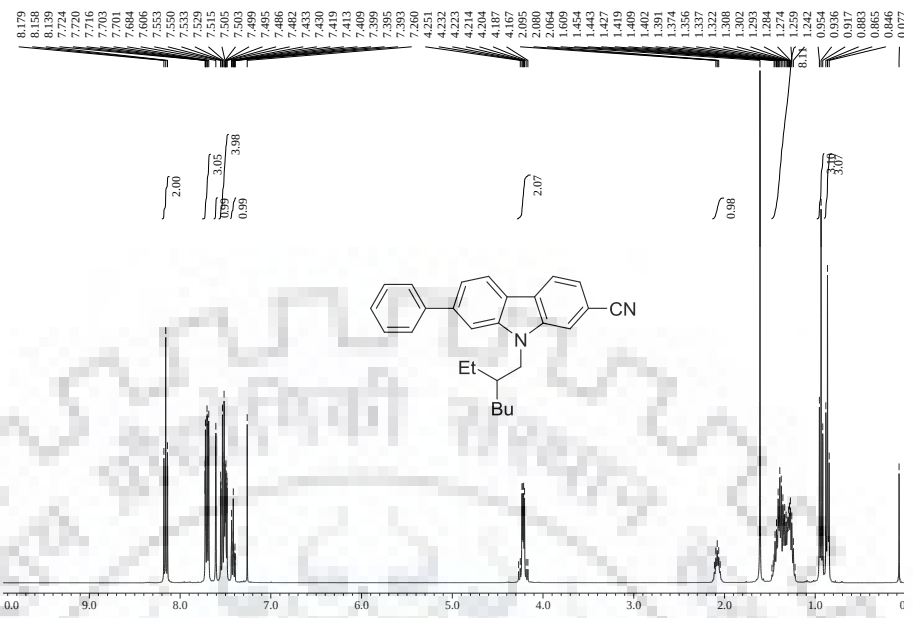

Figure S1 ^{1}H NMR spectrum for **4a** recorded in $CDCl_3$.

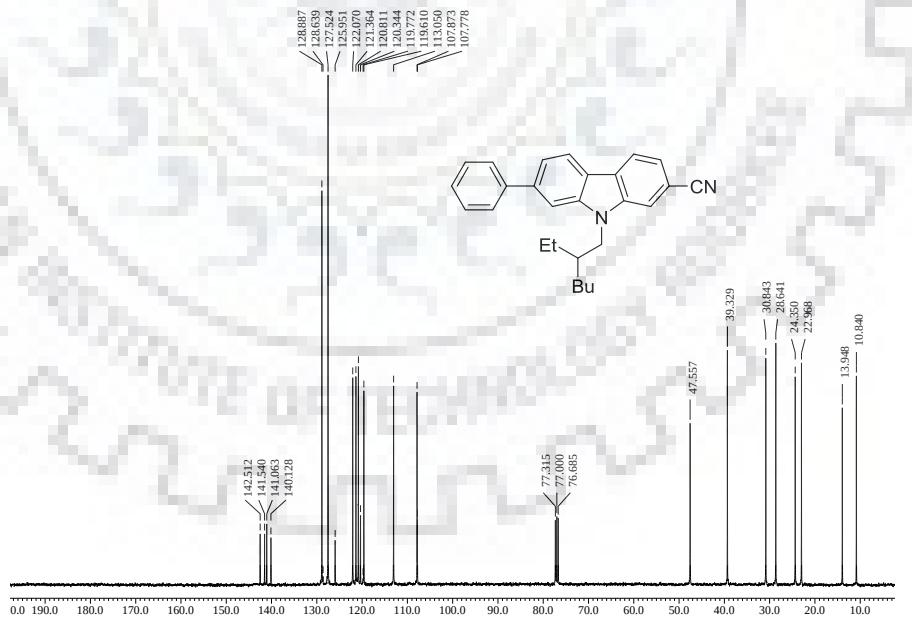

Figure S2 ^{13}C NMR spectrum for **4a** recorded in $CDCl_3$.

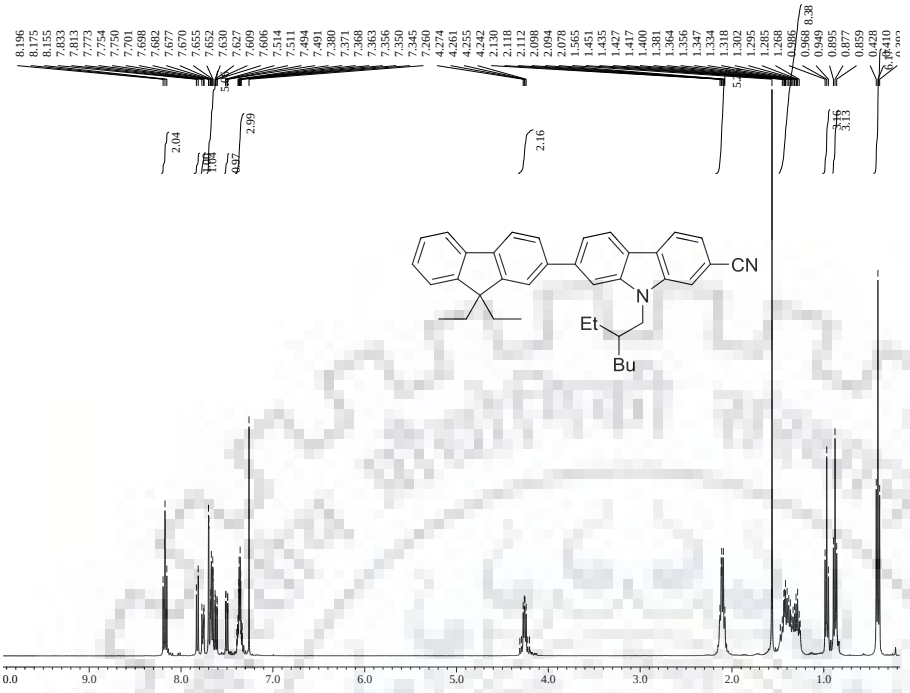

Figure S3 ^{1}H NMR spectrum for **4b** recorded in $CDCl_3$.

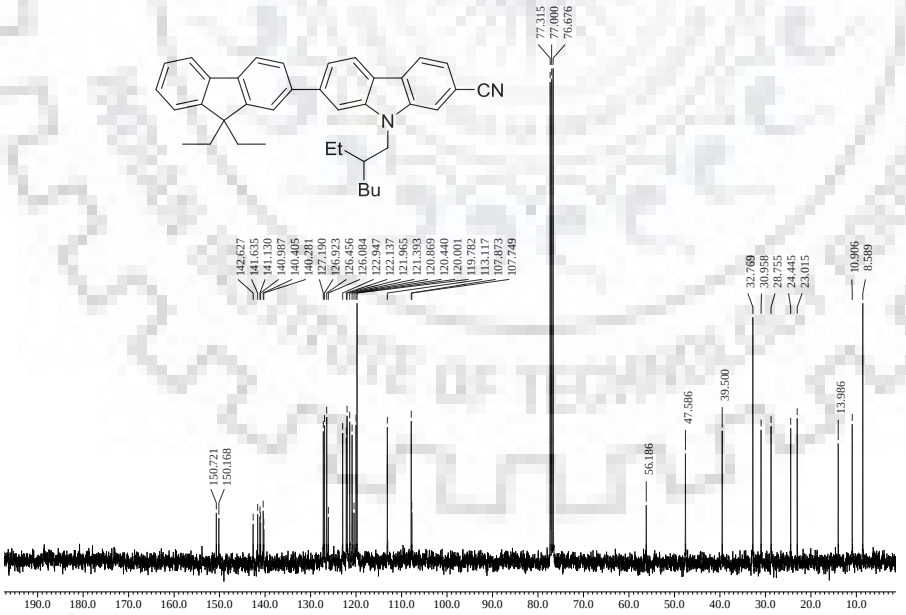

Figure S4 ^{13}C NMR spectrum for **4b** recorded in $CDCl_3$.

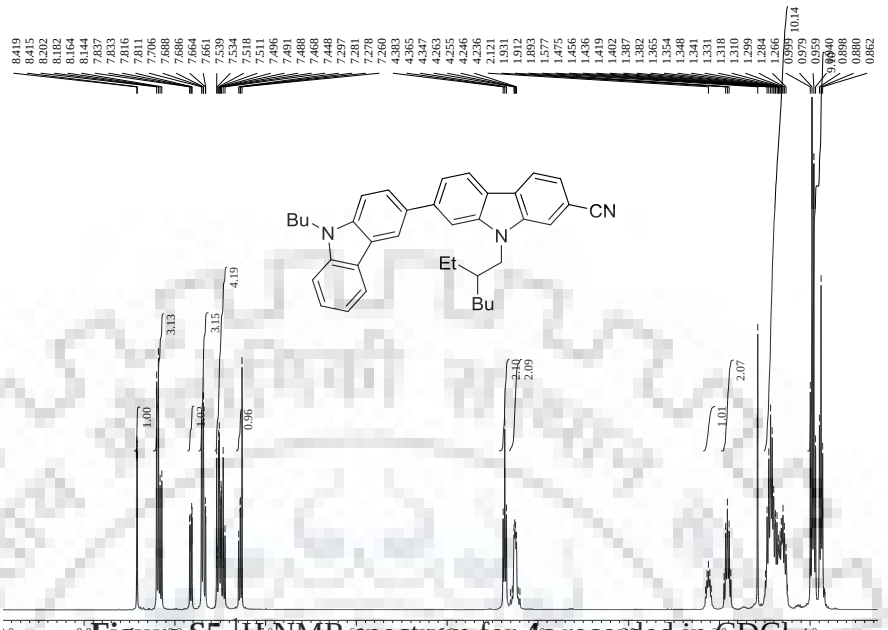

Figure S5 ^{1}H NMR spectrum for **4c** recorded in $CDCl_3$.

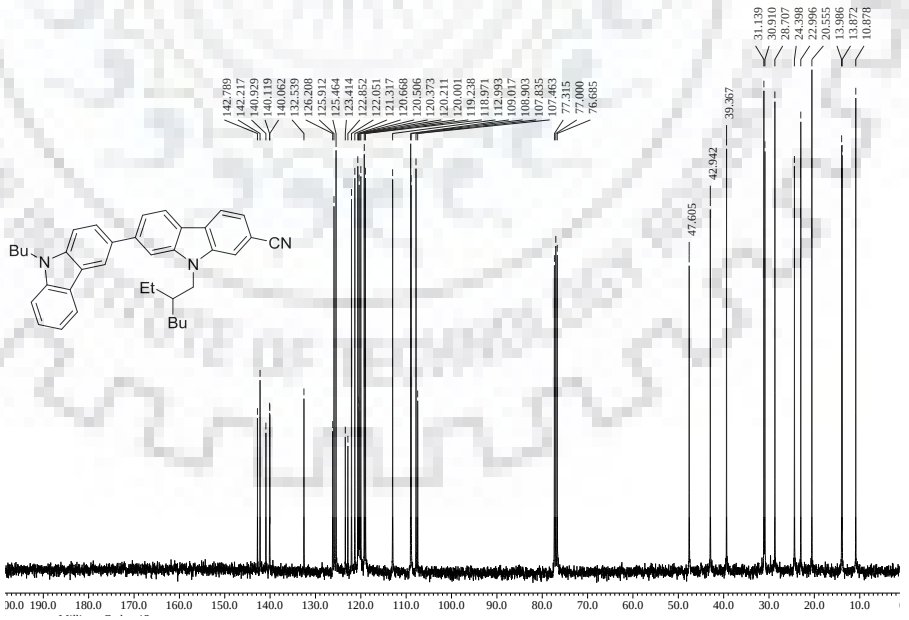

Figure S6 ^{13}C NMR spectrum for **4c** recorded in $CDCl_3$.

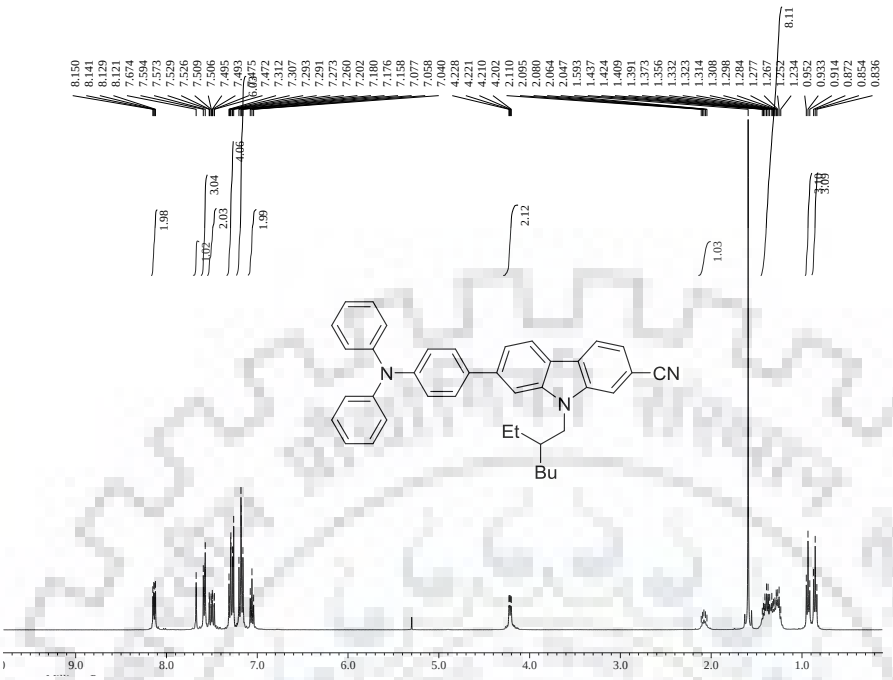

Figure S7 ^{1}H NMR spectrum for **4d** recorded in $CDCl_3$.

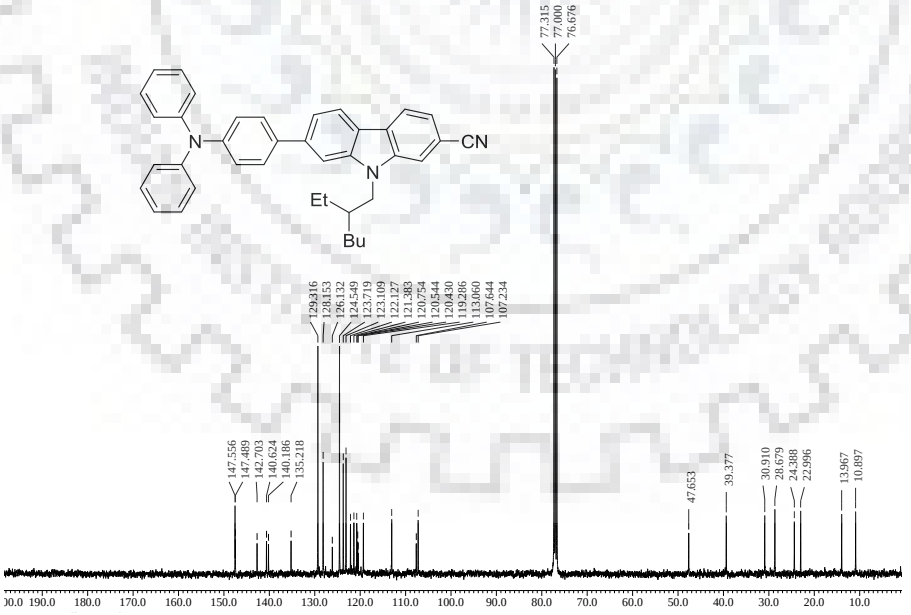

Figure S8 ^{13}C NMR spectrum for **4d** recorded in $CDCl_3$.

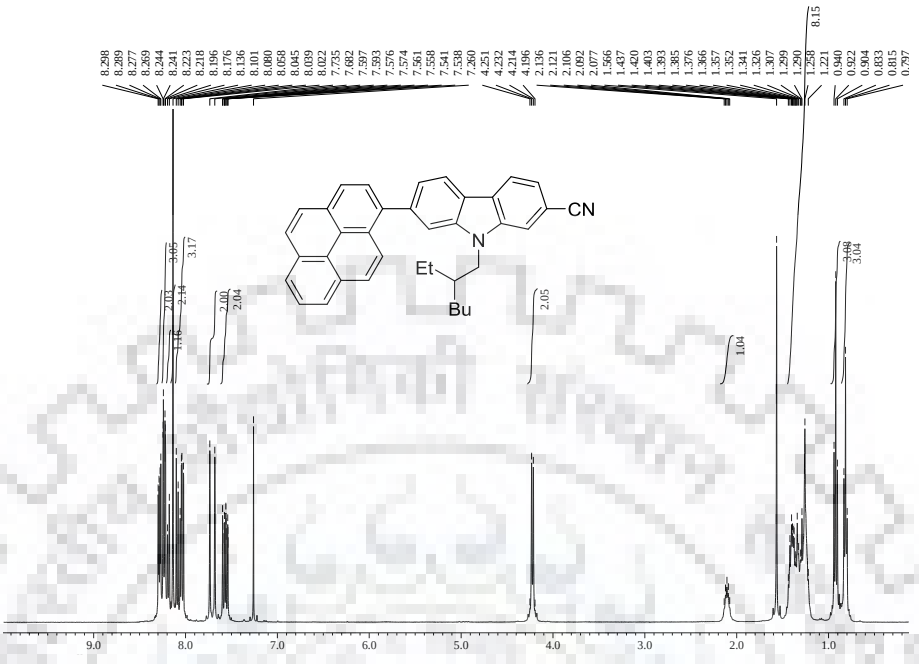

Figure S9 ^{1}H NMR spectrum for **4e** recorded in $CDCl_3$.

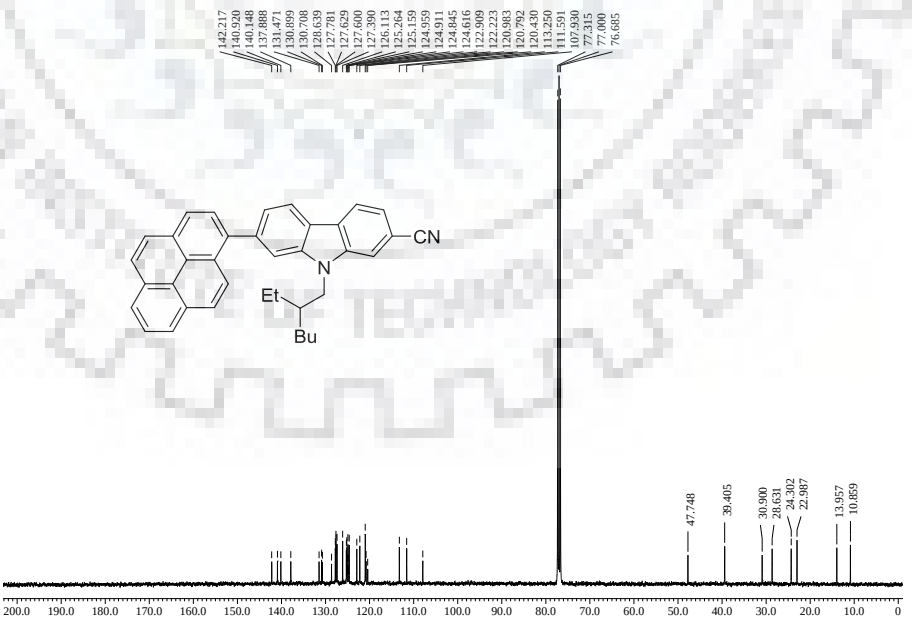

Figure S10 ^{13}C NMR spectrum for **4e** recorded in $CDCl_3$.

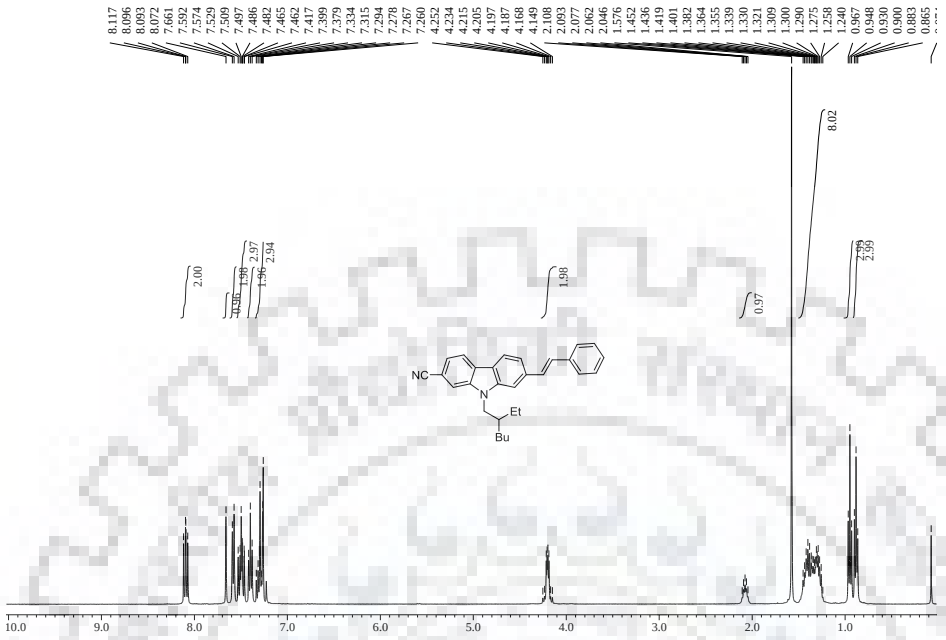

Figure S11 ^{1}H NMR spectrum of **8a** recorded in $CDCl_3$.

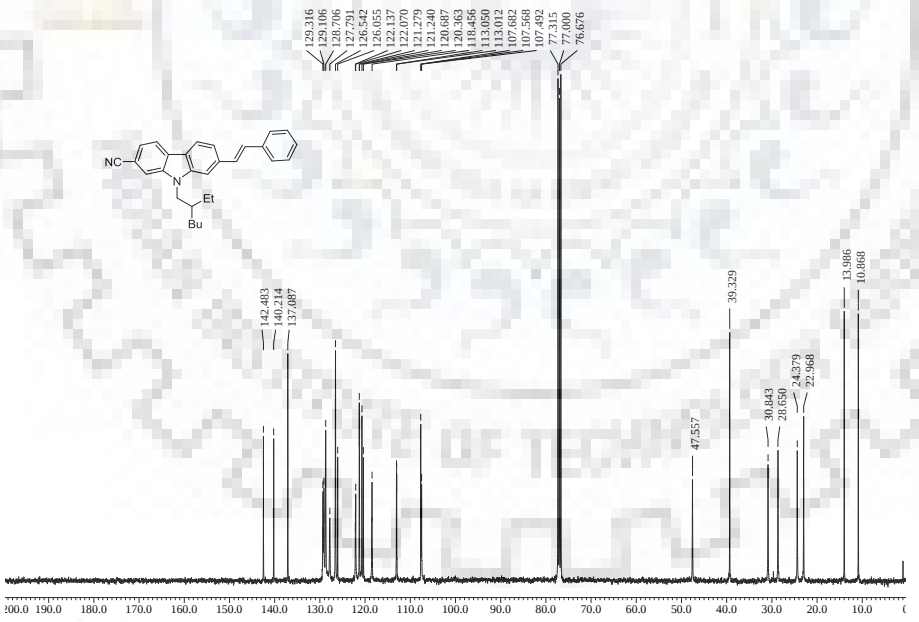

Figure S12 ^{13}C NMR spectrum of **8a** recorded in $CDCl_3$.

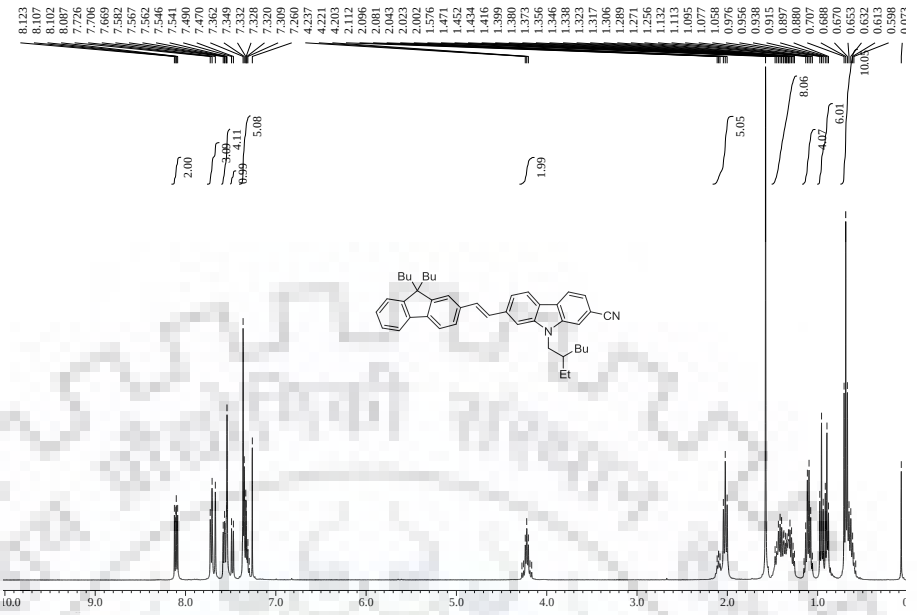

Figure S13 ^{1}H NMR spectrum of **8b** recorded in $CDCl_3$.

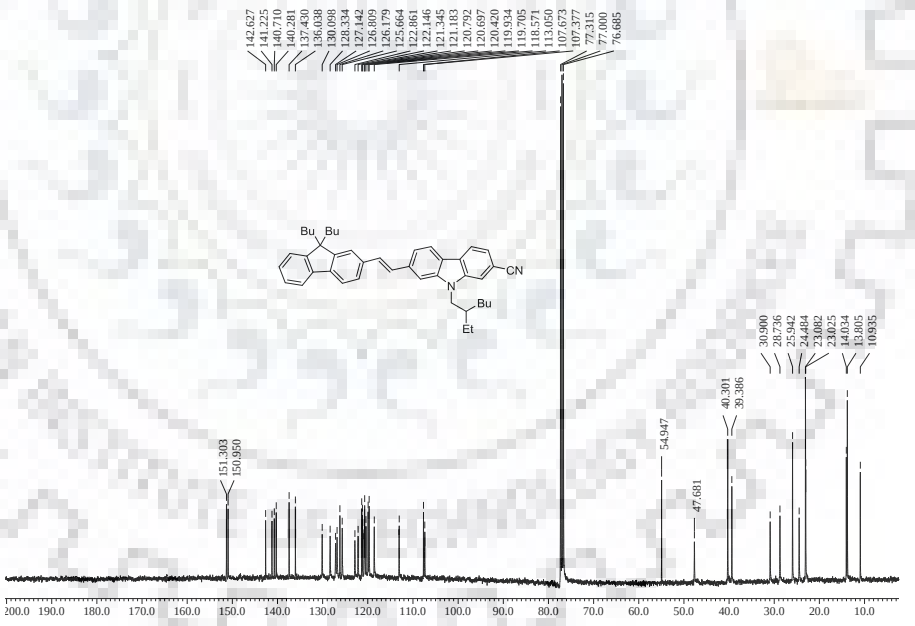

Figure S14 ^{13}C NMR spectrum of **8b** recorded in $CDCl_3$.

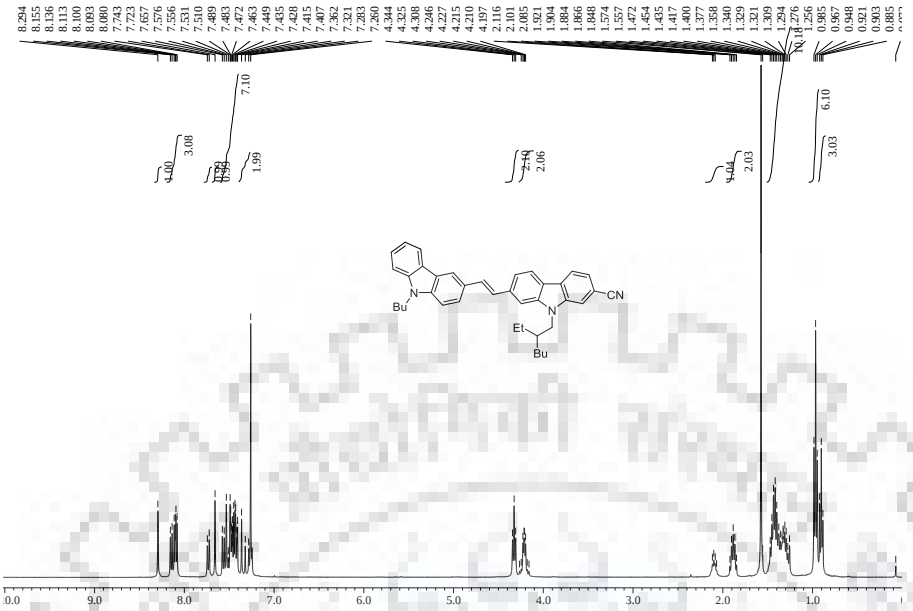

Figure S15 ^{1}H NMR spectrum of **8c** recorded in $CDCl_3$.

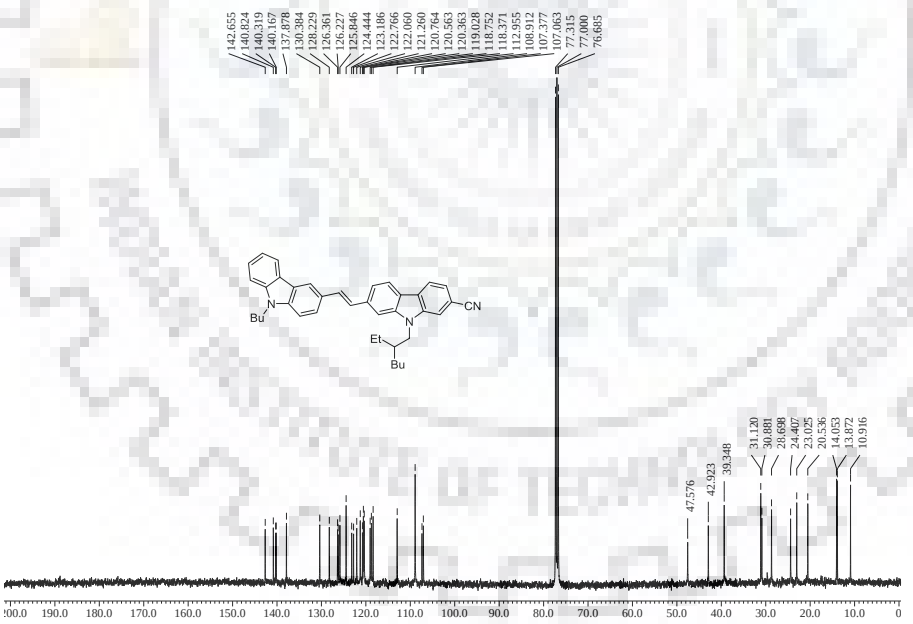

Figure S16 ^{13}C NMR spectrum of **8c** recorded in $CDCl_3$.

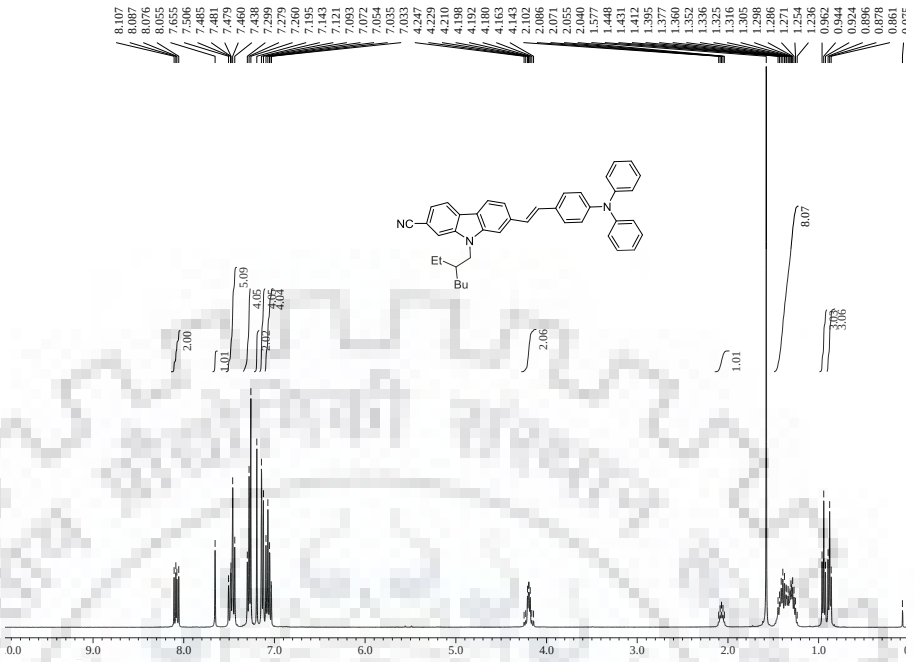

Figure S17 ^{1}H NMR spectrum of **8d** recorded in $CDCl_3$.

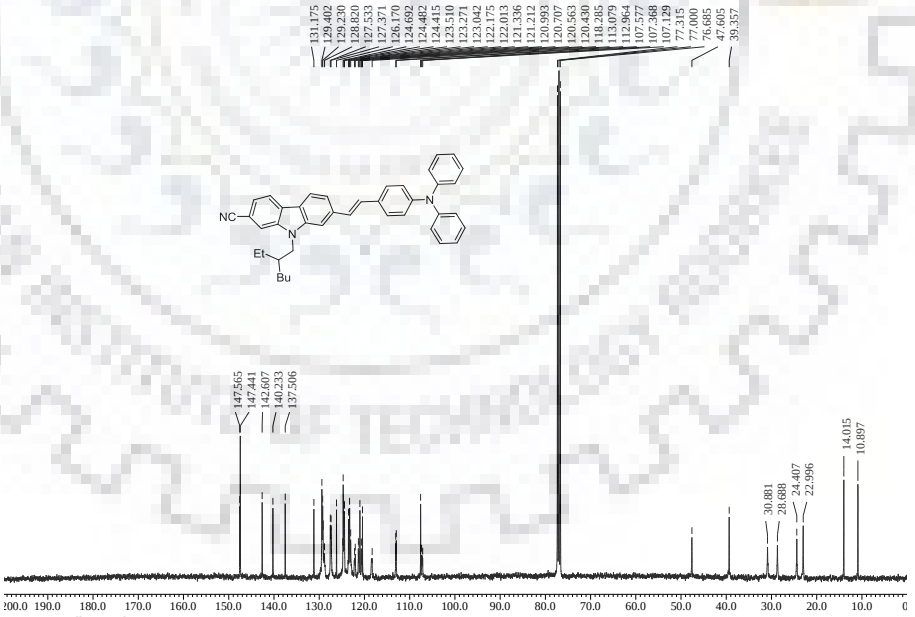

Figure S18 ^{13}C NMR spectrum of **8d** recorded in $CDCl_3$.

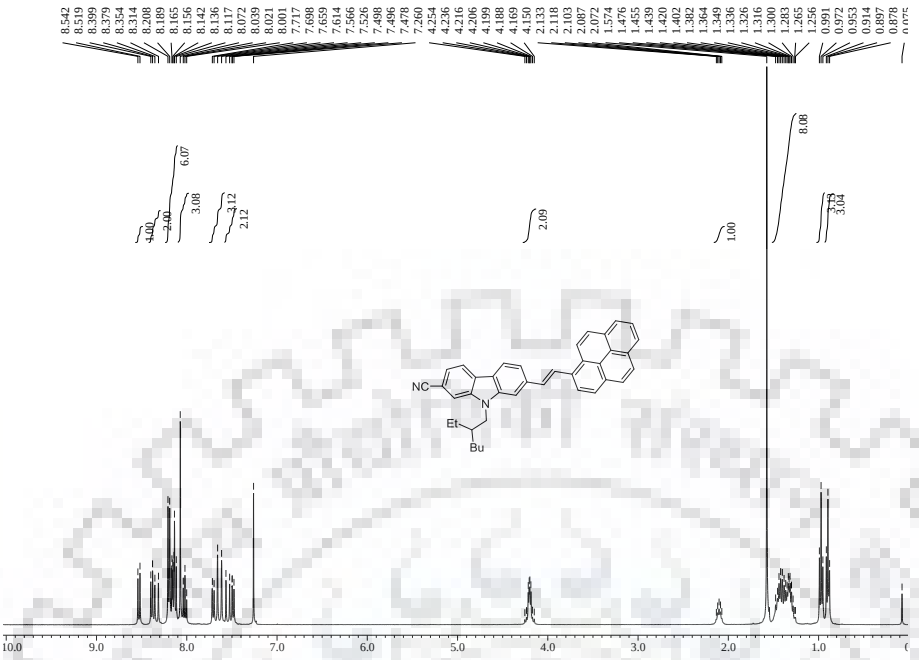

Figure S19 ^{1}H NMR spectrum of **8e** recorded in $CDCl_3$.

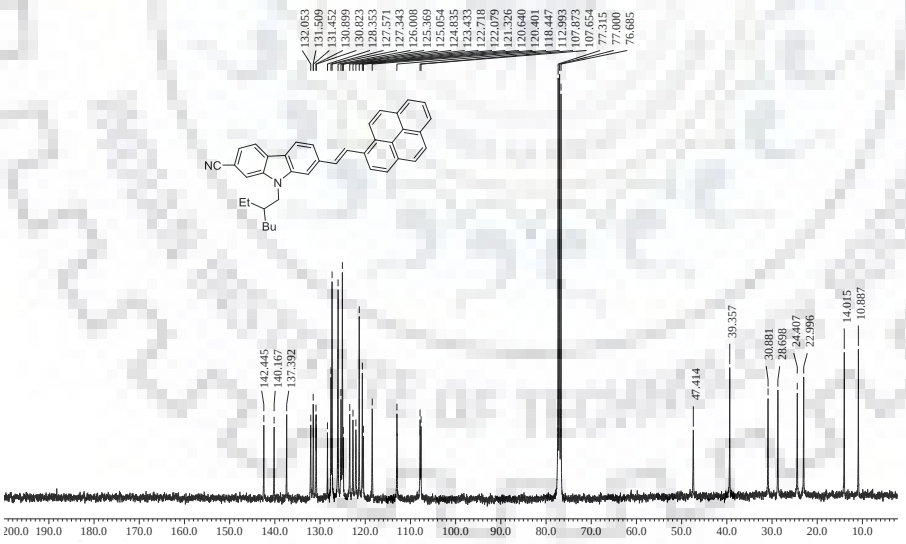

Figure S20 ^{13}C NMR spectrum of **8e** recorded in $CDCl_3$.

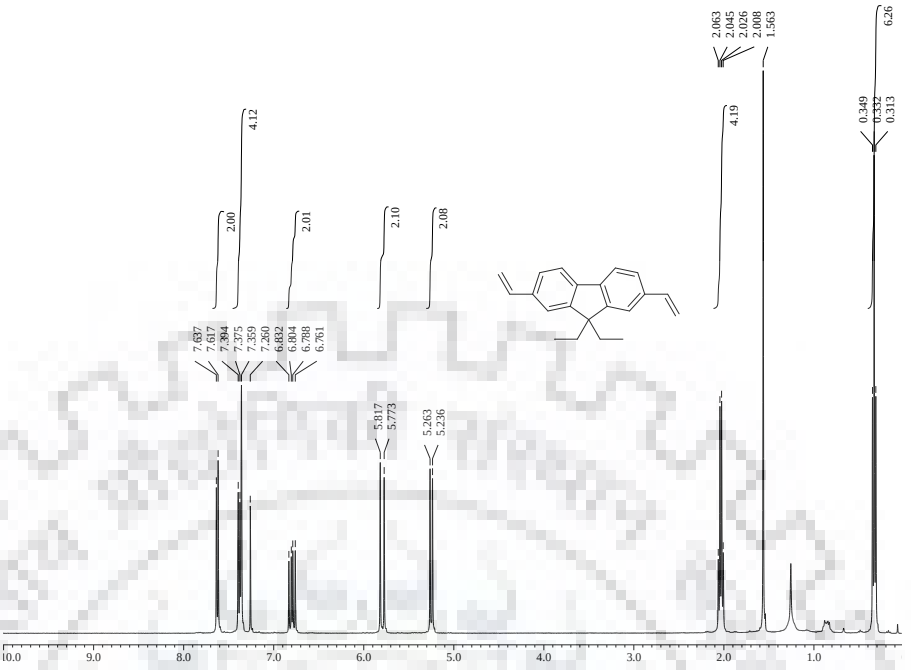

Figure S21 ^{1}H NMR spectrum of **13a** recorded in $CDCl_3$.

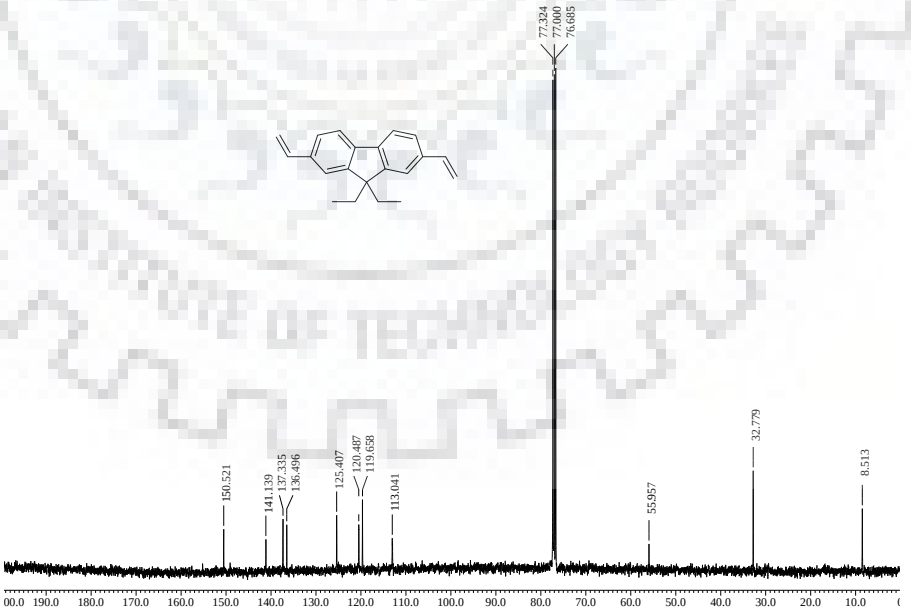

Figure S22 ^{13}C NMR spectrum of **13a** recorded in $CDCl_3$.

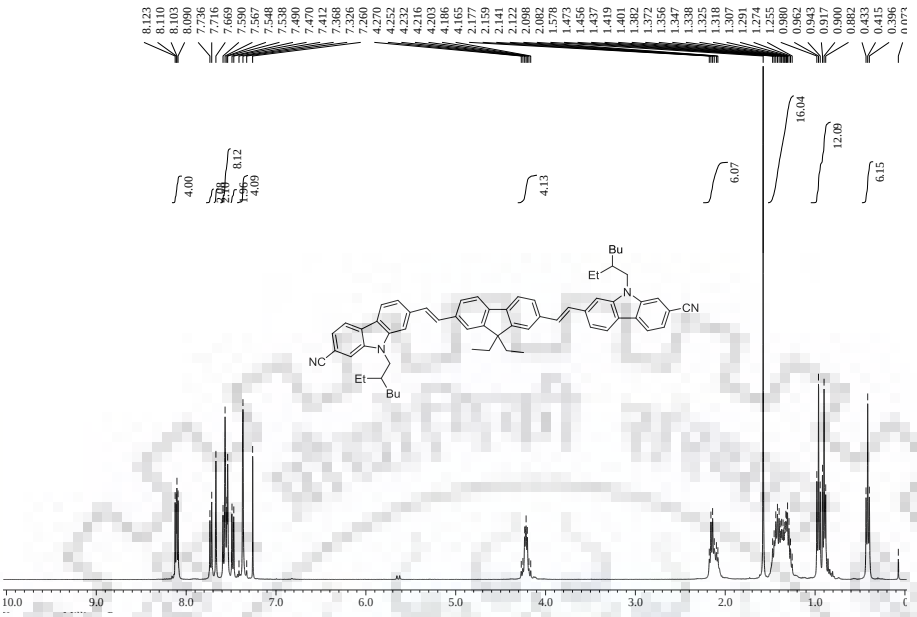

Figure S23 ^{1}H NMR spectrum of **14a** recorded in $CDCl_3$.

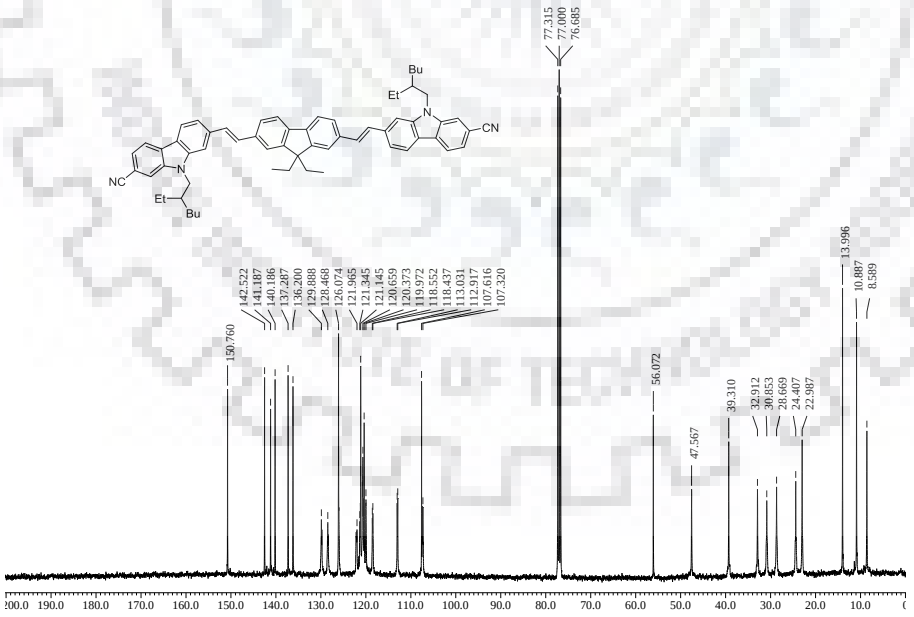

Figure S24 ^{13}C NMR spectrum of **14a** recorded in $CDCl_3$.

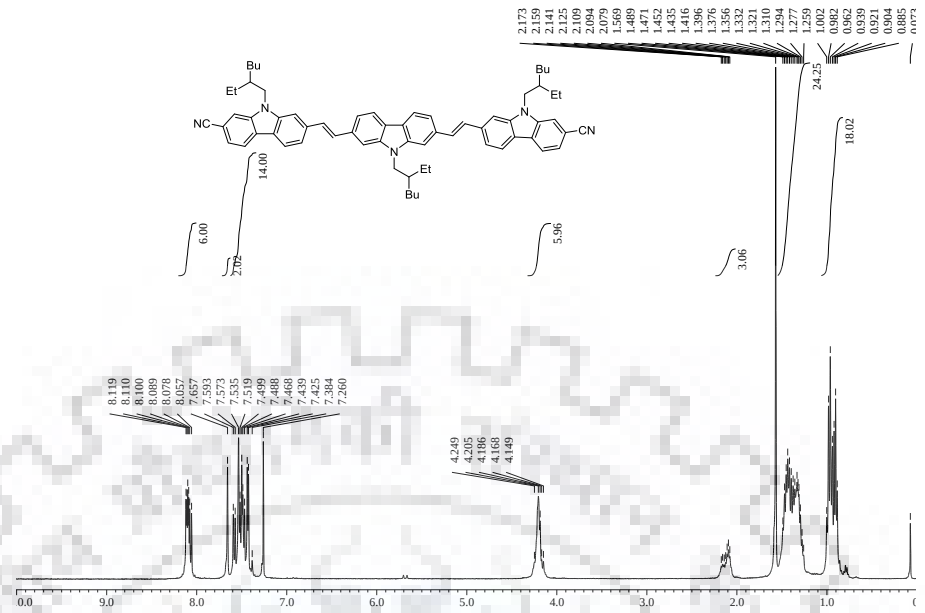

Figure S25 ^{1}H NMR spectrum of **14b** recorded in $CDCl_3$.

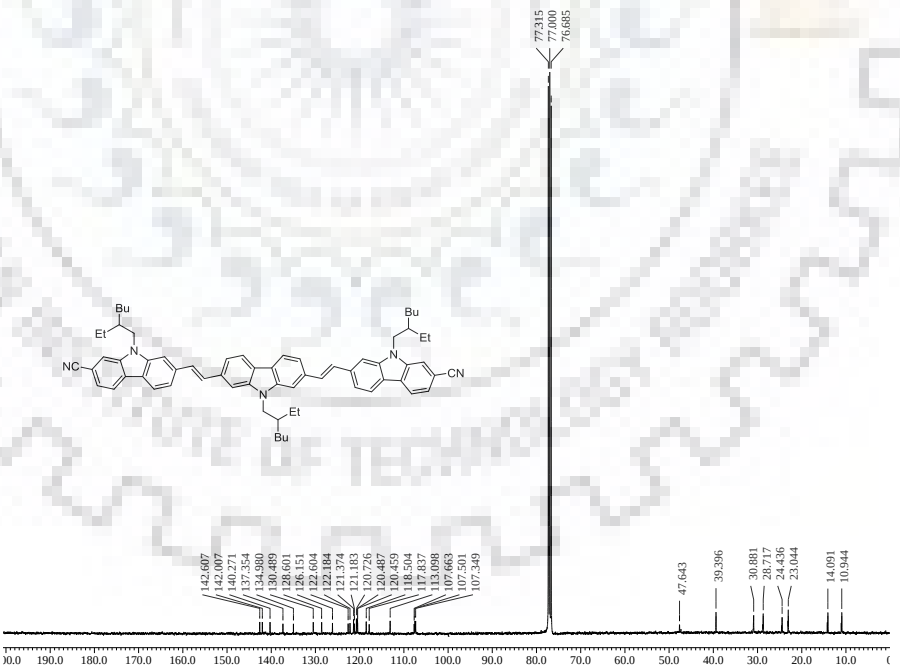

Figure S26 ^{13}C NMR spectrum of **14b** recorded in $CDCl_3$.

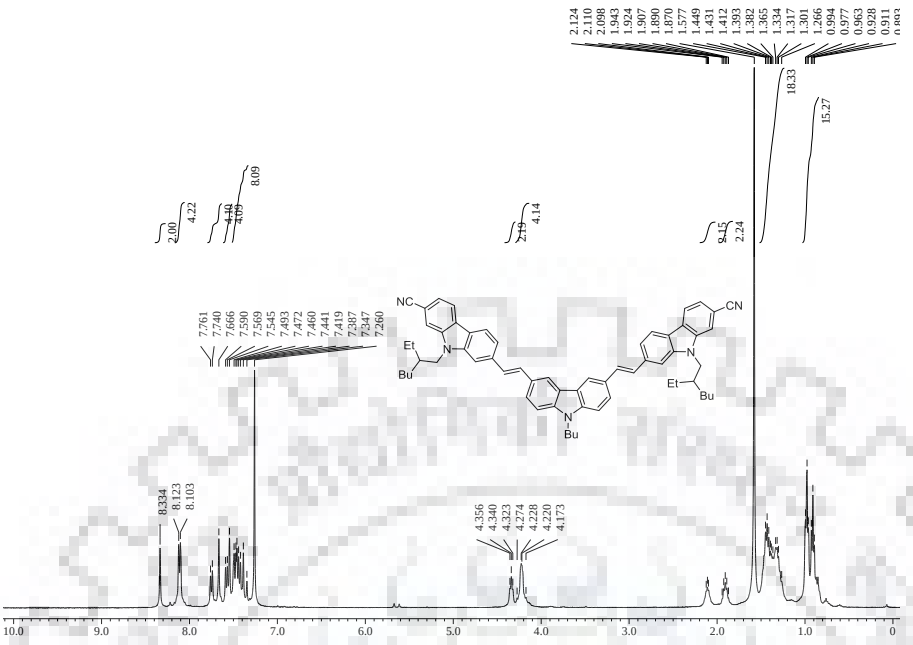

Figure S27 ^{1}H NMR spectrum of **14c** recorded in $CDCl_3$.

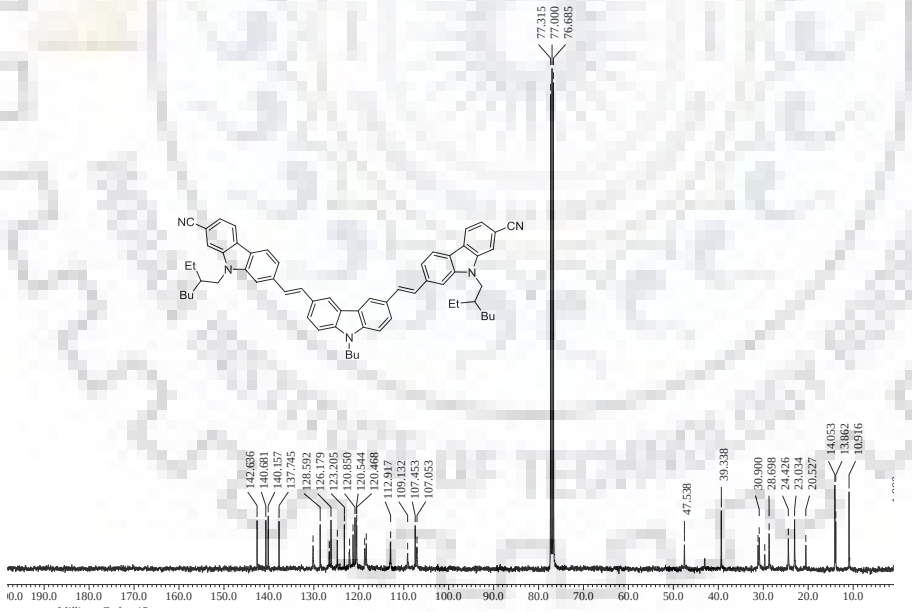

Figure S28 ^{13}C NMR spectrum of **14c** recorded in $CDCl_3$.

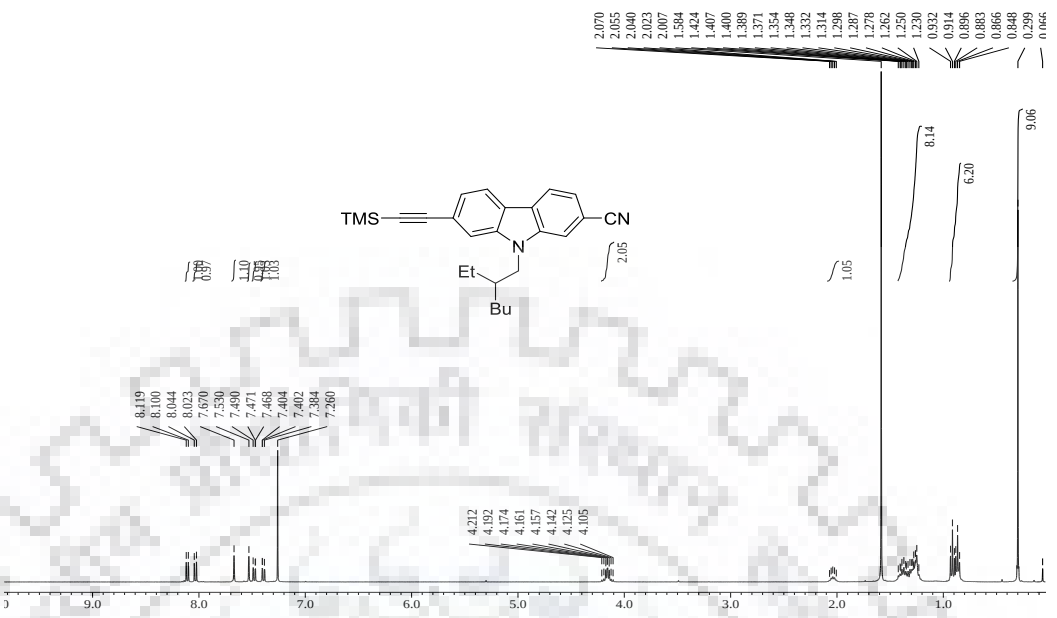

Figure S29 ^{1}H NMR spectrum of **15** recorded in $CDCl_3$.

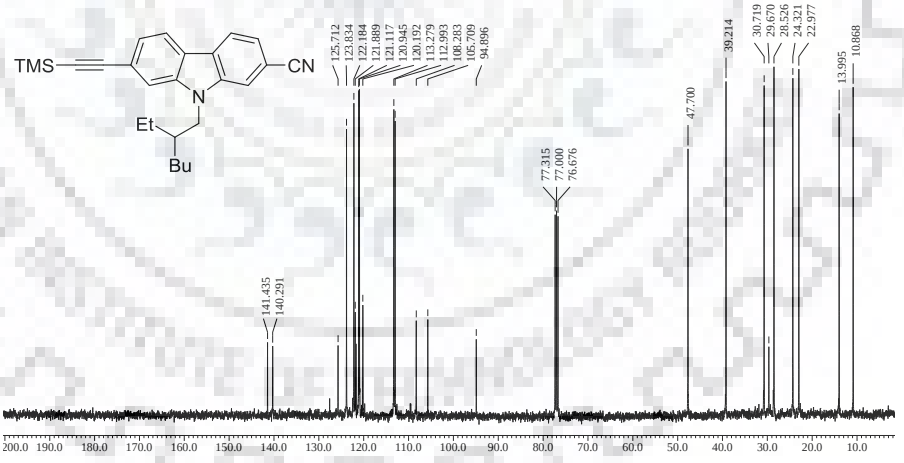

Figure S30 ^{13}C NMR spectrum of **15** recorded in $CDCl_3$.

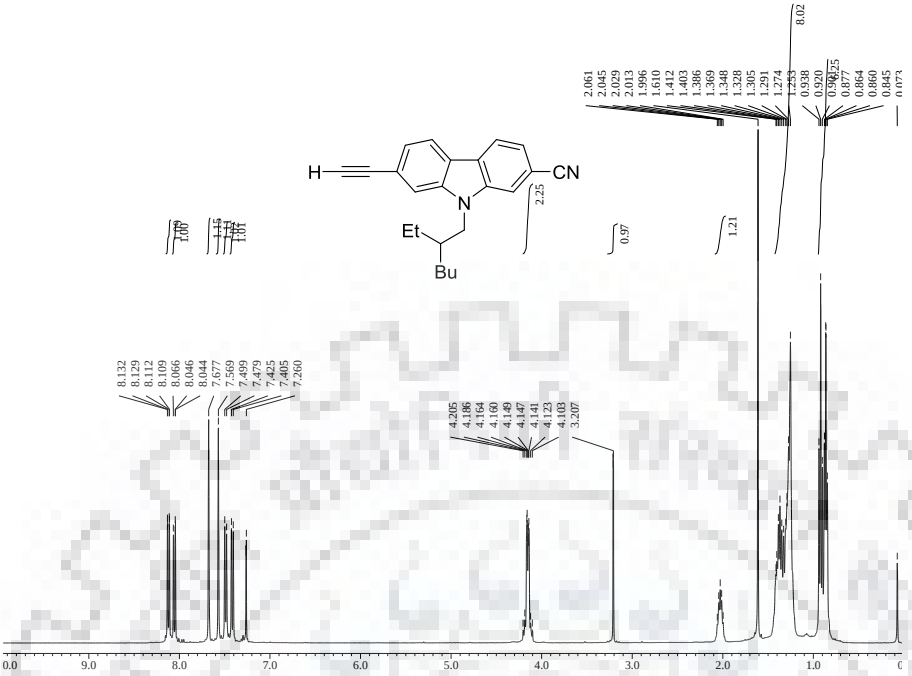

Figure S31 ^{1}H NMR spectrum of **16** recorded in $CDCl_3$.

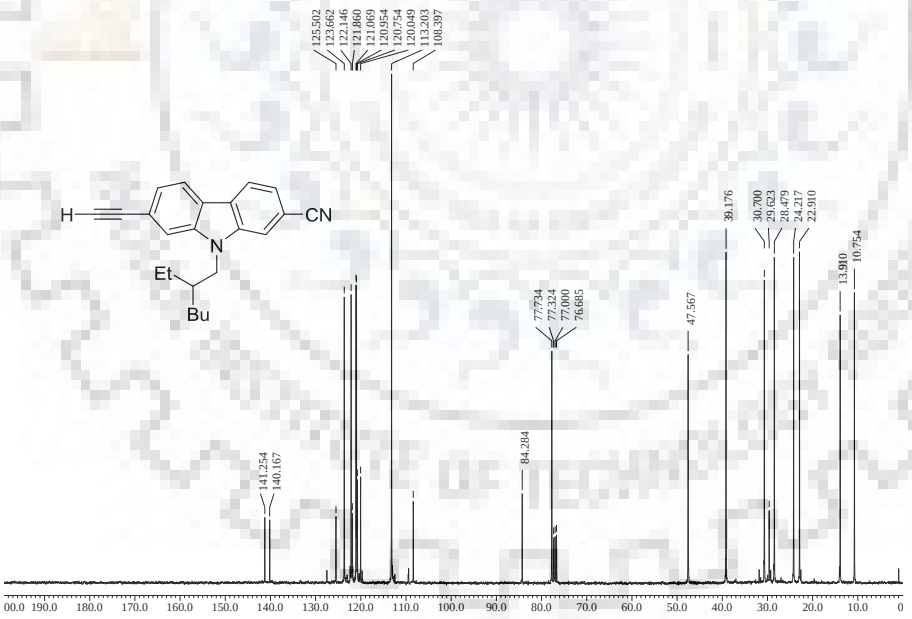

Figure S32 ^{13}C NMR spectrum of **16** recorded in $CDCl_3$.

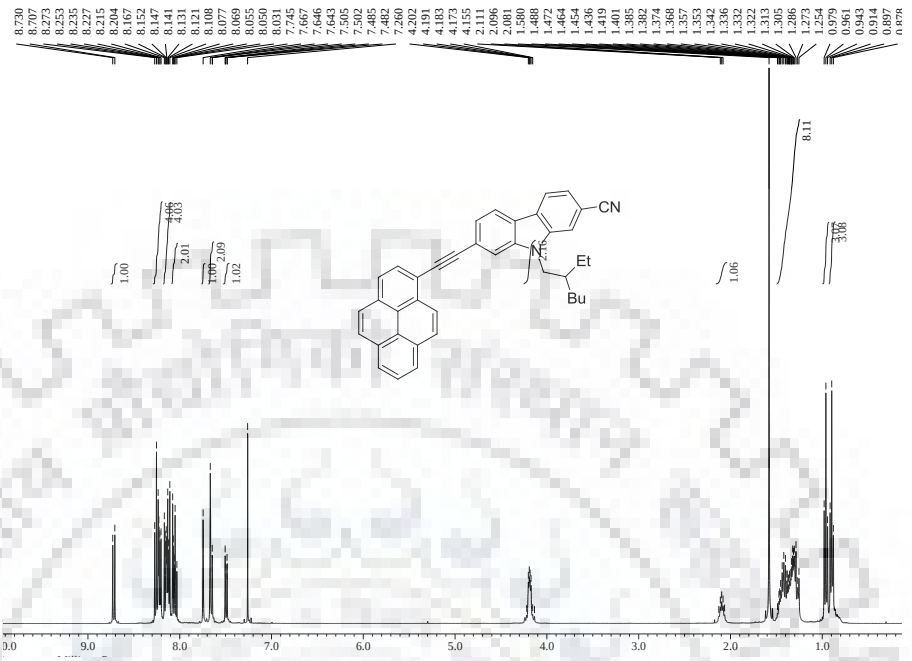

Figure S33 ^{1}H NMR spectrum of **18a** recorded in $CDCl_3$.

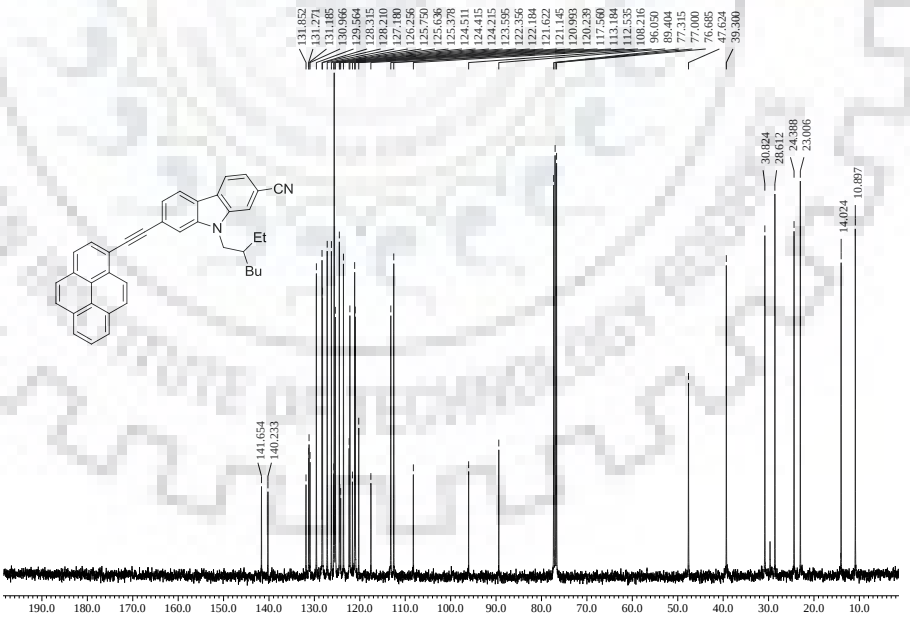

Figure S34 ^{13}C NMR spectrum of **18a** recorded in $CDCl_3$.

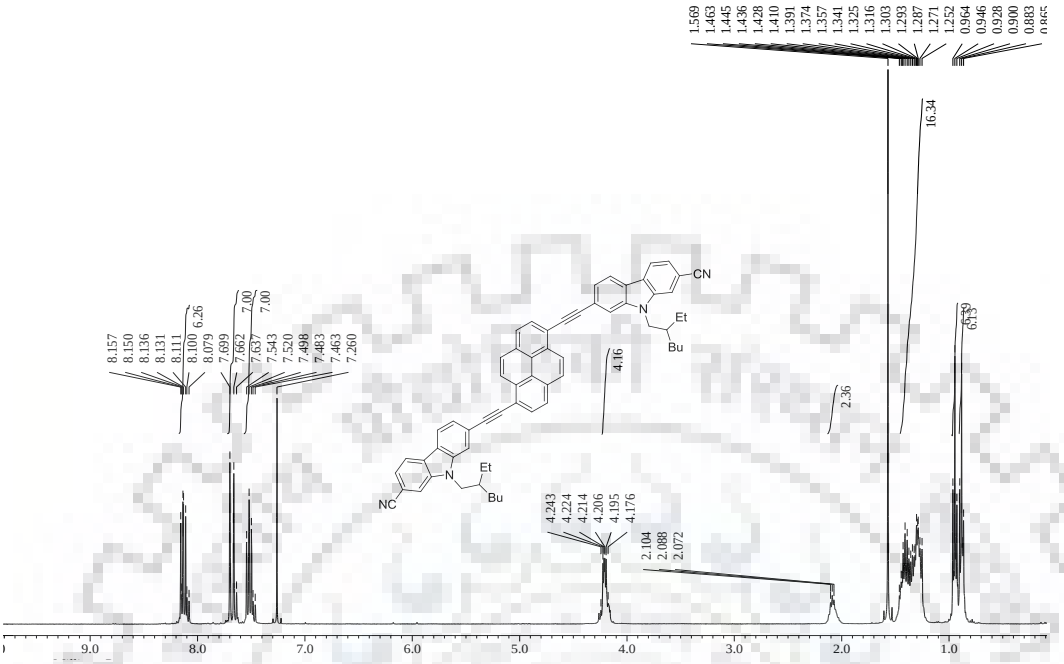

Figure S35 ^{1}H NMR spectrum of **18b** recorded in $CDCl_3$.

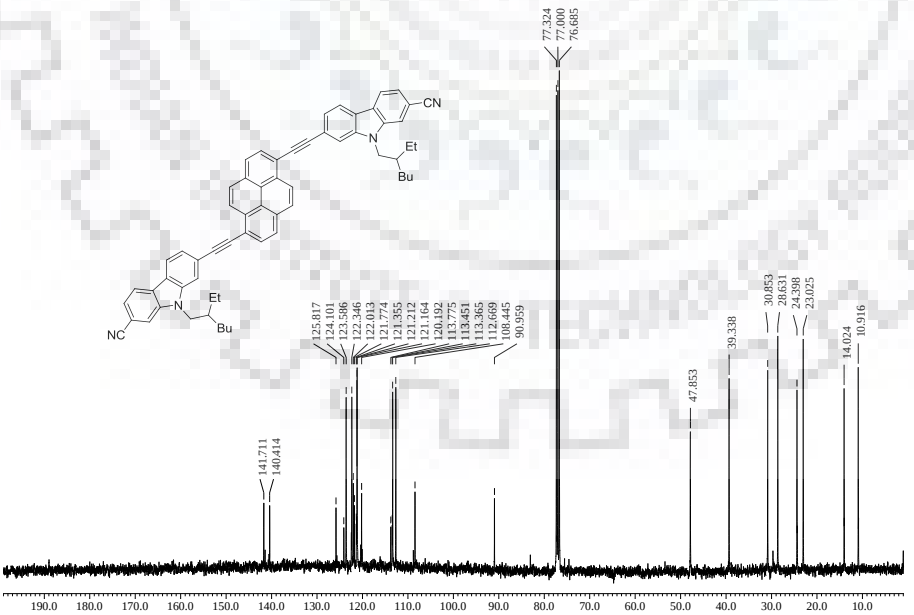

Figure S36 ^{13}C NMR spectrum of **18b** recorded in $CDCl_3$.

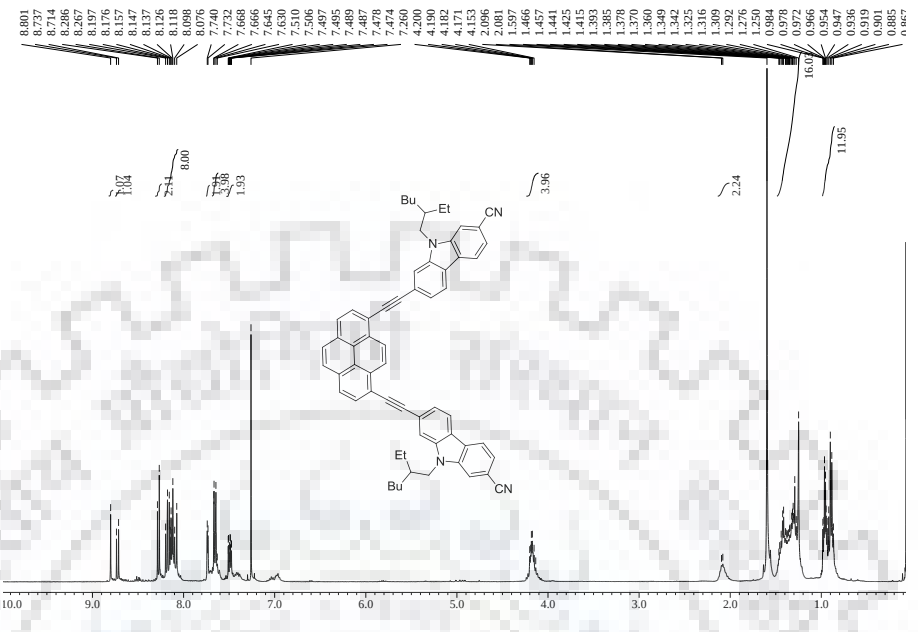

Figure S37 ^{1}H NMR spectrum of **18c** recorded in $CDCl_3$.

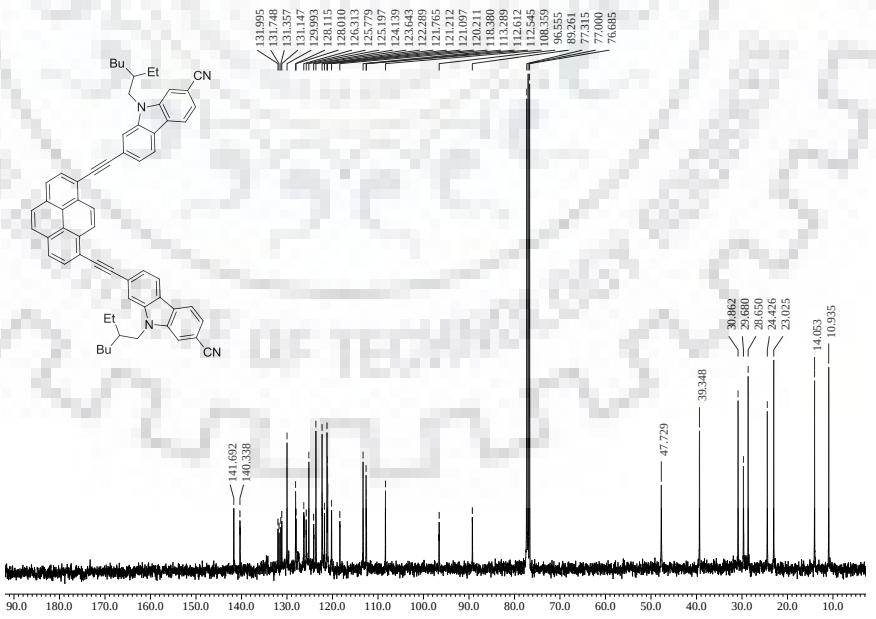

Figure S38 ^{13}C NMR spectrum of **18c** recorded in $CDCl_3$.

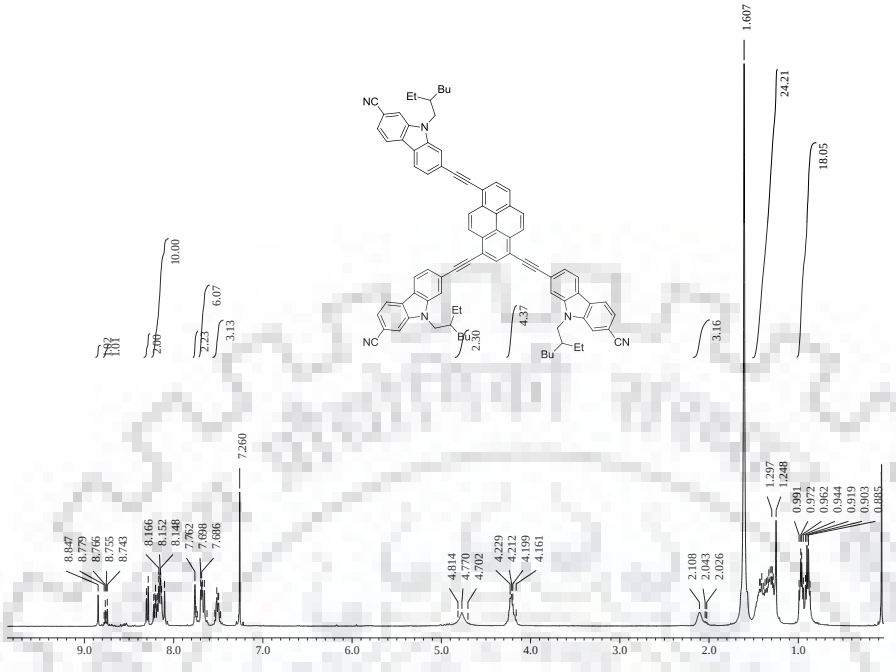

Figure S39 ^{1}H NMR spectrum of **18d** recorded in $CDCl_3$.

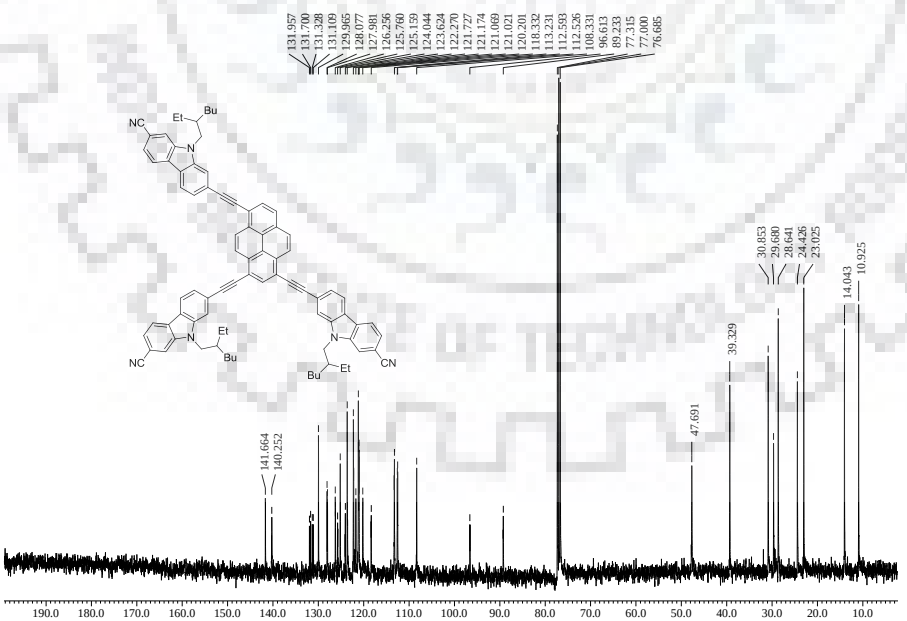

Figure S40 ^{13}C NMR spectrum of **18d** recorded in $CDCl_3$.

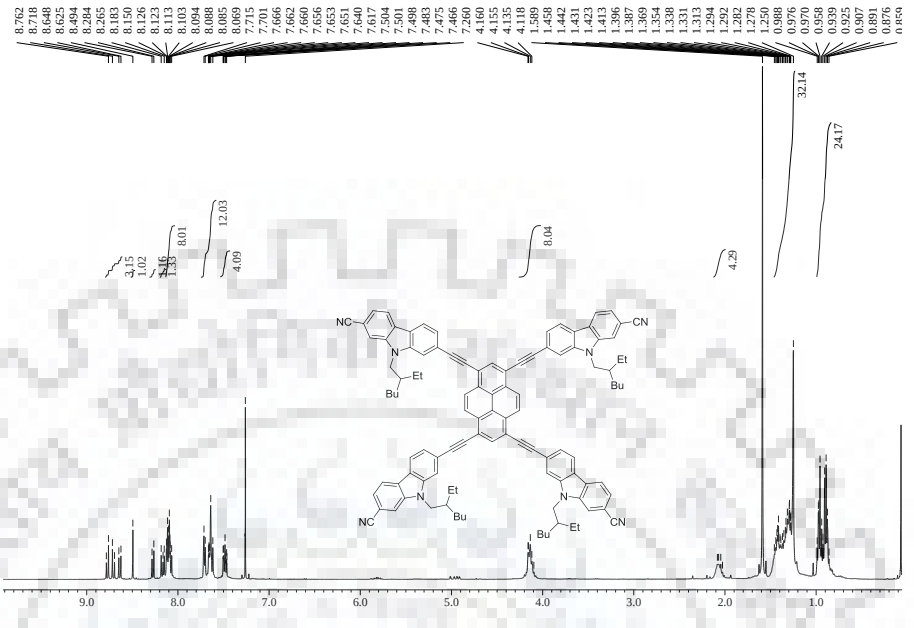

Figure S41 ^{1}H NMR spectrum of **18e** recorded in $CDCl_3$.

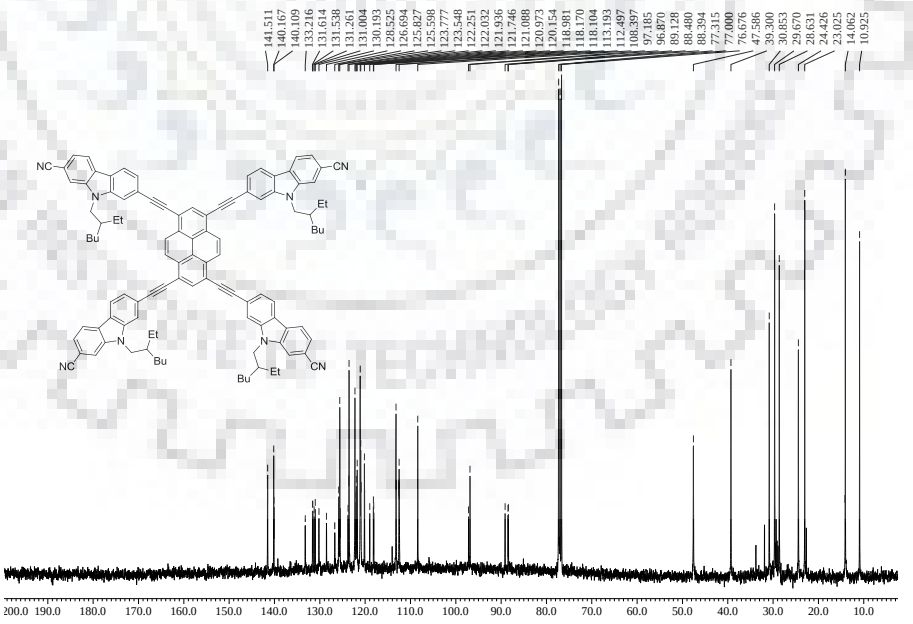

Figure S42 ^{13}C NMR spectrum of **18e** recorded in $CDCl_3$.

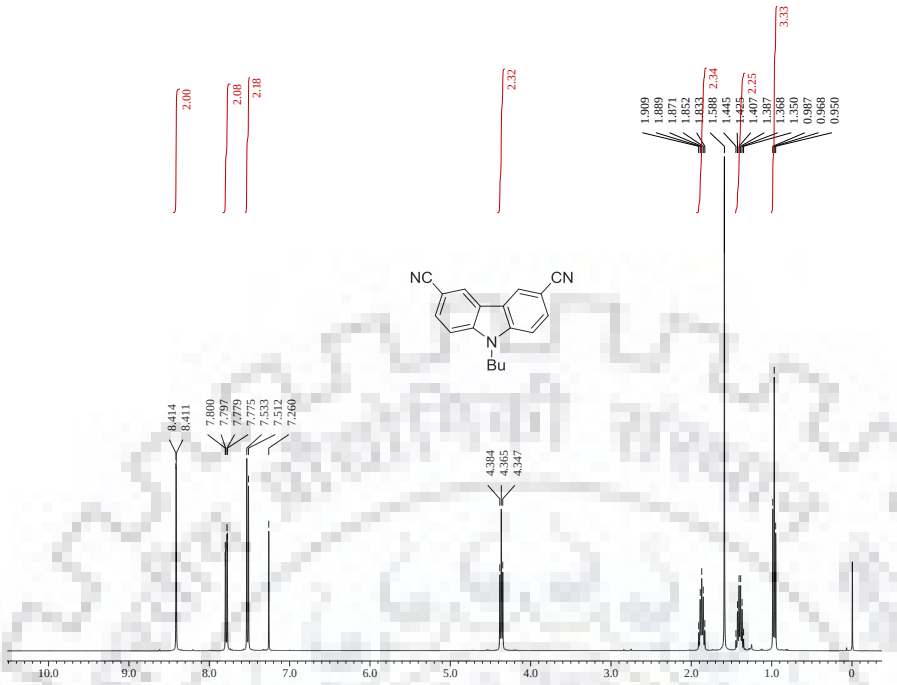

Figure S43 ^{1}H NMR spectrum of **20a** recorded in $CDCl_3$.

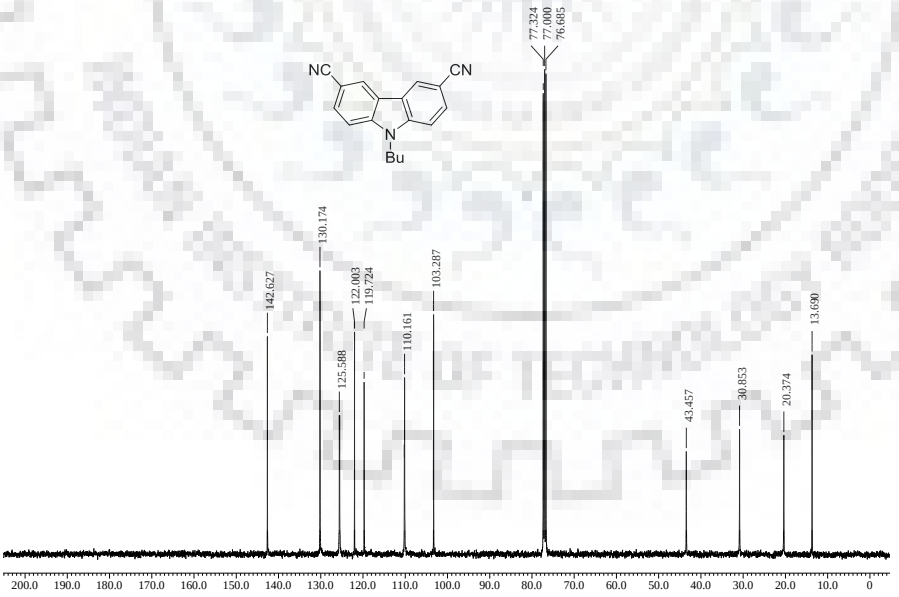

Figure S44 ^{13}C NMR spectrum of **20a** recorded in $CDCl_3$.

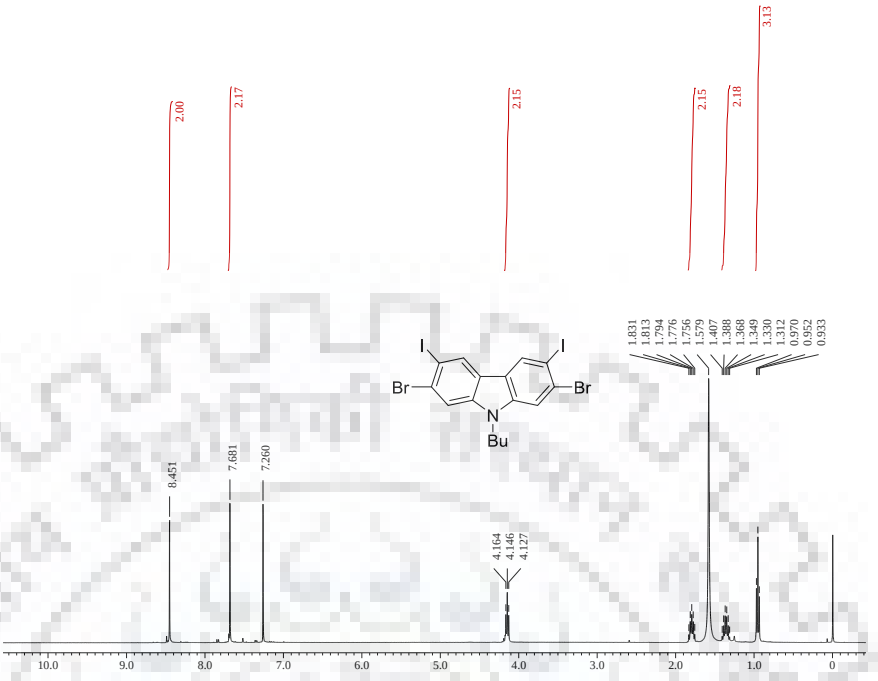

Figure S45 ^{1}H NMR spectrum of **20b** recorded in $CDCl_3$.

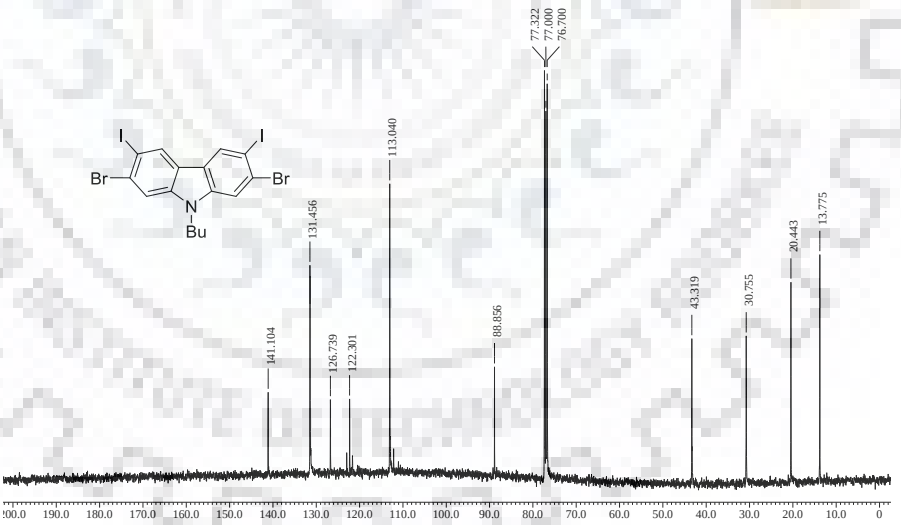

Figure S46 ^{13}C NMR spectrum of **20b** recorded in $CDCl_3$.

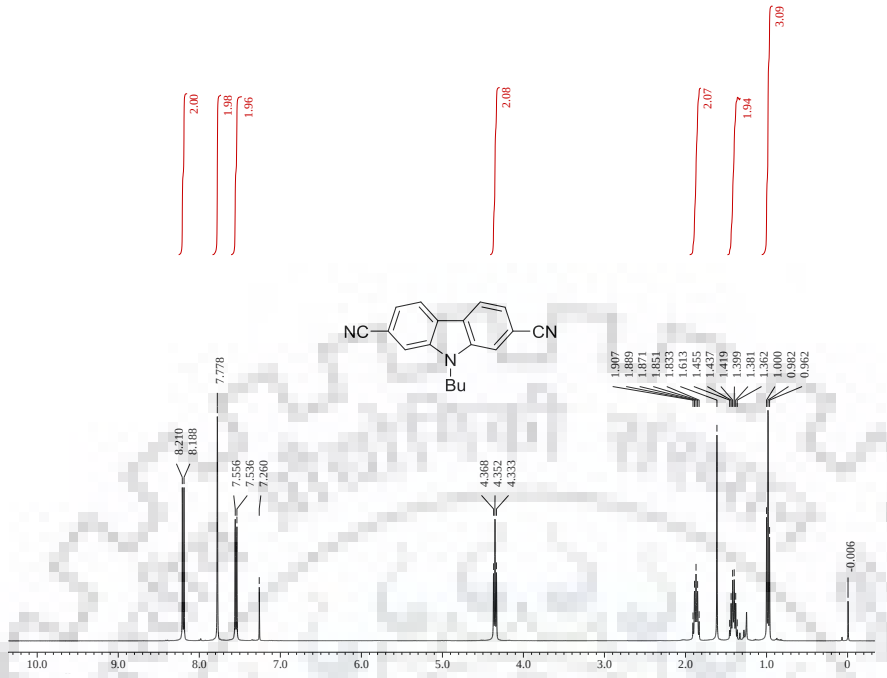

Figure S47 ^{1}H NMR spectrum of **20c** recorded in $CDCl_3$.

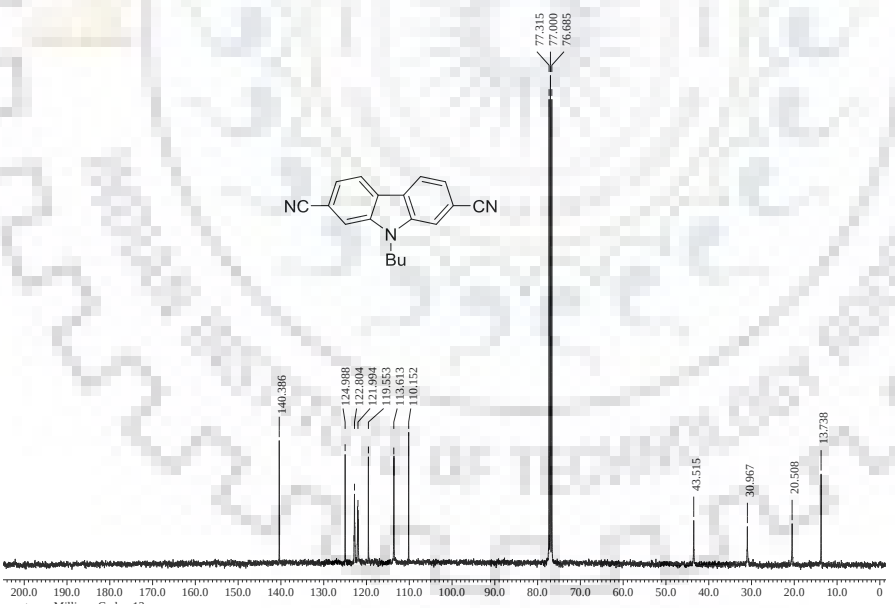

Figure S48 ^{13}C NMR spectrum of **20c** recorded in $CDCl_3$.

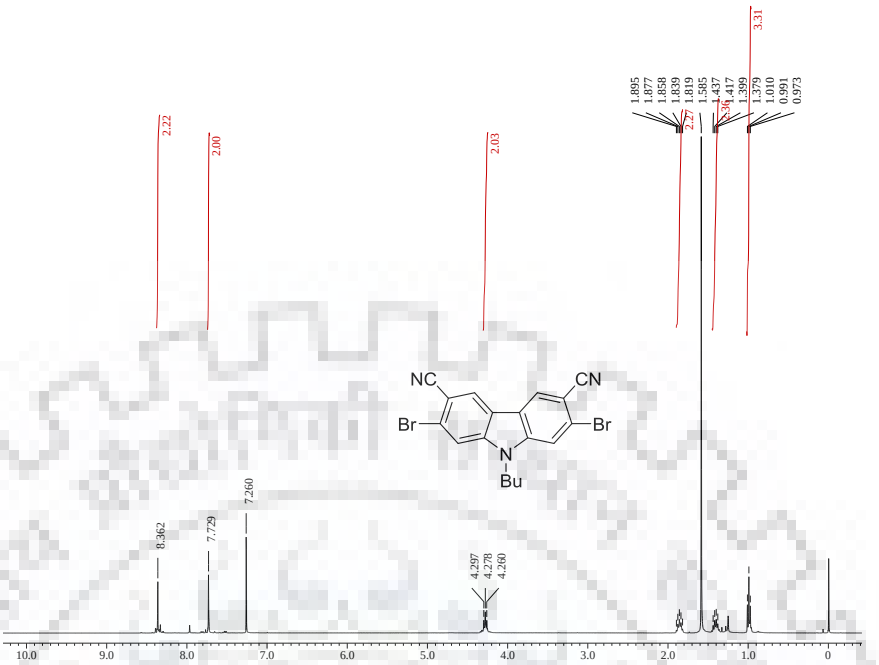

Figure S49 ^{1}H NMR spectrum of **21b** recorded in $CDCl_3$.

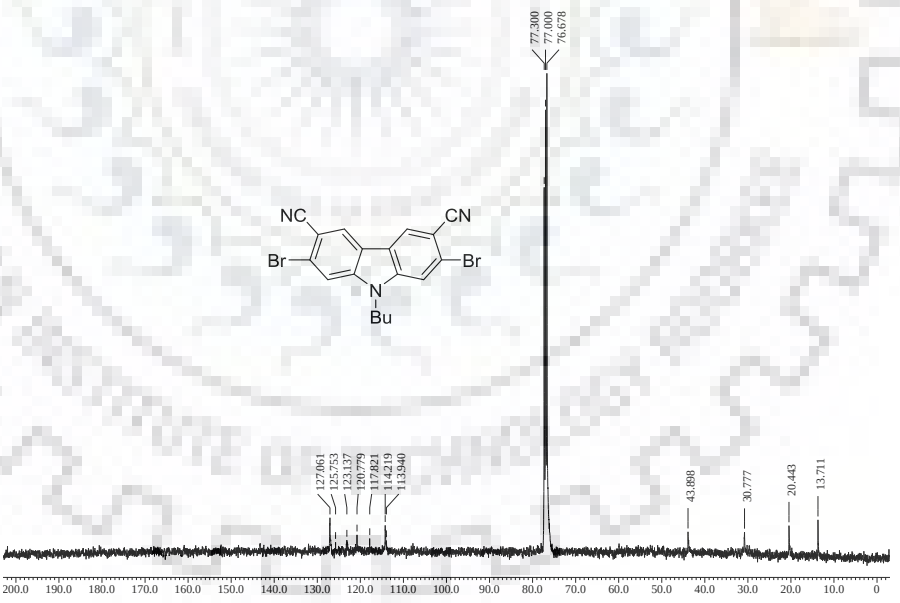

Figure S50 ^{13}C NMR spectrum of **21b** recorded in $CDCl_3$.

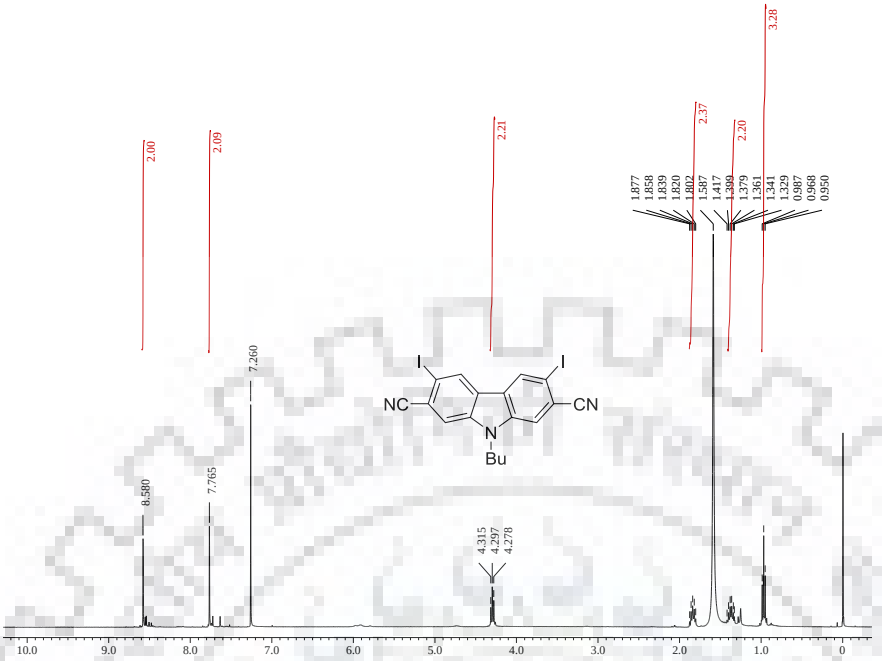

Figure S51 ^{1}H NMR spectrum of **21c** recorded in $CDCl_3$.

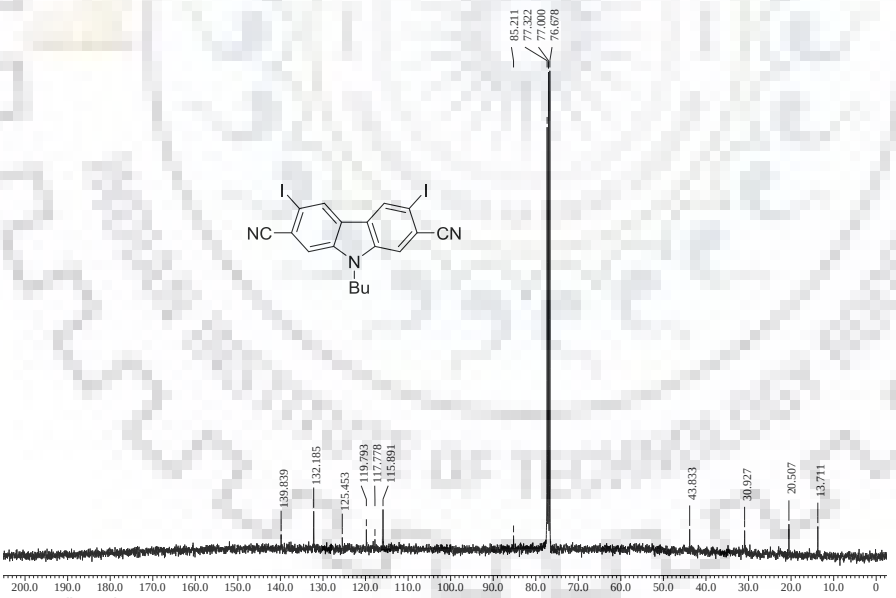

Figure S52 ^{13}C NMR spectrum of **21c** recorded in $CDCl_3$.

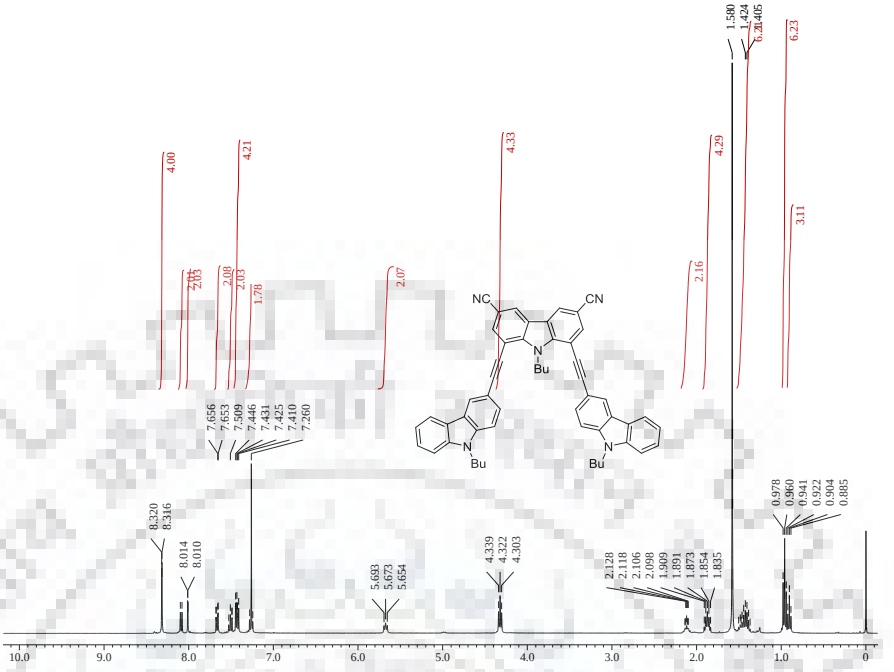

Figure S53 ^{1}H NMR spectrum of **22a** recorded in $CDCl_3$.

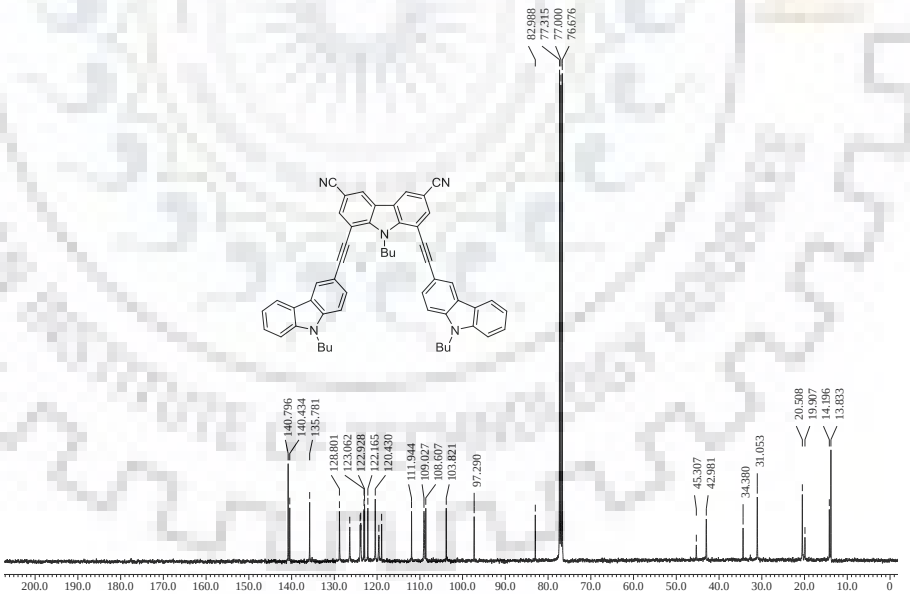

Figure S54 ^{13}C NMR spectrum of **22a** recorded in $CDCl_3$.

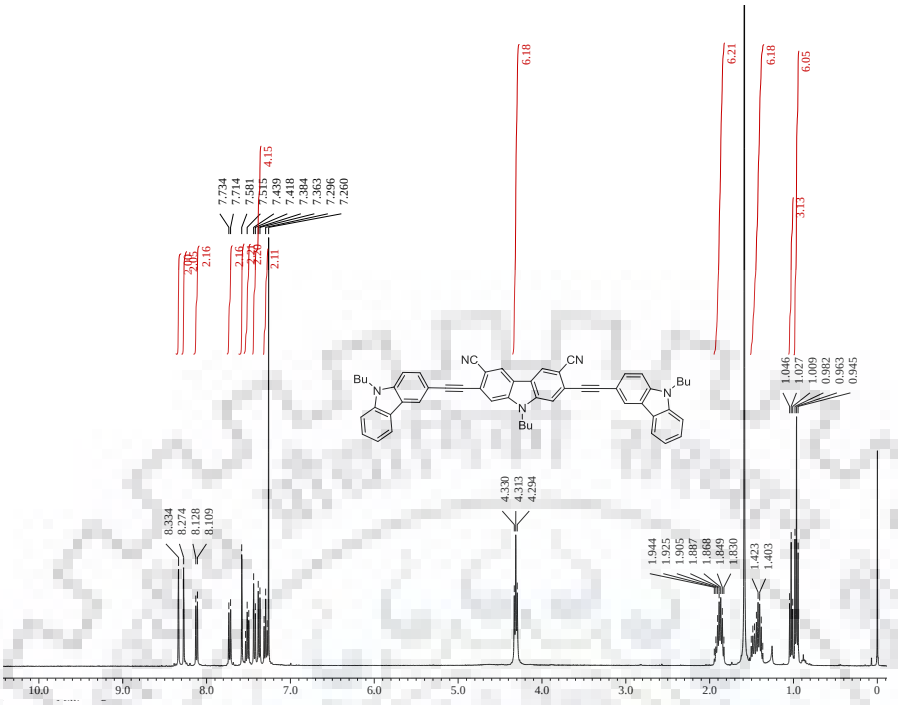

Figure S55 ^{1}H NMR spectrum of **22b** recorded in $CDCl_3$.

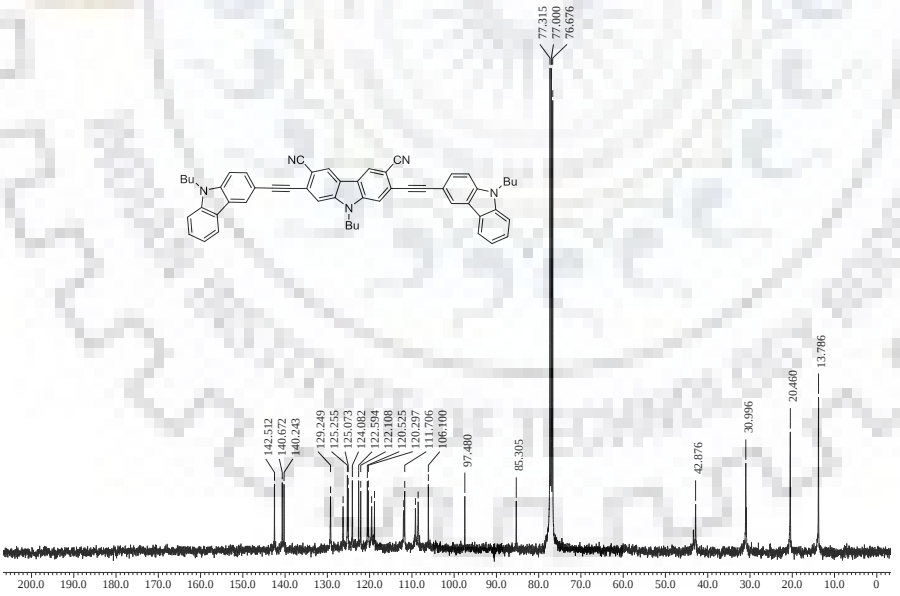

Figure S56 ^{13}C NMR spectrum of **22b** recorded in $CDCl_3$.

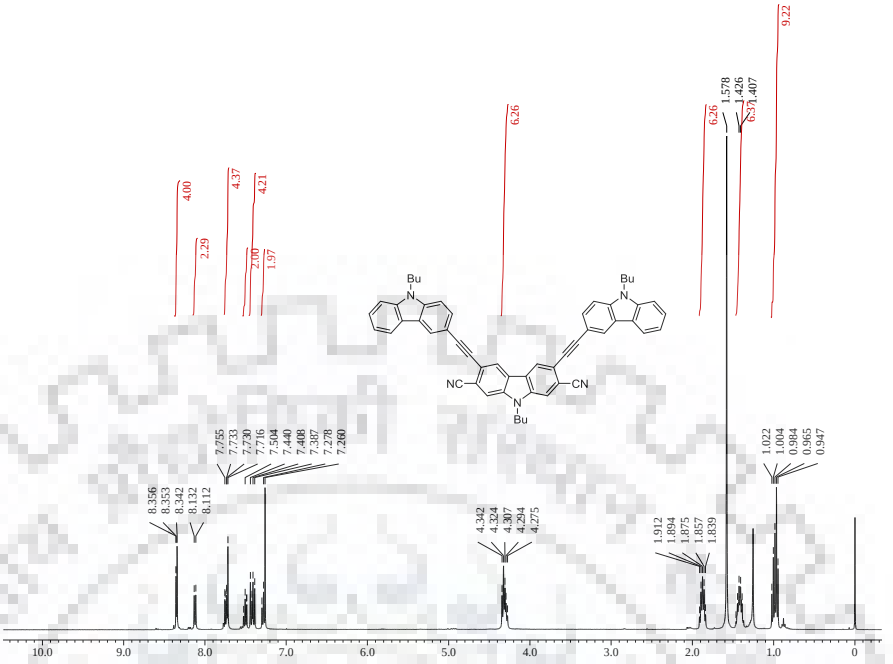

Figure S57 ^{1}H NMR spectrum of **22c** recorded in $CDCl_3$.

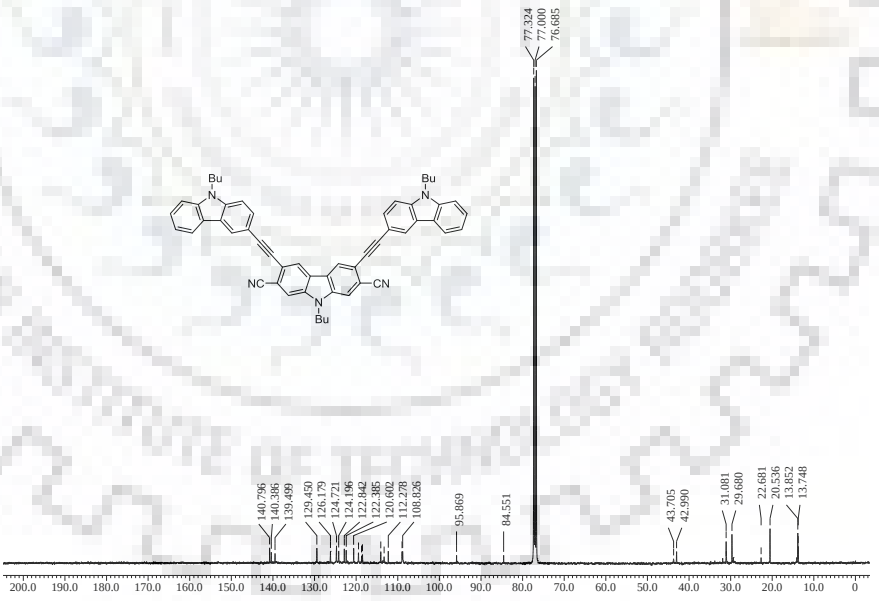

Figure S58 ^{13}C NMR spectrum of **22c** recorded in $CDCl_3$.

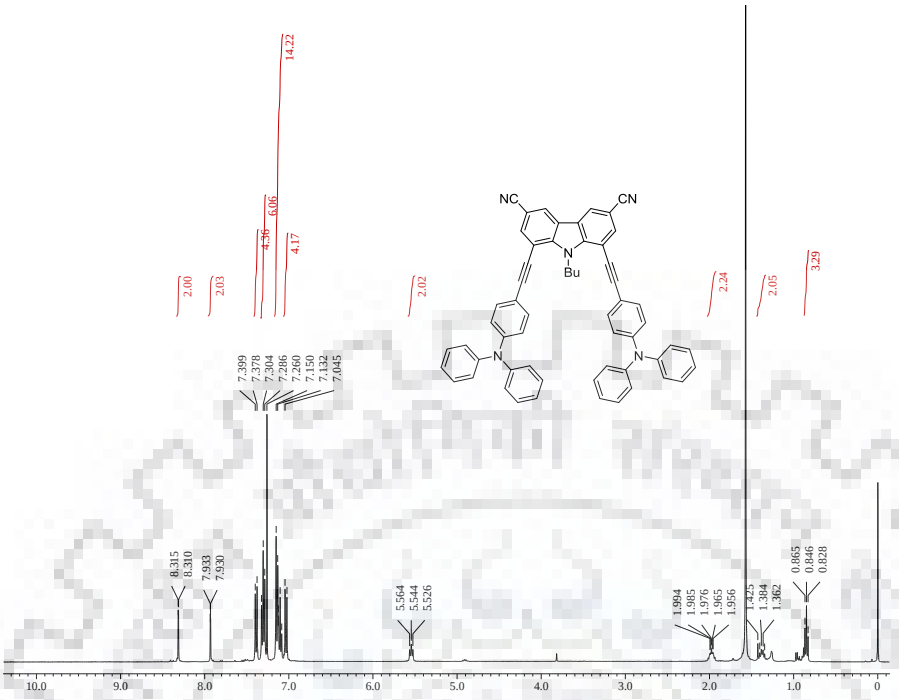

Figure S59 ^{1}H NMR spectrum of **23a** recorded in $CDCl_3$.

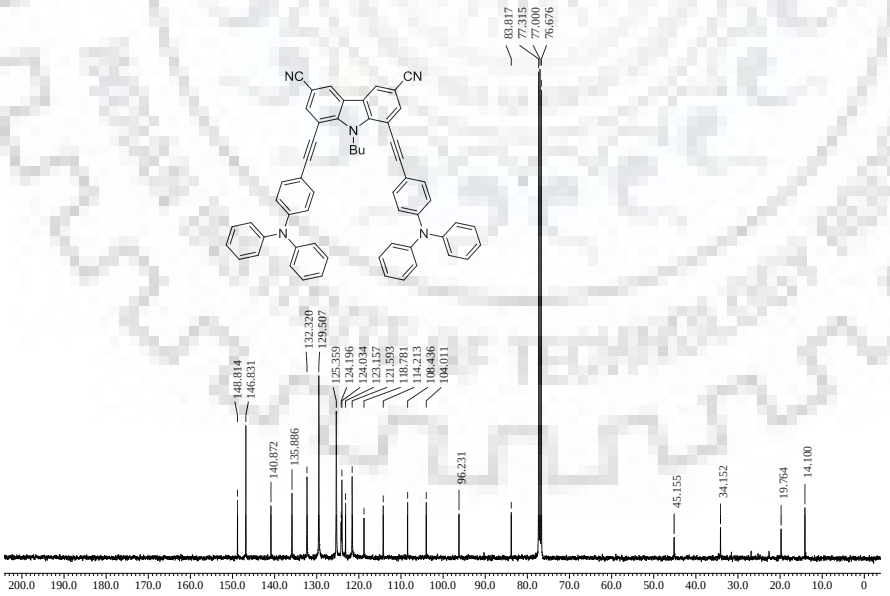

Figure S60 ^{13}C NMR spectrum of **23a** recorded in $CDCl_3$.

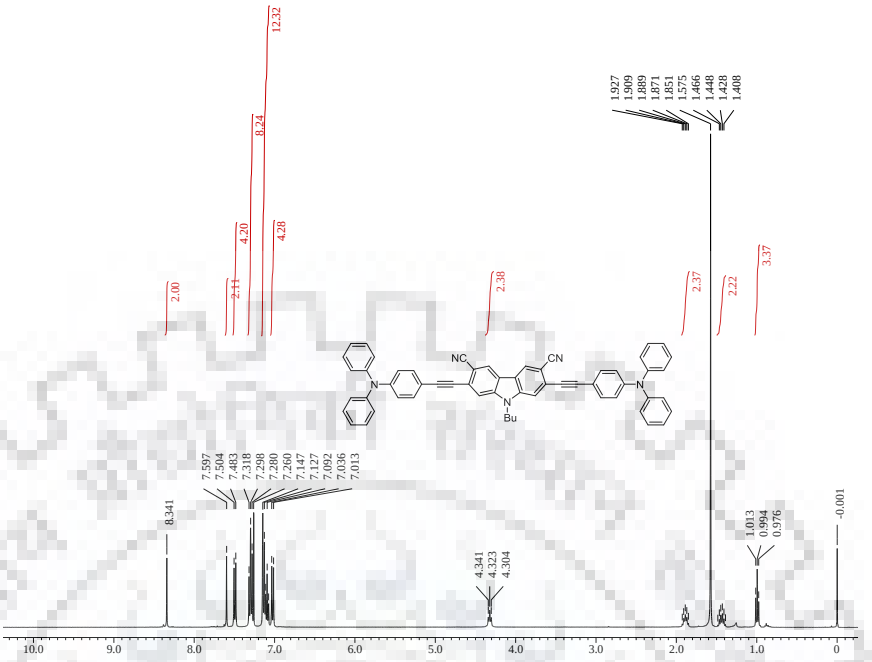

Figure S61 ^{1}H NMR spectrum of **23b** recorded in $CDCl_3$.

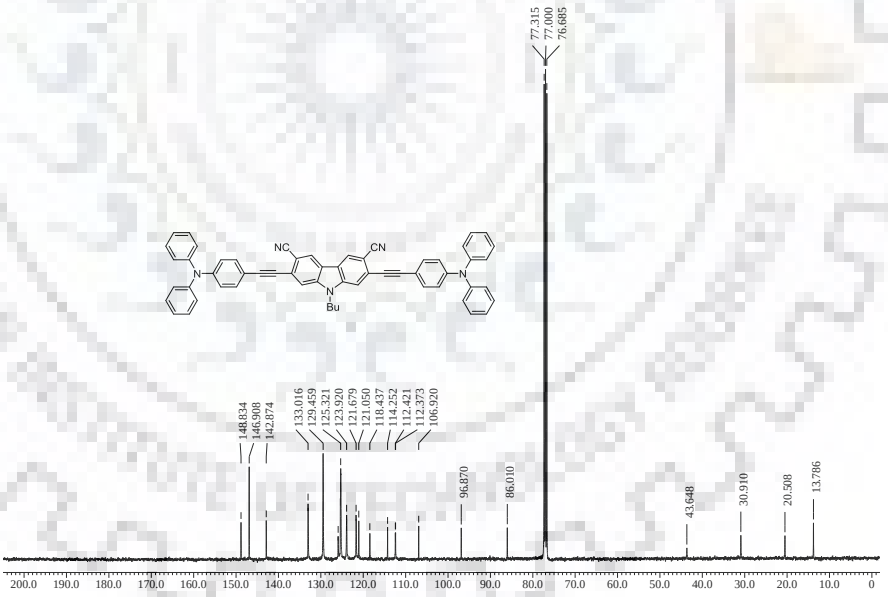

Figure S62 ^{13}C NMR spectrum of **23b** recorded in $CDCl_3$.

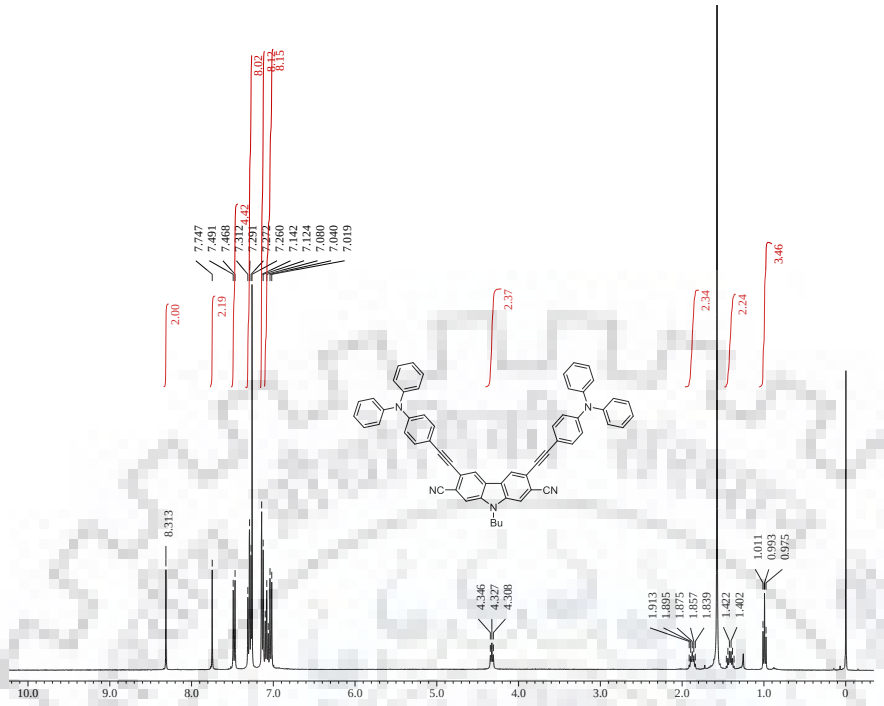

Figure S63 ^{1}H NMR spectrum of **23c** recorded in $CDCl_3$.

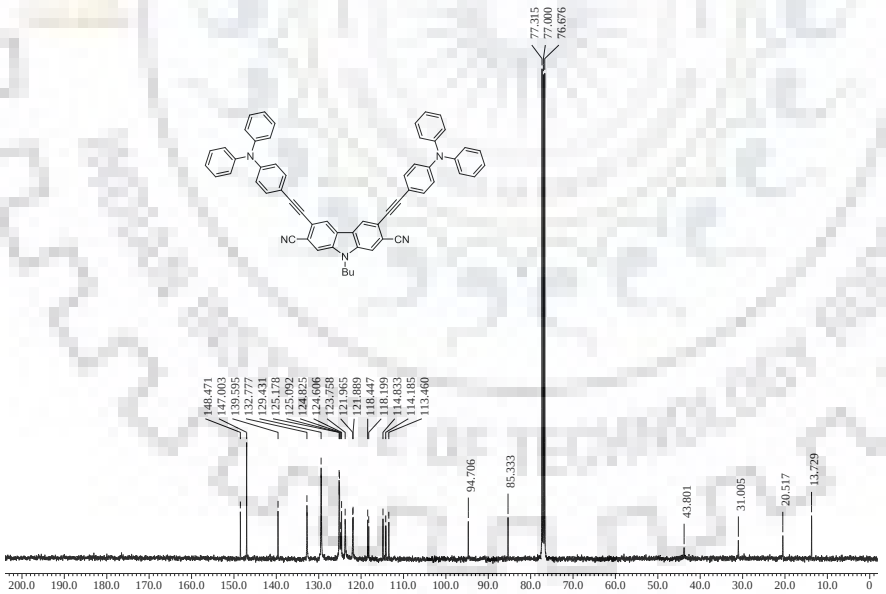

Figure S64 ^{13}C NMR spectrum of **23c** recorded in $CDCl_3$.